Call: NFRP-2019-2020

Topic: NFRP-2019-2020-02 Safety assessments for Long Term Operation (LTO) upgrades of Generation II and III reactors
Funding Scheme: Research and Innovation Action (RIA)

Deliverable No. 4.7

Public Summary Report of WP4

Grant Agreement no.:	945253
Project Title:	**Advanced PTS Analysis for LTO**
Contractual Submission Date:	01/31/2024
Actual Submission Date:	10/09/2024
Responsible partner:	P5: Kiwa

APAL has received funding from the Euratom research and training programme 2019-2020 under grant agreement No 945253.

Grant agreement no.	945253
Project full title	Advanced PTS Analysis for LTO

Deliverable number	**D4.7**
Deliverable title	**Public Summary Report of WP4**
Type[1]	R
Dissemination level[2]	PU
Work package number	WP4
Work package leader	P5: KIWA
Author(s)	Andrey Shipsha, Petter von Unge, Peter Dillström (KIWA), Ralf Tiete, Sébastien Blasset, Vignesh Suryaprakash, Katharina Angermeier (FRA-G), Klaus Heckmann, Jürgen Sievers (GRS), Sándor Kovács (BZN), Diego Fernando Mora Mendez (PSI), David Bouhjiti (IRSN), Susana Flores Holgado, David Flórez del Olmo (TECNATOM), Oriol Costa (JSI), Vladislav Pistora, Miroslav Posta (UJV), Yaroslav Dubyk (IPP)
Keywords	APAL, PTS, LTO, PFM, probabilistic fracture mechanics, probabilistic margin assessment

The research leading to these results has received funding from the Euratom research and training programme 2019-2020 under grant agreement No 945253.

The author is solely responsible for its content, it does not represent the opinion of the European Commission and the Commission is not responsible for any use that might be made of data appearing therein.

[1] **Type**: Use one of the following codes (in consistence with the Description of the Action):
- R: Document, report (excluding the periodic and final reports)
- DEM: Demonstrator, pilot, prototype, plan designs
- DEC: Websites, patents filing, press & media actions, videos, etc.
- OTHER: Software, technical diagram, etc.

[2] **Dissemination level**: Use one of the following codes (in consistence with the Description of the Action)
- PU: Public, fully open, e.g. web
- CO: Confidential, restricted under conditions set out in the Model Grant Agreement
- Cl: Classified, information as referred to in Commission Decision 2001/844/EC

Table of Contents

1 Introduction 9
1.1 Structure of report 10
1.2 Definition of terms used in probabilistic assessments 10
1.3 Alignment/interface between WP3 and WP4 11
2 Definition of probabilistic benchmark 13
2.1 General overview and description of main concepts 13
2.1.1 FAVOR terminology adopted in APAL 13
2.1.2 RPV failure frequency acceptance criterion for APAL 13
2.1.3 Margin definition for PFM assessments 14
2.2 Computational chain for PTS assessment 15
2.2.1 Deterministic assessment 15
2.2.2 Probabilistic assessment 15
2.3 Basic data for RPV probabilistic fracture mechanics assessment 17
2.3.1 RPV design and geometry 18
2.3.2 Flaw type, location and orientation 19
2.3.3 Loads 21
2.3.4 Fracture Toughness Concepts 21
2.3.5 Initial Reference Temperature 23
2.3.6 Reference Temperature Shift 23
2.3.7 Chemical Composition 24
2.3.8 Neutron Fluence 24
2.3.9 Limit Conditions 25
2.3.10 Crack Initiation and Crack Arrest 26
2.3.11 Margin Assessment 28
2.3.12 FAVOR/CAPAL limitations and used assumptions 28
3 Stress and temperature distributions for benchmark performance 34
3.1 Input data 34
3.1.1 RPV geometry 34
3.1.2 Material properties 35
3.1.3 Boundary conditions 36
3.2 Structural analyses of base cases and sensitivity study 36
3.2.1 TH input data from RELAP 36
3.2.2 1D Simulations 39
3.2.3 3D Simulations 40
3.2.4 Other locations 41
3.2.5 Mesh refinement 43
3.2.6 Time steps 44

3.3 Structural analyses of LTO improvements 45
3.3.1 Results from 1D FE analyses 46
3.3.2 Results from 3D FE 52
3.4 Structural analyses for TH uncertainties (Wilks analyses) 58
3.4.1 Uncertainties in TH data analyses for Wilks 58
3.4.2 Typical Wilks TH input data for structural analyses 58
3.4.3 Results for stress and temperature distributions through the RPV wall thickness 60
3.4.4 Discussion of structural analysis results for TH uncertainty 68
4 Baseline probabilistic benchmark 73
4.1 Brief description 73
4.2 Verification of analysis tools 73
4.2.1 Check Random Number Generator (RNG) 73
4.2.2 Check generation of data from a provided tabulated PDF 74
4.2.3 Check generation of tabulated data for UCC (and TCC) 78
4.2.4 Check generation of data from a truncated distribution 83
4.2.5 Check CPI for provided T, K_I and ART 99
4.2.6 Check CPF for provided T, K_I and ART (non-mandatory) 106
4.3 Round-robin benchmarks 108
4.3.1 RR1 – Predict ART for increasing fluence level 109
4.3.2 RR2 – Check CPI for base case transient 114
4.3.3 RR3 – Check CPF for base case transient (non-mandatory) 141
4.3.4 RR4 – Check CPI for base case with distributed crack size 151
4.3.5 RR5 – Check CPF for base case with distributed crack size (non-mandatory) 164
4.4 Discussion and main outcome 173
5 Probabilistic benchmark of LTO improvements 175
5.1 Description of activities 175
5.1.1 Baseline benchmarks (Mandatory) 177
5.1.2 Non-Mandatory benchmarks 178
5.2 Results from probabilistic benchmark of LTO improvements 179
5.2.1 Results for each LTO improvement 179
5.2.2 Plausibility checks 197
5.3 Discussion and main outcome 206
5.4 CPI values for PMA1 and PMA2 207
6 Probabilistic benchmark of uncertainties in the TH data 213
6.1 Description of Activities 213
6.1.1 Baseline benchmarks (Mandatory) 214
6.1.2 Non-Mandatory benchmarks 215
6.2 Results from probabilistic benchmark of TH uncertainties 216

6.2.1 Results overview for PMA1 216
6.2.2 Results overview for PMA2 237
6.2.3 Plausibility checks 251
6.3 Discussion and main outcome 259
7 Probabilistic margin assessment 261
7.1 Objectives 261
7.2 Introduction to margin concepts 262
7.3 Probabilistic Margins Concepts 262
7.3.1 Assessment based on fracture toughness (PMA1) 262
7.3.2 Assessment based on lifetime (PMA2) 263
7.3.3 Assessment based on failure frequency (PMA3) 264
7.3.4 Assessment based on reliability theory (PMA4) 264
7.4 Description of Activities 265
7.4.1 Common approaches for probabilistic assessment 265
7.4.2 Relation to other deliverables and tasks 266
7.4.3 Common template 266
7.4.4 Case selection and connection points to D4.3, D4.4 and D4.5 268
7.5 Probabilistic margin assessment 268
7.5.1 Probabilistic margin assessment for baseline probabilistic cases 269
7.5.2 Probabilistic margin assessment of LTO improvements 274
7.5.3 Probabilistic margin assessment of thermal-hydraulic uncertainties 283
7.6 Conclusion 290
8 General conclusions of WP4 292
9 Lessons-learned in WP4 296
9.1 Tool verification and round robin analyses 296
9.2 Probabilistic analyses and margin assessments 296
10 References 298

List of Abbreviations

ACC	Accumulator
APAL	Advanced PTS Analysis for LTO
ART	Adjusted Reference Temperature
ASME	The American Society of Mechanical Engineers
ATHLET	Analysis of THermal-hydraulics of LEaks and Transients
BFD	Bounding Flaw Depth
BZN	Bay Zoltán Nonprofit Ltd. for Applied Research
CAPAL	Code for APAL (project specific version of FAVOR)
CDF	Cumulative Distribution Function
CFL	Crack Front Length
CPF	Conditional Probability of Failure
CPI	Conditional Probability of Initiation
cpi(t)	Instantaneous conditional probability of initiation
CPNA	Conditional Probability for Non-Arrest
CPSA	Conditional Probability for Stable Arrest
D	Deliverable
DC	Downcomer
EC	Embedded crack
ECC	Emergency core cooling
ECCS	Emergency core cooling system
FAVOR	Fracture Analysis of Vessels – Oak Ridge (software)
FD	Flaw Depth
FE	Finite element (Analysis/method)
FI	Frequency of crack initiation
FF	frequency of failure
FL	Flaw Length
FORM	First Order Reliability Method
FRA-G	Framatome GmbH
GRS	Expert organisation on nuclear safety (Gesellschaft für Anlagen- und Reaktorsicherheit)
HPI	High Pressure Injection
HPSI	High Pressure Safety Injection
ICAS	International Comparative Assessment Study (OECD NEA project)
IPP	IPP Centre LLC
JSI	Jožef Stefan Institute
KIWA	Kiwa Technical Consulting AB
KWU	Kraftwerk Union AG
LB	Lower Bound
LTO	Long Term Operation
MART	Maximum Allowable Reference Temperature
max. all. ART	Maximum Allowable Reference Temperature
MC	Master Curve
MCS-IS	Monte Carlo Simulation with Importance Sampling
MPFP	Most Probable Failure Point
MIX	Mixing
MV	Mean Value
NPP	Nuclear power plant

NRC	(United States) Nuclear Regulatory Commission
OCI	Oak Ridge Consulting International, Inc.
PDF	Probability Density Function
PFM	Probabilistic Fracture Mechanics
PMA	Probabilistic Margin Approach
PNNL	Pacific Northwest National Laboratory
PSI	Paul Scherrer Institut
PTS	Pressurized Thermal Shock
RELAP	Reactor Excursion and Leak Analysis Program (software)
RNG	Random Number Generator
RPV	Reactor Pressure Vessel
RR	Round Robin
SD	Standard Deviation
SIF	Stress Intensity Factor
SSTC	State Scientific and Technical Center for Nuclear and Radiation Safety
TCC	Through-Clad Crack
TCC1	Through-Clad Crack with recommended SIF-solution in APAL
TCC2	Through-Clad Crack with SIF-solution in FAVOR
Tecnatom	Tecnatom S.A.
TH	Thermal Hydraulic
TRACE	TRAC/RELAP Advanced Computational Engine
UCC	Underclad Crack
UJV	ÚJV Řež, a. s. (in English: Nuclear Research Institute, Rez)
u-space	Space of standard normal variables
VB	Visual Basic
WP	Work Package
WPS	Warm Pre-Stressing
WRS	Weld Residual Stress

List of Symbols

a	Crack Depth [mm]
c	Half Crack Length [mm]
d	Distance from cladding/base fusion line (for embedded cracks) [mm]
f_{err}	Error function [°C]
h	RPV wall thickness (excluding cladding) [mm]
i	Index
p	Probability
r	Cladding thickness [mm]
t	RPV wall thickness (including cladding), $h + r$ [mm]
x	Distance from cladding/base fusion line [cm]
y	Random number
B	Crack Front Length used in MC [mm]
Cu	Copper content [%]
F	Neutron fluence [neutron/m²]
F_0	Neutron fluence at cladding/base fusion line [neutron/m²]
K_I	Modus I stress intensity factor [MPa$\sqrt{\text{m}}$]
K_{Ia}	Fracture toughness measured at cleavage crack arrest [MPa$\sqrt{\text{m}}$]
K_{Ic}	Plane strain fracture initiation toughness [MPa$\sqrt{\text{m}}$]
K_{Jc}	K-equivalent of the value of J measured at cleavage crack initiation [MPa$\sqrt{\text{m}}$]
M_p	Inverse standard normal distributed value used in MC
Mn	Manganese content [%]
Ni	Nickel content [%]
P	Phosphorus content [%]
RT_{NDT}	Nil ductility reference temperature [°C]
RT^0_{NDT}	Initial nil ductility reference temperature [°C]
T	temperature [°C]
T_0	MC reference temperature [°C]
T^0_0	Initial MC reference temperature [°C]
T_c	Cold leg temperature under normal full power operating conditions [°C]
T_{KIa}	Temperature at which the K_{Ja} MC has a median value of 100 MPa$\sqrt{\text{m}}$ [°C]
β	Random value
γ	Random value sampled from a continuous uniform distribution between (0, 4)
ΔRT_{NDT}	Reference temperature shift [°C]
μ	Mean value
σ	Standard deviation
φ	Neutron fluence divided by 10^{23} [10^{23}·neutron/m²]
ϕ	Average neutron flux [n/cm²/s]

1 Introduction

APAL (Advanced PTS Analysis for LTO) is a project funded by the EU within HORIZON 2020 programme. One of the most limiting safety assessments for the long-term operation (LTO) of nuclear power plants (NPPs) is the reactor pressure vessel (RPV) integrity assessment for pressurized thermal shock (PTS). The main objectives of APAL project are the following:

- development of advanced deterministic and probabilistic PTS assessment methods,
- quantification of deterministic and probabilistic safety margins,
- development of best-practice guidance.

The APAL project consists of 7 work packages (WP):

- WP1 - LTO improvements relevant for PTS event
- WP2 - Improvement of TH analysis
- WP3 - Deterministic margin assessment
- **WP4 - Probabilistic margin assessment**
- WP5 - Definition of best-practice for advanced PTS analysis
- WP6 - Training, Communication, Dissemination and Exploitation
- WP7 - Scientific coordination and project management

This report summarises the work, main results, conclusions and lessons learned of WP4 “Probabilistic margin assessment”. The main objective of WP4 was to determine the impact of LTO improvements and uncertainties in thermal hydraulic (TH) data on the results of PTS analysis using probabilistic assessment. As a part of this assessment, probabilistic safety margins have been quantified and compared with deterministic safety margins.

The WP4 (Probabilistic margin assessment) consists of six tasks:

- Task 4.1: Structural assessment
- Task 4.2: Definition of a probabilistic benchmark
- Task 4.3: Baseline probabilistic benchmark
- Task 4.4: Probabilistic benchmark related to LTO improvements
- Task 4.5: Probabilistic benchmark related to uncertainties in the TH data
- Task 4.6: Probabilistic margin assessment.

Task 4.1 *Structural assessment*, addresses calculations of stress and temperature distributions through the RPV wall thickness at the prioritized positions [1]. The obtained stress and temperature distributions through the RPV wall provide the key input data for subsequent fracture mechanics analyses as a part of deterministic and probabilistic benchmarks and margin assessments. Most of the efforts regarding structural analyses of the RPV have been carried out and discussed in detail within WP3 [7]. Within WP4, the structural analyses were performed to evaluate the influence of uncertainties in TH analyses and TH data on transient stress and temperature distributions through the RPV wall thickness.

Task 4.2 *Definition of a probabilistic benchmark*, deals with development and definition of the probabilistic benchmark for probabilistic fracture mechanics PTS assessment. This task provides also definitions of all basic concepts, approaches and input data required for probabilistic assessments within APAL. Besides that, the benchmark definition contains the pre-requisite tasks related to verification of probabilistic tools used by APAL partners and several round-robin tasks for baseline probabilistic benchmark carried out within Task 4.3. The probabilistic benchmark in Task 4.2 has been developed in parallel with the deterministic fracture mechanics assessment benchmark within WP3 [7] for ensuring a solid basis for comparison between deterministic and probabilistic analyses.

Task 4.3 *Baseline probabilistic benchmark*, focuses on the analysis work with baseline probabilistic benchmark. All activities within this Task have been divided into two main parts. The first part addresses verification of probabilistic tools and methods used by participants for probabilistic analyses

in the APAL project. The second part contains several round robin benchmarks for testing and adjusting the input data and verifying a complete chain of probabilistic analyses performed in Tasks 4.4-4.5.

Task 4.4 *Probabilistic benchmark related to LTO improvements*, addresses the probabilistic fracture mechanics assessments of max. allowable ART-values and allowable RPV age based on the TH data for selected LTO improvements in comparison with the TH data for the Base case. Task 4.4 is primarily focused on performing and summarising the probabilistic calculations of the selected LTO improvements. A detailed interpretation of the results and probabilistic margin assessments are performed as a part of Task 4.6 in the report D4.6 [6].

Task 4.5 *Probabilistic benchmark related to uncertainties in the TH data,* addresses the probabilistic fracture mechanics calculations of max. allowable ART-values and allowable RPV age related to uncertainties in the TH data. Similarly to Task 4.4, the Task 4.5 is primarily focused on performing and summarising the probabilistic calculations for the TH uncertainties. A detailed interpretation of the results and probabilistic margin assessments are performed as a part of Task 4.6 in the report D4.6 [6].

Task 4.6 *Probabilistic margin assessment*, investigates different probabilistic margin assessments for PTS analyses. Besides the baseline cases, probabilistic margins are quantified and discussed for the LTO improvements and the TH uncertainties.

1.1 Structure of report

Section 2 provides a fundamental basis for all Tasks within WP4 presenting a definition of probabilistic benchmark in APAL along with the main concepts and terminology. This Section also describes the approach for probabilistic fracture mechanics assessment of RPV including necessary input data, conditions, and equations for probabilistic margin assessment.

Section 3 describes the structural analyses in APAL which have been performed to calculate stress and temperature distributions through the RPV wall thickness for the analysed transient event. The obtained distributions provide the key input data for subsequent fracture mechanics analyses as a part of deterministic and probabilistic benchmarks and margin assessments. Within WP4, the structural analyses of stress and temperature distributions through the RPV wall thickness are focused on evaluating the influence of uncertainties in TH analyses and TH data. The structural analyses for investigating the effect of different LTO improvements on stress and temperature distributions through the RPV wall thickness are also covered briefly in Section 3 as they are presented in detail in the Public Summary report for WP3.

Section 4 summarises the work with baseline probabilistic benchmark performed within Task 4.3. All activities within this Task have been divided into two main parts. The first part addresses verification of probabilistic tools and methods used by participants for probabilistic analyses in the APAL project. The second part contains several round robin benchmarks for testing and adjusting the input data and verifying a complete chain of probabilistic analyses in APAL.

Sections 5 and 6 describe the probabilistic assessments for LTO improvements and TH uncertainties performed within Tasks 4.4 and 4.5 respectively. These sections present a summary of probabilistic results obtained by different partners along with performed plausibility checks.

Section 7 provides a detailed interpretation of all probabilistic results along with quantification and comparison of margins.

Sections 8 and 9 provide summarizing remarks (lessons learned) and general conclusions for WP4 in APAL.

1.2 Definition of terms used in probabilistic assessments

This Section provides definitions that have been used for probabilistic assessments within the APAL project:

- **Baseline case** = benchmark case with methods, models and set of parameters to be investigated by all partners (mandatory)
- **Base case TH data set** = new conservative transient (in the meaning to be conservative for the safety assessment) for T2 from ICAS including accumulator, named now APAL-ICAS T2, this is the reference transient
- **Best estimate TH data set** = transient results from Task 2.3 **"**best estimate solution**"** from **"**Wilks set**"** is a solution of TH calculations for the APAL-ICAS T2 transient with all input parameters (both plant parameters and model parameters, as well as human-factor parameters) set to their best estimates if they are available. (Otherwise, the conservative value is applied.)
- **Average transient data set** = transient results from task 2.3 from **"**Wilks set", the term "Wilks set" implies random selection of parameters. This is in contradiction "all input parameters set to their best estimates", hence we select "some average" transient from the Wilks set
- **Base line assessment** = basic assessment considering base case TH loading for structural assessment, RPV location of interest at core weld below cold leg with safety injection
- **Enveloping TH data set** = results from Task 2.3 (enveloping solution from Wilks set of TH calculations) and was evaluated in task 4.5 (margin assessment related to TH uncertainties), from Wilks set
- **Statistical TH data sets** = set of all transients (i.e., coming from Wilks method) resulting from task 2.3 and was evaluated in Task 3.5 (margin assessment related to TH uncertainties)
- **Long term operation (LTO) improvements** = set of transients concerning TH improvement to RPV brittle fracture assessment for long term operation resulting from Task 2.1 and was assessed in Task 4.4 (margin assessment related to LTO improvement)
- **ART** = adjusted reference temperature (from indirect or direct measurement), this is the name chosen for the index of the K_{Ic} curve (RT_{NDT} concept, indirect) as well as for the index from the Master Curve (direct measurement of T_0 + margin = RT_0).
- **max. all. ART =** This is the (calculated from PTS fracture mechanics safety assessment) value being shifted in order to find the highest index fulfilling the limit condition (tangent or WPS). The max. all. ART can be max. all. RT_{NDT} or max. all. RT_0, depending on the adopted concept (RT_{NDT} or Master Curve)
- **margin** (in…against … between … and …due to ...) = the term margin alone does not mean anything, the relation leading to a margin must be always specified. Specifically, in the APAL project the definition of the margin is given by: margin in maximum allowable reference temperature (max. all. ART) against RPV failure (situation leading to crack initiation or non-arresting crack), this is given by the comparison (difference) of maximum allowable ARTs between situation A and situation B due to the change of a given parameter.
- **Inherent margin** = Unquantifiable positive bias in results of some method, calculation, assessment, measurement, etc.
- **RPV failure** = within the APAL project, this is the name of the situation obtained if a postulated crack could initiate under given combination of loading and aging (mandatory task, penalizing) and if a propagating crack cannot stop or growths up to some given proportion of RPV thickness (e.g. 75%) under given combination of loading and aging (aging is non-mandatory task), i.e. RPV failure = crack growth up to 75% of the RPV wall thickness
- **Limit condition** (or limit state): WPS or tangent approach; initiation or unstable (non-arresting) crack growth (or too deep crack, i.e., plastic collapse).

1.3 Alignment/interface between WP3 and WP4

Within APAL, WP3 and WP4 have a strong interaction as the deterministic and probabilistic benchmark definitions are both based on the same technical basis and input data from structural assessment (i.e. stress and temperature field) are identical.

Both benchmarks have the following common input data:

- RPV geometry
- Material properties (mechanical and physical)
- Residual stresses
- Stresses from PTS transient
- SIF solution
- Limit conditions (tangent approach, WPS)

Another common approach is the location of postulated flaw. In both benchmarks a single flaw is assessed located at position of interest (e.g. core weld elevation below cold plume).

Within the probabilistic fracture mechanics benchmark some fracture-mechanics input data are treated as distributed parameters. Starting from sampling exercises, and beginning with only fracture toughness as distributed parameter, the level of complexity of the probabilistic assessment was increased during the benchmark performance and the type of probabilistic margin assessment. Concerning the determination of max. all. ART within the margin assessment, a connection to deterministic benchmark was ensured, as some quantiles (i.e. pre-defined lower bounds) of the fracture toughness (and crack arrest) distribution was used in the deterministic assessment:

- Fracture toughness:
  - RT_{NDT} concept: Use ASME Curve as Mean – 2xStandard deviation (i.e. 2.5% lower bound) for deterministic benchmark
  - Master Curve (T_0) concept: Use 5% lower bound of crack initiation distribution for deterministic benchmark
- Crack Arrest:
  - RT_{NDT} concept: Use ASME Curve as Mean – 2xStandard deviation (i.e. 2.5% lower bound) for deterministic benchmark
  - Master Curve (T_0) concept: Use 5% lower bound of crack arrest distribution for deterministic benchmark

For the case, that fracture toughness is the only parameter assumed distributed, the above-mentioned use of quantiles for the deterministic benchmark led to the artificial effect, that the probabilistic assessment gives more conservative max. all. ART. In such case, the probabilistic margin assessment with a pre-defined allowable cpi of 2.22E-04 can be treated as equivalent to a deterministic margin assessment taking into account a 2.22E-04 (i.e. 0.22%) lower bound fracture toughness, which is more conservative than Mean Value – 2 x standard deviation for ASME K_{IC} or 5% lower-bound Master-Curve K_{IC}. It should be kept into mind, that this is an artificial conservatism, as a full probabilistic fracture mechanics assessment usually leads to higher max. all. ART and can be used to quantify margins of a deterministic assessment in terms of failure probability.

In addition, the quantification of impact of TH uncertainties was done based on both approaches, although it is more related to a full probabilistic assessment. The impact of the TH uncertainties on stress and temperature fields have been determined by assessing all of the Wilks data sets. As the goal of APAL was to determine the impact of TH uncertainties on margin assessment, it was out of scope to derive a stress and temperature uncertainty due to TH input data variation. The APAL approach within WP2 was to determine lower bound TH data sets by Wilks analysis and compare it with the base case TH data set. But it turned out, that the identification of lower bound TH data set requires the full chain of PTS analysis up to final fracture mechanics for margin assessment. Therefore, the assessment of all TH data sets from Wilks analysis was required in both, deterministic and probabilistic margin assessment.

As the structural assessment is a common basis for both deterministic and probabilistic benchmark, the corresponding chapter will be part of both public summary reports.

2 Definition of probabilistic benchmark

This Section provides an overview and definition of the benchmark for probabilistic fracture mechanics PTS assessment developed in Task 4.2 within WP4. This benchmark has been defined in parallel with the deterministic fracture mechanics assessment benchmark within the WP3 [7] for ensuring a solid basis for comparison between deterministic and probabilistic analyses.
The probabilistic benchmark is based on the work performed in DEFI-PROSAFE [20] and further extended in APAL, embracing the following aspects:

- different types of flaws (underclad and through-clad cracks, embedded cracks),
- different crack locations (inside and outside cold plume),
- fracture toughness concepts (ASME RT_{NDT}, Master Curve T_0),
- limit conditions (Tangent and Max WPS approaches).

The probabilistic benchmark also includes the required input data for performing the baseline probabilistic assessment as described in Section 4.

2.1 General overview and description of main concepts

2.1.1 FAVOR terminology adopted in APAL

The terminology used for probabilistic assessments in the previous projects, e.g. PROSIR [22], differs from the FAVOR [23] terminology adopted in APAL. This Section provides definitions for important terms and quantities in the APAL project.

In the FAVOR manual [23] a pressurized-thermal shock (PTS) is defined as the transient condition of combined thermal plus mechanical loading in an overcooling event with high internal pressure of the coolant.

The conditional probability of initiation (CPI) means the probability of fracture by plane-strain cleavage fracture initiation under the condition/assumption that the considered transient occurs. In PROSIR the abbreviation for this parameter is PCI, which has a different meaning in this document.

- PCI, PCA = Probability for crack initiation / crack arrest (used in PROSIR); in APAL no real results just used for abbreviations of benchmark sub-tasks

The goal of probabilistic fracture mechanics (PFM) is to calculate the conditional probability of failure of the vessel (CPF).

FAVOR manual: “The term conditional refers here to the assumption that the specific PTS event under study has in fact occurred. Combined with an estimate of the frequency of occurrence for the event, a predicted frequency of vessel failure can then be calculated.”

- cpi(t) = instantaneous conditional probability of initiation at time t in the selected transient
- CPI = final conditional probability of initiation for a selected transient
- CPF = final conditional probability of failure for a selected transient
- FI = frequency of crack initiation
- FF = frequency of failure

The terms “critical stress intensity”, “crack resistance” and “fracture toughness” are synonyms.

2.1.2 RPV failure frequency acceptance criterion for APAL

One of the fundamental topics for probabilistic assessments is related to the computation of failure initiation or failure frequency (per year) for an RPV. Foremost, it is important to recognise what is considered as a RPV failure from several possible events. The frequency of initiation (FI) is the event frequency causing initiation of one crack. The frequency of failure (FF) is the frequency of a propagation of a non-arresting crack (i.e. crack arrest is taken into account and an initiated but arrested crack does

not add to the failure frequency) reaching a defined portion of the RPV wall or leading to plastic collapse of the RPV. The latter case (considering a crack can arrest) is the more realistic.

We have to set an allowable FI or FF for margin assessment:

$$\text{Base line} = 1 \cdot 10^{-6}$$

The primary PTS acceptance criterion according to Regulatory Guide 1.230 [21] stipulates the acceptable TWCF $< 1 \cdot 10^{-6}$ vessel failures per reactor-operating year.

For a correlation of FI or FF with conditional probability of initiation (CPI) or conditional probability of failure (CPF), the yearly occurrence of the base case transient is needed. In DEFI-PROSAFE [20] the yearly occurrence is defined as given in Table 2.1.

Table 2.1 Occurrence of base case transient (from DEFI-PROSAFE)

Group of scenarios	Representative scenario	mean value of frequency	5% quantile	50% quantile	95% quantile
		[1/year]	[1/year]	[1/year]	[1/year]
Medium LOCA	ICAS T2	$4.39 \cdot 10^{-3}$	$5.28 \cdot 10^{-4}$	$2.43 \cdot 10^{-3}$	$1.43 \cdot 10^{-2}$

The allowable CPI and CPF of $2.28 \cdot 10^{-4}$ has been defined in APAL based on the 10^{-6}acceptance limit according to the NRC Regulatory Guide 1.230 [21] in combination with the mean value of probability of occurrence of the selected transient.

2.1.3 Margin definition for PFM assessments

This Section provides a general definition of margins and margin assessments used in PTS analyses. Foremost, the fundamental distinction between two types of margins should be addressed:

- **Explicit margin:** Difference between maximum allowable value for data of interest (e.g. ART) determined by PTS analysis (either probabilistic or deterministic) and predicted value for data of interest (e.g. material ART for expected operation lifetime).
- **Implicit margin:** Margin that implicitly exists due to used conservative assumptions or conditions (e.g. flaw postulate, loads, boundary conditions, SIF solution). Quantification of an implicit margin can be performed through a comparison of results obtained by using different approaches (e.g. different SIF solutions) or through a comparison of results based on different input data (e.g. conservative versus best-estimate data).

Historically, in deterministic PTS analyses the explicit margin is quantified in terms of difference between the material ART and calculated max. allowable ART from a PTS analysis. For probabilistic fracture mechanics analyses there are mainly two quantifications used: in terms of ageing (e.g. max. all. ART) or in terms of risk of initiation or failure. For these margin quantifications there are several probabilistic approaches possible with different levels of uncertainty consideration.

In DEFI-PROSAFE [20] a methodology has been developed to assess the maximum allowable ageing of the RPV in terms of maximum allowable ART (max. all. ART) which can be used to make comparison and assess margin. The principle is to determine the max. all. ART for which a given probability of failure is calculated.

Within APAL several probabilistic margin approaches (PMA) have been defined and discussed in detail in Section 2.3.11. Different PMA assessments are presented in Section 7 summarizing the Task 4.6 in APAL [6].

2.2 Computational chain for PTS assessment

2.2.1 Deterministic assessment

A general computational chain for the PTS safety assessment of RPVs is shown in Figure 2.1. A detailed overview of deterministic PTS safety analyses along with main results and findings is presented in WP3 Public Summary report [7].

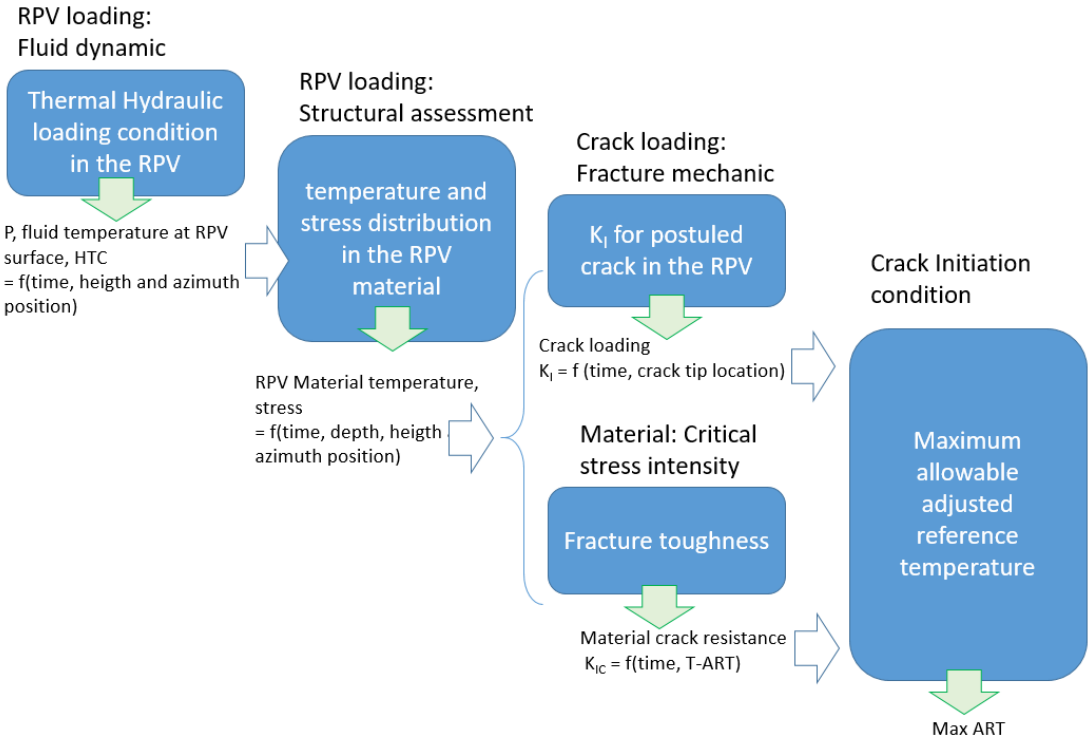

Figure 2.1: Flow chart of the calculation chain for RPV PTS deterministic safety assessment.

2.2.2 Probabilistic assessment

Examples of principal computational chains for the calculation of CPI and CPF are shown in Figure 2.2 and Figure 2.3. Different steps of probabilistic PTS safety assessment will be described in detail in further section of this report.

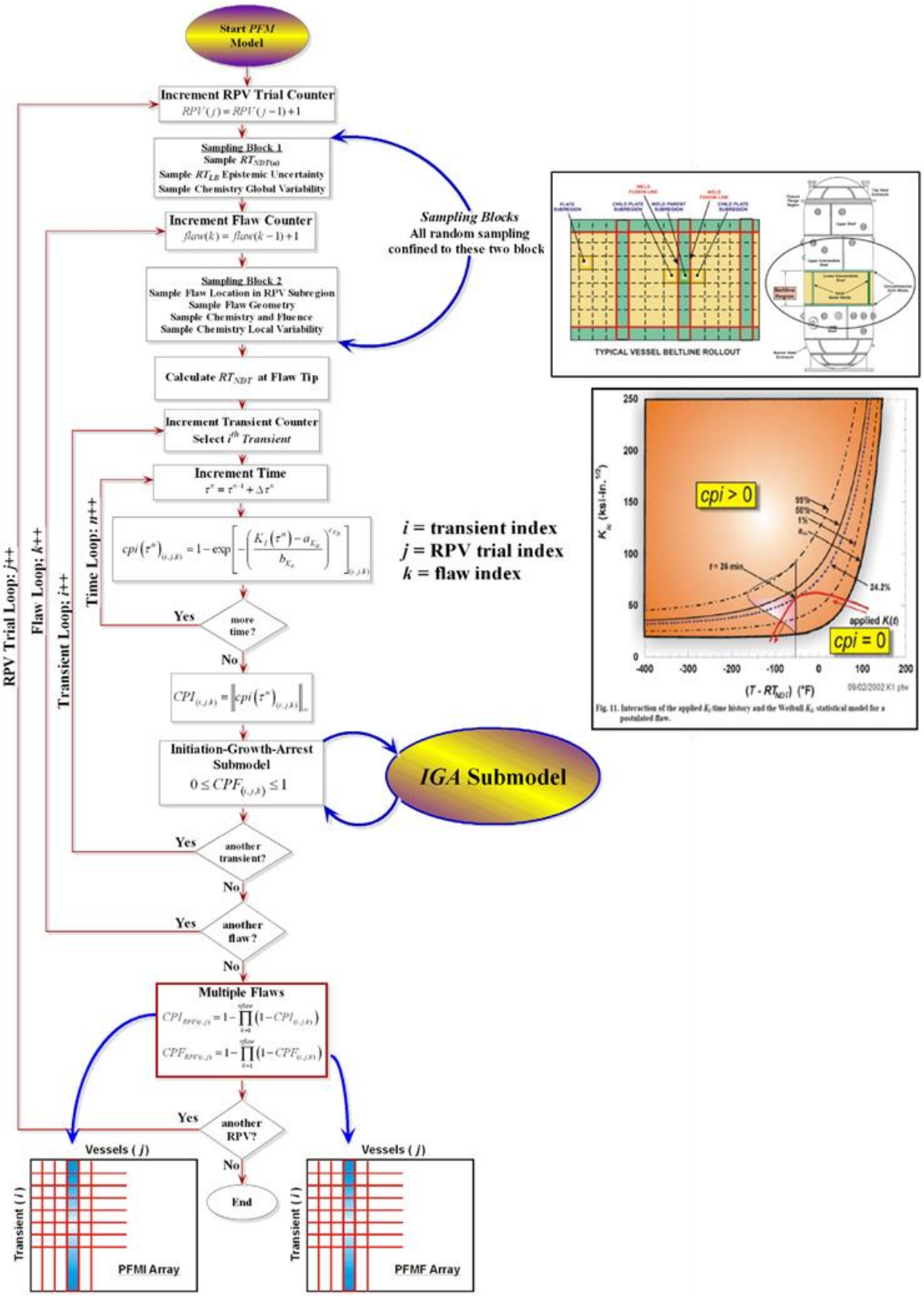

Figure 2.2: Flow chart for CPI and CPF calculation within FAVPFM Module.

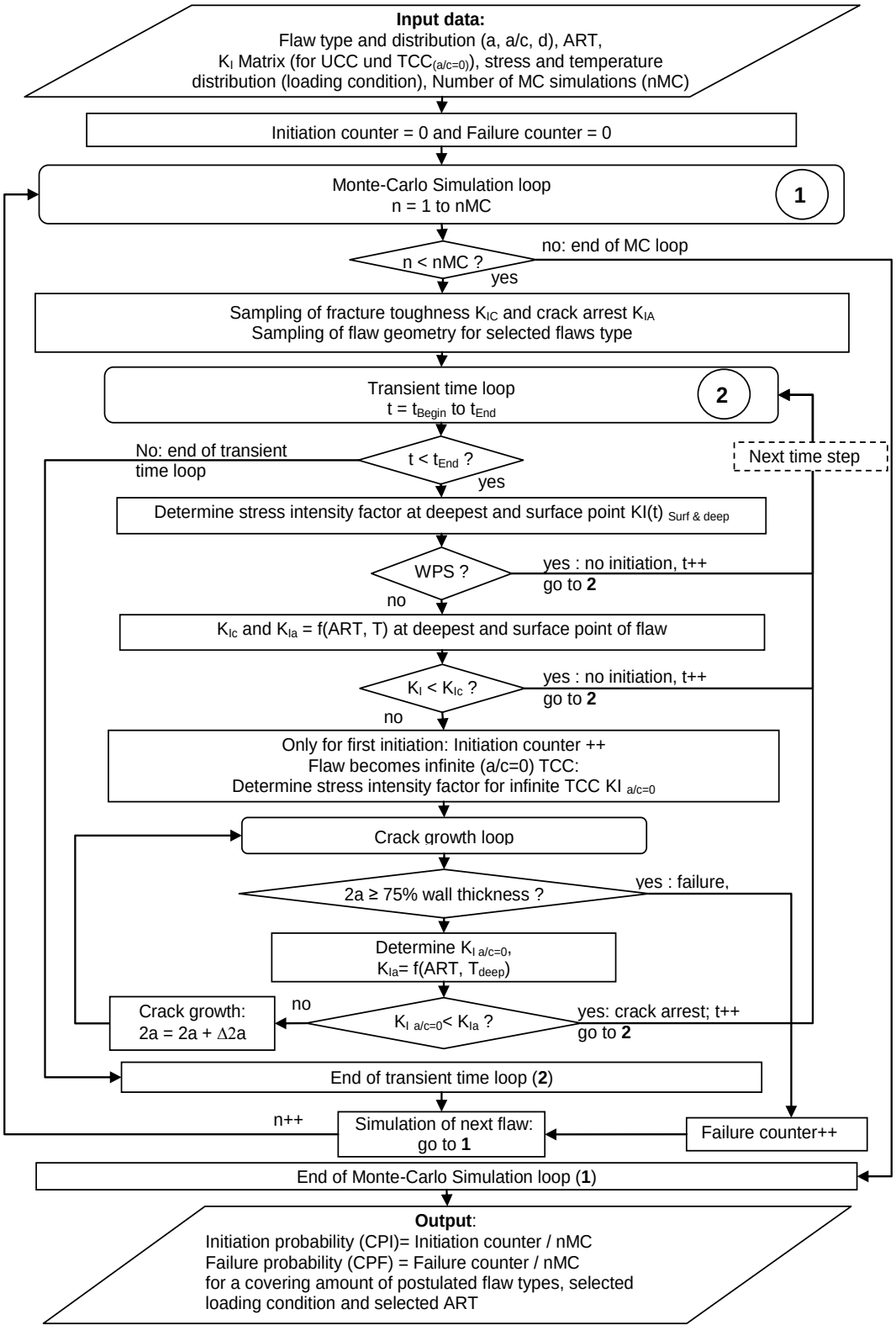

Figure 2.3: Flow chart of CPI and CPF calculation with MC method, FRA-G in-house tool.

2.3 Basic data for RPV probabilistic fracture mechanics assessment

The main data required for a probabilistic PTS assessment is summarised in Table 2.2. The Table also includes an overview of the parameters for several PMAs indicating whether they are treated as

distributed parameters within the APAL benchmark. The following subsections provide a detailed description of input data and associated uncertainties required for probabilistic assessments.

Table 2.2 Overview of input data 1.

Data		Type of uncertainty (epistemic/ aleatory)	Distributed in APAL benchmark (otherwise fixed value)	Required for PMA1	Required for PMA2/4
RPV geometry	PWR 4-loop type	Epistemic			
Properties of base metal, weld and cladding	Thermal	Aleatory		√	
	Tensile	Aleatory		√	
	Toughness: K_{IC}, K_{Ia}, J_{IC}	Both	√	√	
	Chemical composition	Aleatory	√		√
Irradiation effects	Fluence vs. EFPY	Both	√		√
	Irradiation shift formula	Both	√		√
	Irradiation decrease through the RPV wall	Both			√
Defect	Position in RPV, Orientation	Epistemic		√	
	Type: surface, underclad or embedded	Epistemic		√	√
	Size: depth, length, shapes	Epistemic	√	√	√
Transient loads	Stresses and temperature	Both	(√)	√	√
Other loads	residual stresses	Epistemic		√	
Fracture mechanic model	K or J evaluation	Epistemic		√	√
RPV Fracture mechanic assessment	Crack initiation (brittle, ductile) Crack arrest	Both	√	√	√
Limit states for crack initiation and arrest	Condition on K_I, K_{IC}, K_{IA} for initiation and arrest	Epistemic	√	√	√

2.3.1 RPV design and geometry

The investigated RPV in APAL is a 4-loop, 1300 MWe PWR of the type built by Siemens/KWU. A detailed RPV description is given in [7]. In APAL, the geometrical RPV dimensions are considered as deterministic having the following dimensions in the near-core region:

- wall thickness of 243 mm in the base/weld material,

- cladding thickness of 6 mm,
- outer surface radius of 2684 mm.

2.3.2 Flaw type, location and orientation

All cracks for the benchmark were located in the core weld at the vertical distance of -2.638 m from the centerline of the cold-leg nozzle. Cracks oriented in both the axial and circumferential directions of the RPV were considered in the analyses.

Three crack types are studied within APAL: through-clad cracks (TCC), underclad cracks (UCC), and embedded cracks. These cracks are briefly described in the following sections. Details regarding the stress intensity factor (SIF) solutions are provided in [7].

2.3.2.1 Through-Clad Crack (TCC)

The TCC is defined according to Figure 2.4 where *r* is the cladding thickness, *a* is the crack depth within the base metal and 2*c* is the crack length. Two positions on the crack front to be assessed are defined, where *A* is the deepest point of the crack while *C* is the point at the cladding/weld interface.

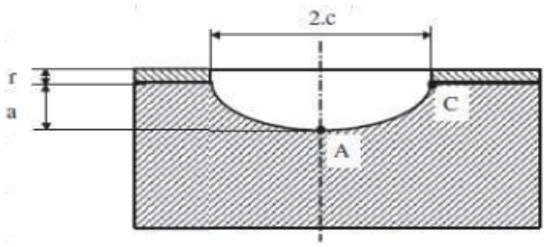

Figure 2.4: Definition of the Through-Clad Crack (TCC).

If other dimensions were not specified, the crack depth and length were $(a + r) = 16$ mm and $2c = 60$ mm, respectively.

Two alternative TCC-shapes are used within APAL, shown in Figure 2.5. Shape 1, sometimes denoted TCC1, is used by most partners. The alternative shape 2, denoted TCC2, is used in the FAVOR code [23]. When simply written as TCC within the deliverable, the shape 1 is implied.

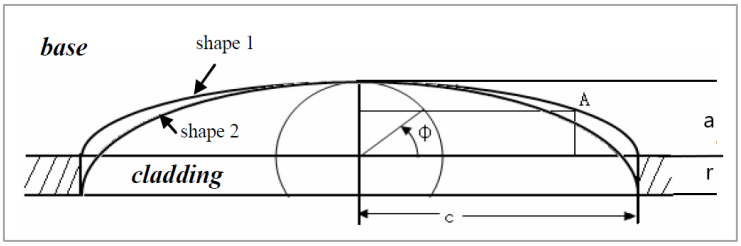

Figure 2.5: Definition of the Through-Clad Crack (TCC).

2.3.2.2 Underclad Crack (UCC)

The UCC is defined according to Figure 2.6 using the same definitions as the TCC in Section 2.3.2.1 with the addition of the third position on the crack front to be assessed – point *B* in the cladding. The position *B* is included as a non-mandatory position when presenting results but is important when correcting for plasticity. Plastic correction should be considered in all analyses for UCC.

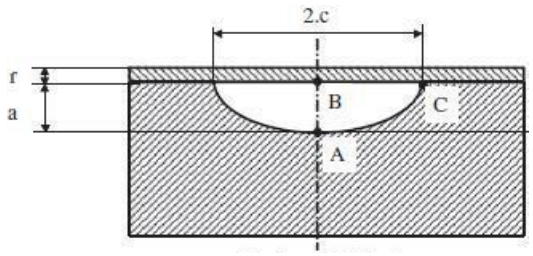

Figure 2.6: Definition of the Underclad Crack (UCC).

If other dimensions were not specified, the crack depth and length were assumed to be $a = 10$ mm and $2c = 60$ mm, respectively.

2.3.2.3 Embedded Crack

The embedded crack is shown in Figure 2.7 where $2a$ is the crack depth, $2c$ is the crack length, r is the cladding thickness and d is the distance to the clad/base interface. Within APAL, embedded cracks are analysed only using the FAVOR code [23] which exposes some limitations for the original definition of embedded cracks (prescribed in the planning phase of the project). These limitations are described below:

- The original distance to clad/base interface was prescribed as $d = 5$ mm or $(d + r) = 11$ mm. This value cannot be fixed as FAVOR distributes the embedded cracks in different locations through the RPV wall thickness. The best approximation found within the simulated cracks is a crack with $(d + r) = 12.45$ mm.
- Crack depth $2a$ is defined in FAVOR as the integer percentage of the RPV wall thickness including the cladding. It implies that the crack depth can differ from the prescribed values that can be used in other PFM codes within APAL. The prescribed value given in APAL was $2a$ = 20 mm. The FAVOR users selected values close to this.
- Flaw shape is defined in FAVOR as $2c/2a = 6$.

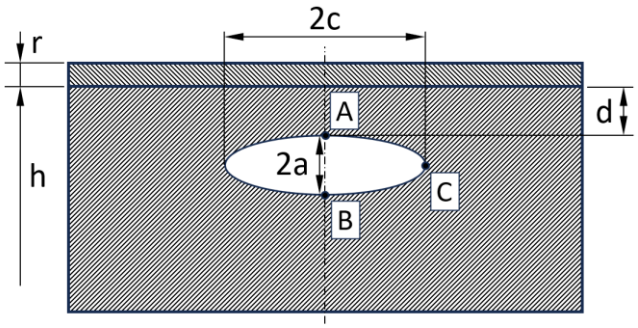

Figure 2.7: Definition of the embedded crack.

2.3.2.4 Distributed Cracks

The UCC crack distribution was studied within one of the tools verification subtasks in Task 4.3, see Section 4. A recommended discrete UCC crack depth distribution is presented in Table 2.3. From this distribution, arbitrary values of a crack depth and corresponding CDFs can be obtained by linear interpolation between the discrete values for a relevant interval. A discrete depth distribution for the TCC cracks can be derived from the UCC distribution by adding 6 mm cladding thickness to the crack depth values.

Table 2.3 Crack depth distribution

Crack Depth [mm]	CDF	Crack Depth [mm]	CDF	Crack Depth [mm]	CDF	Crack Depth [mm]	CDF
0.5	0	1.9	0.821977	3.3	0.981772	4.7	0.99863
0.6	0.019774	2	0.846819	3.4	0.984787	4.8	0.998864
0.7	0.071055	2.1	0.868167	3.5	0.987238	4.9	0.999056
0.8	0.143365	2.2	0.886348	3.6	0.98931	5	0.999219
0.9	0.230056	2.3	0.902412	3.7	0.991136	5.1	0.999363
1	0.327022	2.4	0.916338	3.8	0.992618	5.2	0.999474
1.1	0.420405	2.5	0.928549	3.9	0.993861	5.3	0.999586
1.2	0.500663	2.6	0.938997	4	0.9949	5.4	0.99968
1.3	0.569497	2.7	0.948	4.1	0.995772	5.5	0.999756
1.4	0.628318	2.8	0.955784	4.2	0.996472	5.6	0.99982
1.5	0.679033	2.9	0.96269	4.3	0.997038	5.7	0.999877
1.6	0.7226	3	0.968665	4.4	0.997533	5.8	0.999935
1.7	0.7607	3.1	0.973834	4.5	0.99798	5.9	0.999969
1.8	0.793737	3.2	0.97812	4.6	0.998327	6	1

Within WP4, a fixed length/depth ratio $2c/a = 6$ for distributed cracks was assumed for facilitating comparisons with the deterministic analyses within WP3 [7]. Note that the length/depth ratio excludes the part of the crack depth that is within the cladding for the TCC (see Figure 2.6).

2.3.3 Loads

The base case transient, presented in detail in [8], was considered in the probabilistic baseline benchmark. The same transient was also used in the deterministic baseline analyses [7].

Weld Residual Stresses (WRS) were considered in all mandatory analyses. In APAL, WRS were defined as a cosine shape with the amplitude of 56 MPa for circumferential cracks and as a constant stress of 56 MPa through the RPV wall thickness for axial cracks, as described in detail in [7].

FAVOR users used the WRS distribution implemented in the FAVOR code [23]. It was shown that the FAVOR WRS distribution provides a very similar effect on the stress intensity factor (SIF) as the WRS recommended in APAL for TCC.

2.3.4 Fracture Toughness Concepts

Three different fracture toughness concepts were evaluated in the probabilistic benchmark assessments and summarised in the following subsections.

2.3.4.1 RT_{NDT} Concept

The RT_{NDT} Concept within APAL is based on the ASME Section XI Appendix A definition of the transition region for lower bound (LB) crack initiation fracture toughness curve, K_{Ic}, and crack arrest curve, K_{Ia}, according to:

$$K_{Ic}^{LB} = 36.5 + 3.1e^{0.036(T-RT_{NDT}+55.5)}$$

$$K_{Ia}^{LB} = 29.4 + 1.4e^{0.026(T-RT_{NDT}+88.9)}$$

In this concept, both material parameters are assumed to be normally distributed with a truncation at ±3 standard deviations (SD). For crack initiation, the mean value (MV) and SD are given as:

$$K_{Ic}^{MV} = K_{Ic}^{LB}/0.7$$

$$K_{Ic}^{SD} = 0.15K_{Ic}^{MV}$$

The corresponding quantities for crack arrest are defined as:

$$K_{Ia}^{MV} = K_{Ia}^{LB}/0.8$$

$$K_{Ia}^{SD} = 0.1K_{Ia}^{MV}$$

It means, that the LB curves according to ASME are supposed to be $MV - 2 \cdot SD$.

The reference temperature RT_{NDT} is defined as the initial reference temperature, RT^{0}_{NDT}, combined with the reference temperature shift, ΔRT_{NDT}:

$$RT_{NDT} = RT_{NDT}^{0} + \Delta RT_{NDT}$$

T and all forms of RT_{NDT} are in °C.
All forms of K_{Ic} and K_{Ia} are in MPa$\sqrt{\mathrm{m}}$

2.3.4.2 T_0 Concept

The T_0 Concept within APAL is based on the Master Curve approach which is defined as a Weibull distribution.

$$K_{Jc}^{p} = 20 + \left[ln\left(\frac{1}{1-p}\right)\right]^{1/4} \cdot \{11 + 77exp[0.019(T - T_0)]\}$$

where p is the probability of crack initiation. The equation is valid for the crack front length of 1 inch (about 25 mm) and should be adjusted if the real crack front length, B, in the base metal is longer than 25 mm according to

$$K_{Jc} = 20 + (K_{Jc} - 20) \cdot \left(\frac{25\ \mathrm{mm}}{B}\right)^{1/4}$$

Adjusting of K_{Jc} for the crack front length is only included as non-mandatory additional work and is disregarded in the mandatory work in the probabilistic baseline benchmark.

For crack arrest the mean value is defined as

$$K_{Ia}^{MV} = 30 + 70e^{0.019(T - T_{KIa})}$$

where

$$T_{KIa} = T_0 + 44.97e^{-0.00613T_0}$$

while the upper and lower bound curves are defined as

$$K_{Ia}^{p} = \begin{cases} K_{Ia}^{MV}(1 + 0.18M_p) & \text{Lower bound} \\ K_{Ia}^{MV}(1 - 0.18M_p) & \text{Upper bound} \end{cases}$$

where M_p is the inverse standard normal distributed value for p.

The reference temperature, T_0, is defined as the initial reference temperature, T_0^0, combined with the reference temperature shift. No specific shift functions are defined for the T_0 Concept and the RT_{NDT} Concept shift functions are assumed within APAL to be valid for the T_0 Concept as well:

$$T_0 = T_0^0 + \Delta RT_{NDT}$$

T, T_{Kla} and all forms of T_0 are in °C.
All forms of K_{Jc} and K_{Ia} are in MPa$\sqrt{\mathrm{m}}$.
B is in mm.

2.3.4.3 FAVOR Concept

The FAVOR Concept within APAL is included for FAVOR users and is based on RT_{NDT} using a Weibull distribution. This is described in more detail in the FAVOR theory manual [23].

2.3.5 Initial Reference Temperature

The initial reference temperature is defined as being normally distributed without truncation. Mean values (MV) and standard deviations (SD) are given in Table 2.4.

Table 2.4 Values for normally distributed initial reference temperature

Concept	Value	Initial Reference Temperature [°C]	
		MV	SD
RT_{NDT}	RT^0_{NDT}	-30	9
T_0	T_0^0	-80	9

Truncation: None

2.3.6 Reference Temperature Shift

Reference temperature shift functions used in APAL are summarised below. The base shift functions are defined for base metal as:

$$\Delta RT_{NDT} = [17.3 + 1537 \cdot (\mathrm{P} - 0.008) + 238 \cdot (\mathrm{Cu} - 0.08) + 191 \cdot \mathrm{Ni}^2\mathrm{Cu}] \cdot \left(\frac{F}{10^{23}}\right)^{0.35} + f_{err}$$

and for welds as:

$$\Delta RT_{NDT} = [18 + 823 \cdot (\mathrm{P} - 0.008) + 148 \cdot (\mathrm{Cu} - 0.08) + 157 \cdot \mathrm{Ni}^2\mathrm{Cu}] \cdot \left(\frac{F}{10^{23}}\right)^{0.35} + f_{err}$$

where *P*, *Cu*, and *Ni* represent the percentage of the chemical elements phosphorous, copper and nickel as defined in Section 2.3.7, while the neutron fluence *F*, is given in Section 2.3.8. Note that in some cases the fluence can be denoted as φ using the conversion $\varphi = F/10^{23}$. The shift functions are supplemented by an error function, f_{err}, which is normally distributed with a mean value (MV) and standard deviation (SD) according to Table 2.5.

Table 2.5 Values for normally distributed error function

Material	Error function, f_{err} [°C]	
	MV	SD
Base Metal	0	10
Welds	0	6

Truncation: ±3SD

As the error function f_{err} is independent of the rest of the function, it may cause a negative shift for ΔRT_{NDT} when the neutron fluence is low. This has been discussed during the project and a truncation at ±3SD was decided to be considered to limit this effect. It may still cause a negative shift in some cases, but as this is only relevant when the neutron fluence is very low, it is of little consequence for the cases studied within APAL.

Additional alternative shift functions which have been used for non-mandatory sensitivity analyses are presented in the following equations. Alternative shift formula for RT_{NDT} and corresponding uncertainties according to RSE-M code, the FIM formula:

$$\Delta \mathrm{RT}_{NDT} = 15.8 \cdot [1 + 35.7 \cdot (\mathrm{P} - 0.008) + 6.6 \cdot (\mathrm{Cu} - 0.08) + 5.8 \cdot \mathrm{Ni}^2\mathrm{Cu}] \cdot \left(\frac{F}{10^{23}}\right)^{0.59}$$

Alternative shift formula for RT_{NDT} and corresponding uncertainties according to 10CFR50.61a:

$$\Delta \mathrm{RT}_{NDT} = 1.417 \cdot 10^{-7} \cdot (1 - 0.001718 \cdot \mathrm{T}_c) \cdot (1 + 6.13 \cdot \mathrm{P} \cdot \mathrm{Mn}^{2.471}) \cdot \phi\mathrm{t}^{0.5} + 155.0 \cdot (1 + 3.77 \cdot \mathrm{Ni}^{1.191}) \cdot \mathrm{f}(\mathrm{Cu}, \mathrm{P}) \cdot \mathrm{g}(\mathrm{Cu}, \mathrm{Ni}, \phi\mathrm{t})$$

ΔRT_{NDT} in °F.
T_c in °F is the cold leg temperature under normal full power operating conditions (suppose T_c = 554°F = 290°C).
ϕ is the average neutron flux in n/cm²/sec.
t is the time that the reactor has been in full power operation in sec.
Mn represents the percentage of chemical element manganese.

$$\mathrm{F}(\mathrm{Cu}, \mathrm{P}) = [\mathrm{Cu} - 0.072 + 1.359 \cdot (\mathrm{P} - 0.008)]^{0.668}$$

$$\mathrm{g}(\mathrm{Cu}, \mathrm{Ni}, \phi\mathrm{t}) = 0.5 + 0.5 \cdot \tanh\{[\log_{10}(\phi\mathrm{t}) + (1.1390 \cdot \mathrm{Cu}) - (0.448 \cdot \mathrm{Ni}) - 18.120]/0.629\}$$

2.3.7 Chemical Composition

The mean values and standard deviations for chemical elements in the RPV ferritic steel are specified in Table 2.6. All chemical elements are assumed to be normally distributed with a truncation of ±3SD to avoid non-physical negative values. Note that the standard deviation values in the Table are given as 2SD.

Table 2.6 Values for normally distributed chemical composition [1]

Material	% Copper (Cu)		% Phosphorus (P)		% Nickel (Ni)		% Manganese (Mn)*	
	MV	2SD	MV	2SD	MV	2SD	MV	2SD
Base Metal	0.086	0.02	0.0137	0.002	0.72	0.1	1.45	0.8
Welds	0.12	0.02	0.018	0.002	0.17	0.1	1.63	0.8

*) Manganese distribution according to NRC 10CFR5061.
Truncation: ±3SD

2.3.8 Neutron Fluence

Irradiation embrittlement of base metal and welds in RPVs due to neutron fluence is the dominant aging mechanism as it contributes to a shift in reference temperature and reduces the fracture toughness with operation time.

Neutron fluence values, *F*, at the inner surface of the RPV are assumed as being normally distributed with a one-sided truncation as $F \geq 0$ to avoid non-physical values and presented in Table 2.7. The

original values that were chosen in the planning phase of the APAL project have been complemented with an additional value of $1 \cdot 10^{23}$ for fluence after 1 year of operation. It was also decided that linear extrapolation should be used beyond 80 years of operation, see Figure 2.8.

Table 2.7 Values for normally distributed neutron fluence.

Years of Operation	Maximum Neutron Fluence at inner surface [neutron/m²]	
	MV	SD
1	$1 \cdot 10^{23}$	10% of MV
10	$3 \cdot 10^{23}$	10% of MV
20	$5 \cdot 10^{23}$	10% of MV
40	$7.5 \cdot 10^{23}$	10% of MV
60	$10 \cdot 10^{23}$	10% of MV
80	$12.5 \cdot 10^{23}$	10% of MV

Truncation: ≥ 0

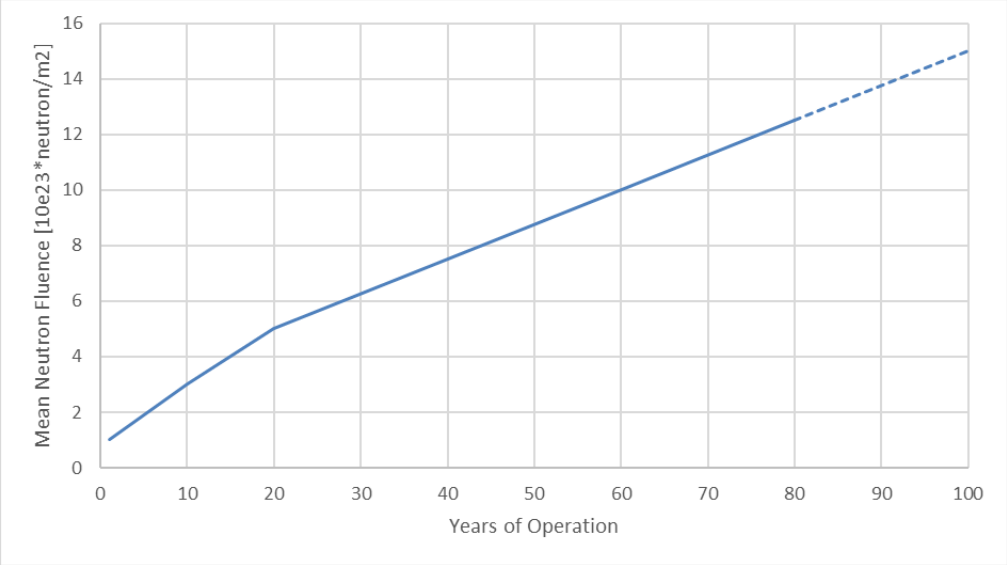

Figure 2.8: Mean neutron fluence as a function of years of operation.

Fluence attenuation through the RPV wall thickness was also considered using the following equation:

$$F = F_0 \cdot e^{-0.125x}$$

where x [cm] represents the distance from the cladding/weld interface and F_0 is the fluence at the cladding/weld interface.

It was decided within the project not to consider any attenuation through the cladding, which results in F_0 being equivalent with values at the inner surface presented in Table 2.7.

2.3.9 Limit Conditions

Two limit conditions, namely the Tangent approach and the maximum Warm Pre-Stressing (WPS) approach were defined as mandatory:

1. The Tangent approach.
   Initiation is assumed to occur when K_I exceeds the fracture toughness, K_{Ic}.
2. The maximum WPS (Baseline WPS) approach.
   The WPS effect is assumed to prevent initiation, provided that K_I remains lower than previous values observed during the transient regardless of temperature. It can be seen as a simplified and very generous WPS approach.

In addition, other WPS approaches given in the FAVOR manual [23] were used in non-mandatory sensitivity studies. These non-mandatory WPS approaches along with the mandatory Baseline WPS approach are described below.

The maximum allowable reference temperature for analysed PTS corresponds to the fracture toughness curve K_{Ic} shifted horizontally up to the point where it intersects at a certain point relative to the maximum value of K_I during the PTS event if warm pre-stressing (WPS) approach is applied.

According to the FAVOR manual [23]:

"*a flaw is assumed to be in a state of WPS when the following condition is met:*

- *a falling applied-K_I field – the time-rate-of-change of the applied-K_I is non-positive (<= 0).*

If a flaw is in a state of WPS, it is not eligible for initiation (or re-initiation if it has arrested) until it leaves the WPS state.

Three conditions can be stated for a flaw not to be in the state of WPS and, thereby, to be eligible for initiation. These three conditions are:

> *Condition (1): the applied-K_I is greater than K_{Ic}(min), where K_{Ic}(min) is defined by the fracture toughness model for the temperature at the flaw tip;*
>
> *Condition (2): a rising applied-K_I field – the time-rate-of-change of the applied-K_I is positive ($dK_I/dt > 0$);*
>
> *Condition (3): in a rising applied-K_I field, the driving force at the flaw tip must exceed some portion of the previously-established maximum applied-K_I (designated as K_I(max)) experienced by the flaw during the transient up to the current point in time under consideration – applied- $K_I(\tau) \geq \alpha\, K_{I(max)}(\tau)$ ".*

Three WPS approaches implemented in FAVOR refer to the different values of the parameter α in the WPS condition 3 above and presented in Table 2.8. More details regarding all three WPS approaches can be found in the FAVOR manual [23] and in [9].

Table 2.8 WPS approaches used in APAL

WPS Approach	Conditions required for initiation (CPI>0)	Mandatory/ non-mandatory
Baseline WPS (Max WPS)	Conditions 1, 2 and 3 ($\alpha = 1$)	Mandatory
Conservative Principle WPS	Conditions 1 and 2 ($\alpha = 0$)	Non-mandatory
Best Estimate WPS	Conditions 1, 2 and 3 (α is sampled from distribution)	Non-mandatory

2.3.10 Crack Initiation and Crack Arrest

Different probability quantities are calculated in APAL. The main analyses consider the probability of initiation of unstable crack growth, while additional non-mandatory analyses also consider the probability of a crack arrest to occur during the transient.

Different probability definitions that have been evaluated in the project are summarised below:

- Conditional Probability of Initiation (CPI):
  The probability that initiation of unstable crack growth occurs during a transient.

- Instantaneous Conditional Probability of Initiation (cpi(t)):
  The probability that initiation of unstable crack growth occurs as a function of time through the transient.

- Conditional Probability of Failure (CPF):
  The probability that failure occurs during a transient. Failure is assumed if the initiated crack is not arrested before it reaches 75% of the wall thickness. This definition is used when crack arrest is considered.

- Conditional Probability for Non-Arrest (CPNA):
  The probability that no crack arrest occurs after first initiation.
  CPNA can be determined as:

$$CPNA = \frac{Simulations\ with\ initiation\ and\ without\ any\ arrest\ after\ first\ initiation}{Total\ number\ of\ simulations}$$

- Conditional Probability for Stable Arrest (CPSA):
  The probability that an initiated crack arrests and does not reach 75% of the wall thickness during the transient. CPSA can be determined as:

$$CPSA = \frac{Simulations\ with\ initiation\ and\ subsequent\ stable\ arrest\ before\ 75\%\ w.t.}{Total\ number\ of\ simulations}$$

The procedure of calculating a crack arrest can be summarised in the following steps:

1. After first (brittle) crack initiation, the crack is assumed to become immediately either infinite (for axial cracks) or fully circumferential (for circumferential cracks). Moreover, UCC is assumed to become TCC (the cladding is broken).

2. Unstable crack growth occurs and crack arrest is checked for the growing crack.

3. If crack is arrested, possibility of re-initiation is checked for the remaining transient time.

4. If crack-reinitiates, revert to step 2.

5. Failure is assumed when the crack has reached 75% of the ferritic thickness of the RPV wall.

It was discussed and concluded between the APAL partners that the cladding thickness should not be included and considered in the 75% limit defined in point 5.

Another important aspect that was also considered during the work is re-sampling of the fracture toughness during the transient. Re-sampling should not be performed as it is important to keep the same probability level throughout each transient analysis. If re-sampling is done for each crack depth or time step, a crack arrest can be overestimated as higher fracture toughness values may be obtained for certain steps than for the step initially leading to initiation. One way of keeping the same probability level throughout the transient is to use a standard normal distribution (MV = 0, SD = 1) that is scaled to the temperature dependent K_{Ic}^{MV} and K_{Ic}^{SD} for each time step throughout the transient and thickness.

As a non-mandatory sensitivity analysis, re-sampling could be considered when transitioning between welds through the RPV wall as the different components welded together may have different fracture toughness. This was however not studied within APAL.

The cpi(t) can be used to illustrate the probability of initiation during the transient and can be defined in different ways. The definition adopted in APAL involves calculations of the conditional probability of initiation for each time step through the transient regardless of history. Using this definition, the maximum value of cpi(t) represents the final CPI. IRSN suggested alternative definitions where one of

the mainly discussed definitions is to consider the transient history. Initiation is assumed to occur only once during each transient run and once the initiation criterion has been met, initiation cannot occur again. Using this definition, the sum of all cpi(t)-values provides the final CPI. Both approaches present different ways for evaluating the probability of initiation during the transient.

2.3.11 Margin Assessment

Three probabilistic margin approaches (PMA) were defined in APAL as presented below. During the work, the originally proposed approach, denoted as PMA3, was excluded and replaced by an alternative approach PMA4.

The approaches can be summarised as:

- PMA1 (Margin definition in terms of maximum allowable ART, also used within DEFI-PROSAFE [20]):
  Determine a maximum allowable ART for a given defined allowable *CPI* = $2.28 \cdot 10^{-4}$ considering the fracture toughness as a statistically distributed parameter and ART as a deterministic parameter.

- PMA2 (Margin definition in terms of lifetime):
  Determine a maximum allowable RPV lifetime for a given defined allowable *CPI* = $2.28 \cdot 10^{-4}$ considering both the fracture toughness and ART as a statistically distributed parameters. The lifetime defines neutron fluence at inner surface of the RPV, and the attenuated fluence at crack tip together with elemental material composition define the ART shift, all of them statistically distributed within the PFM.

- PMA4 (Margin definition in terms of reliability theory; non-mandatory):
  Determine the parameters of most probable failure point, also in standard normal variables, and the reliability index.

The limit of *CPI* = $2.28 \cdot 10^{-4}$, as discussed in Section 2.1.2, was defined from the acceptance limit of 10^{-6} according to the NRC Regulatory Guide 1.230 [21] in combination with the mean value of frequency of occurrence of the selected transient.

PMA 1 has the disadvantage of losing some uncertainty treatment in relation to RPV specific material behaviour (embrittlement), whereas PMA 2 and PMA 4 are using the full scope of probabilistic fracture mechanics. On the other hand, PMA 1 is the preferred approach for quantifying a potential margin gain obtained solely by lowering the uncertainty in the loading path (e.g. related to TH uncertainties) independently of the type of RPV, as a bias due to uncertainties in material embrittlement is excluded. PMA 1 and PMA 2 can be used for comparisons of deterministic and probabilistic assessments and for quantifying the implicit margin in a deterministic PTS analysis. All approaches can be used to quantify the difference in explicit margins related to LTO improvements.

2.3.12 FAVOR/CAPAL limitations and used assumptions

JSI, PSI and Tecnatom are using the FAVOR code [23] to perform many of the analyses within APAL. A project specific version of the code, entitled CAPAL [24][27], was provided by OCI (international partner of APAL) which includes features needed in APAL that are not included in FAVOR. These features include the Master Curve (T_0) concept, fluence attenuation formula and base shift formulas for RT_{NDT}.

However, the FAVOR/CAPAL code has some limitations for performing the analyses which are presented further in this report. These limitations are given below:

- Fracture toughness: FAVOR uses a Weibull distribution for RT_{NDT} concept, not a normal distribution.
- TCC cracks:

- TCC axial cracks cannot be evaluated with FAVOR because the program only considers surface defects with circumferential orientation due to the cladding application.
- Crack tip: FAVOR only calculates the deepest point (point A). Surface point (point C) cannot be evaluated.
- Crack Depth: it is defined as % of thickness in integers. The APAL normalised crack depth as implemented in FAVOR is $(a + r)/t = 16/249 = 0.064$, i.e. 6th or 7th percentiles. Where t is the total wall thickness including cladding.
- Crack Length: the available crack length-to-depth ratios are only 2, 6, 10 and infinite.
- Flaw Shape: FAVOR uses the flaw shape TCC2, see Section 2.3.2.1, with the centre of the ellipse placed on the inner surface of the RPV as opposed to TCC1 where the centre of the ellipse is on the clad/base interface. The TCC2 crack includes the cladding thickness, r, and cannot be fixed as:$2c/(a + r) = 60/16 = 3.75$.

For RR3 PMA2 and RR5 PMA1 and PMA2: CPNA cannot be calculated with FAVOR because it can only be obtained in FAVOR for a specific crack with a fixed value of RT_{NDT}.

- Embedded cracks:
  - Depth: it is defined as a % of wall thickness.
  - Distance of point 1 to the surface: X1 = 11 mm. It cannot be fixed in FAVOR because the program distributes the embedded cracks in different locations in the thickness.

2.3.12.1 Assumptions made by Tecnatom and PSI

The following section gives a short description of assumptions made by Tecnatom and PSI.

RR2/RR3-PMA1/PMA2

- TCC2 cracks:
  - Depth: it is defined as a % of thickness. Values used: 7% of thickness is used $(a + r = 17.43$ mm).
  - Flaw shape: $2c/(a + r) = 60/16 = 3.75$. It cannot be fixed to 3.75. Value used: $2c/(a + r) = 6$ (more conservative).
- Embedded cracks:
  - Depth: it is defined as a % of thickness. Value used: 8% of thickness ($2a = 19.92$ mm).
  - Flaw shape: in FAVOR defined as $2c/2a = 120/20 = 6$. This is the value used.
  - Distance of point 1 to the surface: $d = 11$ mm. It cannot be fixed in FAVOR because the program distributes the embedded cracks in different locations in the thickness. The best approximation found within the simulated cracks is a crack with $d = 12.45$ mm.
  - For PMA2: In this case, as a distribution of RT_{NDT} is needed, in FAVOR it is necessary to consider different cracks and the embedded cracks are distributed through the thickness.

RR4/RR5-PMA1/PMA2:

- TCC2 cracks:
  - Depth: it is defined as a % of thickness. For the distribution given, a S.DAT file has been obtained with the following cracks (1 crack per register = 1000 cracks):
    3%t → 0.294 in → 7.47 mm → 653 cracks (65.3%)
    4%t → 0.392 in → 9.96 mm → 341 cracks (34.1 %)
    5%t → 0.490 in → 12.45 mm → 6 cracks (0.6%)
    These are also presented in Table 2.9 and Figure 2.13.

Table 2.9 Discrete crack size distribution in CAPAL/FAVOR used by Tecnatom and PSI for TCC2

a + r		*(a + r)/t*	2*c* = 2(*a + r*)
[in]	[mm]	[-]	[mm]
0.294	7.4676	0.03	14.9352
0.392	9.9568	0.04	19.9136
0.49	12.446	0.05	24.892

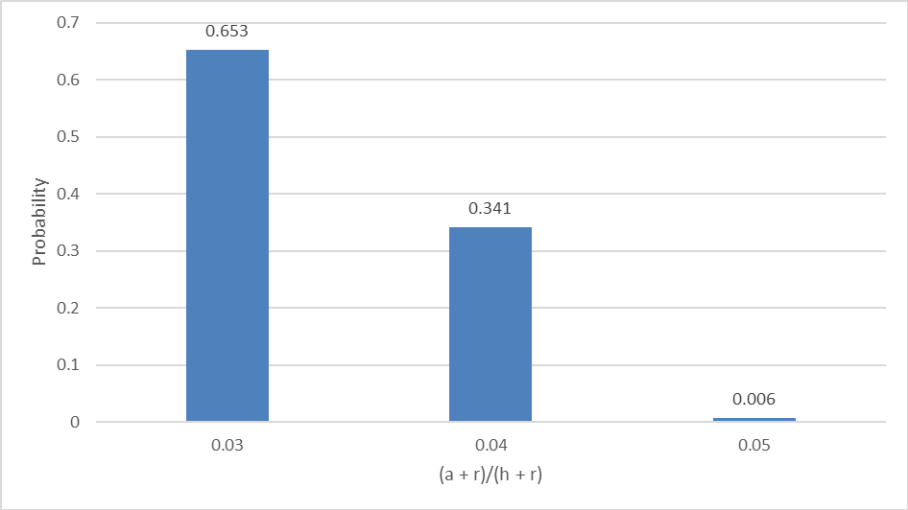

Figure 2.9: CAPAL/FAVOR crack depth distribution used by Tecnatom and PSI for TCC2.

- Flaw shape: In FAVOR the cladding is included, so the flaw shape is $2c/(a+r)$. For the distribution given flaw shapes between 0.46 and 3 are obtained. Value used: fixed flaw shape $2c/(a+r) = 2$.

- For RR5 PMA1 and PMA2: CPNA cannot be calculated with FAVOR because it can only be obtained in FAVOR for a specific crack with a fixed value of RT_{NDT}.

- Embedded cracks:
  - PSI used the following distribution for embedded cracks is presented in Table 2.1 and Figure 2.10.

Table 2.10 Discrete crack size distribution in CAPAL/FAVOR used by PSI for embedded cracks

2a + r +ligament		*(2a + r + ligament)/t*	2*c* = 6(*2a*)
[in]	[mm]	[-]	[mm]
0.49	12.45	0.05	9.0
0.58	14.94	0.06	23.64
0.68	17.43	0.07	38.58
0.78	19.92	0.08	53.52

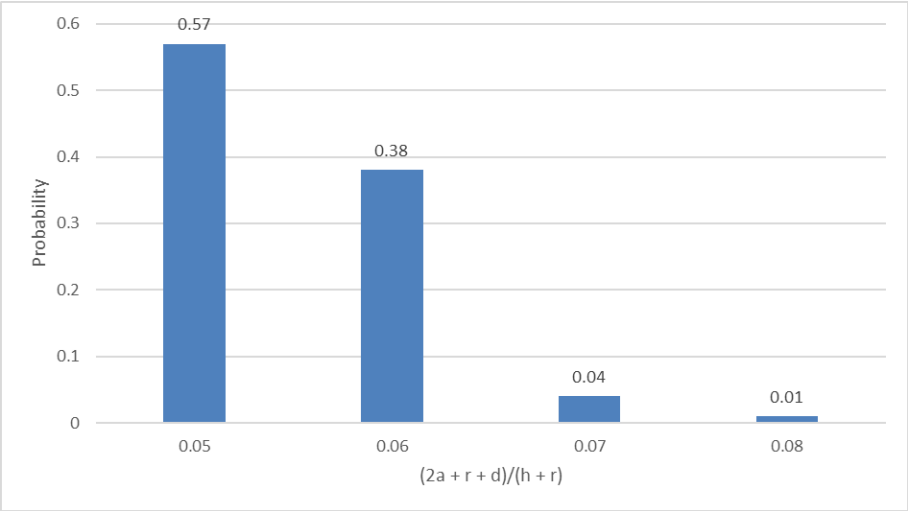

Figure 2.10: CAPAL/FAVOR crack depth distribution used by PSI for embedded cracks.

- Tecnatom treated this in a different manner where depth ($2a$) is defined as a % of thickness according to UCC distribution (Embedded depth ($2a$) is the double of UCC depth (a)).
- Flaw shape: in FAVOR defined as $2c/2a = 120/20 = 6$.
- Distance of point A to the surface: $d = 11$ mm. It can't be fixed in FAVOR because the program distributes the embedded cracks in different locations in the thickness.
- The distribution used by Tecnatom is shown in Table 2.11 and Figure 2.11.

Table 2.11 Discrete crack size distribution in CAPAL/FAVOR used by Tecnatom for embedded cracks

$2a$		$2a/t$	$2c = 6(2a)$
[in]	[mm]	[-]	[mm]
0.098	2.49	0.01	14.94
0.196	4.98	0.02	29.88
0.294	7.47	0.03	44.82
0.392	9.96	0.04	59.76
0.490	12.45	0.05	74.70

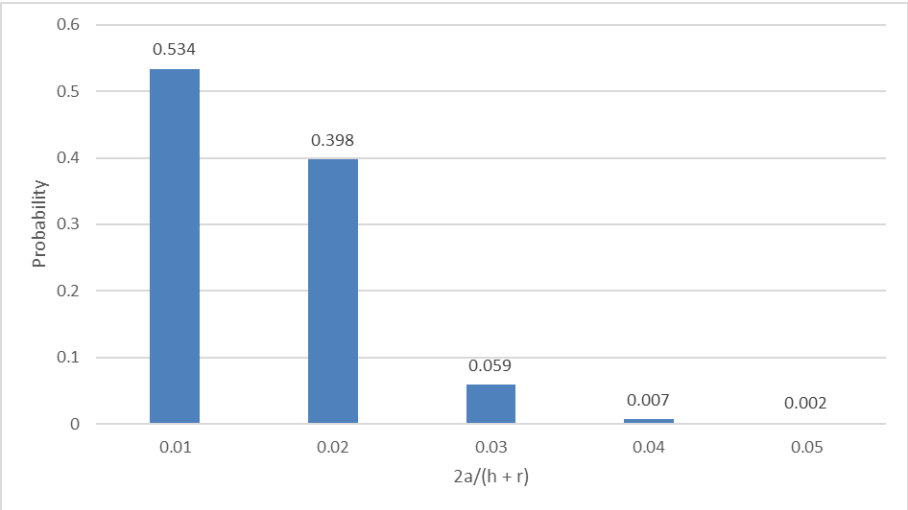

Figure 2.11: CAPAL/FAVOR crack depth distribution used by Tecnatom for embedded cracks.

2.3.12.2 Assumptions made by JSI

JSI initially performed RR2 tasks with a circumferential TCC1 at deepest point (single APAL crack size) using the CEA SIF solutions and an in-house code with the ASME-RTNDT, MC-T0 and FAVOR-RTNDT concepts as well as tangent and Max WPS approaches.

When performing RR4 (distributed crack size) with the CAPAL code, JSI decided to additionally perform RR2 tasks also with CAPAL with a circumferential TCC2 at deepest point (single CAPAL crack size).

RR2 & RR3 circumferential TCC2 size in CAPAL (single)
The chosen dimensions of the crack are:

- $2c/(a + r) = 6$ and $a/t = 0.06$

These were chosen based on Figure 2.12 , where it can be seen that the CAPAL SIFs for the crack (ath6_2ca6) are the closest to CEA SIFs with the APAL crack size (CEA TCC).

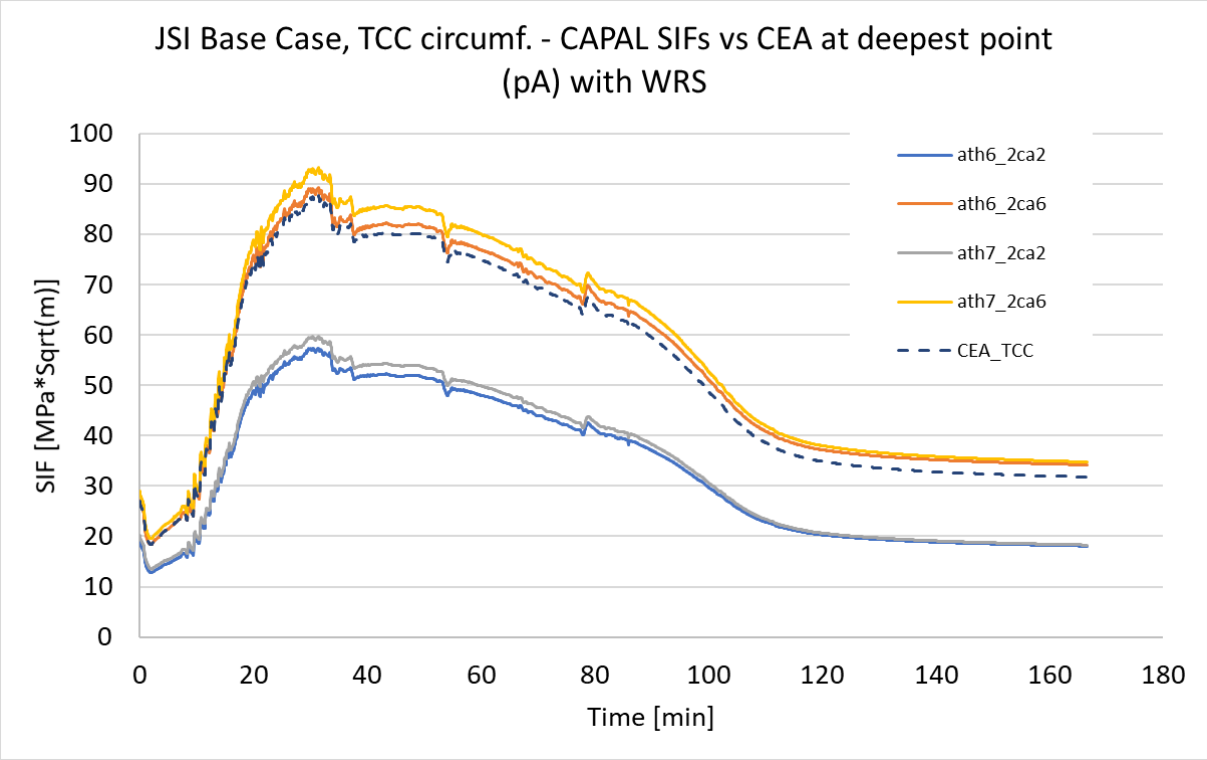

Figure 2.12: Selection of circumferential TCC2 crack size for RR2 with CAPAL code.

RR4 & RR5 circumferential TCC2 crack size in CAPAL (distributed)
Operating on the given APAL TCC crack depth distribution (Figure 4.11, Section 4.2.3.3), one can obtain the median depth ($a + r$) of 7.2 mm, which corresponds to a length ($2c$) of also 7.2mm. This is a ratio $2c/(a + r)$ equal to 1. In CAPAL/FAVOR, the closest ratio available is 2 (see CAPAL/FAVOR limitations above) which was therefore selected:

- $2c/(a + r) = 2$

Full lines in Figure 2.13 compare the available APAL TCC crack sizes in the given distribution with the ones in CAPAL/FAVOR assuming the selected ratio and continuous crack depths.

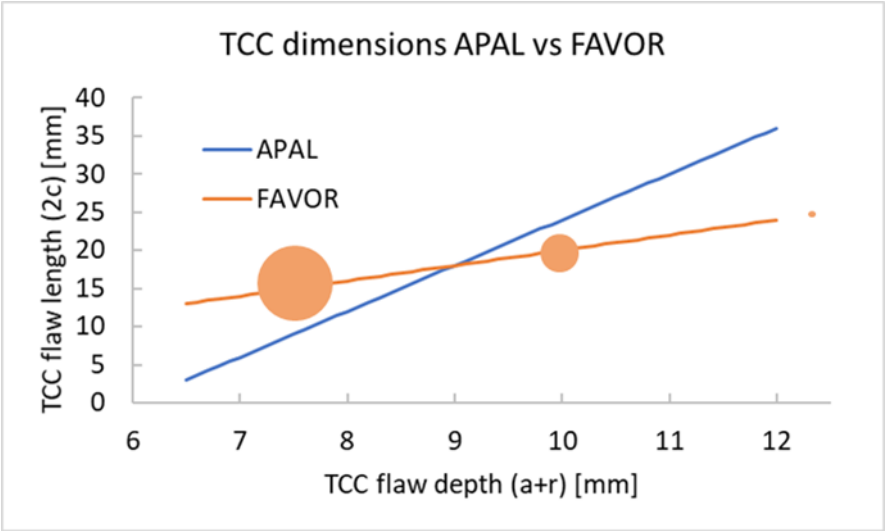

Figure 2.13: Comparison of APAL vs CAPAL crack sizes from available distributions.

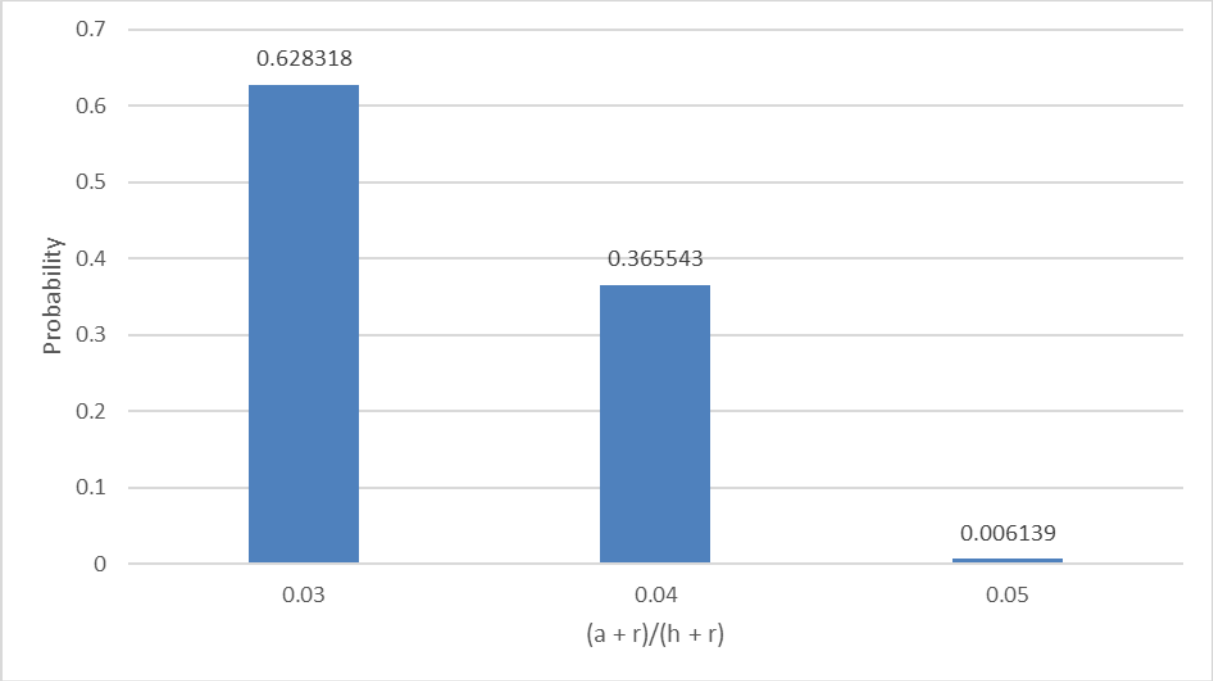

Figure 2.14: CAPAL/FAVOR crack depth distribution used by JSI for TCC2.

As mentioned above, however, crack depths distributions in CAPAL/FAVOR are based on integer-percentiles of normalised wall-thickness. The APAL crack size distribution is therefore transformed to the CAPAL/FAVOR discrete distribution shown in Figure 2.14, the crack size of which are also given in Table 2.12 for completeness. The dots over the FAVOR line in Figure 2.13 represent the discrete crack sizes used in CAPAL/FAVOR that, with the distribution in Figure 2.14, were used to perform tasks in RR4 and RR5.

Table 2.12 Discrete crack size distribution in CAPAL/FAVOR used by JSI for TCC2

$a + r$		$(a + r)/t$	$2c = 2(a + r)$
[in]	[mm]	[-]	[mm]
0.294	7.4676	0.03	14.9352
0.392	9.9568	0.04	19.9136
0.49	12.446	0.05	24.892

3 Stress and temperature distributions for benchmark performance

This Section summarises the structural analyses in APAL which have been performed to calculate stress and temperature distributions through the RPV wall thickness for the analysed transient event. The obtained stress and temperature distributions through the RPV wall provide the key input data for subsequent fracture mechanics analyses as a part of deterministic and probabilistic benchmarks and margin assessments.

Most of the efforts regarding structural analyses of the RPV have been carried out and discussed in detail within WP3 [7]. Foremost, a round-robin benchmark was performed in order to compare and verify finite element (FE) solutions based on 1D, 2D and 3D formulations. The round-robin benchmark also included the analyses of seven different locations in the RPV with specific underlying thermal-hydraulic (TH) data in order to identify a location with most conservative results for PTS assessments.

Further, the structural analyses based on the TH data representing different LTO improvements and human factors have been conducted for analysing the influence on stress and temperature distributions and ultimately, on quantification of safety margins under the PTS event.

Within WP4, the structural analyses were performed to evaluate the influence of uncertainties in TH analyses and TH data on transient stress and temperature distributions through the RPV wall thickness. The TH uncertainties were evaluated within WP2 in APAL covering the TH computer-code uncertainties, plant uncertainties related to initial conditions, boundary conditions and parameters of the NPP systems, and uncertainties connected with human interactions. The TH uncertainties have been treated using statistical methods based on the Wilks approach allowing to define a statistical set of TH data with given confidence level and tolerance limits. More detailed description regarding the construction of statistical TH data sets can be found in WP2 Public Summary report [8] and it is also described in Section 3.4 below.

3.1 Input data

3.1.1 RPV geometry

The investigated reactor is a four-loop, 1300 MWe PWR of the type built by Siemens/KWU, such as the PWR at Grafenrheinfeld. In the near-core region, the proposed four-loop RPV has:

- an internal diameter of 4870 mm in the downcomer,
- a wall thickness of 243 mm in the base/weld material and
- a 6 mm cladding thickness.

Details of the relevant RPV geometry (core region and nozzles) are shown in Figure 3.1.

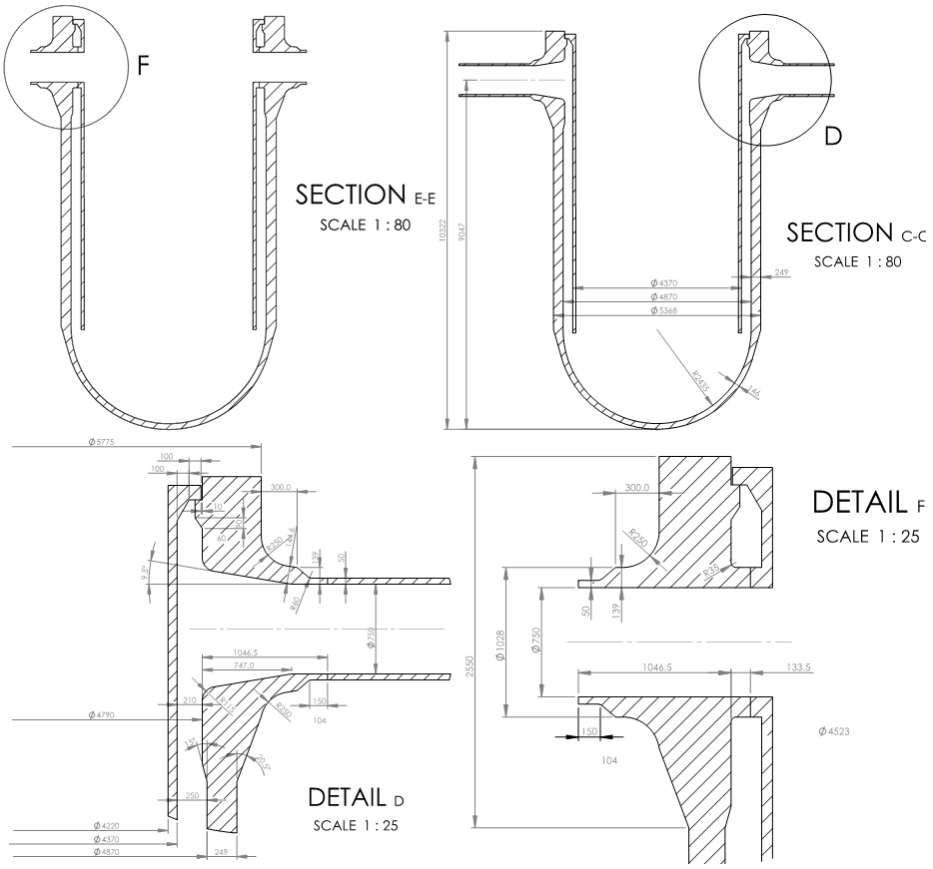

Figure 3.1: Geometry of the RPV and nozzles.

3.1.2 Material properties

The base material is assumed to be ferritic steel 22NiMoCr37, and the material number of the austenitic stainless steel cladding is 1.4551. For the simulations the linear-elastic material model was applied. In this case for the mechanical properties the knowledge of the Young's modulus and the Poisson's ratio is sufficient. The density of the base/weld metal and the cladding was set as 7800 kg/m3.

Furthermore, the relevant temperature dependent material properties of the RPV are presented in Table 3.1 and Table 3.2.

Table 3.1 Material properties of the base metal (22NiMoCr37) and the weld metal

T [°C]	20 (T_m)	100	200	300	350
E [MPa]	206000	199000	190000	181000	172000
ν [-]	0.3	0.3	0.3	0.3	0.3
λ [W/(m·K)]	44.4	44.4	43.2	41.8	39.4
C_p [J/(g·K)]	0.45	0.49	0.52	0.56	0.61
α [10^{-6}/K]	10.3	11.1	12.1	12.9	13.5

Table 3.2 Material properties of the austenitic cladding

T [°C]	20 (T_m)	100	200	300	400
E [MPa]	200000	194000	186000	179000	172000
ν [-]	0.3	0.3	0.3	0.3	0.3
λ [W/(m·K)]	16	16	17	17	18
C_p [J/(g·K)]	0.5	0.5	0.54	0.54	0.59
α [10^{-6}/K]	15	16	17	19	21

In the tables, the reference temperature for thermal expansion is 20°C (the temperature, from which is defined the thermal expansion for establishing the mean thermal expansion coefficient α), however for the consideration of stress-free state in cladding with initial transient temperature (291.042°C), the temperature has to be changed in some cases as the thermal expansion coefficient depends on it.

3.1.3 Boundary conditions

The following boundary conditions were applied for the simulations:

- Thermal conditions at the internal surface of the RPV:
  - Fluid temperature
  - Heat transfer coefficient
  - or RPV inner-surface temperature with $HTC = 10^6\ \mathrm{W/m^2K}$
- Thermal conditions at the external surface of the RPV:
  - Adiabatic or
  - $HTC = 1\ \mathrm{W/m^2K}$ and $T_{\mathrm{outside}} = 40\ ℃$
- Mechanical conditions:
  - Inner pressure at the cladding wet surface
  - Outer pressure: $p_{\mathrm{outside}} = 0\ \mathrm{MPa}$
  - Free end or end cap pressure for axial stress applied to end cross-section of RPV model
  - Necessary and sufficient boundary conditions to prevent a free-body motion.

Stress-free state in RPV was assumed at the initial transient temperature ($291.042°C$).

3.2 Structural analyses of base cases and sensitivity study

3.2.1 TH input data from RELAP

The input data for the benchmark task were received from WP2 [8] where for the generation of thermal hydraulic (TH) data the RELAP5 code was applied. However, due to the geometric limitation it had to be simplified. Therefore, so called 0D/1D/2D simulation TH data were generated. Here the denotation 0D/1D/2D is related to the TH data simplification and has no relationship to the 1D/2D/3D symbols related to the FEM model for structural analyses. Table 3.3 contains the RELAP5 data cases with their explanations.

Table 3.3 RELAP5 TH data variations

Number of Case	Description of the Case	Evaluation of RELAP5 data	
		Elevation (height)	Azimuth (circumference)
Case 1	0D – average	average	average
Case 2	1D – core weld	2638 mm (V05)	average
Case 3	2D – core weld/cold plume	2638 mm (V05)	202.5° (A-095 below HP injection)
Case 4	2D – core weld/ambient	2638 mm (V05)	337.5° (A-098 ambient)
Case 5	1D – flange weld	1130 mm* (V03)	Average
Case 6	2D – flange weld/cold plume	1130 mm* (V03)	202.5° (A-095 below HP injection)
Case 7	2D – flange weld/ambient	1130 mm* (V03)	337.5° (A-098 ambient)

The elevation and azimuth values in the RPV give the position in the downcomer from where the TH data were obtained for the structural analysis. As it can be seen from Figure 3.3, RELAP5 “divides” the geometry height into 11 parts (named from V01 to V11 as is stated in Table 3.5, where the elevations are given in the middle of these volumes). Along the circumference the geometry is divided into 8 parts

(named as DC channels 091-098), where the azimuthal angle (as it is shown in Figure 3.2 and Table 3.4) is given in the middle of these parts. For every cell (in total 11x8 cells), temperature and HTC distributions were generated which are time dependent. Therefore, the 0D/1D/2D cases mean the following:

- 0D simulation: In the whole geometry the TH inputs were averaged and are time dependent.
- 1D simulations: at the given elevation (2638 mm or 1130 mm) the TH input data are averaged along the circumference and are time dependent.
- 2D simulations: the TH inputs are from a specific position of the downcomer (V05 and DC channel 095; V05 and DC channel 098; V03 and DC channel 095; V03 and DC channel 098)

Table 3.4 Azimuthal positions of inlet/outlet nozzles

Nozzle	No of DC channel in R5 model	Azimuthal angle
CL1	A-091	22.5°
HL1	A-092	67.5°
HL2	A-093	112.5°
CL2	A-094	157.5°
CL3	A-095	202.5°
HL3	A-096	247.5°
HL4	A-097	292.5°
CL4	A-098	337.5°

Table 3.5 Elevation of DC volumes

Volume	Elevation [m]
V01	+0.5725
V02	0.0
V03	-1.13
V04	-2.083
V05	-2.638
V06	-3.3215
V07	-3.9745
V08	-4.6275
V09	-5.2809
V10	-5.9335
V11	-6.5155

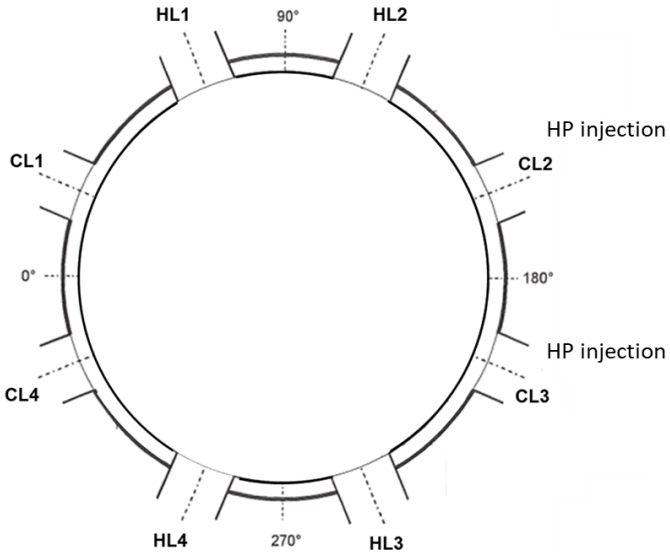

Figure 3.2: Azimuthal position of hot and cold legs.

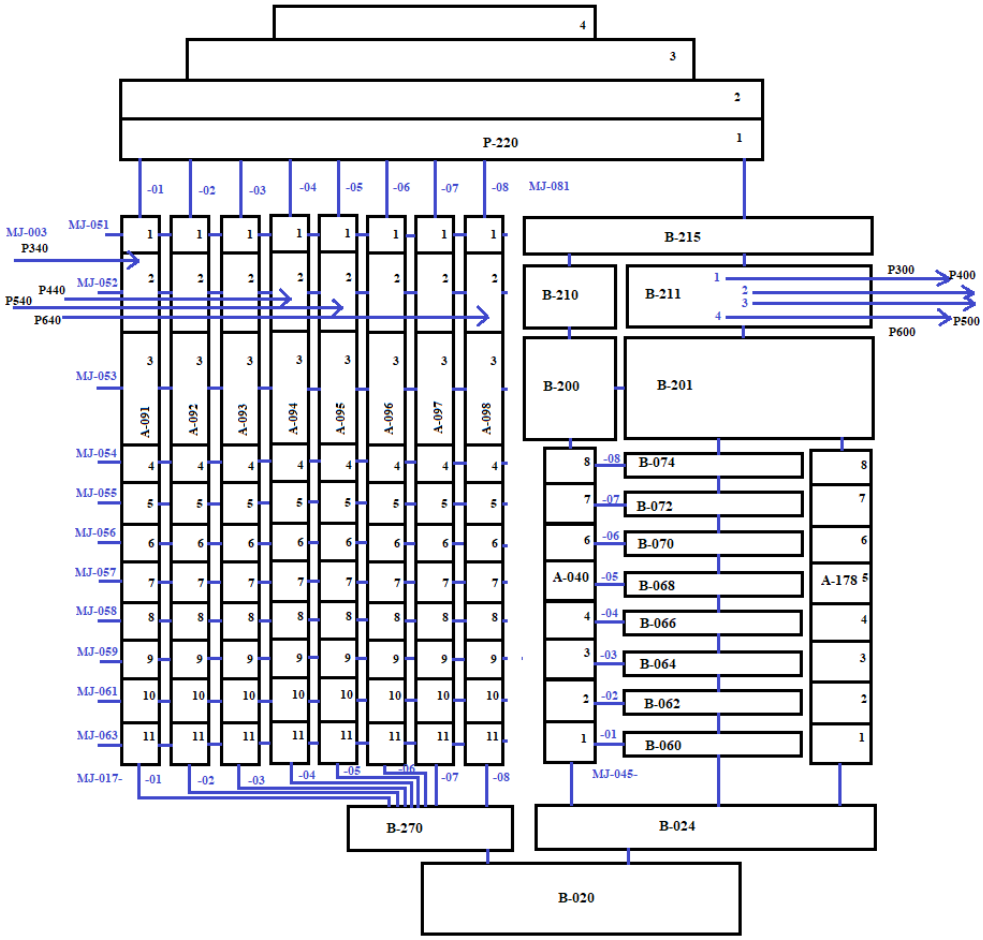

Figure 3.3: RELAP5 Nodalization of reactor.

The aim was to compare the averaging effects and select the appropriate TH data for flange and core welds. The seven cases were therefore compared where the values were generated from the averaging of the results of all the partners. The most relevant thickness for the later parts of WP3 is where the crack tip is located, this was chosen to be 16 mm, therefore Figure 3.4 shows the temperature distribution as a function of time, while Figure 3.5 illustrates the stress profiles at this value for the 7 cases.

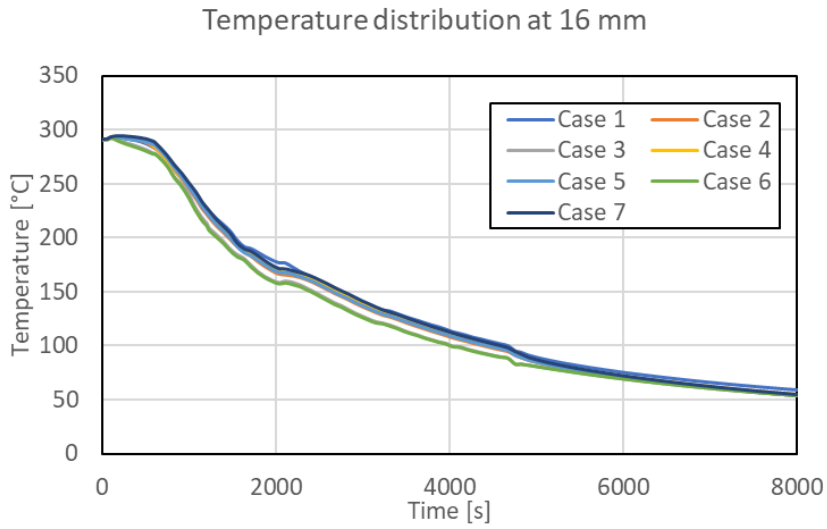

Figure 3.4: Comparison of temperature profiles for the 7 cases

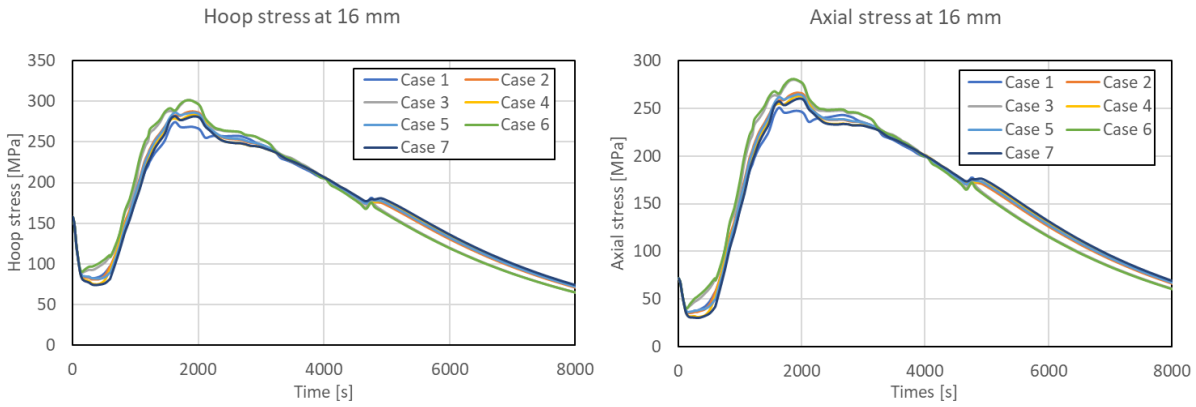

Figure 3.5: Comparison of stress profiles for the 7 cases

From these curves, it is difficult to determine which case gives the most conservative results, so the differences at the given time steps were also compared, which are shown in MPa and in percentages in Figure 3.6, where the comparison was based on Case 3 and therefore its values are zero.

16 mm (crack tip)	T [°C] t=6 s	T [°C] t=30 s	T [°C] t=300 s	T [°C] t=600 s	T [°C] t=1200 s	T [°C] t=2400 s	T [°C] t=3600 s	T [°C] t=4800 s	T [°C] t= 6000 s	T t=6 s	T t=30 s	T t=300 s	T t=600 s	T t=1200 s	T t=2400 s	T t=3600 s	T t=4800 s	T t= 6000 s
Case1	291.0246	290.9865	291.0717	283.0639	227.4962	163.4227	124.0889	94.29672	75.30929	0.00%	0.00%	1.24%	1.66%	6.34%	7.67%	11.90%	13.69%	8.09%
Case2	291.0243	290.9927	291.4319	283.1341	221.5777	159.2739	118.3109	89.47096	70.61129	0.00%	0.00%	1.36%	1.68%	3.58%	4.94%	6.69%	7.87%	1.35%
Case3	291.0361	290.9845	287.5198	278.4552	213.9295	151.7742	110.8964	82.9418	69.67016	0.00%	0.00%	0.00%	0.00%	0.00%	0.00%	0.00%	0.00%	0.00%
Case4	291.0249	291.0525	293.2582	284.9182	224.9799	162.678	121.2822	92.4583	71.75906	0.00%	0.02%	2.00%	2.32%	5.17%	7.18%	9.37%	11.47%	3.00%
Case5	291.0192	290.9871	291.0518	285.6972	222.9435	159.9724	119.2041	89.65766	70.58362	-0.01%	0.00%	1.23%	2.60%	4.21%	5.40%	7.49%	8.10%	1.31%
Case6	291.0315	290.9794	286.3009	278.1714	211.3127	150.1316	109.9942	83.03464	69.19745	0.00%	0.00%	-0.42%	-0.10%	-1.22%	-1.08%	-0.81%	0.11%	-0.68%
Case7	291.0197	291.0484	293.6068	288.4346	227.5466	164.217	122.7935	92.78156	71.89132	-0.01%	0.02%	2.12%	3.58%	6.37%	8.20%	10.73%	11.86%	3.19%

16 mm (crack tip)	Hoop stress [MPa] t=6 s	Hoop stress [MPa] t=30 s	Hoop stress [MPa] t=300 s	Hoop stress [MPa] t=600 s	Hoop stress [MPa] t=1200 s	Hoop stress [MPa] t=2400 s	Hoop stress [MPa] t=3600 s	Hoop stress [MPa] t=4800 s	Hoop stress [MPa] t=6000 s	Hoop stress t=6 s	Hoop stress t=30 s	Hoop stress t=300 s	Hoop stress t=600 s]	Hoop stress t=1200 s	Hoop stress t=2400 s	Hoop stress t=3600 s	Hoop stress t=4800 s	Hoop stress t=6000 s
Case1	157.0024	146.0549	82.13977	96.8638	220.588	257.451	220.8348	178.9129	132.431	-0.18%	-1.21%	-11.68%	-10.84%	-12.19%	-2.46%	-2.07%	2.64%	9.93%
Case2	157.3789	147.9731	81.27159	97.14193	235.7219	255.5607	223.1331	176.0638	130.7793	0.06%	0.09%	-12.61%	-10.59%	-6.16%	-3.18%	-1.05%	1.00%	8.56%
Case3	157.292	147.8386	92.99978	108.6439	251.2081	263.9491	225.5073	174.3122	120.4667	0.00%	0.00%	0.00%	0.00%	0.00%	0.00%	0.00%	0.00%	0.00%
Case4	157.3784	147.7765	75.81684	92.94787	228.4437	251.2199	222.4994	175.7758	133.8294	0.05%	-0.04%	-18.48%	-14.45%	-9.06%	-4.82%	-1.33%	0.84%	11.09%
Case5	157.3789	147.9727	82.41297	89.05106	233.3767	255.862	222.9251	177.9154	132.1585	0.06%	0.09%	-11.38%	-18.03%	-7.10%	-3.06%	-1.15%	2.07%	9.71%
Case6	157.3795	148.0361	96.7818	108.9777	256.8088	264.8204	224.1822	170.977	119.6174	0.06%	0.13%	4.07%	0.31%	2.23%	0.33%	-0.59%	-1.91%	-0.70%
Case7	157.3784	147.7714	74.79291	82.08695	223.8555	251.0138	222.5577	179.0935	135.9854	0.05%	-0.05%	-19.58%	-24.44%	-10.89%	-4.90%	-1.31%	2.74%	12.88%

16 mm (crack tip)	Axial stress [MPa] t=6 s	Axial stress [MPa] t=30 s	Axial stress [MPa] t=300 s	Axial stress [MPa] t=600 s	Axial stress [MPa] t=1200 s	Axial stress [MPa] t=2400 s	Axial stress [MPa] t=3600 s	Axial stress [MPa] t=4800 s	Axial stress [MPa] t=6000 s	Axial stress t=6 s	Axial stress t=30 s	Axial stress t=300 s	Axial stress t=600 s	Axial stress t=1200 s	Axial stress t=2400 s	Axial stress t=3600 s	Axial stress t=4800 s	Axial stress t=6000 s
Case1	71.37985	66.47135	37.57105	57.43013	191.7026	240.7786	212.8636	175.4427	128.0677	-0.22%	-1.27%	-22.34%	-17.12%	-13.90%	-2.69%	-2.23%	2.63%	10.36%
Case2	71.56521	67.3502	36.57778	57.74446	207.0251	238.9794	215.2879	172.7048	126.4278	0.04%	0.03%	-24.39%	-16.67%	-7.02%	-3.42%	-1.11%	1.03%	8.95%
Case3	71.53604	67.3276	48.37658	69.29703	222.6589	247.4465	217.7105	170.9406	116.0406	0.00%	0.00%	0.00%	0.00%	0.00%	0.00%	0.00%	0.00%	0.00%
Case4	71.56463	67.16033	31.09879	53.53791	199.6984	234.6072	214.6472	172.4039	129.4882	0.04%	-0.25%	-35.72%	-22.74%	-10.31%	-5.19%	-1.41%	0.86%	11.59%
Case5	71.56524	67.34988	37.72331	49.60236	204.6727	239.289	215.0924	174.5636	127.8128	0.04%	0.03%	-22.02%	-28.42%	-8.08%	-3.30%	-1.20%	2.12%	10.14%
Case6	71.56578	67.41356	52.1566	69.58723	228.2818	248.3164	216.3701	167.5776	115.1932	0.04%	0.13%	7.81%	0.42%	2.53%	0.35%	-0.62%	-1.97%	-0.73%
Case7	71.56457	67.14756	30.06696	42.62489	195.0737	234.3907	214.6956	175.7414	131.6603	0.04%	-0.27%	-37.85%	-38.49%	-12.39%	-5.28%	-1.38%	2.81%	13.46%

Figure 3.6: Percentage and absolute differences in 7 cases compared to Case 3

The comparisons show that lower values of temperature are only observed in Case 6, where the circumferential angle is the same, but the elevation is different (flange weld). For this reason, higher values are observed for the circumferential and axial stresses in Case 6. The difference between Case 3 (202.5°) and Case 4 (337.5°) is the circumferential position, from where the TH data are taken. As can be seen from the table, Case 3 shows higher stress values and therefore Cases 4 and Case 7 (ambient) have been excluded from the future simulations.

3.2.2 1D Simulations

As described in the previous section, Case 3 was chosen as the focus of Task 3.1. A comparison of the partners' results based on 1D FE simulations is presented for the Case 3.

Comparison of partners' results for temperatures, hoop and axial stresses as a function of time for the crack tip position is shown in Figure 3.7 to Figure 3.9. From the diagrams it can be seen that the final differences between the results of the partners are less than 5% compared to the previously introduced reference curve. The only exception is a 2D axisymmetric model which was done

additionally to 1D model. The core weld is relatively far away from the conical part close to the RPV nozzles, therefore it only has minor effect on resulting stresses. According to other calculations, the conical part has a much more significant effect on the flange weld stress, this will be introduced in more detail further.

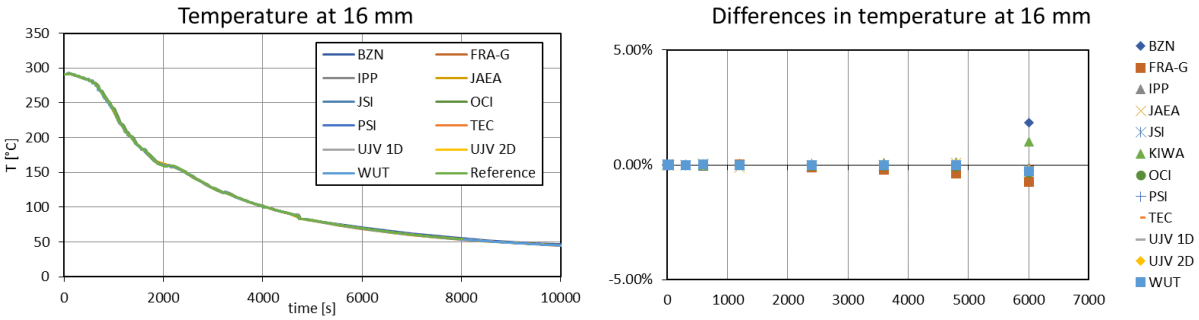

Figure 3.7: Comparison of partners' results of temperature as a function of time (Case 3)

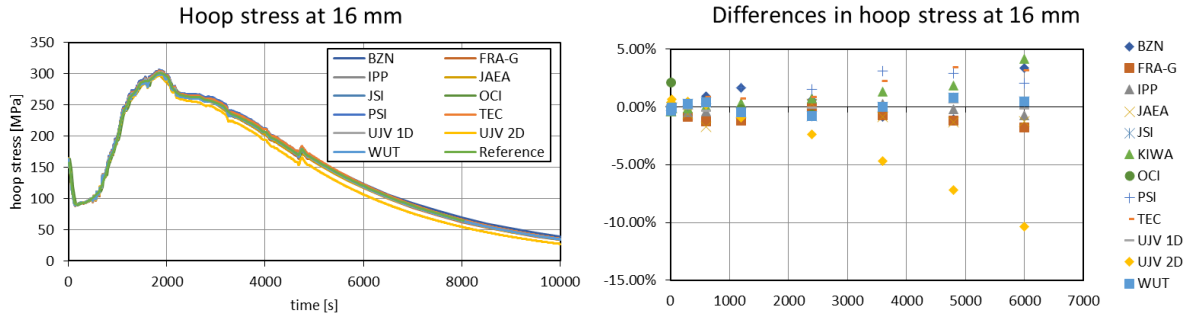

Figure 3.8: Comparison of partners' results of hoop stress as a function of time (Case 3)

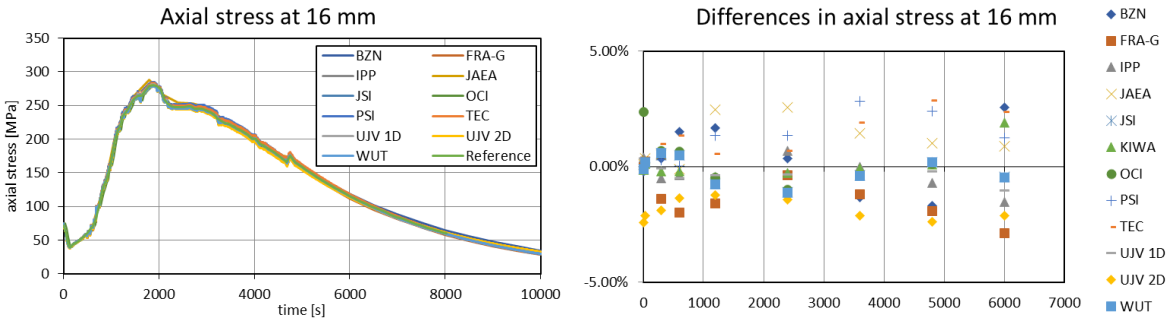

Figure 3.9: Comparison of partners' results of axial stress as a function of time (Case 3)

3.2.3 3D Simulations

Beside the 1D simulations of RPV, 3D calculations were also performed by several partners. In the following text the 3D FE models, the boundary conditions and some of the results are briefly introduced. The following results were taken out from the core weld (2638 mm) and cold leg (202.5°) positions.

The first comparison was done with same RELAP TH input data used. The comparisons of temperature and hoop stress distribution as function of time at the crack tip is shown in Figure 3.10.

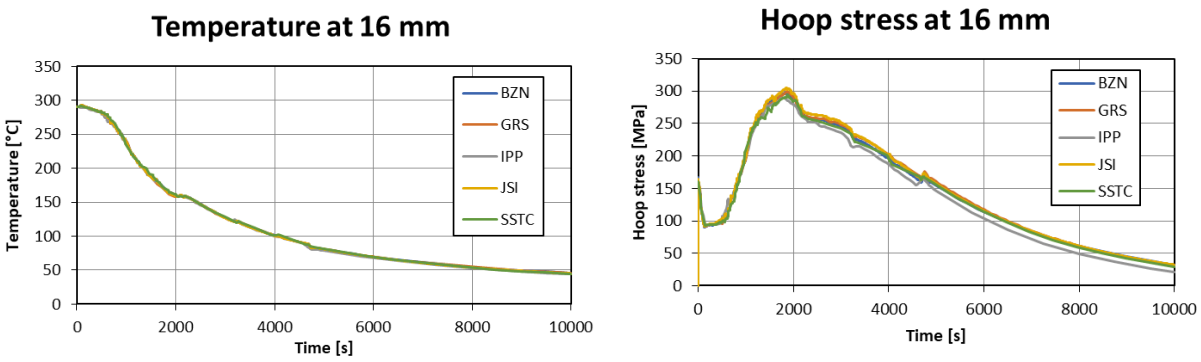

Figure 3.10: Temperature and hoop stress distribution as a function of time for the same TH input data

The second comparison was done with the base case simulation versions of the partners. Here three types of TH data were used RELAP, KWU-MIX and TRACE. The comparisons of temperature and hoop stress distribution as function of time at the crack tip is shown in Figure 3.11. Even in case of the temperature large differences can be seen, which are the resulted from the different TH data. It has to be noted that in case of the TRACE results this large difference is due to the linear extrapolation of the results from the wall thickness of 26 mm and 46.5 mm as there were no other nodes between 6 mm and 26 mm. This should therefore be taken into account when interpreting the curve. Also, in case of the KWU-MIX data the cold plume was also considered therefore the data are taken from 180° where the coldest wall temperatures are occurring in case of the core weld (2638 mm). In the other TH data this circumferential angle was 202.5°.

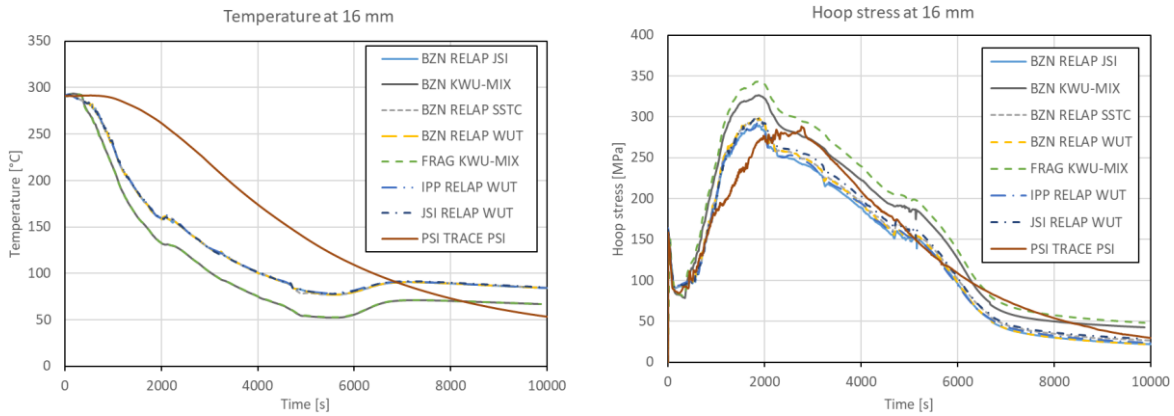

Figure 3.11: Temperature and hoop stress distribution as a function of time with different TH input data

3.2.4 Other locations

3.2.4.1 Flange weld location

As it already was mentioned previously beside the investigation of the core weld the flange weld was also considered. The core weld is placed at the high of 2638 mm where the thickness of the reactor pressure vessel wall is already uniform. The flange weld is located at 1350 mm which is already very close to the nozzle area furthermore the thickness of the vessel increases here, which can modify the stress distribution.

Several partners have investigated the effect of the flange weld location with either 1D or 3D FE method and with either input from system code (e.g. RELAP) or from system in combination with mixing code. All the investigations showed the same trend, but with different quantities. The impact of flange weld location is exemplary shown in Figure 3.12 and Figure 3.13 (results considering RELAP input at relevant locations). The results for the flange weld location from 3D FE with input from RELAP in combination with mixing code are given in Annex Section 8.1 in [7].

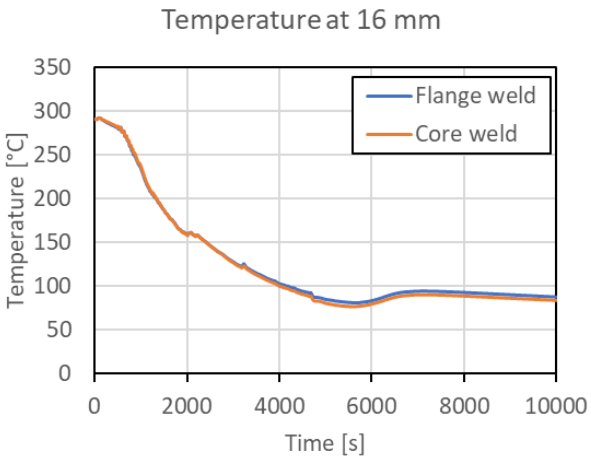

Figure 3.12: Temperature variation at crack tip of the RPV wall for the core weld and the flange weld below the cold leg

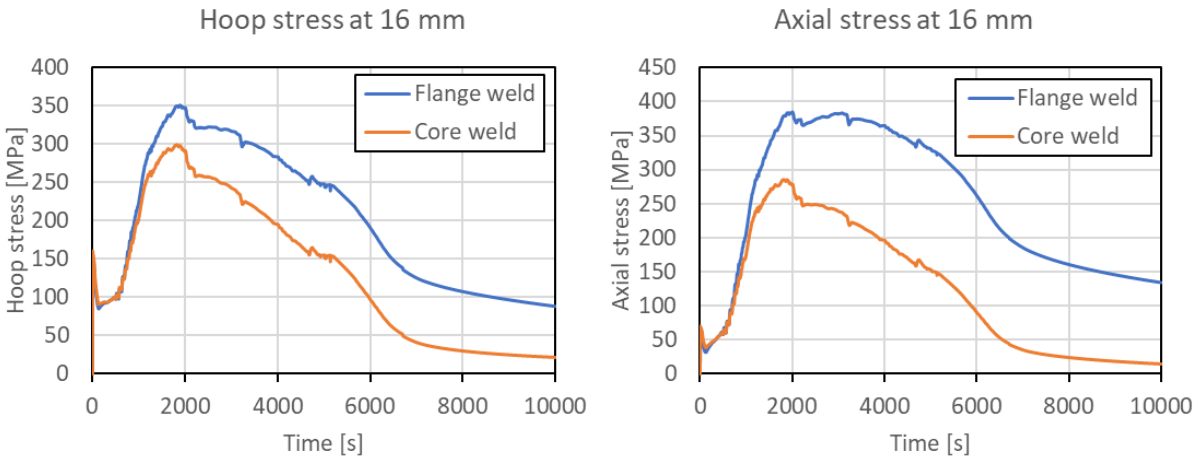

Figure 3.13: Hoop stress and axial stress variation at crack tip of the RPV wall for the core weld and the flange weld below the cold leg

3.2.4.2 Outside cold plume location

The location outside plume was chosen to be below CL4 at azimuth 337.5° (far away from cold injection leg CL2 and CL3), see section 3.1.1. Several partners have investigated the effect of the outside plume location with either 1D or 3D FE method and with either input from system code (e.g. RELAP) or from system in combination with mixing code.

The results and comparison with inside plume location showed, that temperatures below the CL2 and CL3 nozzles (volumes 094-05 and 095-05) where the ECC water is injected and the plume is formed, are lower than the temperatures below other nozzles during most of the transient. As expected, this yields higher stresses in the two plume locations than in the other locations. Results for outside plume location and comparison with inside plume location can be made by considering the results provided in Annex Sections 8.1.1 and 8.1.13 in [7].

Figure 3.14 shows the comparison between 3D (ABAQUS) and 1D (FAVOR) results at the core and flange weld elevations, and both at the outside plume location below CL4 centerline and with the addition of the ABAQUS results for the alternative outside plume location below HL2. The results at the core weld elevation are presented in Figure 3.14 (right), where it is shown that while the inner-surface temperatures of the 2 outside plume locations are practically identical, the stresses below HL2 are slightly lower than below CL4, the latter very well reproduced by FAVOR. Figure 3.14 (left) presents

the results at the two outside plume locations, but at the flange weld elevation. While the temperatures are also very much the same, we can see again some discrepancy on the stresses. As already concluded in section 3.2.4, FAVOR clearly deliver lower stresses at the flange weld since the 1D approximation cannot account for close proximity of the thicker part of the RPV and nozzles. The ABAQUS hoop stresses below HL2 are again lower than below CL4, however, the axial stresses are practically the same as can be seen in the figure inset.

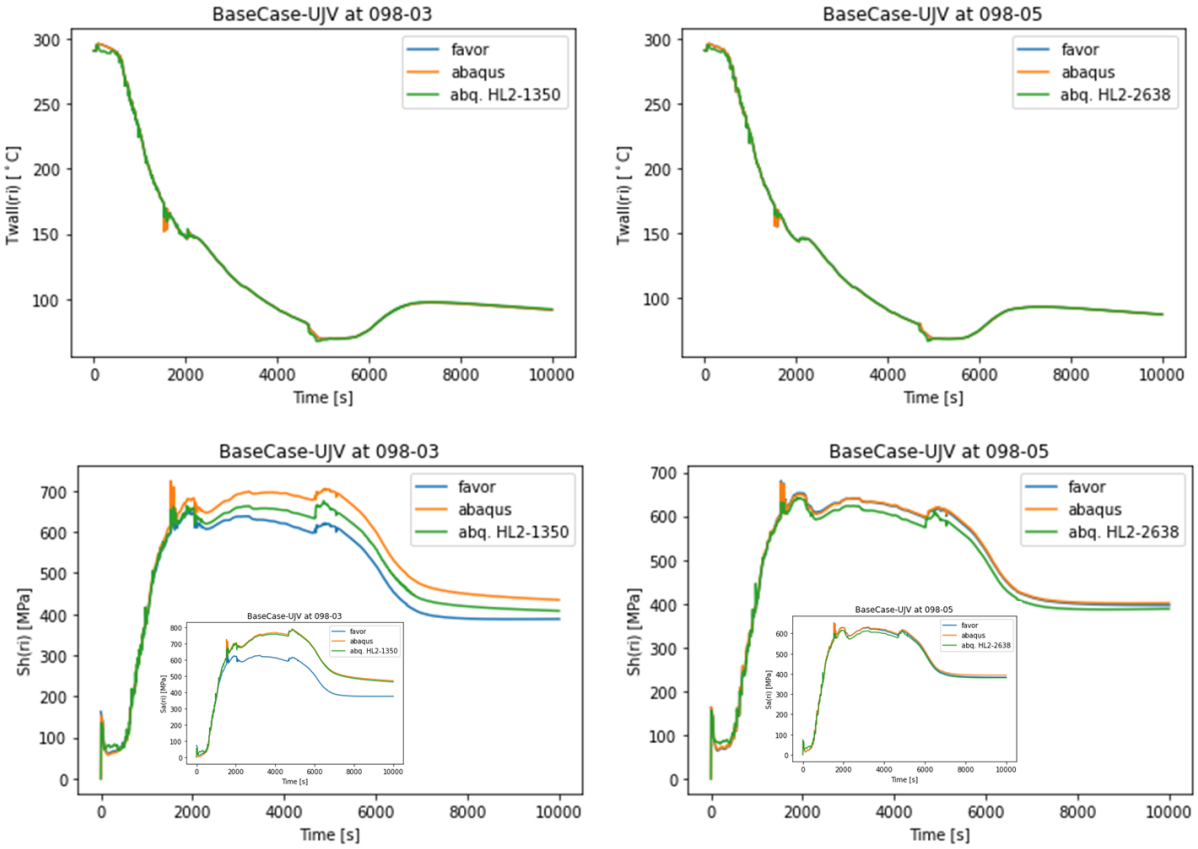

Figure 3.14: RPV inner-surface temperatures (top), hoop (bottom) and axial (bottom-inset) stresses at the core weld (right) and flange weld (left) elevations, both at the outside plume location below CL4 (FAVOR and ABAQUS) and below HL2 (abq. HL2)

3.2.4.3 Nozzle corner

Stress and temperature fields for the nozzle corner (cold leg) have only been calculated with 3D FE. Results for nozzle corner location and comparison with inside plume location at core weld can be made by considering the results provided in Annex Sections 8.1.1 and 8.1.4 in [7].

3.2.5 Mesh refinement

Several partners have investigated the effect of mesh refinement. Different variants of mesh refinement in combination with linear or quadratic elements have been selected and analysed. Details about all results from all partners are given in [13].

Exemplary the results on mesh refinement in case of the 3D simulation is presented, where the FE models listed in Table 3.6 were used. Two type of global model was created, one with linear elements where the full model was made and one with quadratic elements where only half of the reactor pressure vessel was generated. Thereafter from the first version local models were also generated where the number of elements were increased as shown in the table.

Table 3.6: Properties of the investigated mesh types

Name	Model version	Order of refinement	Number of elements in the cladding	Number of elements in the base metal
Mesh 1	Linear model	Linear (full model)	3	10
Mesh 2		Linear (local model)	3	38
Mesh 3		Linear (Local model)	6	76
Mesh 4	Quadratic model	Quadratic (half model)	3	10

The temperature distribution in all 4 mesh versions were in excellent agreement, however in case of the hoop and axial stress larger deviations could be noted as it is also illustrated in Figure 3.15 and Figure 3.16.

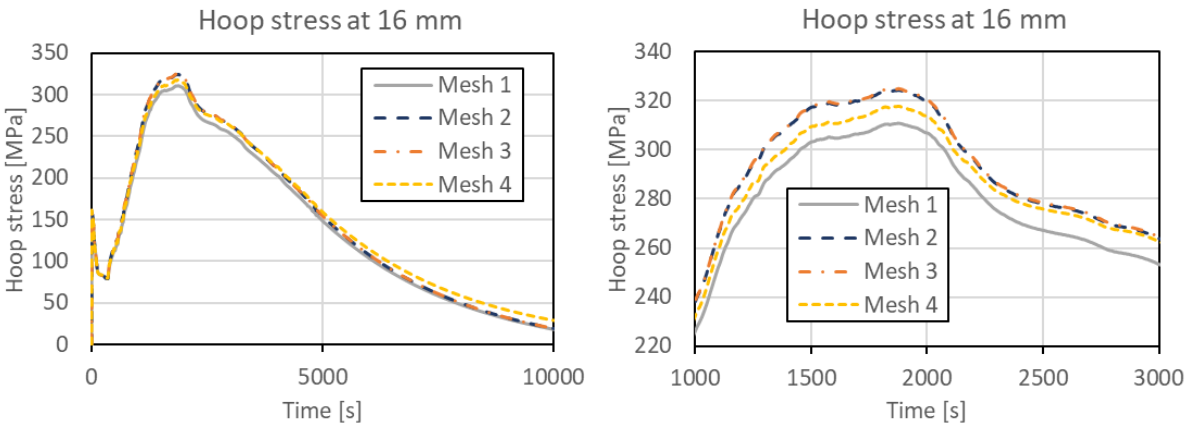

Figure 3.15: Influence of the mesh size on the hoop stress

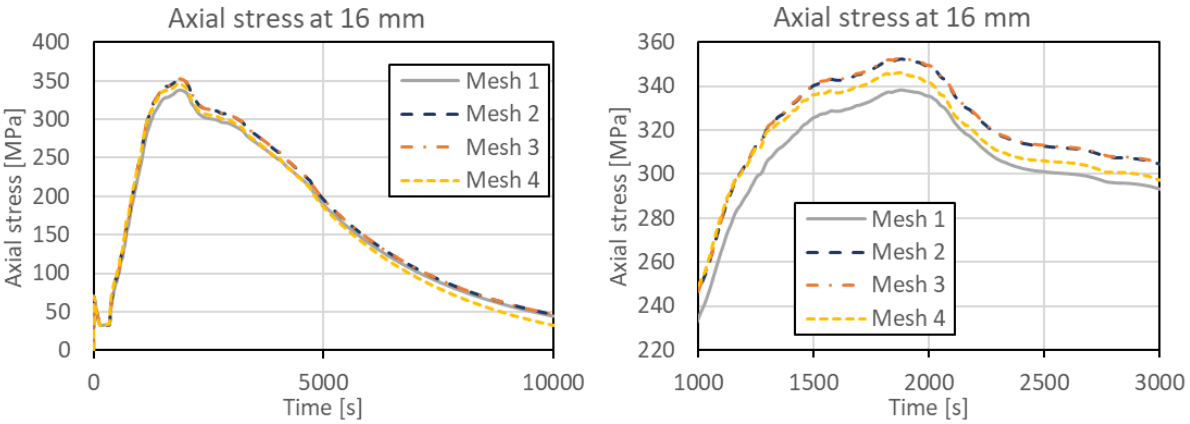

Figure 3.16: Influence of the mesh size on the axial stress

3.2.6 Time steps

The effect of the size of the time step was investigated to see how the simplifications could be applied. The input data – results of TH calculations - had a duration of 10 000 s, where the time step was 1 s. This is not a major problem for 1D simulations, but the runtime of a 3D simulation would be too long, so data simplification was considered. For both 1D and 3D simulations, we used the Case3 presented earlier. For the 1D simulation, 4 different time steps were considered: 1 s, 2 s, 5 s and 10 s. With these values the number of time steps can be reduced from 10000 to 5000, 2000 and 1000. Figure 3.17 and Figure 3.18 show the difference of the hoop stress at the inner surface of the RPV and at crack tip location (16 mm). This shows that the result obtained with 10 s time step is higher/lower than that one with 1 s time step by more than 20 MPa. This results in a relative difference of about 5%. The results

obtained with the 2s time step are in fairly good agreement with the original version, but the number of time steps seems to be too large in this case too.

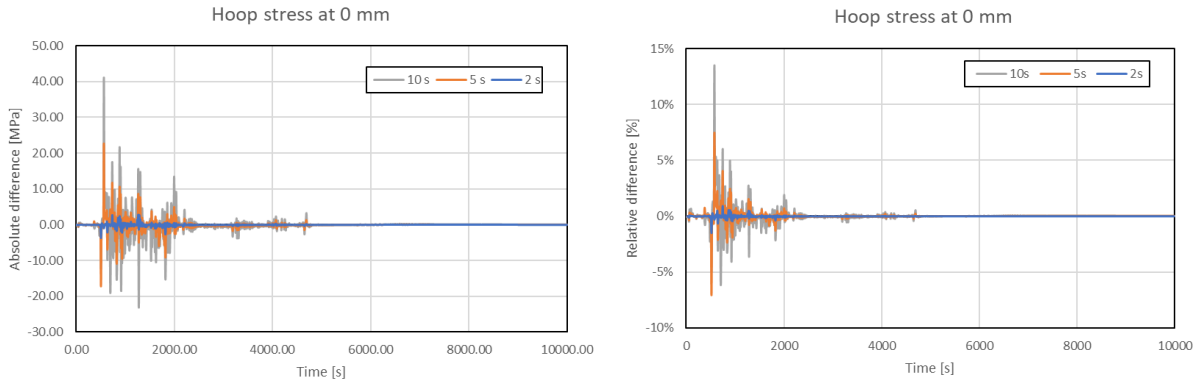

Figure 3.17: Absolute and relative difference of the hoop stress as a function of time step at the inner surface of the RPV

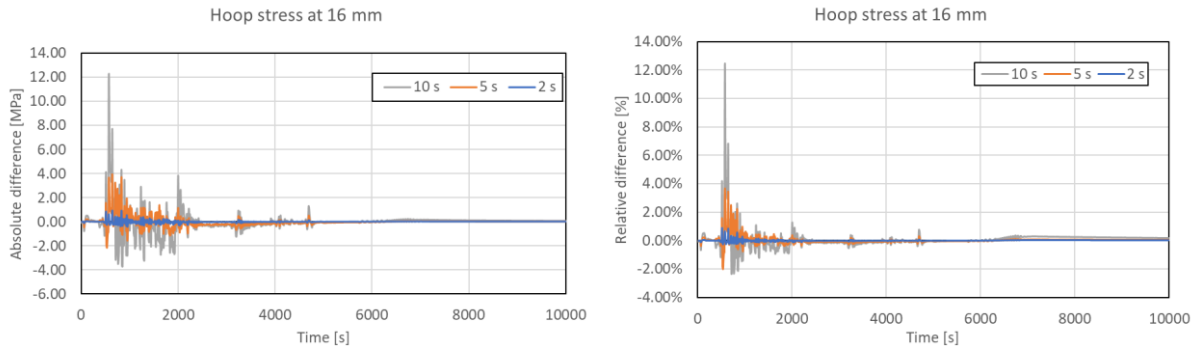

Figure 3.18: Absolute and relative difference of the hoop stress as a function of time step at the crack tip (16 mm)

3.3 Structural analyses of LTO improvements

In WP2 nine types of long-term operation improvements and human actions were simulated which are listed in Table 3.7. The thermohydraulic simulations for Task 2.1 were performed with different system codes and mixing codes, namely ATHLET, RELAP5, TRACE, KWU-MIX, ECC-MIX and Ansys fluent.

Table 3.7: Investigated LTO improvements and human factors

Index Code	Naming in Table	
1	LTO1	Heating of water in the HPSI tanks (T = 45°C)
2	LTO2	Heating of water in the ACCs (T = 50°C)
3	LTO3	Heating of water in the LPSI tanks (T= 45°C)
4	LTO4	Decreasing the HPSI head (75%)
5	LTO5	Decreasing the HPSI capacity (75%)
6	LTO6	Reduction of HPSI flow (operator action) at 1800s
7	LTO7	Decreasing of ACC pressure (20 bar)
8	LTO8	Change of cooldown rate (operator action) at 200 K/h
9	LTO9	Isolation of ACCs (operator action) at 500s

3.3.1 Results from 1D FE analyses

For every LTO improvement included in Table 3.7 1D simulations were performed by the different partners. In every 1D simulation the TH data were generated the same way as in Case 3. In the following subsections the results from one partner are shown exemplary. More details about all results are given in [13].

3.3.1.1 LTO1 – Heating of water in the HPIS tanks (T = 45°C)

In case of the TH data the heating of water in HPIS tanks was simulated by increasing the injection temperature from the reference value of 15°C to the LTO value of 45°C. There calculations showed that the increased injection temperature results in a higher water temperature in the DC during the whole transient. The proposed LTO development until the ACCs start (about 2790 s) has an impact on the break flow and fluid levels. Therefore, it was concluded that the LTO improvement could potentially be beneficial for PTS.

The obtained hoop stress and temperature and the comparison with base case result to see the impact of LTO improvement are shown in Figure 3.19 (TH input from RELAP) and in Figure 3.20 (TH input from TRACE).

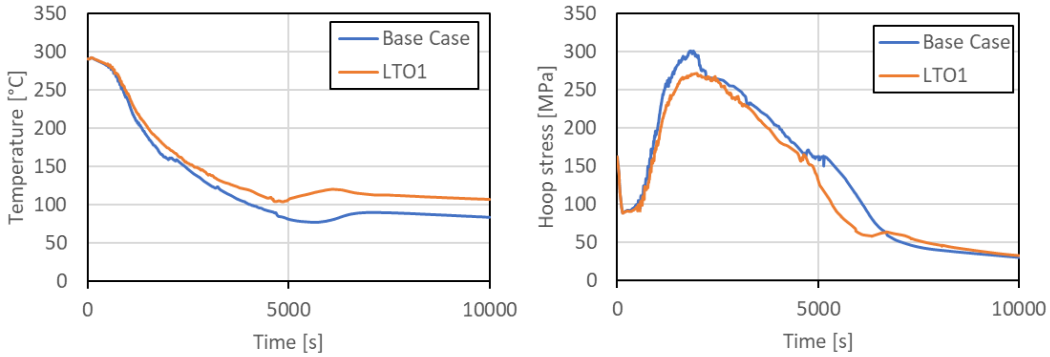

Figure 3.19: LTO1 results of JAEA interpolated to the 16 mm of RPV wall thickness, with RELAP (WUT) TH input data

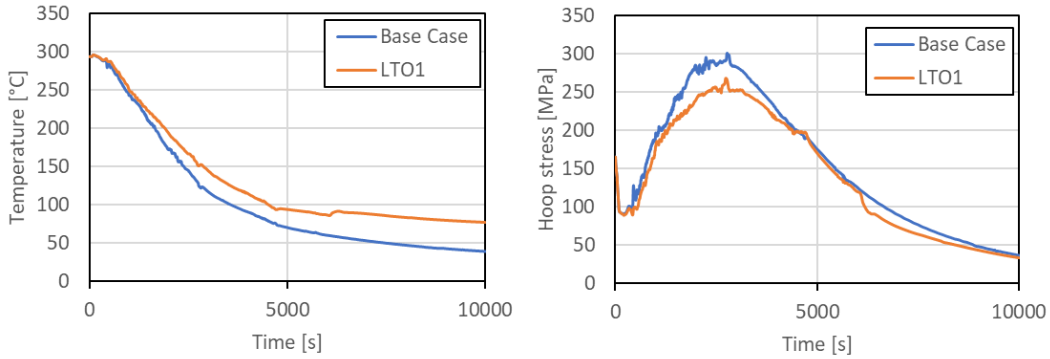

Figure 3.20: LTO1 results of TEC interpolated to the 16 mm of RPV wall thickness, with TRACE (PSI) TH input data

3.3.1.2 LTO2 – Heating of water in the ACCs (T = 50°C)

In case of the thermal hydraulic calculations the heating of the water in the ACCs was simulated by increasing the water injection temperature from the reference value of 20°C to 50°C. The LTO improvement resulted in slightly higher temperature in the DC after the beginning of the flow from ACCs. Therefore, they concluded that the LTO improvement provides no significant benefit from a PTS perspective.

The obtained hoop stress and temperature and the comparison with base case result to see the impact of LTO improvement are shown in Figure 3.21 (TH input from RELAP), in Figure 3.22 (TH input from TRACE) and in Figure 3.23 (TH input from ECC-MIX, plot only up to 6000 sec.).

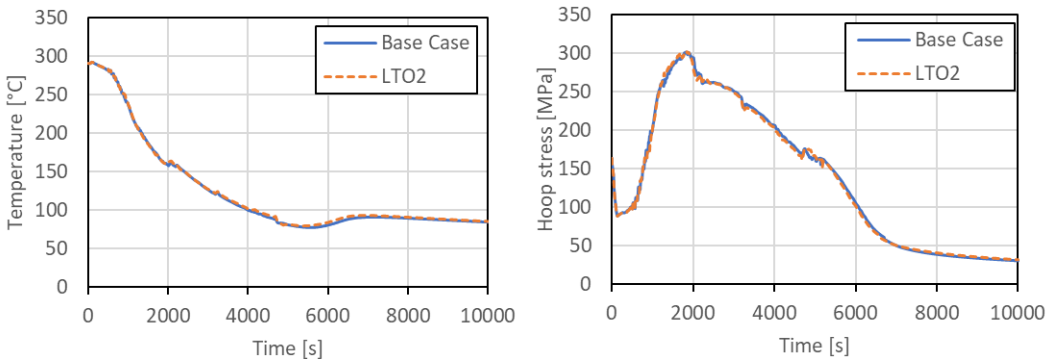

Figure 3.21: LTO2 results of JSI interpolated to the 16 mm of RPV wall thickness, with RELAP (WUT) TH input data

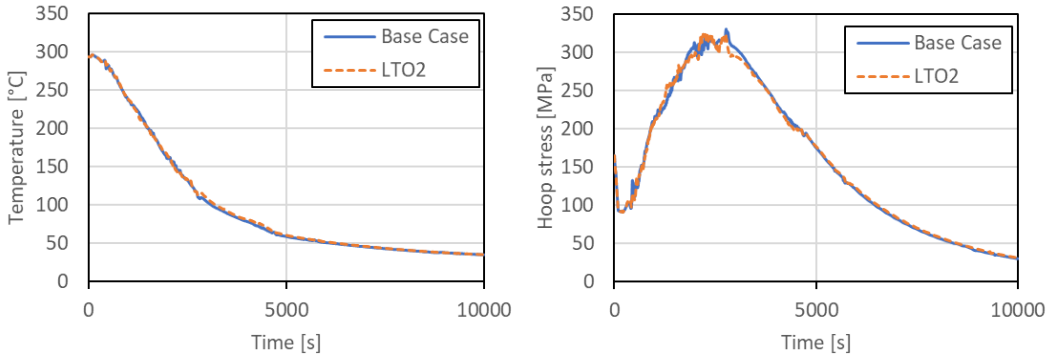

Figure 3.22: LTO2 results of PSI interpolated to the 16 mm of RPV wall thickness, with TRACE (PSI) TH input data

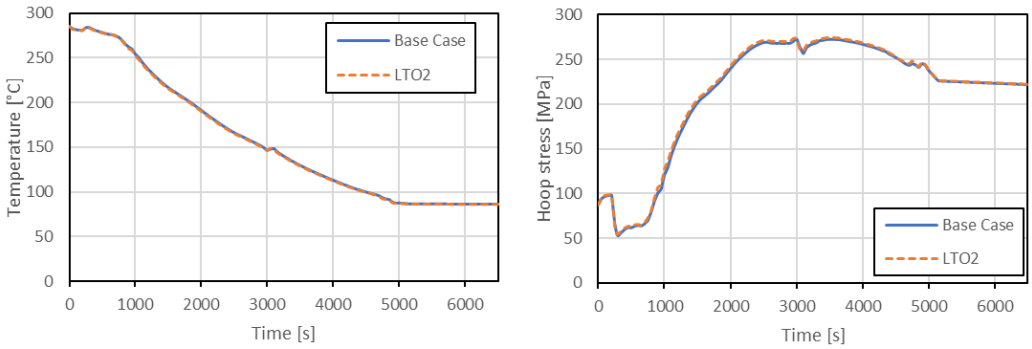

Figure 3.23: LTO2 results of GRS interpolated to the 16 mm of RPV wall thickness, with ECC-MIX (GRS) TH input data

3.3.1.3 LTO3 – Heating of water in the LPIS tanks (T = 45°C)

The heating of the water in the LPI tanks was simulated by increasing the injection temperature from the reference value of 15°C to 45°C. The RELAP calculations showed that there is insignificant impact on the water level and water temperature in the DC till the end of transient (5000 s). Similarly to this, in case of the TRACE simulations, for this particular transient, heating of LPI had only a very small benefit Therefore the studied LTO improvement provided no benefit from a PTS perspective.

The obtained hoop stress and temperature and the comparison with base case result to see the impact of LTO improvement are shown in Figure 3.24 (TH input from RELAP) and in Figure 3.25 (TH input from KWU-MIX).

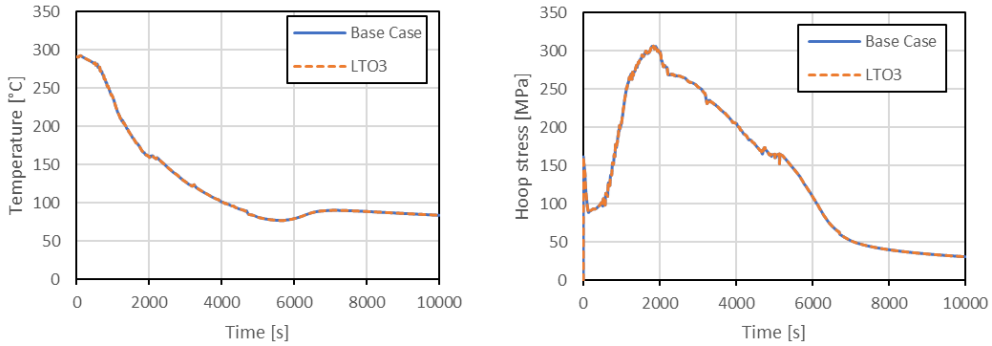

Figure 3.24: LTO3 results of BZN at the 16 mm of RPV wall thickness, with RELAP (WUT) TH input data

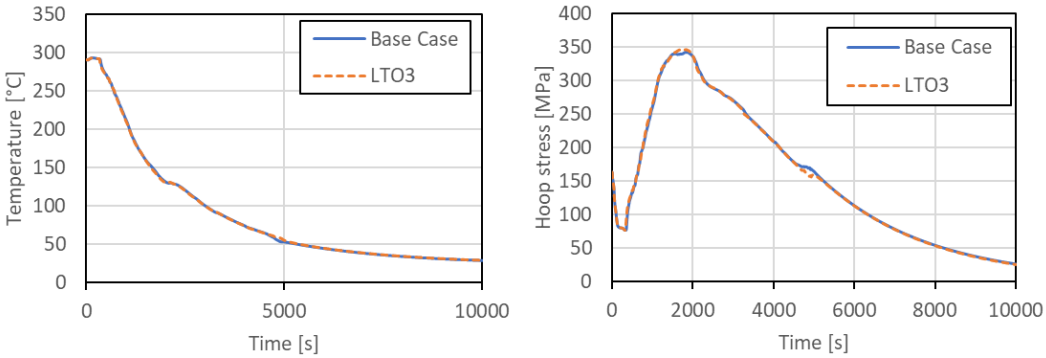

Figure 3.25: LTO3 results of IPP at 16 mm of RPV wall thickness, with KWU-MIX (FRA-G) TH input data

3.3.1.4 LTO4 – Decreasing the HPSI head (75%)

The decreasing of the HPI pump head was simulated by scaling the pressure component of the HPI pump curve down to 75% of the reference value.

The obtained hoop stress and temperature and the comparison with base case result to see the impact of LTO improvement are shown in Figure 3.26 (TH input from RELAP) and in Figure 3.27 (TH input from ECC-MIX).

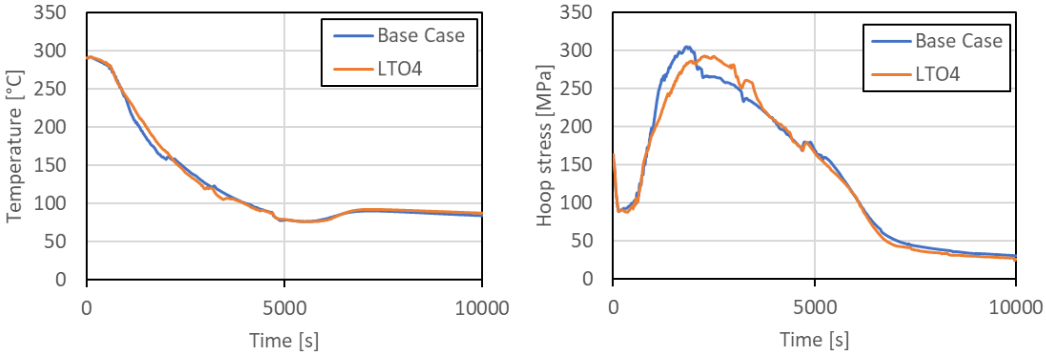

Figure 3.26: LTO4 results of KIWA at 16 mm of RPV wall thickness, with RELAP (SSTC) TH input data

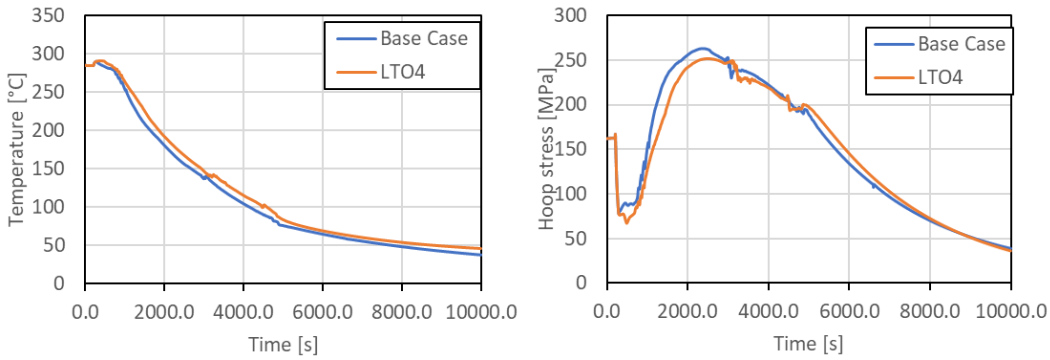

Figure 3.27: LTO4 results of TEC interpolated to the 16 mm of RPV wall thickness, with ECC-MIX (GRS) TH input data

3.3.1.5 LTO5 – Decreasing the HPSI capacity (75%)

The decreasing of the HPI pump capacity was simulated via scaling of the flow component of the HPI pump curve down to 75%. From the TH simulations it was concluded that by decreasing rate of cooling (via HPI pumps) the coolant temperatures can be reduced to some extent as well. Based on the results they assumed that analysed LTO improvement potentially may affect results of RPV strength analysis. However, they stated that the effect needs to be confirmed using thermo-mechanical and fracture mechanics simulations.

The obtained hoop stress and temperature and the comparison with base case result to see the impact of LTO improvement are shown in Figure 3.28 (TH input from RELAP) and in Figure 3.29 (TH input from TRACE).

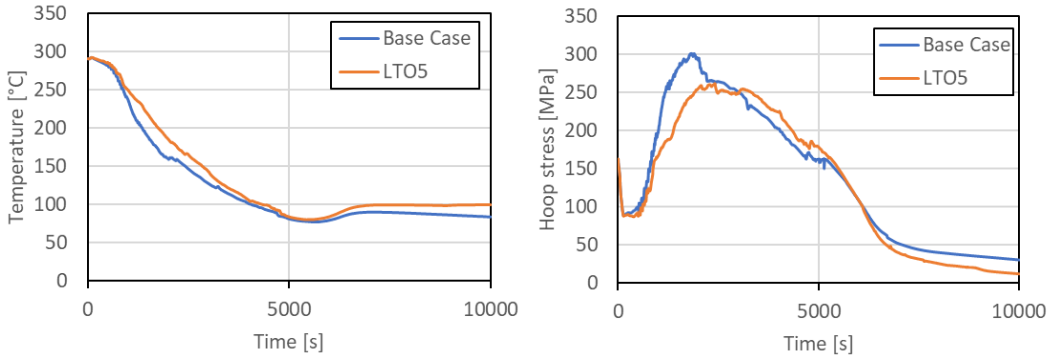

Figure 3.28: LTO5 results of JAEA interpolated to the 16 mm of RPV wall thickness, with RELAP (WUT) TH input data

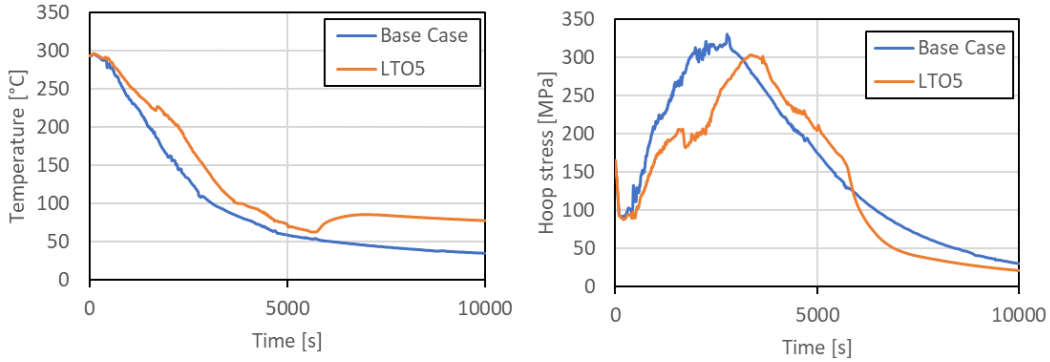

Figure 3.29: LTO5 results of PSI interpolated to the 16 mm of RPV wall thickness, with TRACE (PSI) TH input data

3.3.1.6 LTO6 – Reduction of HPSI flow (operator action) at 1800s

In the TH calculations the reduction of HPSI flow by operator was simulated by switching off 1 of 2 HPIS pumps 1800 s after the initiation of the break. The calculations showed that the reduction of HPI injection results in a higher temperature of the water in the DC starting at 1800 s. Additionally, the lower break flow, the lower water level in the DC and the higher void fraction is observed after this operator action. Therefore, in the TH calculations it was concluded that this LTO improvement could potentially be beneficial from a PTS perspective.

The obtained hoop stress and temperature and the comparison with base case result to see the impact of LTO improvement are shown in Figure 3.30 (TH input from RELAP) and in Figure 3.31 (TH input from KWU-MIX).

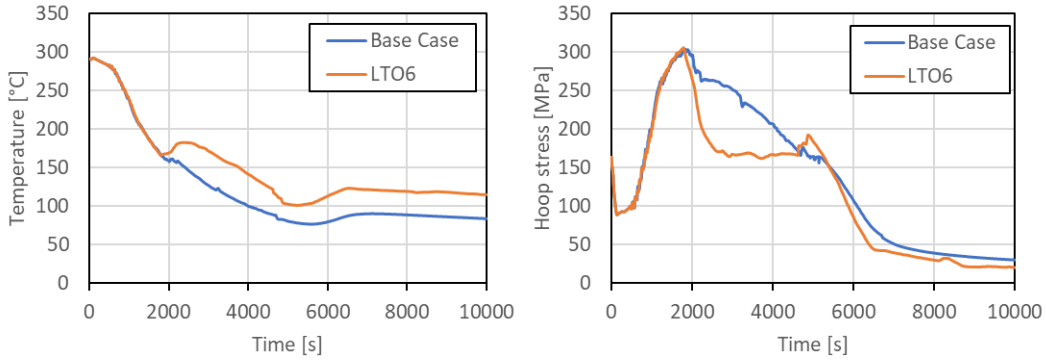

Figure 3.30: LTO6 results of UJV at 16 mm of RPV wall thickness, with RELAP (WUT) TH input data

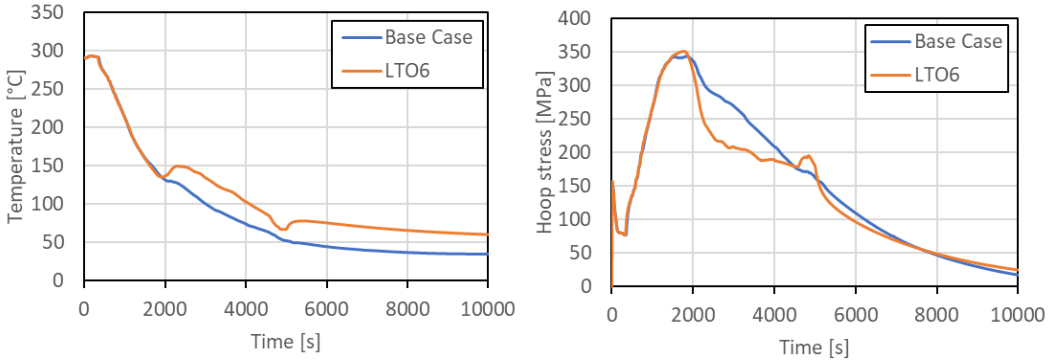

Figure 3.31: LTO6 results of BZN at 16 mm of RPV wall thickness, with KWU-MIX (FRA-G) TH input data in the middle of the plume

3.3.1.7 LTO7 – Decreasing of ACC pressure (20 bar)

In the TH calculations the LTO improvement of decreasing of ACC pressure was modelled by decreasing the initial pressure opening setpoint in the ACCs from the nominal value of 2.6 MPa to 2 MPa. In case of the RELAP calculations the results showed that the decrease of the ACC pressure slightly increases the water temperature in the DC, however they concluded that the studied LTO improvement provides no significant benefit from a PTS perspective.

The obtained hoop stress and temperature and the comparison with base case result to see the impact of LTO improvement are shown in Figure 3.32 (TH input from RELAP) and in Figure 3.33 (TH input from TRACE).

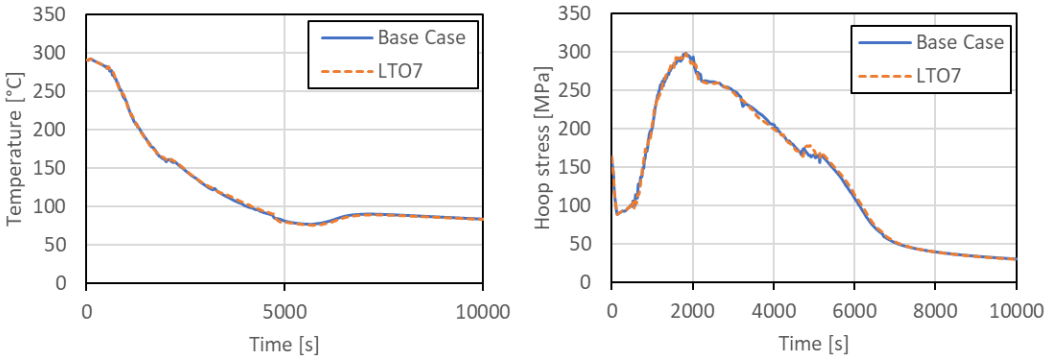

Figure 3.32: LTO7 results of WUT interpolated to the 16 mm of RPV wall thickness, with RELAP (WUT) TH input data

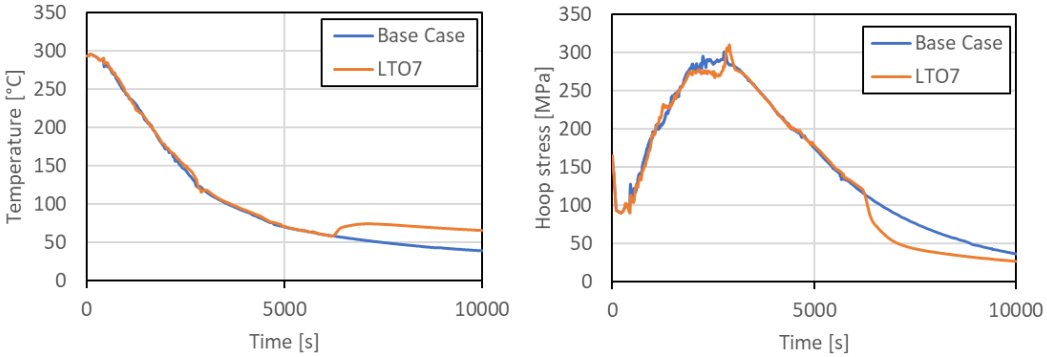

Figure 3.33: LTO7 results of TEC interpolated to the 16 mm of RPV wall thickness, with TRACE (PSI) TH input data

3.3.1.8 LTO8 – Change of cooldown rate (operator action) to 200K/h

During the TH calculation the increase of the secondary side cooldown rate by operator was simulated by increasing the cooldown of the secondary side from 100 K/h to 200 K/h. The proposed LTO improvement resulted in the increase of the water temperature in the DC after 2000 s. In the D2.1 report it was stated that the studied LTO improvement could potentially be beneficial from a perspective of higher water temperature in DC, but at the same time, it could be detrimental from a perspective of the faster pressure drop in DC. Therefore, it was determined that the overall benefit of this LTO improvement should be verified by the structural analysis.

The obtained hoop stress and temperature and the comparison with base case result to see the impact of LTO improvement are shown in Figure 3.34 (TH input from RELAP) and in Figure 3.35 (TH input from KWU-MIX).

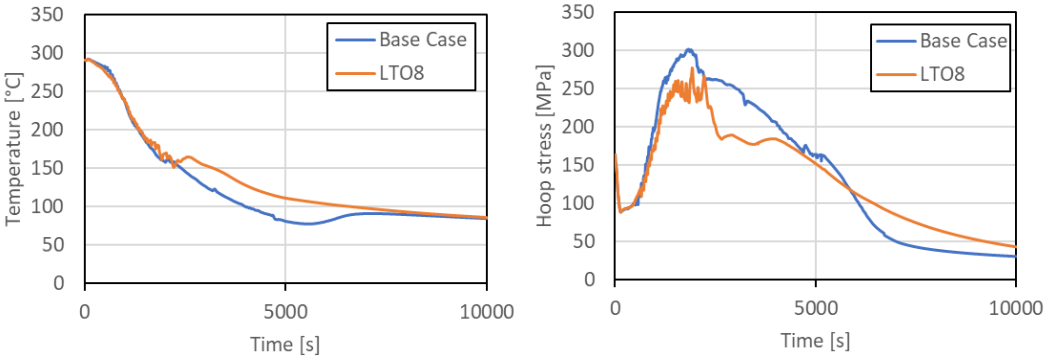

Figure 3.34: LTO8 results of JSI interpolated to the 16 mm of RPV wall thickness, with RELAP (WUT) TH input data

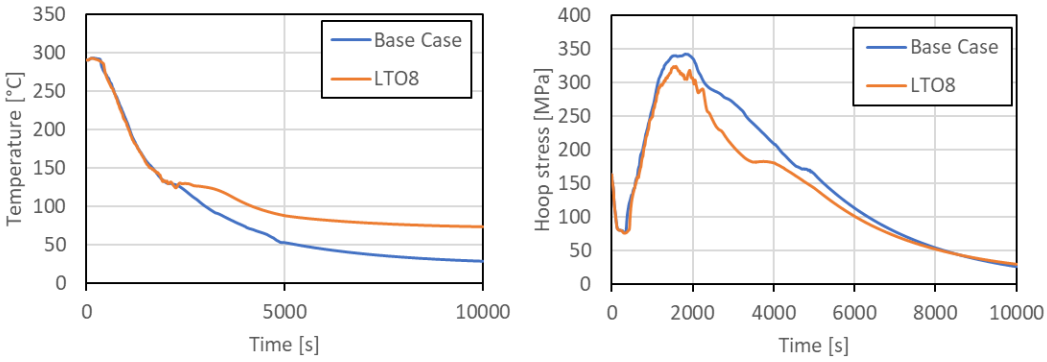

Figure 3.35: LTO8 results of IPP at 16 mm of RPV wall thickness, with KWU-MIX (FRA-G) TH input data

3.3.1.9 LTO9 – Isolation of ACCs (operator action) at 500s

In case of LTO9 the results from the system analysis performed with RELAP5, were repeated with the addition of a time for ACC isolation at 500 s. Because the pressure for this break size does not decrease to 26 bar until after 500 s, the ACCs were isolated before they could inject. The result was a pressure transient. In case of the TH calculations, it was concluded that this action has no significant effect.

The obtained hoop stress and temperature and the comparison with base case result to see the impact of LTO improvement are shown in Figure 3.36 (TH input from RELAP).

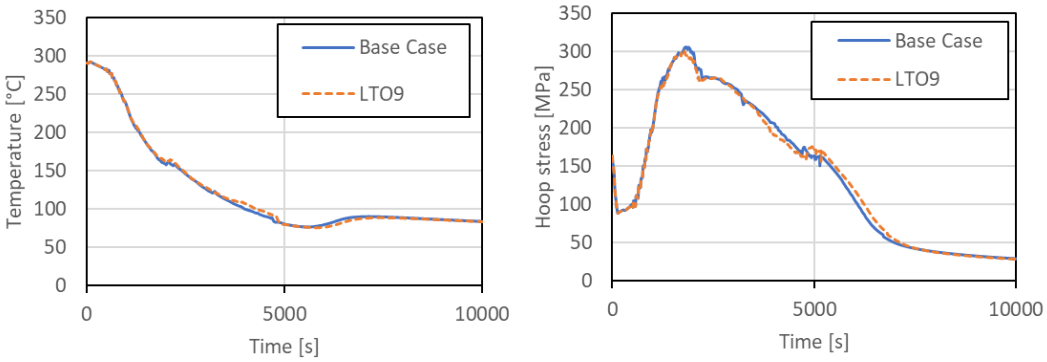

Figure 3.36: LTO9 results of IPP interpolated to the 16 mm of RPV wall thickness, with RELAP (WUT) TH input data

3.3.2 Results from 3D FE

Beside the 1D calculations, 3D simulations were also performed for the LTO cases. In the following chapters, results from 3D simulations are presented for the most important LTO cases (LTO1, LTO4, LTO5, LTO6 and LTO8) and for the other LTO cases can be found in [13]. In general, the results are similar and show the same trend than those from 1D simulations shown in Section 3.3.1 The stresses and temperature profiles given are for core weld elevation under the cold leg position.

3.3.2.1 LTO1 – Heating of water in the HPSI tanks (T = 45°C)

The results at core weld elevation under the cold leg position from 3D calculations are given in Figure 3.37 (TH input from KWU-MIX), in Figure 3.38 (TH input from RELAP) and in Figure 3.39 (TH input from TRACE).

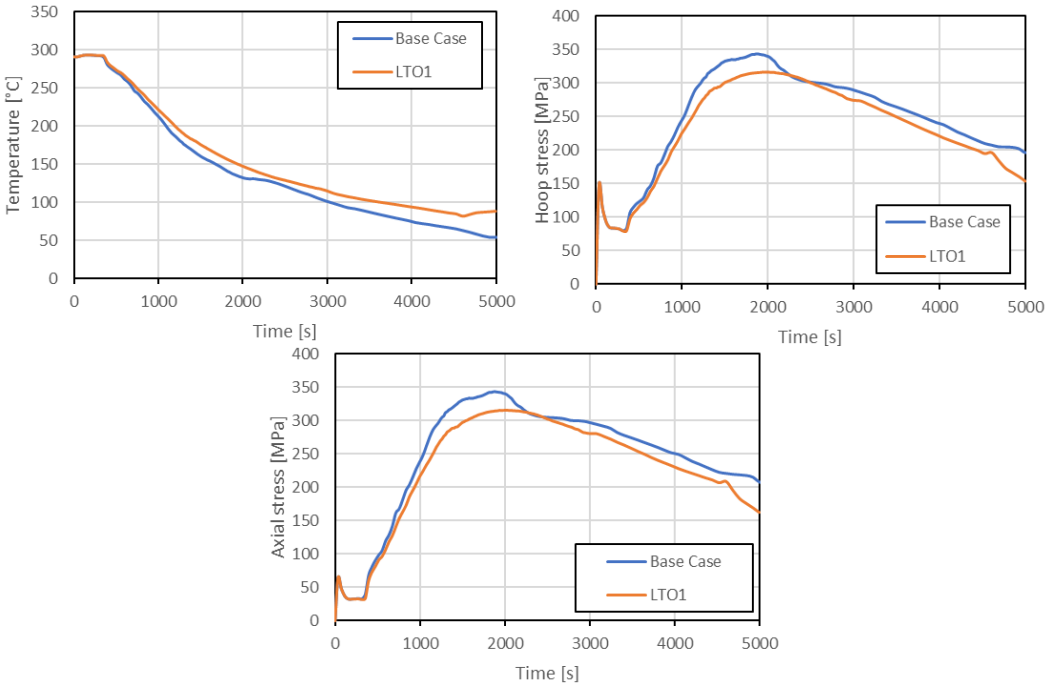

Figure 3.37: LTO1 results of FRA-G at 16 mm of RPV wall thickness, with KWU-MIX (FRA-G) TH input data

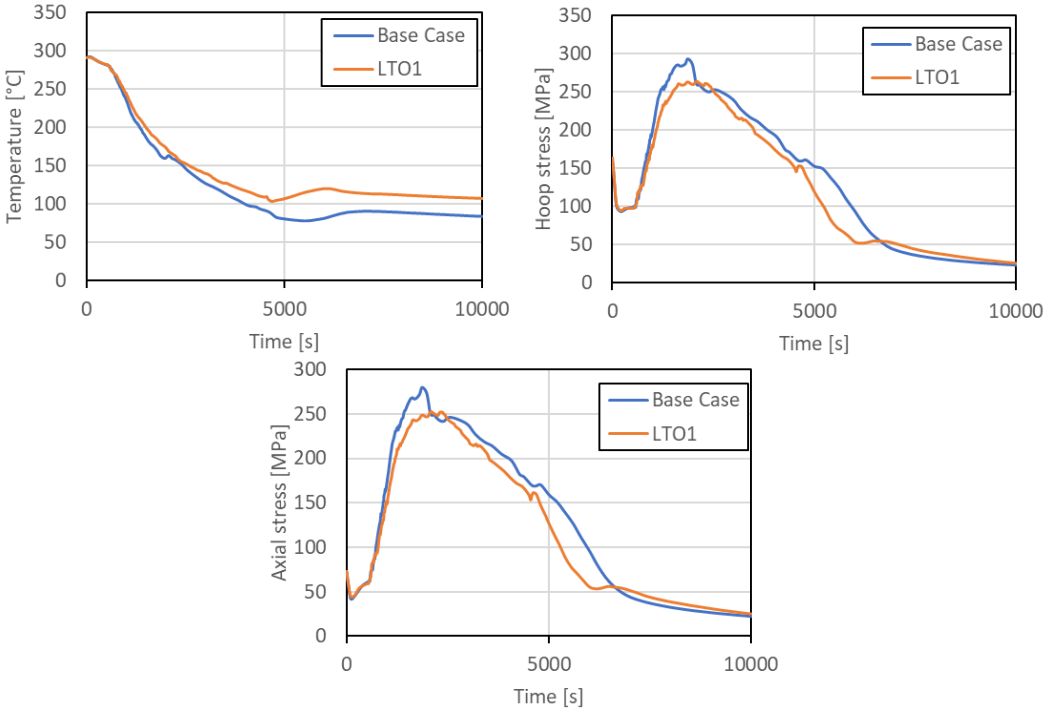

Figure 3.38: LTO1 of IPP at 16 mm of RPV wall thickness, with RELAP (WUT) TH input data.

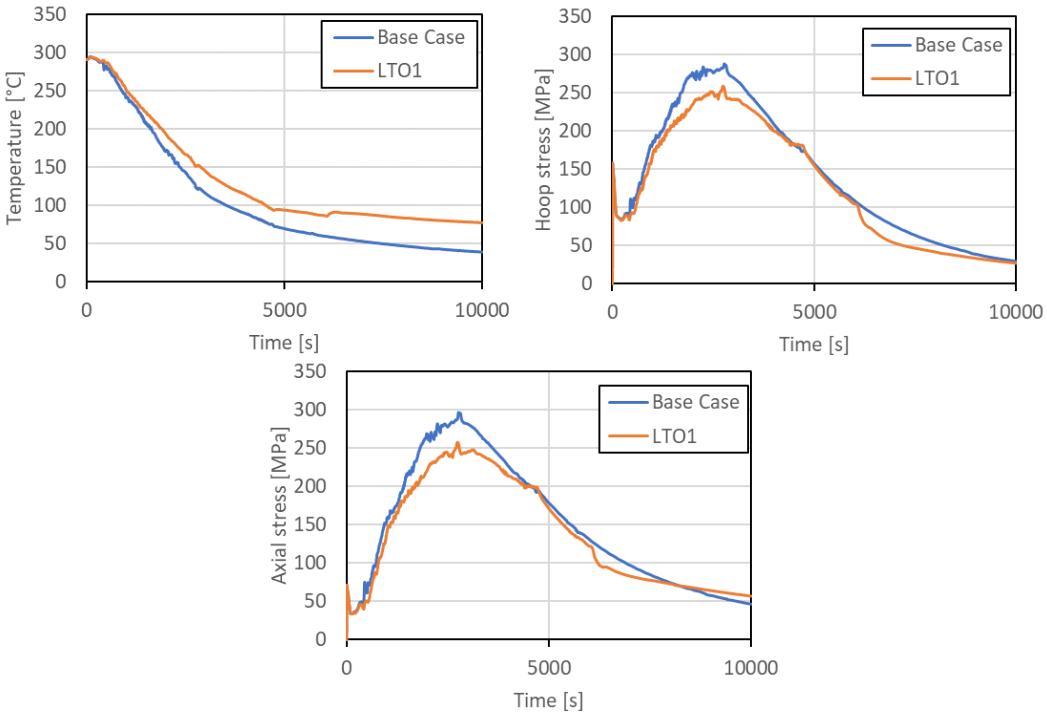

Figure 3.39: LTO1 results of PSI extrapolated to the 16 mm of RPV wall thickness, with TRACE (PSI) TH input data

3.3.2.2 LTO4 – Decreasing the HPSI head (75%)

The results at core weld elevation under the cold leg position from 3D calculations are given in Figure 3.40 (TH input from RELAP) and in Figure 3.41 (TH input from TRACE).

Interestingly in case of the simulations with RELAP input data the resulting temperature and stress fields similarly to the 1D results have some deviation from the base case, however no differences can be noted in case of the simulations done with TRACE input data.

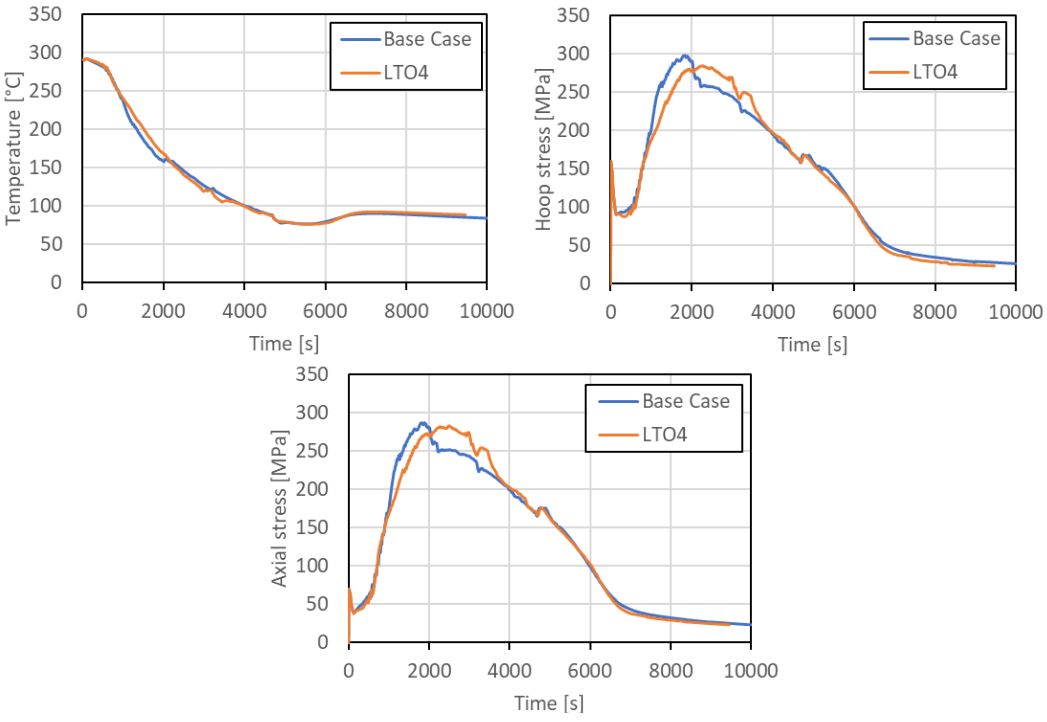

Figure 3.40: LTO4 results of BZN at 16 mm of RPV wall thickness, with RELAP (SSTC) TH input data.

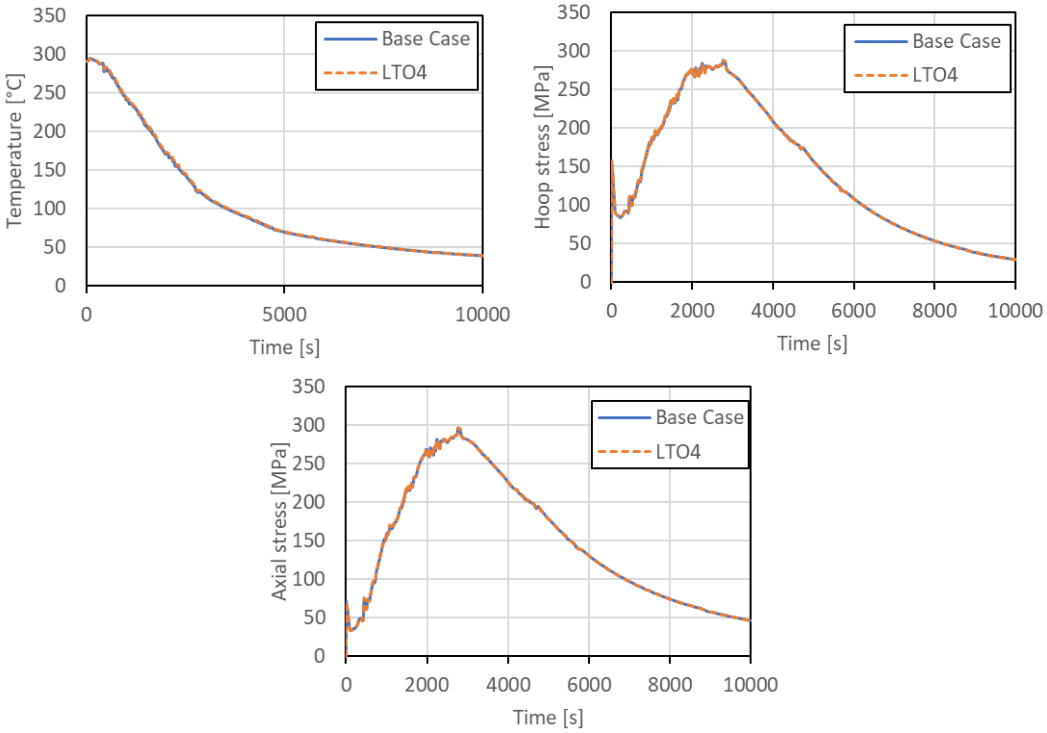

Figure 3.41: LTO4 results of PSI extrapolated to the 16 mm of RPV wall thickness, with TRACE (PSI) TH input data.

3.3.2.3 LTO5 – Decreasing the HPSI capacity (75%)

The results at core weld elevation under the cold leg position from 3D calculations are given in Figure 3.42 (TH input from RELAP).

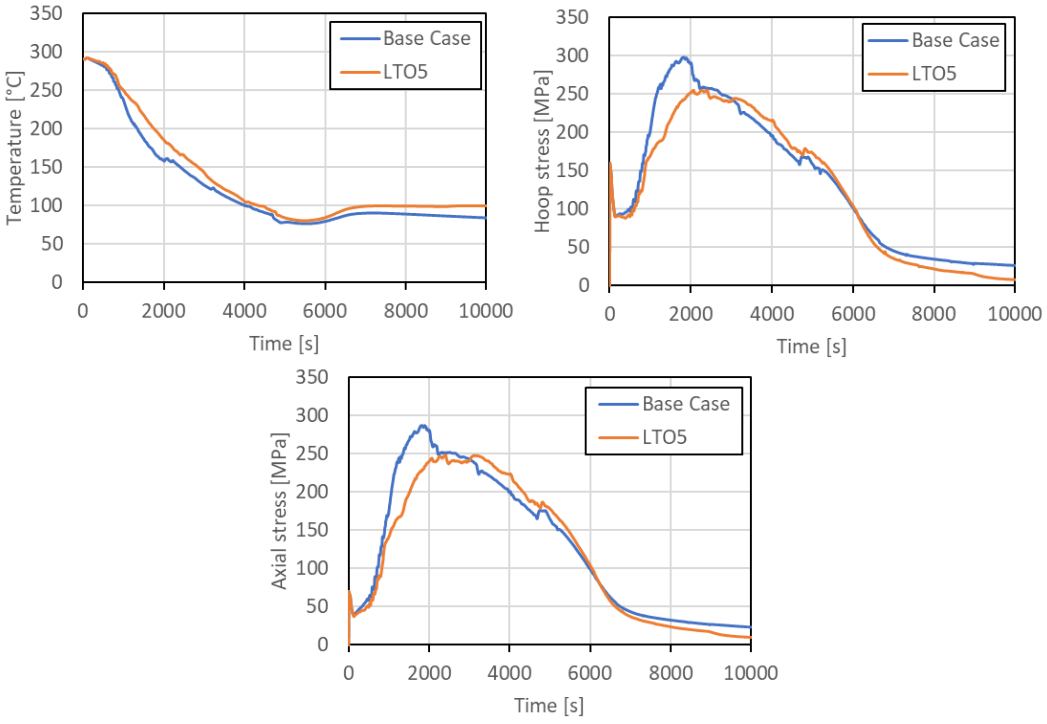

Figure 3.42: LTO5 results of BZN at 16 mm of RPV wall thickness, with RELAP (SSTC) TH input data.

3.3.2.4 LTO6 – Reduction of HPSI flow (operator action) at 1800s

The results at core weld elevation under the cold leg position from 3D calculations are given in Figure 3.43 (TH input from RELAP) and in Figure 3.44 (TH input from KWU-MIX).

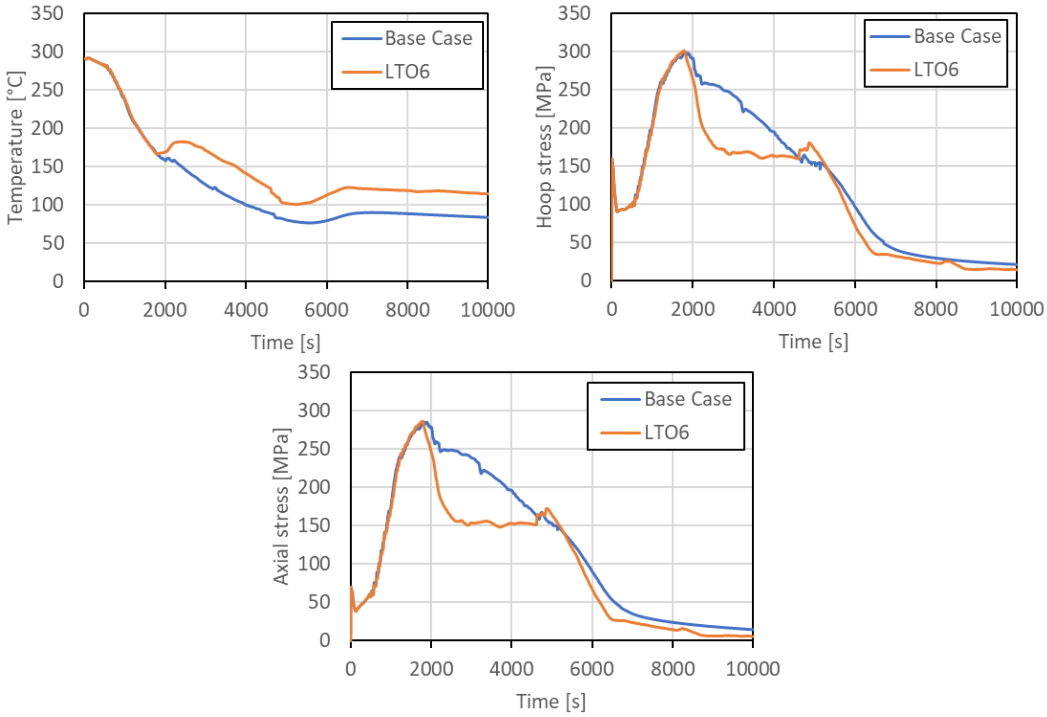

Figure 3.43: LTO6 results of BZN at 16 mm of RPV wall thickness, with RELAP (WUT) TH input data.

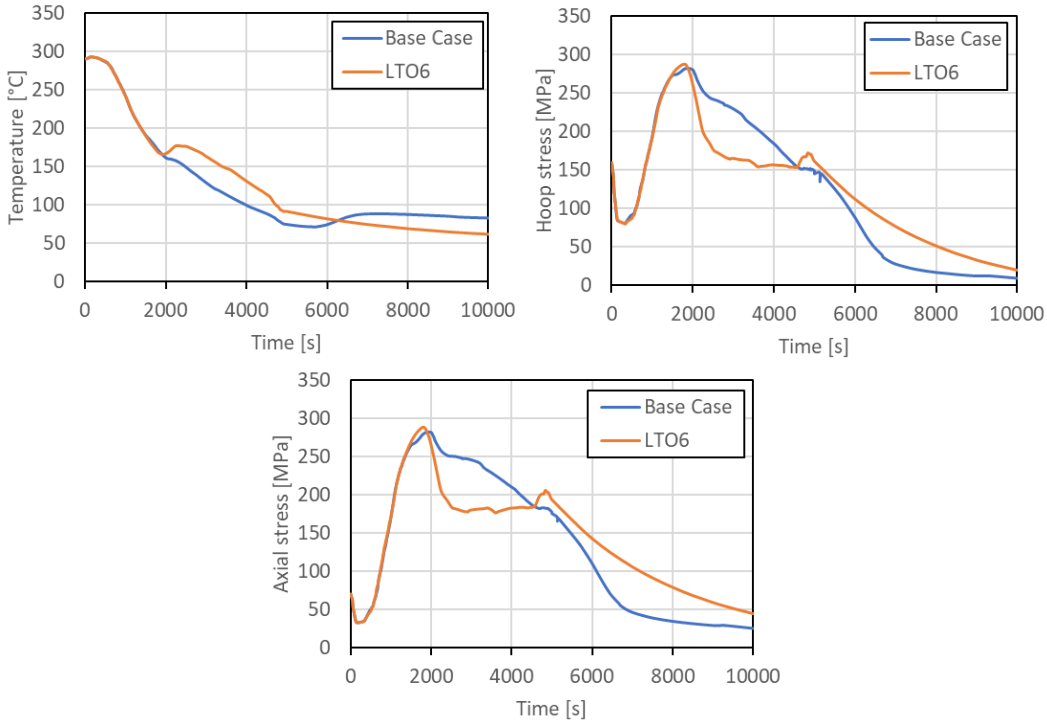

Figure 3.44: LTO6 results of SSTC interpolated to the 16 mm of RPV wall thickness, with KWU-MIX (FRA-G) TH input data.

3.3.2.5 LTO8 – Change of cooldown rate (operator action) to 200K/h

The results at core weld elevation under the cold leg position from 3D calculations are given in Figure 3.45 (TH input from RELAP) and in Figure 3.46 (TH input from KWU-MIX).

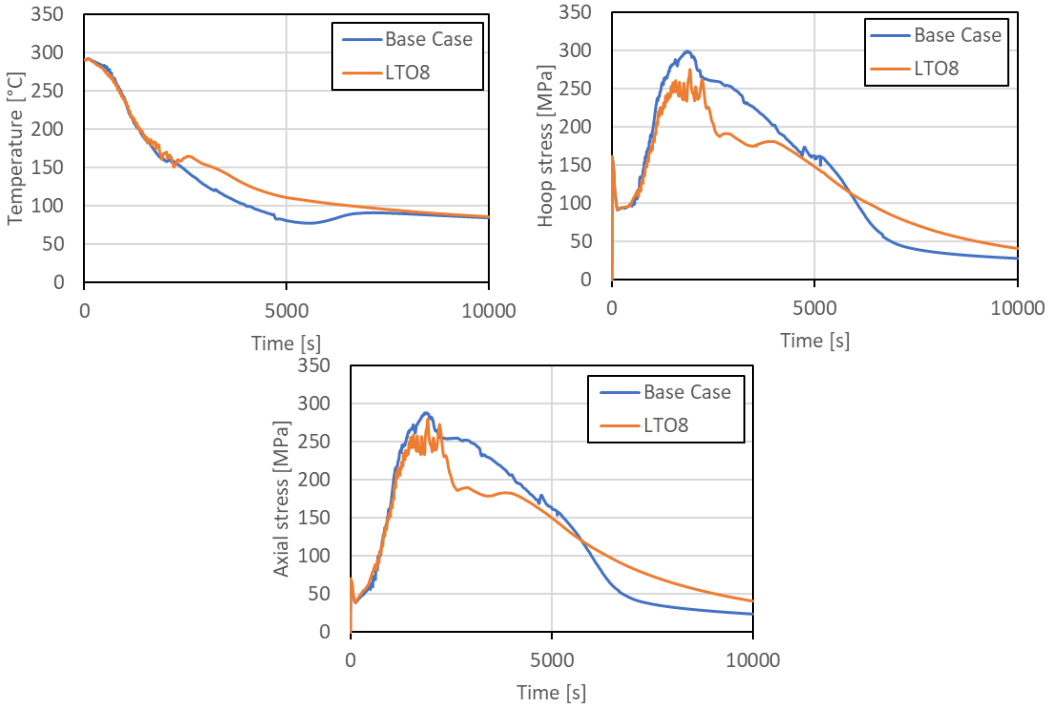

Figure 3.45: LTO8 results of JSI interpolated to the 16 mm of RPV wall thickness, with RELAP (WUT) TH input data

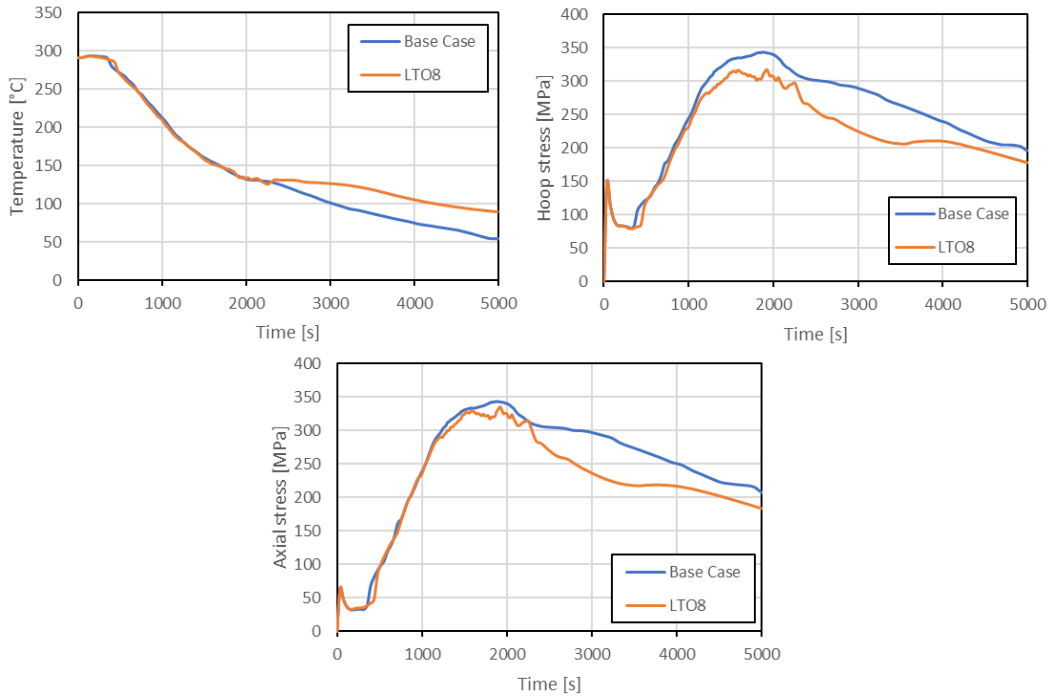

Figure 3.46: LTO8 results of FRA-G at 16 mm of RPV wall thickness, with KWU-MIX (FRA-G) TH input data

3.4 Structural analyses for TH uncertainties (Wilks analyses)

This Section describes the structural analyses of TH uncertainties. The position below the injection nozzle CL3 at the beltline weld at the elevation of -2.638 m was selected as the prioritized location for analyses, see Figure 3.1.

3.4.1 Uncertainties in TH data analyses for Wilks

Evaluation of TH uncertainties and their distributions have been performed in WP2 [8] covering the model and computer-code uncertainties, plant uncertainties related to initial conditions, boundary conditions and parameters of the NPP systems, and uncertainties connected with human interactions. The TH uncertainties have been treated using statistical methods based on the Wilks approach allowing to define a statistical set of TH data with given confidence level and tolerance limits.

Thus, it was shown that using the Wilks method 59 simulations is required to achieve a one-sided tolerance interval with the tolerance limit of $P{=}0.95$, and the confidence level of $1{-}\alpha{=}0.95$. For achieving a double-sided tolerance interval for the same tolerance limit ($P = 0.95$) and the confidence levels of 0.95 or 0.99, Wilks simulations of 93 and 130 samples are required, respectively.

Several system TH codes (RELAP, ATHLET, TRACE) and one mixing TH calculation code (KWU-MIX) were used for TH analyses for best-estimate TH input parameters supplemented with statistically defined TH input data sets with propagated uncertainties according to the Wilks method. A summary of performed Wilks TH analyses by the APAL partners is presented in Table 3.8. The grey cells in the presented summary indicate which Wilks data sets have been used as the TH input data for structural analyses by different partners.

Table 3.8 Summary of TH data sets used for Wilks analyses (per partner).

TH code and partner	ATHLET from GRS	KWU-MIX from FRA-G	RELAP from JSI		RELAP from KIWA	RELAP from SSTC	RELAP from UJV		TRACE from PSI		RELAP from WUT
Wilks sets	59	93*	59	130	59	59	59	93	59	130	93
UJV							x	x			
FRA-G		x									
PSI									x	x	
JSI			x	x							
KIWA					x**						
IPP						x					
WUT											x
GRS	x										
BZN								x			
Tecnatom									x		

* First 59 Sets are treated as 59 Wilks sets.
** KIWA used Base Case from JSI TH data.

3.4.2 Typical Wilks TH input data for structural analyses

In general, all TH results from the Wilks analyses have a similar appearance but certain quantitative differences in the calculated results were observed. It can be explained by a variety of used TH codes, their functionality, differences in nodalisation of TH models and taken assumptions.

It is not feasible to represent all TH results that have been used as the input data for structural analyses. Therefore, typical TH data from the Wilks analyses based on US NRC system TH code TRACE is presented as an example in this Section.

The TH results presented in this report demonstrate the following TH cases:

- Base Case: The conservative reference case based on the adjusted ICAS T2 transient in Task 2.1 in the APAL Deliverable D2.1 [10] and also summarised in WP2 Public Summary [8].

Additionally, the conservative case (CC) was analysed by some partners, where all statistically distributed TH input parameters were taken with their conservative values (described in mor detail in WP3 Public Summary[7]).

- Best Estimate: The best estimate case based on the best-estimate input data for the TH analyses in Task 2.3 as reported in the APAL Deliverable D2.3 [12] and also summarised in WP2 Public Summary [8].
- Wilks: The TH data set based on the best-estimate case with random sampling of distributed selected plant parameters and boundary conditions. The random parameters and sampling methodology are described in D2.3 [12] and [8].

Examples of fluid temperature, RPV pressure and heat transfer coefficient (HTC) time histories are shown for the Wilks sets with 59 and 130 samples in Figure 3.47-Figure 3.49 using the PSI data obtained from the TH code TRACE. The grey curves in all plots represent individual results for each Wilks set.

It can be noticed from the presented TH results that the temperature and HTC time histories demonstrate a large scatter while the RPV pressure variation remains in a rather confined scatter band.

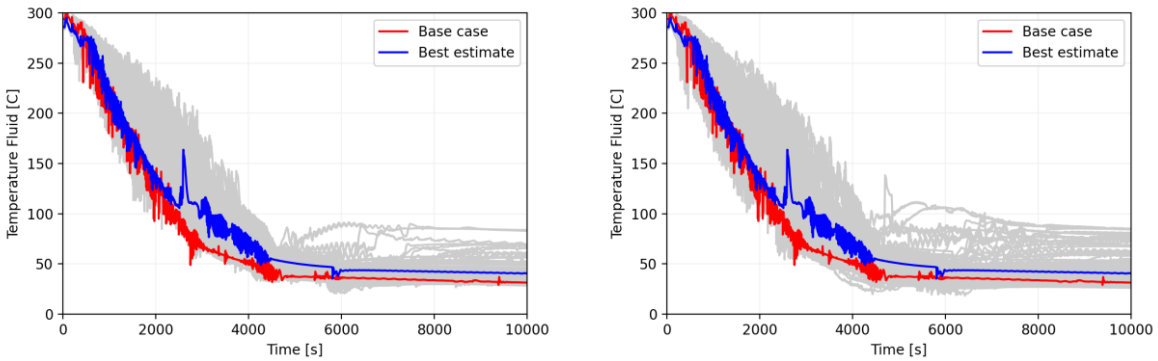

Figure 3.47: Fluid temperature as a function of time for (a) Wilks-59 and (b) Wilks 130 data sets. PSI results based on the TH code TRACE.

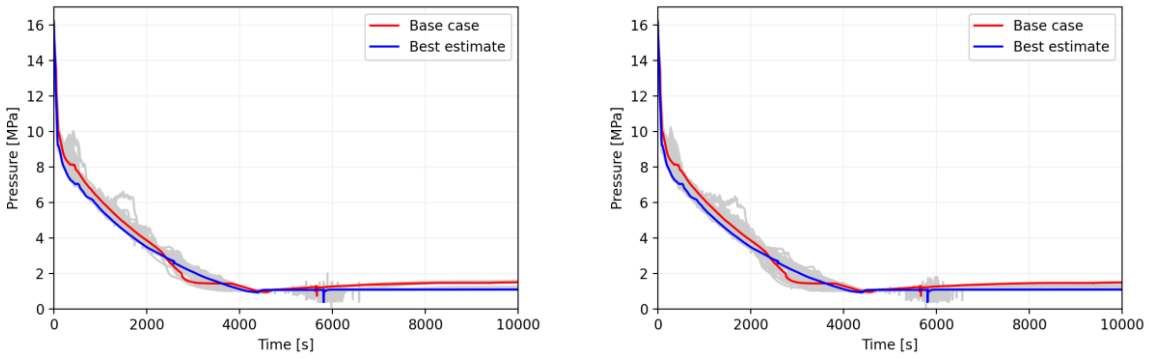

Figure 3.48: Pressure in RPV as a function of time for (a) Wilks-59 and (b) Wilks 130 data sets. PSI results based on the TH code TRACE.

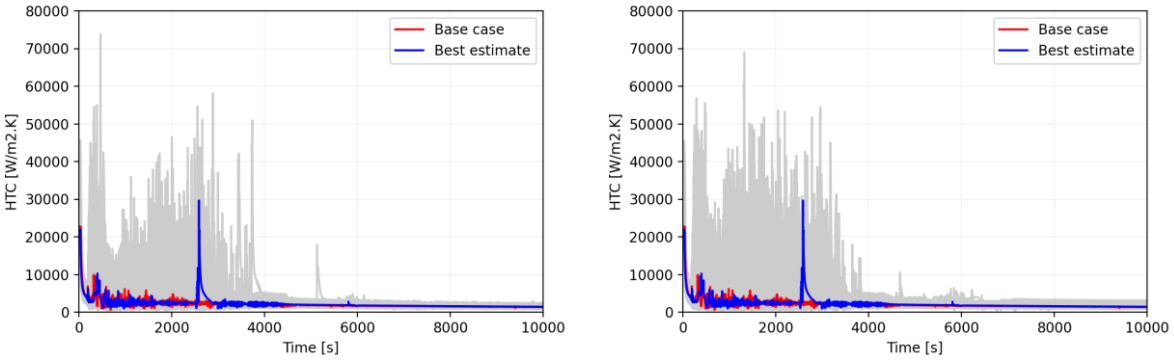

Figure 3.49: Heat transfer coefficient (HTC) as a function of time for (a) Wilks-59 and (b) Wilks 130 data sets. PSI results based on the TH code TRACE.

3.4.3 Results for stress and temperature distributions through the RPV wall thickness

This Section presents the structural analysis results in terms of transient stress and temperature distributions through the RPV wall. The analyses have been performed by partners using the TH input data as given in Table 3.8. The calculated stress and temperature distributions through the RPV wall as a function of time are later used as the input data for fracture mechanics analyses within the deterministic and probabilistic benchmarks.

Again, it is not feasible to present all obtained results due to large amount of data. Only typical results are shown in the following subsections based on the analyses for two Wilks data sets with 59 and 130 samples. A discussion of main trends and deviations in the results from different partners is also provided in this report.

For facilitating a comparison of the results between different partners, the following result plots were requested from each partner;

- Inner RPV wet surface temperatures as a function of time,
- Hoop and axial stresses at the RPV inner surface as a function of time,
- Temperature, hoop and axial stresses at the crack tip as a function of time,
- Hoop and axial stresses at the crack tip as a function RPV wall temperature at the crack tip.

In the analyses the crack tip located at the distance of 16 mm from the inner (wet) surface of the RPV was assumed. The obtained stress distributions include weld residual stresses.

3.4.3.1 Results for Wilks set with 59 samples

Typical plots from the structural analyses of 59 Wilks samples are summarised below using the PSI results obtained by FAVOR. The RPV wall temperature, hoop and axial stresses at the inner (wet) surface of RPV as a function of time are presented in Figure 3.50 - Figure 3.52. The temperature at the crack tip location (crack depth of 16 mm is assumed), hoop and axial stresses at the crack tip location as a function of time are presented in Figure 3.53 - Figure 3.55. The hoop and axial stresses at the crack tip as a function of crack tip temperature are shown Figure 3.56 and Figure 3.57.

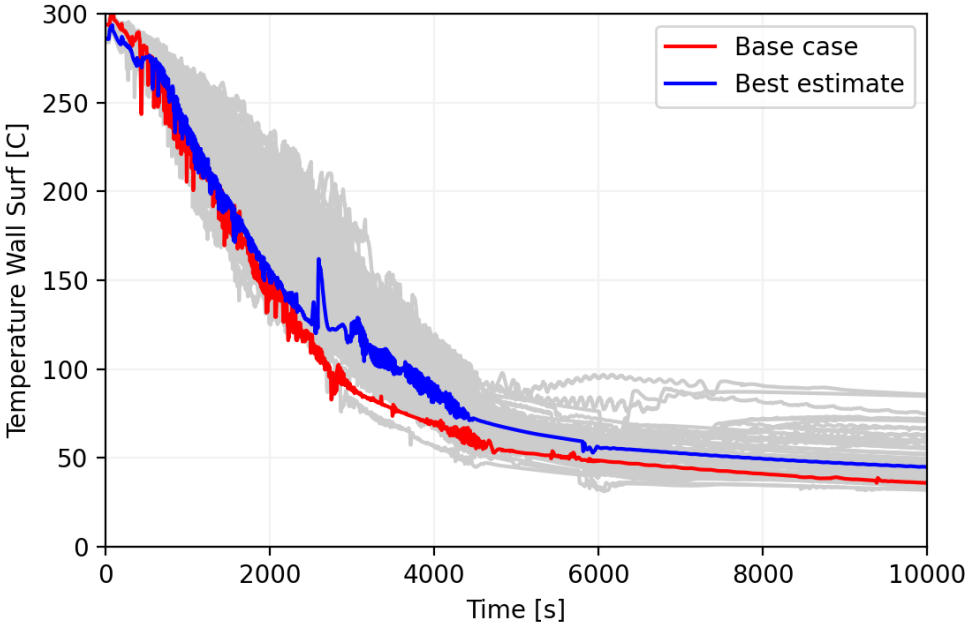

Figure 3.50: Inner surface temperature as a function of time for Wilks-59.

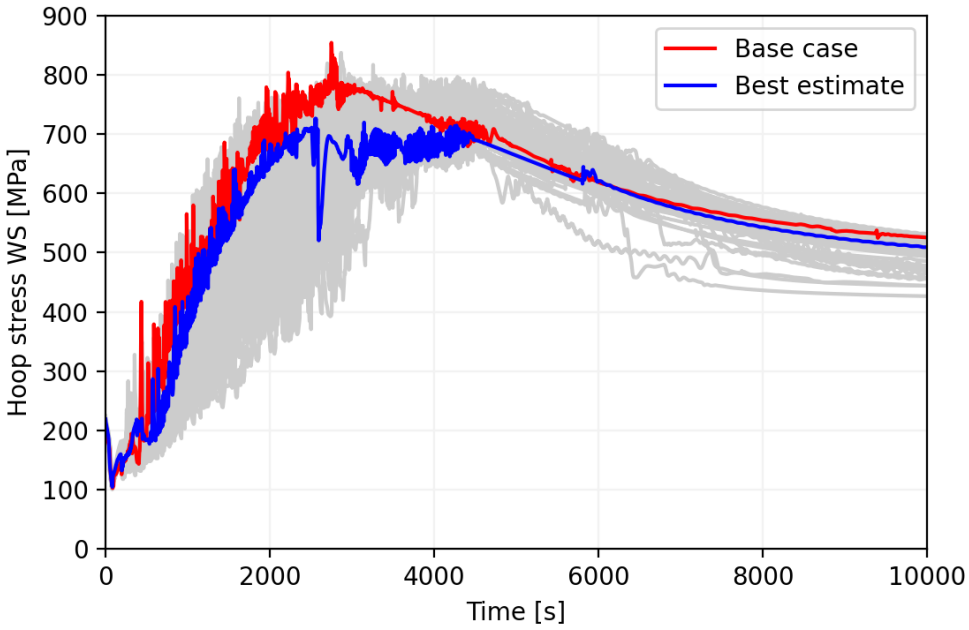

Figure 3.51: Hoop stresses at inner surface as a function of time for Wilks-59 with WRS.

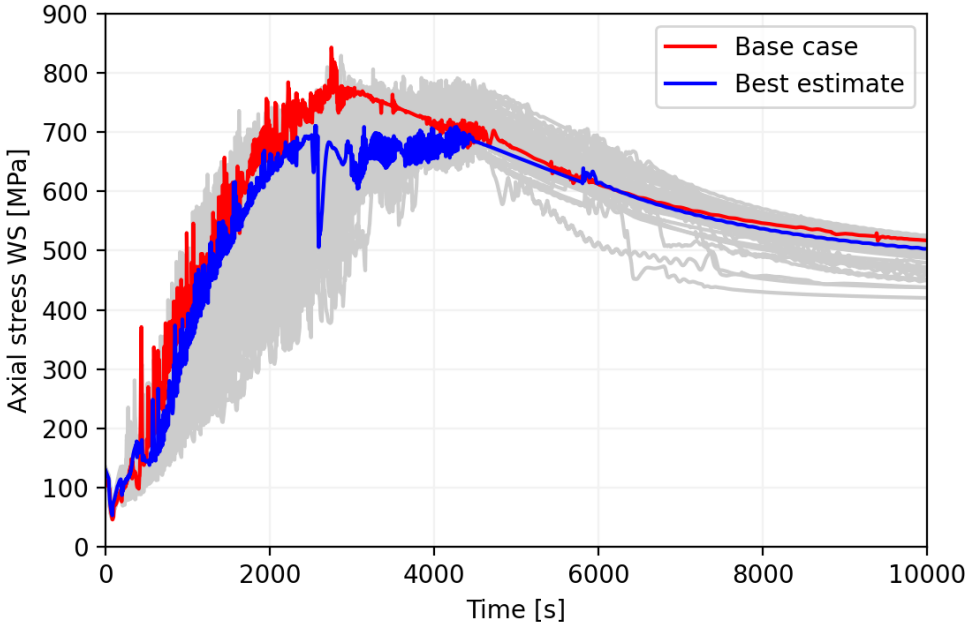

Figure 3.52: Axial stresses at inner surface as a function of time for Wilks-59 with WRS.

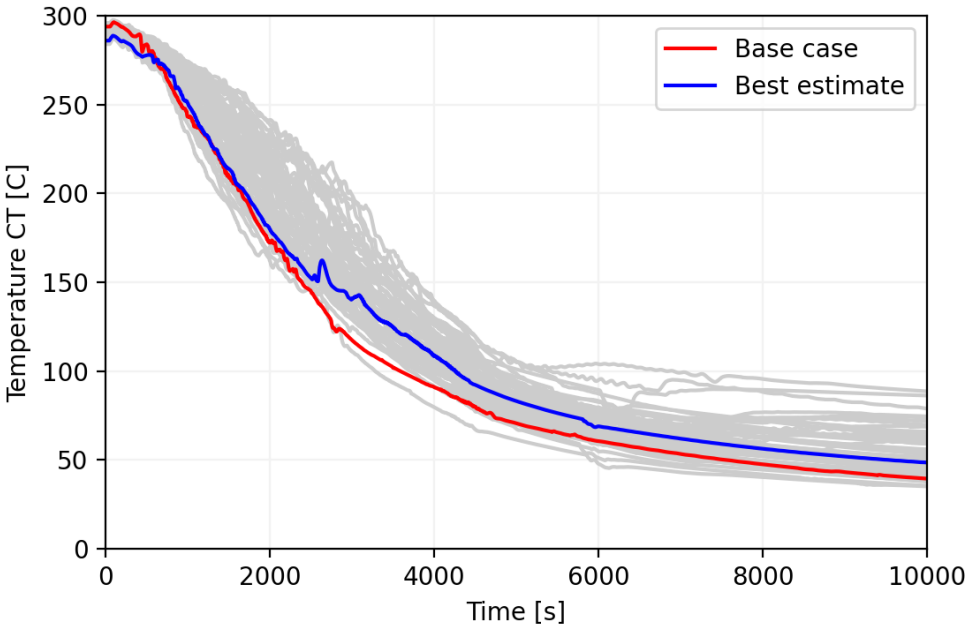

Figure 3.53: Temperature at the crack tip location as a function of time for Wilks-59.

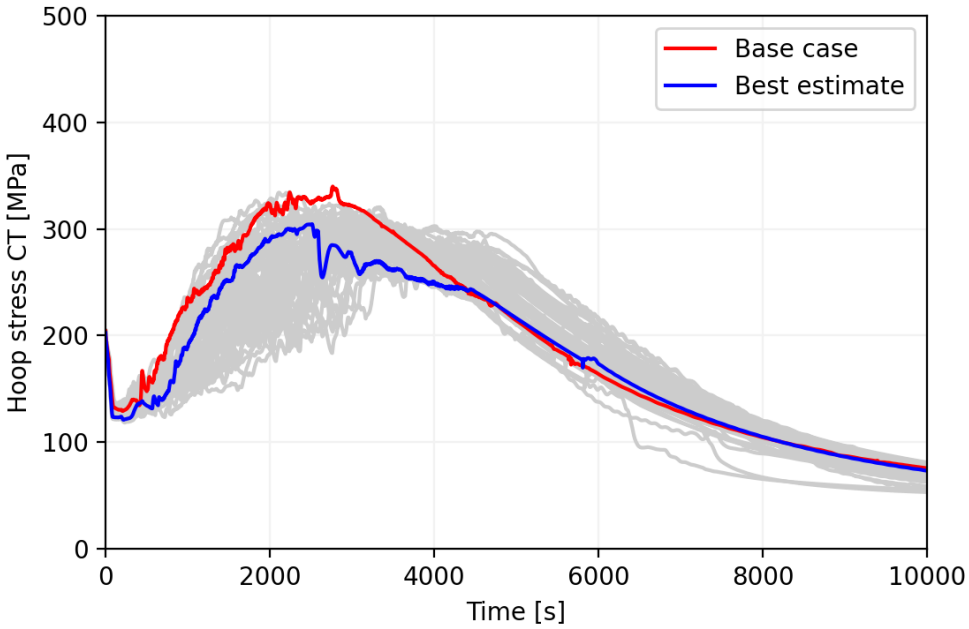

Figure 3.54: Hoop stresses at the crack tip location as a function of time for Wilks-59 with WRS.

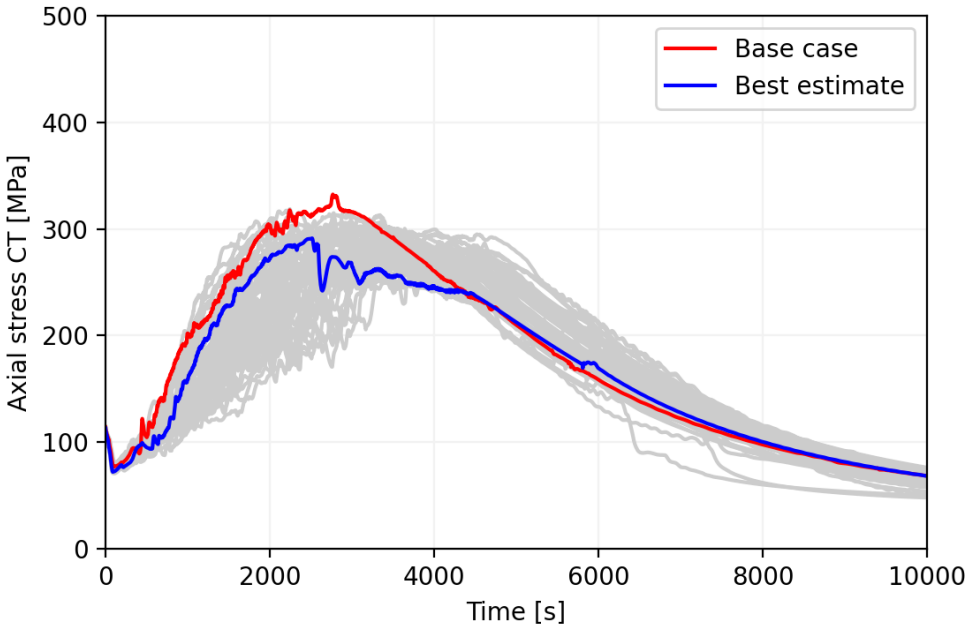

Figure 3.55: Axial stresses at the crack tip location as a function of time for Wilks-59 with WRS.

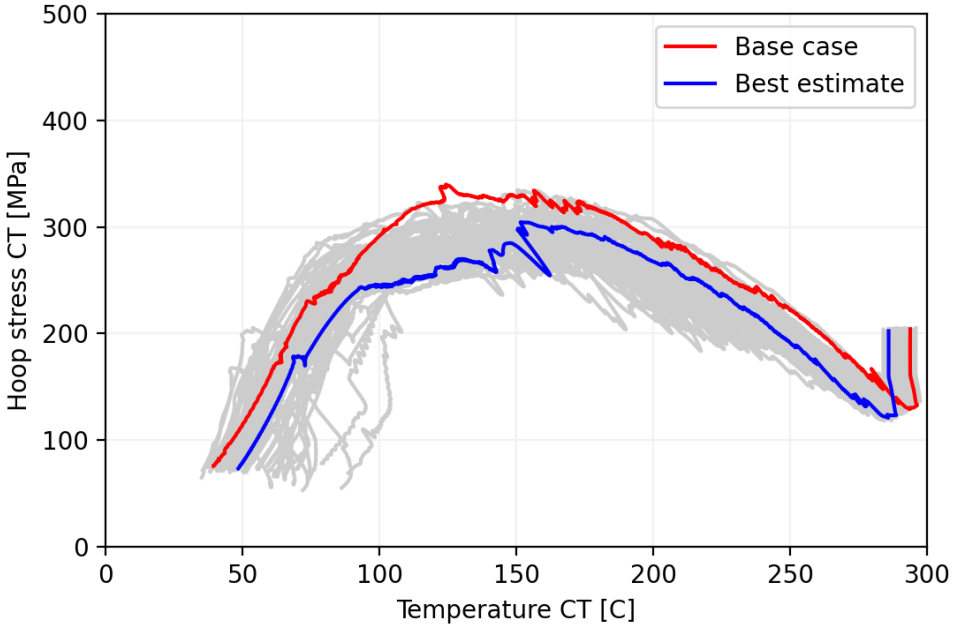

Figure 3.56: Hoop stresses at the crack tip as a function of crack tip temperature for Wilks-59 with WRS.

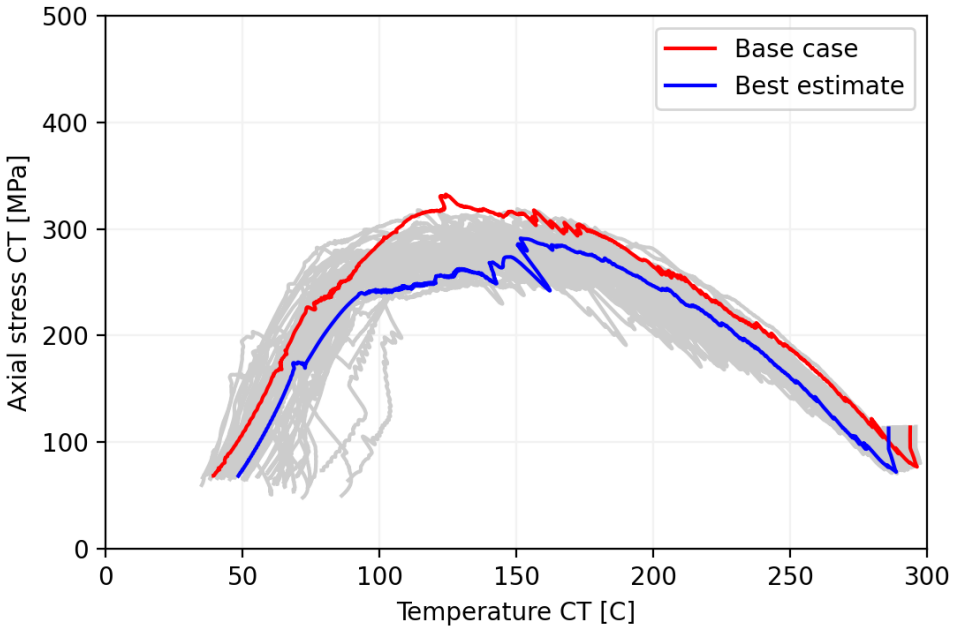

Figure 3.57: Axial stresses at the crack tip as a function of crack tip temperature for Wilks-59 with WRS.

3.4.3.2 Results for Wilks set with 130 samples

Typical plots from the structural analyses of 130 Wilks samples are summarised below using the PSI results obtained by FAVOR. The RPV wall temperature, hoop and axial stresses at the inner (wet) surface of RPV as a function of time are presented in Figure 3.58 - Figure 3.60. The temperature at the crack tip location (crack depth of 16 mm is assumed), hoop and axial stresses at the crack tip location as a function of time are presented in Figure 3.61 - Figure 3.63. The hoop and axial stresses at the crack tip as a function of crack tip temperature are shown Figure 3.64 and Figure 3.65.

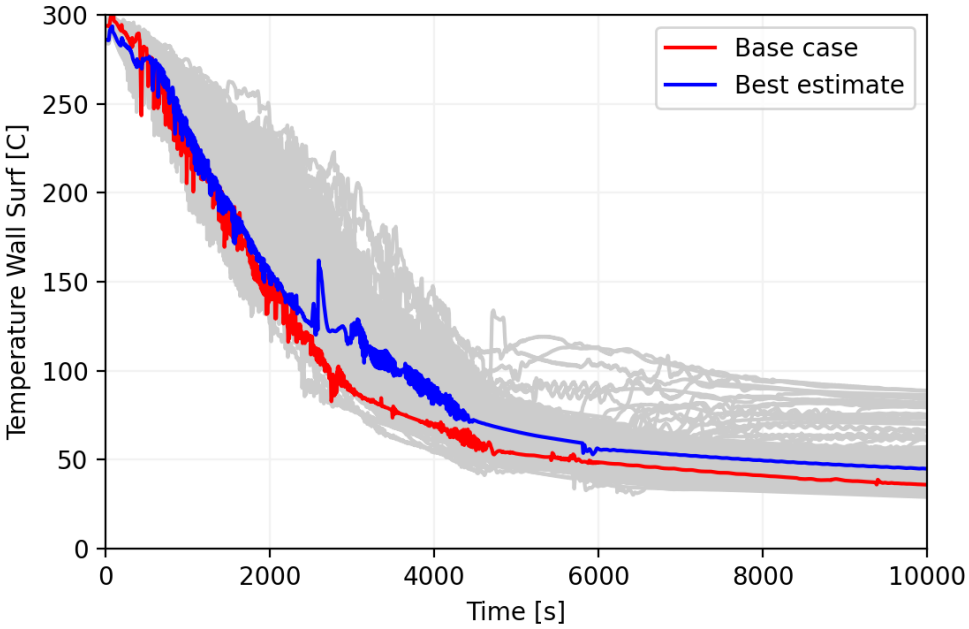

Figure 3.58: Inner surface temperature as a function of time for Wilks-130.

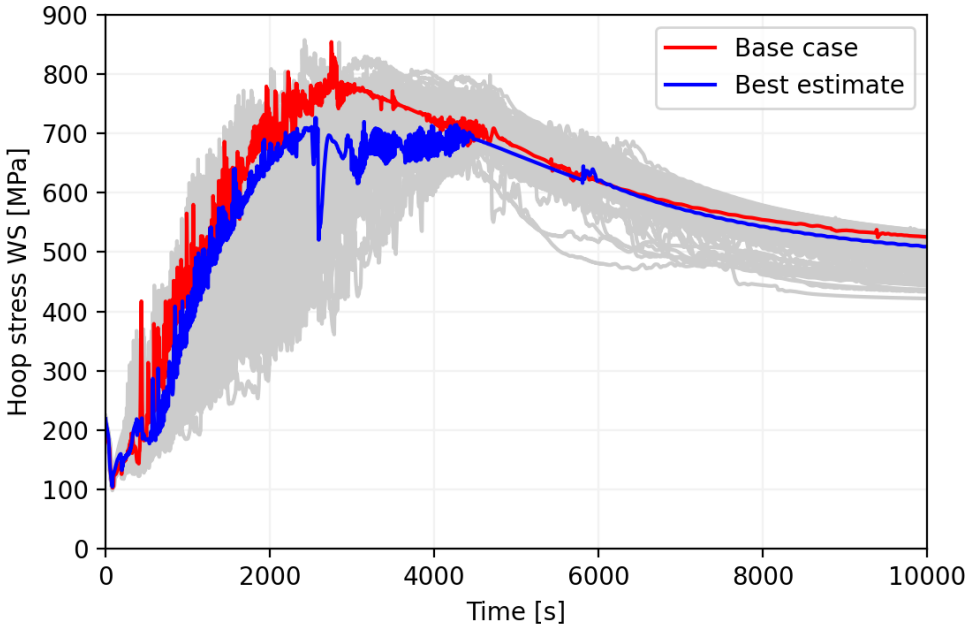

Figure 3.59: Hoop stresses at inner surface as a function of time for Wilks-130 with WRS.

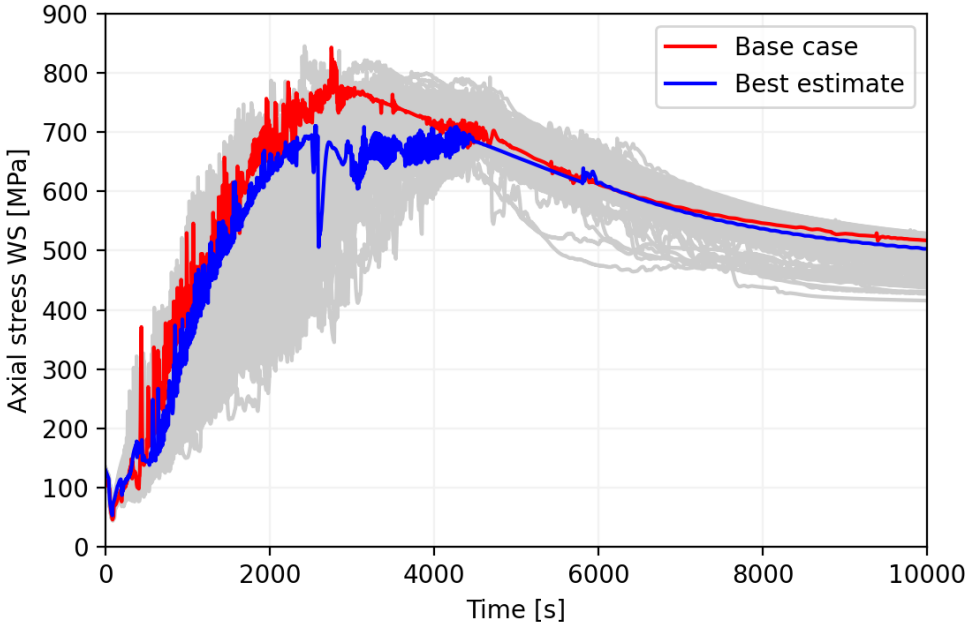

Figure 3.60: Axial stresses at inner surface as a function of time for Wilks-130 with WRS.

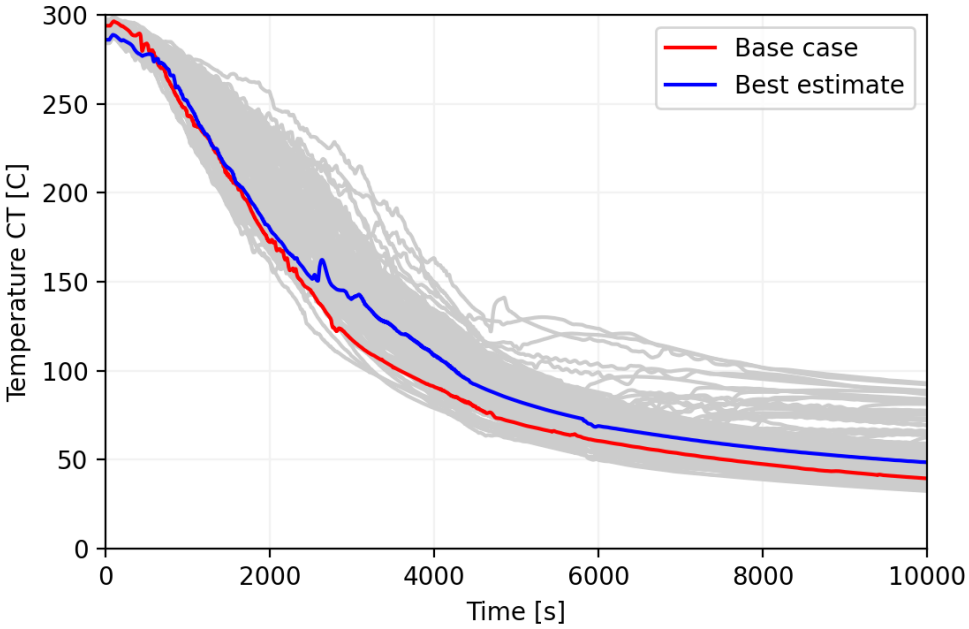

Figure 3.61: Temperature at the crack tip location as a function of time for Wilks-130.

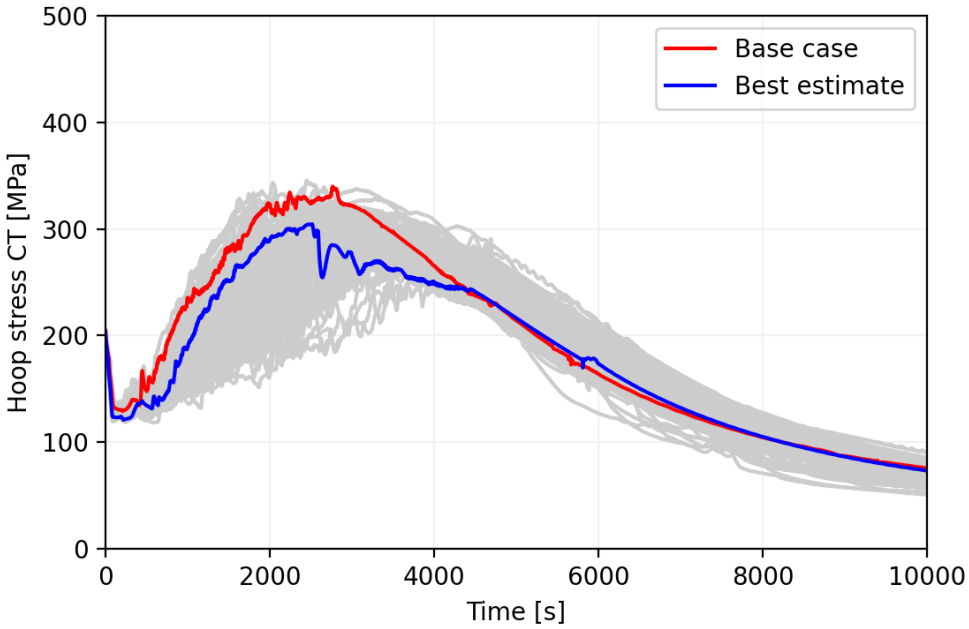

Figure 3.62: Hoop stresses at the crack tip location as a function of time for Wilks-130 with WRS.

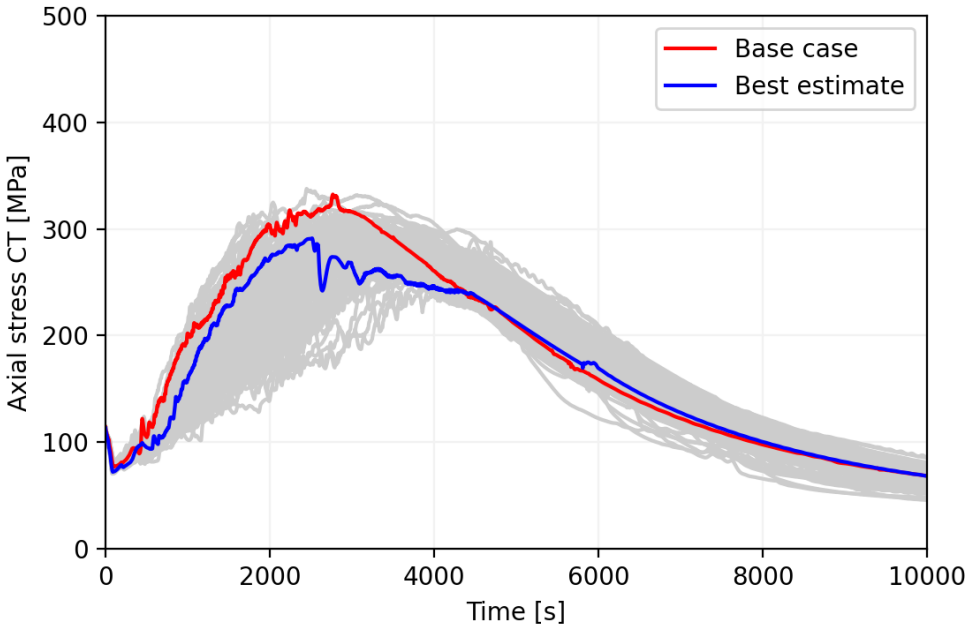

Figure 3.63: Axial stresses at the crack tip location as a function of time for Wilks-130 with WRS.

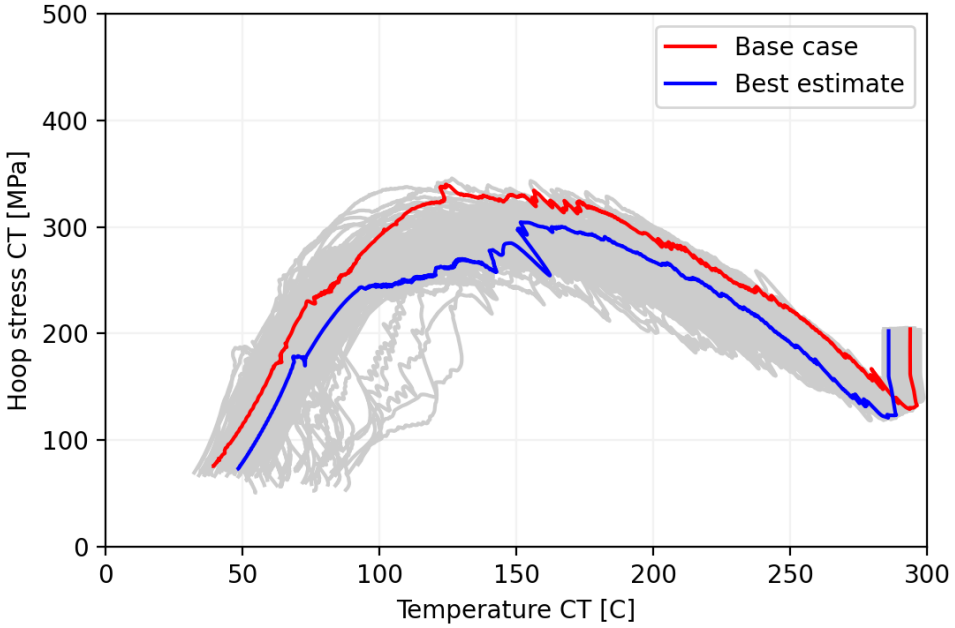

Figure 3.64: Hoop stresses at the crack tip as a function of crack tip temperature for Wilks-130 with WRS.

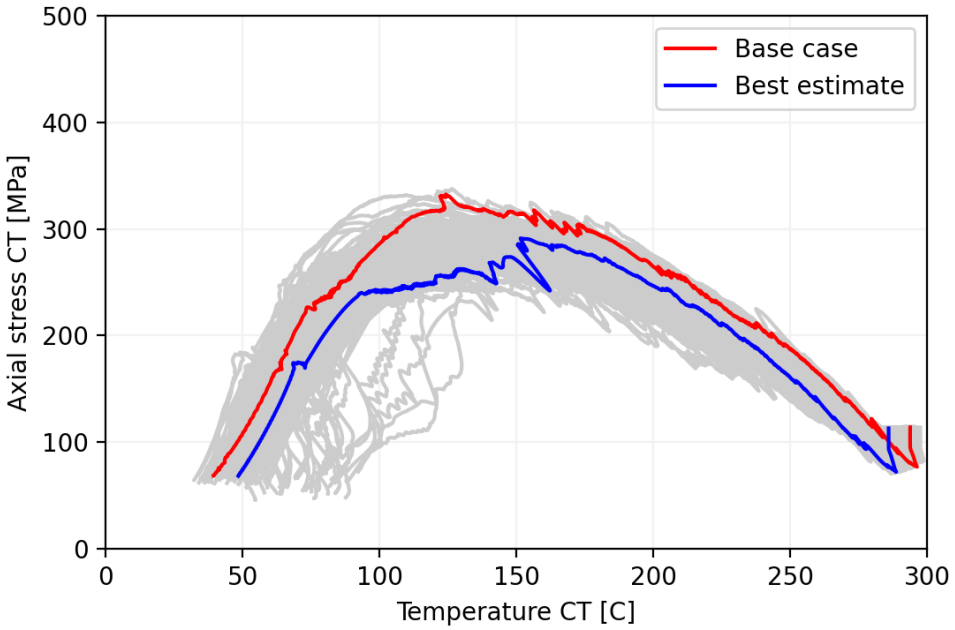

Figure 3.65: Axial stresses at the crack tip as a function of crack tip temperature for Wilks-130 with WRS.

3.4.4 Discussion of structural analysis results for TH uncertainty

3.4.4.1 TH input data

TH input data for structural analyses was obtained from TH uncertainty analyses based on the Wilks method as described in Section 3.4.1. For the TH analyses, different TH codes were used such as RELAP5, ATHLET, TRACE and KWU-MIX (for mixing calculations) together with several tools for uncertainty evaluation, e.g. DAKOTA, SUSA, etc. TH uncertainty analyses were performed for 59, 93 and 130 Wilks data sets.

The TH analysis results used as the TH input data for structural assessments are summarised for each partner in Table 3.8. A detailed review and comparison of the TH results from uncertainty analyses between different partners have been carried out in APAL Deliverable 2.3 [12]. However, it is worth to include a short summary of this comparison and point out some observed differences in the TH data as it has a direct bearing on some deviations in the calculated temperatures and stresses.

Figure 3.66 illustrates a comparison of fluid temperature as a function of time used by JSI, IPP and KIWA as the TH parameter used for the temperature and stress calculations. These partners have been chosen as they performed TH uncertainty analyses based on 59 Wilks data sets using RELAP5 in combination with the uncertainty evaluation software SUSA.

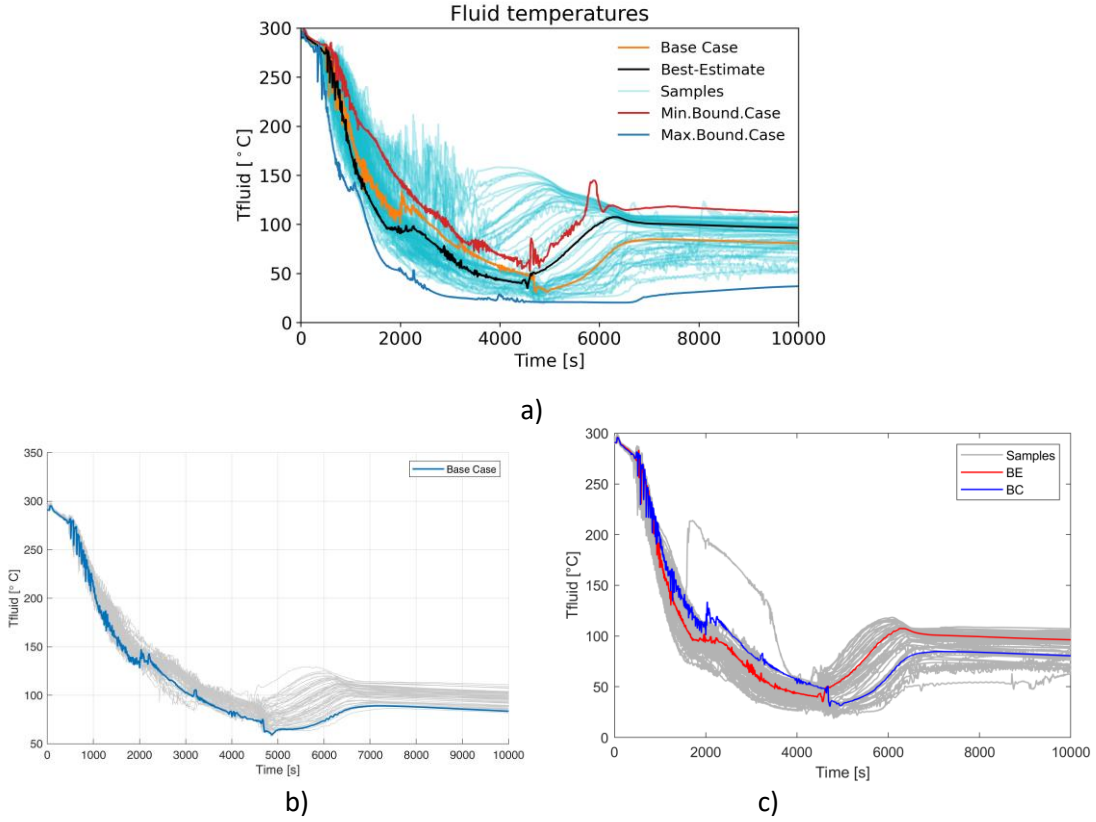

Figure 3.66: Comparison of fluid temperature as a function of time used for structural analyses by a) JSI, b) IPP and c) KIWA. Wilks 59 data samples.

Significant variations in Wilks results can be observed between JSI, IPP and KIWA. JSI results have much wider spread in the Wilks data samples in comparison to the IPP and KIWA data. One of the KIWA Wilks data samples demonstrates a clear deviation in the temperature trend when the fluid temperature increases in the time range between 1800 to 4000 s. Similar trend has also been observed in KIWA results from TH analyses for LTO improvements, namely LTO 05 for high pressure injection flow (HPSI) reduction. KIWA performed the TH analyses by reducing HPSI flow from 100% down to 75% with 5% increments. The characteristic rise of temperature, similar to the one in Figure 3.66, was observed in the results for HPSI reduction to 75%. For higher HPSI levels (80%-100%) the temperature rise in this time range was not observed or it was much lower and less pronounced.

The temperature rise for HPSI at 75% may be explained by the following considerations. By reducing the emergency coolant quantity (HPSI flow) pumped into the reactor primary system the void fraction (ratio of steam to total volume) increases substantially. The void fraction in volume 9101 for HPSI 75% at 1500-3000 s is much larger than that for HPSI 80% which would support this assumption (void fraction values in HPSI cases 100%-80% at around 1500-3000 sec do not change much actually). It means that there is substantially more gas phase in downcomer which causes deterioration of heat

transfer at certain conditions. This in turn leads to higher temperature rise in downcomer as it was obtained in the calculations for 75%. There should be a threshold somewhere between 75% and 80% HPSI reduction levels when the emergency coolant inflow is so low that most of it boils thereby deteriorating heat transfer.

Differences in fluid temperature can also be observed in the TH data for Wilks 93 data sets that have been calculated by FRA-G, UJV and WUT as shown in Figure 3.67.

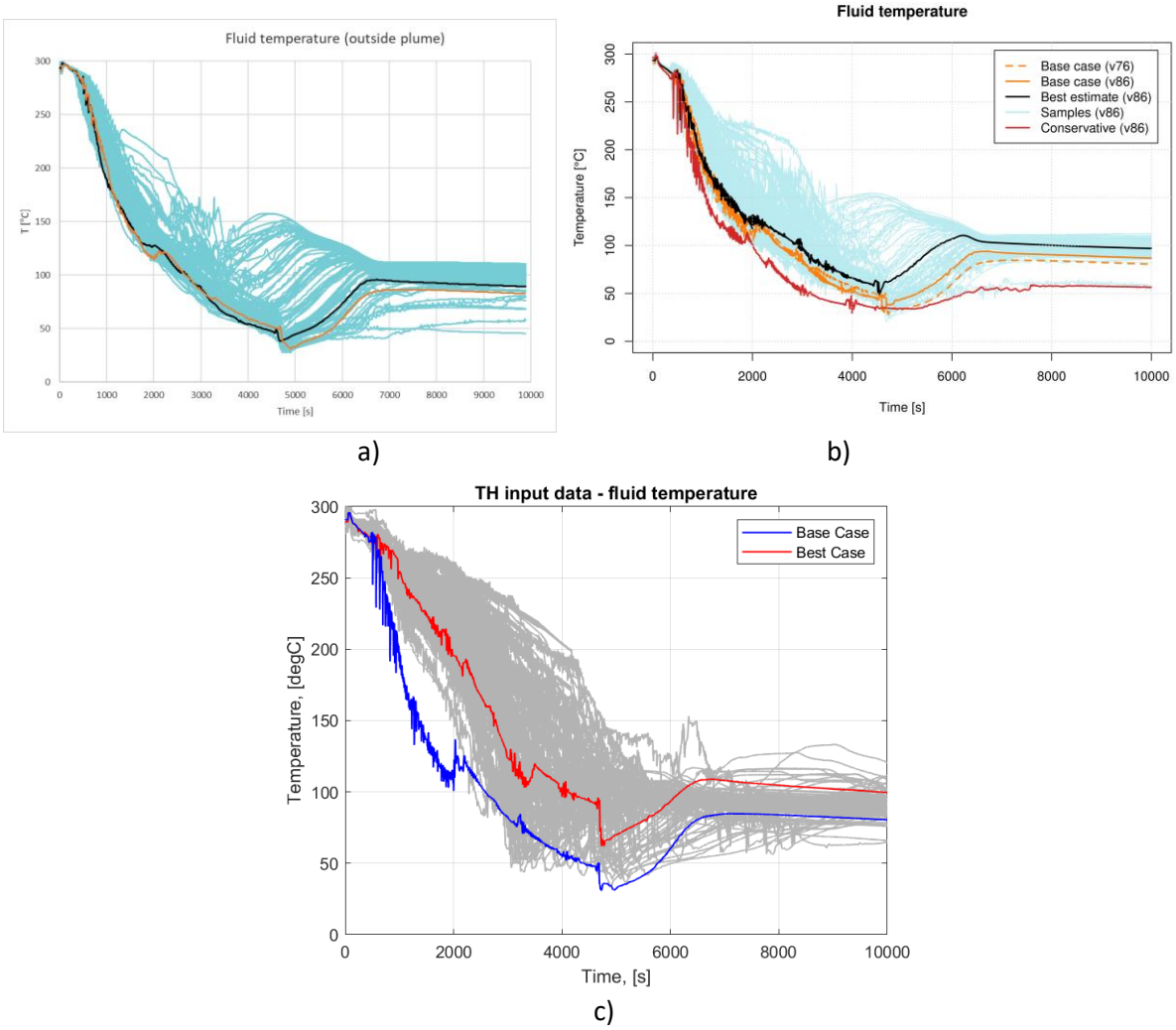

Figure 3.67: Comparison of fluid temperature as a function of time used for structural analyses by a) FRA-G, b) UJV and c) WUT. Wilks 93 data samples.

3.4.4.2 Structural results

It is not feasible to make comparisons of calculated stress and temperature distributions from all or several partners due to large amount of data curves. Therefore, only some qualitative comparisons and observed deviations in the structural results are provided herein.

Temperature at the RPV inner surface for the Best Estimate case analysed by PSI (TH code TRACE) exhibits a local peak with temperature increase at about 2600 s. This temperature peak results in local abrupt decrease in calculated stresses at the inner surface. Thus, hoop stresses exhibit a decrease by about 200 MPa as shown in Figure 3.68. Similar trends for the Best Estimate case can also be found in the results from TECNATOM who used the TH data from PSI for the structural analyses.

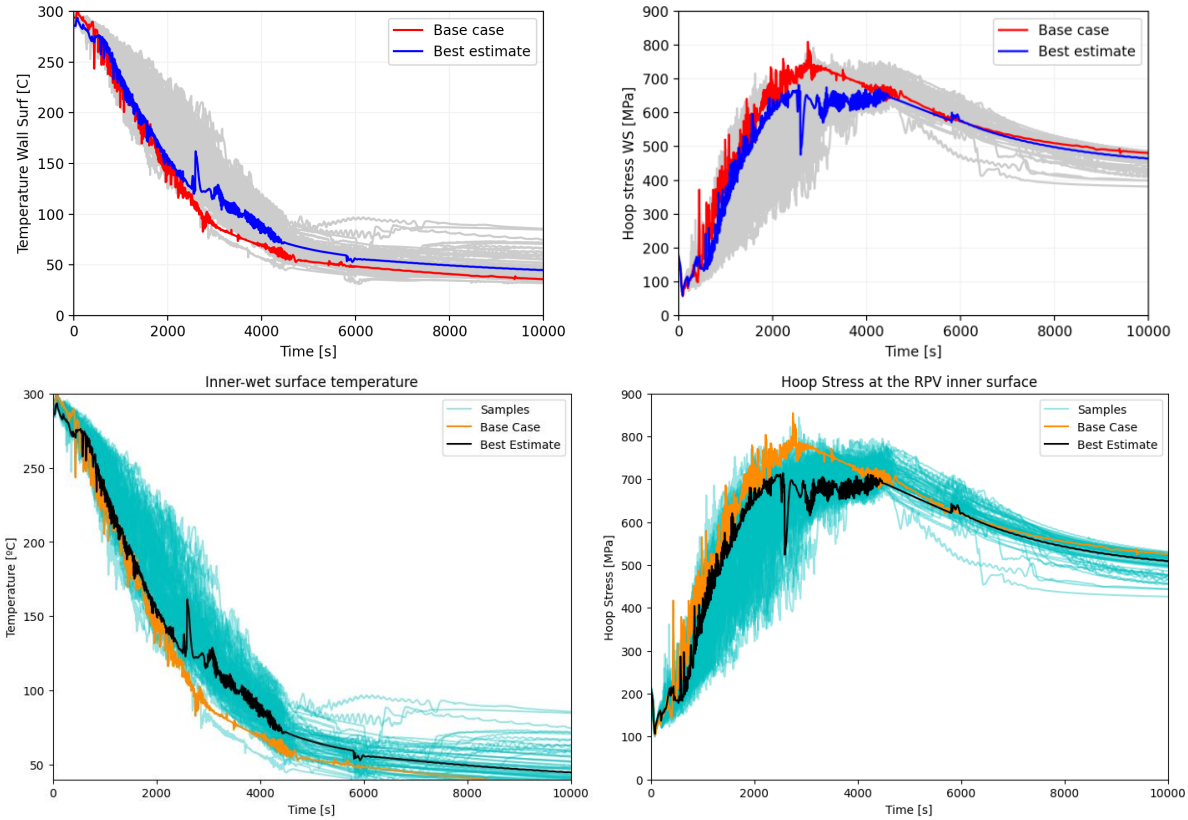

Figure 3.68: RPV inner-surface temperature and hoop stresses at the inner surface as a function of time. PSI vs Tecnatom results for Wilks 59 data samples.

It was described above that one of the KIWA Wilks TH data samples demonstrated a clear deviation in the temperature trend when the fluid temperature increased in the time range between 1,800 to 4,000 s, see Figure 3.66(c). An explanation to this Wilks TH data sample behaviour is given in Section 3.4.4.1. This deviation in the TH data affects also the structural results leading to decrease of calculated stresses in the given time range. An example of this behaviour is presented in Figure 3.69.

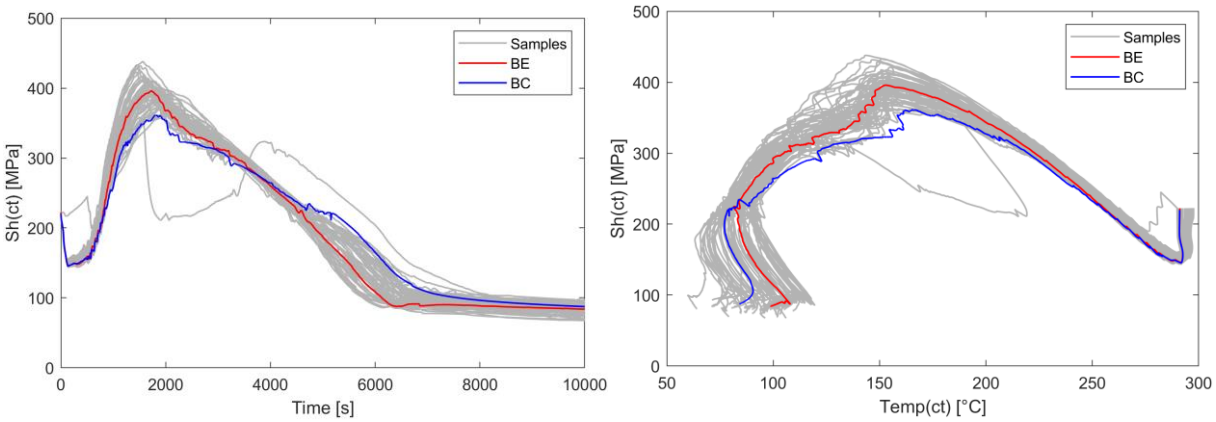

Figure 3.69: Hoop stresses at the crack tip location as a function of time and as a function of crack tip temperature. KIWA results for Wilks 59 data samples.

4 Baseline probabilistic benchmark

4.1 Brief description

This Section summarises the work performed within Task 4.3 dealing with baseline probabilistic benchmark. All activities within this Task were divided into two main parts. The first part addresses verification of probabilistic tools and methods used by participants for probabilistic analyses in the APAL project. The second part contains several round robin benchmarks for testing and adjusting the input data and verifying a complete chain of probabilistic analyses performed in Tasks 4.4-4.5 and presented later in Sections 5 and 6, respectively.

The main parts with underlying tool verifications/benchmarks within Task 4.3 are presented below followed by detailed summary in the forthcoming sections:

1. Tools verification:
   - Check random number generator
   - Check generation of data from a provided tabulated PDF
   - Check generation of tabulated data for UCC (and TCC)
   - Check generation of data from a truncated distribution
   - Check CPI for provided T, K_I and ART
   - Check CPF for provided T, K_I and ART (non-mandatory)

2. Round Robin (RR) benchmarks:
   - RR1 – Predict ART for increasing fluence level
   - RR2 – Check CPI for base case transient
   - RR3 – Check CPF for base case transient (non-mandatory)
   - RR4 – Check CPI for base case with distributed crack size
   - RR5 – Check CPF for base case with distributed crack size (non-mandatory)

4.2 Verification of analysis tools

For verifying that all tools used within WP4 can handle correctly different aspects considered within APAL, several tool verification benchmarks were performed. This Section presents a description of the basis and objectives along with main results and conclusions for each verification task.

4.2.1 Check Random Number Generator (RNG)

For probabilistic analyses based on Monte Carlo Simulation (MCS) methods an appropriate random number generator (RNG) is required, especially for calculations of low probability events. One of the most important characteristics of RNGs is the sequence length or sequence period, i.e. non-repeating sequence of generated random numbers.

The standard Excel RNG, the Visual Basic (VB) function Rnd(), has a sequence length of only 16,777,216 numbers rendering this RNG not suitable for MCS with a large number of samples. Other RNGs with substantially longer sequence length, e.g. Mersenne Twister algorithm [18], may be more appropriate to be used for probabilistic analyses. A performance of the Excel/VB RNG with a clear periodicity due to limited sequence length is compared with the Mersenne Twister RNG in Figure 4.1.

For the determination of maximum allowable ART and CPI/CPF values in the order of magnitude of 10^{-8}, it may be required to perform MCS with a sample size of up to 10^{10}. A simple verification of RNGs used by different partners was performed in this Subtask for ensuring that uncertainty related to insufficient RNGs is eliminated.

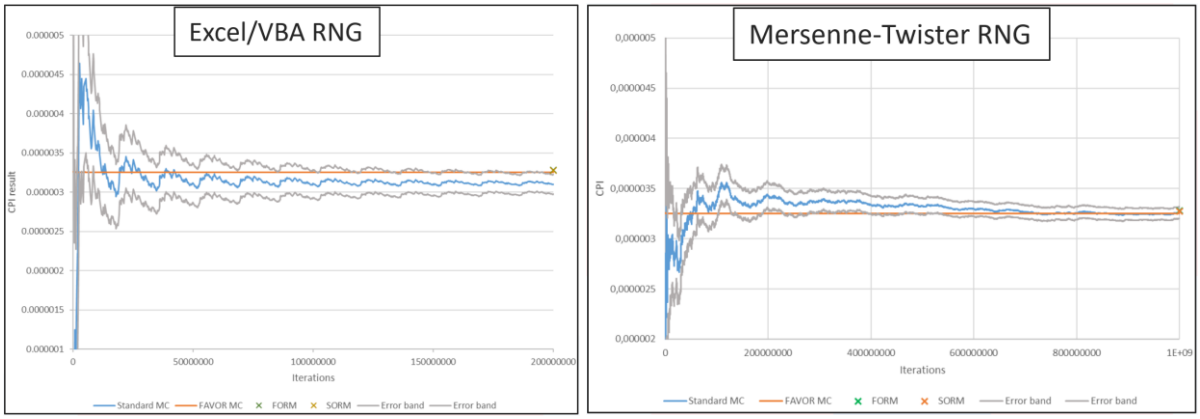

Figure 4.1: Comparison of performance for Excel/Visual Basic RNG and Mersenne Twister RNG.

For performance verification of RNGs, two benchmark cases based on different conditional probability of initiation (CPI) have been analysed. Fracture toughness K_{Ic} was assumed as a normally distributed probabilistic parameter with the mean value $\mu = 80\ \mathrm{MPa}\sqrt{\mathrm{m}}$ and the standard deviation $\sigma = 4\ \mathrm{MPa}\sqrt{\mathrm{m}}$. In both benchmark cases, the probability of fracture initiation (CPI) has been evaluated by solving the limit state function $K_{Ic} - K_I$. The stress intensity factor K_I was assumed as deterministic and equal to $K_I = 61.975\ \mathrm{MPa}\sqrt{\mathrm{m}}$ (for the first case) and $K_I = 56.01\ \mathrm{MPa}\sqrt{\mathrm{m}}$ (for the second case).

This problem can be solved analytically by deriving the inverse of normal cumulative distribution of K_{Ic}. Thus, it can be shown that for $K_I = 61.975\ \mathrm{MPa}\sqrt{\mathrm{m}}$ the conditional probability of fracture initiation $CPI = 3.3 \cdot 10^{-6}$ and for $K_I = 56.01\ \mathrm{MPa}\sqrt{\mathrm{m}}$, the $CPI = 1.0 \cdot 10^{-9}$. Both cases have been evaluated using Monte Carlo simulations with chosen RNGs using a sampling size of 10^8 and 10^{11} for the first and second case, respectively. The verification results for the cases with $CPI = 3.3 \cdot 10^{-6}$ and $CPI = 1.0 \cdot 10^{-9}$ are shown in Figure 4.2.

All RNGs have demonstrated an adequate sequence length ensuring that no periodicity occurs for the chosen sampling size. The probability values in the order of magnitude 10^{-9} can be predicted. All MC simulations have converged to the analytically predicted CPIs.

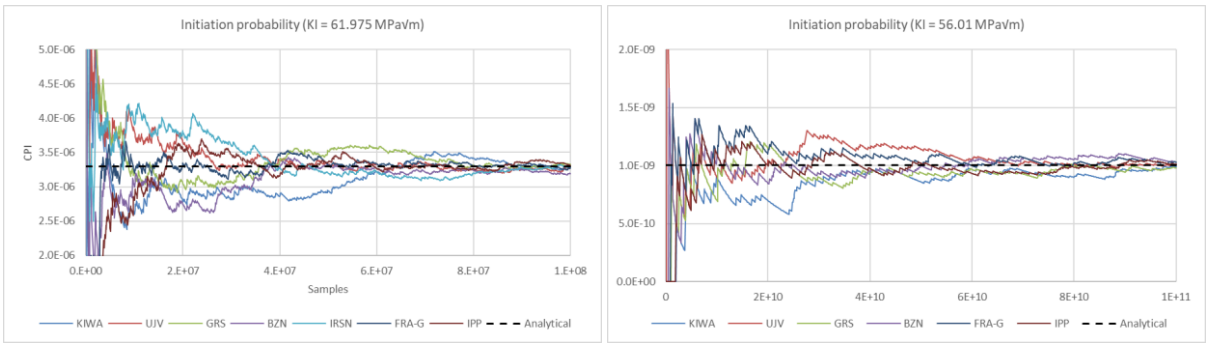

Figure 4.2:Results from RNG verification for CPI=3.3e-6 (sampling size 10^8) and CPI=1.0e-9 (sampling size 10^{11}).

4.2.2 Check generation of data from a provided tabulated PDF

The objective of this subtask was to verify that each partner is able to generate the correct flaw depth distribution from the provided tabulated distribution data given in Table 4.1 and graphically presented in Figure 4.3. The provided tabulated flaw depth distribution data is used only as an example for

verification. The real flaw depth distribution for probabilistic assessments within APAL is reviewed in Section 2.3.2.4 and will be discussed in detail in Section 4.2.3.

Generation of flaw depth distribution should be performed by a Monte Carlo simulation using the algorithm provided in the ICAS project [19]:

- For each flaw, generate a uniformly distributed random number $0 \leq y \leq 1.0$;
- If $y \leq CDF(1) = 0.6446$, then the flaw depth is $a = 2.13$ mm (upper limit);
- If $CDF(1) < y \leq CDF(2)$, then the flaw depth is $a = 4.29$ mm (upper limit);
- In general, if $CDF(i) < y \leq CDF(i+1)$, then the flaw depth is $a(i+1)$.

Table 4.1 Tabulated flaw depth distribution

Crack depth (mm). Lower limit	Crack depth (mm). Upper limit	Probability, that crack depth is in given interval	CDF
0.00	2.13	6.4460E-01	6.446000E-01
2.13	4.29	3.0370E-01	9.483000E-01
4.29	6.43	4.1300E-02	9.896000E-01
6.43	8.59	5.7129E-03	9.953129E-01
8.59	10.72	2.3929E-03	9.977058E-01
10.72	12.85	1.1348E-03	9.988406E-01
12.85	15.01	5.4031E-04	9.993809E-01
15.01	17.15	2.7169E-04	9.996526E-01
17.15	19.30	1.4000E-04	9.997926E-01
19.30	21.44	7.3525E-05	9.998661E-01
21.44	23.57	3.9092E-05	9.999052E-01
23.57	25.73	1.1326E-05	9.999165E-01
25.73	27.86	8.4110E-06	9.999250E-01
27.86	30.02	5.5197E-06	9.999305E-01
30.02	32.16	4.1338E-06	9.999346E-01
32.16	34.29	2.9630E-06	9.999376E-01
34.29	36.45	2.1983E-06	9.999398E-01
36.45	38.58	1.4576E-06	9.999412E-01
38.58	40.74	1.1947E-06	9.999424E-01
40.74	42.88	1.0036E-06	9.999434E-01
42.88	45.01	7.6464E-07	9.999442E-01
45.01	47.17	4.0621E-07	9.999446E-01
47.17	49.30	2.6284E-07	9.999449E-01

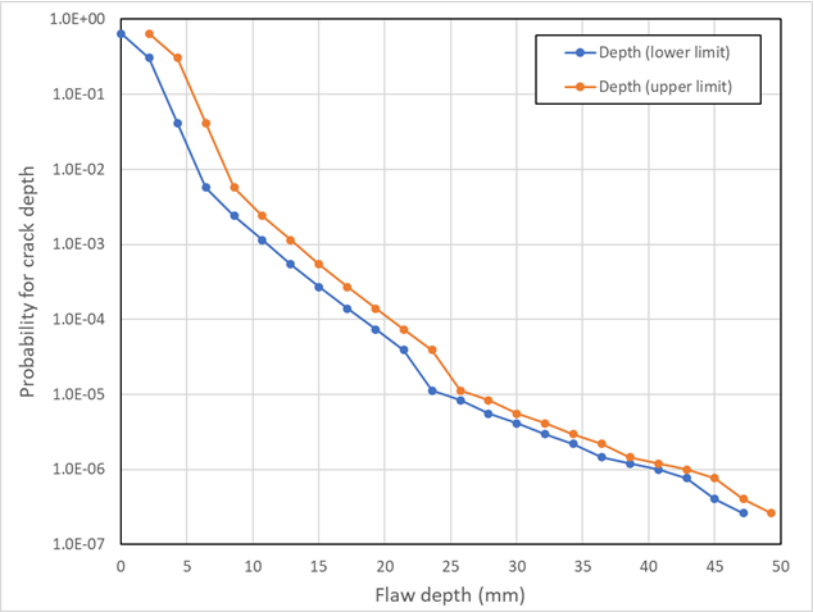

Figure 4.3: Graphical representation of the tabulated flaw depth distribution.

As a part of this subtask, the flaw depth distributions should be generated using a sampling size of 10^4, 10^6, 10^8 and 10^{10} and presented as histograms for comparison between different partners.

All partners have used their own Monte Carlo tools with random number generators verified in the previous Section. Based on the provided input data (see Table 4.1) Kiwa performed the initial Monte Carlo simulation. The obtained flaw depth distribution is shown in Figure 4.4(a) demonstrating unrealistically high sampling frequency for the last flaw depth bin. The CDF values for the input flaw depth distribution in Table 4.1 were obtained by summing up the PDF-values for each flaw depth range. However, the PDF-values have been provided with insufficient precision (only 4-5 significant digits) resulting in $\mathrm{CDF} \neq 1.0$ for the last flaw depth range, see Table 4.2. In the deterministic domain, the CDF-value for the last row may appear to be "very close" to 1.0. However, in a probabilistic context the difference of 5.514161E-05 from $\mathrm{CDF} = 1.0$ is substantial and two orders of magnitude greater than the PDF-value for the flaw depth of 49.3 mm (last row).

The initial flaw depth distribution has been corrected by adding the discrepancy in the CDF to the probability value for crack depth of 2.13 mm (first row) and recalculating the CDF-values, see Table 4.2. It provides a negligible influence on sampling frequencies for small flaws but allows for correct sampling for deep flaws. The computed sampling frequencies from the corrected flaw depth distribution are presented in Figure 4.4(b) along with the results from the initial flaw distribution.

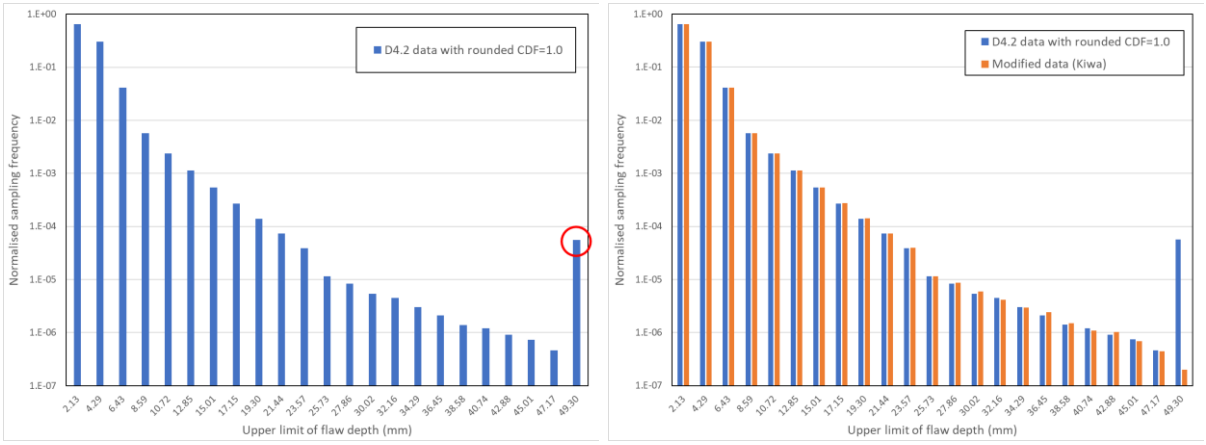

(a) **(b)**

Figure 4.4: Normalised sampling frequencies from the initial and corrected flaw depth distributions. The results are produced with 10^8 MC simulations.

Table 4.2 Initial and corrected flaw depth distributions

Intial tabulated distribution with $\mathbf{CDF \neq 1.0}$

Crack depth (mm). lower limit	Crack depth (mm) upper limit	Probability, that crack depth is in given interval	CDF
0.00	2.13	6.4460E-01	6.446000E-01
2.13	4.29	3.0370E-01	9.483000E-01
4.29	6.43	4.1300E-02	9.896000E-01
6.43	8.59	5.7129E-03	9.953129E-01
8.59	10.72	2.3929E-03	9.977058E-01
10.72	12.85	1.1348E-03	9.988406E-01
12.85	15.01	5.4031E-04	9.993809E-01
15.01	17.15	2.7169E-04	9.996526E-01
17.15	19.30	1.4000E-04	9.997926E-01
19.30	21.44	7.3525E-05	9.998661E-01
21.44	23.57	3.9092E-05	9.999052E-01
23.57	25.73	1.1326E-05	9.999165E-01
25.73	27.86	8.4110E-06	9.999250E-01
27.86	30.02	5.5197E-06	9.999305E-01
30.02	32.16	4.1338E-06	9.999346E-01
32.16	34.29	2.9630E-06	9.999376E-01
34.29	36.45	2.1983E-06	9.999398E-01
36.45	38.58	1.4576E-06	9.999412E-01
38.58	40.74	1.1947E-06	9.999424E-01
40.74	42.88	1.0036E-06	9.999434E-01
42.88	45.01	7.6464E-07	9.999442E-01
45.01	47.17	4.0621E-07	9.999446E-01
47.17	49.30	2.6284E-07	9.999449E-01

≈ 1.0

Corrected tabulated distribution with $\mathbf{CDF = 1.0}$

Crack depth (mm) lower limit	Crack depth (mm) upper limit	Probability, that crack depth is in given interval	CDF
0.00	2.13	6.446551E-01	6.446551E-01
2.13	4.29	3.037000E-01	9.483551E-01
4.29	6.43	4.130000E-02	9.896551E-01
6.43	8.59	5.712900E-03	9.953680E-01
8.59	10.72	2.392900E-03	9.977609E-01
10.72	12.85	1.134800E-03	9.988957E-01
12.85	15.01	5.403100E-04	9.994361E-01
15.01	17.15	2.716900E-04	9.997077E-01
17.15	19.30	1.400000E-04	9.998477E-01
19.30	21.44	7.352500E-05	9.999213E-01
21.44	23.57	3.909200E-05	9.999604E-01
23.57	25.73	1.132600E-05	9.999717E-01
25.73	27.86	8.411000E-06	9.999801E-01
27.86	30.02	5.519700E-06	9.999856E-01
30.02	32.16	4.133800E-06	9.999897E-01
32.16	34.29	2.963000E-06	9.999927E-01
34.29	36.45	2.198300E-06	9.999949E-01
36.45	38.58	1.457600E-06	9.999964E-01
38.58	40.74	1.194700E-06	9.999976E-01
40.74	42.88	1.003600E-06	9.999986E-01
42.88	45.01	7.646400E-07	9.999993E-01
45.01	47.17	4.062100E-07	9.999997E-01
47.17	49.30	2.628400E-07	1.000000E+00

The histograms of sampled flaw depths based on 10^4 and 10^6 MC simulations by all partners are presented in Figure 4.5. For the sampling size of 10^4, the results were consistent between the partners for the first three bins with smallest flaw depths. However, a larger scatter can be seen for deeper flaws, followed by totally unpopulated bins for flaw depths greater than 20 mm. This result is quite expected considering that the first three ranges of flaw depths have a major contribution to the flaw depth distribution with the $\mathrm{CDF} \approx 0.99$ (see Table 4.2).

For larger sampling sizes, the results between partners show a better agreement even for deeper flaws. Figure 4.6 shows the sampling frequencies for flaw depths from 10^8 Monte Carlo simulations. Some deviations in the results can be observed only for the bins with large flaw depths. Analyses with the sampling size of 10^{10} are summarised in Figure 4.7 showing very consistent results between all partners.

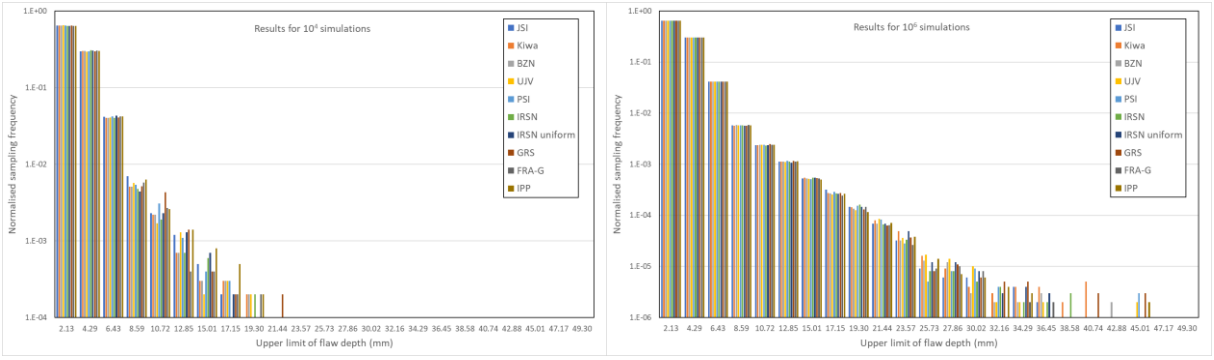

Figure 4.5: Normalised sampling frequencies for flaw depths with 10^4 and 10^6 MC simulations.

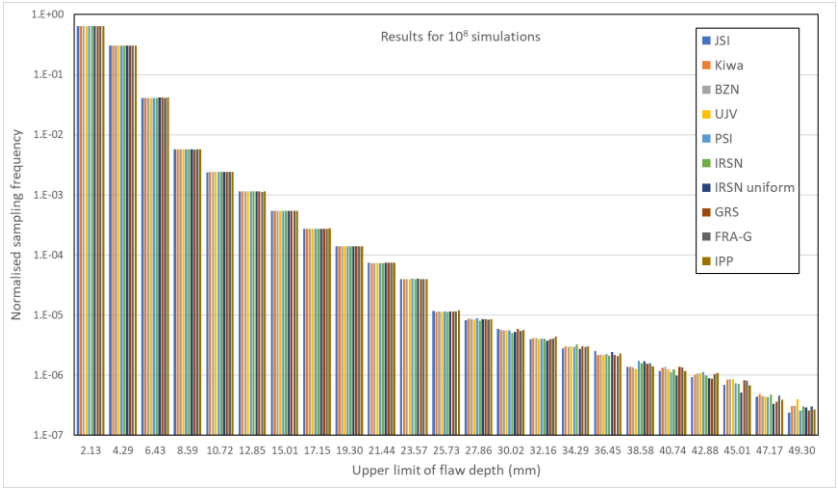

Figure 4.6: Normalised sampling frequencies for flaw depths with 10^8 MC simulations.

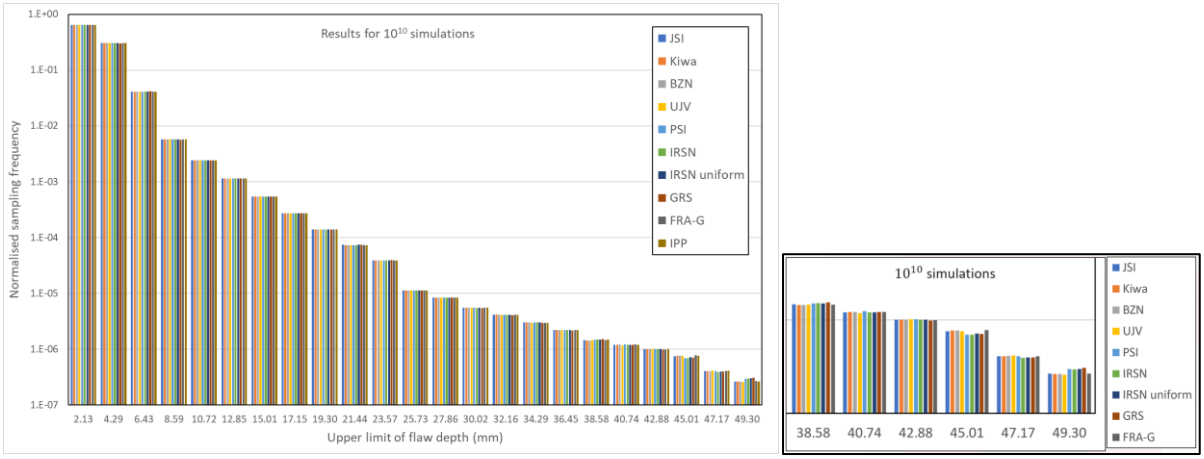

Figure 4.7: Normalised sampling frequencies for flaw depths with 10^{10} MC simulations.

4.2.3 Check generation of tabulated data for UCC (and TCC)

One of the challenges within APAL project was related to developing a realistic flaw distribution for underclad cracks (UCC) that can be used in probabilistic analyses. Significance of UCC cracks for calculated RPV failure probabilities had previously been underestimated in comparison to defects located in welds, base metal, and cladding. Therefore, there is limited and scarce information available in the open literature about statistically validated basis and distribution parameters for UCC.

One of the widely recognised UCC flaw distribution models has been developed by PNNL based on insights from literature review along with a treatment of the uncertainties in estimating the distribution parameters [25]. The PNNL UCC distribution model, as presented in Figure 4.8, includes the following parameters: the maximum (or bounding) through-wall depth of UCC flaws, the conditional distribution of the through-wall depth expressed as a fraction of the bounding depth dimension and the conditional distribution of the length for UCC flaws.

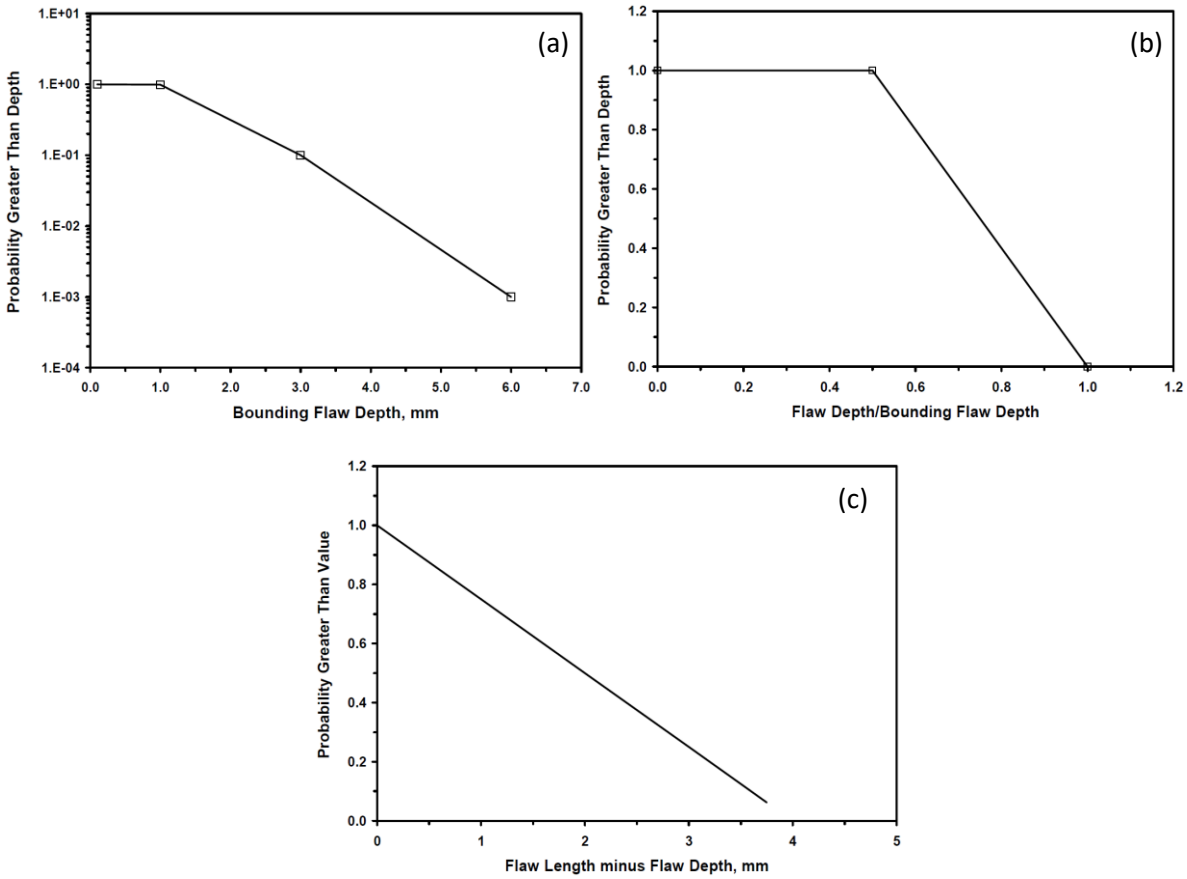

Figure 4.8: The UCC flaw distribution model developed by PNNL with the parameters; (a) the bounding flaw depth, (b) the ratio between the flaw depth and the bounding flaw depth, (c) the flaw length.

Figure 4.8(a) shows the conditional distribution for the bounding flaw depth (BFD) dimension truncated at the maximum BFD of 6 mm. This maximum BFD is assumed to be related to details of the cladding procedure. Ranges for the bounding flaw depths (0-1 mm, 1-3 mm and 3-6 mm) and their probabilities are based on the French work cited in [25] regarding vessel-to-vessel variability for the BFD. Thus, the distribution of bounding flaw depths over the range of 0-6 mm is described by uniform distribution of the logarithm of the probability for given BFD ranges.

The conditional distribution of UCC flaw depth (FD) is assumed to be relatively uniform and is described by a uniform distribution over the range of 50-100% of the BFD as shown by Figure 4.8 (b). The uniform distribution is a reflection of the lack of information on measured FD dimensions. The undertaken approach in the PNNL model, therefore, conservatively assigns a large fraction of the flaws to have depth close to the bounding flaw depth.

Figure 4.8 (c) presents the PNNL conditional uniform distribution of UCC flaw length (FL). This distribution implies that the maximum FL is bounded by a dimension of 10 mm which is much less than 60 mm originally proposed in French work cited in [25]. The French publications provided no motivation for the 60 mm flaw length. Furthermore, discussions of the mechanisms of sub-clad

cracking state that flaws are confined to the overlap region of the heat-affected zones of adjacent passes of the strips of cladding. This mechanistic model would give flaw lengths significantly lower than the 60 mm flaw of the French publications.

The PNNL flaw distribution model is provided in such way that does not allow direct use with an arbitrary probabilistic code. One of the aims with the APAL project is to assess and compare the results produced by various probabilistic codes that have been developed or used by different APAL partners. Therefore, a generic tabulated distribution of UCC (and TCC) flaw depth (in terms of cumulative distribution function (CDF)) needs to be developed from the PNNL distribution model (see Figure 4.8) that can be used as input to an arbitrary probabilistic tool.

A development of the generic CDF for UCC flaw depth has been set up as a round-robin exercise where the involved partners individually interpreted, made necessary assumptions and mathematically treated the PNNL flaw distribution model, see Figure 4.8. Most of the partners have used MCS methods for sampling the UCC flaw depth and length from the PNNL model whereas several partners have used direct integration approach.

4.2.3.1 Monte Carlo approach

Most of the partners have interpreted the PNNL flaw distribution model (see Figure 4.8) in a similar way as described below. The distribution in Figure 4.8(a) represents $(1 - CDF)$ for the bounding flaw depth (BFD) on the logarithmic scale. It can be assumed that BFD values larger than 6 mm have zero probability and BFD=6 mm has a probability of 0.001. Considering the $(1 - CDF)$ distribution, the following equations can be written where x is the BFD:

$F(x) = 0$ for $x < 1$,
$F(x) = 1 - 10^{-\frac{x-1}{2}}$ for $1 \leq x < 3$,
$F(x) = 1 - 10^{-\frac{x-1.5}{1.5}}$ for $3 \leq x < 6$,
$F(x) = 1$ for $6 \leq x$.

Thus, the new CDF for the bounding flaw depth can be plotted on the linear scale as presented in Figure 4.9.

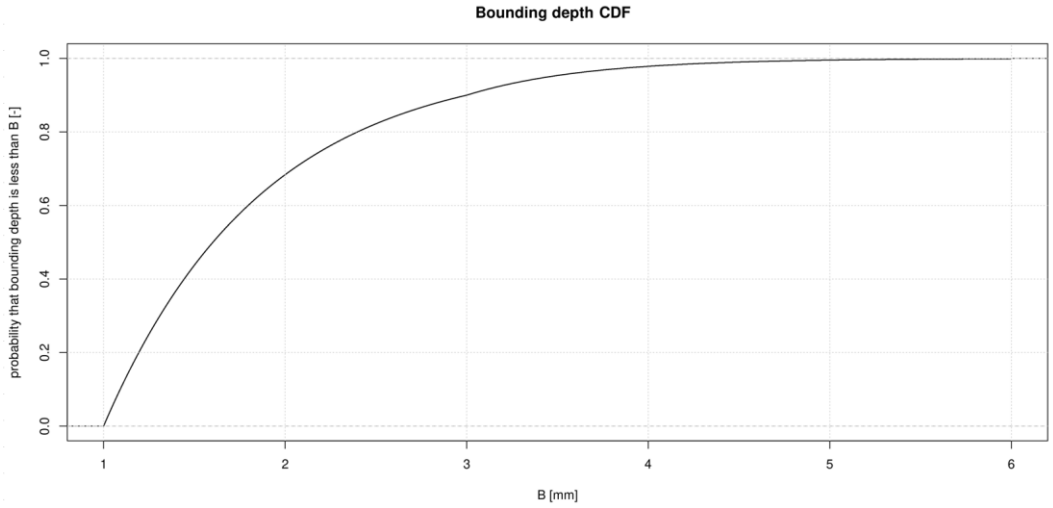

Figure 4.9: The CDF for the bounding flaw depth used for sampling in MCS.

A value of BFD can be randomly sampled from the cumulative distribution function $F(x)$. For that, a random value α is sampled from a continuous uniform distribution between (0, 1) and the BFD value is calculated by the inverse CDF as $BFD = F^{-1}(\alpha)$.

For sampling the flaw depth, FD, a random value β is obtained from a continuous uniform distribution between (0.5, 1). The value β represents a ratio between the flaw depth and the bounding flaw depth, $\frac{FD}{BFD}$ according to Figure 4.8(b). Thus, the flaw depth FD can be calculated as $FD = \beta \cdot BFD$.

The flaw length, *FL*, is implicitly defined in Figure 4.8(c) as a difference between the flaw length FL and the flaw depth FD and can be represented as $\gamma = (FL - FD)$. The value γ is sampled from a continuous uniform distribution between (0, 4). Then, the flaw length can be derived as $FL = \gamma + FD$.

4.2.3.2 Direct integration approach (by BZN)

BZN has proposed an interesting solution for determining the flaw depth distribution based on direct integration. A mathematical representation of the original PNNL flaw distribution given in Figure 4.8 is similar to the one presented for the Monte Carlo approach.

Let y to be the BFD, then the CDF for the BFD can be piecewise described as:
if $y \leq 1$ then $\left(1 - CDF_y\right) = 1$,
if $1 < y \leq 3$ then $\left(1 - CDF_y\right) = 3.640706706 \cdot e^{(-1.151292548y)}$,
if $3 < y \leq 6$ then $\left(1 - CDF_y\right) = 15.35056729 \cdot e^{(-1.53505672y)}$,
if $6 < y$ then $\left(1 - CDF_y\right) =$ Not Available.

Let x is the $\frac{FD}{BFD}$ where X~UNI(0.5,1), and z is the actual crack depth.
Using:

$$\begin{aligned} F_Z(z) &\stackrel{\text{def}}{=} \mathbb{P}(Z \leq z) \\ &= \mathbb{P}(XY \leq z) \\ &= \mathbb{P}(XY \leq z, X \geq 0) + \mathbb{P}(XY \leq z, X \leq 0) \\ &= \mathbb{P}(Y \leq z/X, X \geq 0) + \mathbb{P}(Y \geq z/X, X \leq 0) \\ &= \int_0^{\infty} f_X(x) \int_{-\infty}^{z/x} f_Y(y)\, dy\, dx + \int_{-\infty}^{0} f_X(x) \int_{z/x}^{\infty} f_Y(y)\, dy\, dx \end{aligned}$$

Solving this integral for z (the actual crack depth):

$$CDF_{depth} = P(Z \leq z) = \int_1^{\max(1,z)} \begin{cases} 0 & y \leq 1 \\ 3.640706706 \cdot \mathrm{e}^{-1.151292548 \cdot \mathrm{y}} & 1 < y \leq 3 \\ 15.35056729 \cdot \mathrm{e}^{-1.53505672866285 \cdot \mathrm{y}} & 3 < y \leq 6 \\ 0 & 6 < y \end{cases} dy$$

$$+2 \cdot \left(\int_{\max(1,z)}^{\max(1,2 \cdot z)} \begin{cases} 0 & y \leq 1 \\ 3.640706706 \cdot \mathrm{e}^{-1.151292548 \cdot \mathrm{y}} & 1 < y \leq 3 \\ 15.35056729 \cdot \mathrm{e}^{-1.53505672866285 \cdot \mathrm{y}} & 3 < y \leq 6 \\ 0 & 6 < y \end{cases} \cdot \left(\frac{z}{y} - 0.5\right) dy \right)$$

Let w is the $(FL - FD)$ where w~UNI(0,4), and l is the actual length.
Then applying the convolution integral for add two probability values:

$$CDF_{length} = P(L \leq l) = P(Z + W \leq l) = \int P(Z \leq l - w) \cdot f(w)\, dw$$

So,

$$CDF_{length} = \frac{1}{4}\int_{0}^{4}\left(\int_{1}^{\max(1,l-w)}\begin{cases}0 & y\le 1\\ 3.640706706\cdot e^{-1.151292548\cdot y} & 1<y\le 3\\ 15.35056729\cdot e^{-1.53505672866285\cdot y} & 3<y\le 6\\ 0 & 6<y\end{cases}dy + 2\cdot\left(\int_{\max(1,l-w)}^{\max(1,2\cdot(l-w))}\begin{cases}0 & y\le 1\\ 3.640706706\cdot e^{-1.151292548\cdot y} & 1<y\le 3\\ 15.35056729\cdot e^{-1.53505672866285\cdot y} & 3<y\le 6\\ 0 & 6<y\end{cases}\cdot\left(\frac{l-w}{y}-0.5\right)dy\right)\right)dw$$

4.2.3.3 Flaw depth distribution

Regardless of the used approach, the obtained CDFs of UCC flaw depth have demonstrated a good agreement between the APAL partners as shown in Figure 4.10. Minor differences in the obtained CDFs may be attributed to the different assumptions for interpretation and mathematical treatment of the conditional distribution for the bounding flaw depth, see Figure 4.8(a). Thus, some partners have assumed $\log(1 - CDF(x))$ distribution to be linear in the range 1 - 6 mm, thereby neglecting the intermediate value of $BFD = 3$ mm.

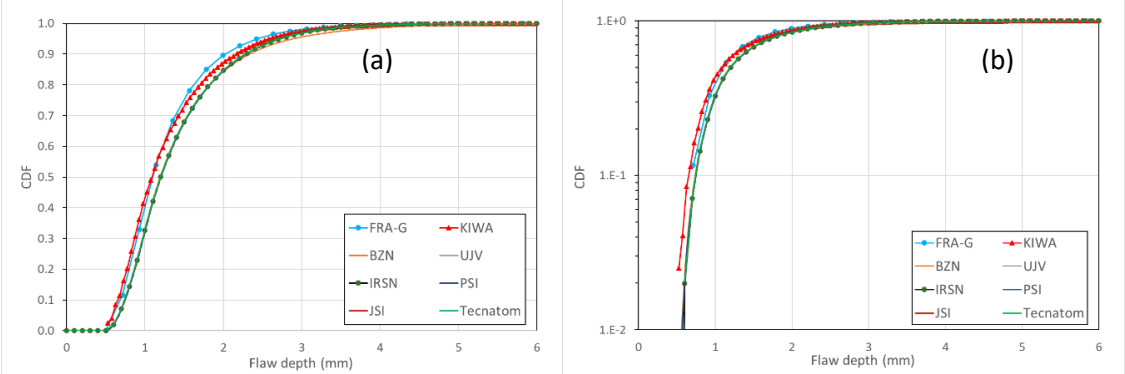

Figure 4.10: The calculated CDFs of UCC flaw depth from different APAL partners; (a) CDFs plotted on linear scale, (b) CDFs plotted on log-scale.

One of the obtained CDFs, judged to be based on most rigorous assumptions, have been selected for further use in probabilistic assessments within the APAL project. The chosen CDF of UCC flaw depth is presented in Figure 4.11. The median flaw depth from this distribution is $a_{\text{median}} = 1.2$ mm. As this CDF is used as input for RR4 and RR5, it is also presented in Table 2.3, Section 2.3.2.4.

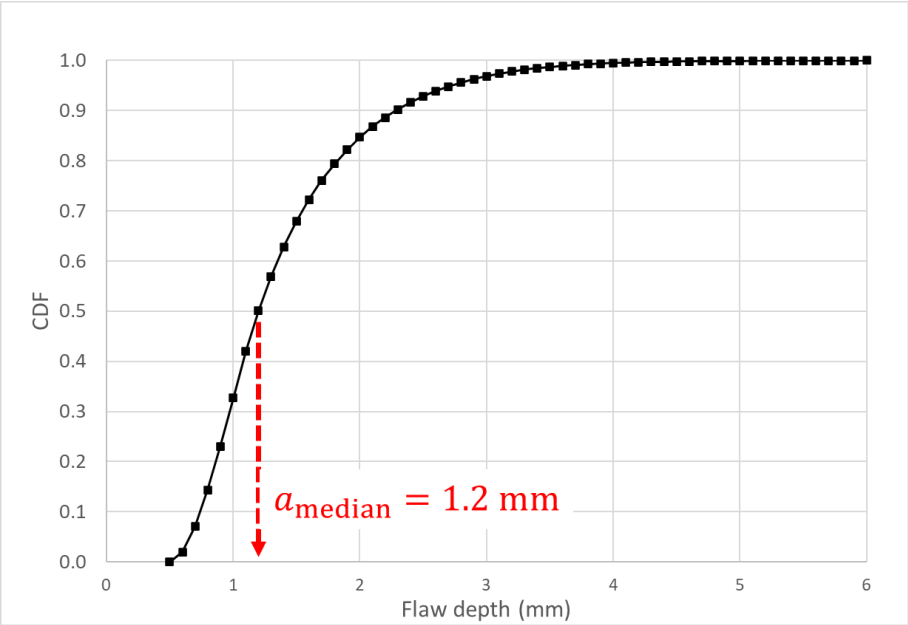

Figure 4.11: The CDF of UCC flaw depth chosen for probabilistic assessments in APAL.

For probabilistic assessments in RR4 and RR5 within APAL, the UCC flaw length is defined as the ratio $2c/a = 6$ (or $2c/a = 3$ for optional analyses). For assessments of TCC flaw growth, the TCC flaw depth distribution was obtained by adding 6 mm cladding thickness to the UCC depth distribution.

4.2.4 Check generation of data from a truncated distribution

Some distributed parameters must be truncated to avoid unrealistic, non-physical samples. Based on experience from previous international probabilistic benchmarks, it has been shown that incorrect treatment of truncated distributions may lead to errors in probabilistic analyses. This subtask is aimed to verify how truncation is handled within the different tools used by the partners.

Verification of a correct sampling for truncated parameters was performed using Monte Carlo simulations with a samplings size ranging from 10^4 to 10^{10}. Histograms from the Monte Carlo simulations were compared for all partners using three different methods:

- Considering the fracture toughness as the only probabilistic parameter,
- Considering the ART as the only probabilistic parameter,
- Considering both the fracture toughness and the ART parameters as probabilistic (up to seven probabilistic parameters). This was not included as one of the cases to check, but was analysed as a sensitivity study by some partners.

For parameters that have been treated deterministically, the mean values were considered.

4.2.4.1 Truncation Approaches

Three different approaches that can be used for truncating a normal distribution have been noted during the project. The recommended method is to use a truncated normal distribution [26] as shown in Figure 4.12.

Another approach is to re-sample values that are outside of the truncation limits. This approach may lead to increased computational time due to the generation of additional random values.

The third approach is to simply cut-off any values outside of the truncation limits and set these values to the truncation limit. This approach is used in FAVOR.

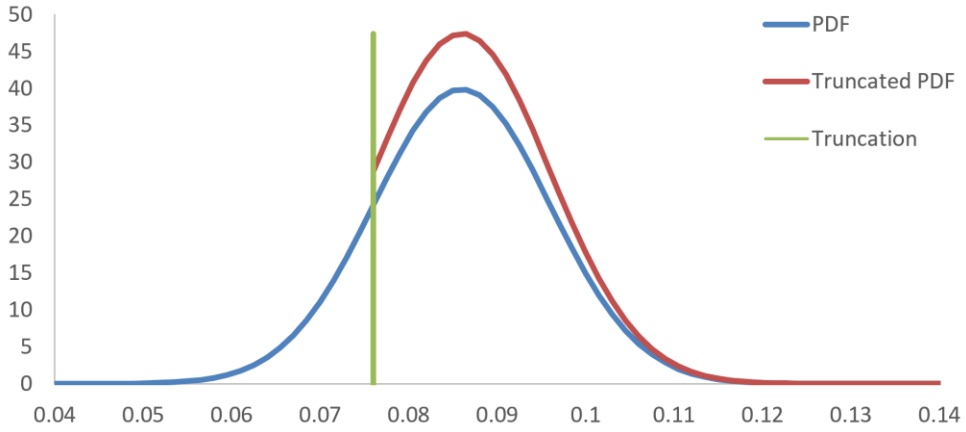

Figure 4.12: Illustration of a truncated distribution.

4.2.4.2 Sensitivity Study of Different Approaches for Truncation

FRA-G made a sensitivity study in which the three different approaches described in Section 4.2.4.1 are compared for three cases using data for copper in base metal according to Section 2.3.7 with three different standard deviations and a one-sided truncation at the physical limit of 0 %. The cases studied are summarised in Table 4.3.

Table 4.3 Cases studied using different truncation methods

Case	MV [%]	SD [%]	One-sided truncation [%]	Trunc. reached for -X SD	Prob. Cu < 0	Effect of truncation
1	0.086	0.01	0	8.6	3.9858e-18	Small
2	0.086	0.03	0	2.9	0.0020741	Medium
3	0.086	0.05	0	1.7	0.04271622	Large

The results for the different truncation methods are presented in Table 4.4 and Figure 4.13. The sensitivity study showed that re-sampling gave a good agreement with a correctly defined truncated distribution. To cut-off any values outside of the truncation limits and set these values to the truncation limit can give large errors when the coefficient of variation is quite large.

Table 4.4 Results for cases studied using different truncation methods

Case	Re-Sampling		Cut-Off		Truncated Distribution	
	MV	Scatter	MV	Scatter	MV	Scatter
1	0.0860	0.0100	0.0860	0.0100	0.0860	0.0100
2	0.0862	0.0297	0.0860	0.0300	0.0862	0.0297
3	0.0908	0.0455	0.0869	0.0481	0.0907	0.0455

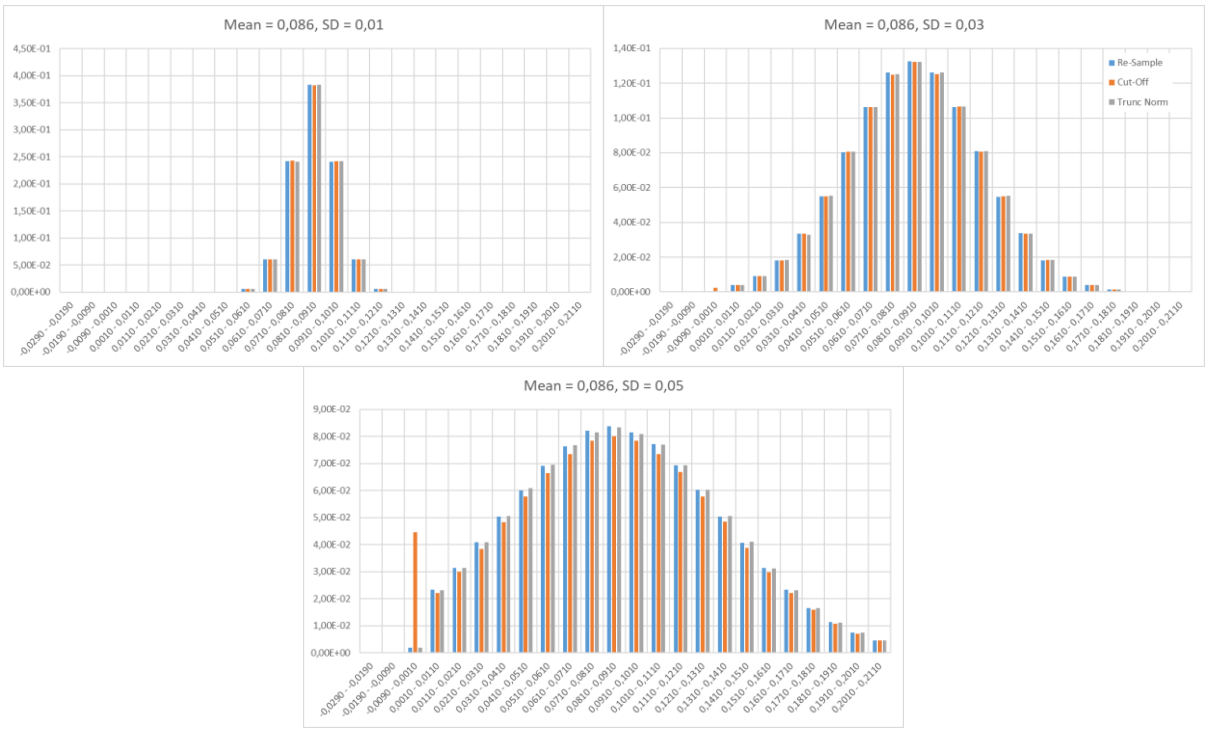

Figure 4.13: Comparison of different truncation methods.

4.2.4.3 Analyses of truncated distributions

Within this subtask the partners developed histograms for several parameters that are based on truncated distributions in order to study the impact of tool specific truncation methods.

Four different sampling sizes were to be considered; 10^4, 10^6, 10^8 and 10^{10}. The impact of sampling size is studied for the first parameter presented; copper in base metal. Based on this, results for the other parameters are only presented for the sampling size deemed sufficient.

The vertical axis for all histograms presented in the following section is normalised against the sampling size to facilitate comparison between different sampling sizes.

The partners who use the FAVOR code did not participate in this subtask as FAVOR cannot readily provide these partial data.

4.2.4.3.1 Chemical composition for base metal: Copper

The results from Monte Carlo simulations for truncated distribution of copper in base metal are summarised in this section. Figure 4.14 – Figure 4.17 show a comparison of the obtained distributions between the partners based on the sampling size of 10^4, 10^6, 10^8 and 10^{10}.

Results for the sampling sizes of 10^4, 10^6, 10^8 and 10^{10} are presented in Figure 4.14 - Figure 4.17. It can be seen that results differ considerably between partners for the smaller sampling size while the agreement in results improves with increasing sampling size. Also, fewer partners provided the results from simulations with larger sampling sizes. Only Kiwa, UJV, BZN and IPP provided results for all sampling sizes up to and including 10^{10}. Such simulations may be very time consuming and may also require a more complex code structure to avoid memory issues due to the large amount of data.

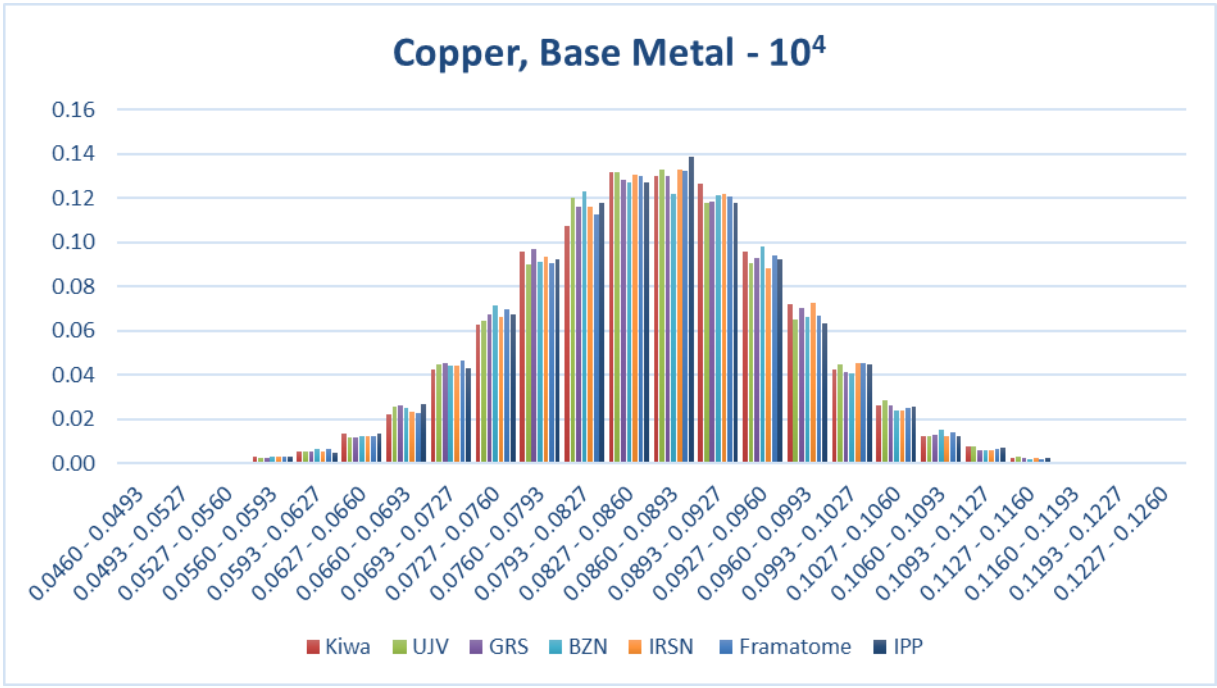

Figure 4.14: Results for truncated distribution for copper in base metal with 10^4 samples.

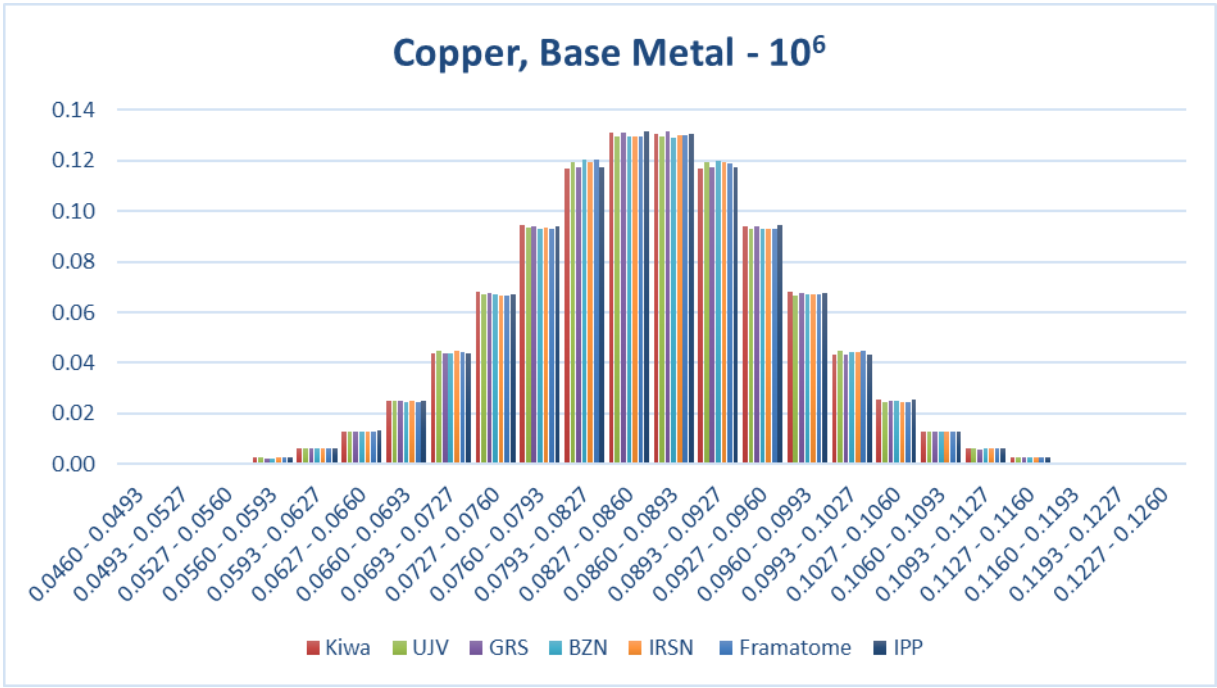

Figure 4.15: Results for truncated distribution for copper in base metal with 10^6 samples.

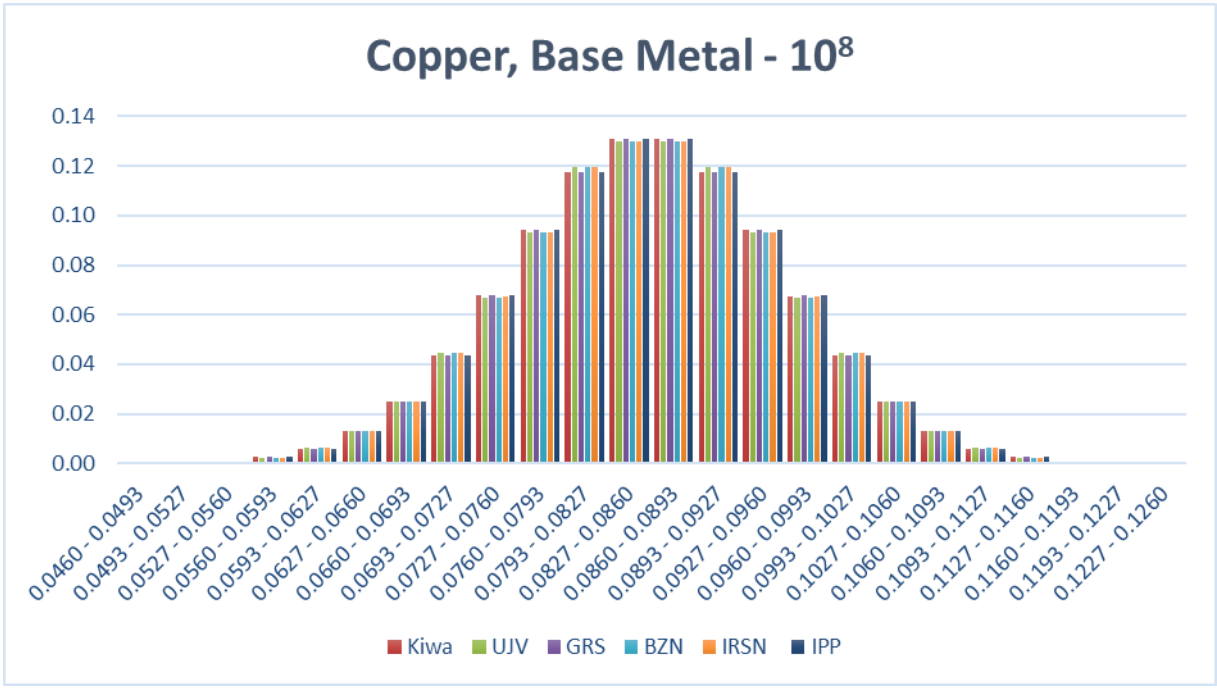

Figure 4.16: Results for truncated distribution for copper in base metal with 10^8 samples.

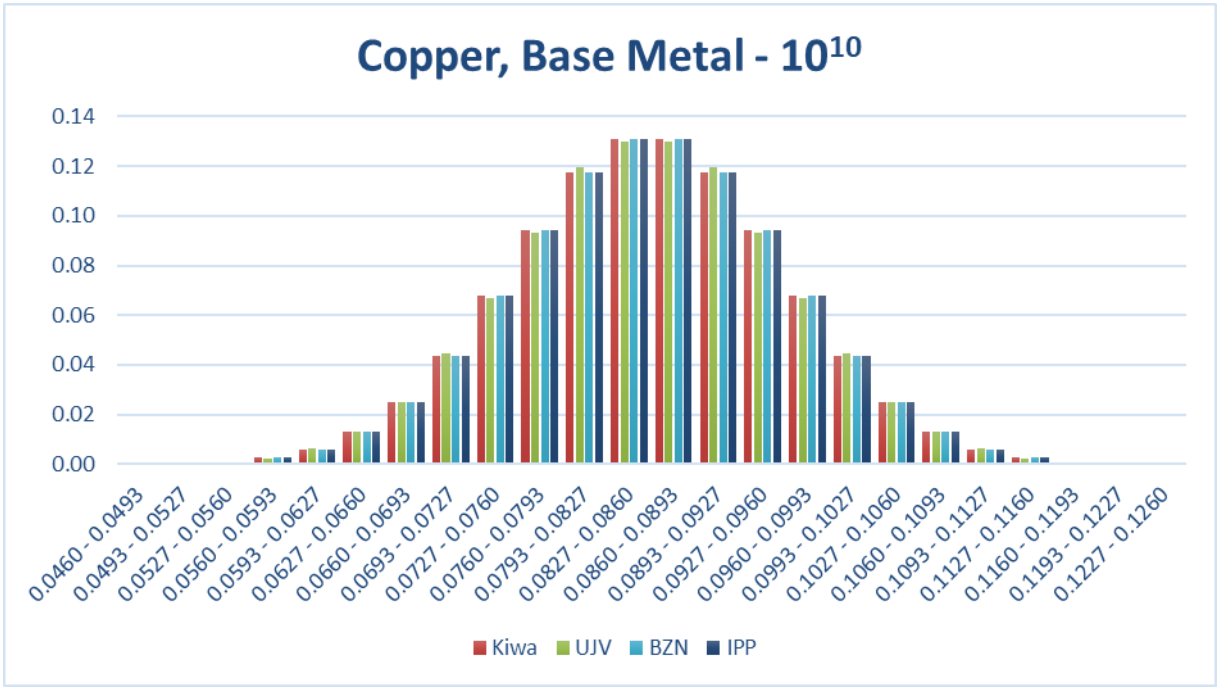

Figure 4.17: Results for truncated distribution for copper in base metal with 10^{10} samples.

Figure 4.18 shows the histograms from BZN and UJV with the distributions for copper in base metal obtained for the full range of requested sample sizes of 10^4-10^{10}. These results show that a convergence is achieved for the sampling sizes of 10^6 and higher.

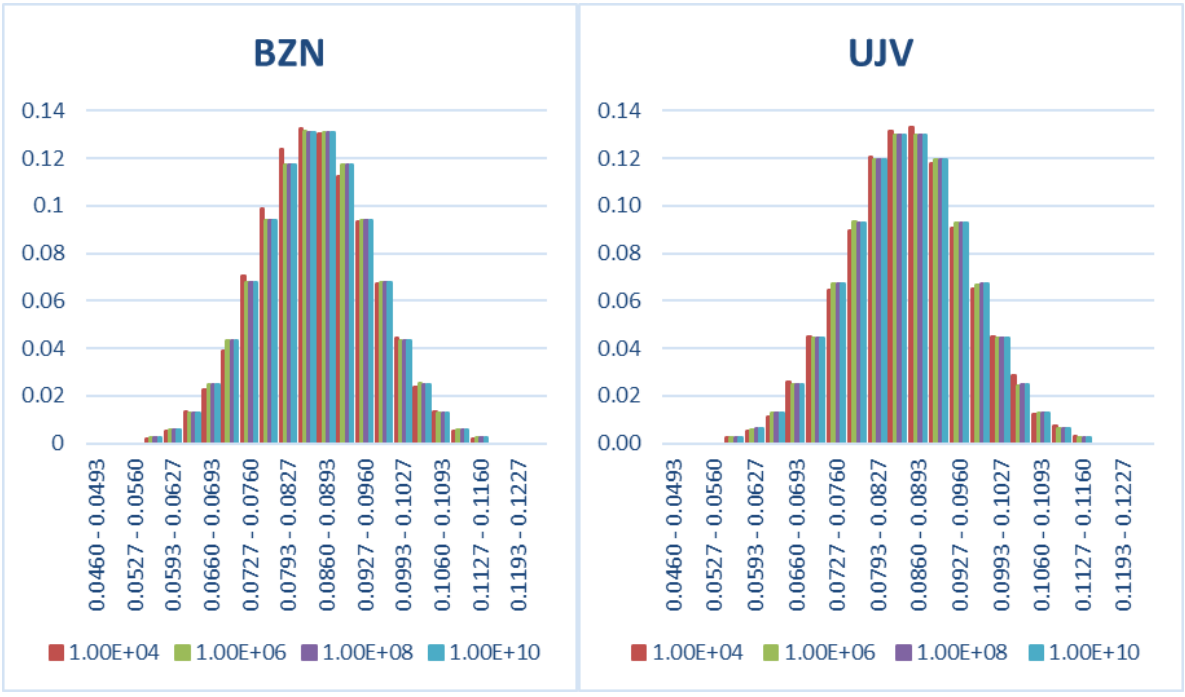

Figure 4.18: Effect of a sampling size on the truncated distribution for copper in base metal.

Based on the comparisons between different sampling sizes and the fact that not all partners that participated within this subtask provided results for sampling sizes higher than 10^6, the results for the other parameters considered are presented for a sampling size of 10^6 only.

The effect of truncation on the distribution of copper for base metal in comparison with untruncated distribution has been investigated using the MCS with 10^8 samples and is shown in Figure 4.19(a). It can be observed that the distribution truncated for ±3SD is almost identical to the untruncated distribution. For amplifying the effect of truncation, a separate simulation of truncation for ±2SD has been performed as presented in Figure 4.19(b).

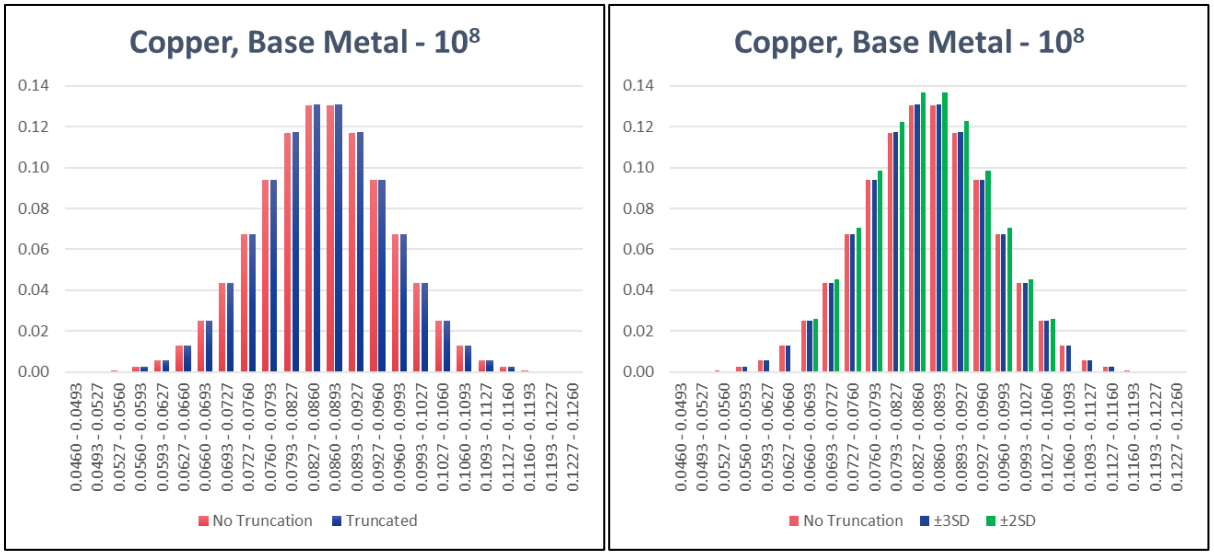

(a) (b)

Figure 4.19: Influence of truncation for a) ±3SD and b) ±2SD in comparison with untruncated distribution for copper in base metal.

4.2.4.3.2 Chemical composition for weld: Copper

Based on the comparison of sampling sizes performed in Section 4.2.4.3.1, results for the copper distribution in welds are only presented for a sampling size of 10^6. Figure 4.20 shows the comparison of the obtained distributions for copper in weld metal between several partners based on the sampling size of 10^4, 10^6 and 10^8. A good agreement among the partners in the sampled distributions can be seen.

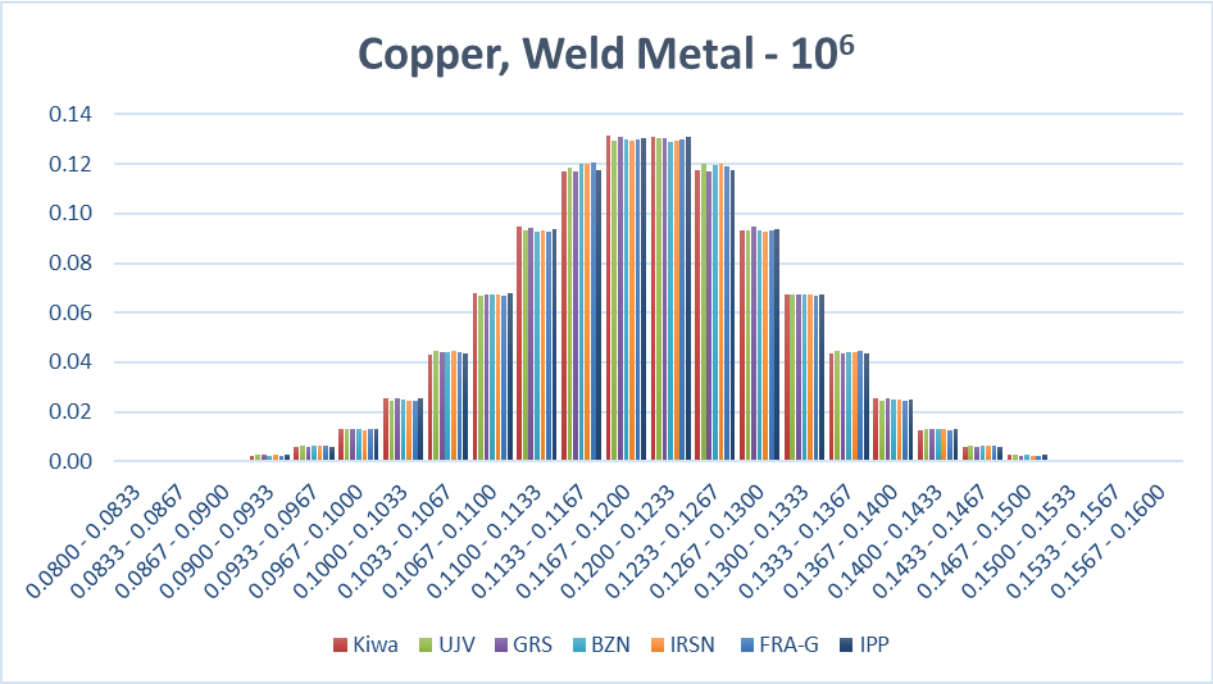

Figure 4.20: Results for truncated distribution for copper in base metal with 10^6 samples.

4.2.4.3.3 Reference temperature transition shift, ΔRT_{NDT} for base metal

The reference temperature shift for the base metal according to Section 2.3.6 where all ingoing parameters are treated probabilistically, with truncations according to the different parts of Section 2, is compared between partners for a sampling size of 10^6 as this was shown as sufficient in Section 4.2.4.3.1. These are shown in Figure 4.21.

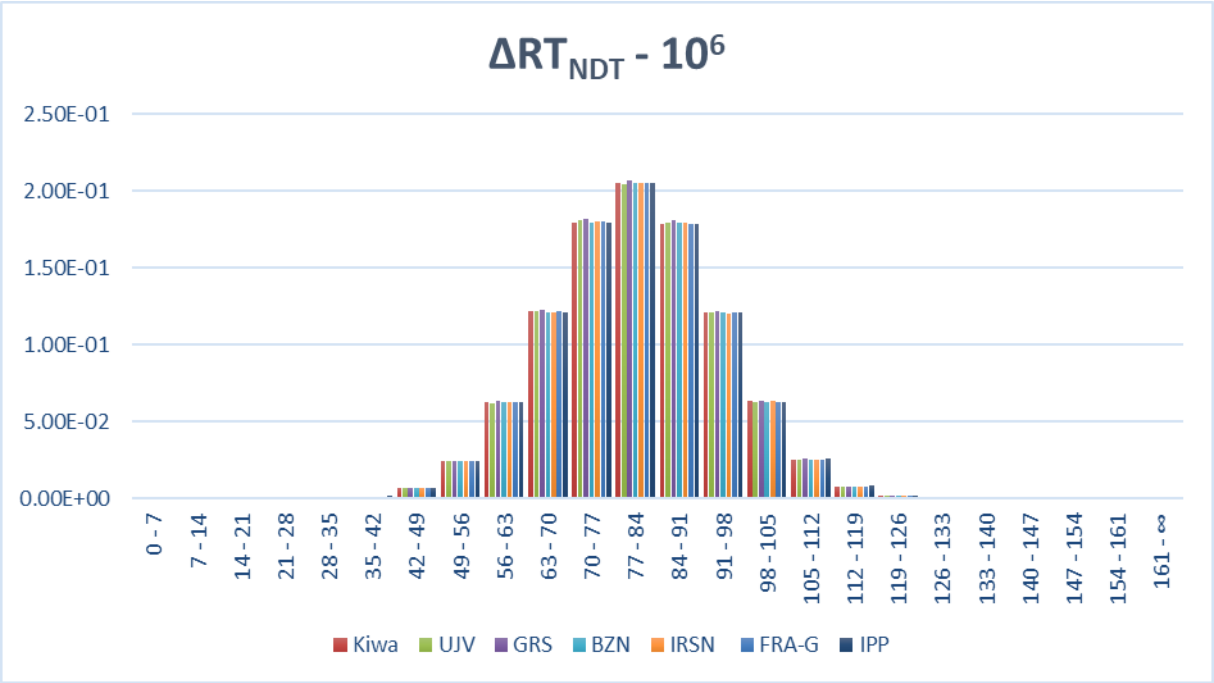

Figure 4.21: Results for truncated distribution for ΔRT_{NDT} in base metal with 10^6 samples.

4.2.4.3.4 Fracture toughness probabilistic and ART deterministic

In this comparison, the fracture toughness is treated probabilistically while ART is considered deterministically using mean values for all ingoing distributed parameters. The calculations are limited to the RT_{NDT} concept.

Results are presented for four different temperatures of 20°C, 50°C, 80°C and 110°C in Figure 4.22 – Figure 4.25 for a sampling size of 10^6. For temperatures above 20°C, the last bin is limited to values above 220 MPa$\sqrt{\text{m}}$ where relevant, in order to limit the results to values relevant for the transition region. For 20°C a limit is set at 110 MPa$\sqrt{\text{m}}$ due to the low fracture toughness results obtained for this temperature.

Figure 4.25 shows that almost all values at a temperature of 110°C are in the upper shelf region. Due to this, the temperature case of 110°C will not be considered in further comparisons within this section.

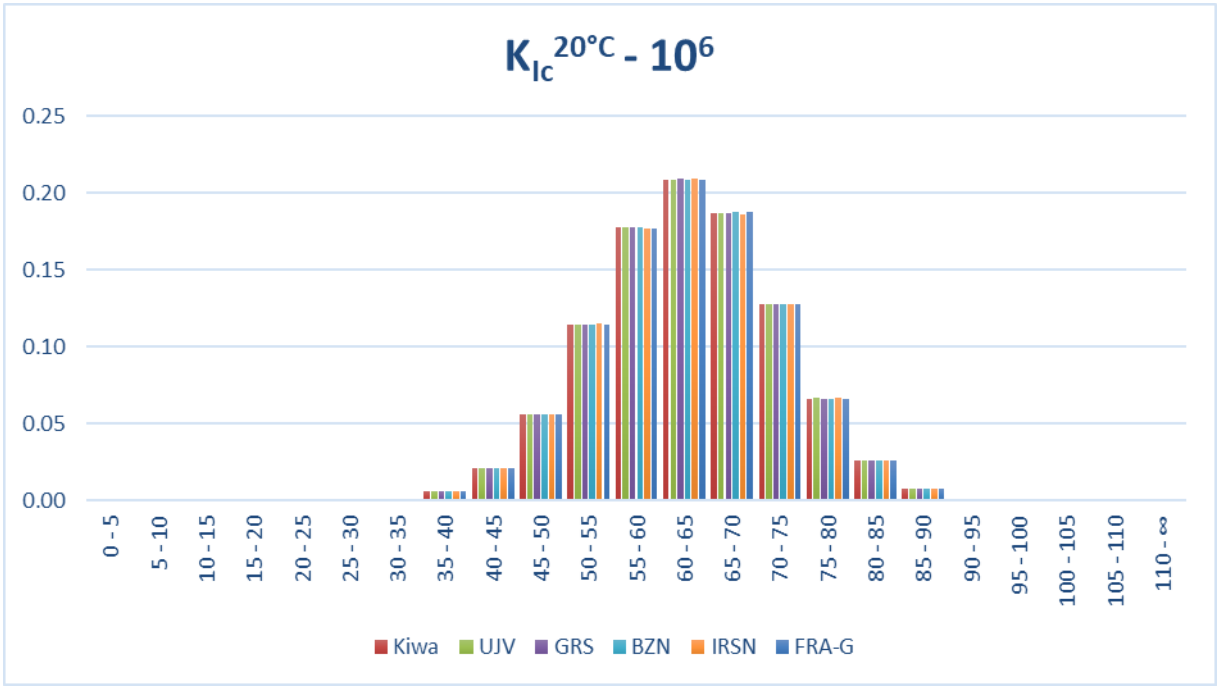

Figure 4.22: Results for truncated distribution for fracture toughness at 20°C with 10^6 samples.

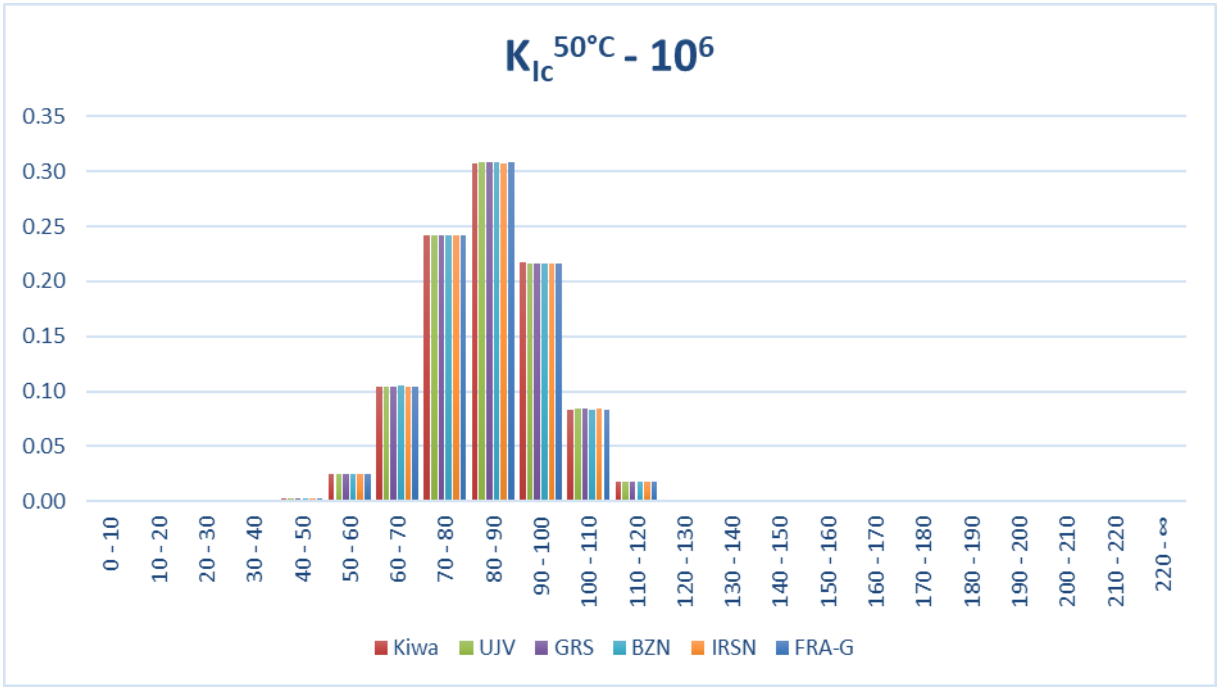

Figure 4.23: Results for truncated distribution for fracture toughness at 50°C with 10^6 samples.

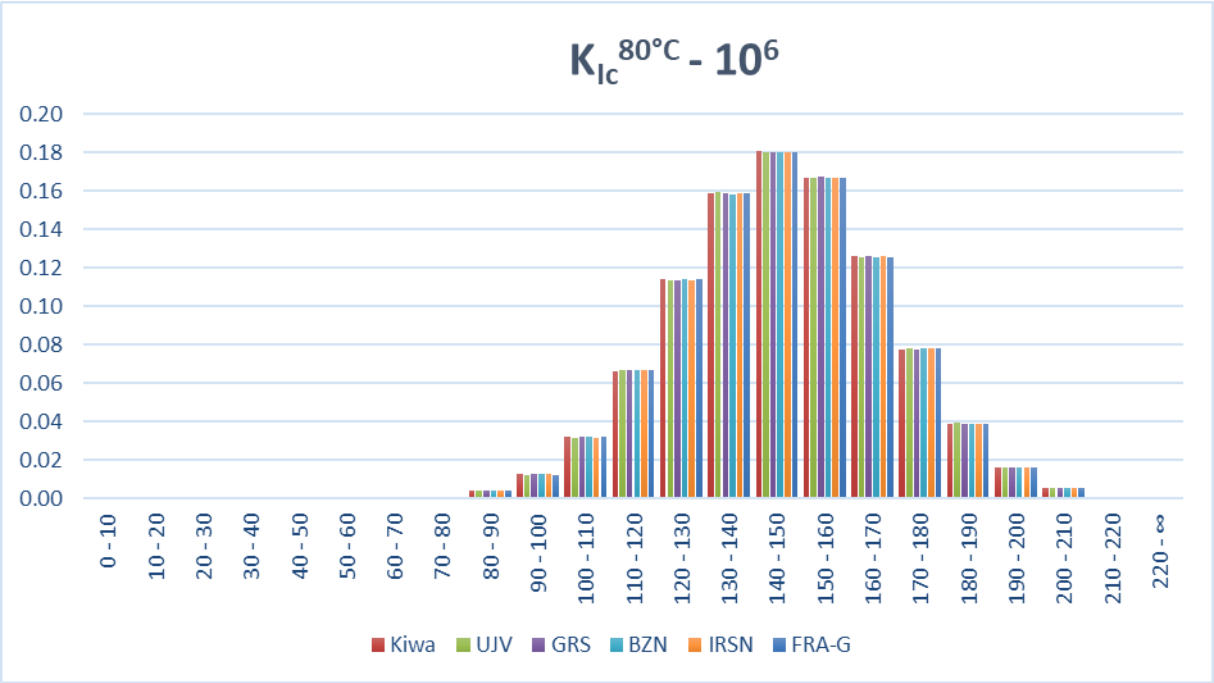

Figure 4.24: Results for truncated distribution for fracture toughness at 80°C with 10^6 samples.

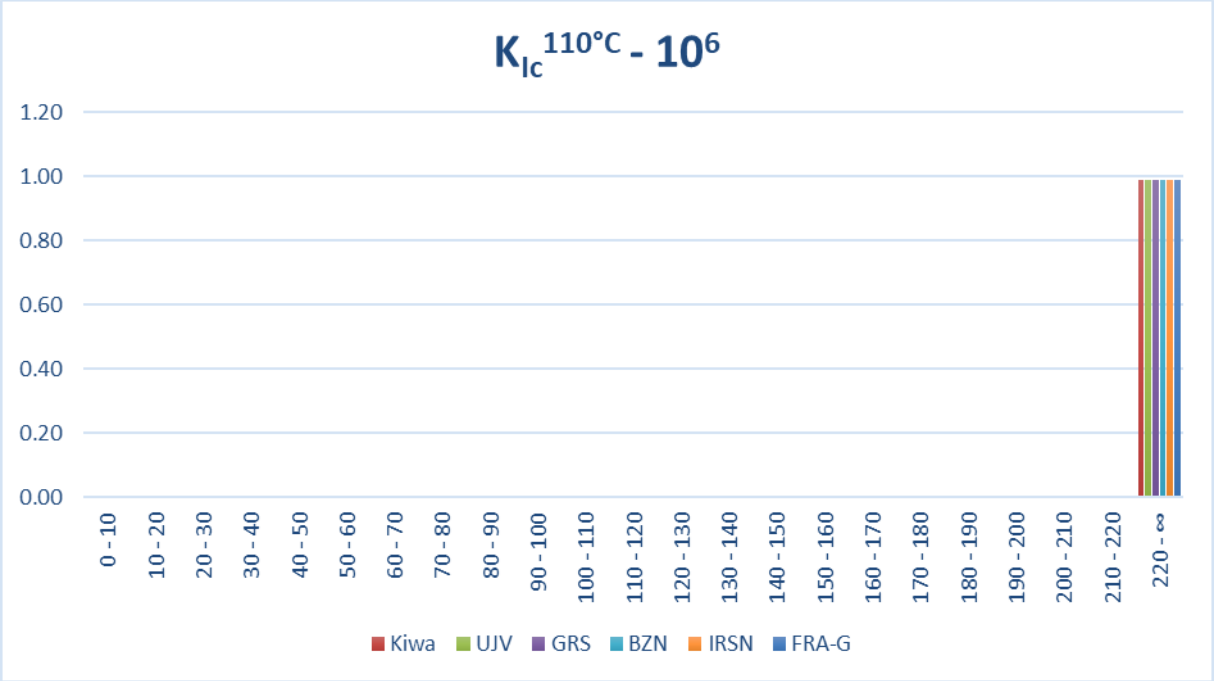

Figure 4.25: Results for truncated distribution for fracture toughness at 110°C with 10^6 samples.

4.2.4.3.5 Fracture toughness deterministic and ART probabilistic

In this comparison, the fracture toughness is treated deterministic using the mean curve, while ART is considered probabilistic where all ingoing parameters are sampled with truncations presented in the different parts of Section 2.

Results are presented for three different temperatures; 20°C, 50°C and 80°C in Figure 4.26 – Figure 4.28 for a sampling size of 10^6. Calculations were made for a temperature of 110°C as well, but as

concluded in Section 4.2.4.3.4, this temperature case is not relevant when studying the transition region.

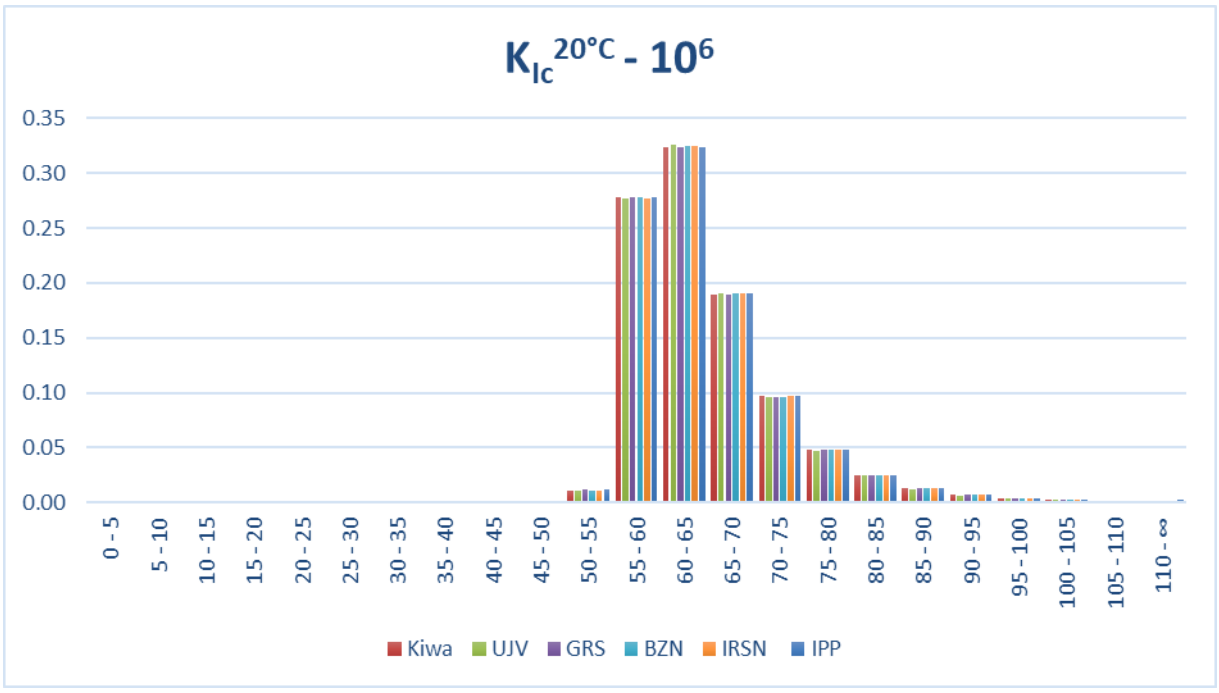

Figure 4.26: Results for fracture toughness with distributed ART at 20°C with 10^6 samples.

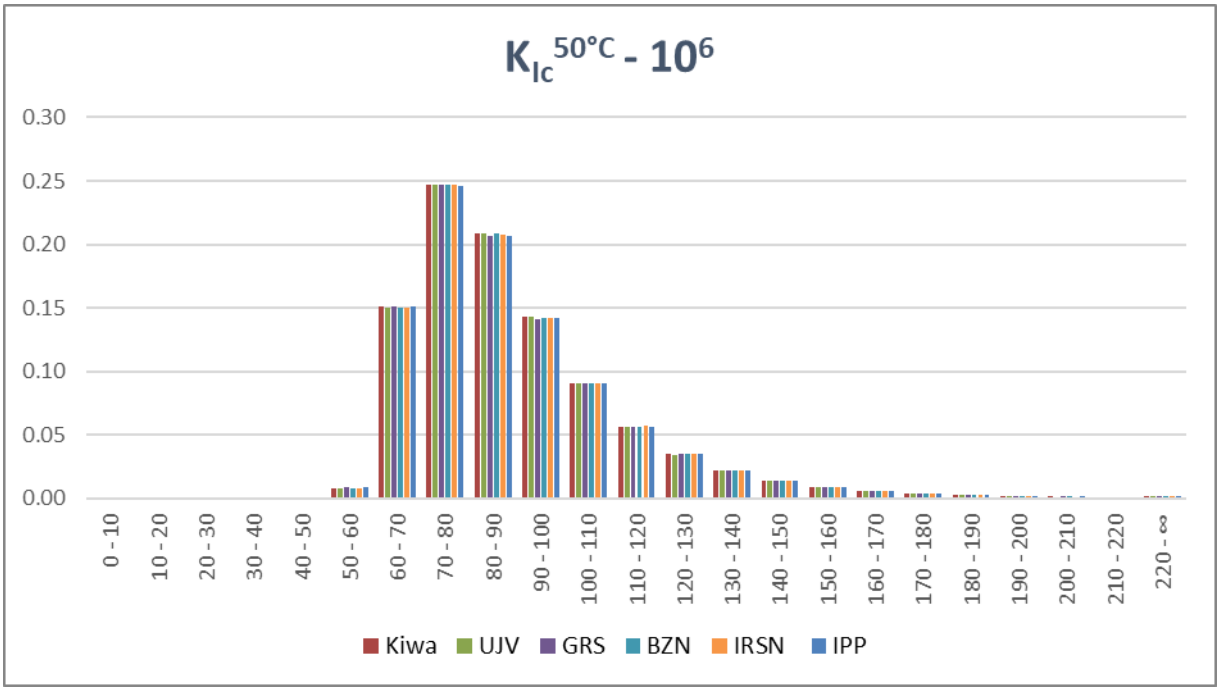

Figure 4.27: Results for fracture toughness with distributed ART at 50°C with 10^6 samples.

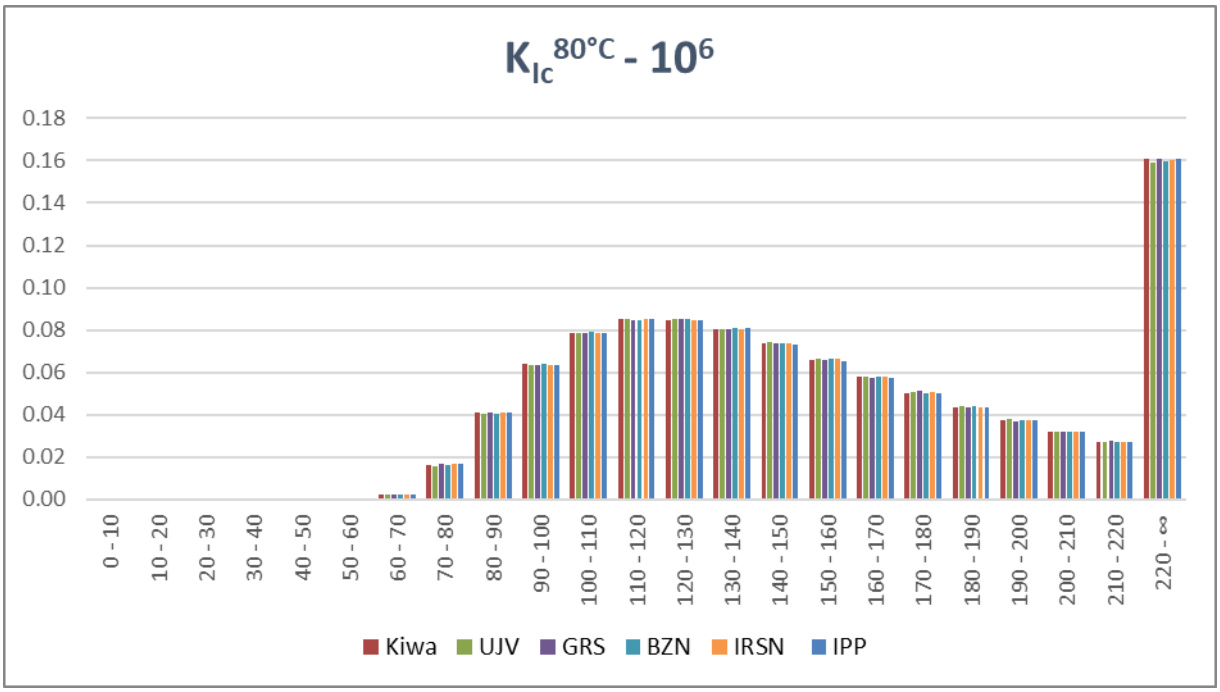

Figure 4.28: Results for fracture toughness with distributed ART at 80°C with 10^6 samples.

4.2.4.3.6 Fracture toughness and ART probabilistic

In this comparison, both the fracture toughness and ART are considered probabilistically. This was not part of the initial definition of the subtask, but was included as a sensitivity study from UJV. FRA-G and Kiwa also analysed this case where all ingoing parameters are considered probabilistic.

Results are presented for three different temperatures; 20°C, 50°C and 80°C in Figure 4.29 – Figure 4.31 for a sampling size of 10^6.

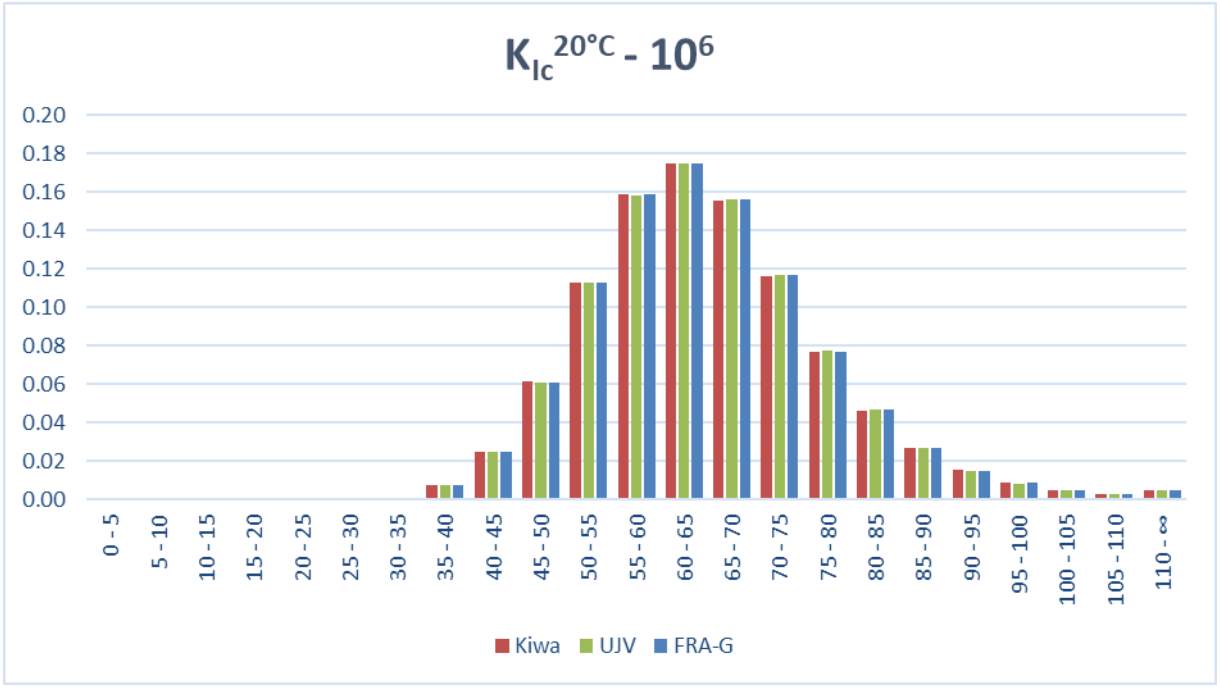

Figure 4.29: Results for fracture toughness with distributed fracture toughness and ART at 20°C with 10^6 samples.

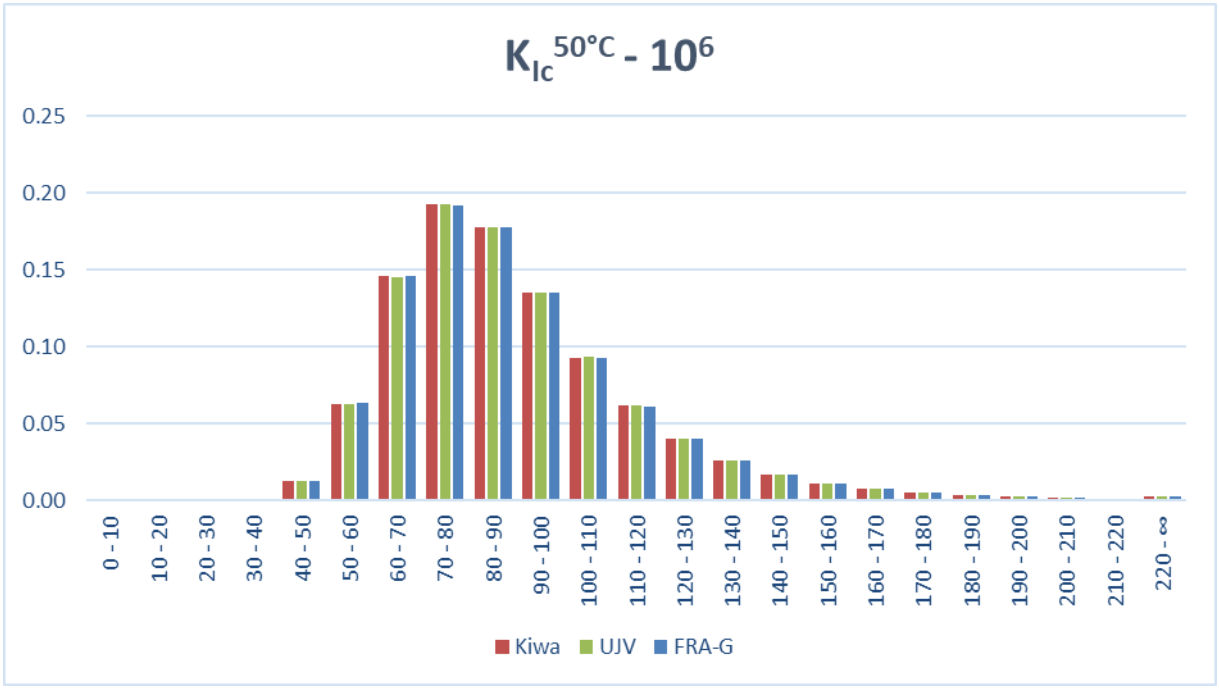

Figure 4.30: Results for fracture toughness with distributed fracture toughness and ART at 50°C with 10^6 samples.

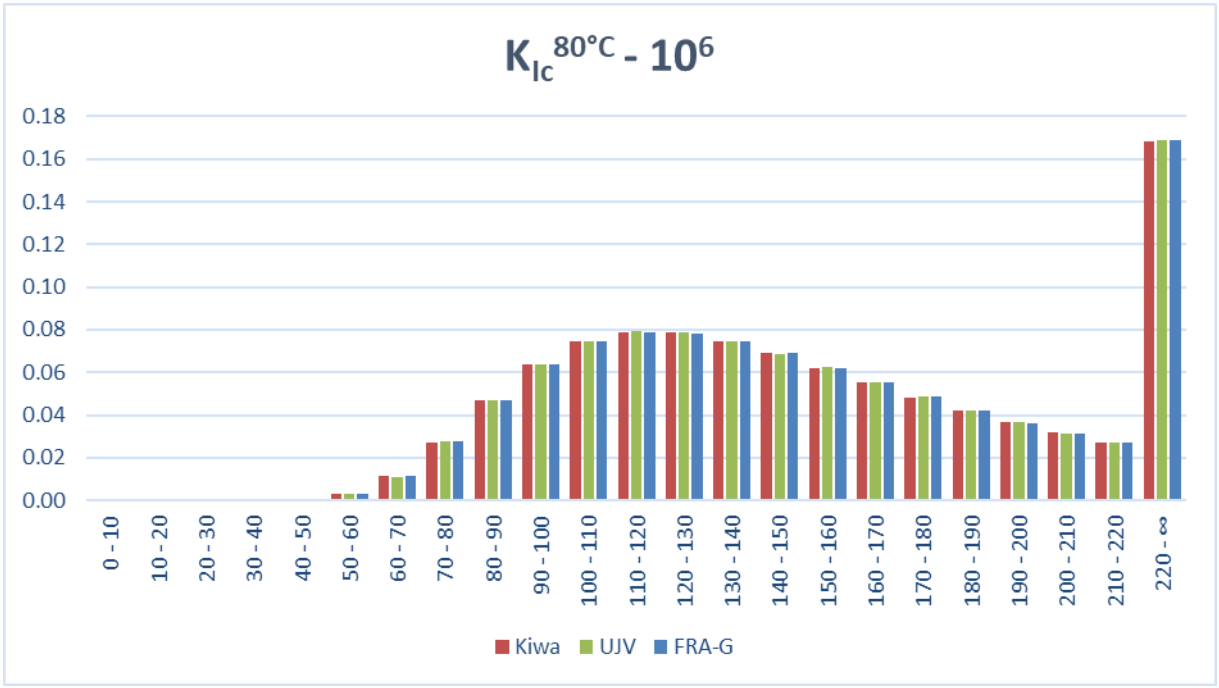

Figure 4.31: Results for fracture toughness with distributed fracture toughness and ART at 80°C with 10^6 samples.

4.2.4.4 Comparison of different methods

The three different cases presented in Section 4.2.4.3.4, 4.2.4.3.5 and 4.2.4.3.6 are compared in the following section. These are denoted; K_{Ic}*-Prob*, *ART-Prob* and *Both-Prob* respectively.

Comparisons between the cases are shown in form of histograms in Figure 4.32 – Figure 4.34 and the probability as a function of fracture toughness, K_{Ic}, are shown in Figure 4.35 – Figure 4.37.

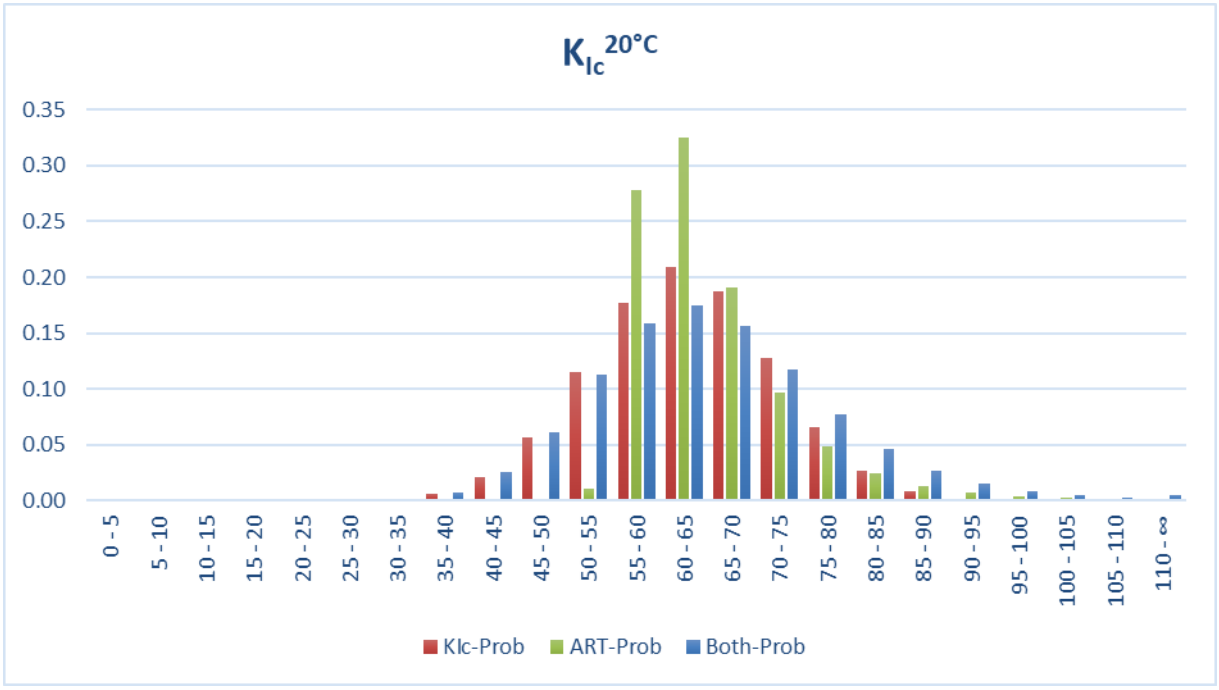

Figure 4.32: Comparison of the three different cases at 20°C.

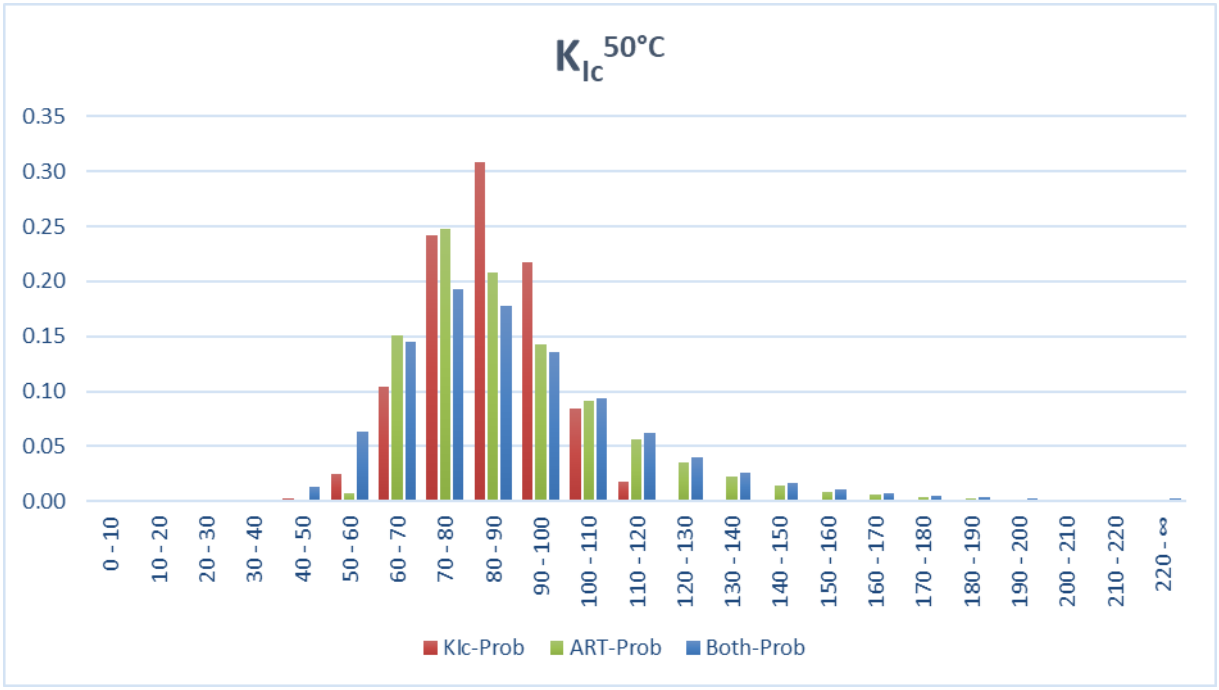

Figure 4.33: Comparison of the three different cases at 50°C.

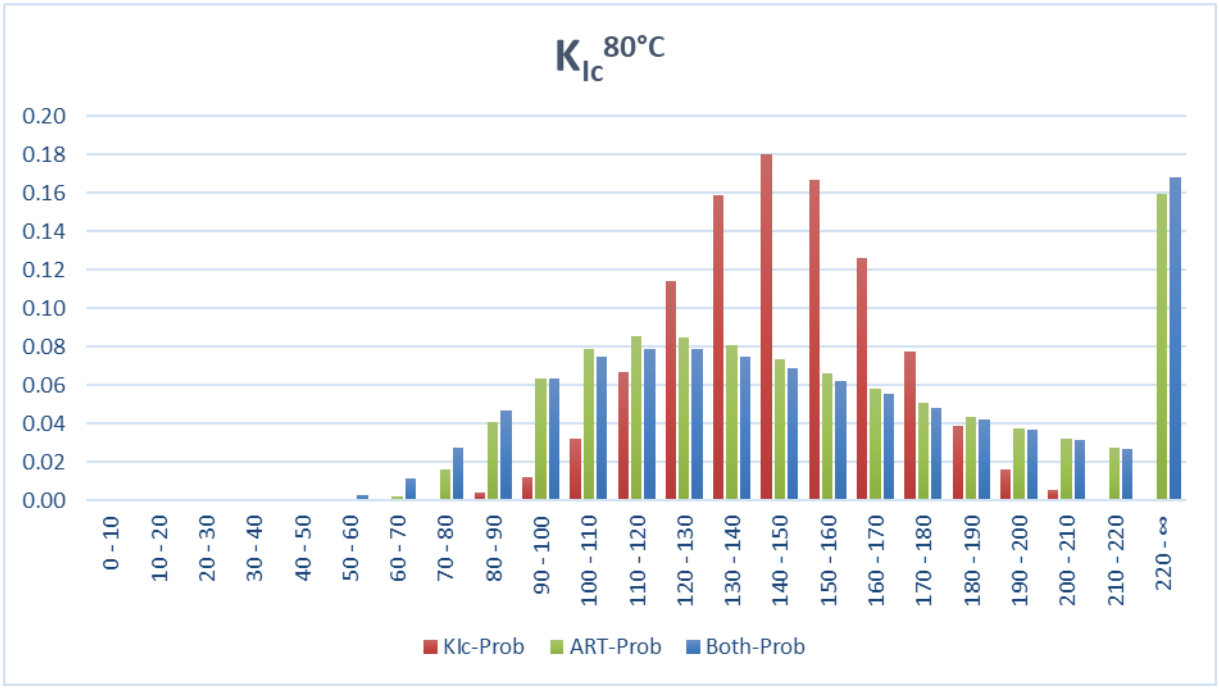

Figure 4.34: Comparison of the three different cases at 80°C.

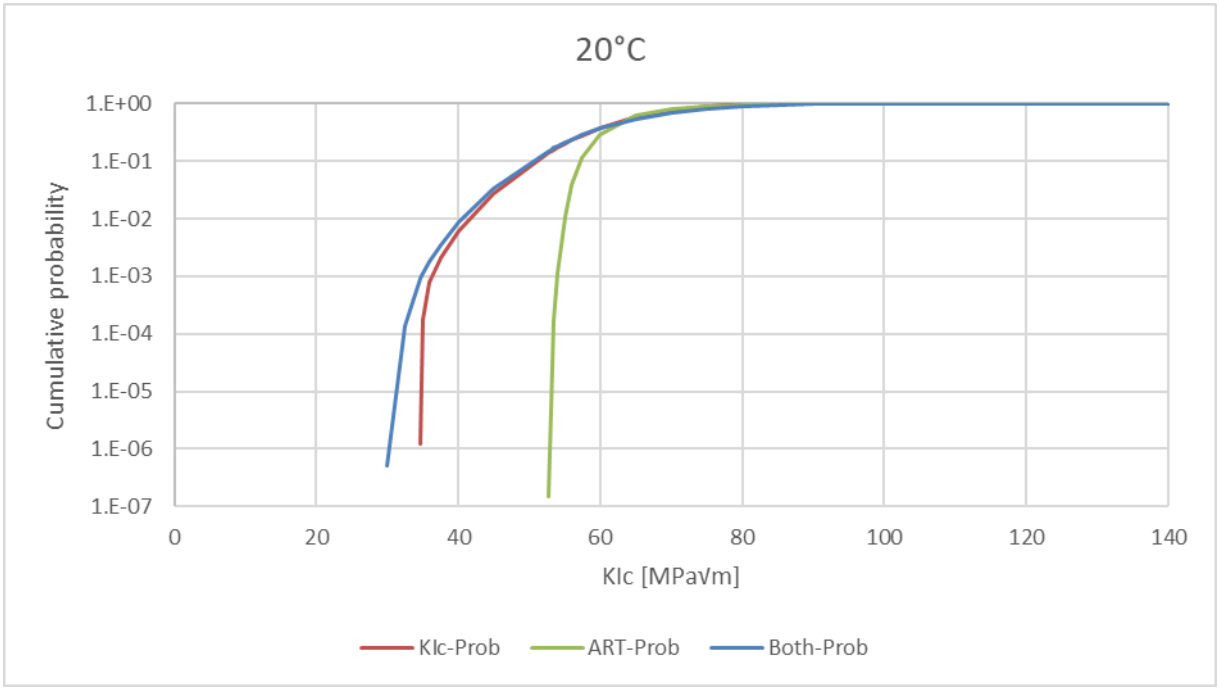

Figure 4.35: Comparison of probability as a function of stress intensity factor for the three different cases at 20°C.

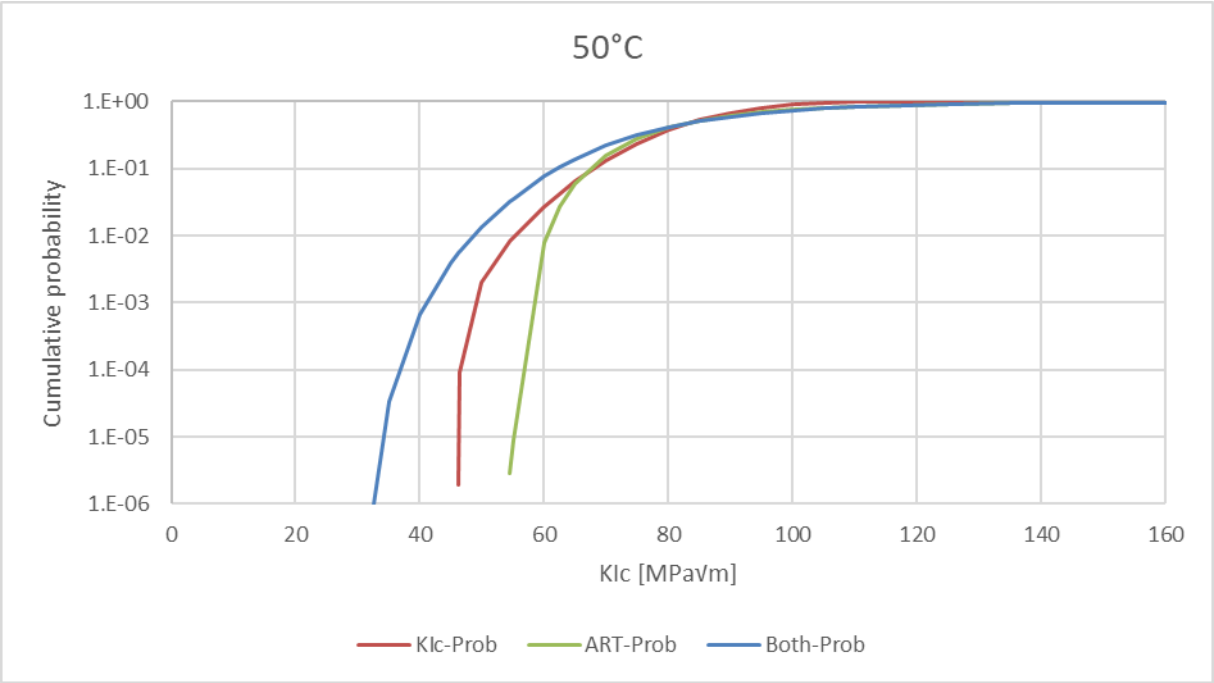

Figure 4.36: Comparison of probability as a function of stress intensity factor for the three different cases at 50°C.

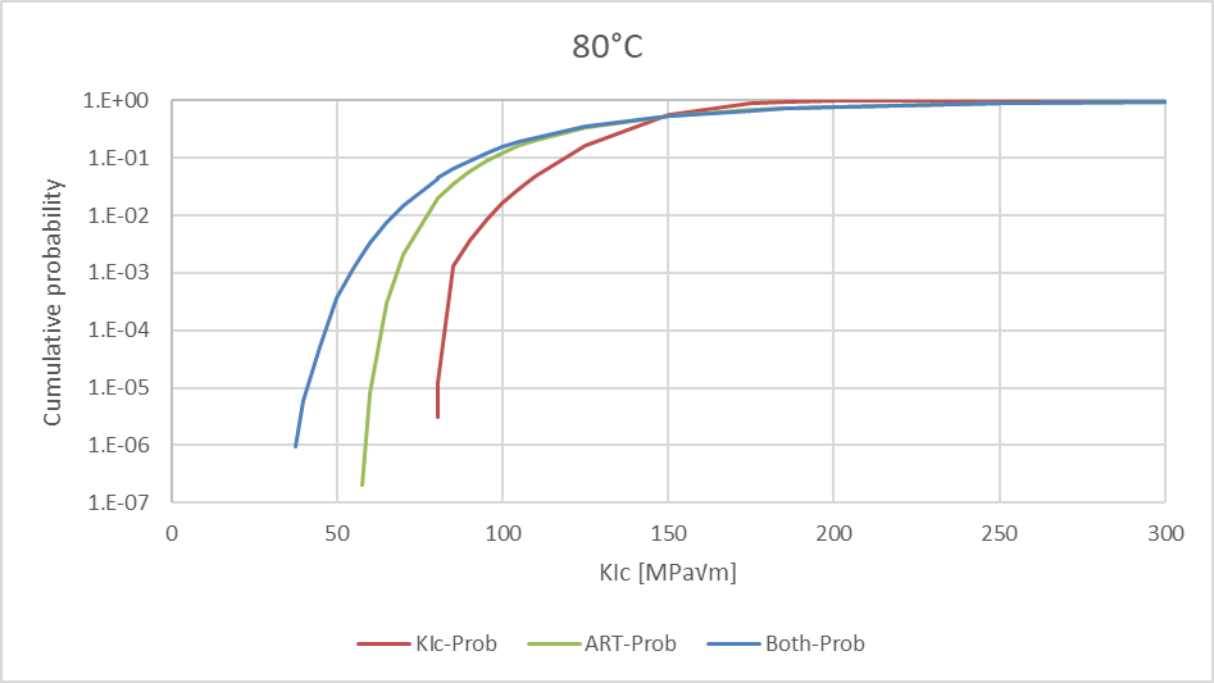

Figure 4.37: Comparison of probability as a function of stress intensity factor for the three different cases at 80°C.

It is seen that cases differs significantly for all temperatures studied where considering both the fracture toughness and ART probabilistically is for all temperatures limiting at lower K_{Ic}-values.

It is seen that probabilities differ significantly between the three cases studied. For most parts except when probabilities are very high, the limiting case is when both fracture toughness and ART are treated probabilistically.

4.2.4.5 Conclusions from truncation study

The difference in results between partners are very small in all cases studied and an effect of different methods used for truncation is hard to notice in the comparison. The conclusion from this comparison is that the truncation methods considered by the partners are sufficient and do not influence the final results.

4.2.5 Check CPI for provided T, K_I and ART

The objective of this subtask was to verify the results from all partners by analysing a pre-defined transient over the time, t, and calculating the conditional probability of initiation (CPI) and instantaneous conditional probability of initiation cpi(t) for a given ART and given transient data in the form of pre-defined stress intensity factors $K_I(t)$ and temperatures at the crack tip, $T(t)$. Only fracture toughness was considered as the distributed parameter. Two cracks in different regions were considered; an inside plume circumferential TCC and an outside plume axial UCC.

Analyses were performed for two limit conditions, namely the Tangent approach and the maximum WPS approach, as described in Section 2.3.9.

Both the RT_{NDT} as well as the T_0 fracture toughness concepts were analysed, the FAVOR fracture toughness concept was additionally used by the FAVOR users. All these concepts are described in Section 2.3.4.

The pre-defined arbitrary chosen ART-values used for the analyses in this subtask are presented in Table 4.5.

Table 4.5 Selected pre-defined ART-values for CPI-calculation

Crack Type	RT_{NDT} [°C]	T_0 [°C]
TCC	105	85
UCC	170	150

All partners contributed with results to this subtask. The FAVOR-partners Tecnatom, JSI and PSI used in house codes. Tecnatom and JSI performed additional analyses with the APAL specific version of FAVOR called CAPAL [24]. IRSN did not participate in analyses involving the WPS approach and have only provided results for the Tangent approach.

The calculated CPI values for the circumferential TCC inside plume and for the axial UCC outside plume are presented in Table 4.6 and Table 4.7, respectively. A very good agreement in calculated CPI values can be seen between all partners.

Table 4.6 Calculated CPI for a circumferential TCC crack inside plume

Partner	RT_{NDT}		T_0	
	Tangent Approach	Max WPS Approach	Tangent Approach	Max WPS Approach
Kiwa	9.933E-01	7.169E-03	7.308E-01	1.873E-02
UJV	9.933E-01	7.168E-03	7.308E-01	1.873E-02
GRS	9.933E-01	7.171E-03	7.308E-01	1.873E-02
BZN	9.933E-01	7.166E-03	7.309E-01	1.873E-02
IRSN	9.932E-01	-	7.308E-01	-
FRA-G	9.932E-01	7.236E-03	7.315E-01	1.772E-02
Tecnatom	9.933E-01	7.168E-03	7.308E-01	1.873E-02
JSI	9.933E-01	7.168E-03	7.308E-01	1.873E-02
PSI	9.933E-01	7.167E-03	7.308E-01	1.873E-02
IPP	9.933E-01	7.195E-03	7.307E-01	1.876E-02

Table 4.7 Calculated CPI for an axial UCC crack outside plume

Partner	RT_{NDT}		T_0	
	Tangent	Max WPS	Tangent	Max WPS
Kiwa	2.114E-01	1.647E-02	2.140E-01	9.217E-03
UJV	2.114E-01	1.647E-02	2.140E-01	9.217E-03
GRS	2.114E-01	1.647E-02	2.140E-01	9.217E-03
BZN	2.113E-01	1.654E-02	2.142E-01	9.228E-03
IRSN	2.112E-01	-	2.140E-01	-
FRA-G	2.121E-01	1.777E-02	2.140E-01	9.217E-03
Tecnatom	2.114E-01	1.647E-02	2.140E-01	9.217E-03
JSI	2.114E-01	1.647E-02	2.140E-01	9.217E-03
PSI	2.114E-01	1.647E-02	2.140E-01	2.140E-01
IPP	2.110E-01	1.644E-02	2.140E-01	9.240E-03

The minor deviations observed in the results between the partners can be explained by different sampling sizes. The results for the T_0 concept by Kiwa, GRS, IRSN and Tecnatom are in perfect agreement as this case has been solved analytically. FRA-G solved it both analytically and using Monte Carlo simulations, the result presented for FRA-G is from their MCS using a sampling size of 10^6. GRS solved the RT_{NDT} concept analytically as well.

Tecnatom and JSI additionally calculated the T_0 concept using CAPAL and CPI values are presented in Table 4.8. Values obtained by Tecnatom are in perfect agreement with the values presented in Table 4.6 and Table 4.7 while results from JSI deviates very slightly with less than 1%.

Table 4.8 Calculated CPI using CAPAL to calculate the T_0 concept.

Partner	TCC		UCC	
	Tangent	Max WPS	Tangent	Max WPS
Tecnatom	7.308E-01	1.873E-02	2.140E-01	9.217E-03
JSI	7.288E-01	1.864E-02	2.125E-01	9.159E-03

Results for the FAVOR concept are presented in Table 4.9 both calculated using In-house codes and CAPAL. The results are in very good comparison and differs less than 1%.

Table 4.9 Calculated CPI using the FAVOR concept.

Partner	Method	TCC		UCC	
		Tangent	Max WPS	Tangent	Max WPS
Tecnatom	In-House	9.258E-01	3.530E-02		
	CAPAL	9.259E-01	3.532E-02	1.58E-01	2.19E-02
JSI	In-House	9.247E-01	3.498E-02	1.570E-01	2.176E-02
	CAPAL	9.247E-01	3.499E-02	1.570E-01	2.176E-02
PSI	In-House	9.259E-01	3.532E-02	1.582E-01	2.196E-02

The cpi(*t*) is also in good agreement between the partners as shown in Figure 4.38 – Figure 4.41 which shows both the RT_{NDT} and T_0 concepts using tangent and max WPS approaches for the TCC. The cpi(*t*) results for the UCC are in equally good agreement.

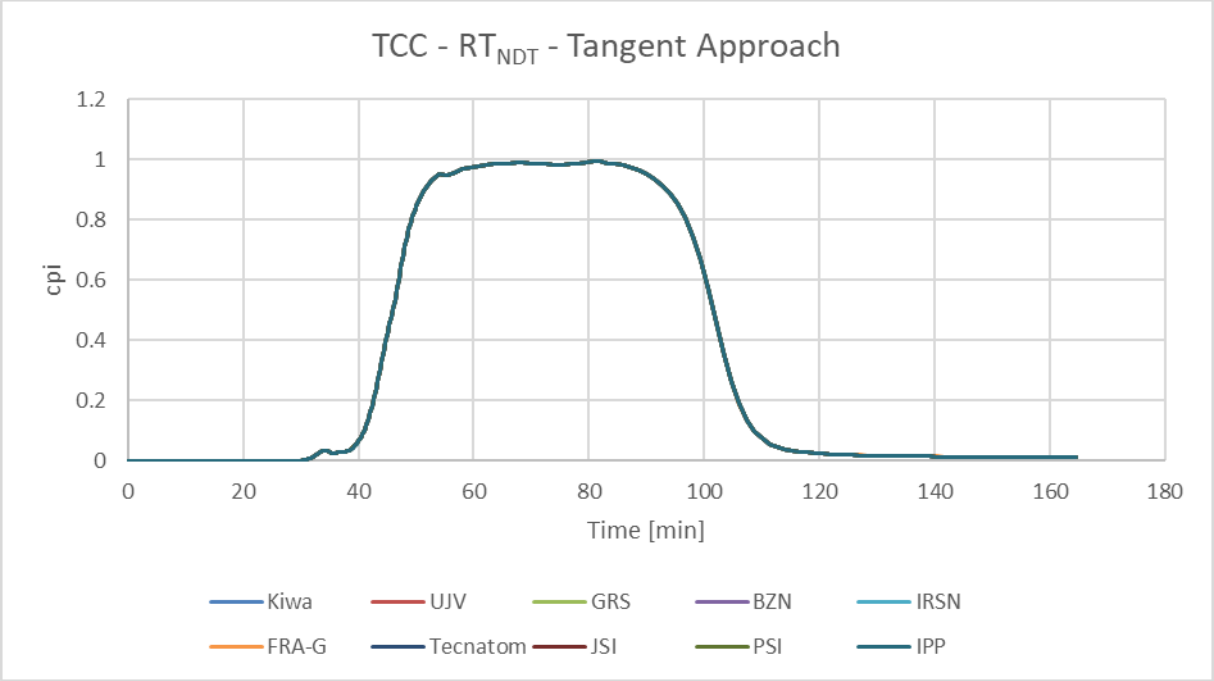

Figure 4.38: Instantaneous cpi(t) TCC using the tangent approach for the RT_{NDT} concept. GRS results are not plotted as GRS did not provide instantaneous cpi-values.

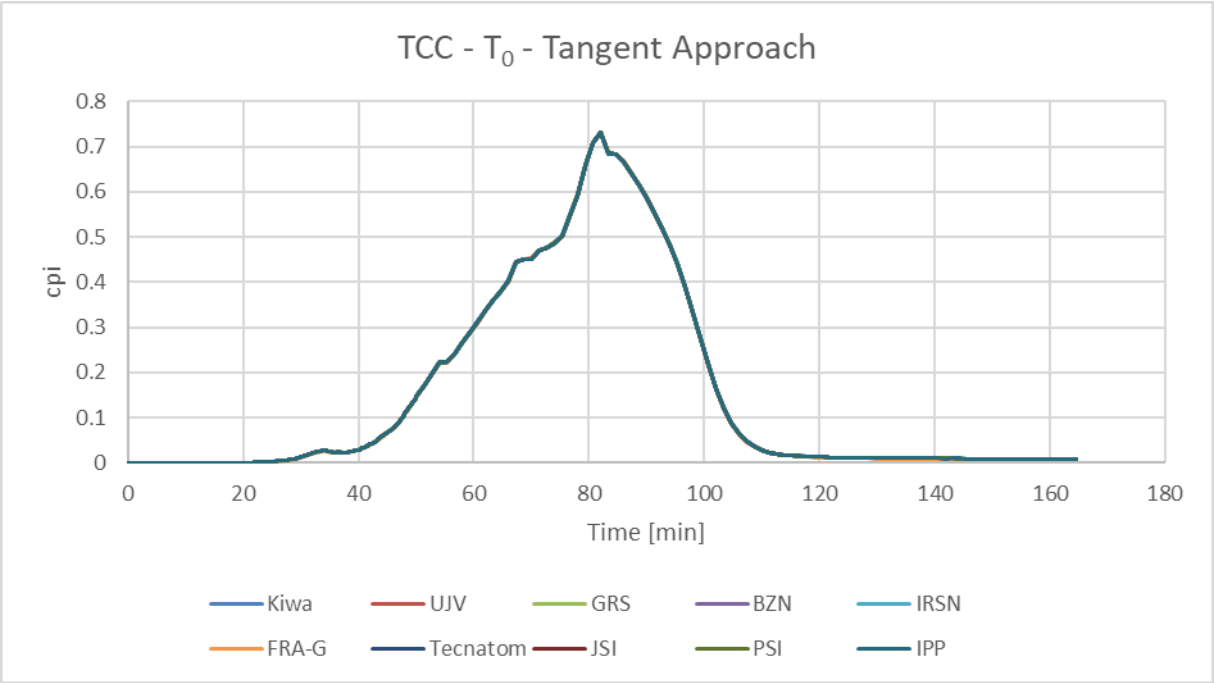

Figure 4.39: Instantaneous cpi(t) TCC using the tangent approach for the T_0 concept. GRS results are not plotted as GRS did not provide instantaneous cpi-values.

Some slight deviances can be seen for FRA-G for the T_0 max WPS analysis. This has been concluded to be due to the limited sampling size of 10^6.

One thing to note when comparing cpi(t) for the max WPS approach, Figure 4.40 and Figure 4.41, is that BZN, JSI and PSI (for the RT_{NDT} concept) have included all values up to the time when maximum K_I is reached, while all others have considered the historically maximum K_I value for each time step. This can be seen by the cpi(t) values drop to zero during times when K_I is lower than it has previously been during the transient. This is of little consequence for the final CPI value as this will always be controlled by the maximum K_I value throughout the full transient.

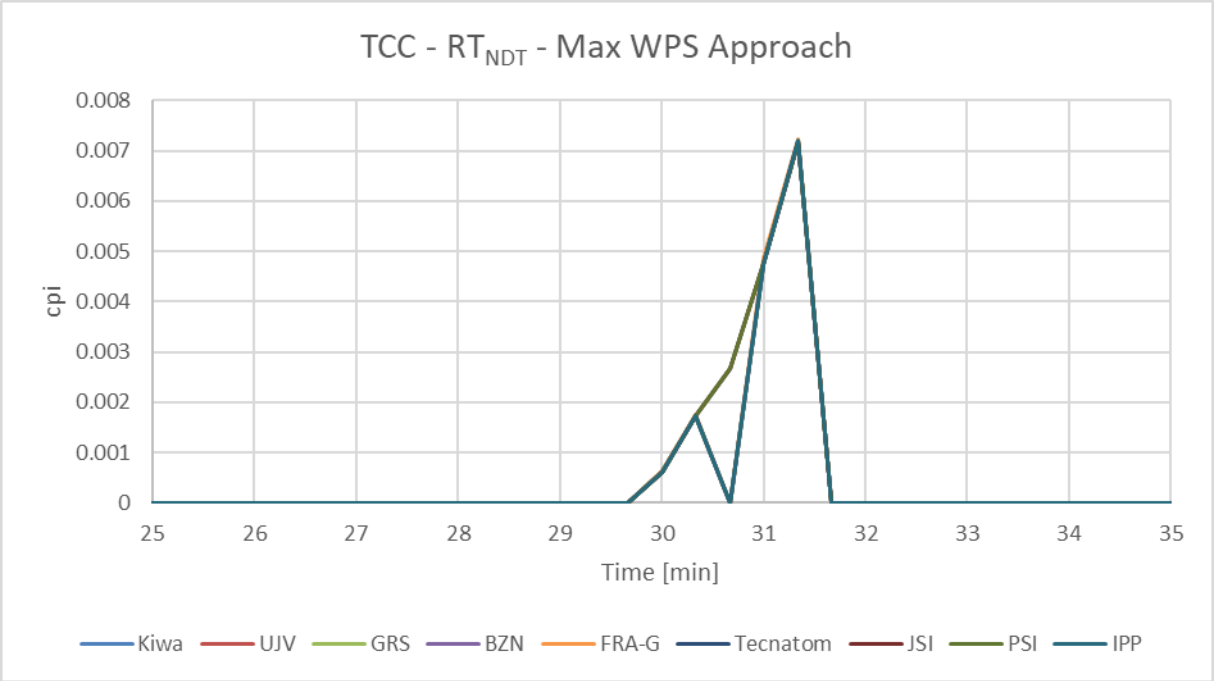

Figure 4.40: Instantaneous cpi(t) TCC using the max WPS approach for the RT_{NDT} concept. The plot is limited to times of interest. GRS results are not plotted as GRS did not provide instantaneous cpi-values.

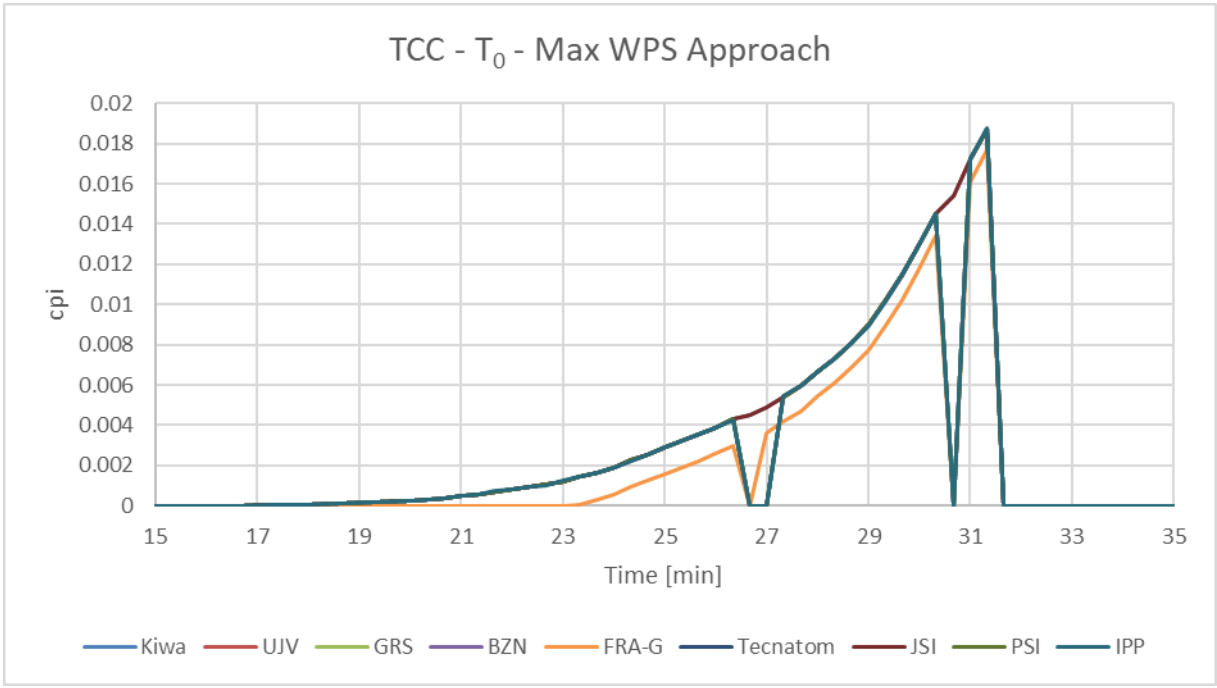

Figure 4.41: Instantaneous cpi(t) TCC using the max WPS approach for the T_0 concept. The plot is limited to times of interest. GRS results are not plotted as GRS did not provide instantaneous cpi-values.

Three different fracture toughness concepts for treating the transition region and distribution of K_{Ic} are compared in Figure 4.42 and Figure 4.43 for the TCC and UCC respectively. It is important to note that the pre-defined ART-values do not necessarily correlate between the RT_{NDT} and T_0 concepts. What may be interesting to note is that the different concepts result in very different shapes of the cpi(t) curves, especially for the UCC where it can be seen that the RT_{NDT} and T_0 concepts result in similar final CPI values, but these occur at completely different times through the transient. The FAVOR concept results in a lower final CPI value which is reached at yet another time during the transient.

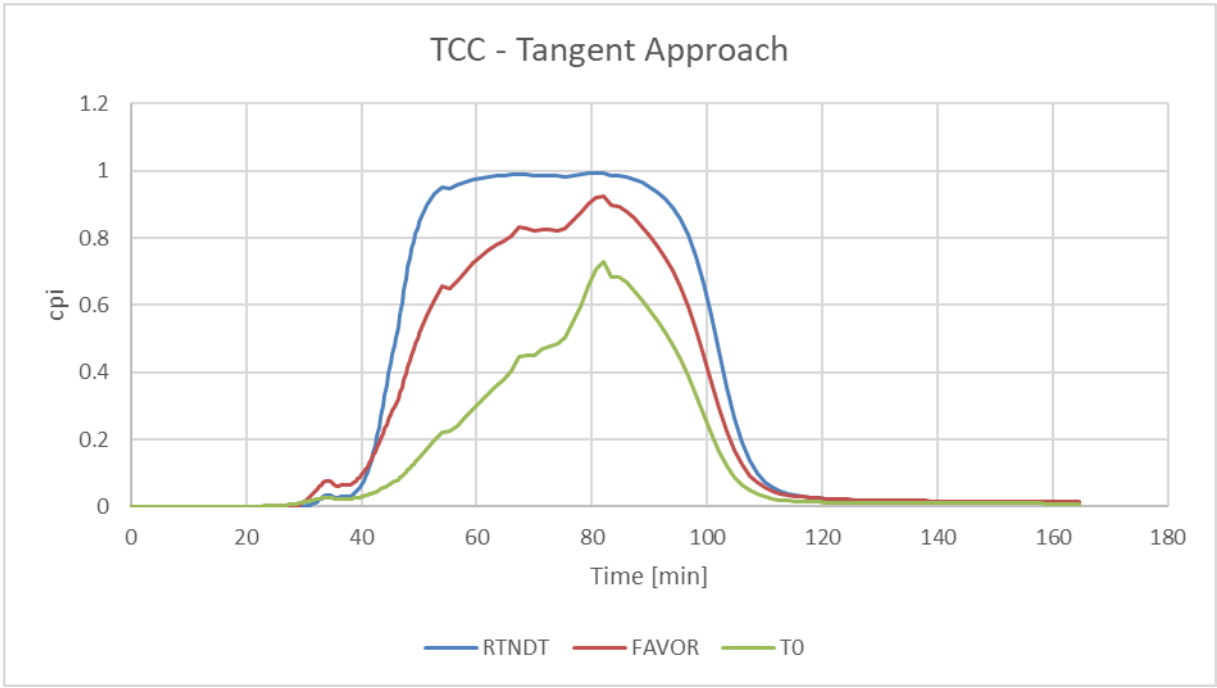

Figure 4.42: Comparison of cpi(t) for a TCC using the tangent approach for the RT_{NDT}, FAVOR and T_0 concepts.

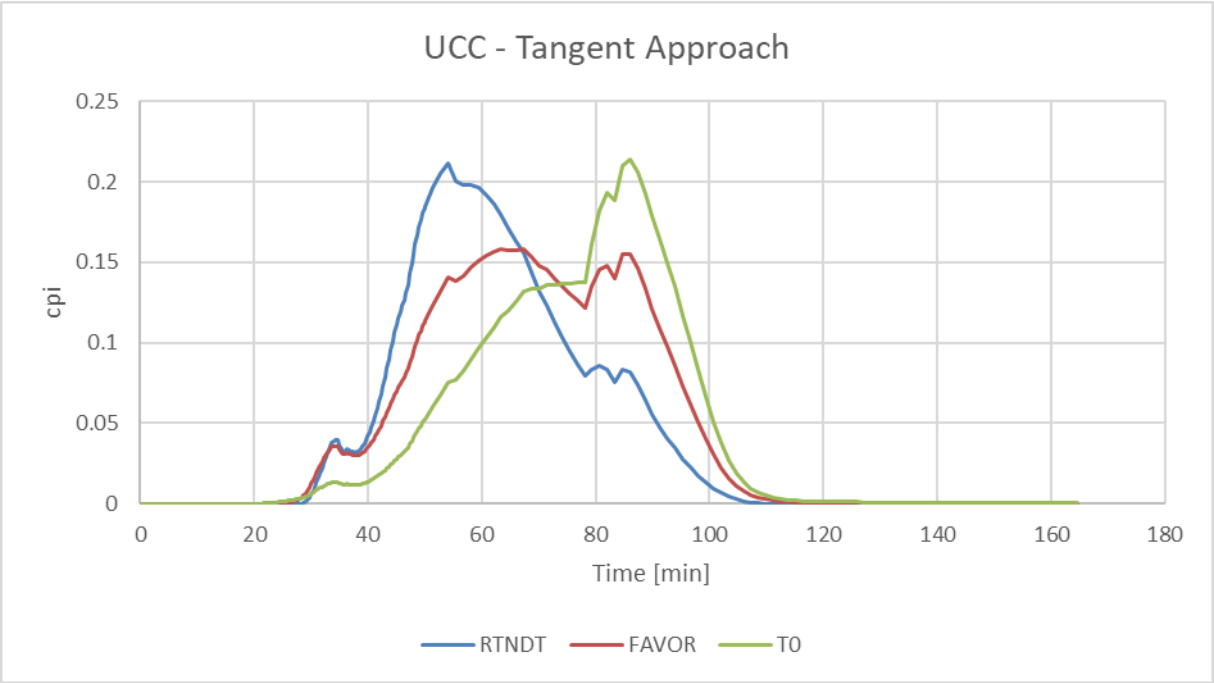

Figure 4.43: Comparison of cpi(t) for a UCC using the tangent approach for the RT_{NDT}, FAVOR and T_0 concepts.

JSI made a sensitivity study using the different WPS approaches implemented in CAPAL [24]. The following WPS approaches described in detail in Section 2.3.9 have been considered:

1. WPS1: Baseline WPS (Max WPS) Approach (mandatory in APAL)
2. WPS2: Conservative WPS Approach (non-mandatory)
3. WPS3: Best Estimate WPS Approach (non-mandatory)

The results for different WPS approaches in terms of calculated CPI-values for circumferential TCC and axial UCC cracks are summarised in Table 4.10. The results from the Tangent approach evaluated using the CAPAL code are also included in the table for comparison.

Table 4.10 Comparison of calculated CPI values from different WPS methods.

Tangent and WPS approaches evaluated by JSI using CAPAL	Calculated CPI			
	TCC circumferential (inside plume)		UCC axial (outside plume)	
	RT_{NDT}	T_0	RT_{NDT}	T_0
Tangent	9.25E-01	7.29E-01	1.57E-01	2.13E-01
WPS1 (Max WPS)	3.499E-02	1.864E-02	2.18E-02	9.16E-03
WPS2 (Conservative)	9.012E-01	6.553E-01	1.54E-01	2.09E-01
WPS3 (Best-estimate)	1.744E-06	4.289E-03	9.73E-04	2.15E-03

It was shown that the CPI-values calculated by max WPS approach (WPS1) are about 1-2 orders of magnitude lower in comparison with the Tangent approach. The Conservative (WPS2) approach predicts the CPI-values similar to the Tangent approach. This result is feasible as the term $\alpha = 0$ in the WPS2 approach definition eliminates the Condition 3 for a crack initiation stating that $K_I(t) \geq \alpha \cdot K_{I(max)}(t)$, see Section 2.3.9 and Table 2.8 for further details. Thus, in some meaning the Conservative WPS2 approach is equivalent to the Tangent approach. The Best-estimate (WPS3) approach with randomly sampled parameter α provides the lowest CPI-values among all evaluated approaches.

Instantaneous cpi(t) for different WPS and Tangent approaches evaluated using the RT_{NDT} and MC T_0 fracture toughness concepts are presented in Figure 4.44-Figure 4.47.

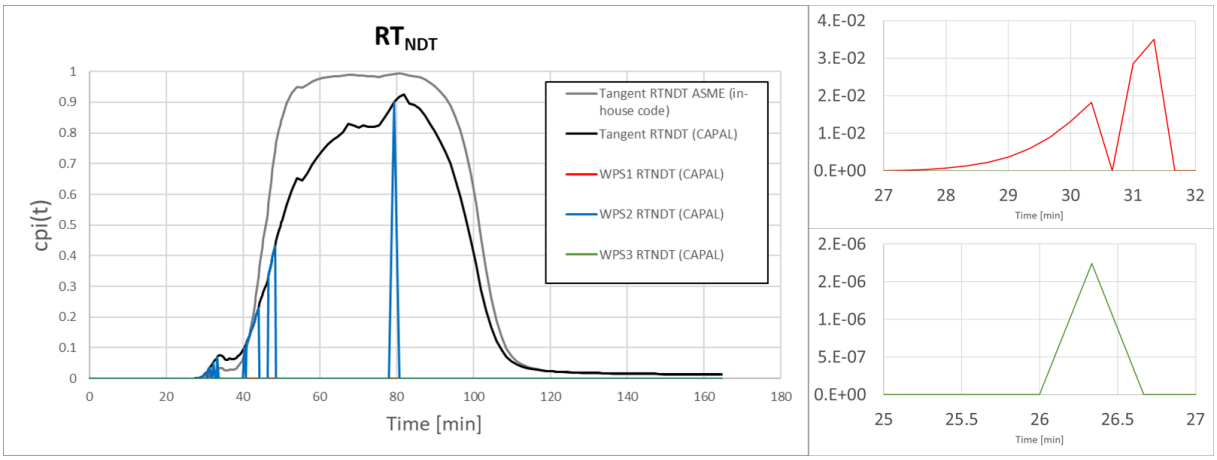

Figure 4.44: Comparison of cpi(t) from different WPS approaches for a circumferential TCC using the RT_{NDT} concept.

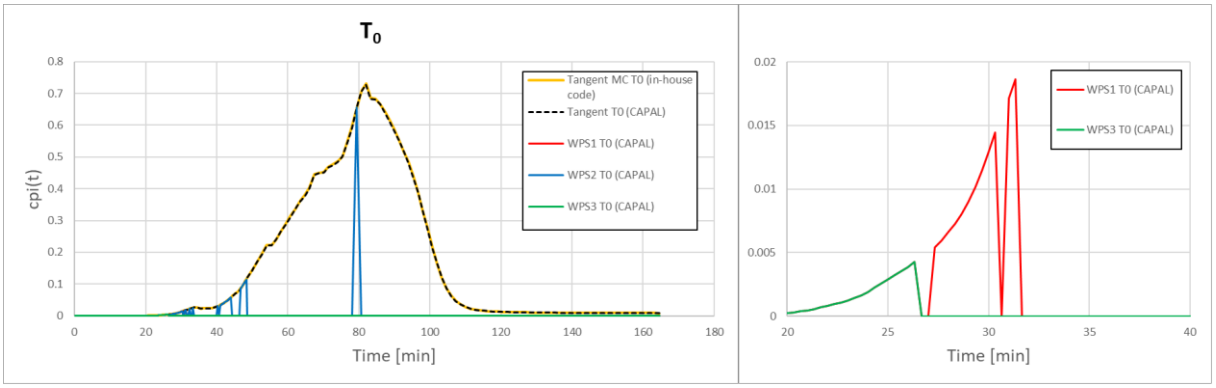

Figure 4.45: Comparison of cpi(t) from different WPS approaches for a circumferential TCC using the T_0 concept.

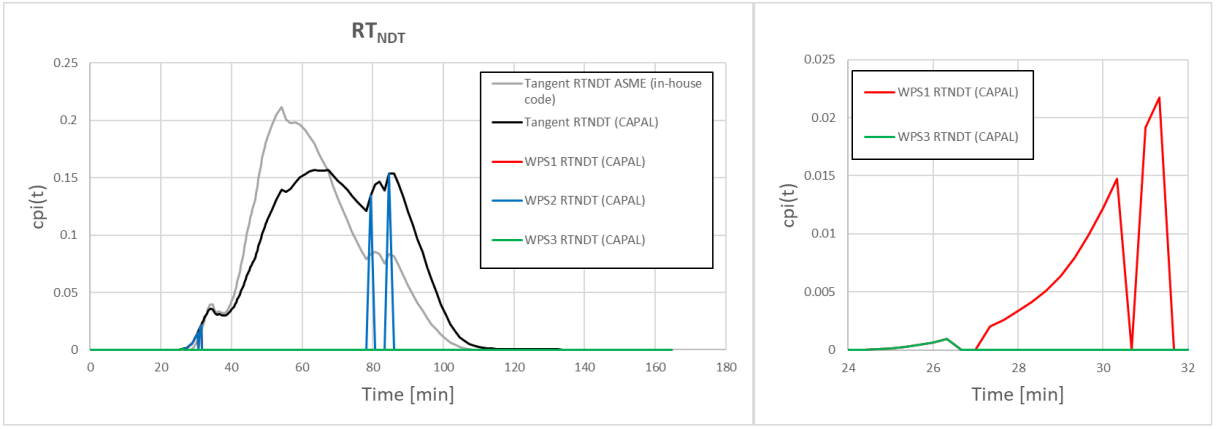

Figure 4.46: Comparison of cpi(t) from different WPS approaches for an axial UCC using the RT_{NDT} concept.

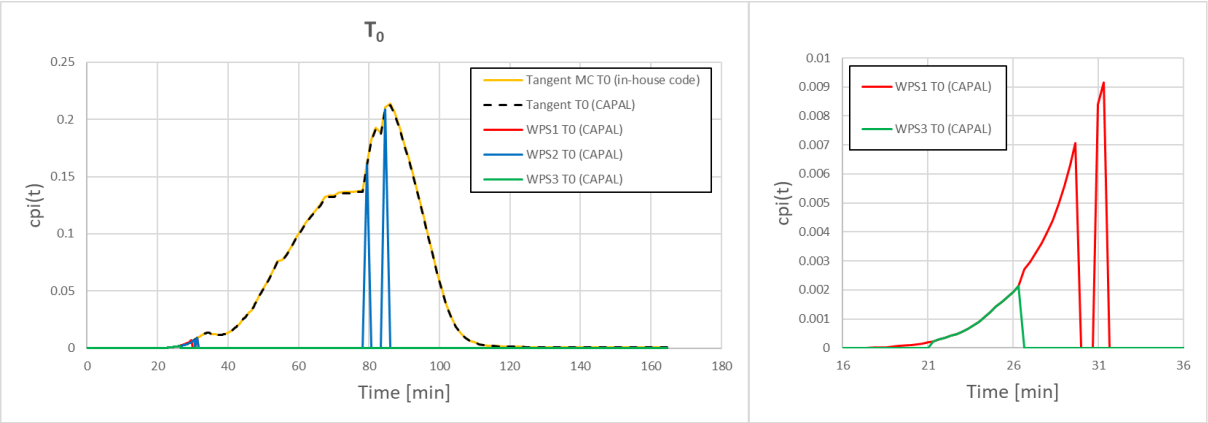

Figure 4.47: Comparison of cpi(t) from different WPS approaches for an axial UCC using the T_0 concept.

4.2.6 Check CPF for provided *T*, K_I and ART (non-mandatory)

This non-mandatory subtask is a continuation on the previous subtask described in Section 4.2.5 with the addition of considering crack arrest. The procedure to be used for crack arrest calculations is given in Section 2.3.10. It was decided during the work to limit this subtask to TCC only.

The main objective of this subtask was to calculate the conditional probability of failure (CPF) using the same pre-defined data as in Section 4.2.5 with the addition of through thickness $K_I(t)$ values for an infinite crack. It was also decided during work on this subtask that the CPI along with the conditional probability of non-arrest (CPNA) and conditional probability of stable arrest CPSA were to be included as results. The definitions of these are given in Section 2.3.10.

Five partners contributed with results for this non-mandatory subtask; FRA-G, Kiwa, UJV, IPP, JSI and Tecnatom. JSI and Tecnatom performed the task using CAPAL including the FAVOR and T_0 fracture toughness concepts while the others performed the task for the RT_{NDT} concept, see Section 2.3.4. UJV solved it for the T_0 concept as well.

For the RT_{NDT} concept, the consideration of crack arrest did not lead to any increase in margin as the CPI = CPF for both the tangent approach, see Table 4.11. The CPI values are identical to the subtask presented in Section 4.2.5 as expected since the same transient has been analysed. UJV got full crack arrest for the max WPS approach with no failure predicted, while FRA-G and IPP got no effect of crack arrest.

Table 4.11 Calculated CPI, CPF, CPNA, and CPSA for a circumferential TCC crack inside plume using the RT_{NDT} concept

Partner	Tangent Approach				Max WPS Approach			
	CPI	CPF	CPNA	CPSA	CPI	CPF	CPNA	CPSA
FRA-G	9.93E-1	9.93E-1	4.81E-2	0	7.11E-3	7.11E-3	7.11E-3	0
Kiwa	9.93E-1	9.93E-1	1.12E-2	0				
IPP	9.93E-1	9.93E-1	3.23E-2	0	7.11E-3	7.11E-3	0	0
UJV	9.93E-1	9.93E-1	3.17E-2	0	7.82E-3	0	0	7.82E-3

The FAVOR concept results are presented in Table 4.12. Different assumptions have been made for these analyses as compared to the subtask presented in Section 4.2.5 which have led to some differences in CPI. It can be seen that Tecnatom obtains a larger impact of crack arrest with no failure for the max WPS approach.

Table 4.12 Calculated CPI, CPF, CPNA, and CPSA for a circumferential TCC crack inside plume using the FAVOR concept

Partner	Tangent Approach				Max WPS Approach			
	CPI	CPF	CPNA	CPSA	CPI	CPF	CPNA	CPSA
Tecnatom	9.19E-1	8.89E-2	1.50E-2	8.30E-1	2.64E-2	0	0	2.64E-2
JSI	9.18E-1	9.12E-1	1.80E-2	0	2.64E-2	1.33E-3	2.10E-2	9.31E-1

The T_0 concept results are presented in Table 4.13. Here as well, different assumptions have been made as compared to the subtask presented in Section 4.2.5 which have led to some differences in CPI. All partners obtain some contribution from crack arrest, especially for the max WPS approach where no failure is obtained by all except IPP who almost gets no contribution from crack arrest.

Table 4.13 Calculated CPI, CPF, CPNA, and CPSA for a circumferential TCC crack inside plume using the T_0 concept

Partner	Tangent Approach				Max WPS Approach			
	CPI	CPF	CPNA	CPSA	CPI	CPF	CPNA	CPSA
Tecnatom	7.10E-1	8.17E-2	3.45E-3	6.29E-1	1.67E-2	0	0	1.66E-2
JSI	7.09E-1	6.99E-1	0	7.00E-3	1.66E-2	0	0	1
IPP	7.31E-1	6.73E-1	1.74E-1	5.81E-2	1.88E-2	1.86E-2	0	1.14E-4
UJV	7.33E-1	6.74E-1	1.73E-1	5.90E-2	1.85E-2	0	0	1.85E-2

4.3 Round-robin benchmarks

Following the verification of different analysis tools presented above, several round robin benchmarks have been designed and carried out as a part of the baseline probabilistic benchmark within Task 4.3. All benchmarks except for the first round-robin benchmark, RR1, were performed using the data from partner-specific base case transients.

The base case transients are presented in D2.1 [10] and WP2 Public Summary [8]. The partner-specific stress and temperature distributions for the base case are presented in D3.1 [13] and WP3 Public Summary [7]. The partner-specific SIF calculations for the base case are presented in D3.3 [15] and WP3 Public Summary [7]. The selected cases by each partner are summarised in Table 4.14. FRA-G is the only partner that considers mixing in the base case analyses which should be taken in consideration when comparing results.

Table 4.14 Base cases used by the partners

Partner	Location	Position	TH-Code	TH-Partner
Kiwa	Core Weld	Inside Plume	RELAP	JSI
UJV	Core Weld	Inside Plume	RELAP	UJV
GRS	Core Weld	Inside Plume	ATHLET	GRS
BZN	Core Weld	Inside Plume	RELAP	WUT
IRSN	Core Weld	Inside Plume	RELAP	JSI
FRA-G	Core Weld	Inside Mixing Plume	KWU-MIX	FRA-G
Tecnatom	Core Weld	Inside Plume	TRACE	PSI
JSI	Core Weld	Inside Plume	RELAP	JSI
PSI	Core Weld	Inside Plume	TRACE	PSI
IPP	Core Weld	Inside Plume	RELAP	SSTC

The different tools and methods used by different partners, including sampling sizes, are presented in Table 4.15. Both UJV and IRSN have solved the parts of PMA1 analytically. GRS have used different methods for different cases including First Order Reliability Method (FORM) and MCS with Importance Sampling (MCS-IS), see descriptions of these methods in Section 3.1.2 and 3.1.3 in D1.4 [17], respectively.

Table 4.15 Calculation methods used by the partners

Partner	Method	Sampling Size
Kiwa	MCS	10^7
UJV	Analytically PMA1; MCS for PMA2	10^6
GRS	MCS-IS / MCS / FORM	$10^3 – 10^4$
BZN	MCS	10^5 for PMA1; 10^6 for PMA2
IRSN	MCS for RT_{NDT}, analytically for T_0; PMA1	$1.2 \cdot 10^4$
FRA-G	MCS	10^6
Tecnatom	FAVOR/CAPAL	
JSI	In-house FAVOR/CAPAL	PMA1: 1; PMA2: 1000-T0, 4000-ASME RR2-PMA1: 1; RR2-PMA2: 5000 RR3-PMA1: 1 with 100 IGA iterations RR4-PMA1: 5000; RR4-PMA2: 10000 RR5-PMA1: 5000 with 100 IGA iterations
PSI	FAVOR/CAPAL	
IPP	MCS	10^7

4.3.1 RR1 – Predict ART for increasing fluence level

This round robin benchmark is aimed at predicting the best-estimate ART-values and quantiles of ART for increasing fluence level. The analyses were carried out for several positions through the RPV wall considering fluence attenuation through the wall according to Section 2.3.8. As it has been pointed above, this round robin benchmark was not based on partner-specific transient data, the participants performed analyses for a pre-defined common data set.

For the baseline (mandatory part) of this benchmark, ART calculations have been performed for both weld and base materials utilizing both the RT_{NDT} and T_0 fracture toughness concepts (see Section 2.3.4).

Predicted mean values of ART along with 5% and 95% quantiles at a location of t/4 from the cladding interface are presented as a function of the RPV age in Figure 4.48 (for base metal) and Figure 4.49 (for welds). The plots show ART-values obtained from the calculations based on the RT_{NDT} and T_0 fracture toughness concepts.

Considering that the analyses were performed using the pre-defined data common for all participants, the results have been shown to be in very good agreement. It can be noted that the FRA-G results differ for the RPV operation time of 0 years as the base shift and hence the error function has not been considered by FRA-G. This was discussed during the project and was the reason for adding a new row to Table 2.7 for 1 year of operation. In the subsequent RR calculations for PMA2, the lowest pre-defined value for years of operation was set to 1 year.

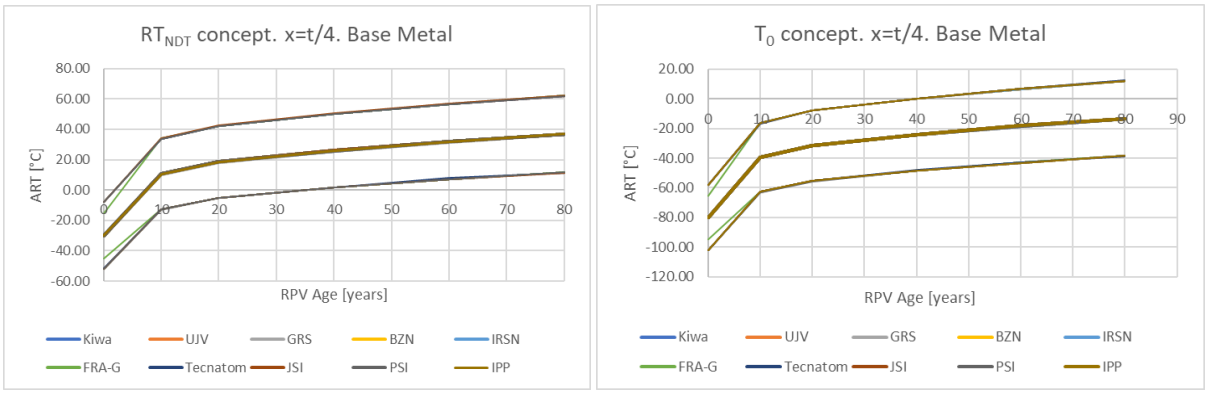

Figure 4.48: Mean values, 5% and 95% quantiles of ART as a function of RPV age at the crack tip position of ¼ of RPV wall thickness for base metal. ART-values are calculated using RT_{NDT} and T_0 fracture toughness concepts.

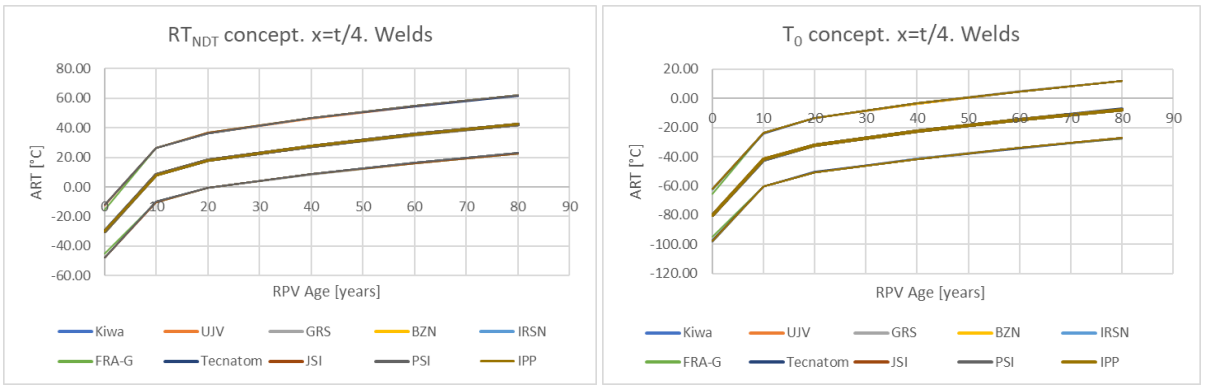

Figure 4.49: Mean values, 5% and 95% quantiles of ART as a function of RPV age at the crack tip position of ¼ of RPV wall thickness for welds. ART-values are calculated using RT_{NDT} and T_0 fracture toughness concepts.

The ART-values plotted as a function of the radial coordinate through the RPV wall for different RPV operation times are shown in Figure 4.50. The plot presents the ART-values for both base metal and welds calculated using the RT_{NDT} concept. It can be observed that ART-values for welds are higher in comparison to base metal for shallow cracks. However, the ART-values for base metal are governing for deeper cracks. This transition occurs at a deeper position through the RPV wall with increasing RPV operation times.

This trend is also illustrated in Figure 4.51 presenting the ART-values as a function of the RPV age at different crack tip locations though the RPV wall. For the crack tip location of about 50% of the RPV wall thickness, the ART-values for base metal become larger than for welds for the whole range of analysed RPV operation times.

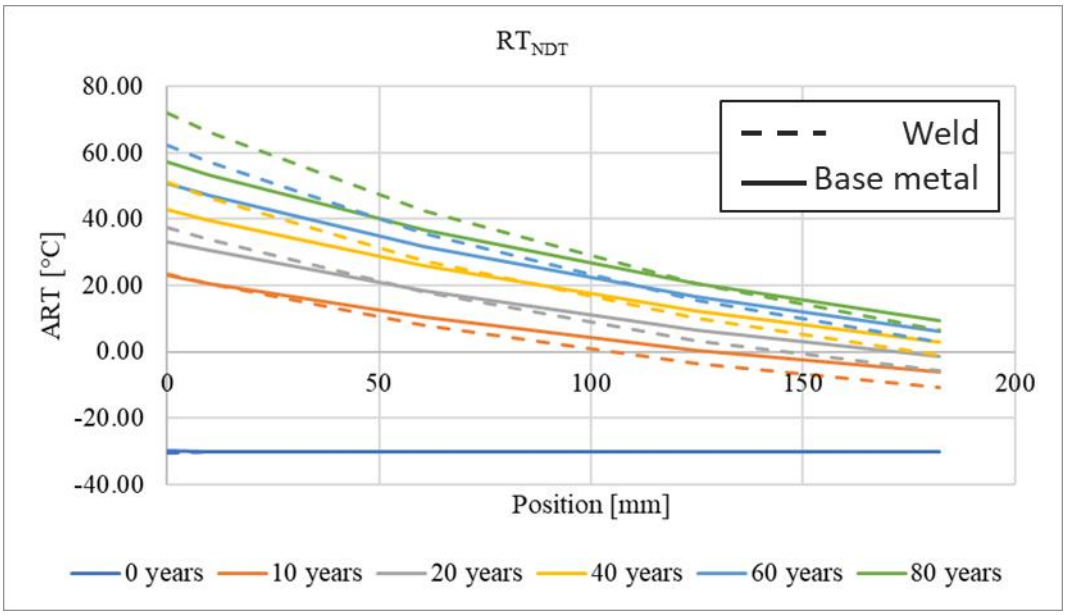

Figure 4.50: ART as a function of crack tip position in base metal and weld through the RPV wall thickness for different RPV operation time. ART-values are calculated using *RT_{NDT}* fracture toughness concept.

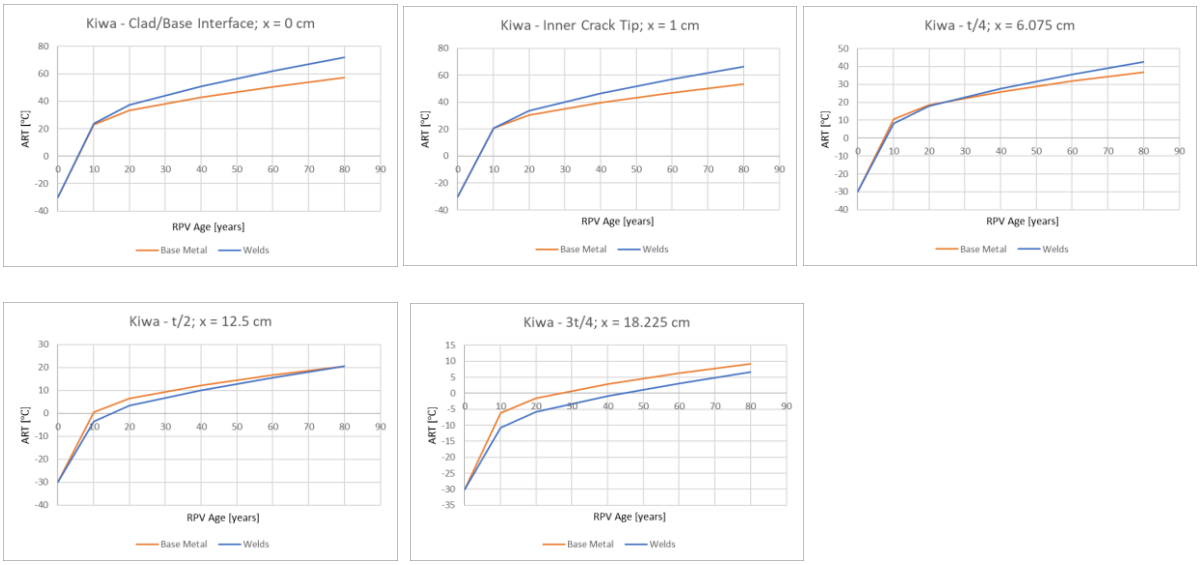

Figure 4.51: ART as a function of the RPV operation time for different crack tip locations through the RPV wall thickness. ART-values are calculated using *RT_{NDT}* fracture toughness concept.

Some partners performed non-mandatory calculations of ART using alternative shift equations according to RSE-M, see Section 2.3.6. The results between partners were in perfect agreement as shown in Figure 4.52. The plots present only the results calculated at the crack tip position of ¼ of RPV wall thickness using the RT_{NDT} fracture toughness concept with RSE-M shift equation. Calculations have been performed for different locations through the RPV wall and using both the RT_{NDT} and T_0 fracture toughness concepts. The perfect agreement between different partners was observed for all results with the RSE-M shift function.

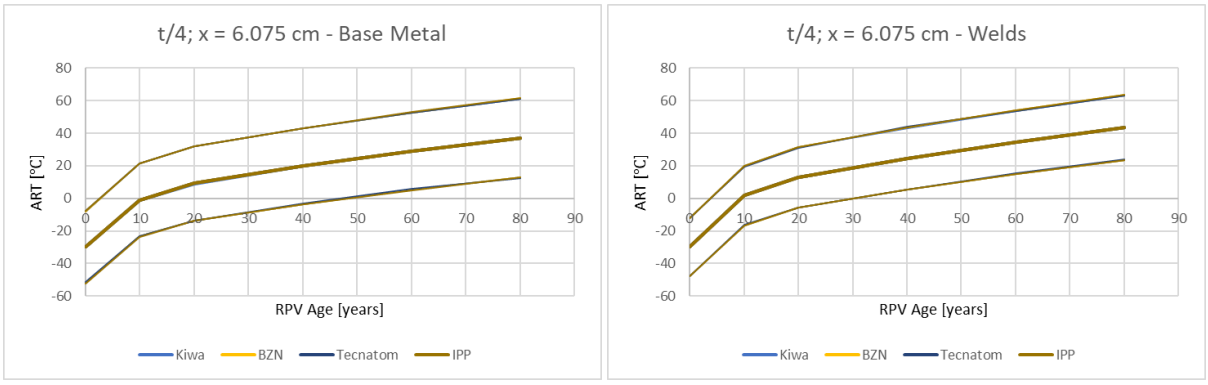

Figure 4.52: Mean values, 5% and 95% quantiles of ART as a function of RPV age at the crack tip position of ¼ of RPV wall thickness for base metal and welds. ART-values are calculated using RT_{NDT} fracture toughness concept with RSE-M shift function.

Only two partners considered the non-mandatory shift function according to 10CFR50.61a in the analyses. The results from this non-mandatory analysis also demonstrated a very good agreement for all considered crack depths. A selection of the plots comparing the results for the 10CFR50.61a shift function is presented in Figure 4.53 and Figure 4.54. The shift and error functions at the operation time of 0 years were not considered by Tecnatom which explains a minor discrepancy in the initial results.

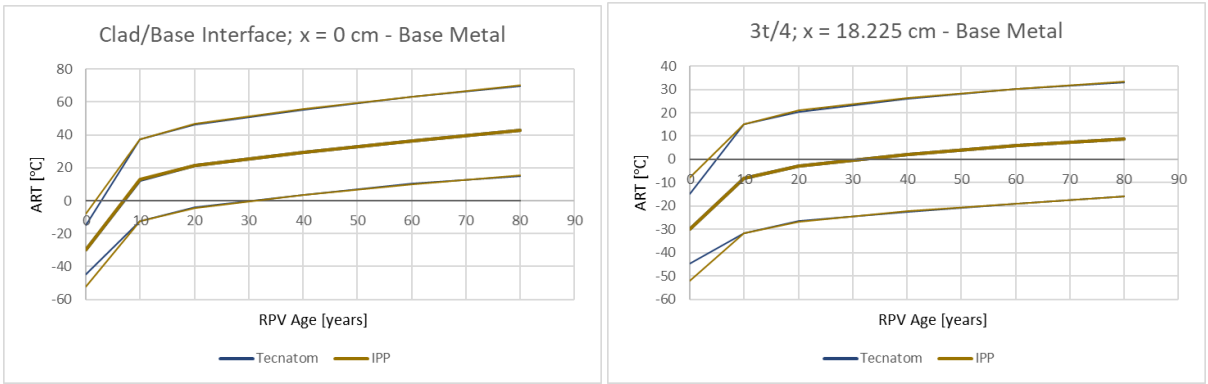

Figure 4.53: ART-values for base metal calculated using RT_{NDT} fracture toughness concept with 10CFR50.61a shift function as a function of RPV age at the clad/base interface and at the depth of ¾ of the RPV wall thickness.

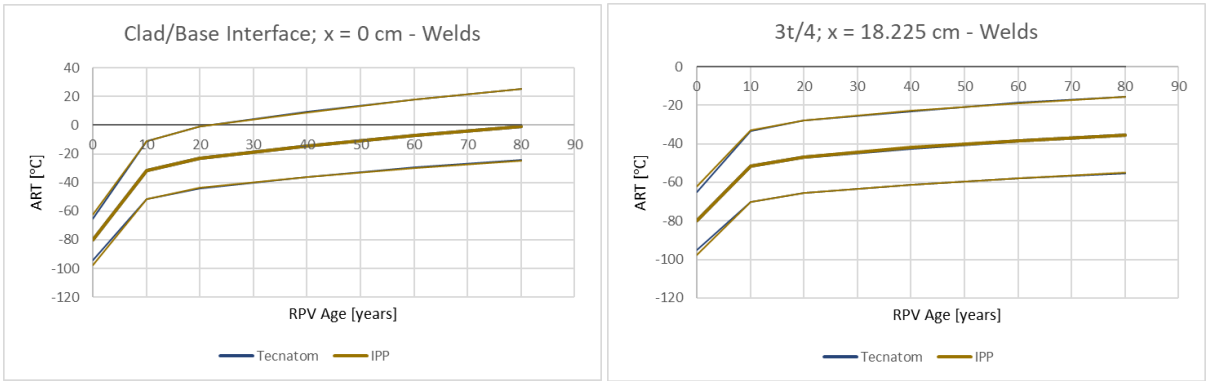

Figure 4.54: ART-values for welds calculated using T_0 fracture toughness concept with 10CFR50.61a shift function as a function of RPV age at the clad/base interface and at the depth of ¾ of the RPV wall thickness.

A comparison of the ART-values obtained by different shift functions using the RT_{NDT} concept is presented in Figure 4.55 based on the results from IPP and Tecnatom. The plots demonstrate the mean ART-values predicted for the base metal and welds at different positions through the RPV wall thickness considering fluence attenuation. It can be observed that the predicted ART-values are governed by different shift functions depending on a crack tip position in the RPV wall. Thus, for shallow cracks being close to the clad/base fusion line (x=0 cm and x=1 cm) the RSE-M shift function predicts highest ART-values for RPV operation time 30+ years while the base shift function governs the ART-values for operation time <30 years. For crack tips located in base metal at ¼ of the RPV wall thickness and deeper, the highest ART-values are predicted using the base shift. For cracks located in welds and having the depth of ½ of the RPV wall thickness and deeper, the 10CFR50.61a shift function predicts the highest ART-values.

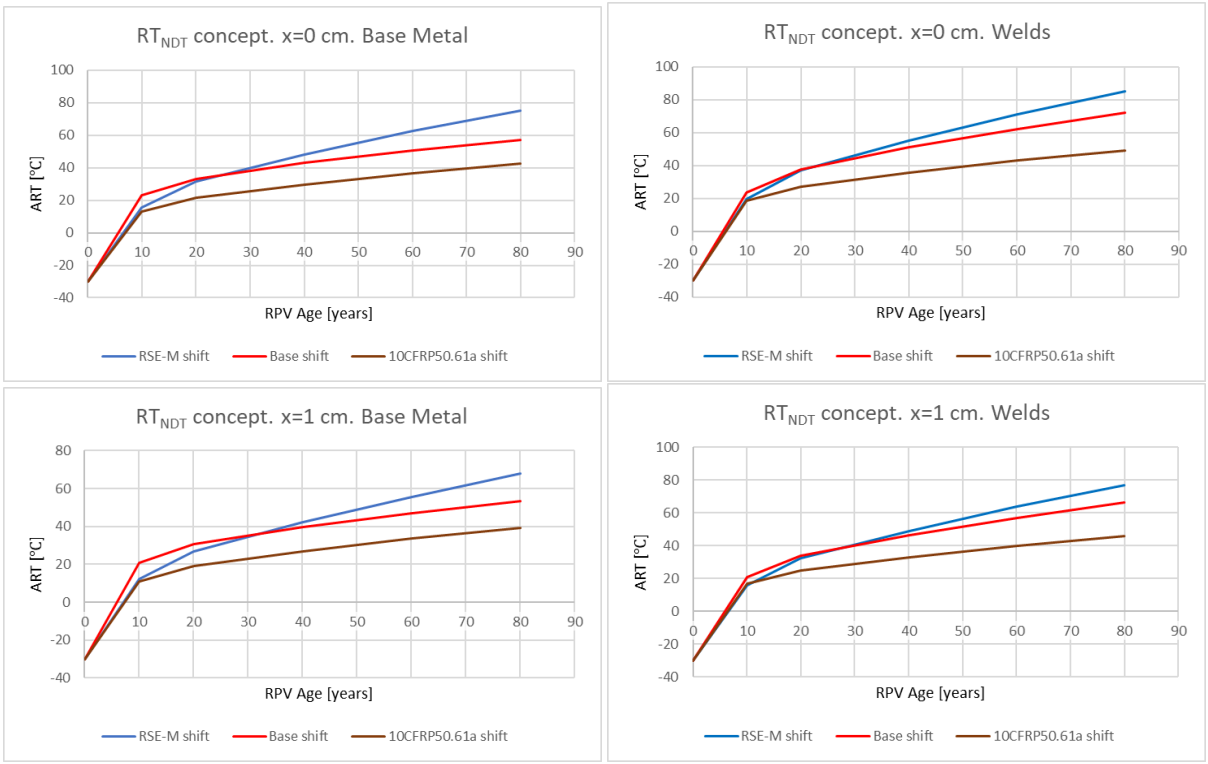

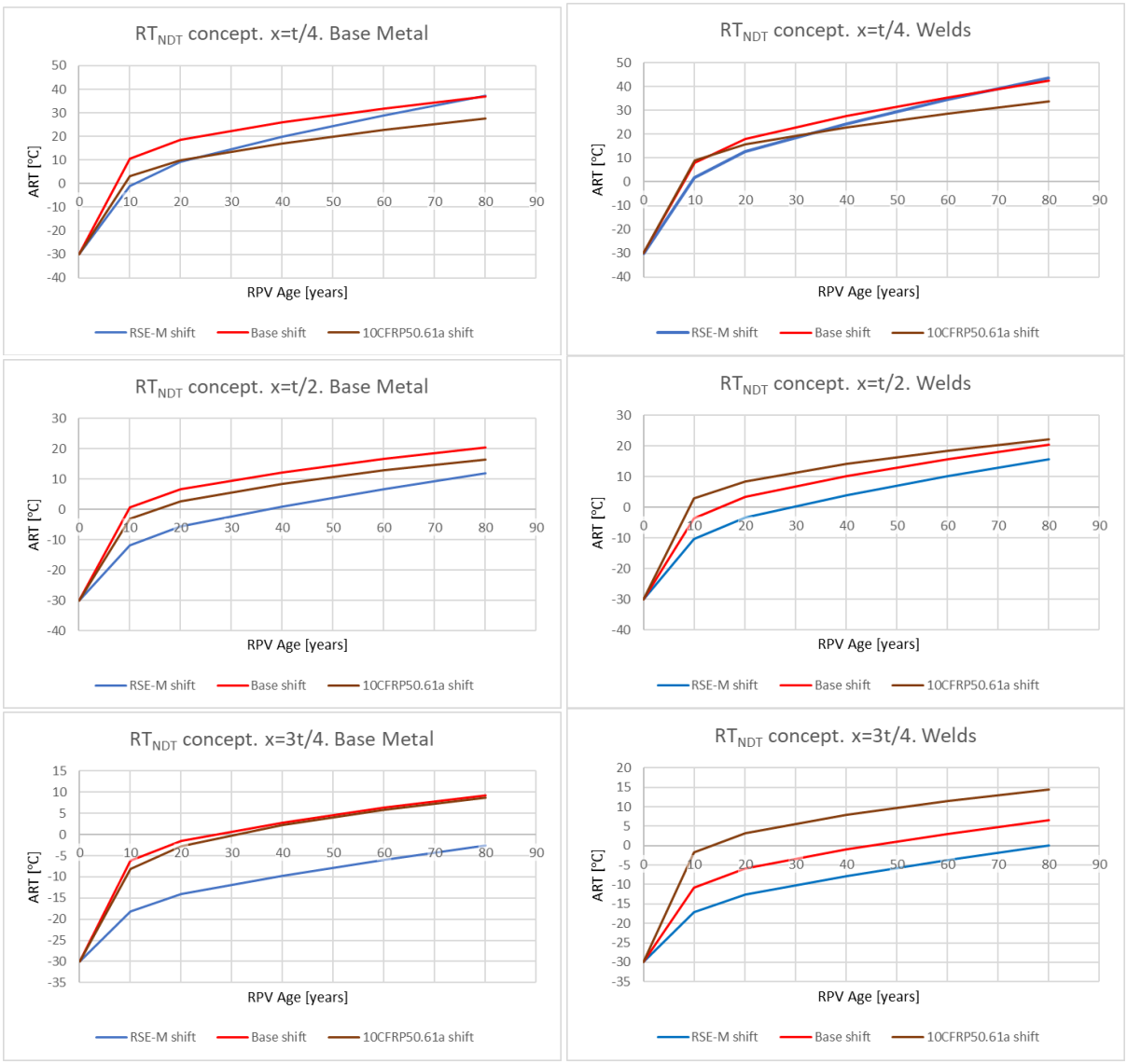

Figure 4.55: IPP and Tecnatom results for mean ART as a function of the RPV operation time at different crack tip positions through the RPV wall thickness. ART-values are calculated using the base shift and alternative shift equations according to RSE-M and 10CFR50.61a for the *RT$_{NDT}$* fracture toughness concept.

4.3.1.1 Conclusions from RR1

The results from this benchmark indicate that ART-values have a clear correlation with fluence level, i.e. the ART-values increase with the RPV age. The ART-values vary through the RPV wall thickness being highest at the inner surface of the RPV. It has also been observed that for shallow cracks the ART-values for welds are higher in comparison to base metal. However, the ART-values for base metal are governing for deeper cracks. This transition occurs at a deeper position through the RPV wall with increasing RPV operation times. The results from RR1 also demonstrate that a choice of shift function has a large influence on the calculated ART-values, where the shift function according to RSE-M governs the ART-values for shallow cracks. For deeper crack the base shift function takes over predicting the highest ART-values for base metal, while the 10CFR50.61a shift function governs the ART-values for welds.

4.3.2 RR2 – Check CPI for base case transient

This round robin benchmark was aimed at calculating CPI values for various crack geometries (TCC, UCC and embedded cracks), orientations within the RPV wall (axial and circumferential), crack tip locations and sizes. User-specific thermal-hydraulic data along with calculated temperatures, stresses and K_I-values have been used in this round robin benchmark, see Table 4.14.

Analyses are performed for both the tangent approach and the max WPS approach as described in Section 2.3.9 and are mandatory for PMA1 and PMA2, while PMA4 is included as a non-mandatory part, see Section 2.3.11.

The RT_{NDT} concept or alternatively the FAVOR concept was considered as mandatory while the T_0 concept was included as a non-mandatory addition to the subtask, see Section 2.3.4.

Iterative calculations were made to find the maximum allowable ART value for PMA1 and the maximum allowable RPV age for PMA2 at CPI = $2.28 \cdot 10^{-4}$ as defined in Section 2.3.11. The partners were requested to present results for both the case chosen as the final result where the CPI value has approximately reached the target probability, as well as intermediate results. In addition, several pre-defined ART and RPV age values needed to be analysed. These are defined in Table 4.16.

Table 4.16 Selected pre-defined ART values and RPV ages to be analysed

PMA-type	Pre-defined values that are to be analysed				
PMA1 [°C]	0	50	100	150	200
PMA2/PMA4 [years]	1	20	40	80	200

It was decided that each partner should calculate and provide the results including the final allowable ART or RPV age for the target CPI-value as well as the instantaneous cpi(t)-values for the transient. For PMA2 the mean value of the fluence at the inner surface should additionally be included as well as the mean value, standard deviation and 5%/95% quantiles for the ART value.

The non-mandatory PMA4 had to be calculated for the pre-defined values according to Table 4.16 and the results should include the CPI value and reliability index, as well as the most probable point of failure (MPF) for each distributed parameter. The PMA4 assessment for RR2 was performed only by GRS and IPP. The PMA4 results are not presented in detail in this Section but will be described and discussed further in Section 7.

4.3.2.1 PMA1

The maximum allowable ART, considering CPI, is calculated for the different geometries and locations for both the tangent and max WPS approaches.

Final allowable ART values for the RT_{NDT} concept are presented in Table 4.17 and Table 4.18 as well as Figure 4.56 and Figure 4.57 for the tangent and max WPS approaches respectively. The results are in quite good agreement between most partners. Kiwa, BZN, UJV and JSI have quite similar results and IPP are quite close to them but have somewhat lower results. FRA-G have much lower values which is to be expected as they are the only partner that have considered mixing in the analyses. GRS and IRSN have higher results than the rest.

As expected, the TCC results are lower than UCC results. For the TCC, the results are quite similar between the two crack positions, and point C at the cladding/base intersection is limiting for most cases. For the UCC, point A at the deepest point is limiting for all cases.

Table 4.17 Maximum allowable ART values for the tangent approach considering the RT_{NDT} concept

Partner	Maximum allowable ART for TCC [°C]				Maximum allowable ART for UCC [°C]			
	Axial		Circumferential		Axial		Circumferential	
	A	C	A	C	A	C	A	C
Kiwa	59.21	57.67	61.42	58.78	79.00	160.55	85.94	190.32
BZN	60.00	57.50	61.50	58.00	82.50	172.00	87.50	197.00
FRA-G	28.00	25.00	27.00	24.00	43.90	90.75	42.79	90.41
GRS	67.50		68.50					
IRSN	67.97	62.21	69.93	62.82	89.74		95.29	
UJV	59.41	57.18	61.33	57.75	79.33	162.30	84.57	191.94
IPP	56.57	53.98	57.31	54.61	75.92	161.22	80.17	190.23
JSI			63					

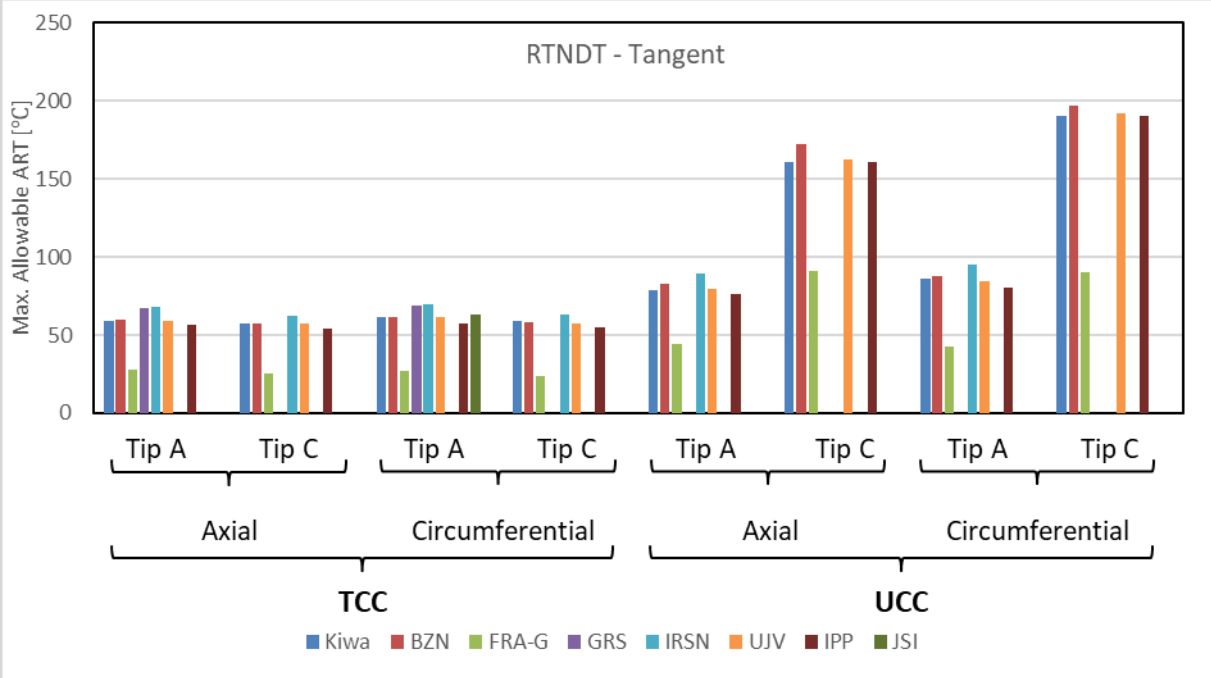

Figure 4.56: Maximum allowable ART values for the tangent approach considering the RT_{NDT} concept.

Table 4.18 Maximum allowable ART values for the max WPS approach considering the RT_{NDT} concept

Partner	Maximum allowable ART for TCC [°C]				Maximum allowable ART for UCC [°C]			
	Axial		Circumferential		Axial		Circumferential	
	A	C	A	C	A	C	A	C
Kiwa	127.15	122.92	129.38	124.91	145.95	186.28	147.20	202.65
BZN	127.50	123.00	129.50	124.00	147.00	192.00	150.50	205.50
FRA-G	99.00	93.00	99.00	94.00	112.90	141.00	113.10	142.30
GRS	125.50		103.50					
UJV	131.02	126.34	133.13	128.36	146.45	184.89	150.55	201.13
IPP	127.51	124.70	129.58	126.72	146.01	186.94	146.80	202.95
JSI			130.00					

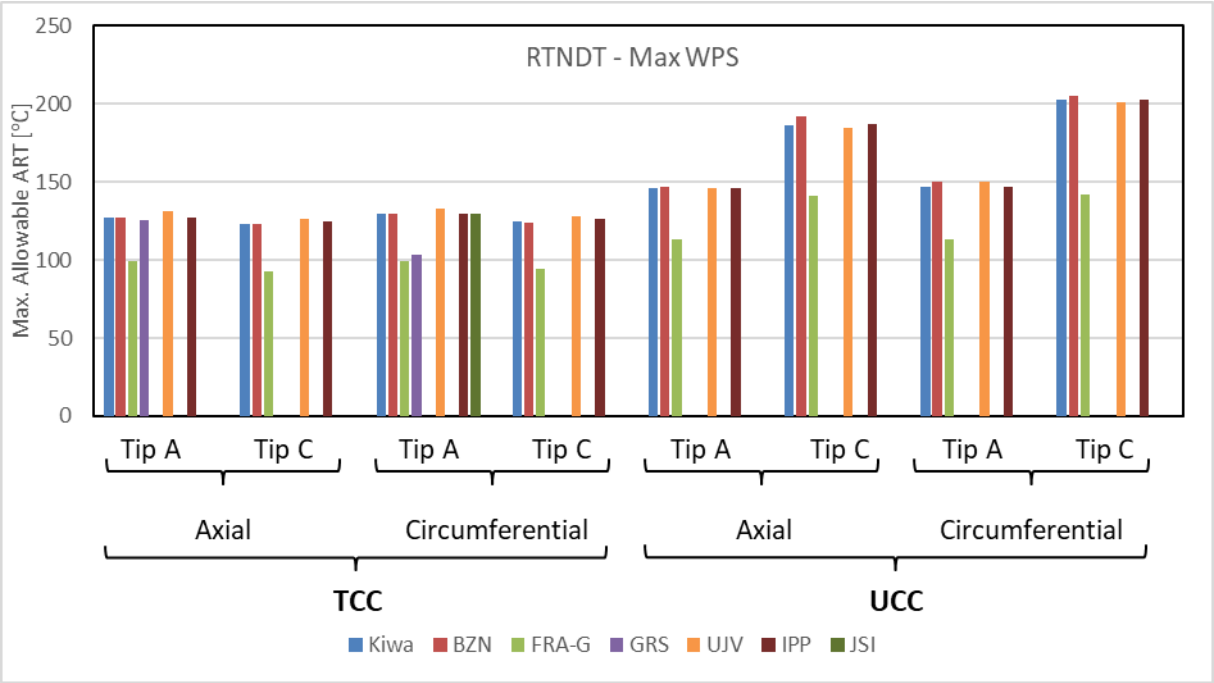

Figure 4.57: Maximum allowable ART values for the max WPS approach considering the RT_{NDT} concept.

Final allowable ART values for the FAVOR concept are presented in Table 4.19 and Table 4.20 as well as Figure 4.58 and Figure 4.59 for a circumferential TCC and embedded cracks respectively. As the pre-defined case in APAL cannot be analysed directly using FAVOR assumptions have been made by the partners described in Section 2.3.12.

For the TCC, different assumptions have been studied by the partners. The first assumption is for the total crack depth including cladding, $(a + r)$, where FAVOR is limited to percentages as integers of the total RPV wall (including cladding). Here, Tecnatom and PSI have used 7% of the wall thickness for most cases, while JSI have used 6%. The second assumption is the crack shape, $2c/(a + r)$ that is limited to the values 2, 6 and 10 in FAVOR.

PSI and JSI also used in-house codes based on the FAVOR methodology to analyse the geometry specified in APAL with $a + r = 16$ mm and $2c/(a + r) = 3.75$. These analyses resulted in quite good agreement.

All partners analysed the cases where $2c/(a + r) = 6$. Here, Tecnatom and PSI, which have used the same transient (see Table 4.14) got very good agreement, while JSI got much higher values for both the tangent and max WPS approaches. It should be noted that JSI are using a smaller crack and a different transient.

It can also be seen from PSI results that the crack shape has a large impact on the end results where the results for a crack shape ratio of 2 results in almost twice as high ART values as the crack shape ratio of 6 for the tangent approach.

Table 4.19 Maximum allowable ART values for the deepest point of a circumferential TCC considering the FAVOR concept

Partner	Crack Depth; a+r [mm]	Crack Shape; 2*c*/(*a*+*r*)	TCC, Circumferential, Point A	
			Tangent [°C]	Max WPS [°C]
Tecnatom	17.43	6	33.5	79.5
PSI	17.43	2	62.5	98.5
	16	3.75	54.6	-
	17.43	6	34.1	79.8
JSI	14.94	6	59	128
	16	3.75	51	120

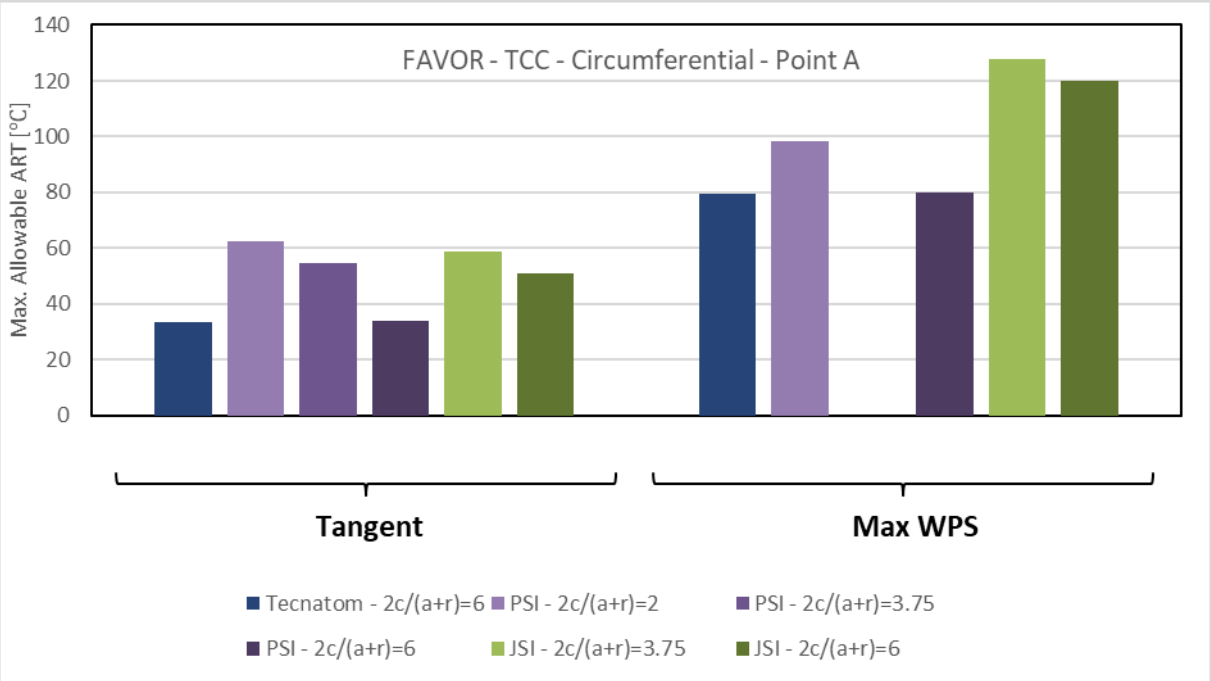

Figure 4.58: Maximum allowable ART values for the deepest point of a circumferential TCC considering the FAVOR concept.

PSI and Tecnatom have analysed the point closest to the cladding for embedded cracks, and the results are presented in Table 4.20 and Figure 4.59. It can be seen from Tecnatom results that the difference between an axial and circumferential crack is slight.

There are some differences in the results between Tecnatom and PSI, especially for the max WPS approach, although they have used the same transient.

Table 4.20 Maximum allowable ART values for the point in embedded cracks closest to the cladding considering the FAVOR concept

Partner	Maximum allowable ART for embedded cracks [°C]			
	Tangent		Max WPS	
	Axial	Circumferential	Axial	Circumferential
Tecnatom	67	68.5	92	93
PSI		77.4		102

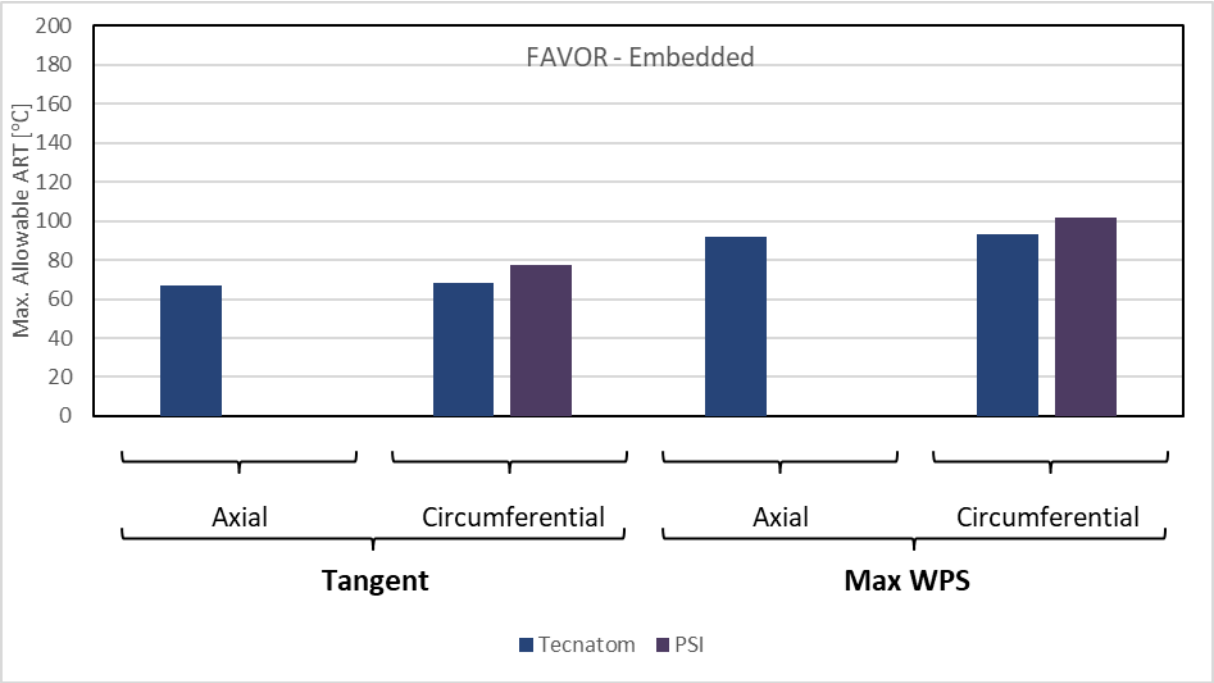

Figure 4.59: Maximum allowable ART values for the point in embedded cracks closest to the cladding considering the FAVOR concept.

Several partners provided non-mandatory results for the T_0 concept which are presented in Table 4.21 and Table 4.22 as well as Figure 4.60 and Figure 4.61 for the tangent and max WPS approaches respectively. Crack front correction was not considered in these calculations. The differences between partners are comparative with those for the RT_{NDT} concept. Some values for the TCC are below 0°C.

BZN have values at 0°C at the lowest due to a limitation in their tool not allowing for negative values. This has been checked and their actual results are close to 0°C. It should be noted that it is important to allow for negative ART values as a cut-off at 0°C leads to non-conservative results.

Table 4.21 Maximum allowable ART values for the tangent approach considering the T_0 concept

Partner	Maximum allowable ART for TCC [°C]				Maximum allowable ART for UCC [°C]			
	Axial		Circumferential		Axial		Circumferential	
	A	C	A	C	A	C	A	C
Kiwa	-1.38	-2.50	1.00	-1.88	26.51	82.87	33.57	100.40
BZN	0.00	0.00	0.50	0.00	30.50	96.00	36.00	106.50
IRSN	10.39	3.76	11.56	4.68	40.17	72.49	46.09	76.30
IPP	-6.48	-6.80	-5.60	-5.80	22.32	81.68	27.65	97.66
JSI			1					

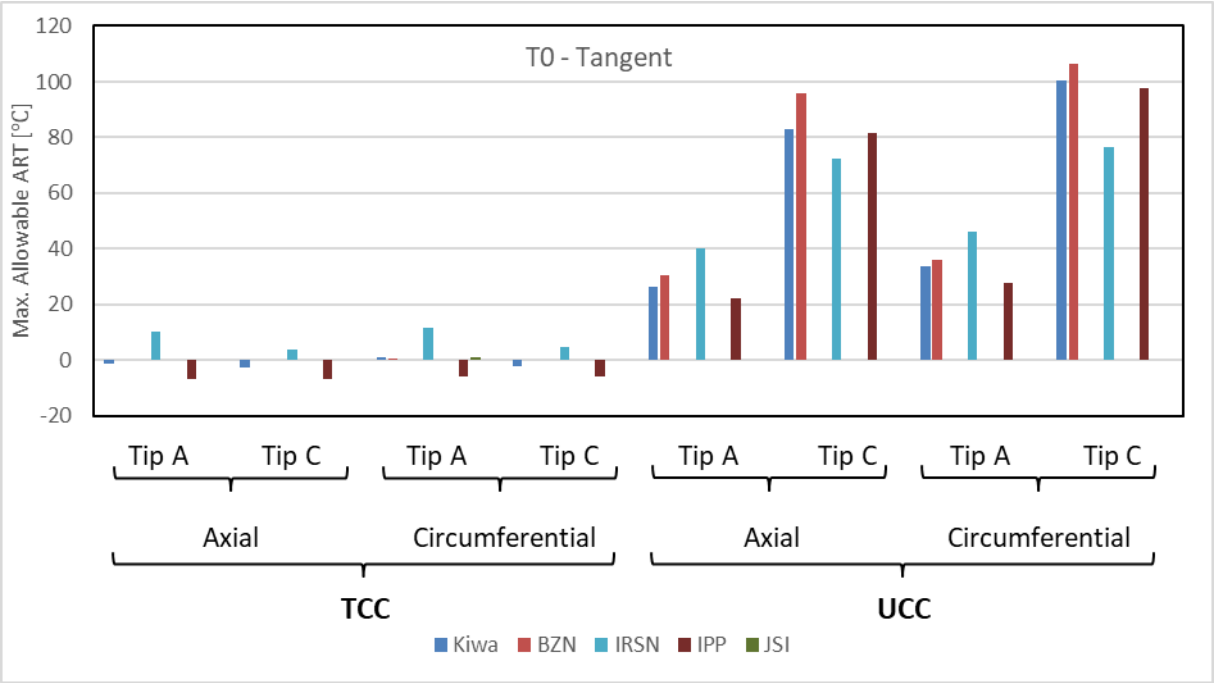

Figure 4.60: Maximum allowable ART values for the tangent approach considering the T_0 concept.

Table 4.22 Maximum allowable ART values for the max WPS approach considering the T_0 concept

Partner	Maximum allowable ART for TCC [°C]				Maximum allowable ART for UCC [°C]			
	Axial		Circumferential		Axial		Circumferential	
	A	C	A	C	A	C	A	C
Kiwa	55.60	56.87	58.30	58.14	84.73	135.82	89.16	149.44
BZN	56.00	56.00	58.50	58.00	86.50	138.00	91.00	147.50
IPP	56.22	58.47	59.55	61.32	83.67	136.35	86.71	148.23
JSI			60.00					

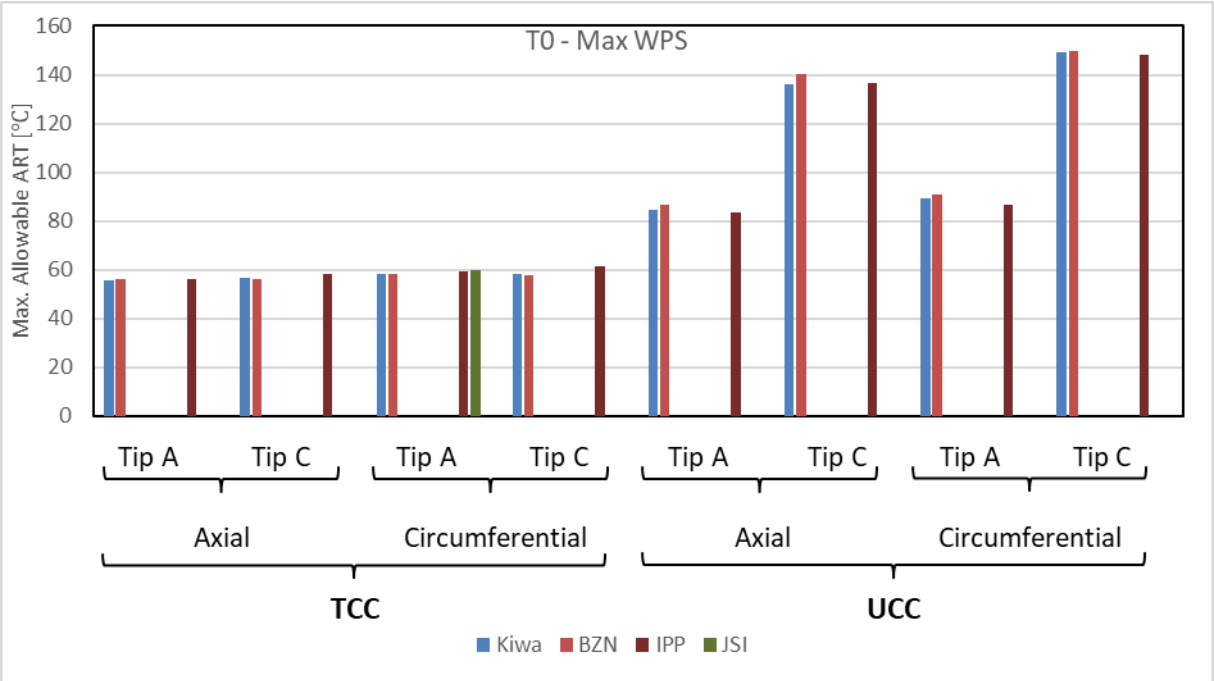

Figure 4.61: Maximum allowable ART values for the max WPS approach considering the T_0 concept.

4.3.2.2 PMA2

The maximum allowable RPV age with regard to the considered allowable CPI was calculated for the different geometries and locations for both the tangent and max WPS approaches.

Final allowable RPV age for the RTNDT concept are presented in Table 4.23 and Table 4.24 as well as Figure 4.62 and Figure 4.63 for the tangent and max WPS approaches respectively.

The partners results relate to each other in a similar way as for PMA1 where Kiwa, BZN, UJV and JSI have quite similar results for most cases while FRA-G have much lower results due to mixing. IRSN gets much higher values than the rest. A difference here as compared to PMA1 is that GRS gets much lower results than most partners. One reason for this could be the use of TH results calculated with ATHLET which differ from TH results of other partners due to differences in the code specific input data sets, assumed distribution functions and boundary conditions as well as TH model assumptions. As GRS used the in-house code PROST, the instantaneous cpi(t) values could not be exported.

In order to verify the calculations, Kiwa analysed several cases with transient data provided by the partners. This is described in further detail in Section 4.3.2.3. The GRS results could not be verified because the instantaneous cpi values were not provided. It should be noted that IRSN did not consider the truncation of K_{Ic} in PMA2. The comparisons in Section 4.3.2.3 shows that if truncation had been considered, IRSN would have gotten even higher results.

As for PMA1 the TCC results are quite similar between axial and circumferential cracks with somewhat higher values for circumferential cracks. Point C is limiting for the TCC crack. Results for the UCC are much higher with point A being limiting for all cases except for the axial UCC where FRA-G gets lower RPV age for point C.

Table 4.23 Maximum allowable RPV age for the tangent approach considering the RT_{NDT} concept

Partner	Max allowable RPV age for TCC [years]				Max allowable RPV age for UCC [years]			
	Axial		Circumferential		Axial		Circumferential	
	A	C	A	C	A	C	A	C
Kiwa	26.6	20.2	30.8	20.9	67.6	330.1	82.9	495.8
BZN	28.8		30.6		75.0		87.5	
FRA-G	3.0	1.0	3.0	1.0	13.0	11.0	12.0	100.0
GRS	19.8		23.0					
IRSN	39.1	25.8	39.0	29.3	83.0		100.2	
UJV	27.6	19.7	30.2	20.2	68.3	337.0	79.8	491.4
IPP	22.3	16.9	23.6	17.6	60.0	335.5	70.1	498.0
JSI			30					

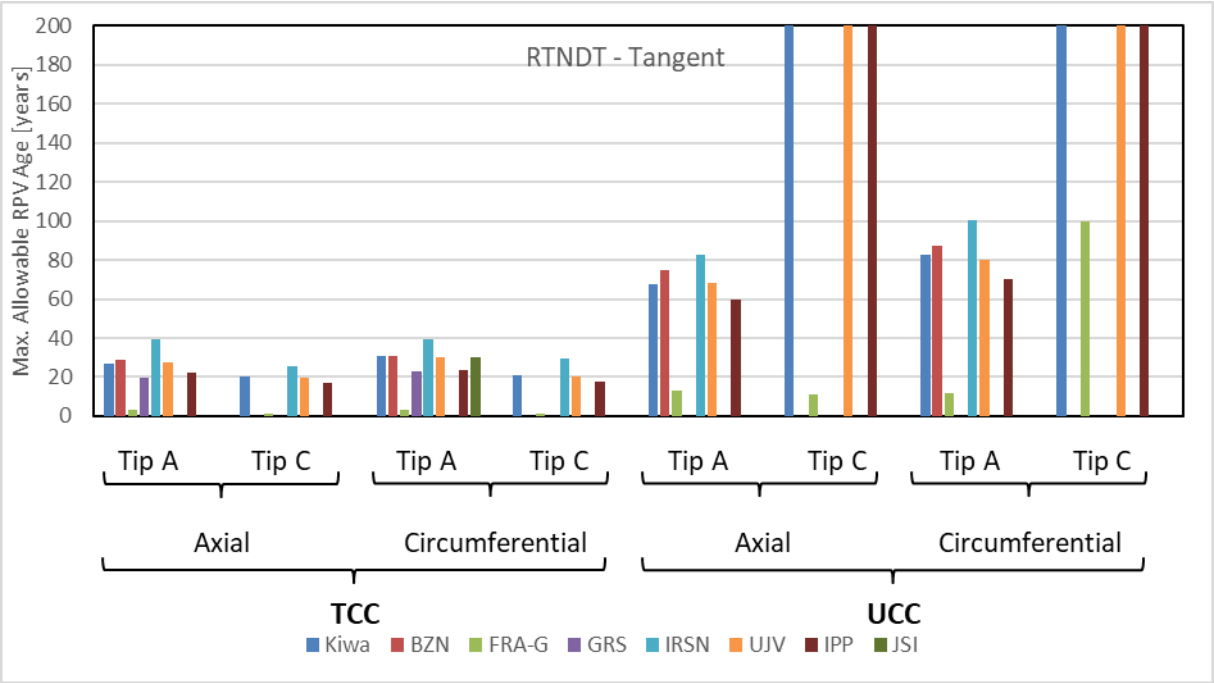

Figure 4.62: Maximum allowable RPV age for the tangent approach considering the RT_{NDT} concept.

Table 4.24 Maximum allowable RPV age for the max WPS approach considering the RT_{NDT} concept

Partner	Max allowable RPV age for TCC [years]				Max allowable RPV age for UCC [years]			
	Axial		Circumferential		Axial		Circumferential	
	A	C	A	C	A	C	A	C
Kiwa	166.7	136.4	174.1	142.0	236.4	416.2	244.3	520.6
BZN	166.5		172.0		239.8		255.0	
FRA-G	93.0	71.0	153.0	72.0	131.0	113.0	132.0	224.0
GRS	175.0		98.0					
UJV	178.0	146.0	185.4	152.3	237.4	409.9	255.9	500.0
IPP	166.4	140.9	173.1	146.8	234.7	416.9	240.9	0.0
JSI			180.0					

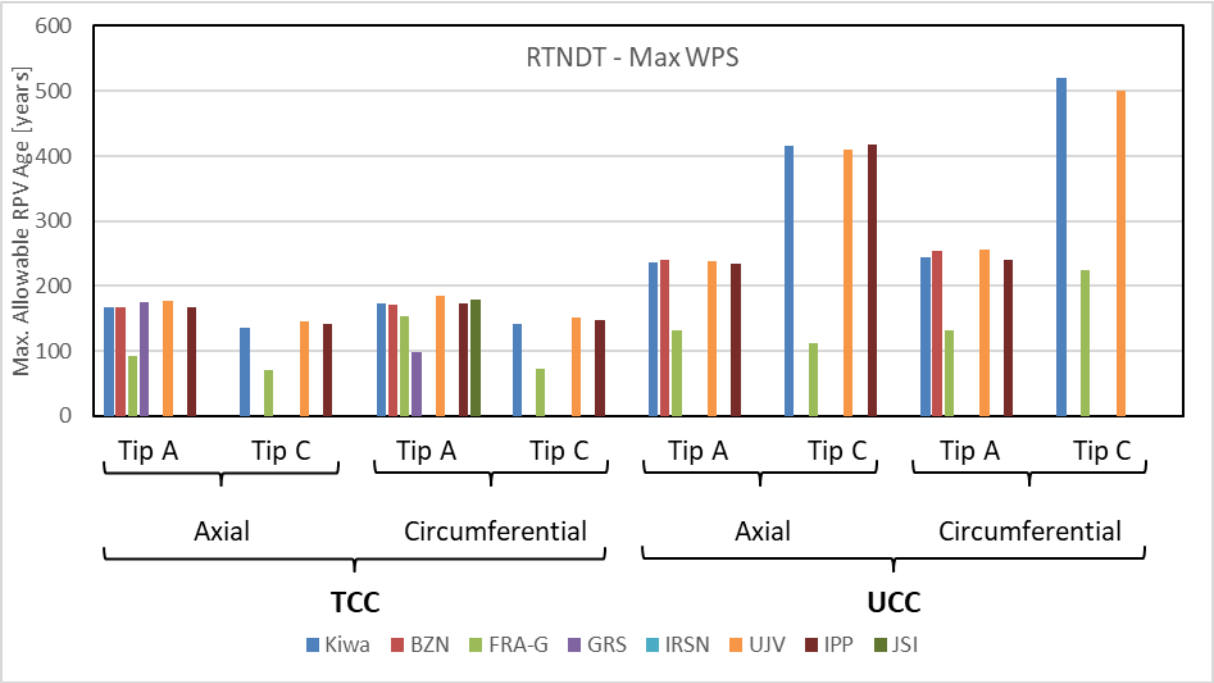

Figure 4.63: Maximum allowable RPV age for the max WPS approach considering the RT_{NDT} concept.

Final allowable RPV ages for the FAVOR concept are presented in Table 4.25 and Table 4.26 as well as Figure 4.64 and Figure 4.65 for a circumferential TCC and embedded cracks respectively.

The assumed crack depth and crack shape ratio for the TCC are included in Table 4.25. JSI gets higher results which may be explained by the smaller crack as well as them using a different transient. PSI and Tecnatom have a good agreement in results.

Table 4.25 Maximum allowable RPV age for the deepest point of a circumferential TCC considering the FAVOR concept

Partner	Crack Depth; a+r [mm]	Crack Shape; 2c/(a+r)	TCC, Circumferential, Point A	
			Tangent [years]	Max WPS [years]
Tecnatom	17.43	6	12	67
PSI	17.43	6	12	69
JSI	14.94	6	25	163

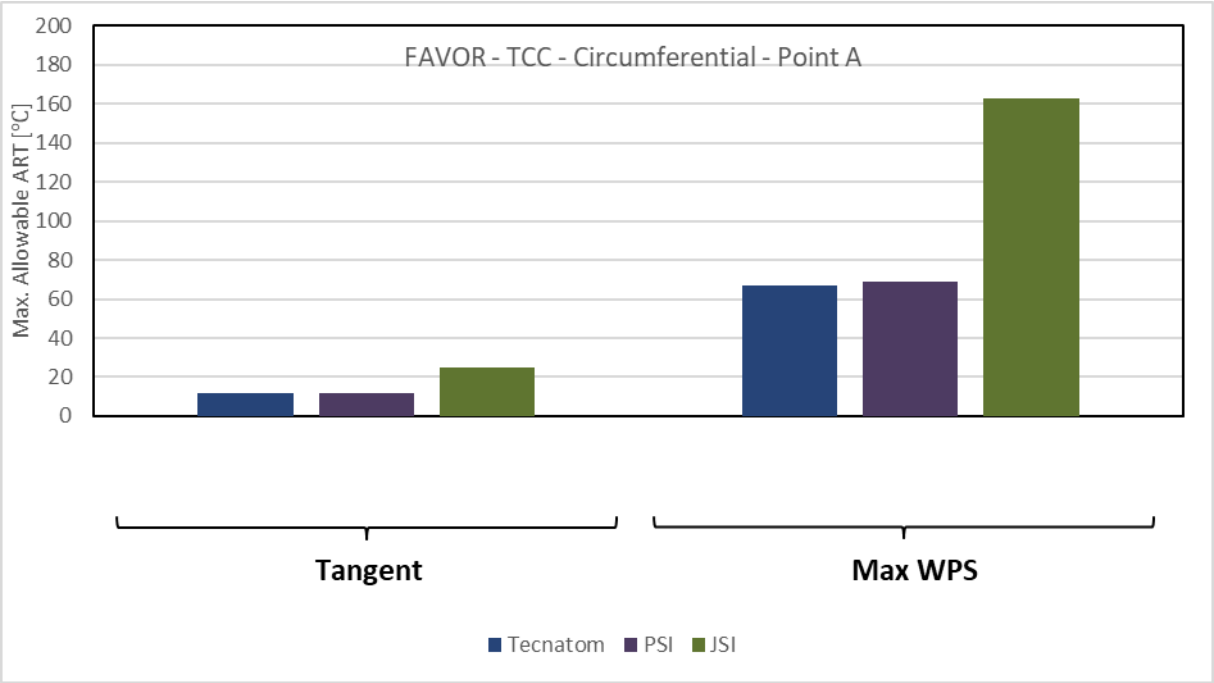

Figure 4.64: Maximum allowable RPV age for the deepest point of a circumferential TCC considering the FAVOR concept.

Table 4.26 Maximum allowable RPV age for the point in embedded cracks closest to the cladding considering the FAVOR concept

Partner	Maximum allowable ART for an embedded crack [years]			
	Tangent		Max WPS	
	Axial	Circumferential	Axial	Circumferential
Tecnatom	85	90	112	116
PSI		72		96

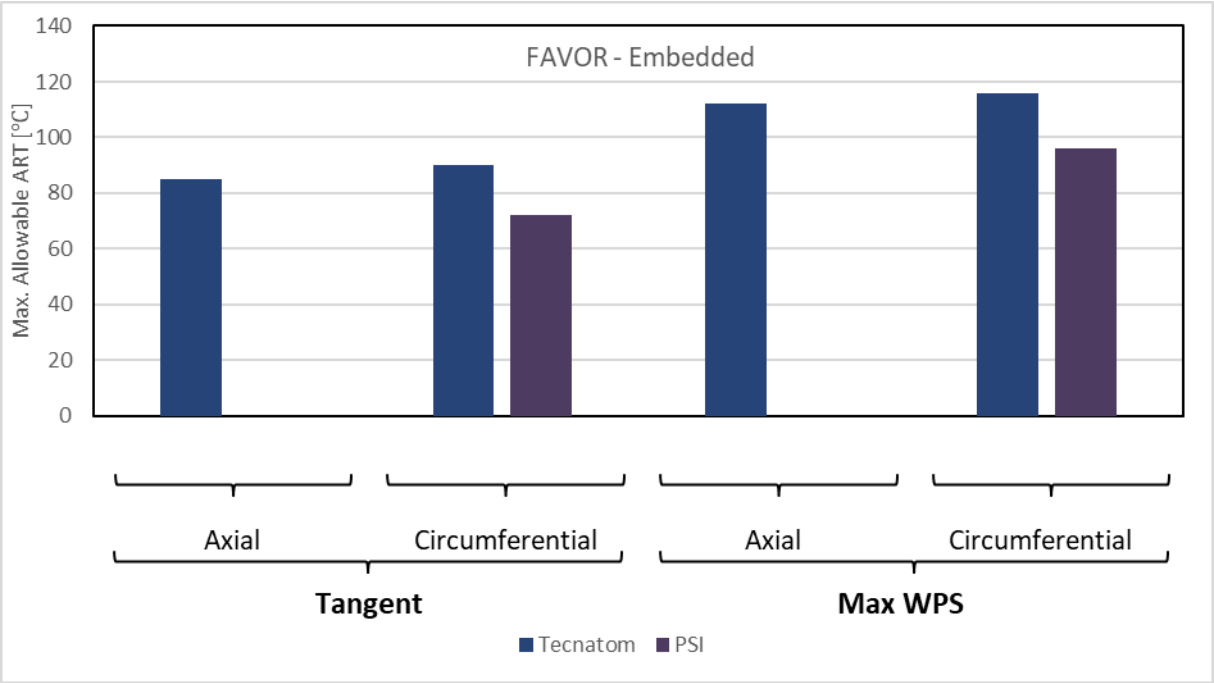

Figure 4.65: Maximum allowable RPV age for the point in embedded cracks closest to the cladding considering the FAVOR concept.

Some partners provided non-mandatory results for the T_0 concept which are presented in Table 4.27 and Table 4.28 as well as Figure 4.66 and Figure 4.67 for the tangent and max WPS approaches respectively. Crack front correction was not considered in these calculations. A sensitivity study of the influence of crack front correction is presented in Section 4.3.2.6.

The T_0 results gives higher RPV ages than the RT_{NDT} results for all relevant cases. The results are lower for the UCC point C which are still limited by point A.

Table 4.27 Maximum allowable RPV age for the tangent approach considering the T_0 concept

Partner	Max allowable RPV age for TCC [years]				Max allowable RPV age for UCC [years]			
	Axial		Circumferential		Axial		Circumferential	
	A	C	A	C	A	C	A	C
Kiwa	32.8	30.3	37.0	34.5	93.5	283.7	107.7	350.1
IPP	26.7	20.6	28.5	21.7	79.6	235.4	94.2	292.7
JSI			40					

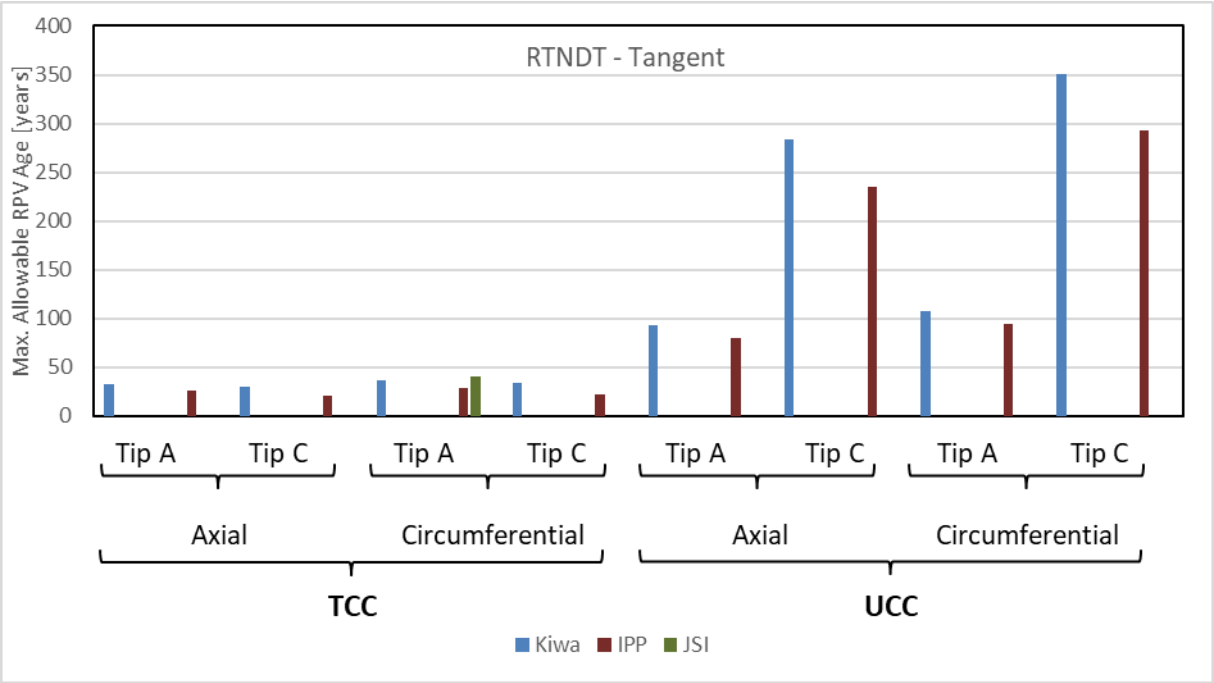

Figure 4.66: Maximum allowable RPV age for the tangent approach considering the T_0 concept.

Table 4.28 Maximum allowable RPV age for the max WPS approach considering the T_0 concept

Partner	Max allowable RPV age for TCC [years]				Max allowable RPV age for UCC [years]			
	Axial		Circumferential		Axial		Circumferential	
	A	C	A	C	A	C	A	C
Kiwa	170.1	169.2	176.6	184.9	271.4	512.3	282.2	582.8
IPP	170.4	153.9	181.5	163.0	270.5	457.0	282.2	>500
JSI			184.0					

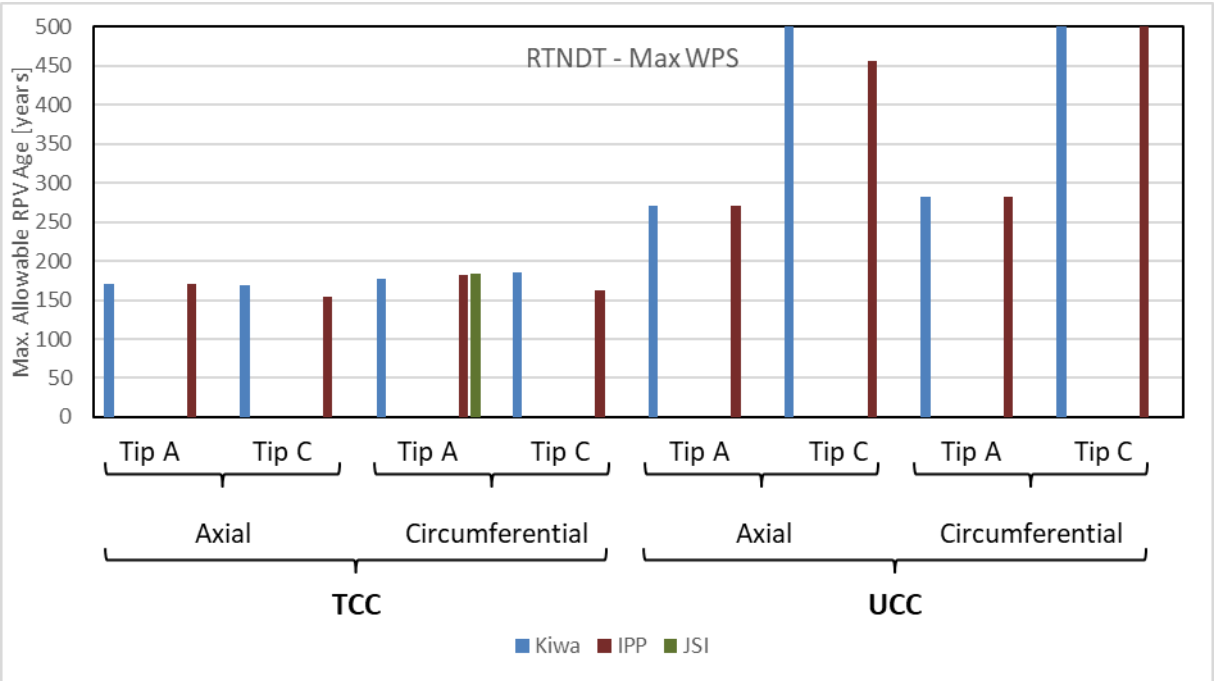

Figure 4.67: Maximum allowable RPV age for the max WPS approach considering the T_0 concept.

4.3.2.3 Calculation verifications

In order to verify the calculations and find reasons for deviances between results, Kiwa performed analyses using transient data from other partners for several of the cases within RR2. During this work, the results for PMA1 could directly be verified while the more complex PMA2 calculations required some iterations in order to obtain good agreement in results.

Verifications were made for all partners who included full transient data (time, temperature and stress intensity factors) in their results for the RT_{NDT} concept. Tecnatom and PSI only analysed the FAVOR concept which could not be verified by Kiwa as it is not included in Kiwa's tool. GRS did not provide instantaneous cpi values, therefore Kiwa could not make comparative analyses for their transient.

During the verification it was found that IRSN does not include truncation of K_{Ic} within their PMA2 calculations. They did furthermore not use the bilinear definition of the neutron fluence as presented in Section 2.3.8 but did instead use a linear approximation. As the effect of their neutron fluence approximation increased with time, and the UCC results gives much longer RPV life than TCC, IRSN updated the UCC results for RR2 with the bilinear description, while the TCC results in RR2 still includes the linear approximation of neutron fluence.

The maximum allowable RPV age calculated by IRSN and Kiwa, including results from Kiwa where K_{Ic} is not truncated, is presented in Table 4.29. These are the final IRSN results where UCC has been updated with the bilinear description of the neutron fluence while the TCC results are still based on the linear approximation. It can be seen that the agreement is very good for the UCC when not including truncation. The results for the TCC are quite close and the linear approximation can be considered sufficient for these cases. It can also be seen that the truncation of K_{Ic} results in longer RPV life-times for the cases considered.

Table 4.29 Maximum allowable RPV age values for the tangent approach considering the RT_{NDT} concept, comparison between IRSN and Kiwa

Partner	TCC, axial [years]	TCC, circumferential [years]	UCC, axial [years]
IRSN	39.1	39.0	83.0
Kiwa	42.9	46.1	96.6
Kiwa, excluding truncation	37.6	40.1	82.6

The cases with and excluding the ±3SD truncation of K_{Ic} are compared in Figure 4.68 where CPI as a function of RPV age is shown for point A of an axial TCC. It can be seen that the truncation has a large influence for lower CPI values while the influence decreases and becomes insignificant as CPI increase. This is due to the tails of the non-truncated distribution having a more significant impact at low probabilities.

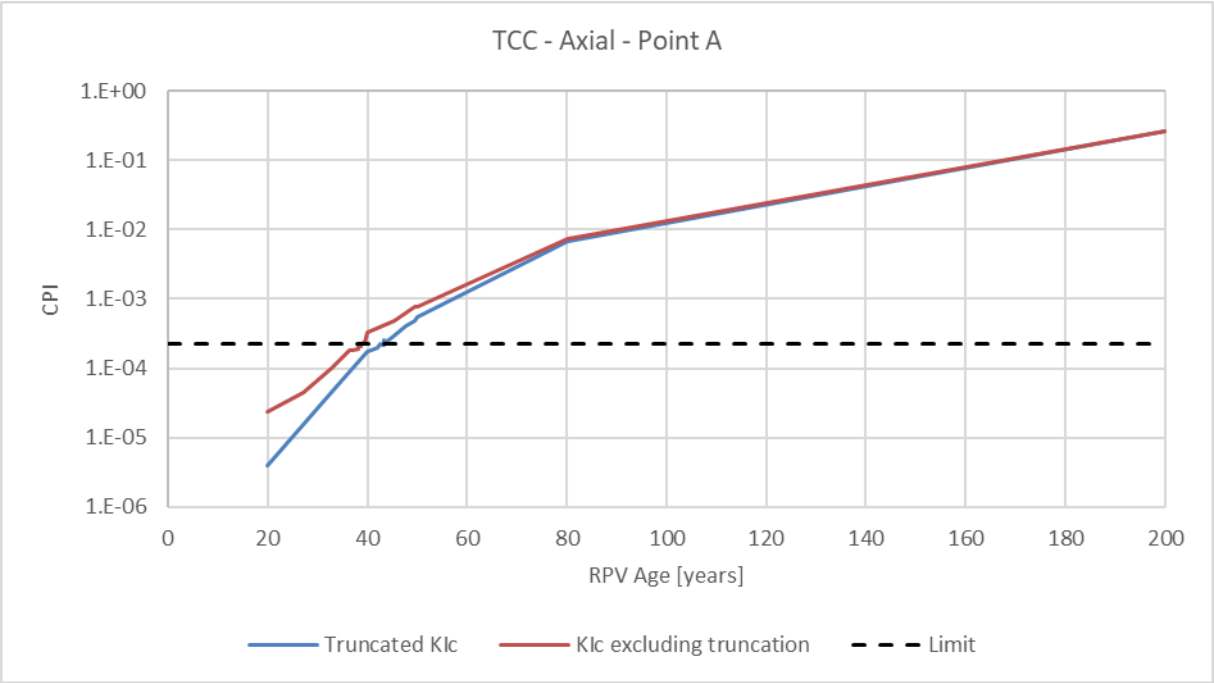

Figure 4.68: Comparison of CPI as a function of RPV age with and excluding the ±3 SD truncation of K_{Ic}.

4.3.2.4 Detailed results for TCC circumferential point A

The point A of a circumferential TCC is analysed by all partners and is therefore selected as case to study in further detail. Figure 4.69 and Figure 4.70 shows CPI as a function of ART (PMA1), using the tangent and max WPS approaches respectively, for the RT_{NDT} concept where the limiting value of CPI = $2.28 \cdot 10^{-4}$ is shown with a dashed line. The figure shows that results from most partners are in quite good agreement. FRA-G, who are considering mixing, gets much higher probabilities throughout the temperature span. GRS have the lowest probabilities for the tangent approach while getting similar results as FRA-G for the max WPS approach as compared to the other partners. This could be due to differences in the TH loading assumptions calculated with the ATHLET code.

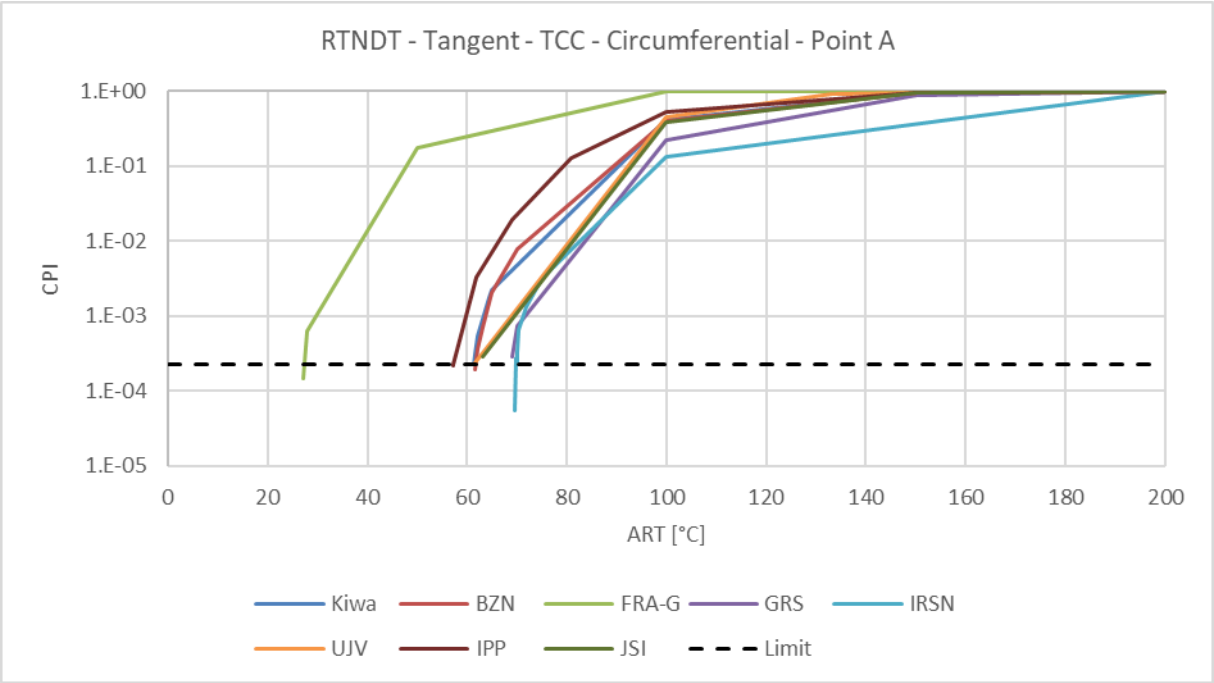

Figure 4.69: CPI as a function of maximum allowable ART for Point A of a circumferential TCC using the tangent approach for the RT_{NDT} concept.

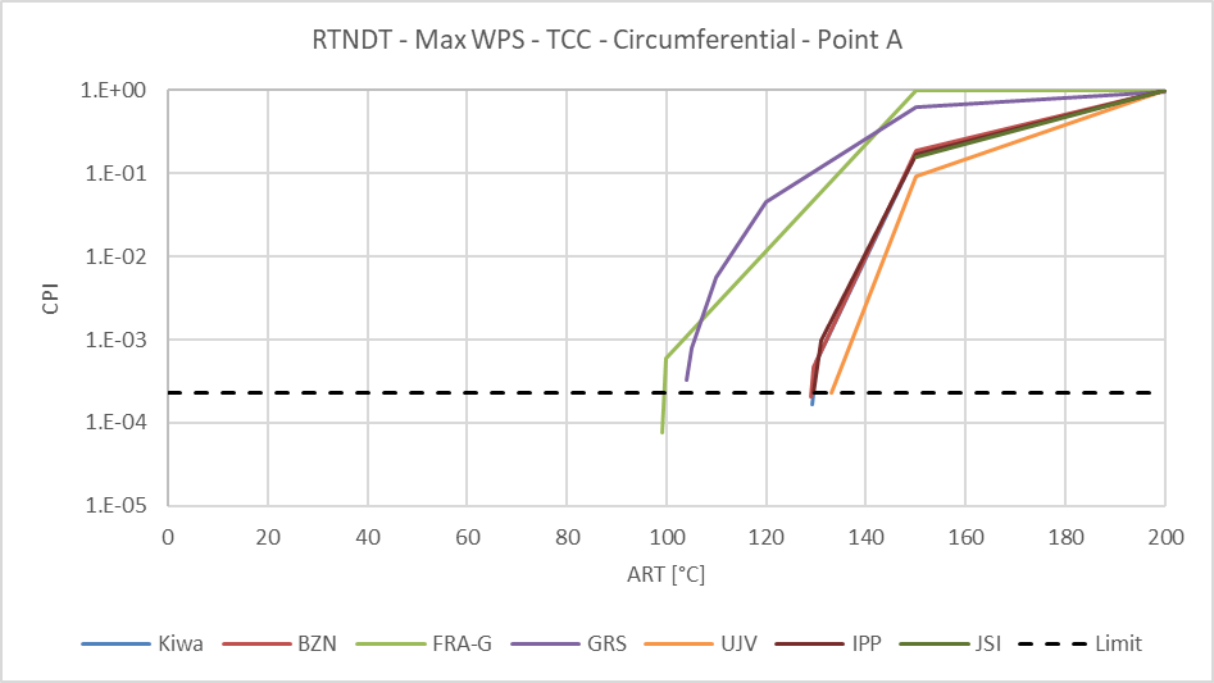

Figure 4.70: CPI as a function of maximum allowable ART for Point A of a circumferential TCC using the max WPS approach for the RT_{NDT} concept.

Figure 4.71 and Figure 4.72 shows corresponding plots for RPV age (PMA2) for the tangent and max WPS approaches respectively. The results between most partners are in quite good agreement here as well with FRA-G as an outlier due to mixing. Here as well, GRS have results close to most partners for the tangent approach, while having results similar to FRA-G for the max WPS approach.

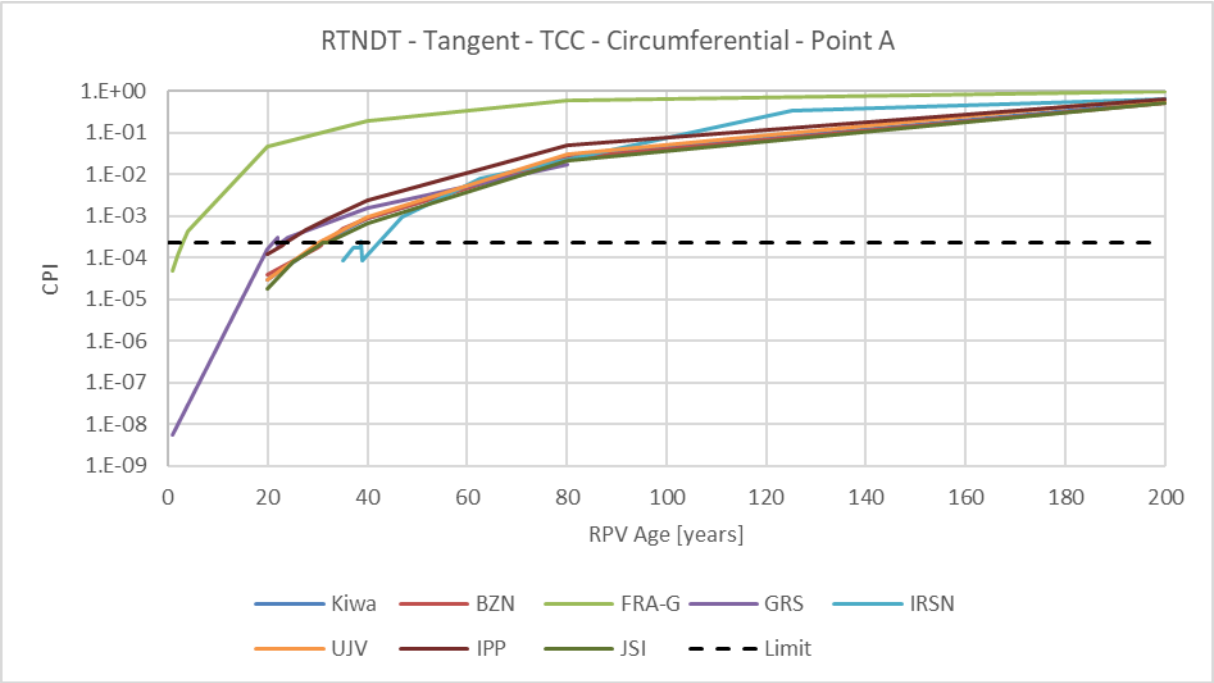

Figure 4.71: CPI as a function of maximum allowable RPV age for Point A of a circumferential TCC using the tangent approach for the RT_{NDT} concept.

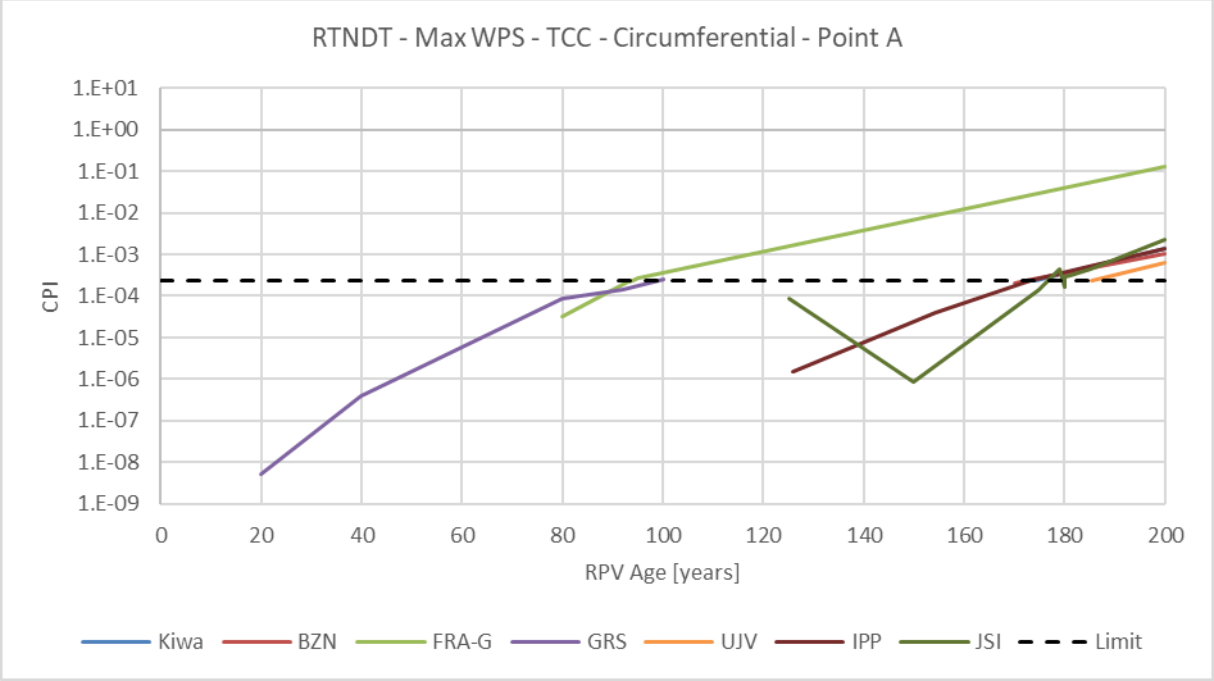

Figure 4.72: CPI as a function of maximum allowable RPV age for Point A of a circumferential TCC using the max WPS approach for the RT_{NDT} concept.

Figure 4.73 and Figure 4.74 shows cpi(t) plots, for PMA1 and PMA2 respectively, both with logarithmic and linear cpi(t) axis, for the time span where cpi(t) values are higher than zero for all partners. The values are for the case where CPI = $2.28 \cdot 10^{-4}$ is approximately reached.

In Figure 4.75 corresponding temperatures and stress intensity factor values are presented. The limiting cpi(t) values occur during a time interval where the temperatures are at their almost lowest while the stress intensity factor values are quite high. It can be seen that most partners have very

similar transient data. FRA-G has a quicker cool-down and lower temperature throughout almost the entire transient, while their K_I values are higher than others. This is due to them analysing a mixing case. IRSN has similar temperatures as most partners, but lower K_I values. This is due to them not including residual stresses in the calculations. GRS did not provide instantaneous cpi values.

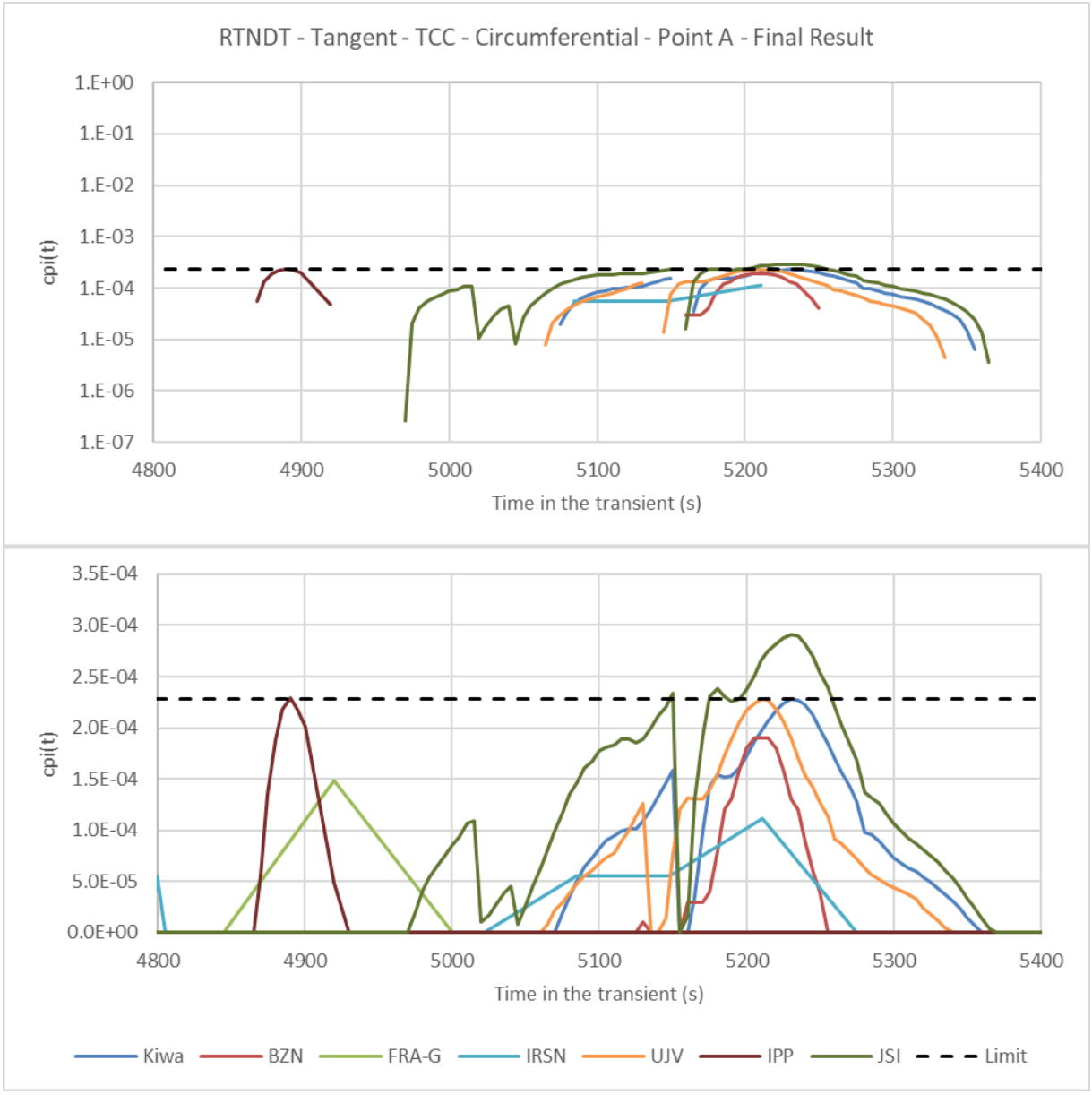

Figure 4.73: PMA1 cpi(t) values as a function of time cases when partners have approximately reached the limit of $2.28 \cdot 10^{-4}$. For point A of a circumferential TCC using the RT_{NDT} concept and tangent approach. The plot is limited to times of interest. The top plot is with logarithmic cpi(t) while the lower is for linear cpi(t).

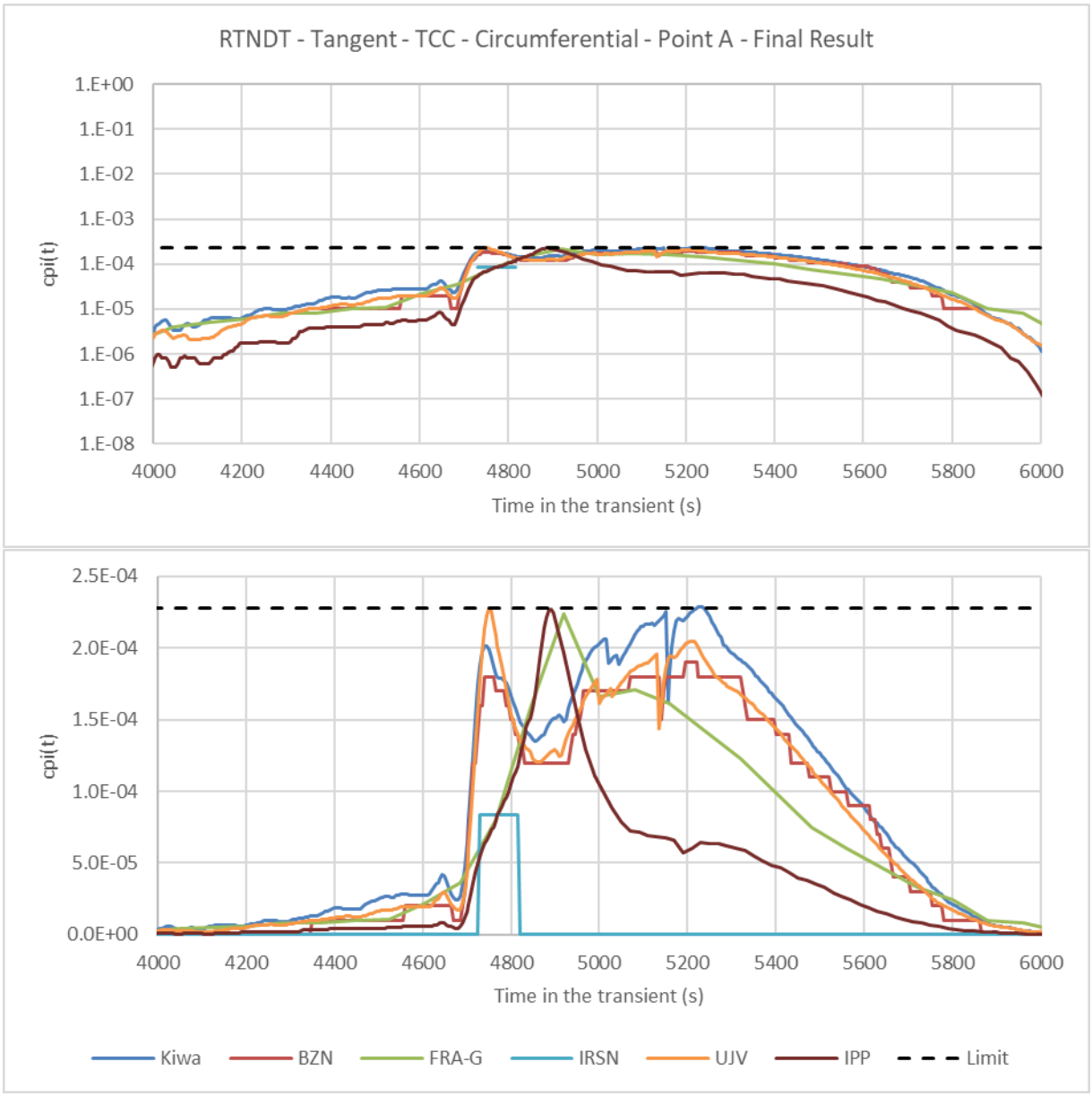

Figure 4.74: PMA2 cpi(t) values as a function of time cases when partners have approximately reached the limit of $2.28 \cdot 10^{-4}$. For point A of a circumferential TCC using the RT_{NDT} concept and tangent approach. The plot is limited to times of interest. The top plot is with logarithmic cpi(t) while the lower is for linear cpi(t).

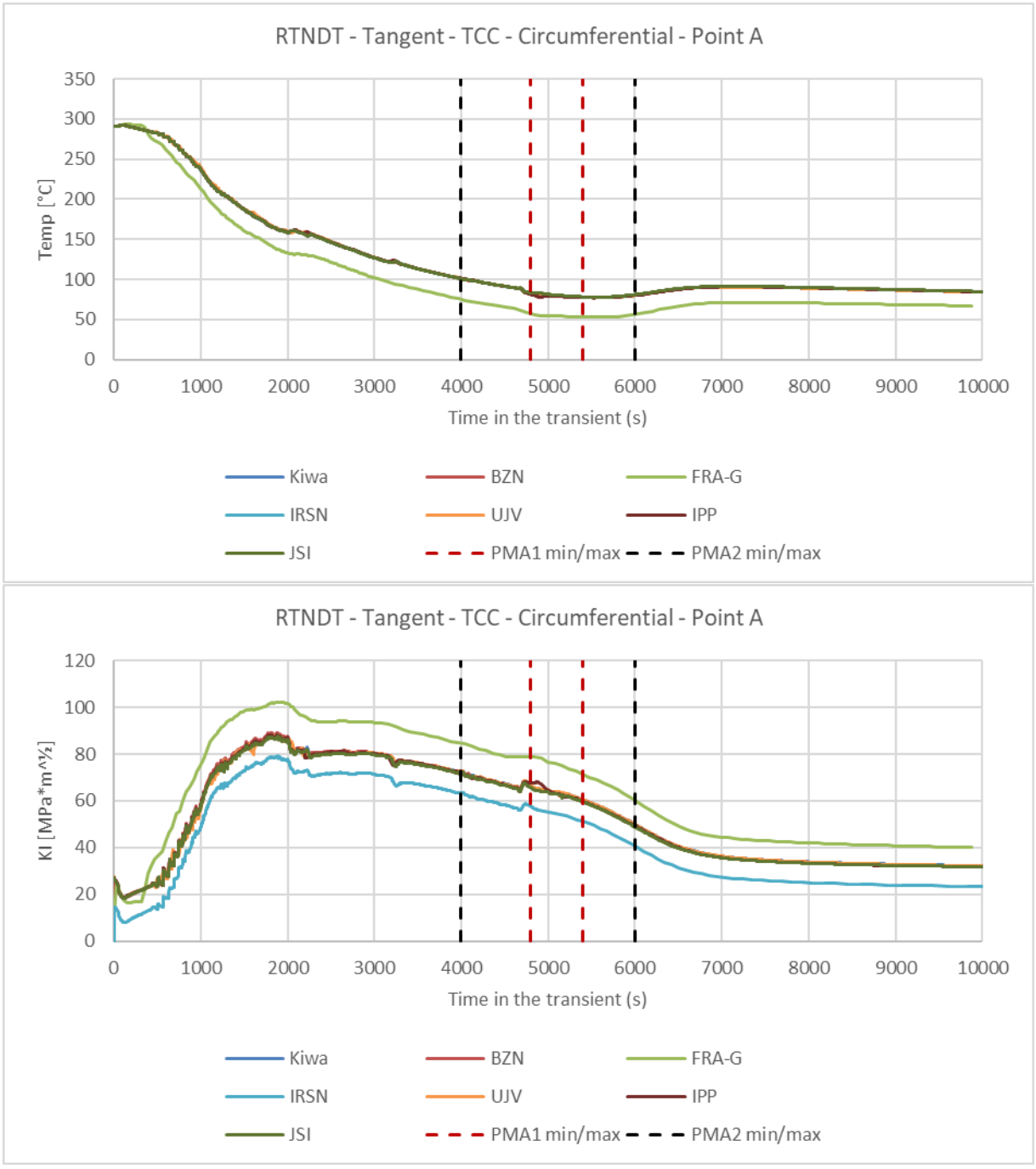

Figure 4.75: Temperature (top) and stress intensity factor values (bottom) for point A of a circumferential TCC using the RT_{NDT} concept. The times where cpi(t) values are of interest is marked with red and black dashed lines for PMA1 and PMA2 respectively.

The distributed ART used in PMA2 is compared between the partners in Figure 4.76 where the thinner lines represent the 5% and 95% quantiles while the thicker lines in the middle represents the mean value. The results are in very good agreement between the partners as expected since they are independent on which transient is being used. The exception is IRSN which can be explained by the different definition of neutron fluence used for the present case, see Section 4.3.2.3. The deviance in neutron fluence due to different definitions is shown in Figure 4.77.

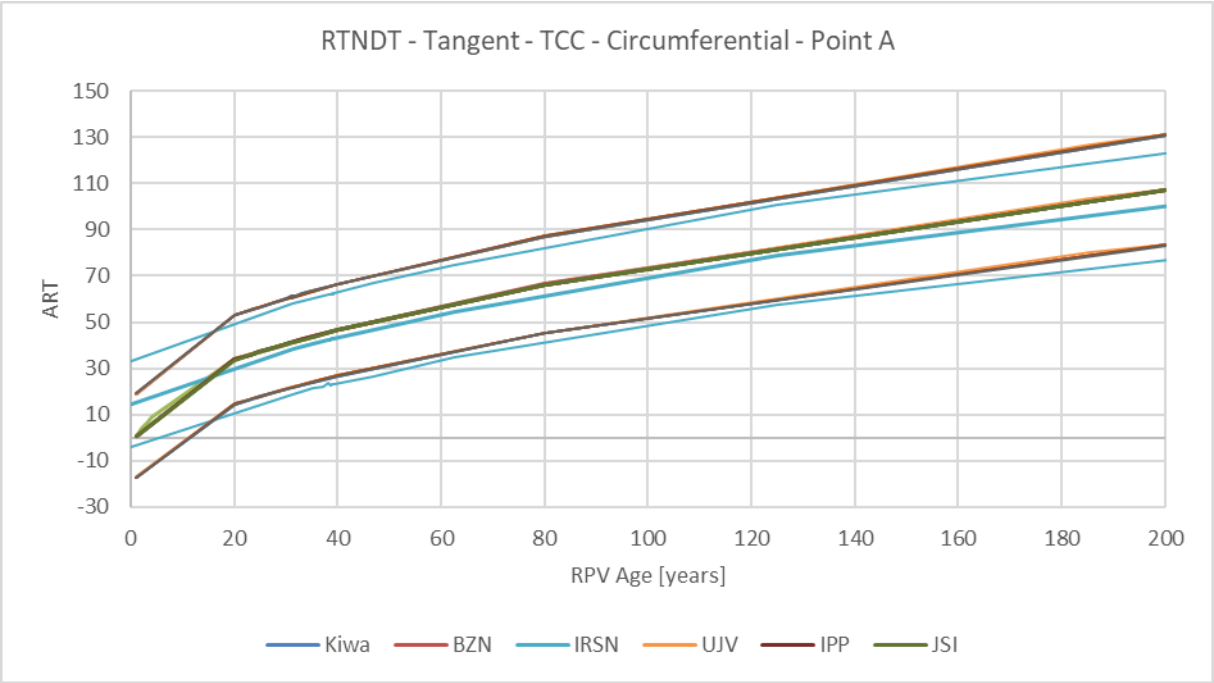

Figure 4.76: ART distribution used within PMA2 presented with mean value as well as 5% and 95% quantiles at the inner surface for point A of a circumferential TCC.

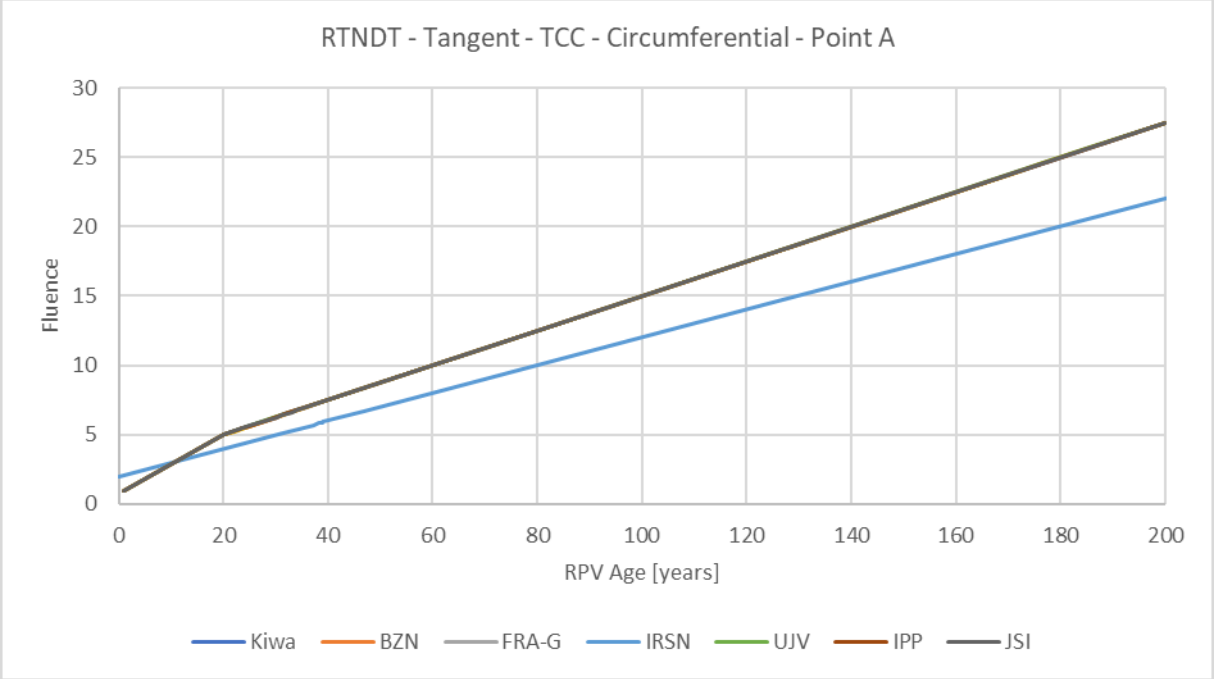

Figure 4.77: Mean neutron fluence used within PMA2 point A of a circumferential TCC.

The same case is studied for the FAVOR concept where a crack shape of $2c/(a + r) = 6$ is used as this case is analysed by all partners using FAVOR.

Figure 4.78 and Figure 4.79 shows CPI as a function of ART (PMA1), using the tangent and max WPS approaches respectively, for the FAVOR concept where the limiting value of CPI = $2.28 \cdot 10^{-4}$ is shown with a dashed line.

The results show a good agreement between Tecnatom and PSI while JSI gets lower CPI values which can be explained by the difference in TH-data.

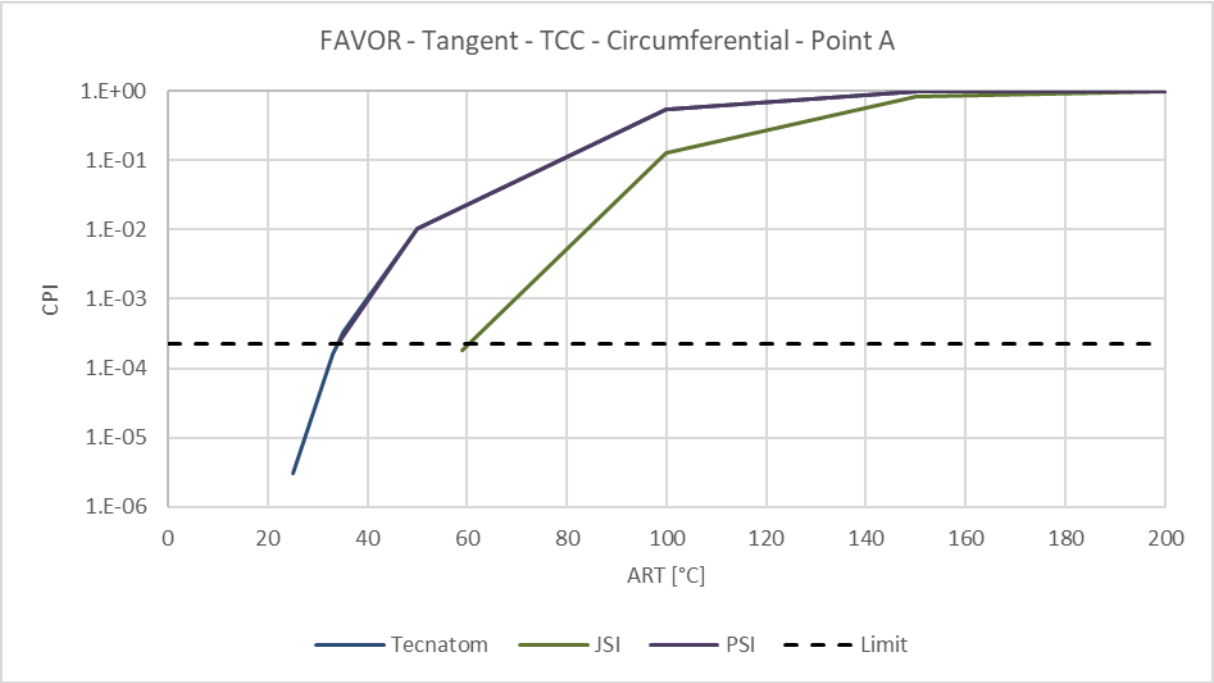

Figure 4.78: CPI as a function of maximum allowable ART for Point A of a circumferential TCC using the tangent approach for the RT_{NDT} concept.

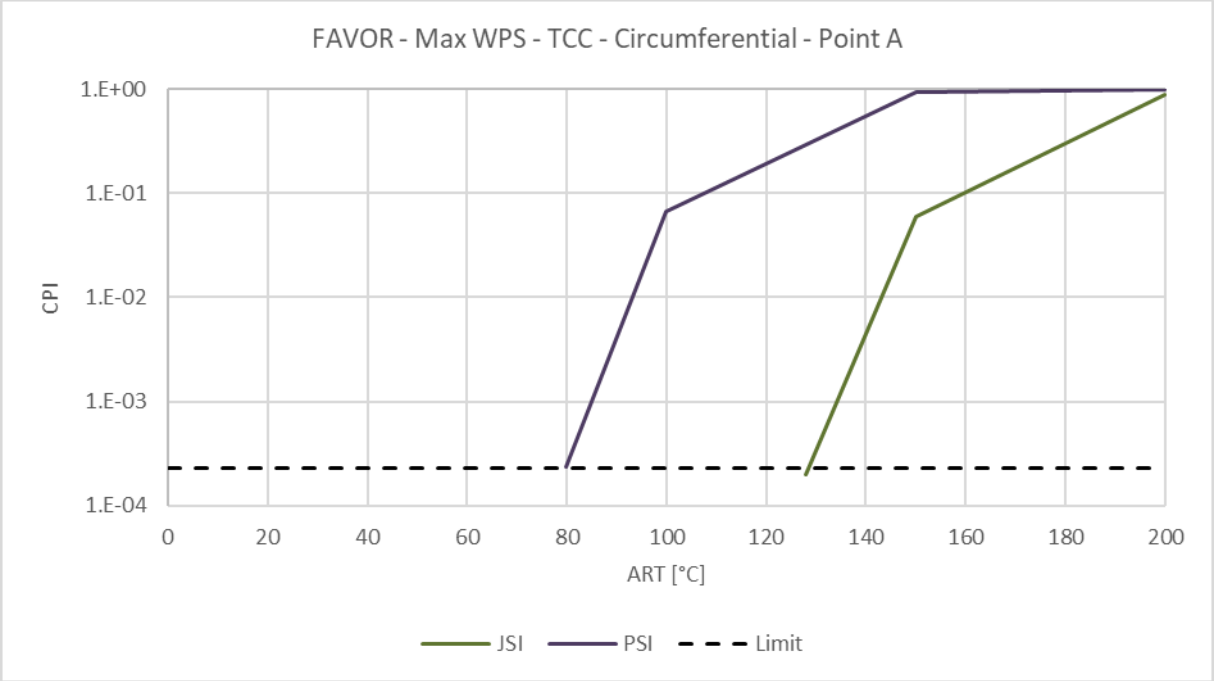

Figure 4.79: CPI as a function of maximum allowable ART for Point A of a circumferential TCC using the max WPS approach for the RT_{NDT} concept.

Figure 4.80 and Figure 4.81 shows CPI as a function of RPV age (PMA2), using the tangent and max WPS approaches respectively, for the FAVOR concept where the limiting value of CPI = $2.28 \cdot 10^{-4}$ is shown with a dashed line.

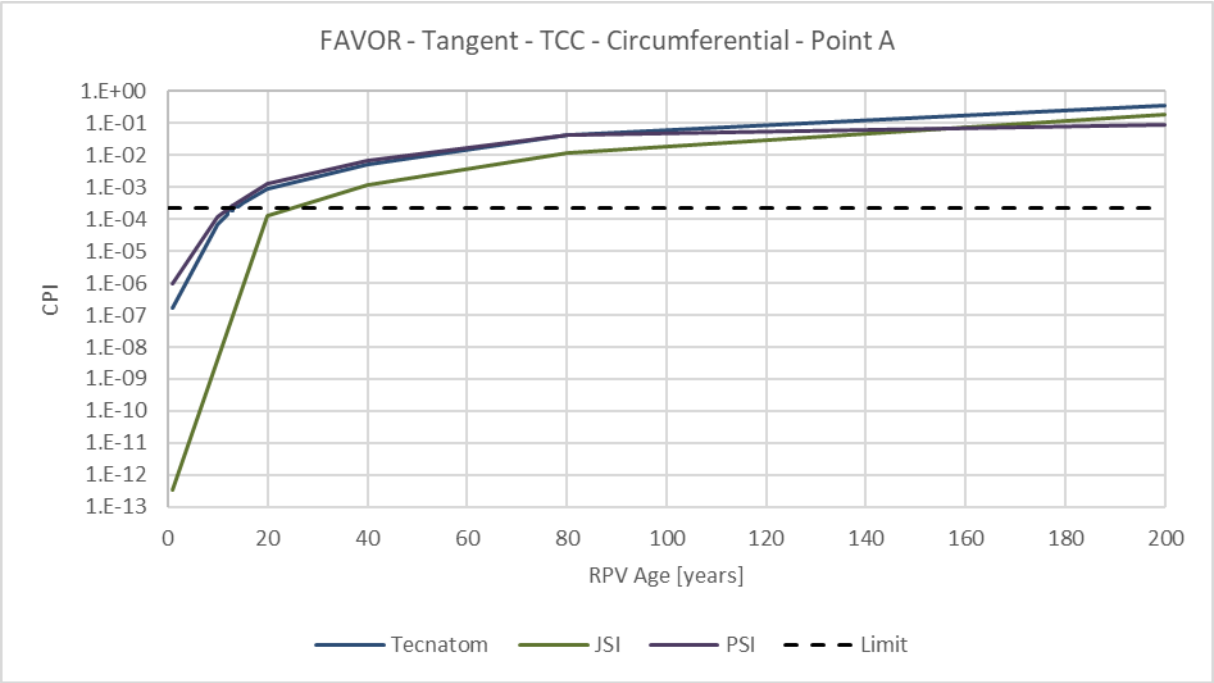

Figure 4.80: CPI as a function of maximum allowable RPV age for Point A of a circumferential TCC using the tangent approach for the RT_{NDT} concept.

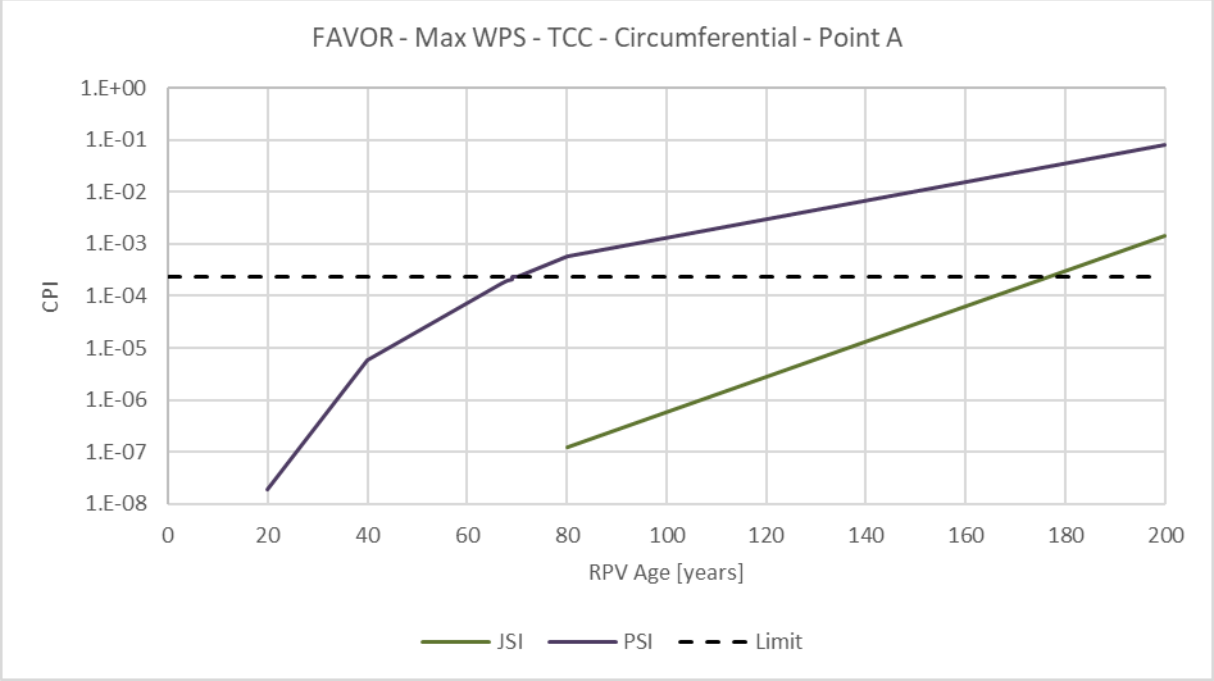

Figure 4.81: CPI as a function of maximum allowable RPV age for Point A of a circumferential TCC using the max WPS approach for the RT_{NDT} concept.

Figure 4.82 shows cpi(t) plots for PMA1, both with logarithmic and linear cpi(t) axis. An oscillating behaviour is seen late in the transient which was not observed for the RT_{NDT} concept. In Figure 4.83 corresponding temperatures and stress intensity factor values are presented.

None of the partners provided cpi(t) curves for PMA2.

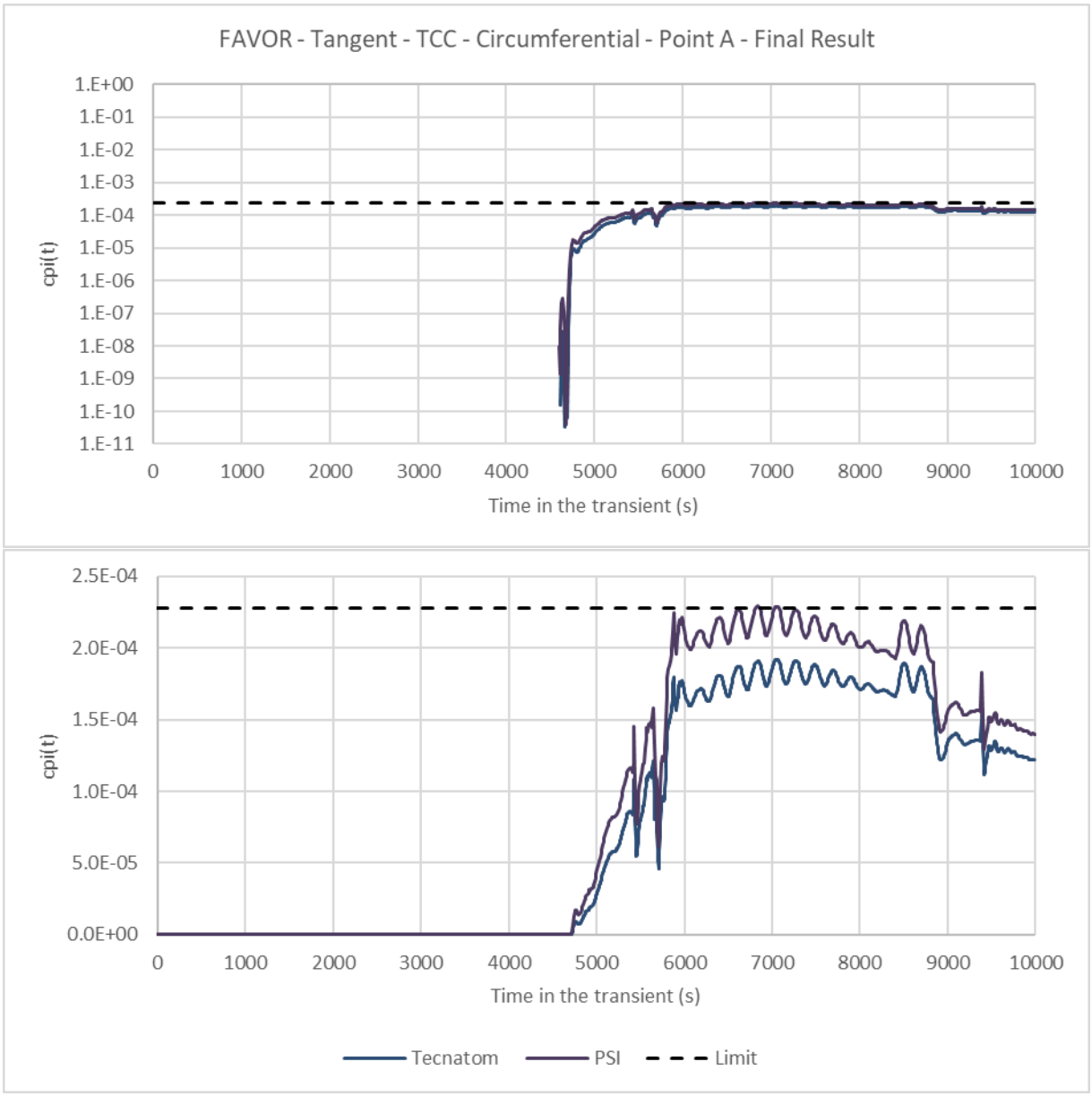

Figure 4.82: PMA1 cpi(t) values as a function of time cases when partners have approximately reached the limit of $2.28 \cdot 10^{-4}$. For point A of a circumferential TCC using the FAVOR concept and tangent approach. The top plot is with logarithmic cpi(t) while the lower is for linear cpi(t).

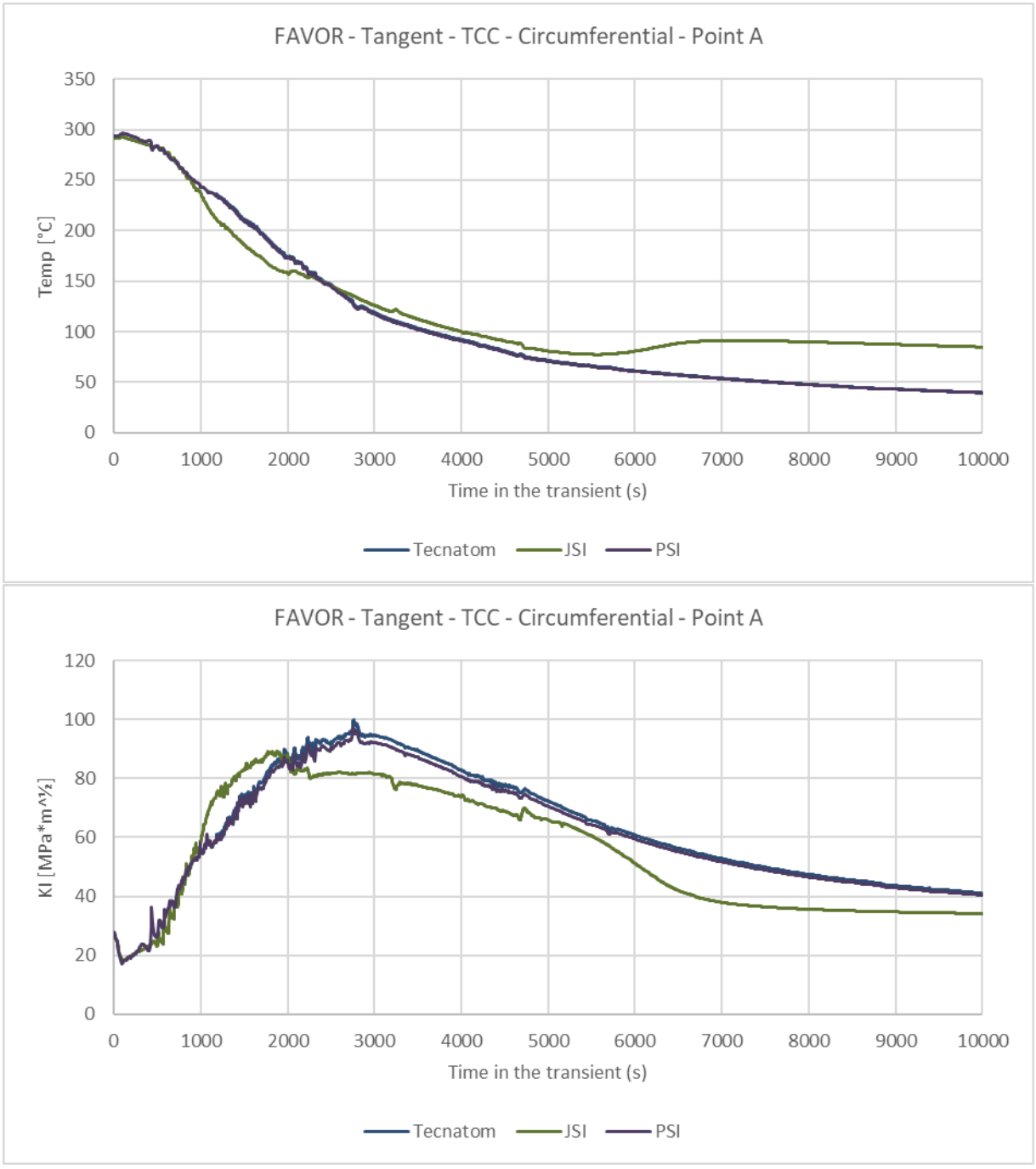

Figure 4.83: Temperature (top) and stress intensity factor values (bottom) for point A of a circumferential TCC using the FAVOR concept.

4.3.2.5 Comparison of fracture toughness concepts

The three different fracture toughness concepts described in Section 2.3.4 are compared in Figure 4.84 for point A of a circumferential TCC using results provided by JSI. Note that for the FAVOR concept, different assumptions for the crack shape have been used according to Section 2.3.12.2. The FAVOR and RTNDT concepts are in relatively good agreement while the T0 concept gives lower probabilities for RPV ages over approximately 25 years.

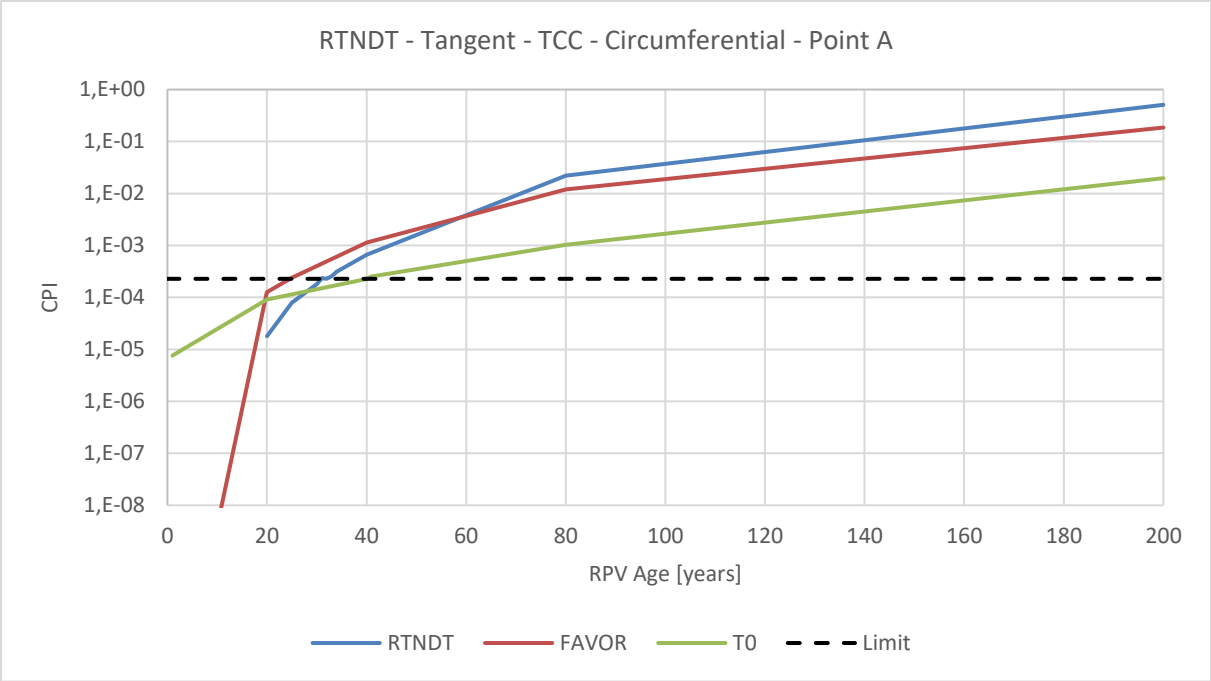

Figure 4.84: Comparison of different fracture toughness concepts using JSI results.

4.3.2.6 Sensitivity study of crack front correction for the T_0 concept

It was decided during the project that the crack front length (CFL) correction for T_0 should be excluded (see Section 2.3.4.2). In this section, a sensitivity study performed by Kiwa is presented to show its impact on the T_0 results.

For the current crack with a depth of 10 mm (excluding cladding) and length of 60 mm, the CFL within the base metal is 124.5 mm. In some countries (e.g. Sweden) the crack front length is recommended to be limited to at most 100 mm, this limit is however not considered in the current study.

In Figure 4.85 the CPI as a function of RPV age is plotted for both the *RT*NDT concept as well as the T_0 concept with and without CFL correction. It can be seen that the probabilities are almost a factor 10 higher when the CFL correction is considered. The T_0 results with CFL correction give higher probabilities than the RT_{NDT} results for up to about 55 years, after which the RT_{NDT} concept is limiting.

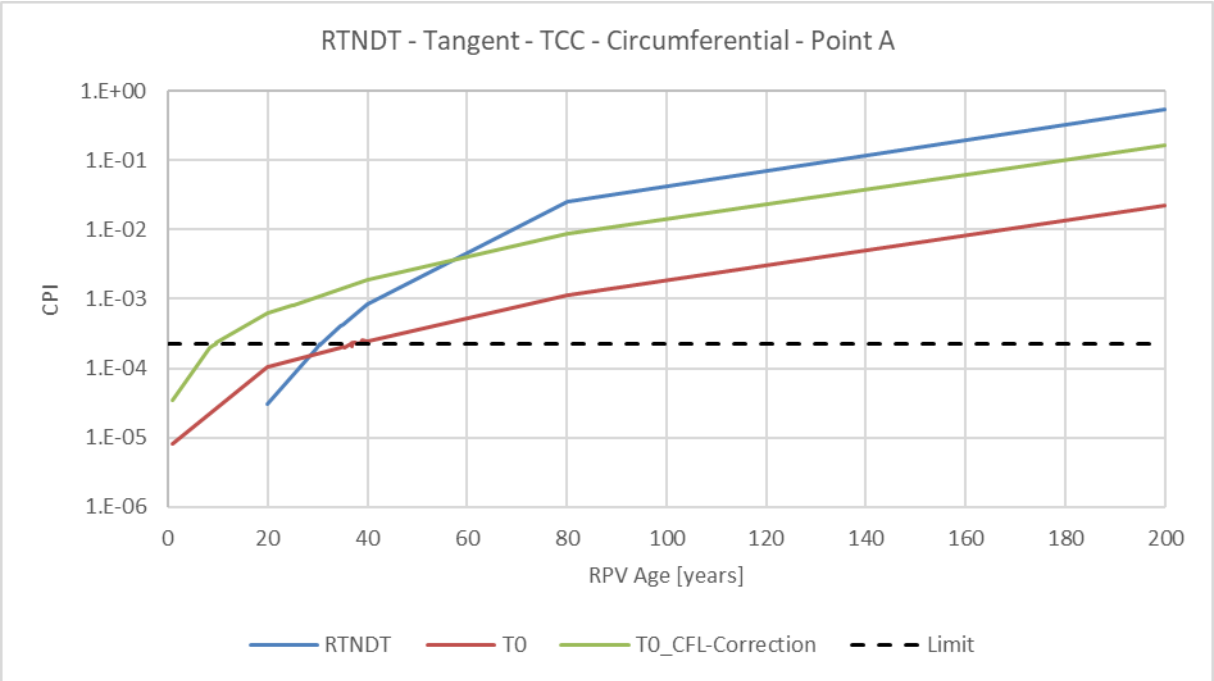

Figure 4.85: Comparison of different fracture toughness concepts using Kiwa results, where the T_0 concept considering crack front length correction is included.

4.3.2.7 Conclusions from RR2

In RR2, fixed crack sizes were analysed for TCC, UCC and embedded cracks according to Section2.3.2.

For TCC, the crack was assumed to have a depth of $a = 16$ mm (including cladding) and length of $2c = 60$ mm. Within the FAVOR code, the TCC shape is defined differently as the TCC2 shape (see Figure 2.5). It is also only available for circumferential cracks and the point C in the clad/base interface is not available. The FAVOR users have therefore only analysed the deepest point for circumferential TCC2. Furthermore, the exact crack shape defined in APAL cannot be used in FAVOR as the crack depth can only be defined as integer percentage values of the full wall thickness, *t* (including cladding). The crack shape is also limited to certain ratios between the crack length and crack depth (including cladding). For PMA1, JSI and PSI studied several crack geometries including the exact shape defined in APAL using in-house code, while for PMA2 all FAVOR users assumed a crack shape of $2c/(a + r) = 6$. Tecnatom and PSI assumed $a = 17.43$ mm (7% of *t*) as a conservative assumption while JSI assumed $a = 14.94$ mm (6% of *t*) based on their comparison of SIF for different crack shapes that showed that this crack depth most resembles the SIF values calculated using the CEA TCC1 definition see Figure 2.12.

For UCC, the crack is assumed as $a = 10$ mm and $2c = 60$ mm. This crack shape is not available within FAVOR, therefore, an alternative embedded crack was defined within APAL with a total crack depth of $2a = 20$ mm and a length of $2c = 120$ mm. The embedded crack was analysed by Tecnatom and PSI who used the assumption of $2a = 19.92$ mm (8% of *t*) and $2c = 119.52$ mm ($2c/2a = 6$), see Section 2.3.12.1. It should also be noted that for embedded cracks, point A represents the position closest to the clad/base interface, while for the other geometries point A is the deepest point of the crack.

The differences between partners can be explained by different TH data used as shown for point A of a circumferential TCC in Figure 4.75 where it can be seen that almost all partners have very similar transient data. FRA-G differs due to the consideration of mixing and IRSN has lower SIF values as they did not include WRS. A corresponding plot for transient data used within FAVOR is shown in Figure 4.83 where it is seen that Tecnatom and PSI have very similar data as they use the same transient data, while JSI have very large differences in their transient data which more closely resembles the TH data

used by other partners (Figure 4.75). GRS did not include instantaneous cpi values, but differences between their results and the other partners are assumed to be due to the use of a different TH code than all others.

It can be seen that the TCC is the most limiting of the geometries studied. For all three fracture toughness concepts, the differences are small between crack orientations for all geometries studied where axial cracks generally give slightly lower values. In most cases point C is limiting for TCC although the differences between the positions are small. For UCC, point A is limiting and point C gives much higher values, except for FRA-G who got shorter RPV lifetimes for point C of the axial UCC. For embedded cracks, only the position closest to the clad/base interface was analysed.

When comparing RT_{NDT} results from FRA-G to the other partners it can be seen that considering mixing has a very large impact on the final results where maximum allowable RPV lifetimes was only 1 year for the tangent approach, where other partners obtained values of about 17 years or more.

IRSN did not include WRS which resulted in lower SIF values. This resulted in RPV lifetimes that were about 20 – 40% longer than the other partners. IRSN also did not include the truncation of the fracture toughness for PMA2 which was shown to be a conservative approach, see Figure 4.68.

JSI analysed all three fracture toughness concepts and these are compared in Section 4.3.2.5 where it was seen that the RT_{NDT} and FAVOR concepts were relatively close while the T_0 concept gave much lower CPI for RPV lifetimes longer than about 30 years. It is important to note however that the crack front length (CFL) correction for the T_0 concept was excluded in the analyses. This was studied in Section 4.3.2.6 where it was shown that if CFL correction is considered, the T_0 concept is much closer to the others.

4.3.3 RR3 – Check CPF for base case transient (non-mandatory)

The RR3 benchmark was planned as a non-mandatory continuation of RR2 by considering crack arrest analyses according to Section 2.3.10 and calculating CPF values for various crack geometries (TCC, UCC and embedded cracks), orientations within the RPV wall (axial and circumferential), crack tip locations and sizes. The calculations in RR3 were performed in the same manner as in RR2, see Section 4.3.2 for both pre-defined values and the final results including intermediate results. The main difference is related to consideration of allowable CPF = $2.28 \cdot 10^{-4}$ instead of CPI.

The partners were requested to report their results for comparison providing the final ART or RPV age for the target CPF-value. Also, the CPI, CPF, CPNA and CPSA values were requested for each calculation.

FRA-G, UJV, IPP, Tecnatom and JSI have performed analyses within this subtask.

4.3.3.1 PMA1

The maximum allowable ART, considering CPF, was calculated for the different crack geometries and locations for both the tangent and max WPS approaches.

Final allowable ART values for the RT_{NDT} concept are presented in Table 4.30 and Table 4.31 as well as Figure 4.86 and Figure 4.87 for the tangent and max WPS approaches respectively. In the figures, the corresponding ART values considering CPI from RR2 are included for comparison.

Results for the RT_{NDT} concept were mainly provided by IPP and FRA-G, with two additional results from UJV as well. Due to the very different transients analysed by FRA-G and the others, the possibility of verifying comparisons is limited. It can be noted that UJV and IPP obtained similar ART values considering CPI in RR2 for point A of both an axial and circumferential TCC. When comparing maximum allowable ART values however, IPP gained much when considering crack arrest, while UJV only have a slight increase.

IPP gains higher maximum allowable ART values for all geometry cases using the tangent approach, while no gain is observed for the max WPS approach. FRA-G only gains higher maximum allowable ART values for the circumferential TCC using the tangent approach.

Table 4.30 Maximum allowable ART values for the tangent approach considering the RT_{NDT} concept

Partner	Maximum allowable ART for TCC [°C]				Maximum allowable ART for UCC [°C]			
	Axial		Circumferential		Axial		Circumferential	
	A	C	A	C	A	C	A	C
FRA-G	28.00	25.00	46.00	45.00	43.90	90.75	42.79	90.41
UJV	59.40		64.00					
IPP	96.06	54.06	96.41	54.59	101.40	161.12	103.08	190.53

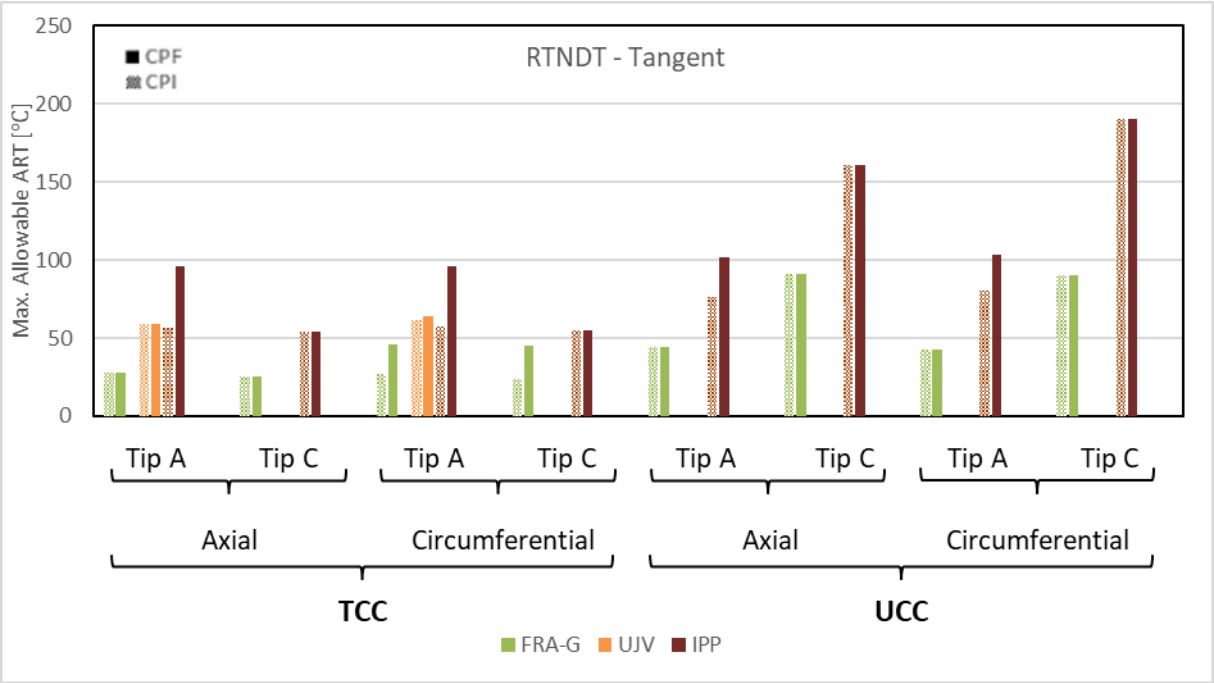

Figure 4.86: Maximum allowable ART values for the tangent approach considering the RT_{NDT} concept.

Table 4.31 Maximum allowable ART values for the max WPS approach considering the RT_{NDT} concept

Partner	Maximum allowable ART for TCC [°C]				Maximum allowable ART for UCC [°C]			
	Axial		Circumferential		Axial		Circumferential	
	A	C	A	C	A	C	A	C
FRA-G	99.00	93.00	99.00	94.00	112.90	141.00	113.10	142.30
IPP	127.49	124.69	129.52	126.69	145.97	186.80	146.74	202.89

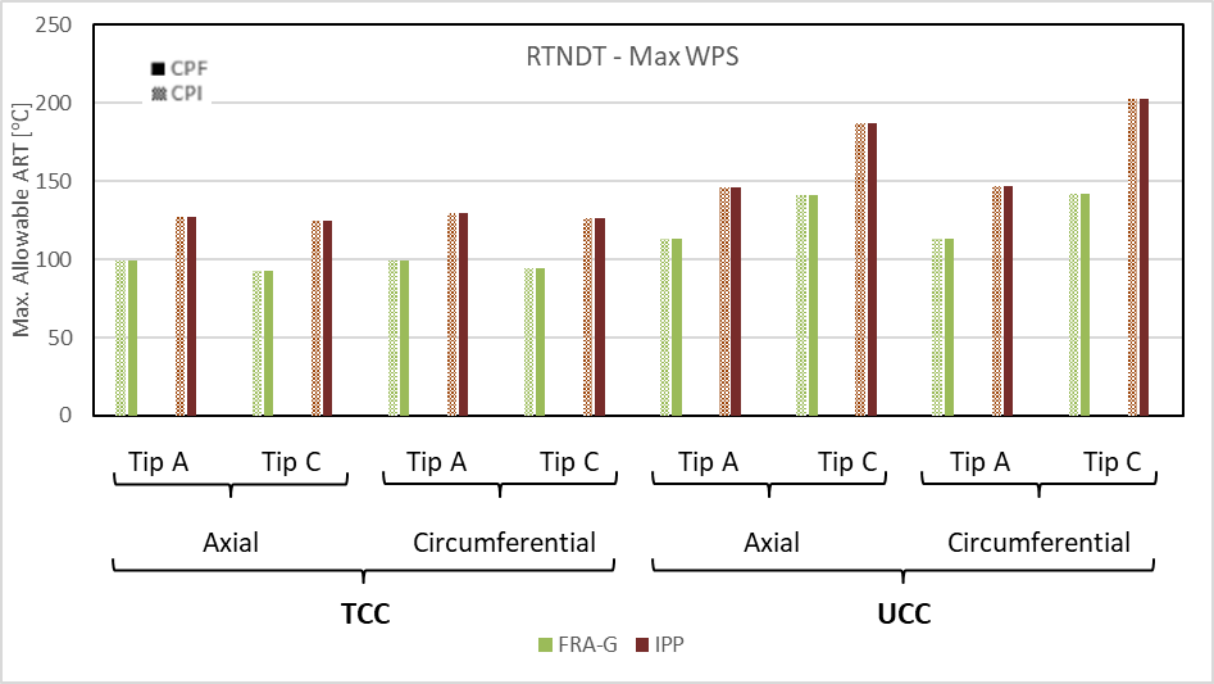

Figure 4.87: Maximum allowable ART values for the max WPS approach considering the RT_{NDT} concept.

Final allowable ART values for the FAVOR concept are presented in Table 4.32 and Table 4.33 as well as Figure 4.88 and Figure 4.89 for a circumferential TCC and embedded cracks respectively. In the figures, the corresponding ART values for given CPI in RR2 are included for comparison.

The gain in maximum allowable ART is similar between Tecnatom and JSI for both the tangent and max WPS approaches.

A noticeable difference as compared to the *RT*NDT concept results is that here, the max WPS approach gains substantially when considering crack arrest.

Table 4.32 Maximum allowable ART values for a circumferential TCC using the FAVOR concept

Partner	Max allowable ART for a circumferential TCC [°C]	
	Tangent	Max WPS
Tecnatom	52	97
JSI	75	138

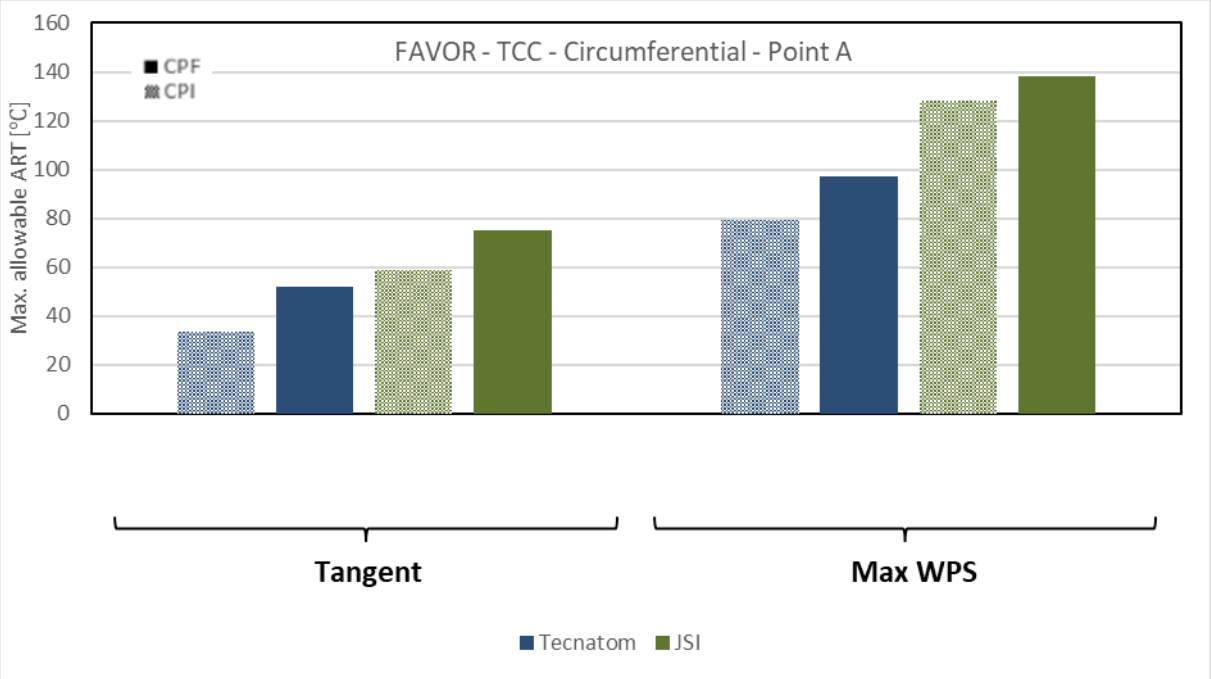

Figure 4.88: Maximum allowable ART values for a circumferential TCC using the FAVOR concept.

Table 4.33 Maximum allowable ART values for a circumferential embedded crack using the FAVOR concept

Partner	Max allowable ART for a circumferential embedded crack [years]	
	Tangent	Max WPS
Tecnatom	178	589

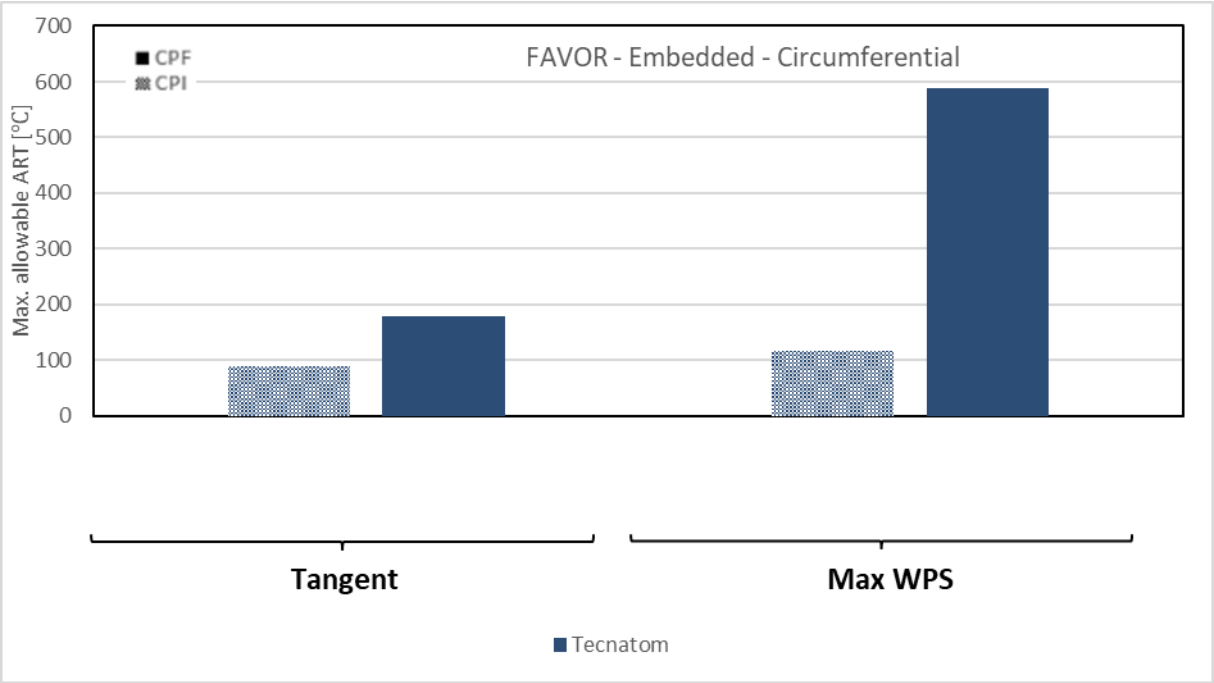

Figure 4.89: Maximum allowable ART values for a circumferential embedded crack using the FAVOR concept.

Final allowable ART values for the T_0 concept are presented in Table 4.34 and Table 4.35 as well as Figure 4.90 and Figure 4.91 for the tangent and max WPS approaches respectively. In the figures, the corresponding values for CPI given in RR2 are included for comparison.
IPP was the only partner who provided results for the T_0 concept, thus comparisons with other partners for verifying the results were not possible. It can be seen that for the T_0 concept, a large gain in maximum allowable ART is obtained for all geometry cases and both the tangent and max WPS approaches.

Table 4.34 Maximum allowable ART values for the tangent approach considering the T_0 concept

Partner	Maximum allowable ART for TCC [°C]				Maximum allowable ART for UCC [°C]			
	Axial		Circumferential		Axial		Circumferential	
	A	C	A	C	A	C	A	C
IPP	94.95	27.28	95.82	27.83	100.01	83.08	100.79	97.09

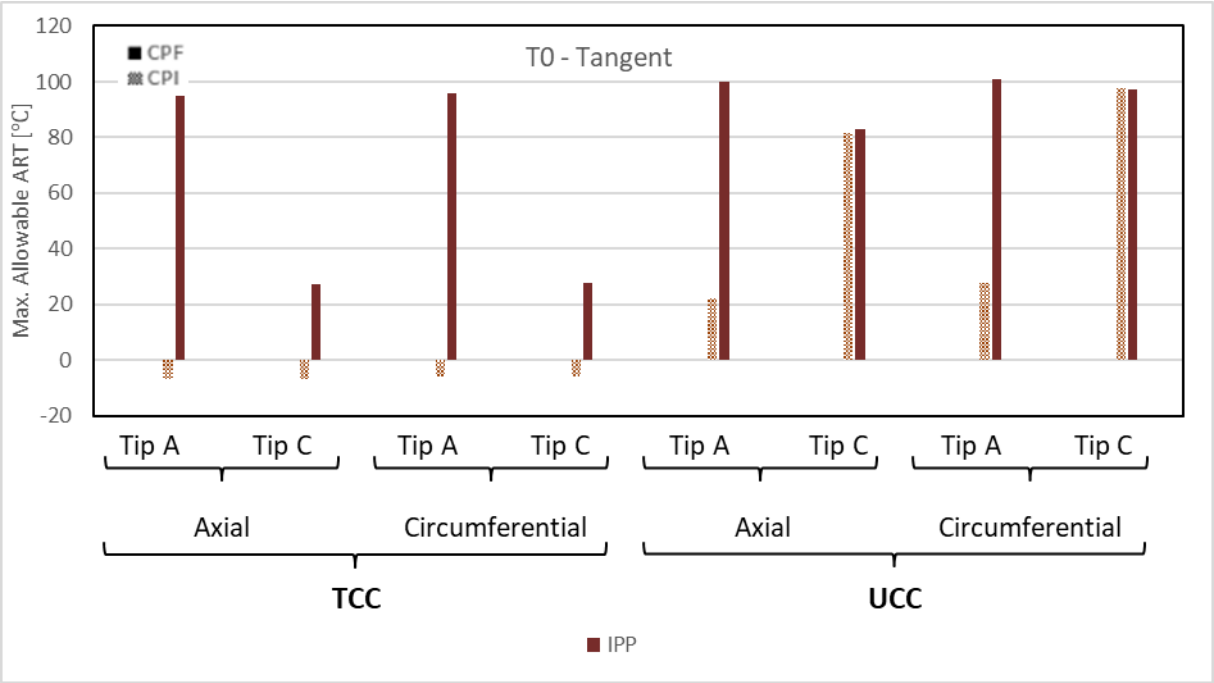

Figure 4.90: Maximum allowable ART values for the tangent approach considering the T_0 concept.

Table 4.35 Maximum allowable ART values for the max WPS approach considering the T_0 concept

Partner	Maximum allowable ART for TCC [°C]				Maximum allowable ART for UCC [°C]			
	Axial		Circumferential		Axial		Circumferential	
	A	C	A	C	A	C	A	C
IPP	105.95	61.60	108.11	65.80	119.21	136.60	120.49	148.98

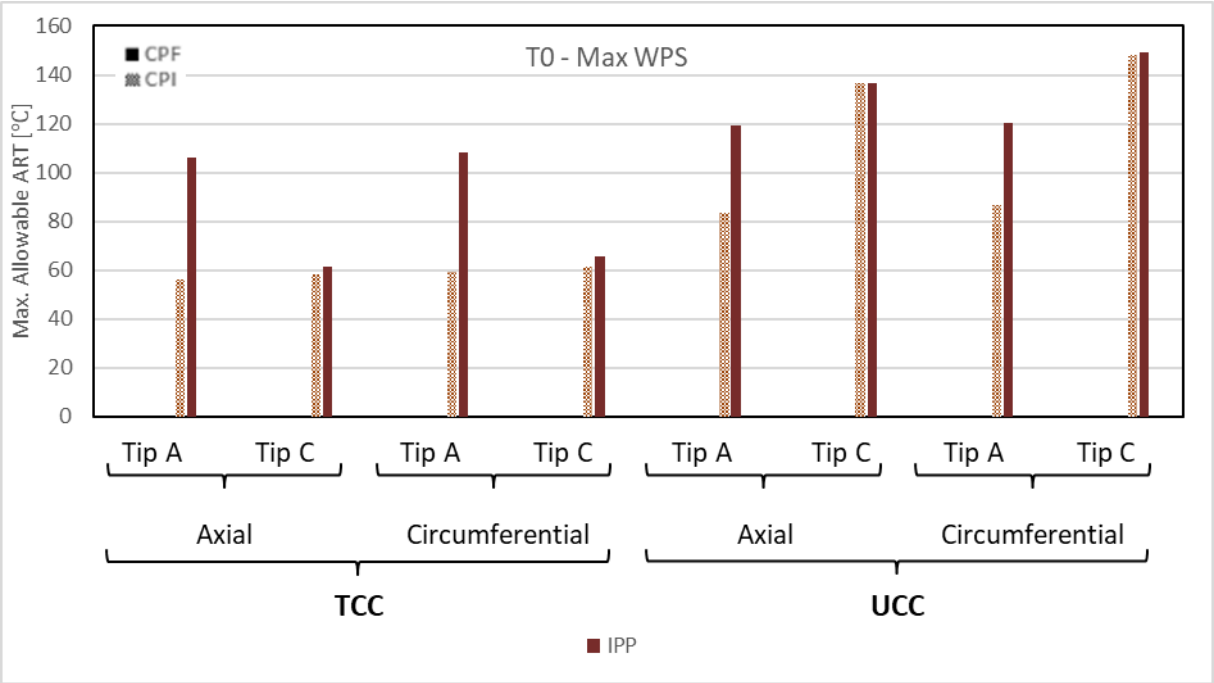

Figure 4.91: Maximum allowable ART values for the max WPS approach considering the T_0 concept.

4.3.3.2 PMA2

The maximum allowable RPV age, considering CPF, is calculated for the different geometries and locations for both the tangent and max WPS approaches.

Final allowable RPV age for the RT_{NDT} concept are presented in Table 4.36 and Table 4.37 as well as Figure 4.92 and Figure 4.93 for the tangent and max WPS approaches respectively. In the figures, the corresponding age values considering CPI from in RR2 are included for comparison.

IPP was the only partner who provided results for PMA2 using the RT_{NDT} concept, thus comparisons with other partners for verifying the results were not possible. It can be seen that for the RT_{NDT} concept, a substantial gain in maximum allowable RPV age is obtained for all geometry cases when considering the tangent approach, while no gain is obtained when using the max WPS approaches. This corresponds well with PMA1.

Table 4.36 Maximum allowable RPV age for the tangent approach considering the RT_{NDT} concept

Partner	Max allowable RPV age for TCC [years]				Max allowable RPV age for UCC [years]			
	Axial		Circumferential		Axial		Circumferential	
	A	C	A	C	A	C	A	C
IPP	95.9	16.8	95.6	17.7	112.2	330.3	118.7	471.7

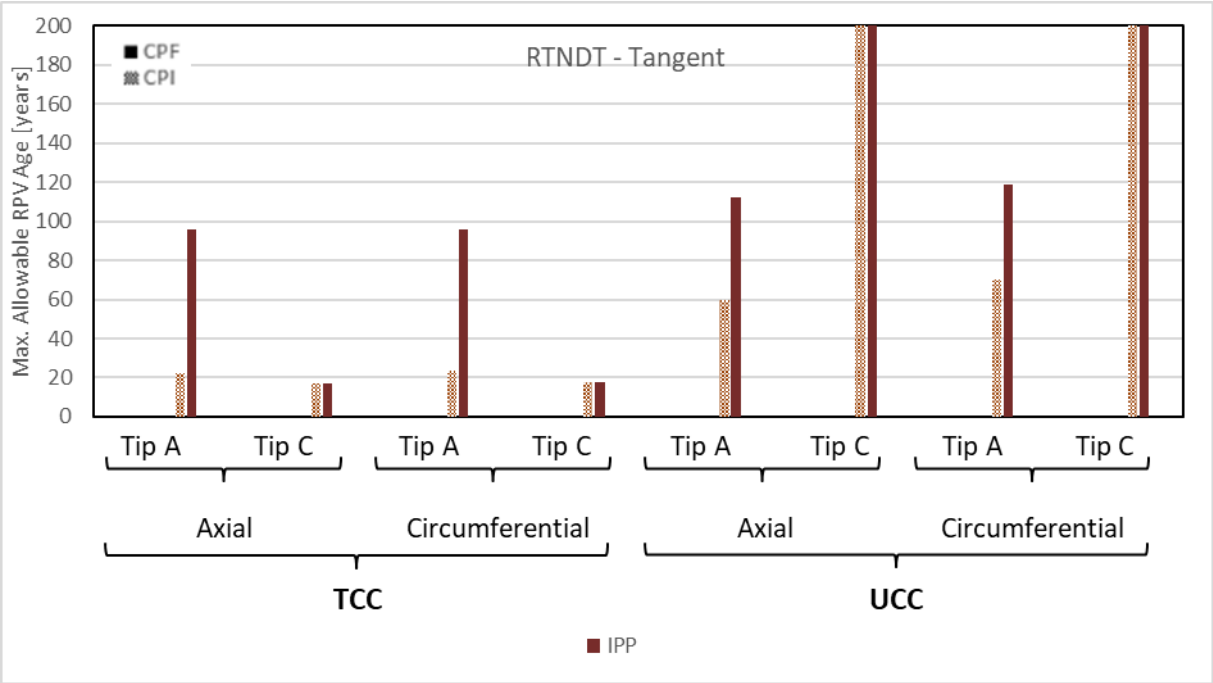

Figure 4.92: Maximum allowable RPV age for the tangent approach considering the RT_{NDT} concept.

Table 4.37 Maximum allowable RPV age for the max WPS approach considering the RT_{NDT} concept

Partner	Max allowable RPV age for TCC [years]				Max allowable RPV age for UCC [years]			
	Axial		Circumferential		Axial		Circumferential	
	A	C	A	C	A	C	A	C
IPP	165.8	141.5	172.4	147.9	233.0	415.4	243.3	>500

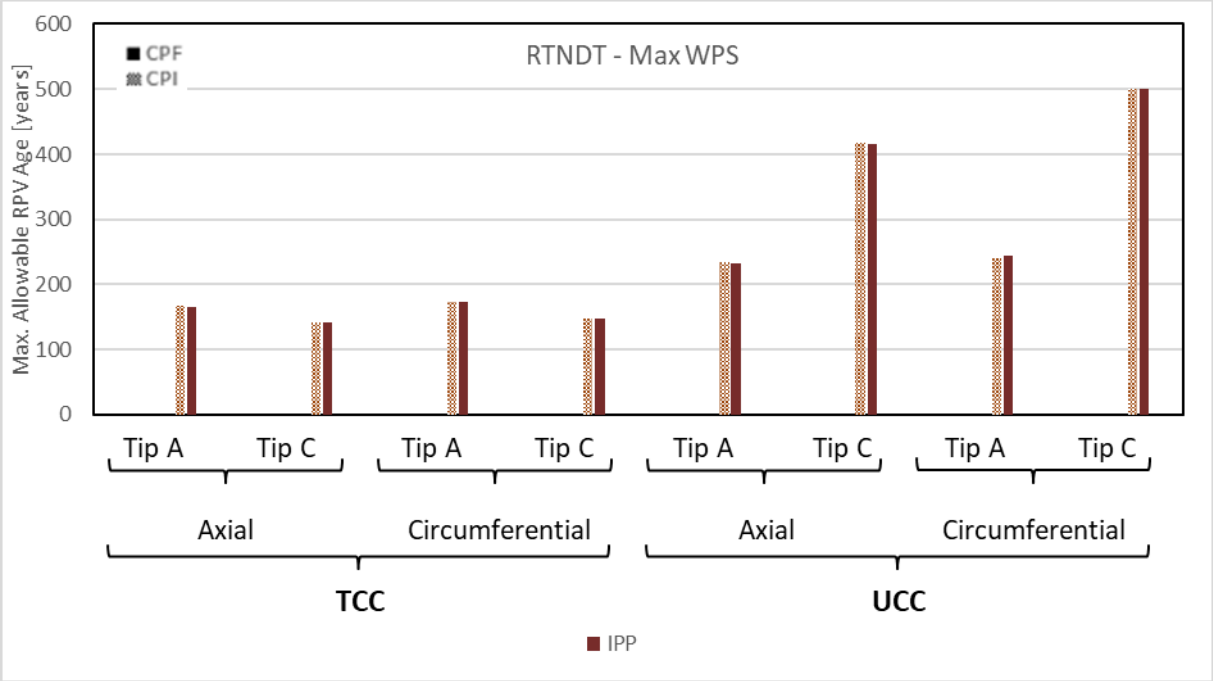

Figure 4.93: Maximum allowable RPV age for the max WPS approach considering the RT_{NDT} concept.

Final allowable RPV age for the FAVOR concept are presented in Table 4.38 as well as Figure 4.94 for a circumferential embedded crack.

Tecnatom was the only partner who provided results for PMA2 using the FAVOR concept, thus comparisons with other partners for verifying the results were not possible. It can be seen that a large gain is obtained both for the tangent and max WPS approaches just like in PMA1.

Table 4.38 Maximum allowable RPV age for a circumferential embedded crack using the FAVOR concept

Partner	Max allowable RPV age for a circumferential embedded crack [years]	
	Tangent	Max WPS
Tecnatom	178	589

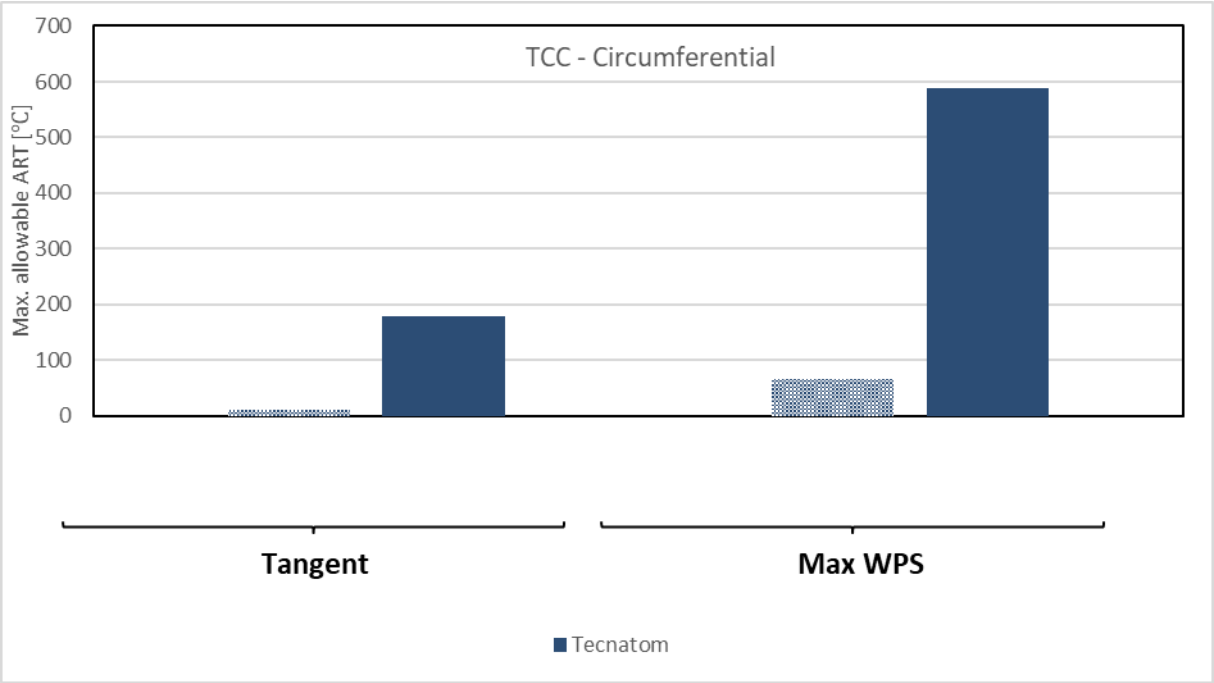

Figure 4.94: Maximum allowable RPV age for a circumferential embedded crack using the FAVOR concept.

Final allowable RPV age values for the T_0 concept are presented in Table 4.39 and Table 4.40 as well as Figure 4.95 and Figure 4.96 for the tangent and max WPS approaches respectively. In the figures, the corresponding age values considering CPI from RR2 are included for comparison.

IPP was the only partner who provided results for the T_0 concept, thus comparisons with other partners for verifying the results were not possible. It can be seen that for the T_0 concept, a substantial gain in maximum allowable RPV age is obtained for all geometry cases and both the tangent and max WPS approaches. This corresponds well with PMA1.

Table 4.39 Maximum allowable RPV age for the tangent approach considering the T_0 concept

Partner	Max allowable RPV age for TCC [years]				Max allowable RPV age for UCC [years]			
	Axial		Circumferential		Axial		Circumferential	
	A	C	A	C	A	C	A	C
IPP	277.1	67.0	277.7	67.5	294.0	236.9	292.7	297.7

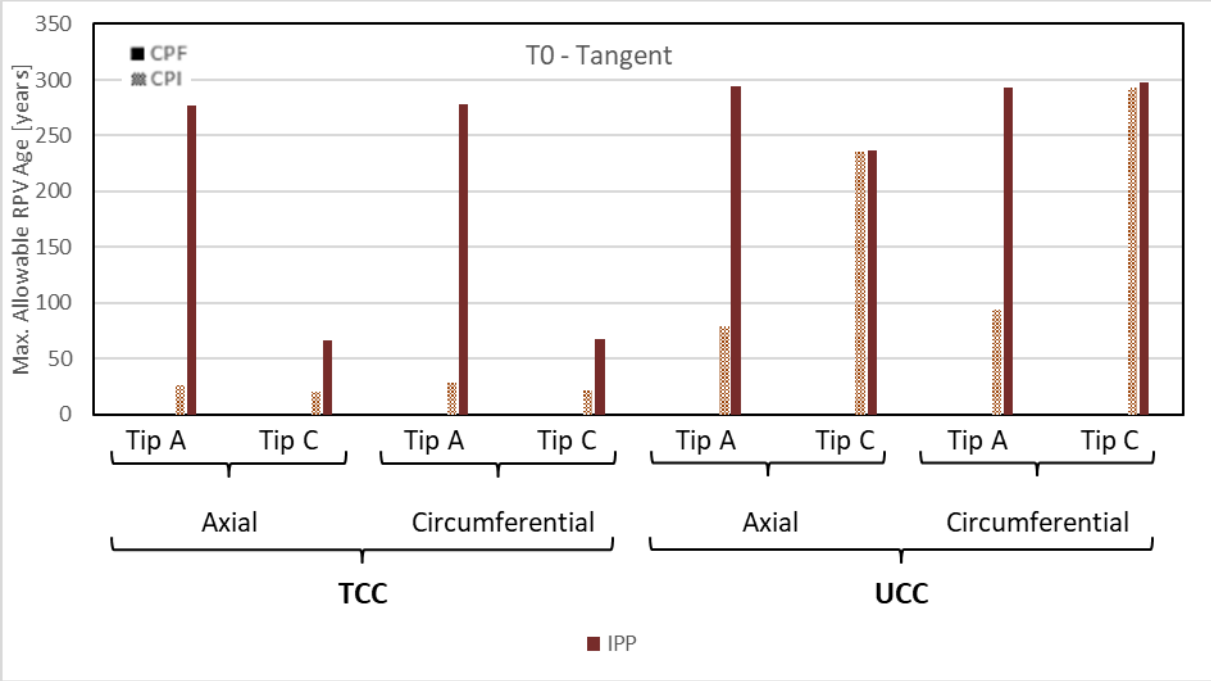

Figure 4.95: Maximum allowable RPV age for the tangent approach considering the T_0 concept.

Table 4.40 Maximum allowable RPV age for the max WPS approach considering the T_0 concept

Partner	Max allowable RPV age for TCC [years]				Max allowable RPV age for UCC [years]			
	Axial		Circumferential		Axial		Circumferential	
	A	C	A	C	A	C	A	C
IPP	317.3	165.2	328.4	168.9	382.1	461.5	391.2	>500

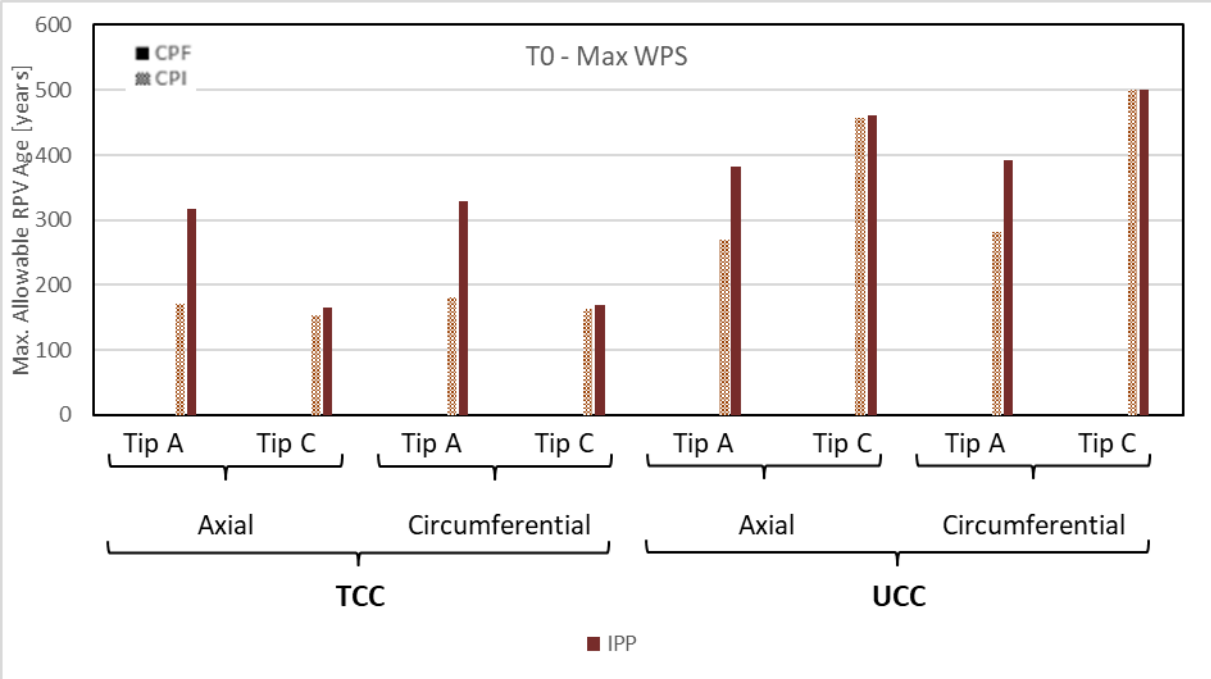

Figure 4.96: Maximum allowable RPV age for the max WPS approach considering the T_0 concept.

4.3.3.3 Conclusions from RR3

RR3 was a non-mandatory continuation of the RR2 by considering the crack arrest and the limit was the conditional probability of failure, CPF.

Only a few partners participated in RR3 using rather different transient data, which makes comparison and verification of the results challenging. Instead, the results were compared to the corresponding results in RR2 in order to see the effect of crack arrest.

For the RT_{NDT} concept, FRA-G had some benefit from crack arrest for a circumferential TCC when considering the tangent approach. IPP had some benefit for UCCs when considering the tangent approach. They had also some benefit for point A for TCC, but not for the limiting point C. No benefit was seen for the max WPS approach.

Fort the FAVOR concept, there was a noticeable benefit for all cases considered by both Tecnatom and JSI.

Only IPP performed the analyses considering the T_0 concept. For this concept, a large benefit was shown in most cases.

4.3.4 RR4 – Check CPI for base case with distributed crack size

This round robin benchmark was defined identical to RR2 but considering a distributed crack according to Section 2.3.2.4. Similar results as in RR2 had to be reported, with addition for providing also the mean value and 5%/95% quantiles for the crack depth.

It should be noted that the distributed crack is much smaller than the deterministic crack used in RR2. The maximum crack size for the distributed crack is 6 mm deep (excluding cladding for the TCC) and 36 mm long, while the deterministic crack in RR2 is 10 mm deep (excluding cladding for the TCC) and 60 mm long.

Mean values as well as 5% and 95% quantiles of the crack depth distribution are presented in Table 4.41. There are some small differences between most partners where Kiwa and IPP have similar values while BZN, FRA-G and PSI have similar values as well. UJV have values in-between these. These differences have not been explained, but may be due to differences in treatment of the pre-defined crack depth distribution in Section 2.3.2.4. Some partners have assumed linear behaviour between data in Table 2.3, while others have assumed discrete steps between the values.

Tecnatom have values quite a lot higher than the others. This is due to the assumptions made for the distribution to be compatible with CAPAL, see Section 2.3.12.1.

Table 4.41 Crack depth distributions calculated by each partner.

Partner	Crack Depth [mm]		
	MV	5% Quantile	95% Quantile
Kiwa	1.385	0.659	2.725
BZN	1.432	0.700	2.800
FRA-G	1.435	0.659	2.725
UJV	1.409	0.700	2.750
Tecnatom	2.346	1.468	3.957
IPP	1.385	0.659	2.726
JSI	1.468	1.468	3.957
PSI	1.436	0.700	2.800

The stress intensity factor (SIF) solution for TCC used by all partners not using the CAPAL code is limited to the crack depth $a \geq 0.75$ mm. There is therefore a need to extrapolate the solution for the smallest crack sizes included in Table 2.3. This has been done differently by the different partners.

Kiwa and IRSN used linear extrapolation of the K_I values while BZN used linear extrapolation of the influence coefficients of the SIF-solution.

FRA-G and IPP used constant extrapolation of the K_I values at 0.75 mm while UJV used constant extrapolation of the influence coefficients of the SIF-solution.

4.3.4.1 PMA1

The maximum allowable ART, considering CPI, is calculated for the different crack geometries and locations for both the tangent and max WPS approaches.

Final allowable ART values for the RT_{NDT} concept are presented in Table 4.42 and Table 4.43 as well as Figure 4.97 and Figure 4.98 for the tangent and max WPS approaches respectively. The results are in quite good agreement between most partners and the pattern is similar to RR2.

Table 4.42 Maximum allowable ART values for the tangent approach considering the RT_{NDT} concept

Partner	Maximum allowable ART for TCC [°C]				Maximum allowable ART for UCC [°C]			
	Axial		Circumferential		Axial		Circumferential	
	A	C	A	C	A	C	A	C
Kiwa	78.80	90.15	79.92	91.49	176.05	>1000	201.93	>1000
BZN	78.52	110.94	78.91	93.75	191.02	>500	204.69	>500
FRA-G	43.00	54.00	42.00	53.00	112.00	>400	110.00	>400
GRS	87.89		89.45					
IRSN	81.54	90.33	82.52	91.31				
UJV	77.74	89.26	78.59	90.29	174.32	>500	200.02	>500
IPP	72.74	86.08	74.87	87.01	191.92	>500	214.70	>500

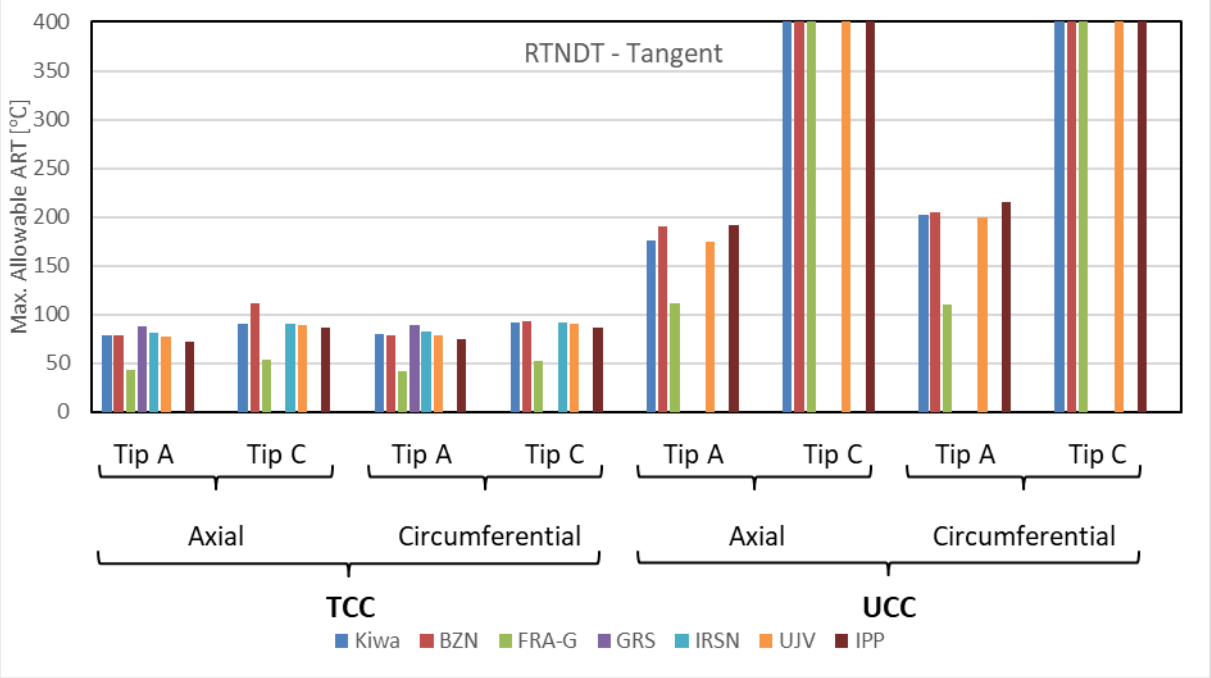

Figure 4.97: Maximum allowable ART values for the tangent approach considering the RT_{NDT} concept.

Table 4.43 Maximum allowable ART values for the max WPS approach considering the RT_{NDT} concept

Partner	Maximum allowable ART for TCC [°C]				Maximum allowable ART for UCC [°C]			
	Axial		Circumferential		Axial		Circumferential	
	A	C	A	C	A	C	A	C
Kiwa	139.59	150.03	142.22	152.94	190.78	>1000	207.29	>1000
BZN	139.06	150.78	141.02	152.73	194.14	>500	202.34	>500
FRA-G	109.00	122.00	110.00	122.00	144.00	>400	144.00	>400
GRS	121.48		121.48					
UJV	143.11	153.54	145.70	156.69	187.46	>500	202.04	>500
IPP	139.43	151.27	141.98	154.43	196.35	>500	217.40	>500

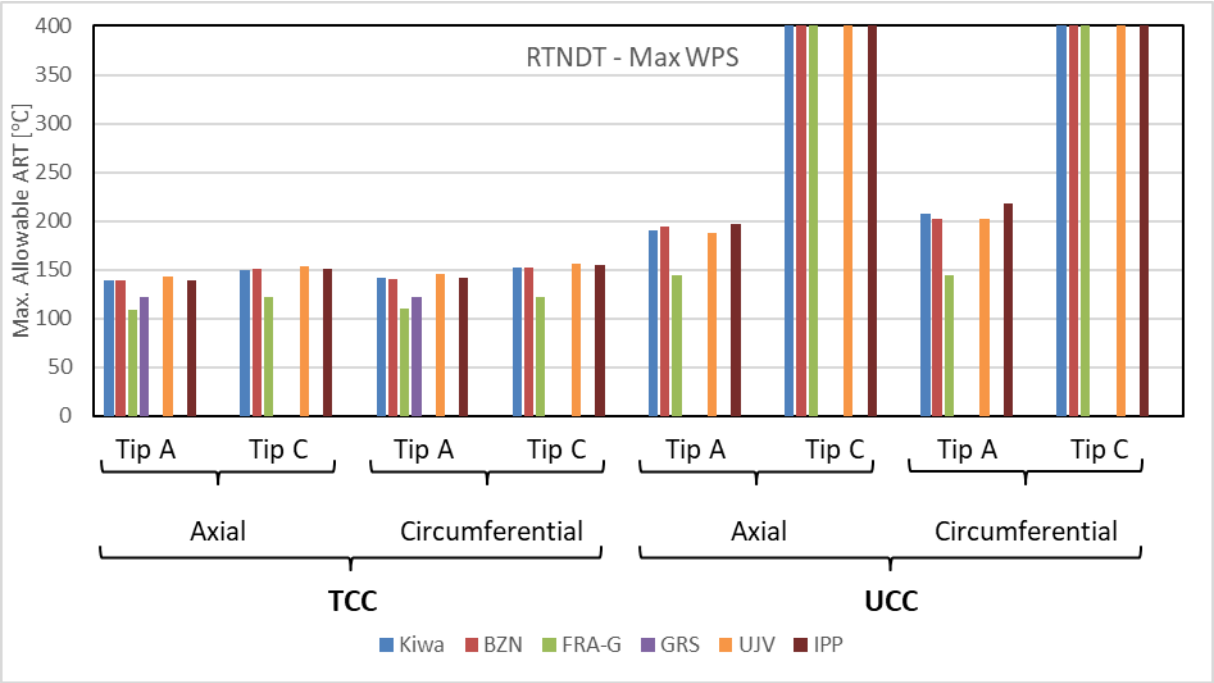

Figure 4.98: Maximum allowable ART values for the max WPS approach considering the RT_{NDT} concept.

Final allowable ART values for the FAVOR concept are presented in Table 4.44 as well as Figure 4.99. As the pre-defined case in APAL cannot be analysed directly using FAVOR, assumptions have been made by the partners described in Section 2.3.12.

Tecnatom and PSI have quite similar results for a circumferential TCC, while JSI have higher values, probably due to the different TH-data. For the circumferential embedded crack, Tecnatom gets about twice as high values as PSI, this may be explained by the different assumptions regarding the crack distribution for embedded cracks, see Section 2.3.12.1.

Table 4.44 Maximum allowable ART values the FAVOR concept

Partner	Max allowable ART for a circumferential TCC [°C]		Maximum allowable ART for an embedded crack [°C]			
			Axial		Circumferential	
	Tangent	Max WPS	Tangent	Max WPS	Tangent	Max WPS
Tecnatom	20	59	131	131	135	135
PSI	18	61			68	76
JSI	60	127				

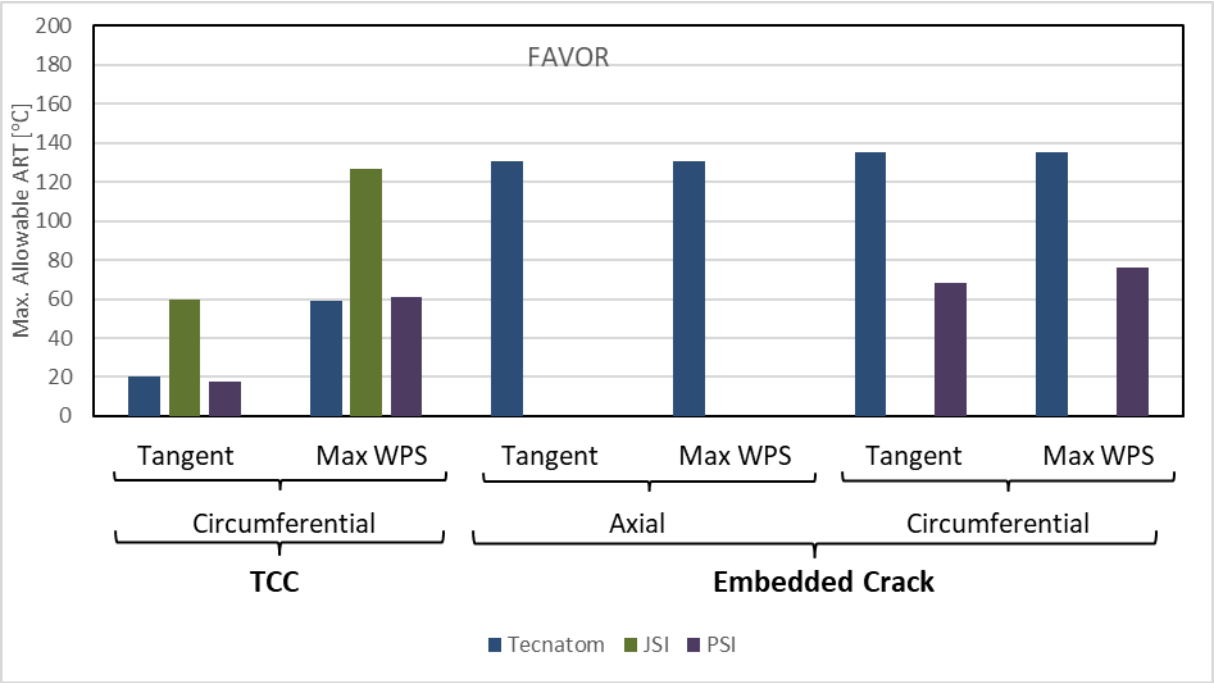

Figure 4.99: Maximum allowable ART values the FAVOR concept.

Kiwa and IPP provided non-mandatory results for the T_0 concept which are presented in Table 4.45 and Table 4.46 as well as Figure 4.100 and Figure 4.101 for the tangent and max WPS approaches respectively. Crack front correction was not considered in these calculations. The differences between partners are comparative with those for the RT_{NDT} concept.

Table 4.45 Maximum allowable ART values for the tangent approach considering the T_0 concept

Partner	Maximum allowable ART for TCC [°C]				Maximum allowable ART for UCC [°C]			
	Axial		Circumferential		Axial		Circumferential	
	A	C	A	C	A	C	A	C
Kiwa	44.61	61.79	45.85	63.33	137.49	4602.50	151.14	12402.20
IPP	41.80	57.02	43.49	59.72	148.63	>500	161.10	>500

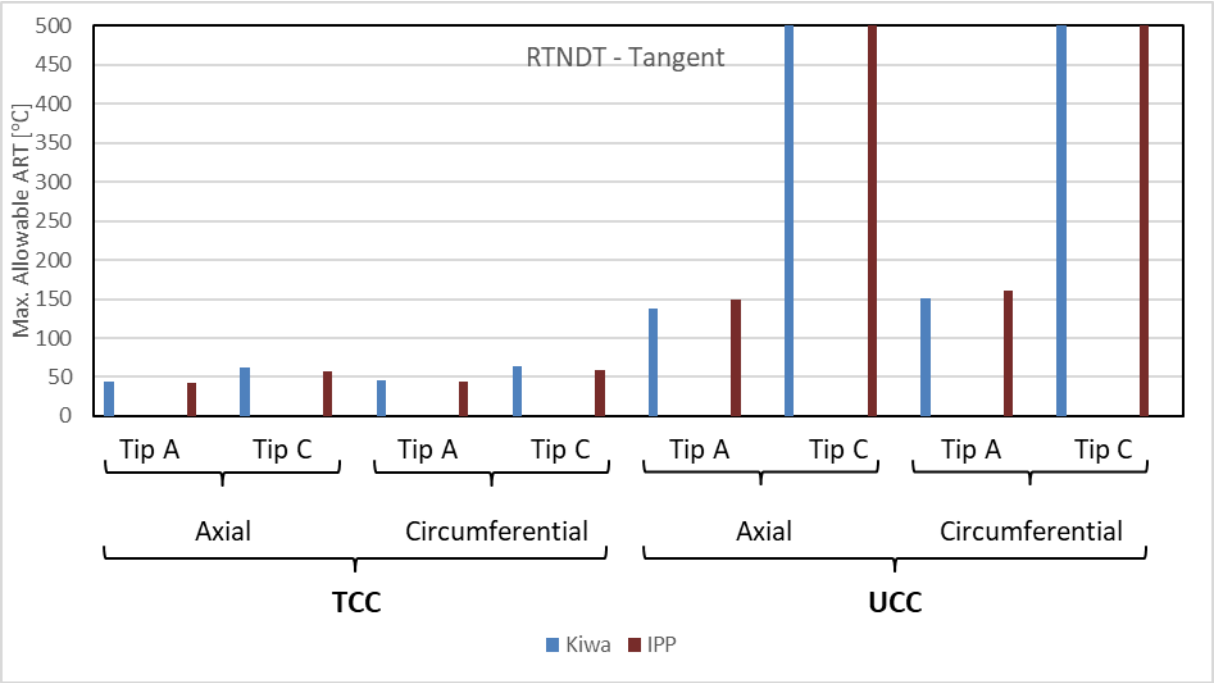

Figure 4.100: Maximum allowable ART values for the tangent approach considering the T_0 concept.

Table 4.46 Maximum allowable ART values for the max WPS approach considering the T_0 concept

Partner	Maximum allowable ART for TCC [°C]				Maximum allowable ART for UCC [°C]			
	Axial		Circumferential		Axial		Circumferential	
	A	C	A	C	A	C	A	C
Kiwa	97.57	117.19	101.69	122.22	166.03	2562.50	178.58	11500.00
IPP	100.61	118.21	104.69	123.71	183.89	>500	196.88	>500

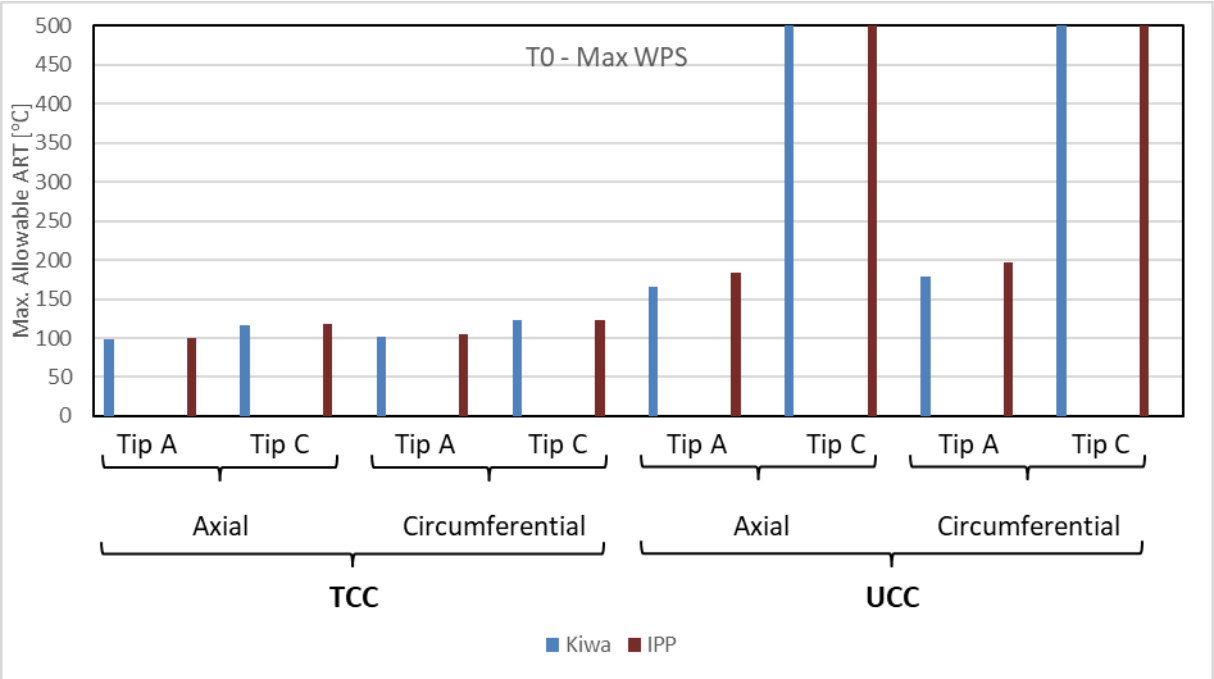

Figure 4.101: Maximum allowable ART values for the max WPS approach considering the T_0 concept.

4.3.4.2 PMA2

The maximum allowable RPV age, considering CPI, is calculated for the different crack geometries and locations for both the tangent and max WPS approaches.

Final allowable RPV age for the RT_{NDT} concept are presented in Table 4.47 and Table 4.48 as well as Figure 4.102 and Figure 4.103 for the tangent and max WPS approaches respectively.

The scatter is overall larger than for RR2 PMA2 and RR4 PMA1. GRS got higher results than all other partners, especially for the tangent approach. This could be due to the use of different TH code than other partners.

It should be noted that FRA-G has a limit on 250 years in their calculations, but since many results are above this limit for the max WPS approach, the Figure 4.103 plots values up to 500 years. The FRA-G bars for UCC may therefore be misleading in Figure 4.103.

Table 4.47 Maximum allowable RPV age for the tangent approach considering the RT_{NDT} concept

	Max allowable RPV age for TCC [years]				Max allowable RPV age for UCC [years]			
	Axial		Circumferential		Axial		Circumferential	
	A	C	A	C	A	C	A	C
Kiwa	81.1	101.8	83.4	105.6	517.0	1000.0	660.5	1000.0
BZN	72.5	90.3	67.5	89.4	444.4	>500	529.4	>500
FRA-G	16.0	32.0	15.0	29.0	186.0	>250	183.0	>250
GRS	124.8		136.5					
IRSN	64.5	110.4	66.7	111.4				
UJV	70.6	99.8	73.1	102.8	448.1	>500	>500	>500
IPP	62.5	91.9	66.4	95.1	>500	>500	>500	>500

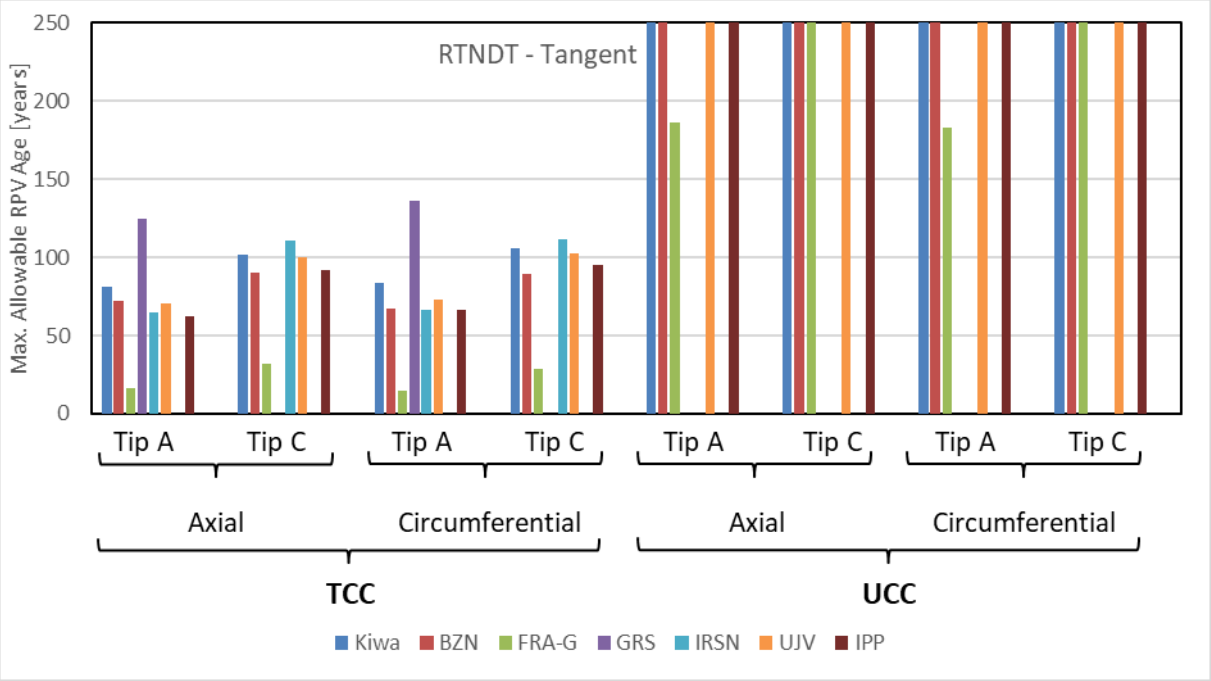

Figure 4.102: Maximum allowable RPV age for the tangent approach considering the RT_{NDT} concept.

Table 4.48 Maximum allowable RPV age for the max WPS approach considering the RT_{NDT} concept

Partner	Max allowable RPV age for TCC [years]				Max allowable RPV age for UCC [years]			
	Axial		Circumferential		Axial		Circumferential	
	A	C	A	C	A	C	A	C
Kiwa	241.5	264.6	254.8	280.2	563.2	>1000	706.3	>1000
BZN	210.6	250.5	215.9	263.8	521.4	>500	534.7	>500
FRA-G	130.0	168.0	131.0	172.0	>250	>250	>250	>250
GRS	284.8		304.3					
UJV	231.9	278.3	244.4	294.0	499.3	>500	>500	>500
IPP	224.2	270.2	235.8	288.3	>500	>500	>500	>500

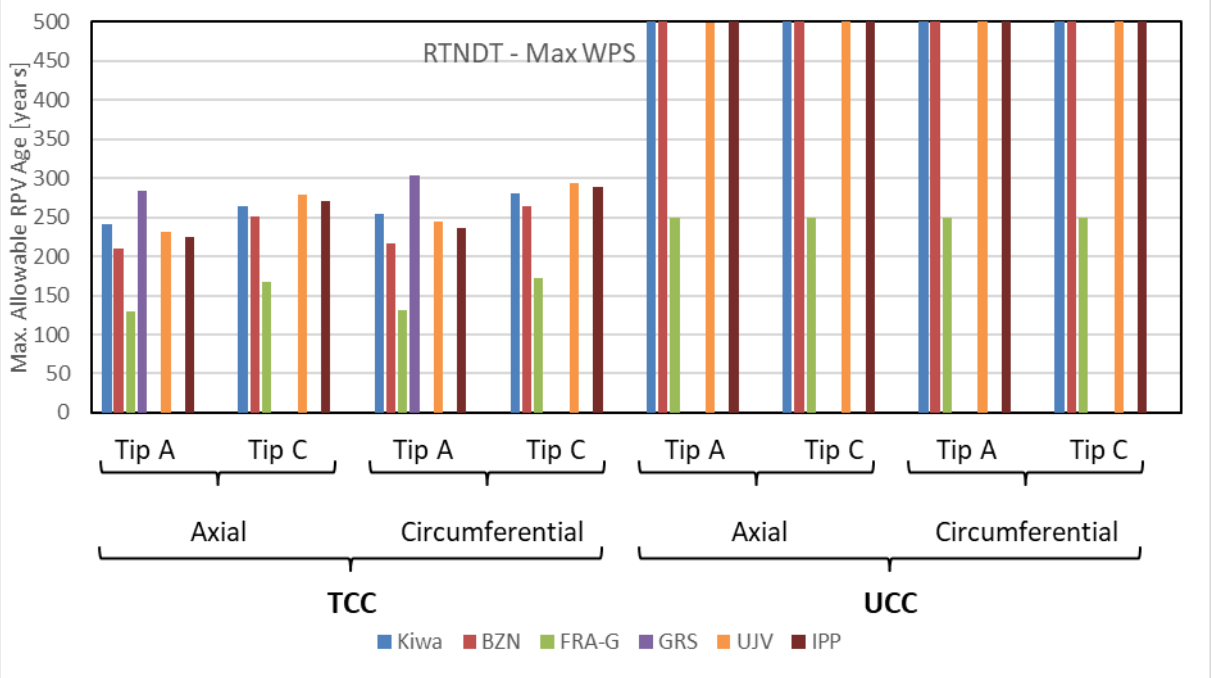

Figure 4.103: Maximum allowable RPV age for the max WPS approach considering the RT_{NDT} concept. Note that FRA-G limited their calculations to ≤250 years.

Final allowable RPV age for the FAVOR concept are presented in Table 4.49 as well as Figure 4.103. As the pre-defined case in APAL cannot be analysed directly using FAVOR assumptions have been made by the partners described in Section 2.3.12.

It can be seen that the good agreement between Tecnatom and PSI that was seen for the circumferential TCC for PMA1 is not observed in PMA2. PSI gets very low maximum allowable RPV age for the tangent approach, while getting very high for the max WPS approach, as compared to Tecnatom. For the circumferential embedded crack, PSI gets higher values than Tecnatom for both approaches, while the opposite was observed for PMA1. The relation between JSI and the other partners is similar as for PMA1.

Table 4.49 Maximum allowable RPV age for the FAVOR concept

Partner	Max allowable RPV age for a circumferential TCC [years]		Maximum allowable RPV age for an embedded crack [years]			
			Axial		Circumferential	
	Tangent	Max WPS	Tangent	Max WPS	Tangent	Max WPS
Tecnatom	20	83	343	345	361	363
PSI	3	118			>400	>400
JSI	44	204				

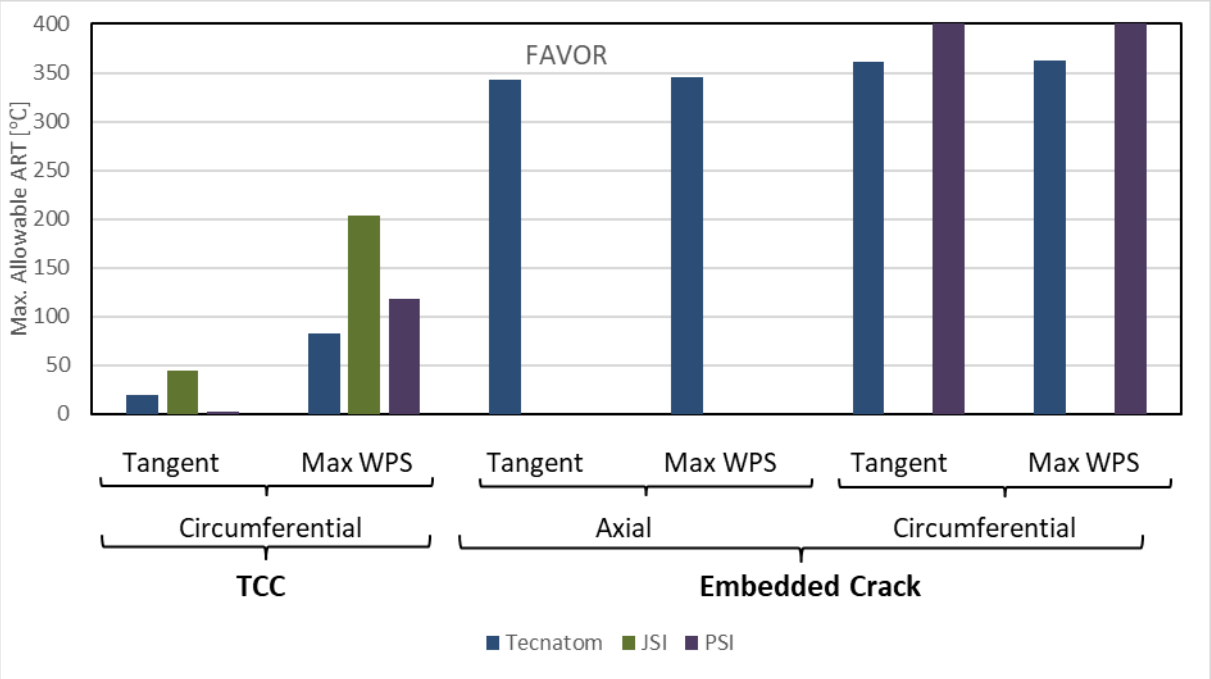

Figure 4.104: Maximum allowable RPV age for the FAVOR concept.

Kiwa and IPP provided non-mandatory results for the T_0 concept which are presented in Table 4.50 and Table 4.51 as well as Figure 4.105 and Figure 4.106 for the tangent and max WPS approaches respectively. Crack front correction was not considered in these calculations. The differences between partners are comparative with those for the RT_{NDT} concept.

Table 4.50 Maximum allowable RPV age for the tangent approach considering the T_0 concept

	Max allowable RPV age for TCC [years]				Max allowable RPV age for UCC [years]			
	Axial		Circumferential		Axial		Circumferential	
	A	C	A	C	A	C	A	C
Kiwa	136.5	166.0	141.1	170.9	536.4	190500.0	622.8	>1000
IPP	113.7	158.8	112.9	159.4	>500	>500	>500	>500

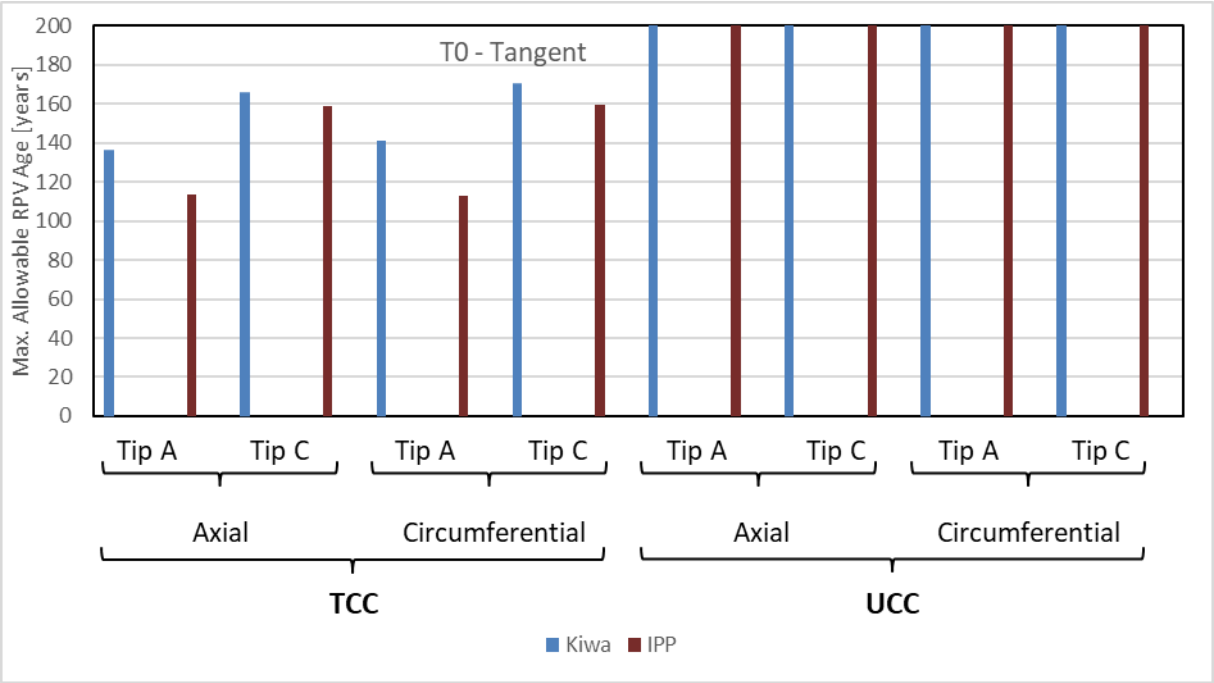

Figure 4.105: Maximum allowable RPV age for the tangent approach considering the T_0 concept.

Table 4.51 Maximum allowable RPV age for the max WPS approach considering the T_0 concept

Partner	Max allowable RPV age for TCC [years]				Max allowable RPV age for UCC [years]			
	Axial		Circumferential		Axial		Circumferential	
	A	C	A	C	A	C	A	C
Kiwa	325.8	367.7	345.4	389.8	697.9	114500.0	791.1	>1000
IPP	309.6	378.3	323.0	395.9	>500	>500	>500	>500

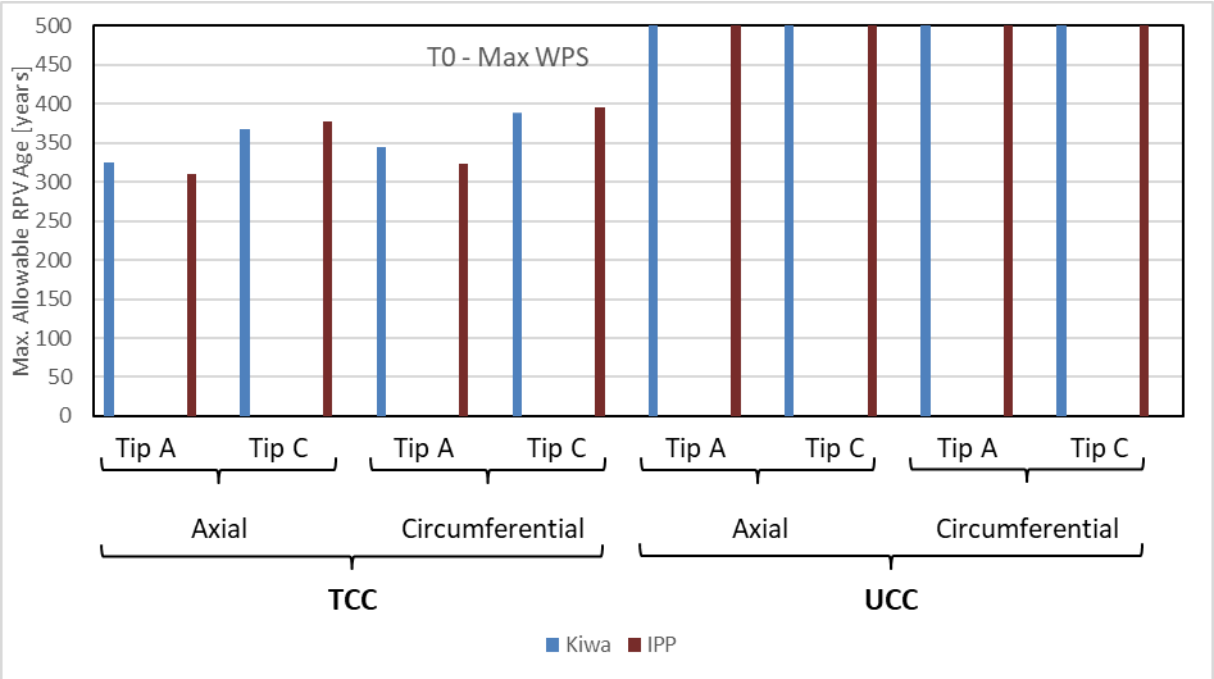

Figure 4.106: Maximum allowable RPV age for the max WPS approach considering the T_0 concept.

4.3.4.3 Sensitivity analysis of temperature assumptions

Since the crack is distributed in the RR4 analyses, the deepest point of the crack is not constant. This consequently means that the temperature and fluence attenuation are not constant for each time step, but rather dependent of the distributed crack.

IPP performed a sensitivity analysis where two cases were compared:

1. Temperature and fluence attenuation are taken at the centre value of the distribution of 3 mm from the clad/base interface resulting in constant temperature and fluence attenuation for each time step.
2. Temperature and fluence attenuation are taken for the corresponding crack depth for each generated set according to the flaw depth distribution.

The sensitivity study was made for both PMA1 and PMA2 and both the RT_{NDT} and T_0 concepts and the results are presented in Table 4.52 – Table 4.55 where it can be seen that the effect is slight and that the assumptions made have an insignificant impact on the end results.

Table 4.52 Comparison of assumptions for temperature and fluence attenuation position for PMA1, RT_{NDT}

Case	Tangent				Max WPS			
	TCC		UCC		TCC		UCC	
	Axial	Circumf	Axial	Circumf	Axial	Circumf	Axial	Circumf
1 [°C]	73.34	74.59	171.68	195.96	139.56	142.04	187.34	199.11
2 [°C]	73.78	75.00	172.42	197.41	140.02	142.79	188.42	200.47
Diff. [%]	0.60	0.54	0.43	0.73	0.33	0.53	0.57	0.68

Table 4.53 Comparison of assumptions for temperature and fluence attenuation position for PMA1, T_0

Case	Tangent				Max WPS			
	TCC		UCC		TCC		UCC	
	Axial	Circumf	Axial	Circumf	Axial	Circumf	Axial	Circumf
1 [°C]	42.58	42.70	129.26	144.22	100.70	104.70	164.40	173.86
2 [°C]	42.56	42.97	129.81	144.65	100.26	104.25	164.60	174.14
Diff. [%]	0.04	0.64	0.42	0.30	0.44	0.43	0.12	0.16

Table 4.54 Comparison of assumptions for temperature and fluence attenuation position for PMA2, RT_{NDT}

Case	Tangent				Max WPS			
	TCC		UCC		TCC		UCC	
	Axial	Circumf	Axial	Circumf	Axial	Circumf	Axial	Circumf
1 [years]	62.67	66.13	451.06	>500	221.99	233.90	491.64	>500
2 [years]	63.47	66.69	460.82	>500	222.02	233.81	>500	>500
Diff. [%]	1.26	0.83	2.12	-	0.01	0.04	-	-

Table 4.55 Comparison of assumptions for temperature and fluence attenuation position for PMA2, T_0

Case	Tangent				Max WPS			
	TCC		UCC		TCC		UCC	
	Axial	Circumf	Axial	Circumf	Axial	Circumf	Axial	Circumf
1 [years]	114.02	121.46	455.01	>500	305.01	326.83	>500	>500
2 [years]	112.77	120.31	463.77	>500	300.73	321.57	>500	>500
Diff. [%]	1.11	0.95	1.89	-	1.42	1.64	-	-

4.3.4.4 Comparison of RR2 and RR4

The results in RR4 are compared with results from RR2 for point A of a circumferential TCC.

This is done for the RT_{NDT} concept in Figure 4.107 and Figure 4.108 for PMA1 and PMA2 respectively, and it can clearly be seen that the case studied in RR4 gives much lower probabilities. This can be explained by the deterministic crack studied within RR2, which is much larger than even the largest limit of the distributed crack used in RR4.

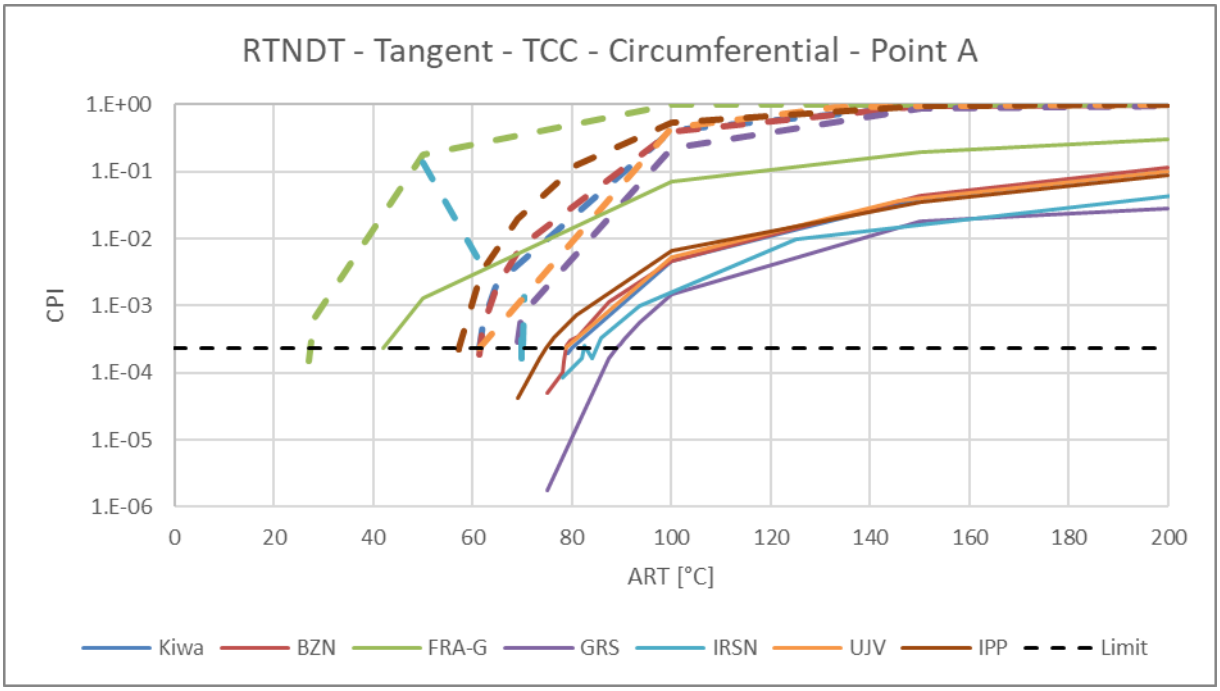

Figure 4.107: Comparison between RR4 (full lines) and RR2 (dashed lines) for PMA1, RT_{NDT}.

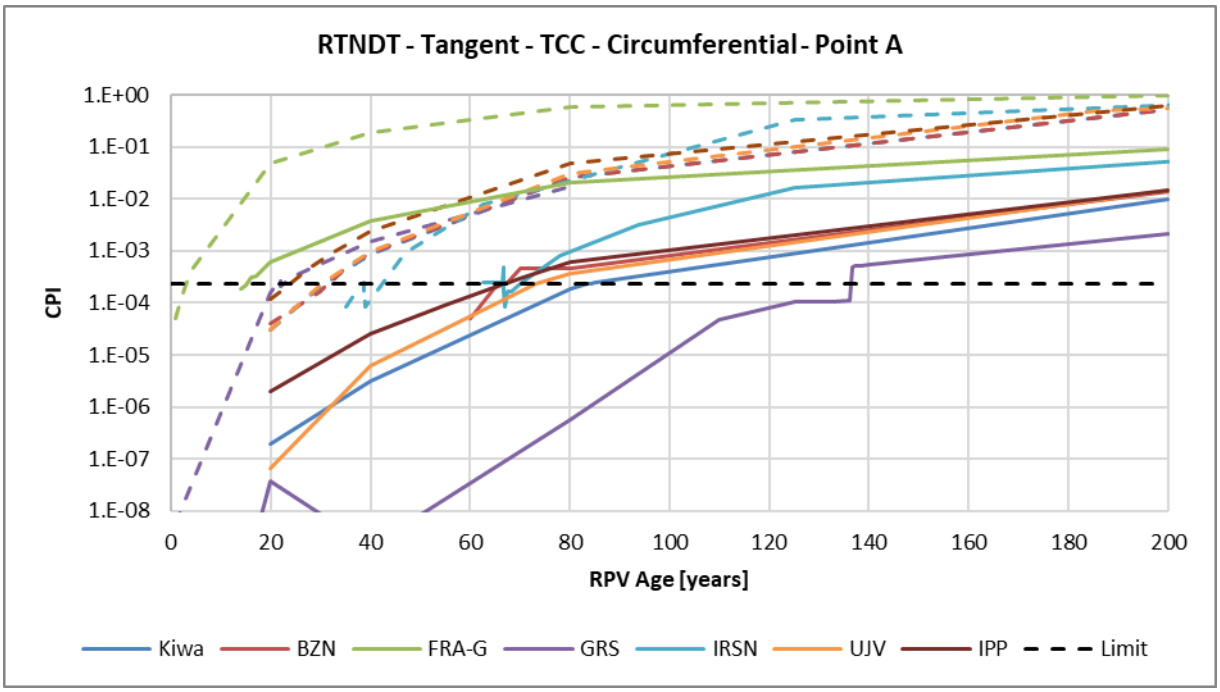

Figure 4.108: Comparison between RR4 (full lines) and RR2 (dashed lines) for PMA2, RT_{NDT} .

For the FAVOR concept, the same comparison is made in Figure 4.109 and Figure 4.110 for PMA1 and PMA2 respectively. It should be noted that different crack aspect ratios have been used in RR2 and RR4, where the RR2 results used in the comparison are for $2c/(a + r) = 6$. For the FAVOR concept, the margins between RR2 and RR4 are much smaller than for the RT_{NDT} concept and for some cases RR4 gives more limiting results than RR2. Tecnatom investigated this closer and found the explanation to be that for the smaller cracks, lower temperatures at the crack tip due to it being closer to the inside of the RPV wall. Less attenuation for the neutron fluence for smaller cracks has been considered as an additional explanation for PMA2.

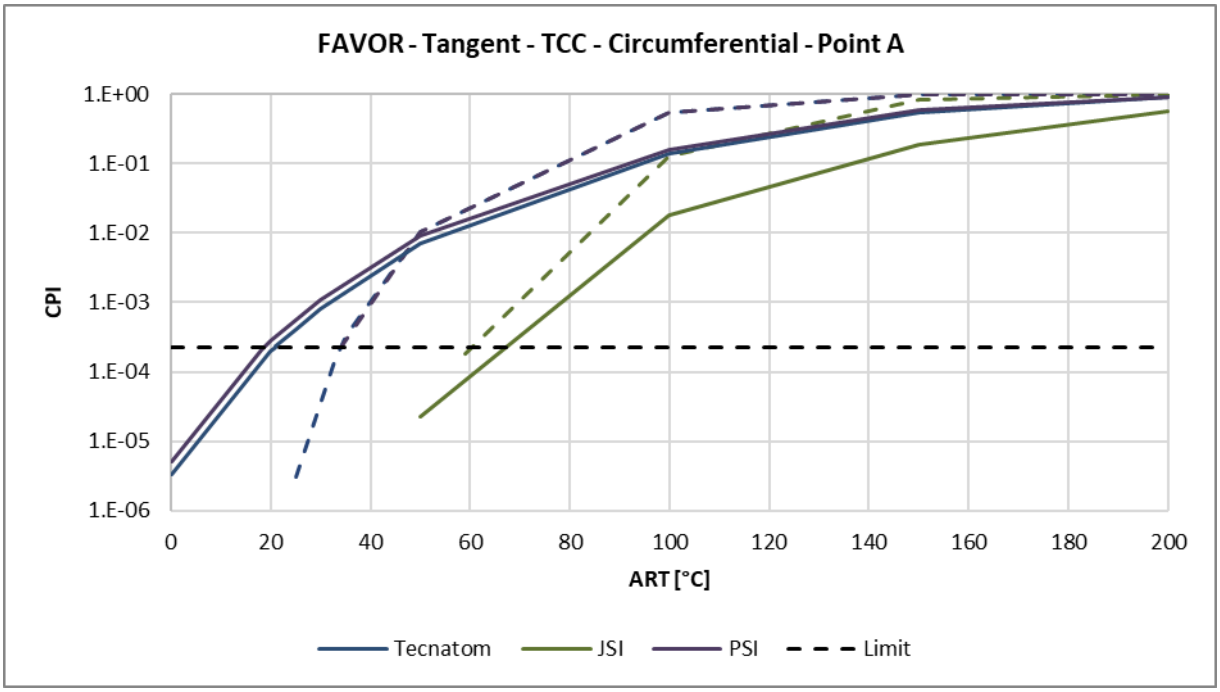

Figure 4.109: Comparison between RR4 (full lines) and RR2 (dashed lines) for PMA1, FAVOR.

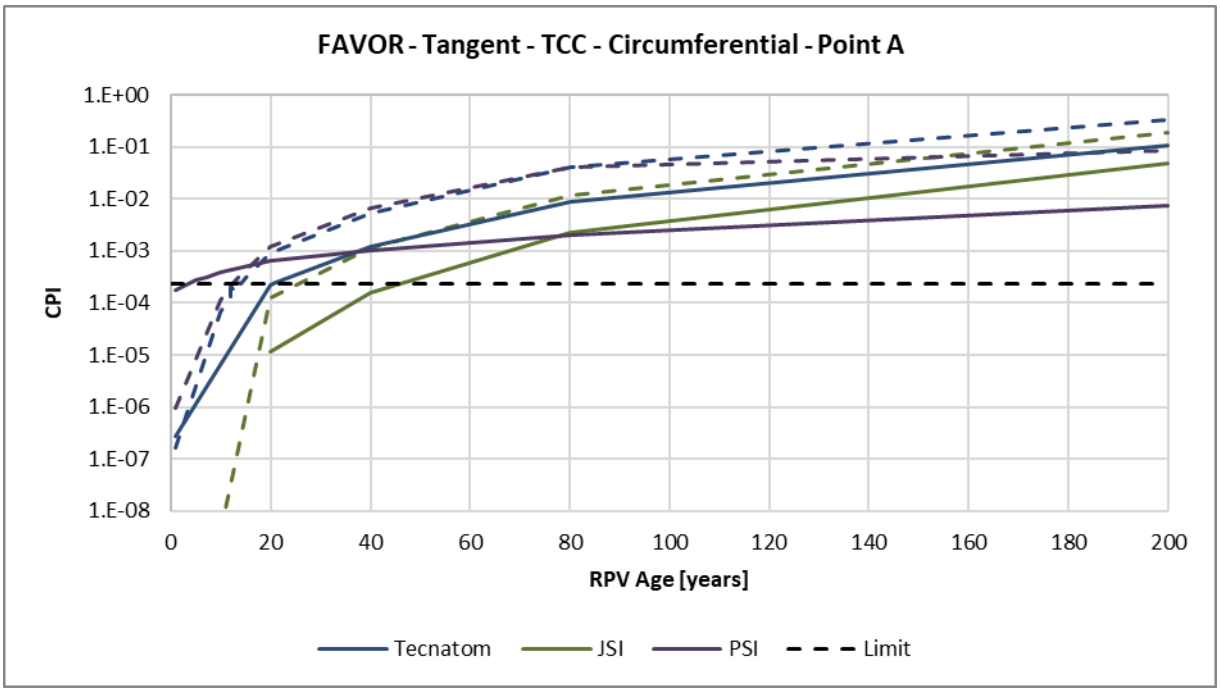

Figure 4.110: Comparison between RR4 (full lines) and RR2 (dashed lines) for PMA2, FAVOR.

4.3.4.5 Conclusions from RR4

RR4 is an alternative to RR2 where distributed cracks are analysed. The distribution to be used is given in Table 2.3. This distribution is not possible to include in FAVOR, approximations of this distribution is therefore used as described in Section 2.3.12.

Besides the distribution approximations made by FAVOR users, there were some additional differences in how the distributed crack was treated. Some partners assumed the distribution to be linear in-between table values, while others considered discrete values.

An additional aspect that had to be considered was the lower limit of crack size for the TCC SIF solution used by all non-FAVOR partners. The smallest crack depth for this solution was 0.75 mm, while the smallest depth crack in the distribution is 0.5 mm. Some partners used linear extrapolation for this while others used constant extrapolation. Furthermore, some partners extrapolated the influence coefficients while others extrapolated the K_I-values. No in-depth study of the effects of these different assumptions were made.

Different temperature assumptions were compared in Section 4.3.4.3 for Point A since this point is not constant. It was shown that the effect of different assumptions had an insignificantly small impact on the end result.

When comparing RR4 with RR2, it is important to note that the crack considered in RR2 was much larger than the largest crack in the crack distribution.

For the RT_{NDT} and T_0 concepts, RR4 gives much higher allowable values than RR2. For the FAVOR concept, this difference was not as large however and in some cases RR4 was more limiting than RR2. This was found to be due to the lower temperatures for smaller cracks as well as less neutron attenuation than for larger cracks.

4.3.5 RR5 – Check CPF for base case with distributed crack size (non-mandatory)

The RR5 benchmark was defined as a non-mandatory extension of RR4 by considering crack arrest analyses according to Section 2.3.10 and calculating CPF values for various crack geometries (TCC, UCC and embedded cracks), orientations within the RPV wall (axial and circumferential).

The calculations in RR5 were performed in the same manner as in RR3, but additionally providing the mean value and 5%/95% quantiles for the crack depth.

IPP was the only partner who provided results for the RT_{NDT} and T_0 concepts, thus comparisons with other partners for verifying the results were not possible. For the FAVOR concept, JSI and Tecnatom provided results.

Note that the results for geometry point C have been included in the comparisons where calculated by the partners. These are however irrelevant as the crack is assumed to immediately become infinite at first initiation of unstable crack growth.

4.3.5.1 PMA1

The maximum allowable ART, considering CPF, is calculated for the different crack geometries and locations for both the tangent and max WPS approaches.

Final allowable ART values for the RT_{NDT} concept are presented in Table 4.56 and Table 4.57 as well as Figure 4.111 and Figure 4.112 for the tangent and max WPS approaches respectively. In the figures, the corresponding ART values considering CPI from RR4 are included for comparison.

IPP gets higher maximum allowable ART values for most cases using the tangent approach, while little gain is seen for the max WPS approach. This is similar to what was seen in RR3.

Table 4.56 Maximum allowable ART values for the tangent approach considering the RT_{NDT} concept

Partner	Maximum allowable ART for TCC [°C]				Maximum allowable ART for UCC [°C]			
	Axial		Circumferential		Axial		Circumferential	
	A	C	A	C	A	C	A	C
IPP	105.45	109.80	106.00	109.55	191.25	>500	212.13	>500

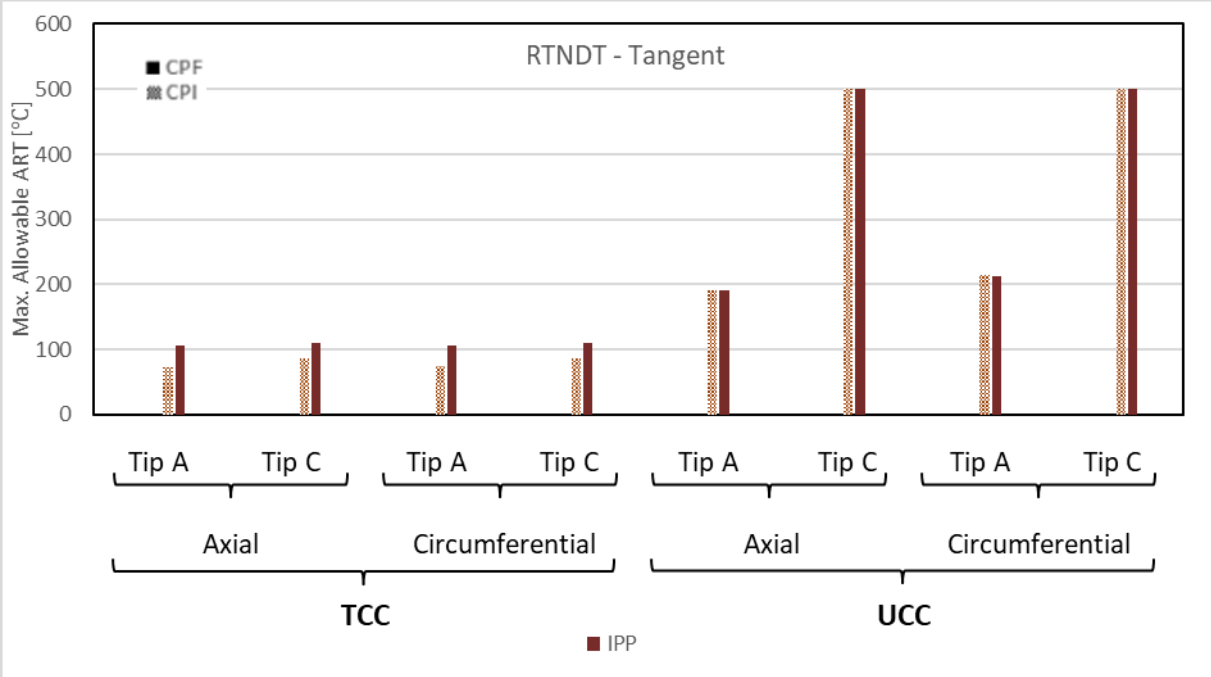

Figure 4.111: Maximum allowable ART values for the tangent approach considering the RT_{NDT} concept.

Table 4.57 Maximum allowable ART values for the max WPS approach considering the RT_{NDT} concept

Partner	Maximum allowable ART for TCC [°C]				Maximum allowable ART for UCC [°C]			
	Axial		Circumferential		Axial		Circumferential	
	A	C	A	C	A	C	A	C
IPP	139.65	151.19	141.80	154.61	197.21	>500	216.65	>500

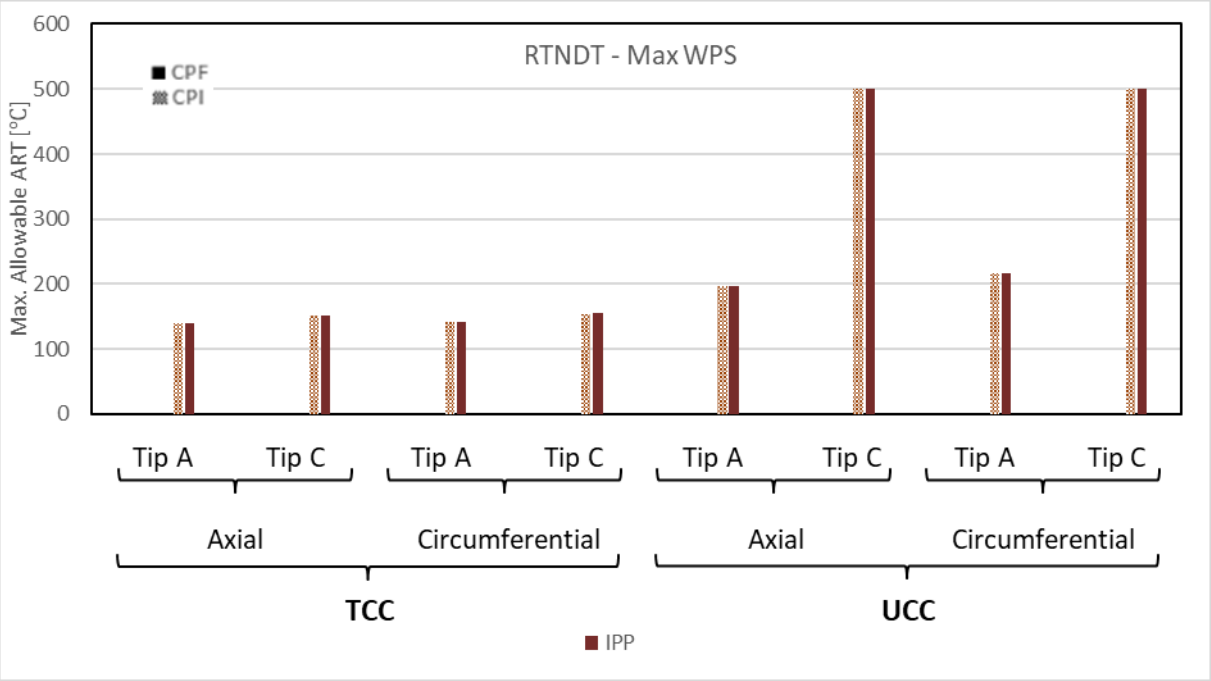

Figure 4.112: Maximum allowable ART values for the max WPS approach considering the RT_{NDT} concept.

Final allowable ART values for the FAVOR concept are presented in Table 4.58 and Figure 4.113 for a circumferential TCC. In the figure, the corresponding values considering CPI from RR4 are included for comparison. The gain in maximum allowable ART is similar between Tecnatom and JSI for both the tangent and max WPS approaches. A noticeable difference as compared to the RT_{NDT} concept results is that the max WPS approach gains substantially when considering crack arrest. These results are in good agreement with the corresponding results in RR3.

Table 4.58 Maximum allowable ART values for a circumferential TCC using the FAVOR concept

Partner	Max allowable ART for a circumferential TCC [°C]	
	Tangent	Max WPS
Tecnatom	49	92
JSI	86	148

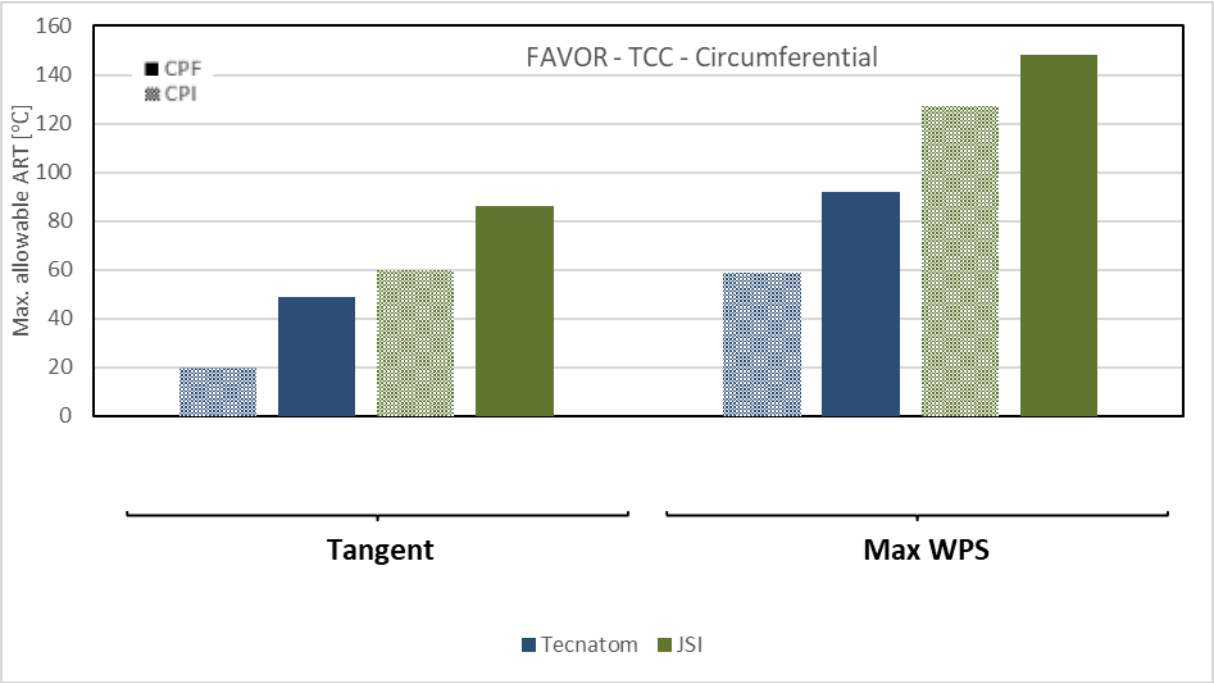

Figure 4.113: Maximum allowable ART values for a circumferential TCC using the FAVOR concept.

Final allowable ART values for the T_0 concept are presented in Table 4.59 and Table 4.60 as well as Figure 4.114 and Figure 4.115 for the tangent and max WPS approaches respectively. In the figures, the corresponding ART values considering CPI from RR4 are included for comparison.

IPP was the only partner who provided results for the T_0 concept, thus comparisons with other partners for verifying the results were not possible. It can be seen that for the T_0 concept, a large gain in maximum allowable ART is obtained for all geometry cases for the tangent approach. There is some gain as well for the max WPS approaches for the TCC.

Table 4.59 Maximum allowable ART values for the tangent approach considering the T_0 concept

Partner	Maximum allowable ART for TCC [°C]				Maximum allowable ART for UCC [°C]			
	Axial		Circumferential		Axial		Circumferential	
	A	C	A	C	A	C	A	C
IPP	106.63	112.01	107.13	112.18	156.06	>500	165.47	>500

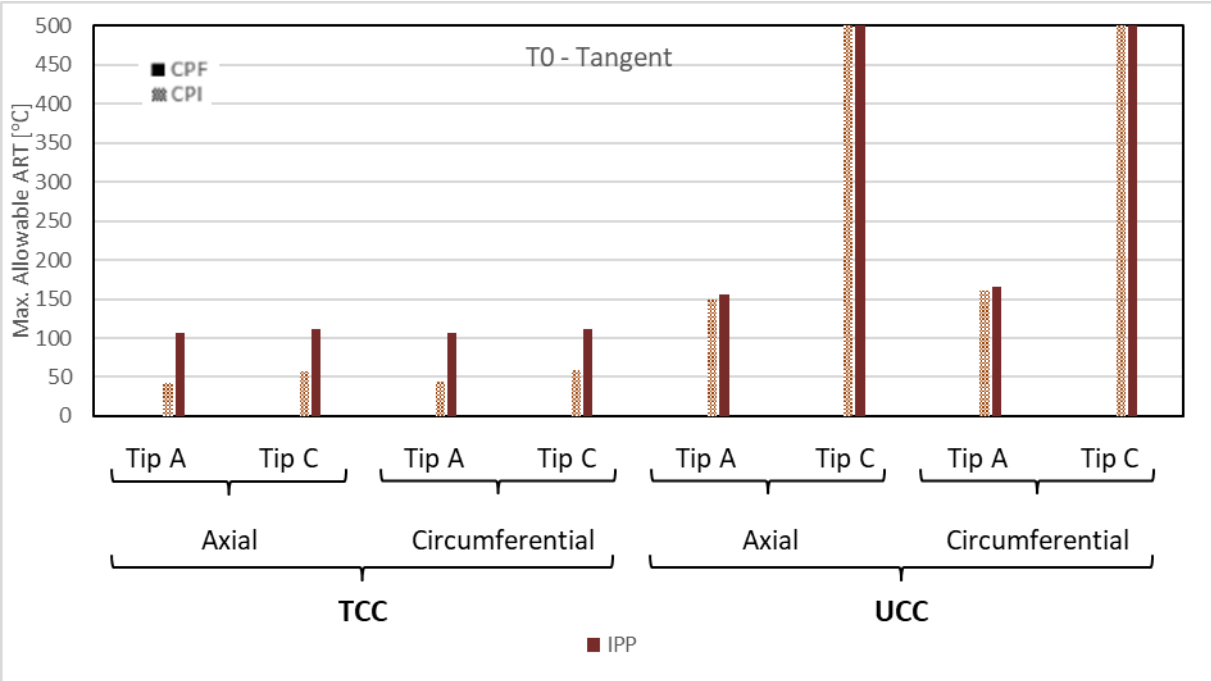

Figure 4.114: Maximum allowable ART values for the tangent approach considering the T_0 concept.

Table 4.60 Maximum allowable ART values for the max WPS approach considering the T_0 concept

Partner	Maximum allowable ART for TCC [°C]				Maximum allowable ART for UCC [°C]			
	Axial		Circumferential		Axial		Circumferential	
	A	C	A	C	A	C	A	C
IPP	126.23	136.60	127.99	139.15	183.39	>500	194.98	>500

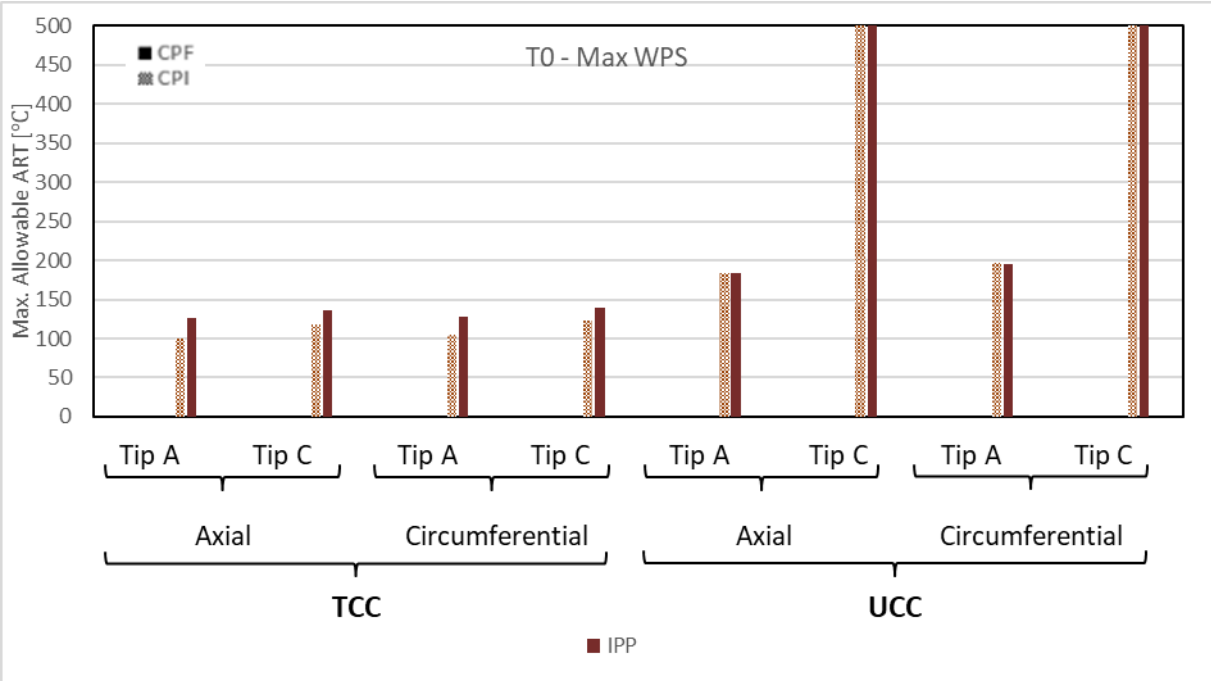

Figure 4.115: Maximum allowable ART values for the max WPS approach considering the T_0 concept.

4.3.5.2 PMA2

The maximum allowable RPV age, considering CPF, is calculated for the different crack geometries and locations for both the tangent and max WPS approaches.

Final allowable RPV age for the RT_{NDT} concept are presented in Table 4.61 and Table 4.62 as well as Figure 4.116 and Figure 4.117 for the tangent and max WPS approaches respectively. In the figures, the corresponding age values considering CPI from RR4 are included for comparison.

IPP was the only partner who provided results for PMA2 using the RT_{NDT} concept, thus comparisons with other partners for verifying the results were not possible. It can be seen that for the RT_{NDT} concept, a large gain in maximum allowable RPV age is obtained for all geometry cases when considering the tangent approach, while no gain is obtained when using the max WPS approaches. This corresponds well with PMA1 as well as PMA2 for RR3.

Table 4.61 Maximum allowable RPV age for the tangent approach considering the RT_{NDT} concept

Partner	Max allowable RPV age for TCC [years]				Max allowable RPV age for UCC [years]			
	Axial		Circumferential		Axial		Circumferential	
	A	C	A	C	A	C	A	C
IPP	120.9	137.4	122.7	138.8	>500	>500	>500	>500

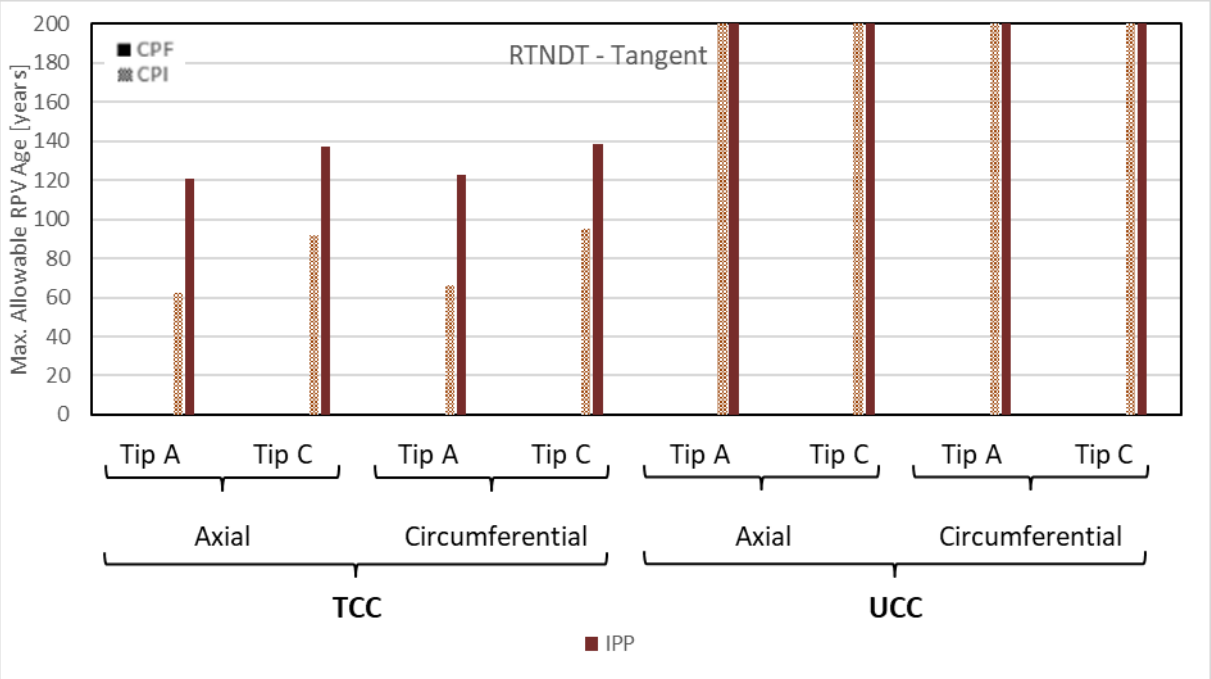

Figure 4.116: Maximum allowable RPV age for the tangent approach considering the RT_{NDT} concept.

Table 4.62 Maximum allowable RPV age for the max WPS approach considering the RT_{NDT} concept

Partner	Max allowable RPV age for TCC [years]				Max allowable RPV age for UCC [years]			
	Axial		Circumferential		Axial		Circumferential	
	A	C	A	C	A	C	A	C
IPP	221.8	271.7	232.4	285.3	>500	>500	>500	>500

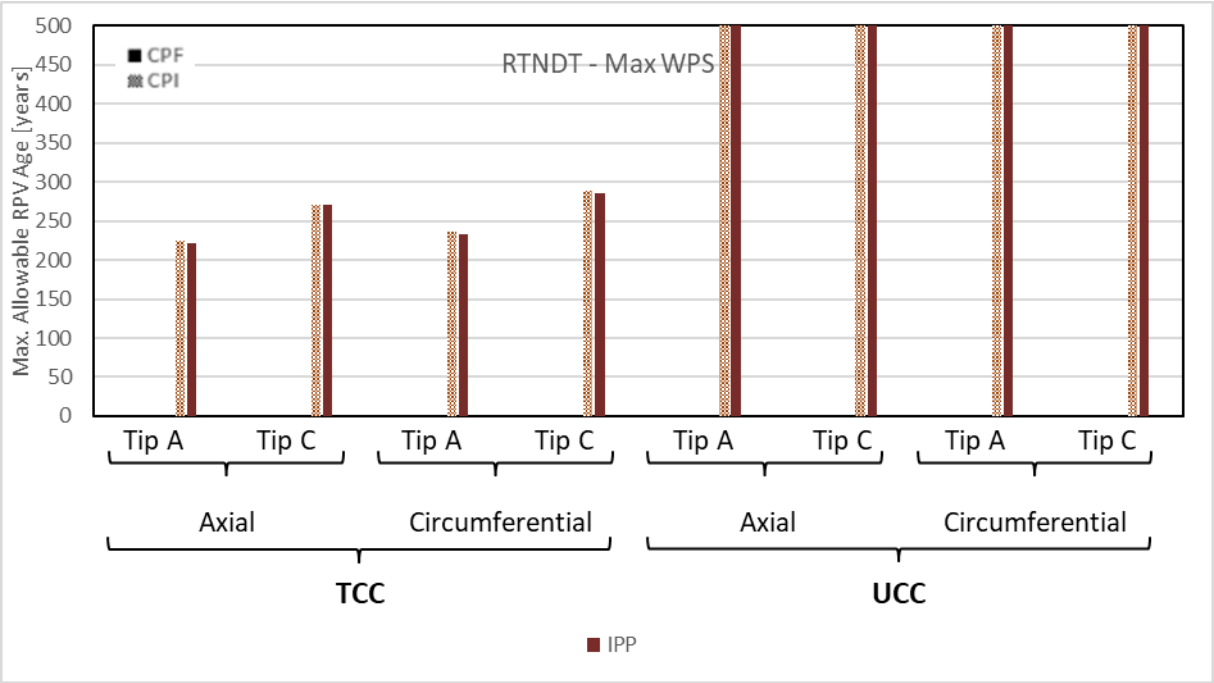

Figure 4.117: Maximum allowable RPV age for the max WPS approach considering the RT_{NDT} concept.

Final allowable RPV age for the FAVOR concept are presented in Table 4.63 and Figure 4.118 for a circumferential embedded crack.

Tecnatom was the only partner who provided results for PMA2 using the FAVOR concept, making verifying comparisons impossible. It can be seen that a large gain is obtained both for the tangent and max WPS approaches which corresponds well with PMA1 as well as RR3.

Table 4.63 Maximum allowable ART values for a circumferential TCC using the FAVOR concept

Partner	Max allowable ART for a circumferential TCC [°C]	
	Tangent	Max WPS
Tecnatom	213	616

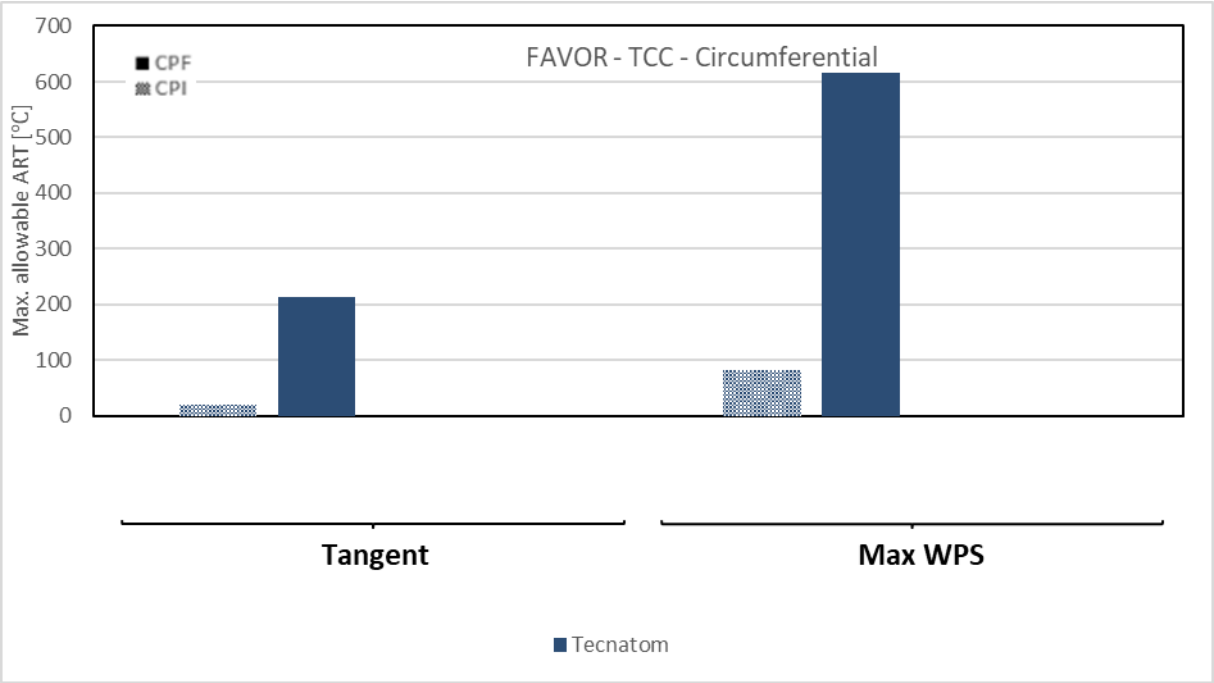

Figure 4.118: Maximum allowable ART values for a circumferential TCC using the FAVOR concept.

Final allowable RPV age for the T_0 concept are presented in Table 4.64 and Table 4.65 as well as Figure 4.119 and Figure 4.120 for the tangent and max WPS approaches respectively. In the figures, the corresponding age values considering CPI from RR4 are included for comparison.

IPP was the only partner who provided results for the T_0 concept, making verifying comparisons impossible. It can be seen that for the T_0 concept, a large gain in maximum allowable RPV age is obtained for all geometry cases using the tangent approach. There is some gain as well for the max WPS approaches for the TCC. For the UCC, all results are above the limiting value of 500 years used by IPP.

Table 4.64 Maximum allowable RPV age for the tangent approach considering the T_0 concept

Partner	Max allowable RPV age for TCC [years]				Max allowable RPV age for UCC [years]			
	Axial		Circumferential		Axial		Circumferential	
	A	C	A	C	A	C	A	C
IPP	297.3	311.0	301.9	315.9	>500	>500	>500	>500

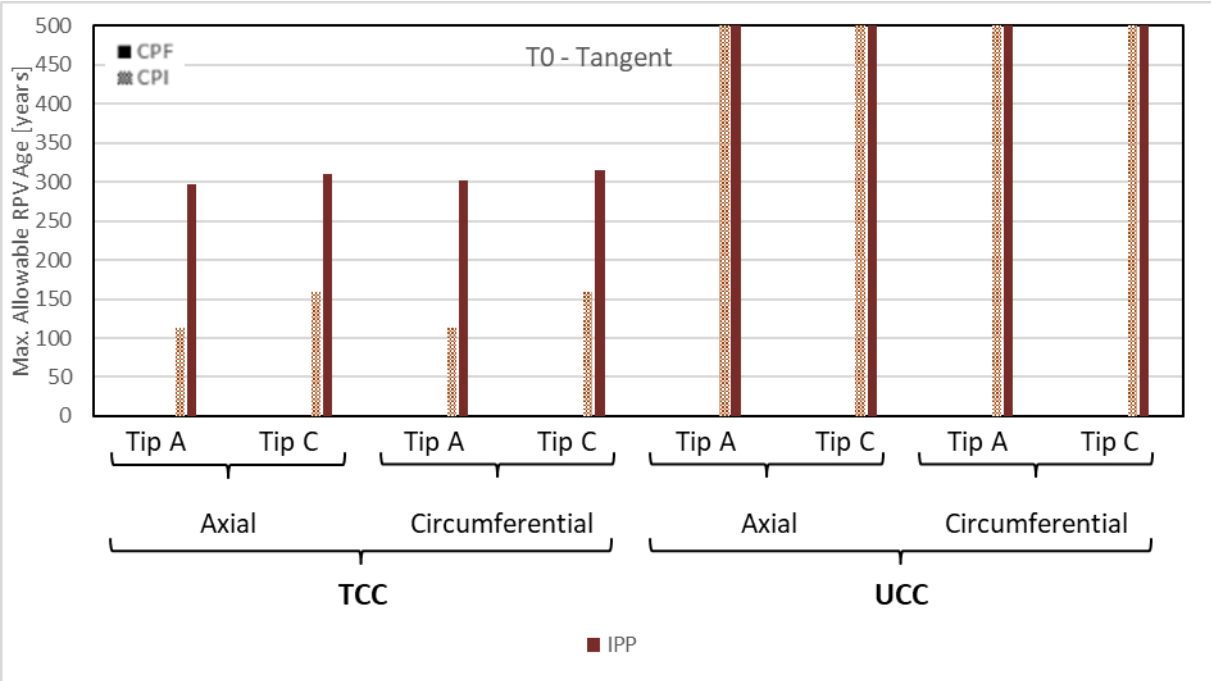

Figure 4.119: Maximum allowable RPV age for the tangent approach considering the T_0 concept.

Table 4.65 Maximum allowable RPV age for the max WPS approach considering the T_0 concept

Partner	Max allowable RPV age for TCC [years]				Max allowable RPV age for UCC [years]			
	Axial		Circumferential		Axial		Circumferential	
	A	C	A	C	A	C	A	C
IPP	388.6	433.6	396.8	446.5	>500	>500	>500	>500

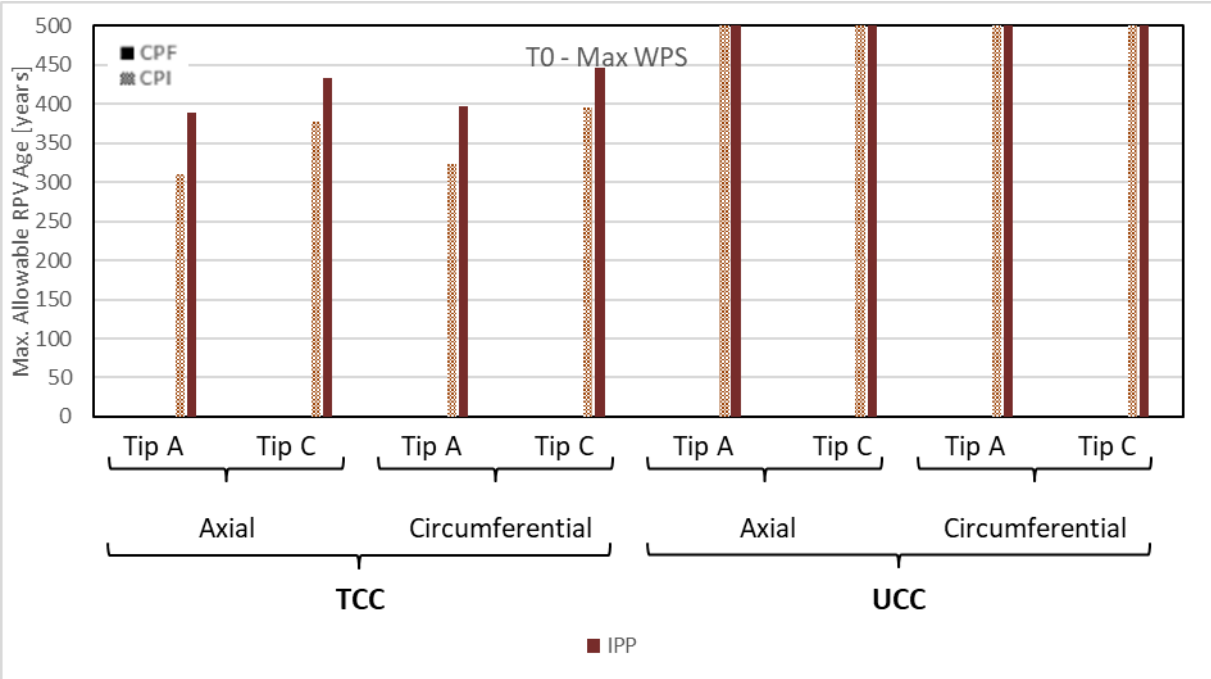

Figure 4.120: Maximum allowable RPV age for the max WPS approach considering the T_0 concept.

4.3.5.3 Conclusions from RR5

RR5 is a non-mandatory continuation of RR4 where crack arrest is considered and the limit is the CPF. Only IPP contributed with results for the RT_{NDT} and T_0 concept, while both JSI and Tecnatom contributed with results for a circumferential TCC2 using the FAVOR concept.

For the RT_{NDT} concept, IPP gets a benefit from considering crack arrest for TCC:s when using the tangent approach, while no benefit is seen for the max WPS approach. The results are similar for the T_0 concept, with the addition that a small benefit for TCC:s is seen for the max WPS approach as well.

For the FAVOR concept, a benefit from considering crack arrest is seen for all cases studied.

4.4 Discussion and main outcome

This Section summarises the main results and findings made within Task 4.3 of Work Package 4. The task included both tools verification and round robin (RR) analyses of a baseline transient where all partners used their base case transient data. The tools verification part was included as a lessons learned from previous international benchmarks where the different aspects have previously caused difficulties when doing comparisons of results from different partners.

The first tools verification was to verify that all partners use sufficient random number generators (RNG) that have a long enough period so that random values without repetition are obtained for Monte Carlo simulations made within the project. All partners used RNGs with sufficient sequence lengths and converged towards the analytically predicted CPIs used for the RNG verification. It should also be noted that the target CPI value used in the RR subtasks is $2.28 \cdot 10^{-4}$ which is much higher than what was used in this subtask, requiring lower sampling sizes and thus not as long sequence lengths for the RNG as within this verification.

One of the challenges within the APAL project was related to developing a realistic flaw depth distribution for UCC cracks that can be used in probabilistic analyses. The PNNL flaw distribution model was chosen as a basis, however, the original PNNL model does not allow a direct use with an arbitrary probabilistic code. The generic CDF for UCC flaw depth has been developed through a round-robin exercise where the involved partners individually interpreted, made necessary assumptions and mathematically treated the PNNL flaw distribution model. Based on these results, the CDF for UCC flaw depth was defined for probabilistic assessments in APAL.

Several distributions used within APAL are truncated normal distributions. The fourth tools verification was therefore to compare calculations made by the partners where truncated distributions were considered. No significant differences were seen between the partners as a result of truncation of distributions. It should be noted that the FAVOR users did not participate in this tools verification and thus, the truncation method used within FAVOR was not considered in the comparisons.

Calculation of CPI and cpi(t) for a pre-defined transient was performed in the fifth tools verification. After several iterations all partners managed to get similar results. This subtask cleared out several questions regarding how the analyses should be performed which was very beneficial before doing the RR analyses with partner specific transients.

The sixth and final tools verification was a non-mandatory continuation of the previous, but considering crack arrest and calculate CPF instead of CPI. Only a few partners participated in this subtask and several results were updated late in the project, which led to the differences not being fully explained.

Following the tools verifications, five round robin subtasks were performed.

RR1 was aimed at predicting ART for an increasing fluence level. The results indicate that ART-values have a clear correlation with fluence level, i.e. the ART-values increase with the RPV age. The ART-values vary through the RPV wall thickness being highest at the inner surface of the RPV. It has also been observed that for shallow cracks the ART-values for welds are higher in comparison to base metal. However, the ART-values for base metal are governing for deeper cracks. This transition occurs at a deeper position through the RPV wall with increasing RPV operation times. The results from RR1 also demonstrate that a choice of shift function has a large influence on the calculated ART-values, where the shift function according to RSE-M governs the ART-values for shallow cracks. For deeper crack the base shift function takes over predicting the highest ART-values for base metal, while the 10CFR50.61a shift function governs the ART-values for welds.

RR2 was the first benchmark based on partner specific transient data, and thus the first benchmark where differences in results were to be expected. The agreement was good between partners after some iterations and the differences can be explained by different transient data. The TCC gives the

shortest lifetimes and in most cases, point C at the clad/base interface was limiting. Detailed conclusions of RR2 are given in Section 4.3.2.7.

RR3 was a non-mandatory extension of RR2 where crack arrest was considered. Only a few partners participated in this subtask which made comparative verification difficult. Some benefits could be seen when considering crack arrest, especially for the FAVOR users, but crack arrest did not lead to longer lifetimes for all cases. Detailed conclusions of RR3 are given in Section 4.3.3.3.

RR4 was similar to RR2, but with a distributed crack. It should be noted that even the largest size in the distribution was smaller than the crack used in RR2. Much higher results were obtained for the RT_{NDT} and T_0 concepts, while the differences were much smaller for the FAVOR concept. Detailed conclusions of RR4 are given in Section 4.3.4.5.

RR5 was a non-mandatory extension of RR4 where crack arrest was considered. Only IPP contributed with results for the RT_{NDT} and T_0 concept, while both JSI and Tecnatom contributed with results for a circumferential TCC2 using the FAVOR concept. For the RT_{NDT} concept, IPP gets a benefit from considering crack arrest for TCC:s when using the tangent approach, while no gain is seen for the max WPS approach. The results are similar for the T_0 concept, with the addition that a small benefit for TCC:s is seen for the max WPS approach as well. For the FAVOR concept, a benefit from considering crack arrest is seen for all cases studied.

5 Probabilistic benchmark of LTO improvements

This Section presents the results obtained from each partner for the probabilistic assessment of the LTO improvements (Task 4.4) along with few plausibility checks. Task 4.4 was primarily focused on performing and summarising the probabilistic calculations of the selected LTO improvements shown in Table 5.1. A detailed interpretation of the results and margin assessments were performed as a part of Task 4.6 in the report D4.6 [6] which is also summarised in Section 7 of this report.

The main objective of the probabilistic benchmark spread between Tasks 4.4 and 4.6 was to quantify:

- Increase (or decrease) of explicit margin by taking into account TH data sets related to LTO improvements or human factor (from Task 2.1).

Table 5.1 Investigated LTO improvements.

Index Code	Naming in Table	Description of LTO improvement
1	LTO1	Heating of water in the HPSI tanks (T = 45°C)
2	LTO2	Heating of water in the ACCs (T = 50°C)
3	LTO3	Heating of water in the LPSI tanks (T= 45°C)
4	LTO4	Decreasing the HPSI head (75%)
5	LTO5	Decreasing the HPSI capacity (75%)
6	LTO6	Reduction of HPSI flow (operator action) at 1800s
7	LTO7	Decreasing of ACC pressure (20 bar)
8	LTO8	Change of cooldown rate (operator action) at 200 K/h
9	LTO9	Isolation of ACCs (operator action) at 500s

The probabilistic assessment of LTO improvements is schematically illustrated in Figure 5.1. It has to be noted that “safety margin” is not always necessarily an explicit margin (i.e. comparison of allowable value with actual RPV value). The comparison can also be done in terms of allowable values, as this gives the increase of explicit margin.

The TH data sets for LTO improvements have been defined in WP2 [8] (selection of potentially most influencing ones). The LTO improvements that have been analysed in WP3 and subsequently also in WP4 are listed in Table 5.1.

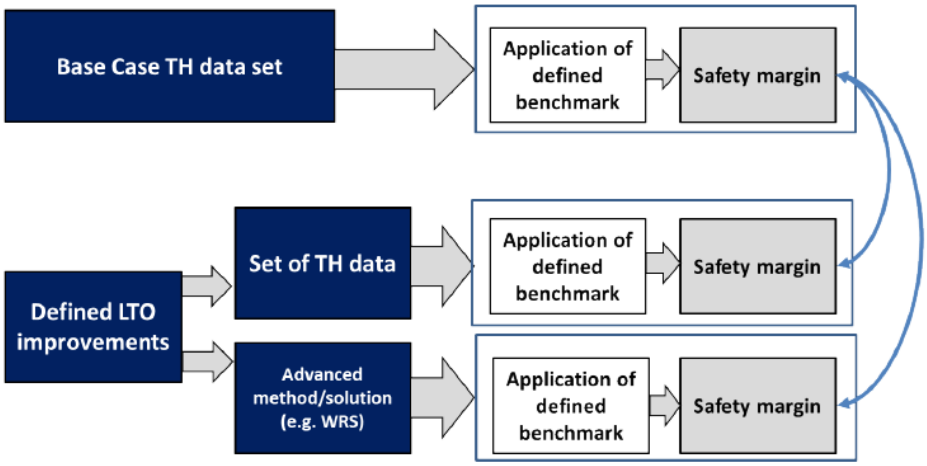

Figure 5.1: Comparison to be performed in Task 4.4.

5.1 Description of activities

Each partner was assigned a set of LTO improvements to be calculated and the final allocation of the LTOs is given in Table 5.2. The blue coloured cells show the source of the TH data that was used by the partners.

Table 5.2 Distribution of LTO improvements among partners.

					LTO improvements								
Partner	**SA**	**TH Input**		**Tool for Probabilistic FM**	**LTO1**	LTO2	LTO3	LTO4	LTO5	**LTO6**	LTO7	**LTO8**	LTO9
		1D/3D	**Source**										
BZN	1D	1D	RELAP	FEA			RELAP UJV/WUT						
PSI	1D	1D	TRACE	FAVOR	TRACE	TRACE					TRACE		
UJV	1D	1D	RELAP	PROVER	RELAP					RELAP WUT		RELAP WUT	
KIWA	1D	1D	RELAP	ISAAC+1D/2D FEA				RELAP SSTC	RELAP	RELAP WUT			
JSI	1D	1D	RELAP	In-house	RELAP WUT	RELAP WUT						RELAP WUT	
GRS	1D	1D	ECC-MIX	PROST		ATHLET (with ECC-MIX option)	ATHLET (with ECC-MIX option)	ATHLET (with ECC-MIX option)					
Tecnatom	1D	1D	TRACE/ECC-MIX	FAVOR	TRACE PSI			ATHLET (with ECC-MIX option) GRS	TRACE PSI				
IPP	1D	1D	Any	SIF-Master			KWU-MIX FRA-G	RELAP SSTC				KWU-MIX FRA-G	RELAP UJV/WUT
BZN	**3D**	**3D**	RELAP	FE with crack+in-house						RELAP WUT	RELAP JSI/WUT		
FRA-G	**3D**	**3D**	KWU-MIX	In-house						KWU-MIX		KWU-MIX	KWU-MIX
IPP	**3D**	**3D**	RELAP	FE with crack	RELAP UJV/WUT								

APAL has received funding from the Euratom research and training programme 2019-2020 under grant agreement No 945253.

In Figure 5.2 the work to be performed by each partner is represented. The mandatory case for this task was the round-robin benchmark RR2 (see Section 4.3.2) which was aimed at calculating the conditional probability of Initiation (CPI) for a given crack type, crack tip location and crack size.

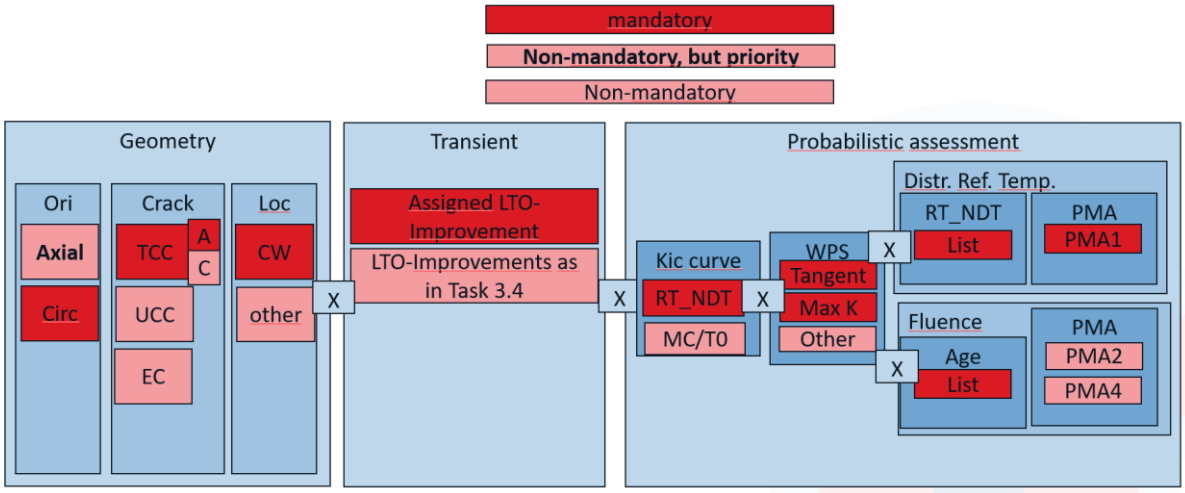

Figure 5.2: Overview of the work to be performed in Task 4.4.

5.1.1 Baseline benchmarks (Mandatory)

A short definition of the benchmarks to be performed for Task 4.4 is presented below. Detailed definition of the probabilistic benchmark is given in Section 2.

PMA1: Compute allowable ART for CPI=2.28e-4

- Assessment of Through clad crack (TCC)
  - Orientation: Circumferential
  - Size:
    - TCC: a in base metal = 10 mm i.e., total depth = 16 mm (10mm + 6mm cladding through); a/c=1/3; shape 1; 2c = 60 mm
  - Location:
    - Inside plume at height of core weld -2638mm from nozzle centerline
    - Inside merging plumes (when using mixing code) at elevation of core weld -2638 mm
- Limit condition:
  - Tangent approach
  - Simplified WPS (max approach)
- Embrittlement (brittle fracture) to be used for PMA1
  - Fixed reference temperature (non-distributed)
  - Use RT_{NDT} approach for distributed fracture toughness K_{IC}
- Calculate CPI for selected RT_{NDT} (0, 50, 100, 150, 200 °C)
- Accuracy of 1°C is recommended to calculate the final max. allowable ART
- Template of PMA1 to be used for the results (See Table 5.3).

APAL has received funding from the Euratom research and training programme 2019-2020 under grant agreement No 945253.

Table 5.3: Output table for PMA1

			Results for pre-defined fixed ART:					Final result
Fixed ART			0	50	100	150	200	
Final CPI for the transient								
Number of MC runs								
Convergence criterion used (y/n)								
Time in the transient (s)	Temp [°C]	KI [MPa√m]	Instantaneous cpi (t)					
0								
…								
10000								

PMA2: Compute allowable RPV age for CPI=2.28e-4

In addition to the mandatory work to be performed by each partner (see Figure 5.2), it was later decided that each partner identify the leading LTO improvement based on their own PMA1 calculations (either tangent approach or simplified WPS) and perform PMA2 assessment for the identified LTO improvement.

- Embrittlement (brittle fracture) to be used for PMA2
- Neutron fluence for selected RPV ages
  - Fluence at inner surface depending on given lifetime
  - Fluence decrease (attenuation) through RPV wall (to finally get ART at crack tip)
- Use RT_{NDT} approach for ART and fracture toughness distribution
  - Core Weld:
    - Chemical composition of weld (see Section 2.3.7)
    - Base shift formula for weld to be used for ΔRT_{NDT} (see Section 2.3.6)
- Calculate CPI for selected RPV ages (1, 20, 40, 80, 200 years, i.e. for corresponding fluences)
- Accuracy of 1 year is recommended to calculate the final allowable RPV age
- PMA2 template for the results (see Table 5.4).

Table 5.4: Output table for PMA2

			Results for pre-defined RPV age:					Final result
RPV age			1	20	40	80	200	
Mean value fluence IS (10^{23} n/m²)			1	5	7.5	12.5	27.5	
ART	MV							
	SD							
	5% Quantile							
	95% Quantile							
Final CPI for the transient								
Number of MC runs								
Convergence criterion used (y/n)								
Time in the transient (s)	Temp [°C]	KI [MPa√m]	Instantaneous cpi (t)					
0								
…								
10000								

5.1.2 Non-Mandatory benchmarks

- PMA2 (determine max. allowable lifetime) except for the leading LTO improvement
- PMA4 (determine reliability index)
- PR-PCA-RR3 (i.e., Determination of CPF for fixed crack size)
- PR-PCI-RR4 (i.e., Determination of CPI with distributed crack depth)

- PR-PCA-RR5 (i.e., Determination of CPF with distributed crack depth)
- TCC, axial
- UCC, circ. and axial
- Embedded, circ. and axial.
- Nozzle Corner
- Point C
- Sophisticated WPS
- T0 concept, FAVOR concept
- Other locations (e.g., flange weld)

5.2 Results from probabilistic benchmark of LTO improvements

In this chapter, the results of the individual LTO improvements are presented. The margins (benefits) of the individual LTO improvements, i.e. differences between the LTO cases and the base case are calculated in D4.6 [6] and also summarised in section 7.

5.2.1 Results for each LTO improvement

5.2.1.1 LTO1 – Heating of water in the HPSI tanks (T = 45°C)

In case of the TH data the heating of water in HPSI tanks was simulated by increasing the injection temperature from the reference value of 15°C to the LTO value of 45°C. The calculations showed that the increased injection temperature results in a higher water temperature in the DC during the whole transient. The proposed LTO development until the ACCs start (about 2790 s) has an impact on the break flow and fluid levels. Therefore, it was concluded in WP2 based TH data that this LTO improvement could potentially be beneficial for PTS. PSI, UJV, JSI, Tecnatom and IPP analysed LTO1 and the obtained results are summarised below. The results for LTO1 for PMA1 and PMA2 assessments of TCC cracks are shown in Table 5.5 - Table 5.8 and in Table 5.9 - Table 5.12 for UCC cracks.

Table 5.5: LTO 1 Final max. all. ART (PMA1) for TCC (RT_{NDT} Approach)

	Final max. all. ART (°C) -RT_{NDT} Approach							
	TCC							
	Axial				Circumferential			
	Point A		Point C		Point A		Point C	
Partner	Tangent	WPS	Tangent	WPS	Tangent	WPS	Tangent	WPS
PSI					58.5			
UJV	85.6	136.2			86.3	138.3		
JSI					86	126		
Tecnatom					58	112		
IPP	87	138.3	81.5	123.1	86.6	126.9	80.7	121.3

Table 5.6: LTO 1 Final max. all. ART (PMA1) for TCC (T_0 Approach)

	Final max. all. ART (°C) -T_0 Approach							
	TCC							
	Axial				Circumferential			
	Point A		Point C		Point A		Point C	
	Tangent	WPS	Tangent	WPS	Tangent	WPS	Tangent	WPS
Partner								
JSI					25	59		
IPP	26.5	68.5	23	60.2	25.8	58.8	22.2	57.9

Table 5.7: LTO 1 Final all. RPV Age (PMA2) for TCC (RT_{NDT} Approach)

	Final Allowable RPV Age (years) - RT_{NDT} Approach							
	TCC							
	Axial				Circumferential			
	Point A		Point C		Point A		Point C	
	Tangent	WPS	Tangent	WPS	Tangent	WPS	Tangent	WPS
Partner								
PSI					130			
UJV	72.78	195.5			74.4	203.2		
Tecnatom					37			
IPP	77.1	200.7	56.6	139.7	74.4	166.9	54.3	134.9

Table 5.8: LTO 1 Final all. RPV Age (PMA2) for TCC (T_0 Approach)

	Final Allowable RPV Age (years) - T_0 Approach							
	TCC							
	Axial				Circumferential			
	Point A		Point C		Point A		Point C	
	Tangent	WPS	Tangent	WPS	Tangent	WPS	Tangent	WPS
Partner								
IPP	87.6	223.2	71	150.8	87.7	180.2	67.3	156.1

Table 5.9: LTO 1 Final max. all. ART (PMA1) for UCC (RT_{NDT} Approach)

	Final max. all. ART (°C) -RT_{NDT} Approach							
	UCC							
	Axial				Circumferential			
	Point A		Point C		Point A		Point C	
	Tangent	WPS	Tangent	WPS	Tangent	WPS	Tangent	WPS
Partner								
IPP	113.8	157.8	223.6	231.6	114.6	160.74	0	0

Table 5.10: LTO 1 Final max. all. ART (PMA1) for UCC (T_0 Approach)

	Final max. all. ART (°C) -T_0 Approach							
	UCC							
	Axial				Circumferential			
	Point A		Point C		Point A		Point C	
	Tangent	WPS	Tangent	WPS	Tangent	WPS	Tangent	WPS
Partner								
IPP	62.6	97.0	140.7	158.45	63.7	104.9	149.2	169.4

Table 5.11: LTO 1 Final all. RPV Age (PMA2) for UCC (RT_{NDT} Approach)

	Final Allowable RPV Age (years) - RT_{NDT} Approach							
	UCC							
	Axial				Circumferential			
	Point A		Point C		Point A		Point C	
	Tangent	WPS	Tangent	WPS	Tangent	WPS	Tangent	WPS
Partner								
IPP	159.7	285.2	0	0	162.7	298.1	>500	>500

Table 5.12: LTO 1 Final all. RPV Age (PMA2) for UCC (T_0 Approach)

	Final Allowable RPV Age (years) - T_0 Approach							
	UCC							
	Axial				Circumferential			
	Point A		Point C		Point A		Point C	
	Tangent	WPS	Tangent	WPS	Tangent	WPS	Tangent	WPS
Partner								
IPP	199.5	338.4	477.1	0	198.9	356.6	>500	>500

5.2.1.2 LTO2- Heating of water in the ACCs (T=50°C)

In case of the thermal hydraulic calculations the heating of the water in the ACCs was simulated by increasing the water injection temperature from the reference value of 20°C to 50°C. The LTO improvement resulted in slightly higher temperature in the DC after the beginning of the flow from ACCs. Therefore, it was concluded in WP2 based on TH data that this LTO improvement could potentially provide no significant benefit from a PTS perspective. PSI, JSI and GRS analysed LTO2 and the obtained results are summarised below. The results for LTO2 for PMA1 of TCC cracks are shown in Table 5.13- Table 5.14 and PMA2 assessment of TCC crack in Table 5.15.

Table 5.13: LTO 2 max. all. ART (PMA1) for TCC (RT_{NDT} Approach)

	Final max. all. ART (°C) -RT_{NDT} Approach							
	TCC							
	Axial				Circumferential			
	Point A		Point C		Point A		Point C	
	Tangent	WPS	Tangent	WPS	Tangent	WPS	Tangent	WPS
Partner								
PSI					34.4			
JSI					61	131		
GRS	80.9	137.11			81.65	139.5		

Table 5.14: LTO 2 Final max. all. ART (PMA1) for TCC (T_0 Approach)

	Final max. all. ART (°C) -T_0 Approach							
	TCC							
	Axial				Circumferential			
	Point A		Point C		Point A		Point C	
	Tangent	WPS	Tangent	WPS	Tangent	WPS	Tangent	WPS
Partner								
PSI								
JSI					0	61		
GRS								

Table 5.15: LTO 2 Final all. RPV Age (PMA2) for TCC (RT_{NDT} Approach)

	Final Allowable RPV Age (years) - RT_{NDT} Approach							
	TCC							
	Axial				Circumferential			
	Point A		Point C		Point A		Point C	
	Tangent	WPS	Tangent	WPS	Tangent	WPS	Tangent	WPS
Partner								
PSI								
JSI								
GRS	43.44	225.21			45.93	234.8		

5.2.1.3 LTO3- Heating of water in the LPSI tanks (T = 45°C)

The heating of the water in the LPSI tanks was simulated by increasing the injection temperature from the reference value of 15°C to 45°C. The RELAP calculations showed that there is insignificant impact on the water level and water temperature in the DC till the end of transient. Similarly, in case of the TRACE simulations, for this transient, heating of LPI had only a very small benefit. BZN, GRS and IPP analysed LTO3 and the obtained results are summarised below. The results for LTO3 for PMA1 and PMA2 assessments of TCC and UCC cracks are shown in Table 5.16- Table 5.23.

Table 5.16: LTO 3 Final max. all. ART (PMA1) for TCC (RT_{NDT} Approach)

	Final max. all. ART (°C) -RT_{NDT} Approach							
	TCC							
	Axial				Circumferential			
	Point A		Point C		Point A		Point C	
	Tangent	WPS	Tangent	WPS	Tangent	WPS	Tangent	WPS
Partner								
BZN	60.93	138.67	58.20	128.51	61.32	133.59	58.20	129.68
GRS	81.65	137.11			83.2	115.23		
IPP	33.18	98.2	30.1	92.6	34.33	99.95	31.03	94.3

Table 5.17: LTO 3 Final max. all. ART (PMA1) for UCC (RT_{NDT} Approach)

	Final max. all. ART (°C) -RT_{NDT} Approach							
	UCC							
	Axial				Circumferential			
	Point A		Point C		Point A		Point C	
	Tangent	WPS	Tangent	WPS	Tangent	WPS	Tangent	WPS
Partner								
BZN	80.46	153.51	158.59	190.6	83.59	156.64	173.43	200
IPP	48.1	122.42	102.1	149	53.11	114.9	119.3	146.13

Table 5.18: LTO 3 Final max. all. ART(PMA1) for TCC (T_0 Approach)

	Final max. all. ART (°C) -T_0 Approach							
	TCC							
	Axial				Circumferential			
	Point A		Point C		Point A		Point C	
	Tangent	WPS	Tangent	WPS	Tangent	WPS	Tangent	WPS
Partner								
BZN	0	67.18	0	61.71	0	63.28	0	63.67
IPP	-27.75	22.15	-32.37	21.55	-26.79	25.53	-27.82	25.66

Table 5.19: LTO 3 Final all. ART (PMA1) for UCC (T_0 Approach)

	Final max. all. ART (°C) -T_0 Approach							
	UCC							
	Axial				Circumferential			
	Point A		Point C		Point A		Point C	
	Tangent	WPS	Tangent	WPS	Tangent	WPS	Tangent	WPS
Partner								
BZN	28.91	91.79	88.28	141.01	31.25	96.48	98.04	148.82
IPP	-6.13	55.97	43.78	99.67	0.18	50.70	58.06	95.69

Table 5.20: LTO 3 Final all. RPV Age (PMA2) for TCC (RT_{NDT} Approach)

	Final Allowable RPV Age (years) - RT_{NDT} Approach							
	TCC							
	Axial				Circumferential			
	Point A		Point C		Point A		Point C	
	Tangent	WPS	Tangent	WPS	Tangent	WPS	Tangent	WPS
Partner								
GRS	45.94	225.77			50.31	138.83		
IPP	6.59	89.65	4.31	69.01	6.93	94.80	4.62	71.44

Table 5.21: LTO 3 Final all. RPV Age (PMA2) for UCC (RT_{NDT} Approach)

	Final Allowable RPV Age (years) - RT_{NDT} Approach							
	UCC							
	Axial				Circumferential			
	Point A		Point C		Point A		Point C	
	Tangent	WPS	Tangent	WPS	Tangent	WPS	Tangent	WPS
Partner								
IPP	17.52	156.90	127.56	>200	24.21	139.45	181.22	>200

Table 5.22: LTO 3 Final all. RPV Age (PMA2) for TCC (T_0 Approach)

	Final Allowable RPV Age (years) - T_0 Approach							
	TCC							
	Axial				Circumferential			
	Point A		Point C		Point A		Point C	
	Tangent	WPS	Tangent	WPS	Tangent	WPS	Tangent	WPS
Partner								
IPP	8.00	81.60	5.69	68.84	8.42	87.08	6.66	73.91

Table 5.23: LTO 3 Final all. RPV Age (PMA2) for UCC (T_0 Approach)

	Final Allowable RPV Age (years) - T_0 Approach							
	UCC							
	Axial				Circumferential			
	Point A		Point C		Point A		Point C	
	Tangent	WPS	Tangent	WPS	Tangent	WPS	Tangent	WPS
Partner								
IPP	29.23	172.05	123.26	>200	36.26	156.04	158.34	>200

5.2.1.4 LTO4- Decreasing the HPSI head (75%)

To get the relevant TH data for the SA simulations in WP2.1 the decreasing of the HPI pump head was simulated by scaling the pressure component of the HPI pump curve down to 75% of the reference value. KIWA, GRS, Tecnatom and IPP analysed LTO4 and the obtained results are summarised below. The results for LTO4 for PMA1 and PMA2 assessments of TCC and UCC cracks are shown in Table 5.24 - Table 5.31.

Table 5.24: LTO 4 max. all. ART (PMA1) for TCC (RT_{NDT} Approach)

	Final max. all. ART (°C) -RT_{NDT} Approach							
	TCC							
	Axial				Circumferential			
	Point A		Point C		Point A		Point C	
	Tangent	WPS	Tangent	WPS	Tangent	WPS	Tangent	WPS
Partner								
KIWA	58.6	107.1	55.5	102.7	59.6	108.8	56.2	82.4
GRS	81.64	139.45			82.4	141		
Tecnatom					38	102		
IPP	59.4	107.4	56.2	103.34	60.1	109	56.9	82.79

Table 5.25: LTO 4 Final max. all. ART (PMA1) for UCC (RT_{NDT} Approach)

	Final max. all. ART (°C) -RT_{NDT} Approach							
	UCC							
	Axial				Circumferential			
	Point A		Point C		Point A		Point C	
	Tangent	WPS	Tangent	WPS	Tangent	WPS	Tangent	WPS
Partner								
KIWA	80	136.1	149.3	182.1	84.4	128.05	169.2	187.1
IPP	80.7	136.2	149.3	181	84.1	127.5	169.4	185.6

Table 5.26: LTO 4 Final max. all. ART (PMA1) for TCC (T_0 Approach)

	Final max. all. ART (°C) -T_0 Approach							
	TCC							
	Axial				Circumferential			
	Point A		Point C		Point A		Point C	
	Tangent	WPS	Tangent	WPS	Tangent	WPS	Tangent	WPS
Partner								
KIWA	-3.46	36	-4.86	35.3	-3.25	38.7	-3.99	15.9
IPP	-4.5	35.2	-4.43	36.2	-3.48	38.6	-3.86	16.8

Table 5.27: LTO 4 Final max. all. ART (PMA1) for UCC (T_0 Approach)

	Final max. all. ART (°C) -T_0 Approach							
	UCC							
	Axial				Circumferential			
	Point A		Point C		Point A		Point C	
	Tangent	WPS	Tangent	WPS	Tangent	WPS	Tangent	WPS
Partner								
KIWA		75.5		132.1		67.9		127.7
IPP	27.3	75	90.2	127.7	31.65	67.7	99.8	125.8

Table 5.28: LTO 4 Final all. RPV Age (PMA2) for TCC (RT_{NDT} Approach)

	Final Allowable RPV Age (years) - RT_{NDT} Approach							
	TCC							
	Axial				Circumferential			
	Point A		Point C		Point A		Point C	
	Tangent	WPS	Tangent	WPS	Tangent	WPS	Tangent	WPS
Partner								
KIWA	25.93	113.82	21.84	106.01	27.03	119.53	23.43	63.59
GRS	45.93	225.7			50.3	138.4		
IPP	26.1	113.2	18.6	91.4	26.9	117.3	19.4	53.01

Table 5.29: LTO 4 Final all. RPV Age (PMA2) for UCC (RT_{NDT} Approach)

	Final Allowable RPV Age (years) - RT_{NDT} Approach							
	UCC							
	Axial				Circumferential			
	Point A		Point C		Point A		Point C	
	Tangent	WPS	Tangent	WPS	Tangent	WPS	Tangent	WPS
Partner								
KIWA	68.5946	206.10	331.158	468.36	80.7938	184.47	449.30	520.24
IPP	69.1	>200	>200	>200	79.3	178.3	>200	>200

Table 5.30: LTO 4 Final all. RPV Age (PMA2) for TCC (T_0 Approach)

	Final Allowable RPV Age (years) - T_0 Approach							
	TCC							
	Axial				Circumferential			
	Point A		Point C		Point A		Point C	
	Tangent	WPS	Tangent	WPS	Tangent	WPS	Tangent	WPS
Partner								
KIWA	30.6	66.1	29.9	63.1	32.3	71	29.6	28.2
IPP	29.9	111	23.11	96.3	31.4	118.6	24.06	58.9

Table 5.31: LTO 4 Final all. RPV Age (PMA2) for TCC (T_0 Approach)

	Final Allowable RPV Age (years) - T_0 Approach							
	UCC							
	Axial				Circumferential			
	Point A		Point C		Point A		Point C	
	Tangent	WPS	Tangent	WPS	Tangent	WPS	Tangent	WPS
Partner								
KIWA		165.6		362.7		142.5		127.7
IPP	90.6	>200	>200	>200	102.9	178.3	>200	>200

5.2.1.5 LTO5- Decreasing the HPSI capacity (75%)

In WP2 Task 2.1 the decreasing of the HPI pump capacity was simulated via scaling of the flow component of the HPI pump curve down to 75%. From the TH simulations it was concluded that by decreasing rate of cooling (via HPI pumps) the coolant temperatures can be reduced to some extent. Based on the results, it was assumed that analysed LTO improvement potentially may affect results of RPV strength analysis. KIWA and Tecnatom analysed LTO5 and the obtained results are summarised below. The results for LTO5 for PMA1 assessment of TCC cracks are shown in Table 5.32 - Table 5.33.

Table 5.32: LTO 5 Final max. all. ART (PMA1) for TCC (RT_{NDT} Approach)

	Final max. all. ART (°C) -RT_{NDT} Approach							
	TCC							
	Axial				Circumferential			
	Point A		Point C		Point A		Point C	
	Tangent	WPS	Tangent	WPS	Tangent	WPS	Tangent	WPS
Partner								
KIWA	64.6	93.4			65.5	94.5		
Tecnatom					41	72		

Table 5.33: LTO 5 Final all. RPV Age (PMA1) for TCC (T_0 Approach)

	Final Allowable RPV Age (years) - RT_{NDT} Approach							
	TCC							
	Axial				Circumferential			
	Point A		Point C		Point A		Point C	
	Tangent	WPS	Tangent	WPS	Tangent	WPS	Tangent	WPS
Partner								
KIWA	32.3	84.3			34.4	86.1		

5.2.1.6 LTO6- Reduction of HPSI flow (operator action) at 1800s

In the TH calculations the reduction of HPSI flow by operator was simulated by switching off 1 of 2 HPIS pumps at 1800 s after the initiation of the break. The calculations showed that the reduction of HPI injection results in a higher temperature of the water in the DC starting at 1800 s. Additionally, the lower break flow, the lower water level in the DC and the higher void fraction are observed after this operator action. Therefore, in the TH calculations it was concluded that this LTO improvement could potentially be beneficial from a PTS perspective. UJV, KIWA, BZN and FRA-G analysed LTO6 and the obtained results are summarised below. The results for LTO6 for PMA1 and PMA2 assessments of TCC and UCC cracks are shown in Table 5.34 - Table 5.41.

Table 5.34: LTO 6 Final max. all. ART (PMA1) for TCC (RT_{NDT} Approach)

	Final max. all. ART (°C) -RT_{NDT} Approach							
	TCC							
	Axial				Circumferential			
	Point A		Point C		Point A		Point C	
	Tangent	WPS	Tangent	WPS	Tangent	WPS	Tangent	WPS
Partner								
UJV	80.82	132			81.5	134.1		
KIWA	81.4	134.3	79	128.8	82.4	136.6	79.8	131
BZN	81.25	132.4	76.5	127.3	82.8	134	77.7	128.9

Table 5.35: LTO 6 Final max. all. ART (PMA1) for UCC (RT_{NDT} Approach)

	Final max. all. ART (°C) -RT_{NDT} Approach							
	UCC							
	Axial				Circumferential			
	Point A		Point C		Point A		Point C	
	Tangent	WPS	Tangent	WPS	Tangent	WPS	Tangent	WPS
Partner								
KIWA	100	149.4	183.5	186.7	104.2	154.1	202.8	203.6
BZN	101.7	148.4	194.1	194.1	106	152	202.3	202.3

Table 5.36: LTO 6 Final max. all. ART (PMA1) for TCC (T0 Approach)

	Final max. all. ART (°C) -T_0 Approach							
	TCC							
	Axial				Circumferential			
	Point A		Point C		Point A		Point C	
	Tangent	WPS	Tangent	WPS	Tangent	WPS	Tangent	WPS
Partner								
KIWA	16.7273	61.9508	18.4578	59.9787	18.5912	66.0239	18.9323	64.3993
BZN	17.97	60.9375	14.8	60.15	20.31	63.67	16.797	62.5

Table 5.37: LTO 6 Final max. all. ART (PMA1) for UCC (T_0 Approach)

	Final max. all. ART (°C) -T_0 Approach							
	UCC							
	Axial				Circumferential			
	Point A		Point C		Point A		Point C	
	Tangent	WPS	Tangent	WPS	Tangent	WPS	Tangent	WPS
Partner								
KIWA	43.2635	88.64	103.50	135.63	52.2634	94.47	116.76	149.47
BZN	47.656	87.5	114.84	142.578	53.9	92.578	123.44	148.05

Table 5.38: LTO 6 Final all. RPV Age (PMA2) for TCC (RT_{NDT} Approach)

	Final Allowable RPV Age (years) - RT_{NDT} Approach							
	TCC							
	Axial				Circumferential			
	Point A		Point C		Point A		Point C	
	Tangent	WPS	Tangent	WPS	Tangent	WPS	Tangent	WPS
Partner								
UJV	62	180.4			63.4	188.2		
KIWA	62.3	187	60.49	174.8	64.9	194.7	61.1	183.5
BZN					60.62	189.6		
FRA-G					7	98		

Table 5.39: LTO 6 Final all. RPV Age (PMA2) for UCC (RT_{NDT} Approach)

	Final Allowable RPV Age (years) - RT_{NDT} Approach							
	UCC							
	Axial				Circumferential			
	Point A		Point C		Point A		Point C	
	Tangent	WPS	Tangent	WPS	Tangent	WPS	Tangent	WPS
Partner								
KIWA	111	250	476.7	471	125.7	268.7	598.2	597.3

Table 5.40: LTO 6 Final all. RPV Age (PMA2) for TCC (T_0 Approach)

	Final Allowable RPV Age (years) - T_0 Approach							
	TCC							
	Axial				Circumferential			
	Point A		Point C		Point A		Point C	
	Tangent	WPS	Tangent	WPS	Tangent	WPS	Tangent	WPS
Partner								
KIWA	72.8653	189.13	71.22	192.10	71.06	207.80	69.99	198.26

Table 5.41: LTO 6 Final all. RPV Age (PMA2) for UCC (T_0 Approach)

	Final Allowable RPV Age (years) - T_0 Approach							
	UCC							
	Axial				Circumferential			
	Point A		Point C		Point A		Point C	
	Tangent	WPS	Tangent	WPS	Tangent	WPS	Tangent	WPS
Partner								
KIWA	138.08	281.98	353.68	519.77	157.90	310.11	426.06	589.53

5.2.1.7 LTO7- Decreasing of ACC pressure (20 bar)

In the TH calculations the LTO improvement of decreasing of ACC pressure was modelled by decreasing the initial pressure opening setpoint in the ACCs from the nominal value of 2.6 MPa to 2 MPa. In case of the RELAP calculations, the results showed that the decrease of the ACC pressure slightly increases the water temperature in the DC, however, it was concluded that the studied LTO improvement provides no significant benefit from a PTS perspective. The SA simulations carried out with RELAP input data in WP3 also confirmed this conclusion. PSI and BZN analysed LTO7 and the obtained results are summarised below. The results for LTO7 for PMA1 assessment of TCC crack using the RT_{NDT} approach is shown in Table 5.42.

Table 5.42: LTO 7 Final max. all. ART (PMA1) for TCC (RT_{NDT} Approach)

	Final max. all. ART (°C) -RT_{NDT} Approach							
	TCC							
	Axial				Circumferential			
	Point A		Point C		Point A		Point C	
	Tangent	WPS	Tangent	WPS	Tangent	WPS	Tangent	WPS
Partner								
PSI					33			
BZN	59.4	133			59.8	134.4		

5.2.1.8 LTO8- Change of cooldown rate (operator action) to 200K/h

During the TH calculation the increase of the secondary side cooldown rate by operator was simulated by increasing the cooldown of the secondary side from 100 K/h to 200 K/h. The proposed LTO improvement resulted in the increase of the water temperature in the DC after 2000 s. In the D2.1 report it was stated that the studied LTO improvement could potentially be beneficial from a perspective of higher water temperature in DC, but at the same time, it could be detrimental from a perspective of the faster pressure drop in DC. The overall benefit of this LTO improvement is studied under WP3 and WP4. UJV, JSI, IPP and FRA-G analysed LTO8 and the obtained results are summarised below. The results for LTO8 for PMA1 and PMA2 assessments of TCC and UCC cracks are shown in Table 5.43 - Table 5.50.

Table 5.43: LTO 8 Final max. all. ART (PMA1) for TCC (RT_{NDT} Approach)

	Final max. all. ART (°C) -RT_{NDT} Approach							
	TCC							
	Axial				Circumferential			
	Point A		Point C		Point A		Point C	
	Tangent	WPS	Tangent	WPS	Tangent	WPS	Tangent	WPS
Partner								
UJV	95.7	129.1			98.2	129.8		
JSI					99	130		
IPP	73.6	115.3	72.6	89.13	75.8	96.53	74.5	89.73
FRA-G					68	96		

Table 5.44: LTO 8 Final max. all. ART (PMA1) for UCC (RT_{NDT} Approach)

	Final max. all. ART (°C) -RT_{NDT} Approach							
	UCC							
	Axial				Circumferential			
	Point A		Point C		Point A		Point C	
	Tangent	WPS	Tangent	WPS	Tangent	WPS	Tangent	WPS
Partner								
IPP	89.3	128.8	139.7	161.3	93.8	130.8	144.8	163.1
FRA-G								

Table 5.45: LTO 8 Final max. all. ART (PMA1) for TCC (T_0 Approach)

	Final max. all. ART (°C) -T_0 Approach							
	TCC							
	Axial				Circumferential			
	Point A		Point C		Point A		Point C	
	Tangent	WPS	Tangent	WPS	Tangent	WPS	Tangent	WPS
Partner								
JSI					40	60		
IPP	14.2	43.2	15.3	19.9	16.5	22.4	18.6	23.1

Table 5.46: LTO 8 Final max. all. ART (PMA1) for UCC (T_0 Approach)

	Final max. all. ART (°C) -T_0 Approach							
	UCC							
	Axial				Circumferential			
	Point A		Point C		Point A		Point C	
	Tangent	WPS	Tangent	WPS	Tangent	WPS	Tangent	WPS
Partner								
IPP	36.7	66.5	90.35	113	42.6	67.04	97	114

Table 5.47: LTO 8 Final all. RPV Age (PMA2) for TCC (RT_{NDT} Approach)

	Final Allowable RPV Age (years) - RT_{NDT} Approach							
	TCC							
	Axial				Circumferential			
	Point A		Point C		Point A		Point C	
	Tangent	WPS	Tangent	WPS	Tangent	WPS	Tangent	WPS
Partner								
UJV	96.56	173.3			102.8	175.6		
JSI					100	177		
IPP	51.07	131.8	42.5	63.2	56	88	45	64.3

Table 5.48: LTO 8 Final all. RPV Age (PMA2) for UCC (RT_{NDT} Approach)

	Final Allowable RPV Age (years) - RT_{NDT} Approach							
	UCC							
	Axial				Circumferential			
	Point A		Point C		Point A		Point C	
	Tangent	WPS	Tangent	WPS	Tangent	WPS	Tangent	WPS
Partner								
IPP	88.5	178	>200	>200	101	183	>200	>200

Table 5.49: LTO 8 Final all. RPV Age (PMA2) for TCC (T_0 Approach)

	Final Allowable RPV Age (years) - T_0 Approach							
	TCC							
	Axial				Circumferential			
	Point A		Point C		Point A		Point C	
	Tangent	WPS	Tangent	WPS	Tangent	WPS	Tangent	WPS
Partner								
IPP	64.11	131.6	56	68.8	67.3	85.3	62	68.6

Table 5.50: LTO 8 Final all. RPV Age (PMA2) for UCC (T_0 Approach)

	Final Allowable RPV Age (years) - T_0 Approach							
	UCC							
	Axial				Circumferential			
	Point A		Point C		Point A		Point C	
	Tangent	WPS	Tangent	WPS	Tangent	WPS	Tangent	WPS
Partner								
IPP	113.5	197	>200	>200	129	205.3	>200	>200

5.2.1.9 LTO9- Isolation of ACCs (operator action) at 500s

In case of LTO9 the results from the system analysis performed with RELAP5, were repeated with the addition of a time for ACC isolation at 500 s. Because the pressure for this break size does not decrease to 26 bar until after 500 s, the ACCs were isolated before they could inject. The result was a pressure transient. In case of the TH calculations, it was concluded that this action has no significant effect. The SA results from WP3 also indicated that this action has a very small effect on the temperature and stress distributions at the crack tip. IPP and FRA-G analysed LTO9 and the obtained results are summarised below. The results for LTO9 for PMA1 and PMA2 assessments of TCC and UCC cracks are shown in Table 5.51 - Table 5.58.

Table 5.51: LTO 9 Final max. all. ART (PMA1) for TCC (RT_{NDT} Approach)

	Final max. all. ART (°C) -RT_{NDT} Approach							
	TCC							
	Axial				Circumferential			
	Point A		Point C		Point A		Point C	
	Tangent	WPS	Tangent	WPS	Tangent	WPS	Tangent	WPS
Partner								
IPP	55.76	133.2	52	129.1	56.4	135.4	52.6	131.2
FRA-G					29	99		

Table 5.52: LTO 9 Final max. all. ART (PMA1) for UCC (RT_{NDT} Approach)

	Final max. all. ART (°C) -RT_{NDT} Approach							
	UCC							
	Axial				Circumferential			
	Point A		Point C		Point A		Point C	
	Tangent	WPS	Tangent	WPS	Tangent	WPS	Tangent	WPS
Partner								
IPP	75.14	148.4	162.2	186.13	79.34	152.7	193.19	>200

Table 5.53: LTO 9 Final max. all. ART (PMA1) for TCC (T_0 Approach)

	Final max. all. ART (°C) -T_0 Approach							
	TCC							
	Axial				Circumferential			
	Point A		Point C		Point A		Point C	
	Tangent	WPS	Tangent	WPS	Tangent	WPS	Tangent	WPS
Partner								
IPP	-6.5	62.3	-9.4	63.2	-8.4	66.1	-9.14	65.8

Table 5.54: LTO 9 Final max. all. ART (PMA1) for UCC (T_0 Approach)

	Final max. all. ART (°C) -T_0 Approach							
	UCC							
	Axial				Circumferential			
	Point A		Point C		Point A		Point C	
	Tangent	WPS	Tangent	WPS	Tangent	WPS	Tangent	WPS
Partner								
IPP	21	86	81.9	135.6	26.62	94	95.3	148

Table 5.55: LTO 9 Final all. RPV Age (PMA2) for TCC (RT_{NDT} Approach)

	Final Allowable RPV Age (years) - RT_{NDT} Approach							
	TCC							
	Axial				Circ			
	Point A		Point C		Point A		Point C	
	Tangent	WPS	Tangent	WPS	Tangent	WPS	Tangent	WPS
Partner								
IPP	21.2	184	15.5	152.5	22.4	189.7	16	159

Table 5.56: LTO 9 Final all. RPV Age (PMA2) for UCC (RT_{NDT} Approach)

	Final Allowable RPV Age (years) - RT_{NDT} Approach							
	UCC							
	Axial				Circumferential			
	Point A		Point C		Point A		Point C	
	Tangent	WPS	Tangent	WPS	Tangent	WPS	Tangent	WPS
Partner								
IPP	58	>200	>200	>200	68.9	>200	>200	>200

Table 5.57: LTO 9 Final all. RPV Age (PMA2) for TCC (T_0 Approach)

	Final Allowable RPV Age (years) - T_0 Approach							
	TCC							
	Axial				Circumferential			
	Point A		Point C		Point A		Point C	
	Tangent	WPS	Tangent	WPS	Tangent	WPS	Tangent	WPS
Partner								
IPP	25	190	18.9	169.6	25.6	194.2	19.3	179

Table 5.58: LTO 9 Final all. RPV Age (PMA2) for UCC (T_0 Approach)

	Final Allowable RPV Age (years) - T_0 Approach							
	UCC							
	Axial				Circumferential			
	Point A		Point C		Point A		Point C	
	Tangent	WPS	Tangent	WPS	Tangent	WPS	Tangent	WPS
Partner								
IPP	77	>200	>200	>200	88.7	>200	>200	>200

5.2.2 Plausibility checks

A few simple plausibility checks have been performed for the mandatory case (see Section 5.1.1), PMA1 for circumferential TCC with assessed deepest point of the crack (point A), by comparing the results with deterministic results from Task 3.4 [16]. Please note that the comparison here is just a consistency check of the results and not a margin assessment, which is covered in Section 7. This is simply an attempt to assess relation between deterministic and probabilistic results that could indicate the plausibility of the results.

The CPI for pre-defined RT_{NDT} values (PMA1) and CPI for pre-defined RPV Age (PMA2) are summarised for circumferential TCC with assessed deepest point of the crack (point A) for each LTO improvement in Appendix provided in Section 5.4.

5.2.2.1 LTO 1

The following conclusions and justifications can be made for LTO1 from Table 5.59:

1. PSI and Tecnatom have obtained comparable final ARTs for both deterministic and probabilistic approach which is expected since they both have used TRACE TH input and FAVOR code in their calculations. The probabilistic final allowable ARTs are much lower due a different crack size used in FAVOR due to code limitation. The crack depth (a) used by PSI and Tecnatom is 17.43 mm and the crack length (2c) is 104.8 mm, whereas a= 10 mm and 2c = 60 mm as per the task definition (see 5.1.1).
2. UJV and JSI have obtained comparable final ARTs from both deterministic and probabilistic analysis which is explainable as both partners have used RELAP TH input in their calculations.
3. IPP performed both deterministic and probabilistic calculations with stresses taken from a 3D SA which accounts for effects from cold plume. Moreover, IPP performed the deterministic calculations with and without WRS. The deterministic results shown here are, however, without WRS. This explains why IPP has obtained higher max.all.ART in the deterministic analysis. The probabilistic max.all.ARTs are, however, comparable to other RELAP users which is expected since all the RELAP TH input users in LTO1 accounted for WRS in their probabilistic assessment.
4. The difference between WPS and tangent approach is higher for the probabilistic analysis compared to the deterministic analysis for all the partners. However, the absolute difference between probabilistic and deterministic for these differences has some scatter (see Figure 5.3).

Table 5.59: Max. all. ART (PMA1) for LTO1. For TCC_Circumferential_Point A

	LTO1 - Final Max.all.ART °C (RT_{NDT} Approach) - TCC_Circ_pA				**Difference (WPS - Tangent)**	
	Deterministic		**Probabilistic**			
Partner	**Tangent**	**WPS**	**Tangent**	**WPS**	**Deterministic**	**Probabilistic**
PSI	95.49	143.54	58.5	N/A	48.05	N/A
UJV	99.27	148.93	86.38	138.37	49.6	51.9
JSI	99.49	137.01	86	126	37.52	40
Tecnatom	95.69563	143.6266	58	112	47.93097	54
IPP	109.8	143.3558	86.7	126.9	33.55	40.2

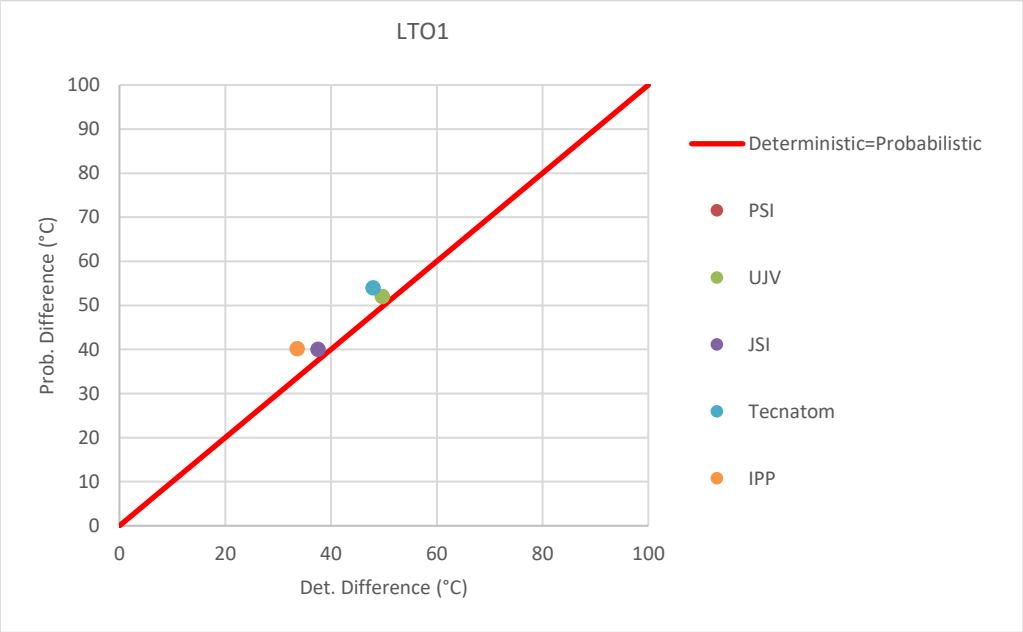

Figure 5.3: Difference in max.all.ART between WPS and Tangent Approach for LTO 1. PSI results are not presented in the plot due to lack of data for probabilistic analysis with WPS approach.

5.2.2.2 LTO 2

The following conclusions and justifications can be made for LTO2 from Table 5.60:

1. In the deterministic analysis, JSI (TH input RELAP) has the most conservative max.all.ART compared to PSI (TH input TRACE) and GRS (TH input ATHLET (with ECC-MIX)) for the tangent approach. However, PSI (TH input TRACE) has the most conservative max.all.ART for the WPS approach. GRS has obtained higher max.all.ART since they do not consider weld residual stresses.
2. The probabilistic analysis results are challenging to compare since each partner has used a different TH input. Additionally, PSI used a different crack size due to limitations in FAVOR code. The crack depth (a) used by PSI is 17.43 mm and the crack length (2c) is 104.8 mm, whereas a= 10 mm and 2c = 60 mm as per the task definition (see 5.1.1).
3. For each partner, the difference between WPS and tangent approach is higher for the probabilistic analysis compared to the deterministic analysis. However, the absolute difference between probabilistic and deterministic for these differences is not very high (<3°C) indicating that the probabilistic results are plausible (see Figure 5.4).

Table 5.60: Max. all. ART (PMA1) for LTO2. For TCC_Circumferential_Point A

	LTO2 - Final max. all. ART °C (RT_{NDT} Approach) - TCC_Circ_pA				**Difference (WPS - Tangent)**	
	Deterministic		**Probabilistic**			
Partner	**Tangent**	**WPS**	**Tangent**	**WPS**	**Deterministic**	**Probabilistic**
PSI	77.6	112.04	34.4	N/A	34.44	N/A
JSI	73.19	141.4	61	131	68.21	70
GRS	95.65	151.6152	81.65	139.5	55.9652	57.85

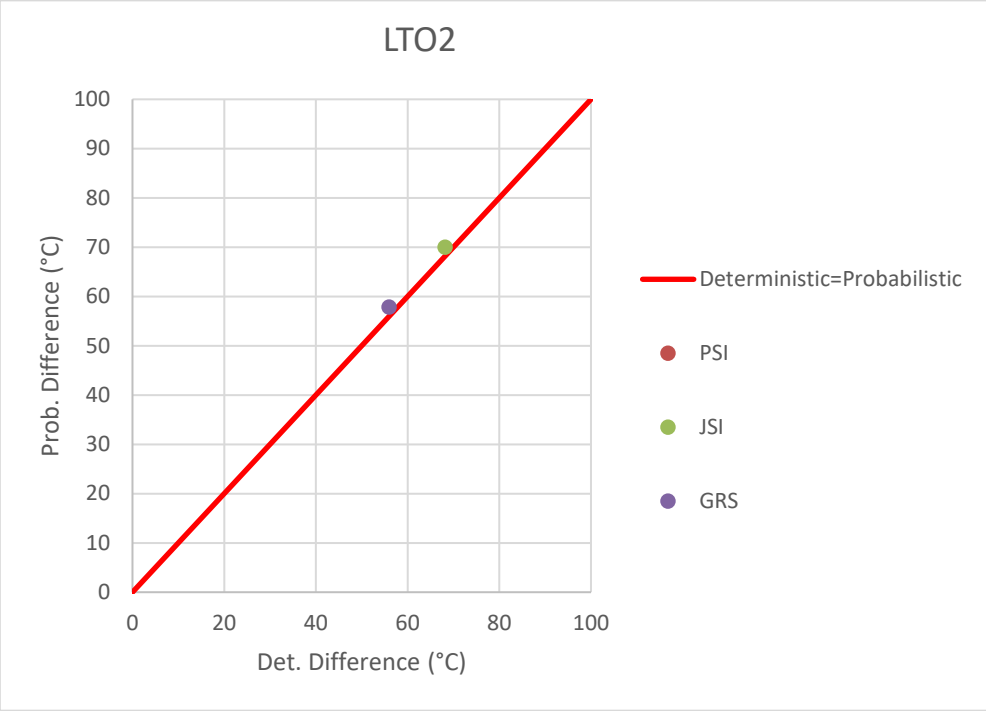

Figure 5.4: Difference in max.all.ART between WPS and Tangent Approach for LTO 2. PSI results are not presented in the plot due to lack of data for probabilistic analysis with WPS approach.

5.2.2.3 LTO 3

The following conclusions and justifications can be made for LTO3 from Table 5.61:

1. BZN (TH input RELAP) and GRS (TH input ATHLET (with ECC-MIX)) have obtained comparable final ARTs for the WPS approach in both deterministic and probabilistic analysis.
2. IPP (TH input KWU MIX) is very conservative due to the TH input coming from KWU-MIX.
3. For each partner, the difference between WPS and tangent approach is higher for the probabilistic analysis compared to the deterministic analysis. However, the absolute difference between probabilistic and deterministic for these differences is not very high (<5°C) indicating that the probabilistic results are plausible (see Figure 5.5).

Table 5.61: Max. all. ART for LTO3 (PMA1). For TCC_Circumferential_Point A

	LTO3 - Final max. all. ART °C (RT_{NDT} Approach) - TCC_Circ_pA				**Difference (WPS - Tangent)**	
	Deterministic		**Probabilistic**			
Partner	**Tangent**	**WPS**	**Tangent**	**WPS**	**Deterministic**	**Probabilistic**
BZN	68.52884	129.3163	55.5	119.1	60.78746	63.6
GRS	96.83993	127.571	83.2	115.23	30.73107	32.03
IPP	47.88691	109.4407	34.33	99.95	61.55379	65.62

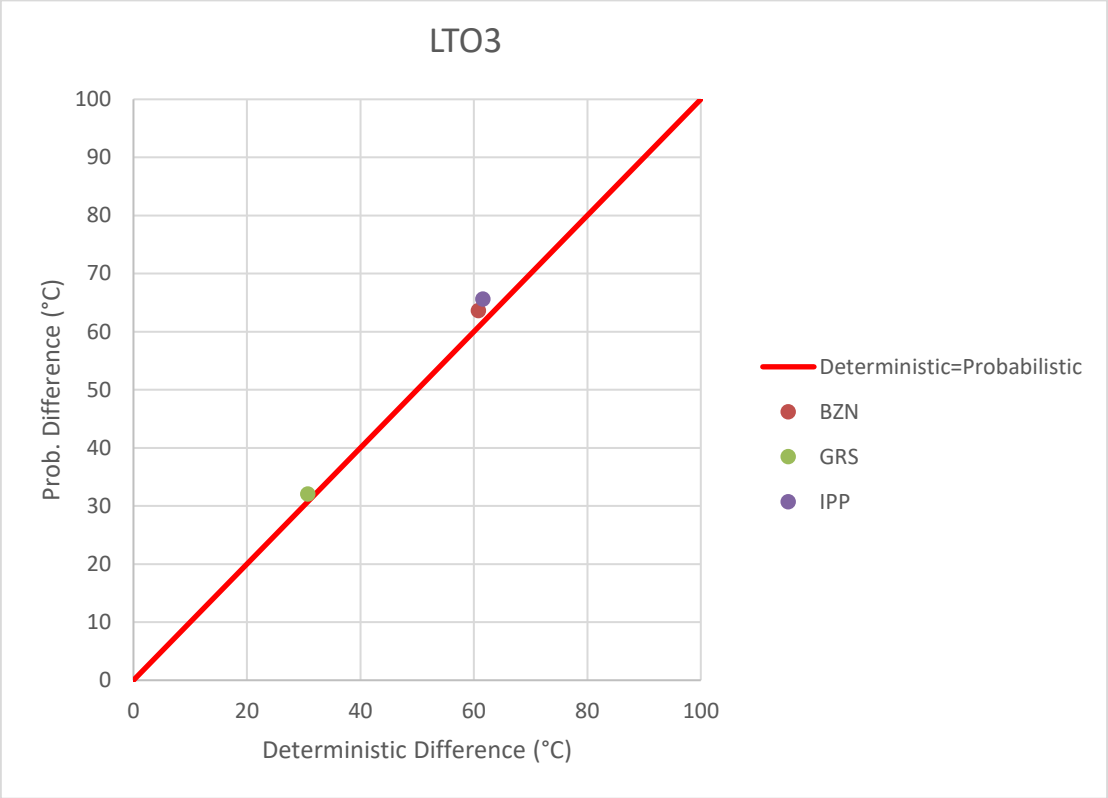

Figure 5.5: Difference in max.all.ART between WPS and Tangent Approach for LTO 3

5.2.2.4 LTO 4

The following conclusions and justifications can be made for LTO4 from Table 5.62:

1. KIWA and IPP who both use RELAP TH input have obtained comparable final ARTs from both deterministic and probabilistic analysis except for WPS approach results from probabilistic analysis.
2. Tecnatom's results are conservative compared to GRS even though both partners use the same ECC-MIX TH input. This could be due to the different crack size used by Tecnatom in FAVOR code. The crack depth (a) used by Tecnatom is 17.43 mm and the crack length (2c) is 104.8 mm, whereas a= 10 mm and 2c = 60 mm as per the task definition (see 5.1.1).
3. For each partner, the difference between WPS and tangent approach is higher for the probabilistic analysis compared to the deterministic analysis. However, the absolute difference between probabilistic and deterministic for these differences is not very high (<3°C) for IPP and GRS indicating that the probabilistic results are plausible (see Figure 5.6).

Table 5.62: Max. all. ART for LTO4 (PMA1). For TCC_Circumferential_Point A

	LTO4-Final max. all. ART °C (RT_{NDT} Approach) - TCC_Circ_pA				Difference (WPS - Tangent)	
	Deterministic		Probabilistic			
Partner	**Tangent**	**WPS**	**Tangent**	**WPS**	**Deterministic**	**Probabilistic**
KIWA	71.91323	118.9227	59.6	108.8	47.00947	49.2
GRS	95.36543	153.2979	82.4	141	57.93247	58.6
Tecnatom	82.49114	135.9704	38	102	53.47926	64
IPP	72.52136	119.0589	60.1	109	46.53754	48.9

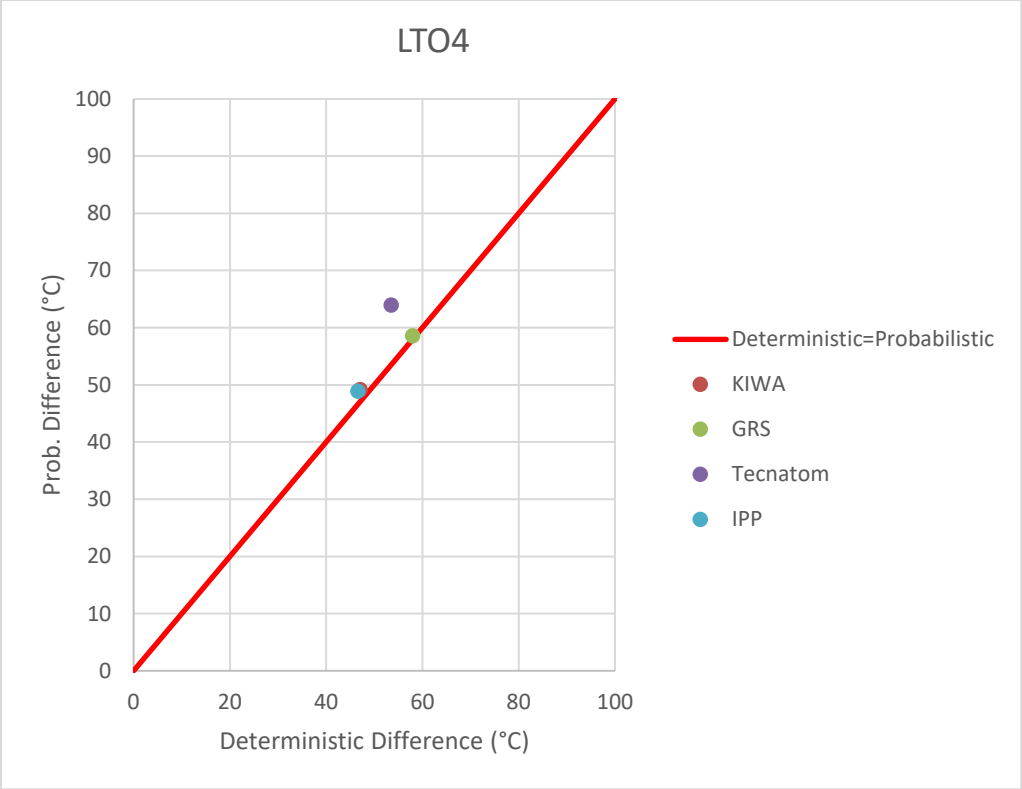

Figure 5.6: Difference in max.all.ART between WPS and Tangent Approach for LTO 4

5.2.2.5 LTO 5

The following conclusions and justifications can be made for LTO5 from Table 5.63:

1. The final ARTs calculated with deterministic analysis seem to be comparable. The probabilistic results from Tecnatom (TH input TRACE) are conservative possibly due to the different crack size used in FAVOR. The crack depth (a) used by Tecnatom is 17.43 mm and the crack length (2c) is 104.8 mm, whereas a= 10 mm and 2c = 60 mm as per the task definition (see 5.1.1).
2. For each partner, the difference between WPS and tangent approach is higher for the probabilistic analysis compared to the deterministic analysis. However, the absolute difference between probabilistic and deterministic for these differences is quite high for Tecnatom (see Figure 5.7).

Table 5.63: Max. all. ART for LTO5 (PMA1). For TCC_Circumferential_Point A

	LTO5 - Final max. all. ART °C (RT_{NDT} Approach) - TCC_Circ_pA				Difference (WPS - Tangent)	
	Deterministic		Probabilistic			
Partner	**Tangent**	**WPS**	**Tangent**	**WPS**	**Deterministic**	**Probabilistic**
KIWA	76.78276	104.7894	65.5	94.5	28.00664	28.9
Tecnatom	80.69427	103.4974	41	72	22.80313	31

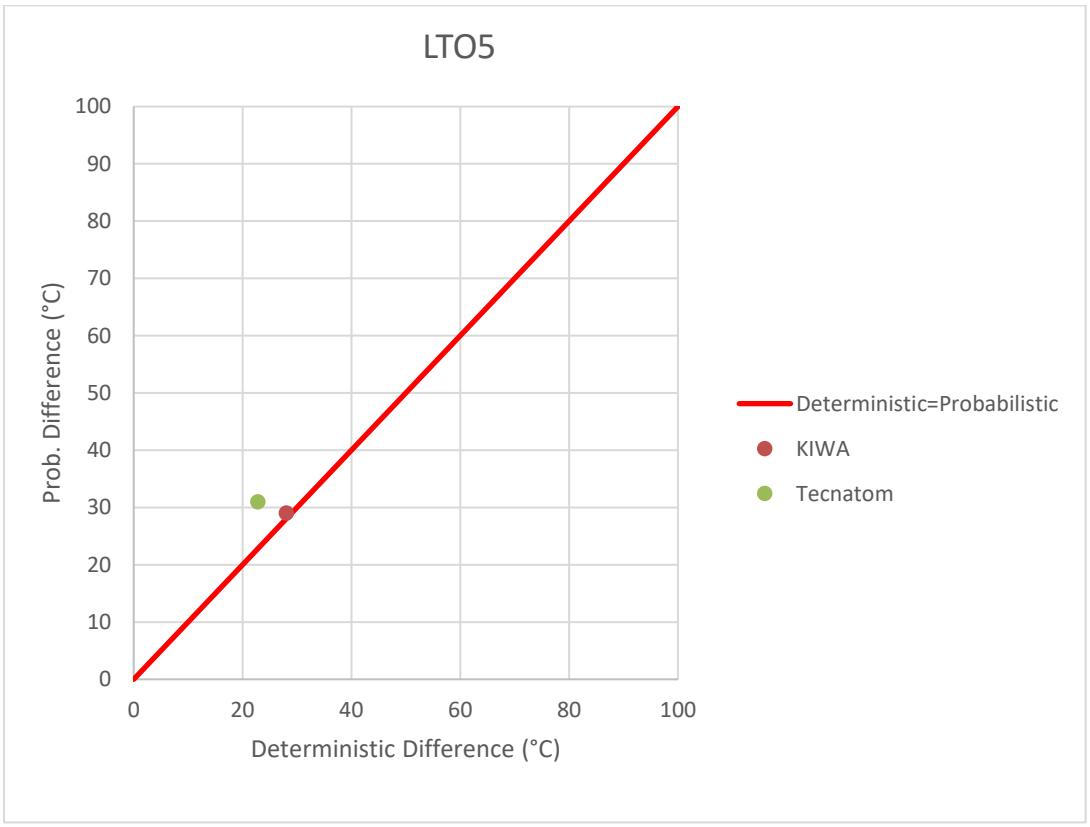

Figure 5.7: Difference in max.all.ART between WPS and Tangent Approach for LTO 5

5.2.2.6 LTO 6

The following conclusions and justifications can be made for LTO6 from Table 5.64:

1. The final ARTs calculated by UJV, KIWA and BZN are comparable for both deterministic and probabilistic analysis. This is expected as these partners use the same TH input from RELAP.
2. FRA-G results are very conservative which is also expected due to KWU-MIX TH input data.
3. For each partner, the difference between WPS and tangent approach is higher for the probabilistic analysis compared to the deterministic analysis. However, the absolute difference between probabilistic and deterministic for these differences is quite small (<2°C) (see Figure 5.8).

Table 5.64: Max. all. ART (PMA1) for LTO6. For TCC_Circumferential_Point A

	LTO6 - Final max. all. ART °C (RT_{NDT} Approach) - TCC_Circ_pA				Difference (WPS - Tangent)	
	Deterministic		Probabilistic			
Partner	**Tangent**	**WPS**	**Tangent**	**WPS**	**Deterministic**	**Probabilistic**
UJV	93.44795	144.10219	81.5	134.1	50.65424	52.6
KIWA	94.73354	146.67027	82.4	136.6	51.93673	54.2
BZN	95.21543	144.24959	82.8	134	49.03416	51.2
FRA-G	48	110	38	101	62	63

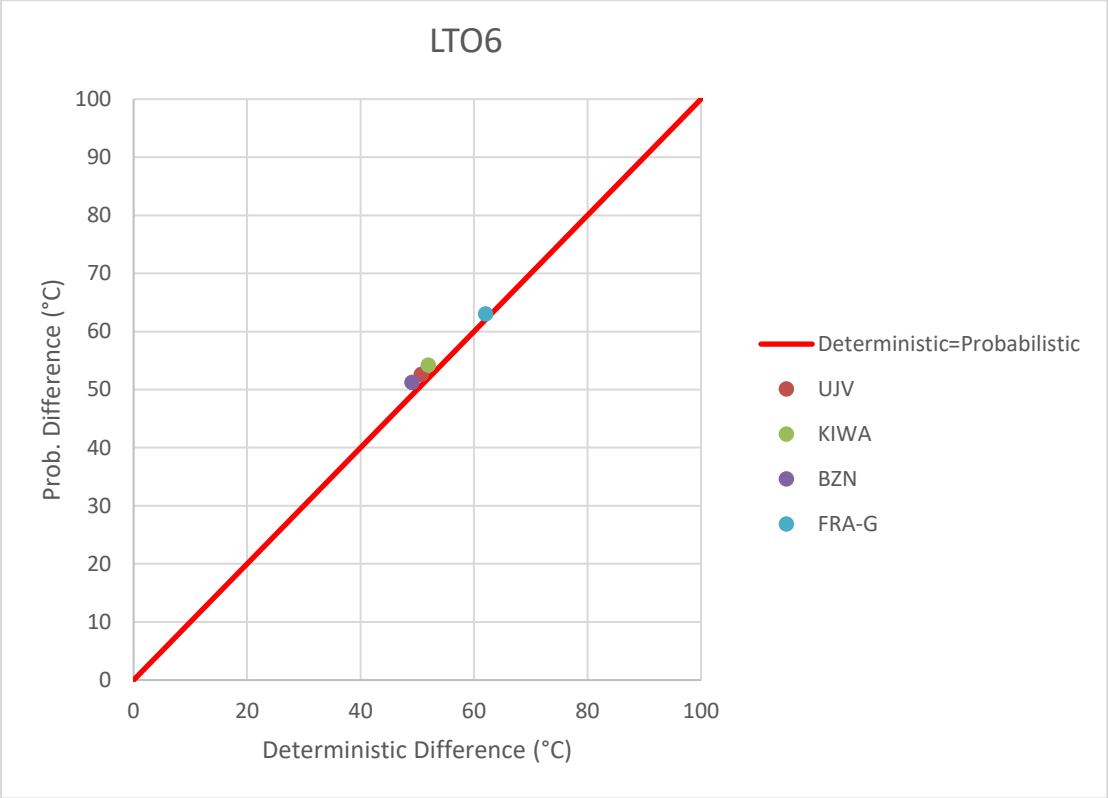

Figure 5.8: Difference in max.all.ART between WPS and Tangent Approach for LTO 6

5.2.2.7 LTO 7

The following conclusions and justifications can be made for LTO7 from Table 5.65:

1. The final ARTs calculated by PSI (TH input TRACE) and BZN (TH input RELAP) are comparable only for the deterministic tangent case. The use of a different crack size in FAVOR by PSI gives conservative final ART in the probabilistic analysis. The crack depth (a) used by PSI is 17.43 mm and the crack length (2c) is 104.8 mm, whereas a= 10 mm and 2c = 60 mm as per the task definition (see 5.1.1).
2. The difference between WPS and tangent approach for BZN is higher for the probabilistic analysis compared to the deterministic analysis. However, the absolute difference between probabilistic and deterministic for these differences is quite small (<3°C) (see Figure 5.9).

Table 5.65: Max. all. ART (PMA1) for LTO7. For TCC_Circumferential_Point A

	LTO7 - Final max. all. ART °C (RT_{NDT} Approach) - TCC_Circ_pA				Difference (WPS - Tangent)	
	Deterministic		Probabilistic			
Partner	Tangent	WPS	Tangent	WPS	Deterministic	Probabilistic
PSI	75	100.25	33	NA	25.25	
BZN	72.30403	144.51011	59.8	134.4	72.20608	74.6

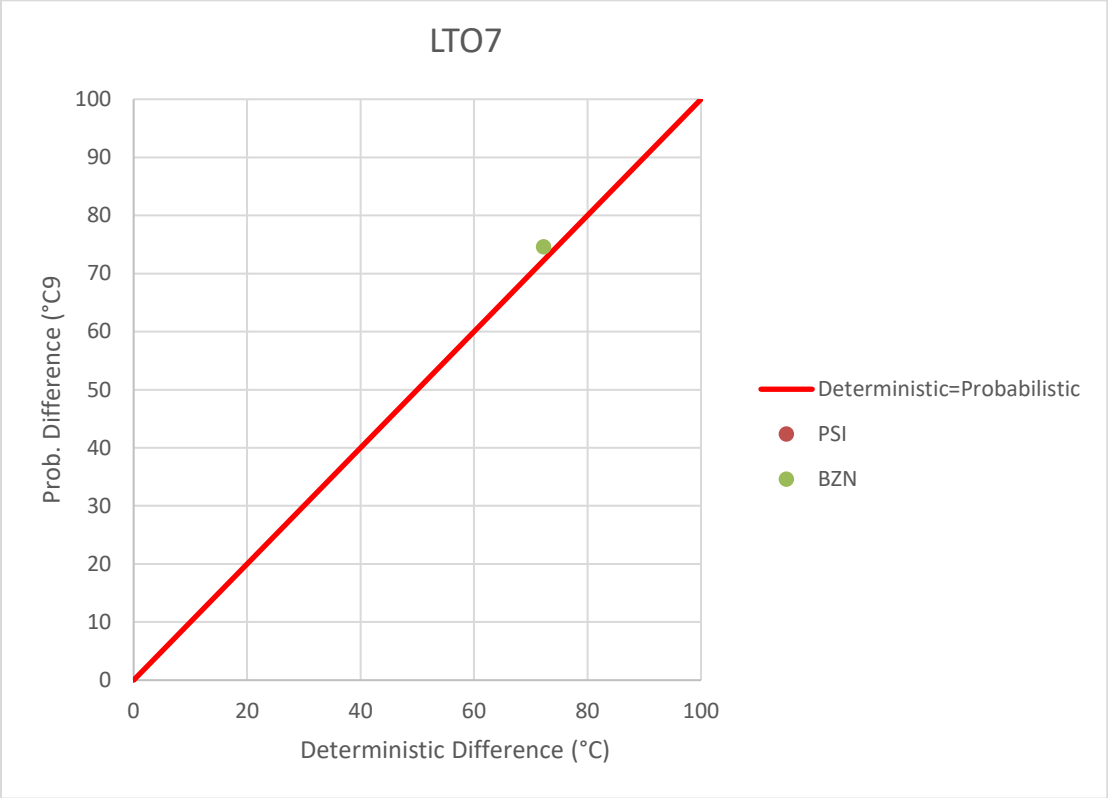

Figure 5.9: Difference in max.all.ART between WPS and Tangent Approach for LTO 8

5.2.2.8 LTO 8

The following conclusions and justifications can be made for LTO8 from Table 5.66:

1. The final ARTs calculated by UJV (TH input RELAP WUT) and JSI (TH input RELAP WUT) are comparable for both deterministic and probabilistic analysis.
2. FRA-G (TH input KWU-MIX) and IPP (KWU-MIX) have comparable final ARTs calculated with WPS approach for both deterministic and probabilistic analysis. FRA-G is conservative for the tangent approach which could be due to 3D structural analysis, whereas IPP has used 1D structural analysis without plume correction.
3. The difference between WPS and tangent approach is higher for the probabilistic analysis compared to the deterministic analysis. However, the absolute difference between probabilistic and deterministic for these differences is small and quite comparable (<5°C) for all the partners (see Figure 5.10).

Table 5.66: Max. all. ART (PMA1) for LTO8. For TCC_Circumferential_Point A

	LTO8 -Final max. all. ART °C (RT_{NDT} Approach) - TCC_Circ_pA				Difference (WPS - Tangent)	
	Deterministic		Probabilistic			
Partner	**Tangent**	**WPS**	**Tangent**	**WPS**	**Deterministic**	**Probabilistic**
UJV	112.70465	139.9002	98.2	129.8	27.19555	31.6
JSI	113.46	140.4	99	130	26.94	31
IPP	90.45298	106.1145	75.8	96.53	15.66152	20.73
FRA-G	80	105	68	96	25	28

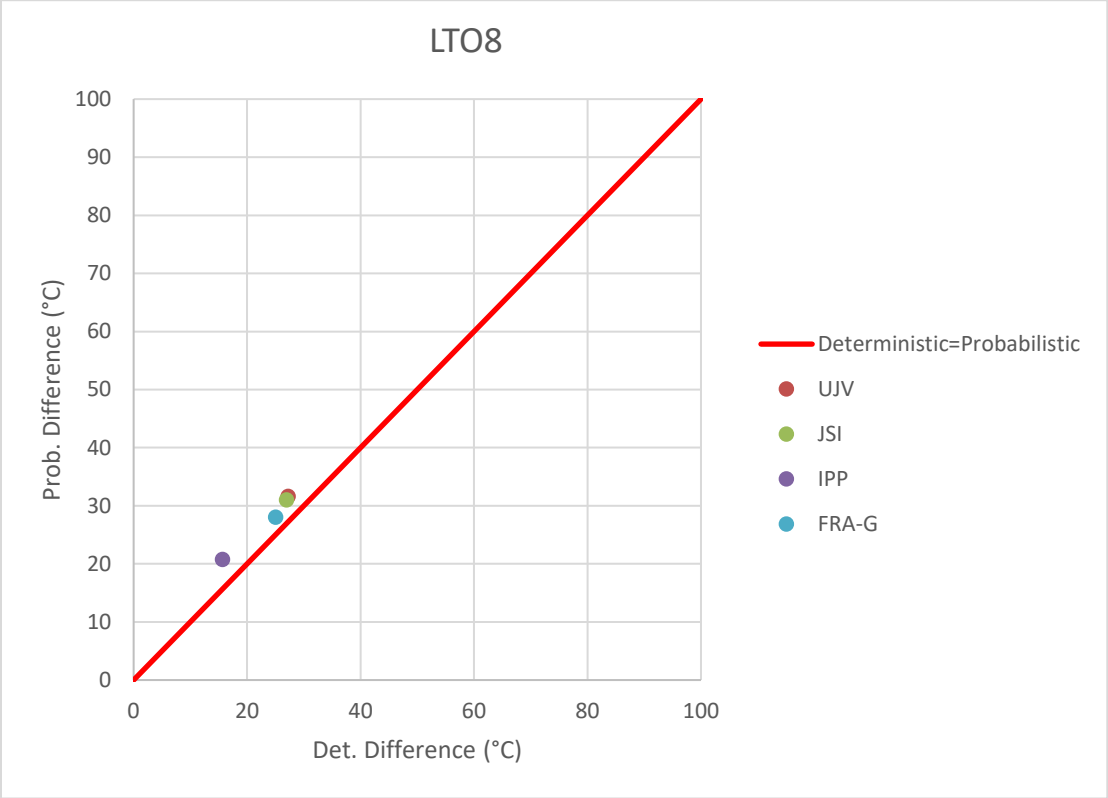

Figure 5.10: Difference in max.all.ART between WPS and Tangent Approach for LTO 8

5.2.2.9 LTO 9

The following conclusions and justifications can be made for LTO9 from Table 5.67:

1. The final ARTs calculated by IPP (TH input RELAP WUT) are less conservative than FRA-G (TH input KWU-MIX) for both deterministic and probabilistic analysis.
2. The difference between WPS and tangent approach is higher for the probabilistic analysis compared to the deterministic analysis. However, the absolute difference between probabilistic and deterministic for these differences is quite small (<2°C) for both partners (see Figure 5.11).

Table 5.67: Max. all. ART (PMA1) for LTO9. For TCC_Circumferential_Point A

	LTO9 - Final max. all. ART °C (RT_{NDT} Approach) - TCC_Circ_pA				Difference (WPS - Tangent)	
	Deterministic		Probabilistic			
Partner	**Tangent**	**WPS**	**Tangent**	**WPS**	**Deterministic**	**Probabilistic**
IPP	68.59582	145.5276	56.4	135.4	76.93178	79
FRA-G	40	109	29	99	69	70

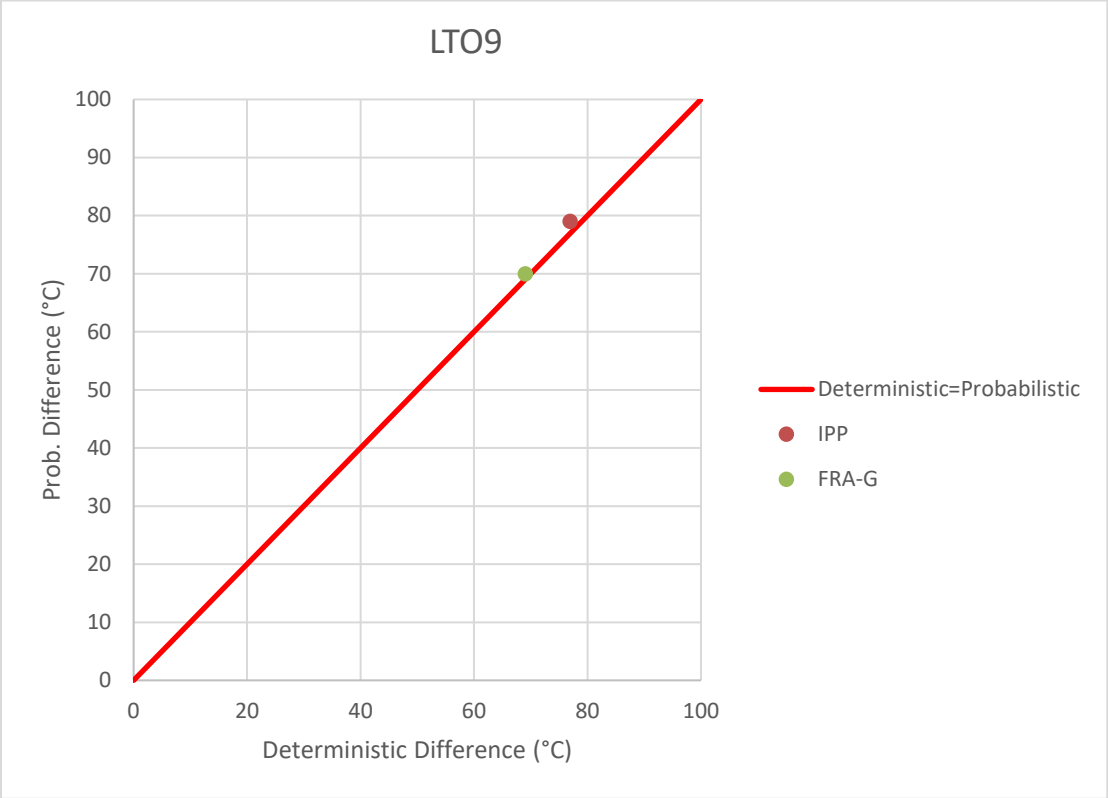

Figure 5.11: Difference in max.all.ART between WPS and Tangent Approach for LTO 9

5.3 Discussion and main outcome

Task 4.4 within APAL WP4 was focused on probabilistic fracture mechanics calculations of the LTO improvements identified in WP2. In this Section, a brief description of performed calculations have been provided. All the results obtained from the partners are presented in Section 5.2 along with some plausibility checks (see Section 5.2.2) for the mandatory case. The results presented herein have been transferred to Task 4.6 for a final margin assessment (see Section 7 in this report).

In general, the results for the mandatory case are consistent and reasonable when compared to the deterministic results from WP3, although the initiation frequency (CPI) used in the deterministic and probabilistic assessments are different. Moreover, only the PMA1 max.all.ART results for a fixed crack depth and length are compared with the deterministic results in this report. The reader is therefore advised to exercise caution before drawing any safety-related conclusions from these comparisons.

Most of the differences between the partners can be attributed to either the source of the TH input data (see Table 5.2 for overview) or the code used in the probabilistic assessments. The partners who used FAVOR in their probabilistic calculations have used a crack size different from that defined for the benchmark due to certain limitations in the FAVOR code when performing PMA1.

5.4 CPI values for PMA1 and PMA2

This Section contains a summary of CPI for pre-defined RT_{NDT} values (PMA1) and CPI for pre-defined RPV Age (PMA2) for circumferential TCC with assessed deepest point of the crack (point A) for each LTO improvement, see Table 5.68 - Table 5.75.

Table 5.68: LTO1 results – conditional probabilities of crack initiation (CPI) for pre-defined RT_{NDT} (PMA1) and RPV age (PMA2) – for circumferential TCC Deepest Point

	Pre-defined RT_{NDT} °C - Tangent				
Partner	**0**	**50**	**100**	**150**	**200**
PSI	0	0	0.00451	0.1057	0.4239
UJV	0	0	0.024477209	0.756457626	0.996636657
JSI	0	0	0.02351	0.73321	0.99578
Tecnatom	0	0	0.2003	0.9284	1
IPP	0	0	0.023482	0.743841	0.995987

	Pre-defined RT_{NDT} °C - WPS				
Partner	**0**	**50**	**100**	**150**	**200**
PSI					
UJV	0	0	0	0.027387869	0.981858055
JSI	0	0	0	0.21059	0.99497
Tecnatom	0.00E+00	0.00E+00	0.00E+00	2.42E-01	9.82E-01
IPP	0	0	0	0.201683	0.996061

	Pre-defined RPV Age (years) - Tangent				
Partner	**1**	**20**	**40**	**80**	**200**
PSI	0	0	0	0	3.94E-03
UJV	0	6.36434E-10	7.95531E-07	0.00041009	0.139490073
JSI					
Tecnatom	0	0.000006942	0.0002019	0.004724	0.14
IPP	0	0	0.000002	0.000425	0.135779

	Pre-defined RPV Age (years) - WPS				
Partner	**1**	**20**	**40**	**80**	**200**
PSI					
UJV	0	0	0	0	0.000183951
JSI					
Tecnatom					
IPP	0	0	0	0	0.001974

Table 5.69: LTO2 results – conditional probabilities of crack initiation (CPI) for pre-defined RT_{NDT} (PMA1) and RPV age (PMA2)- for circumferential TCC Deepest Point

	Pre-defined RT_{NDT} °C - Tangent				
Partner	**0**	**50**	**100**	**150**	**200**
PSI	0	0.008716	0.4763	0.9923	1
JSI	0.00E+00	0.00E+00	4.33E-01	9.41E-01	1.00E+00
GRS	0	0	0.04265235	0.784	0.949

	Pre-defined RT_{NDT} °C - WPS				
Partner	**0**	**50**	**100**	**150**	**200**
JSI	0.00E+00	0.00E+00	0.00E+00	1.26E-01	1.00E+00
GRS	0	0	0	0.01545602	0.807

	Pre-defined RPV Age (years) - Tangent				
Partner	**1**	**20**	**40**	**80**	**200**
GRS	4.36367E-13	5.67937E-06	8.84958E-05	0.00243314	0.097170705

	Pre-defined RPV Age (years) - WPS				
Partner	**1**	**20**	**40**	**80**	**200**
GRS	3.18017E-59	1.27224E-17	5.56419E-14	6.90063E-10	4.71931E-05

Table 5.70: LTO3 results – conditional probabilities of crack initiation (CPI) for pre-defined RT_{NDT} (PMA1) and RPV age (PMA2) - for circumferential TCC Deepest Point

	Pre-defined RT_{NDT} °C - Tangent				
Partner	**0**	**50**	**100**	**150**	**200**
BZN	0	0	0.4128	0.972	1
GRS	0	0	0.03510551	0.756	0.957
IPP	0	0.030778	0.859558	1	1

	Pre-defined RT_{NDT} °C - WPS				
Partner	**0**	**50**	**100**	**150**	**200**
BZN	0	0	0	0.08374	0.99971
GRS	0	0	0	0.3565575	0.942
IPP	0	0	0.000246	0.993473	1

	Pre-defined RPV Age (years) - Tangent				
Partner	**1**	**20**	**40**	**80**	**200**
GRS	7.22078E-12	4.27635E-06	7.83676E-05	0.001953521	0.085240217
IPP	0	0.009178	0.049585	0.254244	0.864649

	Pre-defined RPV Age (years) - WPS				
Partner	**1**	**20**	**40**	**80**	**200**
GRS	6.2589E-22	2.34509E-11	7.66525E-09	2.8805E-06	0.003745335
IPP	0	0	0	0.000032	0.118349

Table 5.71: LTO5 results – conditional probabilities of crack initiation (CPI) for pre-defined RT_{NDT} (PMA1) and RPV age (PMA2) - for circumferential TCC Deepest Point

	Pre-defined RT_{NDT} °C - Tangent				
Partner	**0**	**50**	**100**	**150**	**200**
KIWA	0	0	4.69E-01	9.97E-01	1
Tecnatom	0.00E+00	4.03E-03	4.53E-01	9.94E-01	1.00E+00

	Pre-defined RT_{NDT} °C - WPS				
Partner	**0**	**50**	**100**	**150**	**200**
KIWA	0	0	5.75E-03	9.74E-01	1
Tecnatom	0.00E+00	0.00E+00	1.28E-01	9.67E-01	1.00E+00

	Pre-defined RPV Age (years) - Tangent				
Partner	**1**	**20**	**40**	**80**	**200**
KIWA	0	1.00E-05	4.87E-04	2.36E-02	6.07E-01

	Pre-defined RPV Age (years) - WPS				
Partner	**1**	**20**	**40**	**80**	**200**
KIWA	0	0	0	1.24E-04	1.48E-01

Table 5.72: LTO6 results – conditional probabilities of crack initiation (CPI) for pre-defined RT_{NDT} (PMA1) and RPV age (PMA2) - for circumferential TCC Deepest Point

	Pre-defined RT_{NDT} °C - Tangent				
Partner	**0**	**50**	**100**	**150**	**200**
UJV	0	0	0.068042347	0.91560478	0.999238564
KIWA	0	0	0.055058	0.88981	0.997584
BZN	0	0	0.04944	0.86184	0.99958
FRA-G	0	0.030598	0.990362	1	1

	Pre-defined RT_{NDT} °C - WPS				
Partner	**0**	**50**	**100**	**150**	**200**
UJV	0	0	0	0.078500227	0.999238564
KIWA	0	0	0	0.046339	0.997411
BZN	0	0	0	0.07631	0.99949
FRA-G	0	0	0	0.994645	1

	Pre-defined RPV Age (years) - Tangent				
Partner	**1**	**20**	**40**	**80**	**200**
UJV	0	1.26444E-08	4.68252E-06	0.001360847	0.24982794
KIWA	0	0	0.000004	0.001085	0.220616
BZN	0	0	0.00001	0.00271	0.41251
FRA-G	0.000001	0.011047	0.074614	0.4201	0.977092

	Pre-defined RPV Age (years) - WPS				
Partner	**1**	**20**	**40**	**80**	**200**
UJV	0	0	0	0	0.000534006
KIWA	0	0	0	0	0.000306
BZN	0	0	0	0	0.00056
FRA-G	0	0	0	0.000014	0.106724

Table 5.73: LTO7 results - conditional probabilities of crack initiation (CPI) for pre-defined RT_{NDT} (PMA1) and RPV age (PMA2) -for circumferential TCC Deepest Point

	Pre-defined RT_{NDT} °C - Tangent				
Partner	**0**	**50**	**100**	**150**	**200**
PSI	0	0.01095	0.511	0.9954	1
BZN	0	0	0.47103	0.9483	1

	Pre-defined RT_{NDT} °C - WPS				
Partner	**0**	**50**	**100**	**150**	**200**
BZN	0	0	0	0.07261	0.99938

Table 5.74: LTO8 results – conditional probabilities of crack initiation (CPI) for pre-defined RT_{NDT} (PMA1) and RPV age (PMA2)

	Pre-defined RT_{NDT} °C - Tangent				
Partner	**0**	**50**	**100**	**150**	**200**
UJV	0	0	0.00098165	0.48621168	1
JSI	0.00E+00	0.00E+00	6.77E-04	4.64E-01	1.00E+00
IPP	0	0	0.077249	0.996141	1
FRA-G	0	0	0.27908	1	1

	Pre-defined RT_{NDT} °C - WPS				
Partner	**0**	**50**	**100**	**150**	**200**
UJV	0	0	0	0.161461853	1
JSI	0.00E+00	0.00E+00	0.00E+00	1.47E-01	1.00E+00
IPP	0	0	0.003118	0.996304	1
FRA-G	0	0	0.003286	0.998989	1

	Pre-defined RPV Age (years) - Tangent				
Partner	**1**	**20**	**40**	**80**	**200**
UJV	0	0	9.58195E-09	1.87437E-05	0.036702747
JSI	0.00E+00	0.00E+00	0.00E+00	2.17E-05	3.35E-02
IPP	0	0	0.000025	0.002329	0.223252

	Pre-defined RPV Age (years) - WPS				
Partner	**1**	**20**	**40**	**80**	**200**
UJV	0	0	0	0	0.001230978
JSI	0.00E+00	0.00E+00	0.00E+00	0.00E+00	1.08E-03
IPP	0	0	0	0.000092	0.158227

Table 5.75: LTO9 results – conditional probabilities of crack initiation (CPI) for pre-defined RT_{NDT} (PMA1) and RPV age (PMA2) - for circumferential TCC Deepest Point

	Pre-defined RT_{NDT} °C - Tangent				
Partner	**0**	**50**	**100**	**150**	**200**
IPP	0	0	0.568337	0.959169	1
FRA-G	0	0.136921	0.990956	1	1

	Pre-defined RT_{NDT} °C - WPS				
Partner	**0**	**50**	**100**	**150**	**200**
IPP	0	0	0	0.05915	0.997974
FRA-G	0		0.000269	0.9971	1

	Pre-defined RPV Age (years) - Tangent				
Partner	**1**	**20**	**40**	**80**	**200**
IPP	0	0.000154	0.002884	0.056573	0.650495

	Pre-defined RPV Age (years) - WPS				
Partner	**1**	**20**	**40**	**80**	**200**
IPP	0	0	0	0	0.000477

6 Probabilistic benchmark of uncertainties in the TH data

This Section presents the results obtained from each partner for the probabilistic assessment of uncertainties in TH data (Task 4.5) along with few plausibility checks. A detailed interpretation of the results and margin assessments are performed in the report D4.6 [6] and summarised in Section 7 of this report.

The main objective of the probabilistic benchmark spread between Tasks 4.5 and 4.6 was to quantify:

i. Implicit margin related to the use of envelope TH data set. This will be done by comparison of results based on the envelope TH data set (determined from envelope TH input data) with results from best-estimate TH data set (determined from best-estimate TH input data).
ii. Verification of (i) by assessing all TH data sets from Wilks method (from Task 2.3): Determine the best-estimate and envelope result for all TH data sets from Wilks method and compare it with results from (i).

The probabilistic assessment of TH data uncertainties is schematically illustrated in Figure 6.1. It has to be noted that "safety margin" is not always necessarily an explicit margin (i.e. comparison of allowable value with actual RPV value). The comparison can also be done in terms of allowable values, as this gives the increase of explicit margin.

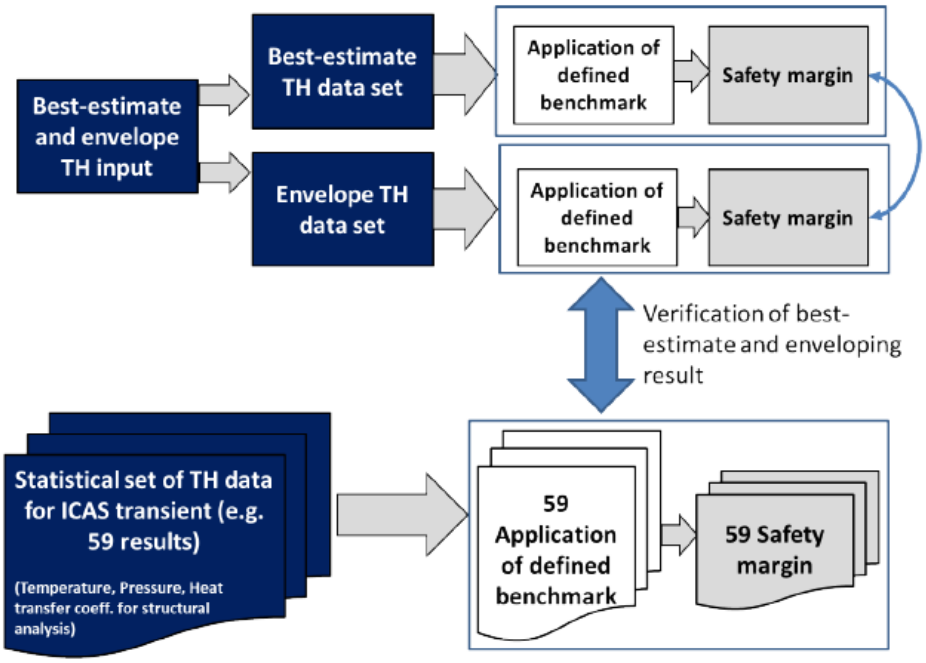

Figure 6.1: Comparison and verification to be performed in Task 4.5.

6.1 Description of Activities

The main goal of Task 4.5 was to perform the probabilistic fracture-mechanics calculations related to the uncertainties in the thermal hydraulic data. The mandatory tasks of each partner were to assess the best-estimate TH data set and the 95% quantile TH data set from Wilks.

The 95% quantile is defined as the 95% conservative quantile:

- 1st rank for 59 Wilks
- 2nd rank for 93 Wilks
- 3rd rank for 130 Wilks
- Ranking of individual transients for Wilks set is based on max. all. ART from Task 3.5 [16].

The above listed ranks are the estimated 95%-quantiles with a 95% confidence, i.e., a conservative estimate of the quantile. The quantile definition used in this report means that the 5% quantile RT_{NDT} is higher (less conservative) than the 95% quantile RT_{NDT}.

An overview of all cases for task 4.5 is shown in Figure 6.2.

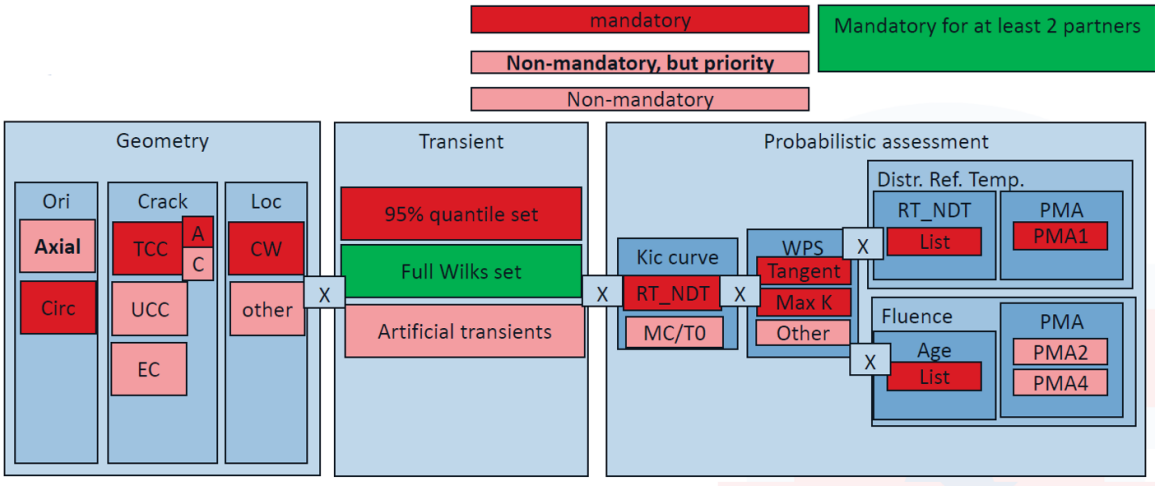

Figure 6.2: Case matrix of task 4.5

The assessment of all Wilks TH data sets is non-mandatory. The mandatory case for this task was the round-robin benchmark RR2 (see Section 4.3.2) which was aimed at calculating the conditional probability of Initiation (CPI) for a given crack type, crack tip location and crack size.

6.1.1 Baseline benchmarks (Mandatory)

PMA1: Compute allowable ART for CPI=2.28e-4

- Assessment of Through clad crack (TCC)
  - Orientation: Circumferential
  - Size:
    - TCC: a in base metal = 10 mm i.e., total depth = 16 mm (10mm + 6mm through cladding); a/c=1/3; shape 1; 2c = 60 mm
  - Location:
    - inside plume at height of core weld -2638mm from nozzle centerline
    - inside merging plumes (when using mixing code) at elevation of core weld -2638 mm
- Limit condition:
  - Tangent approach
  - Simplified WPS (max approach)
- Embrittlement (brittle fracture) to be used for PMA1
  - Fixed reference temperature (non-distributed)
  - Use RT_{NDT} concept for distributed fracture toughness K_{IC}
- Calculate CPI for selected RT_{NDT}s (0, 50, 100, 150, 200 °C)
- Accuracy of 1°C is recommended to calculate the final max. allowable ART
- Template of PMA1 to be used for the results (see Table 6.1).

Table 6.1: Output table for PMA1

			Results for pre-defined fixed ART:				
Fixed ART			0	50	100	150	200
Final CPI for the transient							
Number of MC runs							
Convergence criterion used (y/n)							
Time in the transient (s)	Temp [°C]	KI [MPavm]	Instantaneous cpi (t)				
0							
...							
10000							

PMA2: Compute allowable RPV age for CPI=2.28e-4

Same input as for PMA1 considering either Tangent or simplified WPS approach.

- Embrittlement (brittle fracture) to be used for PMA2
- Neutron fluence for selected RPV ages
  - Fluence at inner surface depending on given lifetime
  - Fluence decrease (attenuation) through RPV wall (to finally get ART at crack tip)
- Use RT_{NDT} concept for ART and fracture toughness distribution
  - Core Weld:
    - Chemical composition of weld (see Section 2.3.7)
    - Base shift formula for weld to be used for ΔRT_{NDT} (see Section 2.3.6)
- Calculate CPI for selected RPV ages (1, 20, 40, 80, 200 years i.e., for corresponding fluences)
- Accuracy of 1 year is recommended to calculate the final allowable RPV age
- PMA2 template for the results (see Table 6.2).

Table 6.2: Output table for PMA2

			Results for pre-defined RPV age:				
RPV age			1	20	40	80	200
Mean value fluence IS (10^{23} n/m²)							
ART	MV						
	SD						
	5% Quantile						
	95% Quantile						
Final CPI for the transient							
Number of MC runs							
Convergence criterion used (y/n)							
Time in the transient (s)	Temp [°C]	KI [MPavm]	Instantaneous cpi (t)				
0							
...							
10000							

6.1.2 Non-Mandatory benchmarks

Non-Mandatory tasks that have been performed within APAL:

- All Wilks TH sets
- Other Quantiles
- Mean/Median/Covering value
- TCC, axial
- UCC, circ. and axial
- Point C (surface point)
- T_0 concept, FAVOR concept

Tasks that could be assessed in addition to the work in the APAL project:

- PMA4 (determine reliability index)
- Artificial transients
- Embedded, circ. and axial.
- Nozzle Corner
- Sophisticated WPS
- Other locations (e.g., flange weld)

6.2 Results from probabilistic benchmark of TH uncertainties

In this chapter, the results obtained from the partners for the different Wilks TH sets such as the base case and best estimate transients are summarised. Within Task 4.5 only PMA1 and PMA2 were assessed:

PMA 1	Determination of max. allowable ART for defined allowable CPI or CPF (2.28E-04)
PMA 2	Determination of max. allowable lifetime for defined allowable CPI or CPF (2.28E-04)
PMA 4	Determination of reliability index for given lifetime

6.2.1 Results overview for PMA1

6.2.1.1 BZN

The assessed cases for BZN include TCC of both axial and circumferential orientation at the deepest point for the CW-IP location. The max. all. ART was evaluated with the RT_{NDT} concept for both the tangent and the Max WPS approach. The results were obtained by Monte-Carlo-Simulation with 10^5 runs.

An overview of all results for BZN is given in Table 6.3. The assessed Wilks transients are the UJV base case, UJV best estimate, and UJV 93 2nd rank (from deterministic assessment) for the 95% quantile.

Table 6.3: Overview of BZN results for max. all. ART in °C – TCC, RT_{NDT} concept

		Base Case	Best Estimate	95% Quantile
Circumferential	**Tangent**	58.6	71.1	58.2
	Max WPS	142.2	137.5	91.8
Axial	**Tangent**	58.6	71.1	58.2
	Max WPS	140.6	139.8	94.1

6.2.1.2 FRA-G

The Framatome results are all for TCC circumferential orientation at the deepest point for the CW-CL-IMP location. The max. all. ART was evaluated with the RT_{NDT} concept for both the tangent and the Max WPS approach. The results were obtained by Monte-Carlo-Simulation with 1000000 runs. The assessed 93 Wilks transients are the Framatome KWU-MIX transients. An overview of all results for Framatome is given in Table 6.4.

Table 6.4: Overview of Framatome results for max. all. ART in °C – TCC, RT_{NDT} concept

	Base Case	Best Estimate	95% Quantile
Tangent	24	36	31
Max WPS	96	122	74

6.2.1.3 GRS

The results provided by GRS are for TCC axial and circumferential orientation at the deepest point for the CW-IP location. The max. all. ART was evaluated with the RT_{NDT} concept for both the tangent and the Max WPS approach. The results were obtained by the FORM method. The assessed 59 Wilks transients are the GRS transients calculated with ECC-MIX. The probability of each reference temperature is plotted for all cases in Figure 6.3. An overview of all results for GRS is given in Table 6.5.

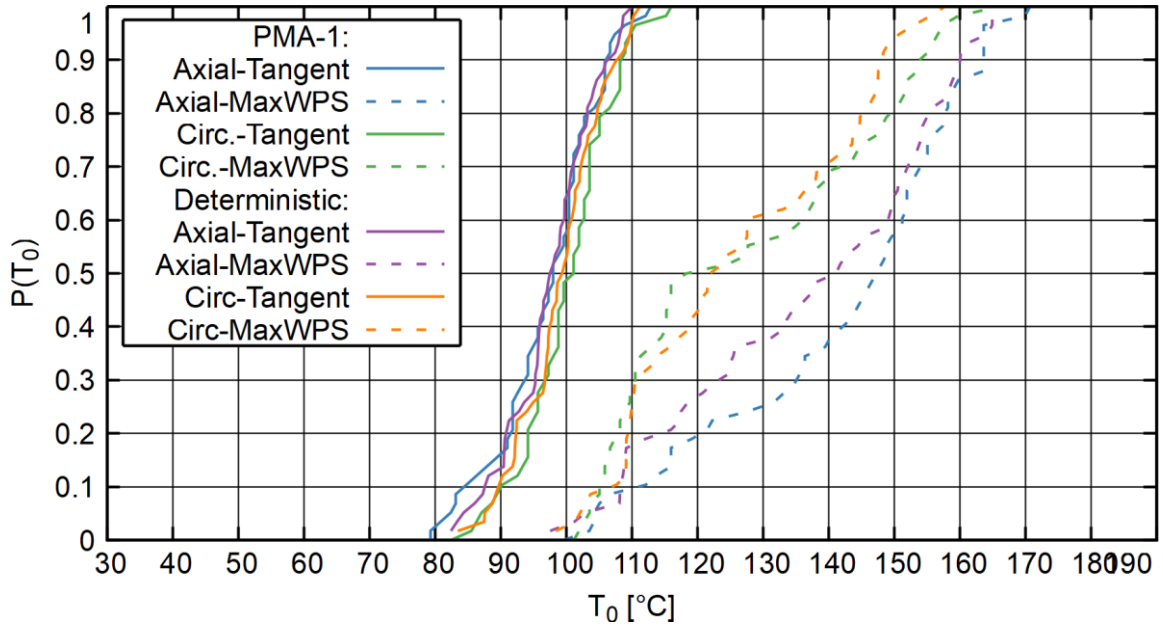

Figure 6.3: GRS results probability of reference temperature – TCC, RT_{NDT} concept

Table 6.5: Overview of GRS results for max. all. ART in °C – TCC, RT_{NDT} concept

		5% Quantile	95% Quantile
Circumferential	**Tangent**	116	82
	Max WPS	166	101
Axial	**Tangent**	113	79
	Max WPS	171	100

6.2.1.4 IPP

The calculations of IPP are based on 59 transients which were generated considering the TH uncertainties. The RELAP computation by SSTC NRC was used. The calculations were performed using the IPP in-house tool SIF-Master with the SIF solutions of Marie & Chapuliot (2008) and plastic correction of Marie & Nedelec (2007). The initial data for the core weld position 95-05 inside plume are shown in Figure 6.4. T_{wall} in the figure corresponds to the inner (wet) surface. The calculations for RR2 PMA1 were performed for UCC/TCC + axial/circumferential + deepest/surface point, always with WRS. For the probabilistic assessment the golden-section search method was used.
The results for final max. allowable ART are shown in Figure 6.5, Figure 6.6, Table 6.6 and Table 6.7 for the RT_{NDT} concept, and in Figure 6.7, Figure 6.8, Table 6.8 and Table 6.9 for the Master Curve concept.

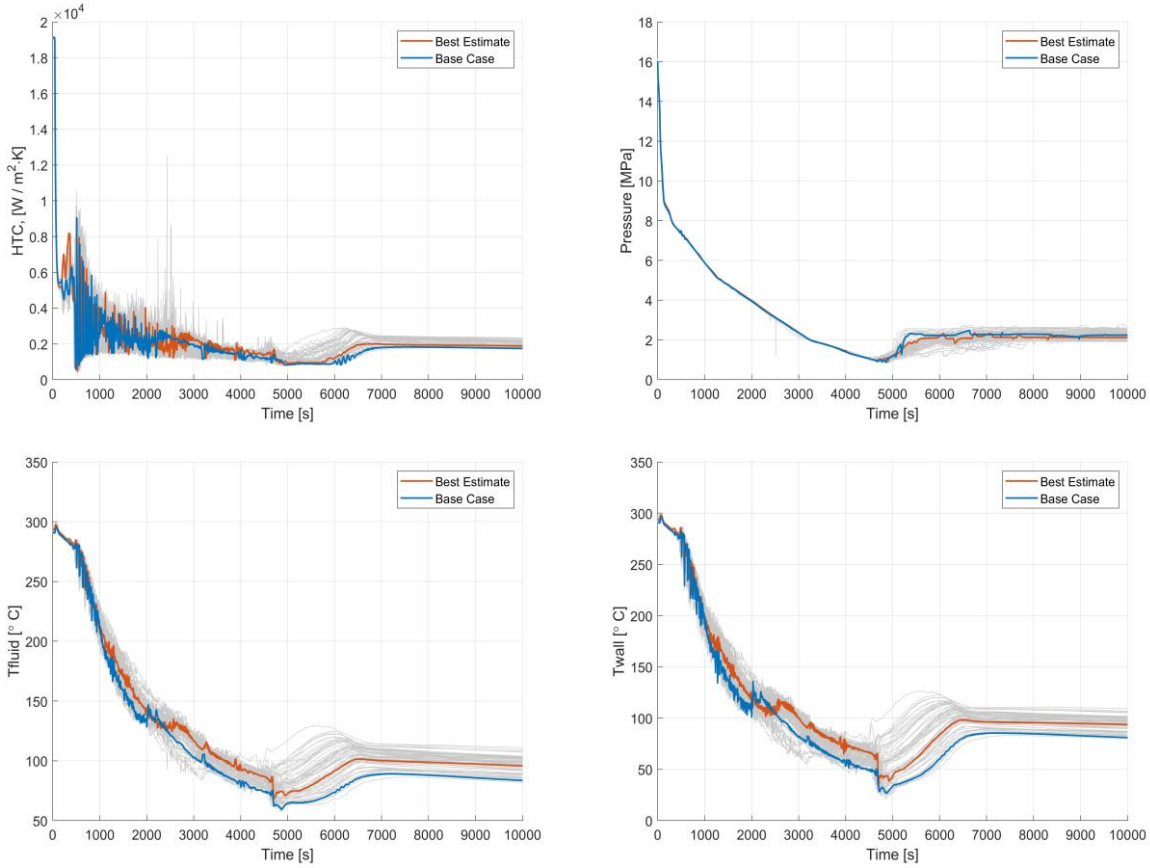

Figure 6.4: Initial TH Data – Relap 59 Wilks (SSTC NRC)

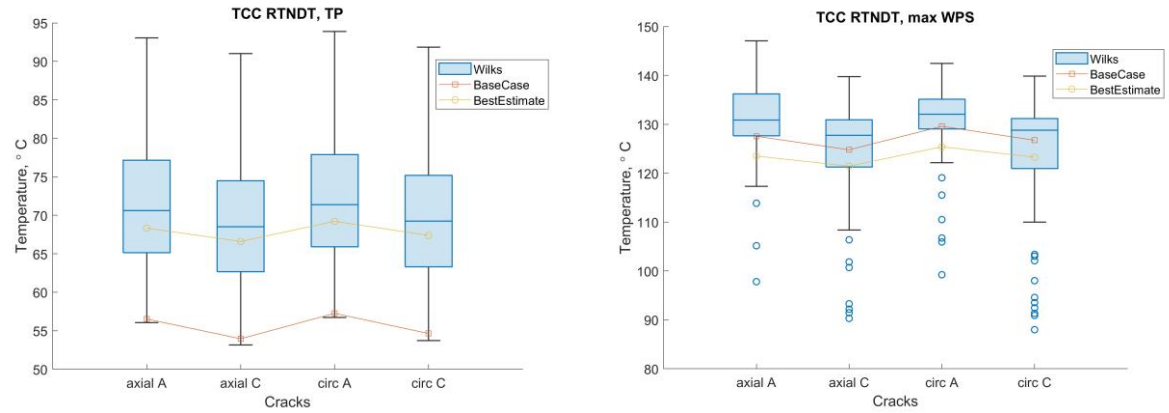

Figure 6.5: Final max. allowable ART results (IPP) for TCC, RT_{NDT} concept

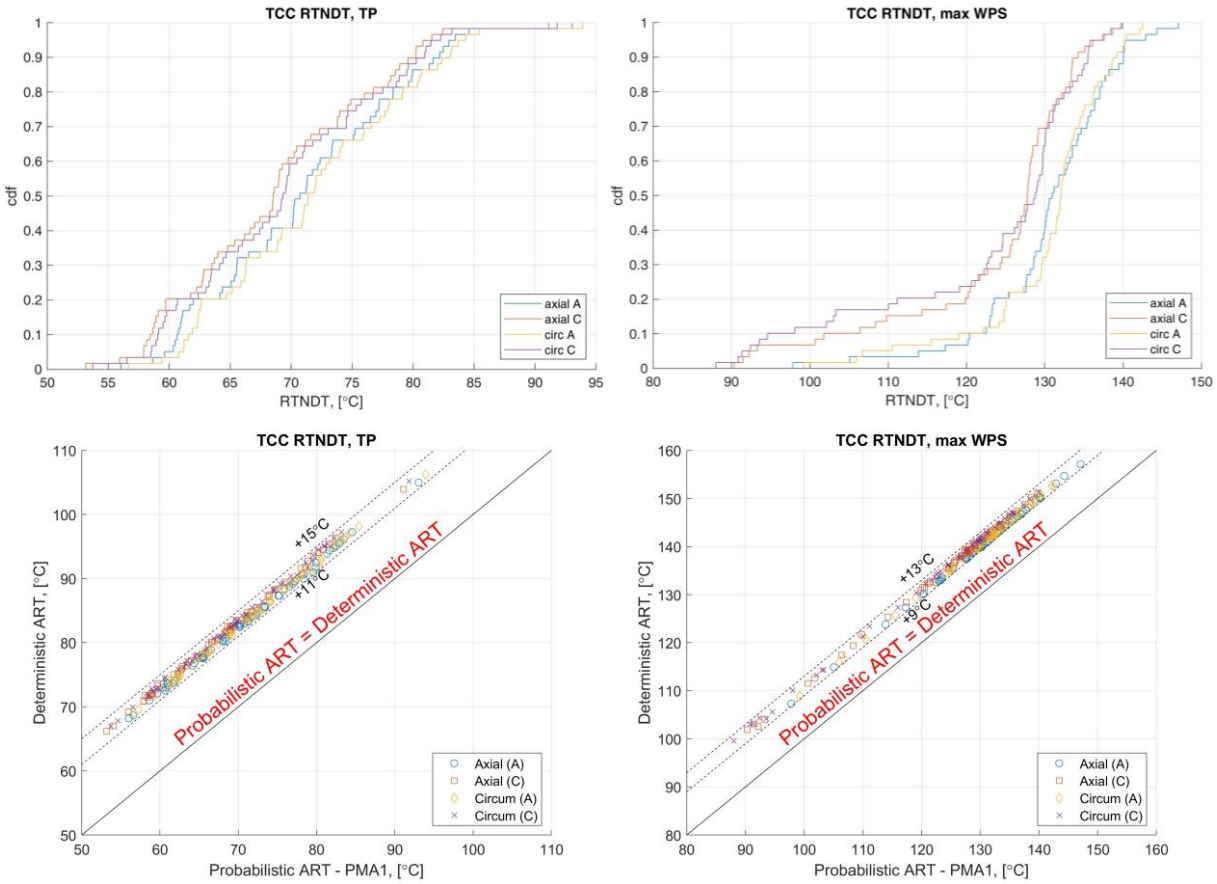

Figure 6.6: Statistical examination of final max. allowable ART results (IPP) for TCC, RT_{NDT} concept

Table 6.6: Final allowable ART results (IPP) for TCC crack, RT_{NDT} concept

	Axial Crack				Circumferential Crack			
	Deepest Point		Surface Point		Deepest Point		Surface Point	
	TP	maxWPS	TP	maxWPS	TP	maxWPS	TP	maxWPS
base case transient:	56.59	127.48	54.04	124.72	57.26	129.58	54.65	126.76
best estimate transient:	68.31	123.55	66.56	121.43	69.15	125.43	67.45	123.24
smallest value of Wilks set:	56.03	97.80	53.16	90.33	56.67	99.22	53.72	88.02
mean of Wilks set:	71.05	130.53	68.73	123.99	71.86	130.35	69.43	122.99
median from Wilks set:	70.72	130.92	68.52	127.78	71.39	132.09	69.33	128.78

Table 6.7: Final allowable ART results (IPP) for UCC crack, RT_{NDT} concept

	Axial Crack				Circumferential Crack			
	Deepest Point		Surface Point		Deepest Point		Surface Point	
	TP	maxWPS	TP	maxWPS	TP	maxWPS	TP	maxWPS
base case transient:	76.00	145.94	161.28	186.95	80.13	146.79	190.56	202.88
best estimate transient:	89.82	152.77	189.70	201.25	94.40	149.78	215.70	221.41
smallest value of Wilks set:	74.45	113.21	141.62	147.85	77.71	115.98	151.44	156.86
mean of Wilks set:	91.72	151.79	182.21	199.98	96.02	151.23	229.43	236.24
median from Wilks set:	91.24	152.10	184.44	197.20	95.55	151.35	212.93	216.86

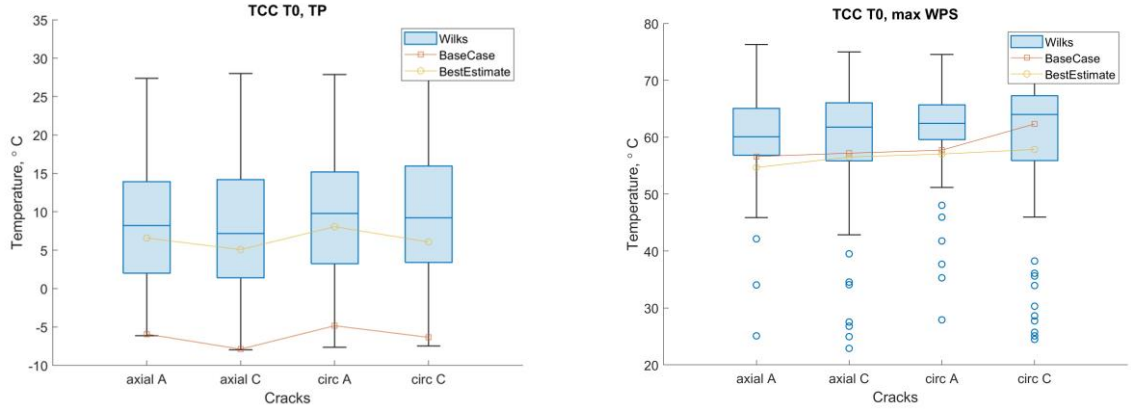

Figure 6.7: Final max. allowable ART results (IPP) for TCC, Master Curve concept

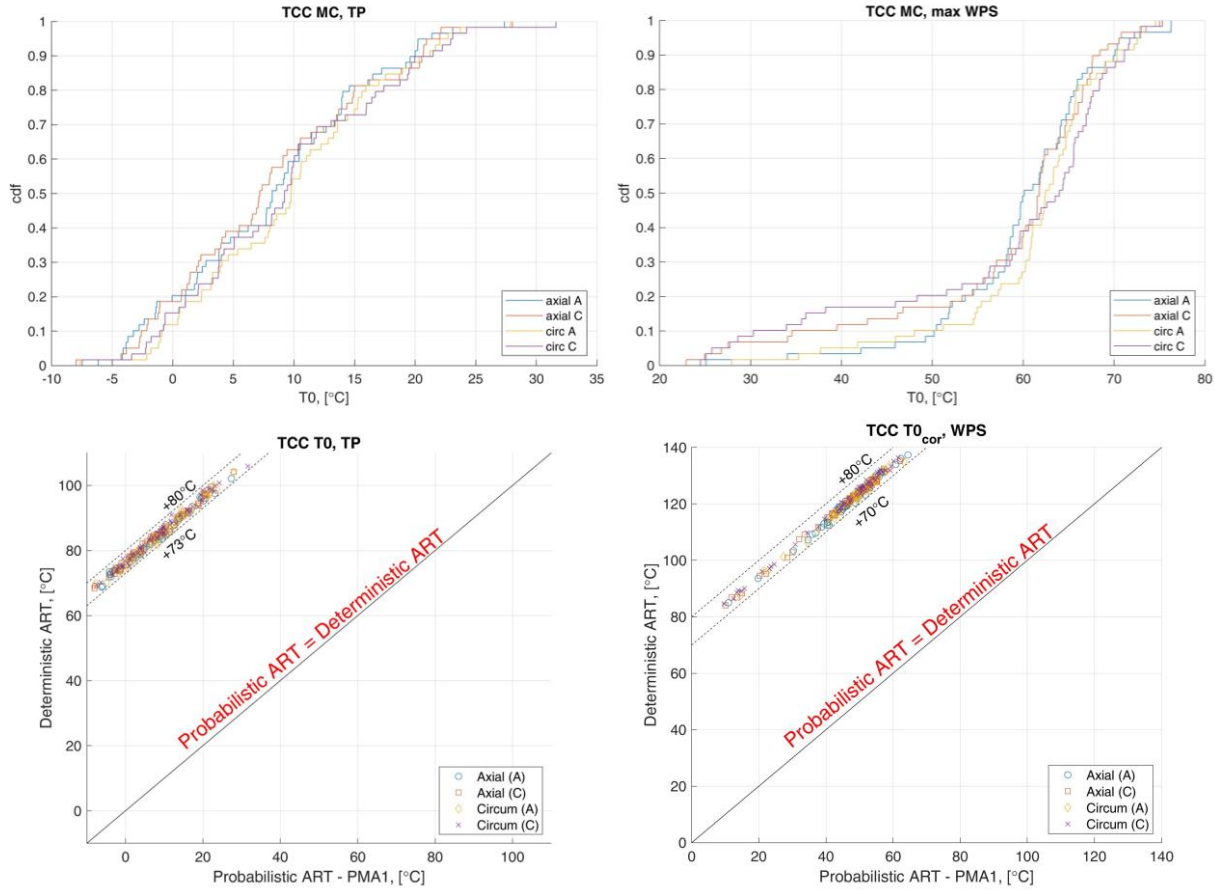

Figure 6.8: Statistical examination of final max. allowable ART results (IPP) for TCC, Master Curve concept

Table 6.8: Final max. allowable ART results (IPP) for TCC crack, Master curve approach

	Axial Crack				Circumferential Crack			
	Deepest Point		Surface Point		Deepest Point		Surface Point	
	TP	maxWPS	TP	maxWPS	TP	maxWPS	TP	maxWPS
base case transient:	-5.93	56.61	-7.90	57.20	-4.85	57.73	-6.35	62.33
best estimate transient:	6.58	54.70	5.07	56.52	8.06	57.04	6.06	57.86
smallest value of Wilks set:	-6.16	25.10	-7.98	22.90	-7.64	27.91	-7.48	24.48
mean of Wilks set:	8.21	59.80	8.06	58.16	9.63	61.03	9.38	58.26
median from Wilks set:	8.20	60.10	7.17	61.78	9.77	62.44	9.22	63.99

Table 6.9: Final max. allowable ART results (IPP) for UCC crack, Master curve approach

	Axial Crack				Circumferential Crack			
	Deepest Point		Surface Point		Deepest Point		Surface Point	
	TP	maxWPS	TP	maxWPS	TP	maxWPS	TP	maxWPS
base case transient:	20.73	85.63	80.00	138.56	28.87	85.57	97.15	148.74
best estimate transient:	36.42	92.31	102.69	145.50	44.17	91.77	119.04	151.47
smallest value of Wilks set:	21.21	50.13	79.27	98.37	24.75	56.23	88.86	106.39
mean of Wilks set:	38.71	91.27	103.10	146.04	44.13	92.86	118.92	154.77
median from Wilks set:	38.89	91.06	104.11	146.22	44.28	93.23	120.00	155.12

6.2.1.5 IRSN

The inputs used by IRSN were the 93 Wilks data sets "CW-CL-IP-180°" of Framatome from KWU-MIX and the 59 Wilks data sets CW + Best case + Conservative case + Best estimate from UJV from RELAP. As for Task 4.3 RR2 the dichotomy method with precision of 0.01°C was applied. Convergence was achieved in less than 15 iterations. The results were all calculated for the tangent approach. The results are given with the corresponding confidence interval (IC).

Results based on Framatome 93 Wilks data sets

The results of IRSN for max. all. ART based on the Framatome Wilks data sets are shown in Figure 6.9 and Figure 6.10 and summarised in Table 6.10. All the results based on the Framatome Wilks data sets are given in Table 6.11.

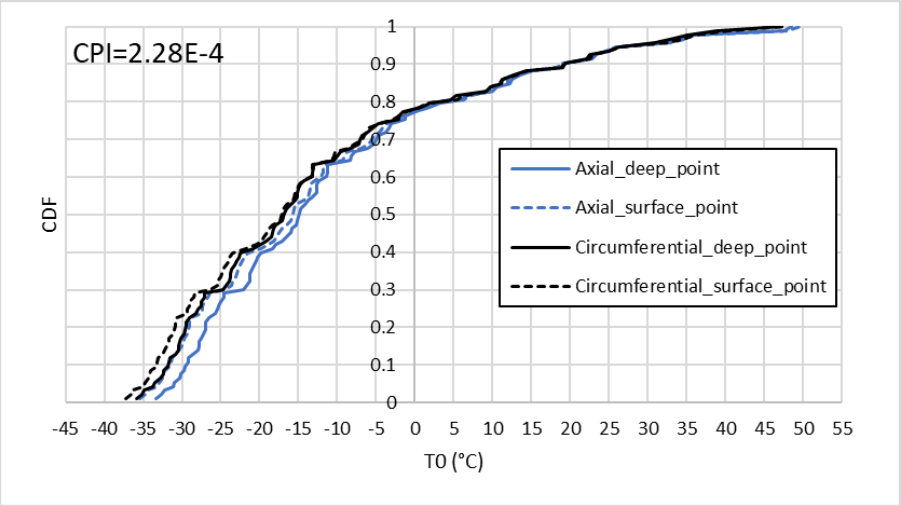

Figure 6.9: IRSN results for max. all. ART based on FRA 93 Wilks data sets – T_0 concept

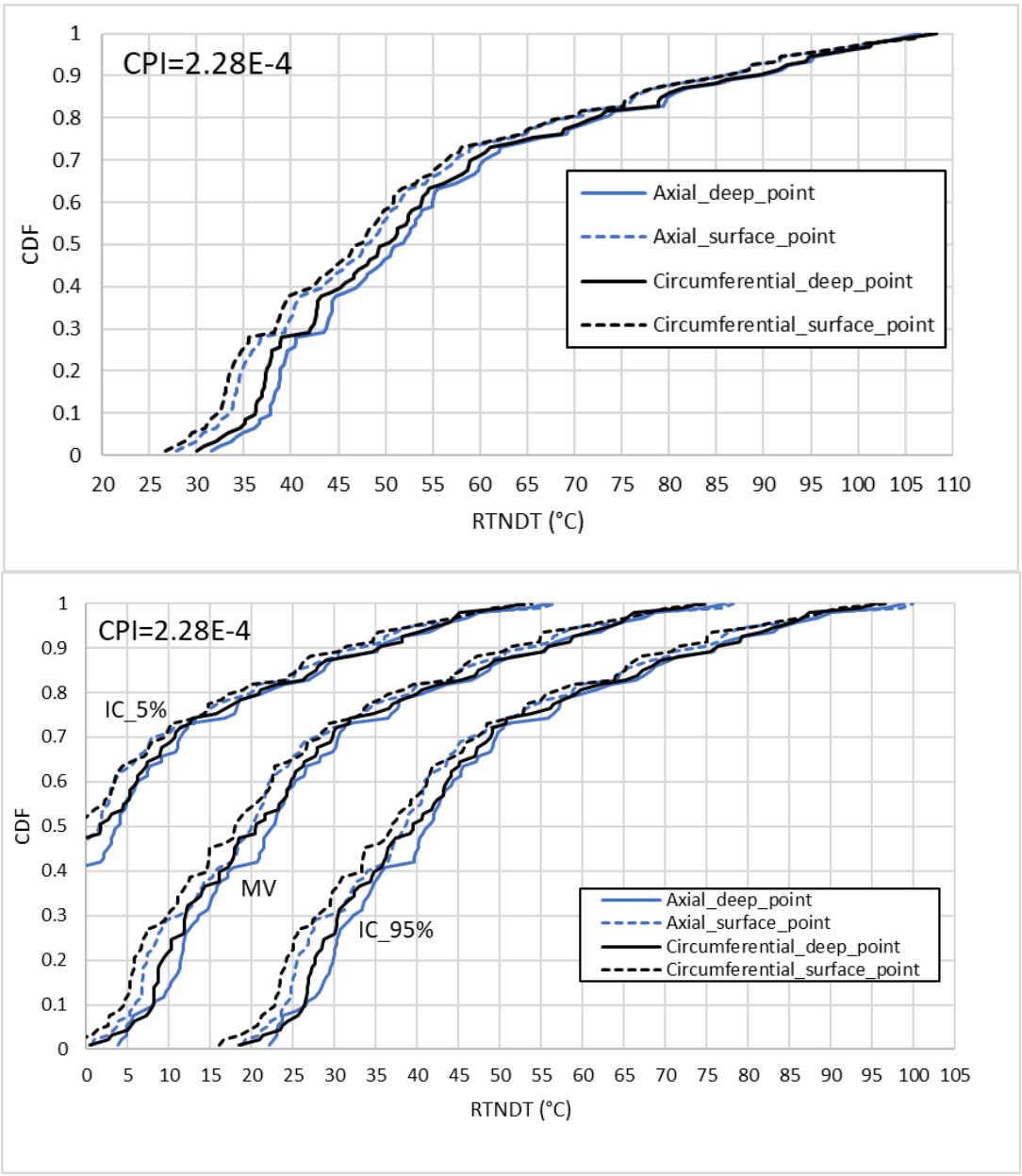

Figure 6.10: IRSN results for max. all. ART based on FRA 93 Wilks data sets – RT_{NDT} concept (results are shown for RTNDT>0°C). The curves represent the empirical cumulative density functions for the median values and the confidence intervals at 5% and 95%.

Table 6.10: Summary of IRSN results for max. all. ART based on FRA 93 Wilks data sets

			T_0				RT_{NDT}			
			med (°C)	min(°C)	max(°C)	cov	med (°C)	min(°C)	max(°C)	cov
TCC	Axial	deep	-9.9	-33.34	48.49	194%	56.56	31.60	106.53	34%
		surf	-10.99	-35.41	49.57	182%	53.06	27.81	107.63	38%
	Circum	deep	-11.87	-35.83	47.22	165%	55.42	30.06	108.34	36%
		surf	-12.46	-37.24	47.36	163%	52.18	26.66	106.00	39%

Table 6.11: IRSN results for TCC (RT_{NDT}) based on FRA 93 Wilks data sets – RT_{NDT} concept

		Wilks									
		RTNDT(°C)									
		med	min	max	cov	std	cov std	IC_5%	cov_IC_5%	IC_95%	Cov_IC_95%
Axial	A	26.81	3.81	77.29	68%	11.59	4%	7.76	2.24	45.90	0.41
	C	24.25	0.68	78.19	0.8	11.52	4%	5.30	3.36	43.19	0.449
Circ	A	25.59	0.44	73.98	0.7	11.56	4%	6.60	2.64	44.61	0.428
	C	22.90	-1.99	75.28	0.8	11.49	4%	4.02	4.43	41.81	0.464

Results based on UJV 59 Wilks data sets + BC/CONS/BE

The results of IRSN for max. all. ART based on the UJV Wilks data sets are shown in Figure 6.11, Figure 6.12 and Figure 6.13, and also summarised in Table 6.12 and Table 6.13. All the results for the UJV Wilks data sets are given in Table 6.14.

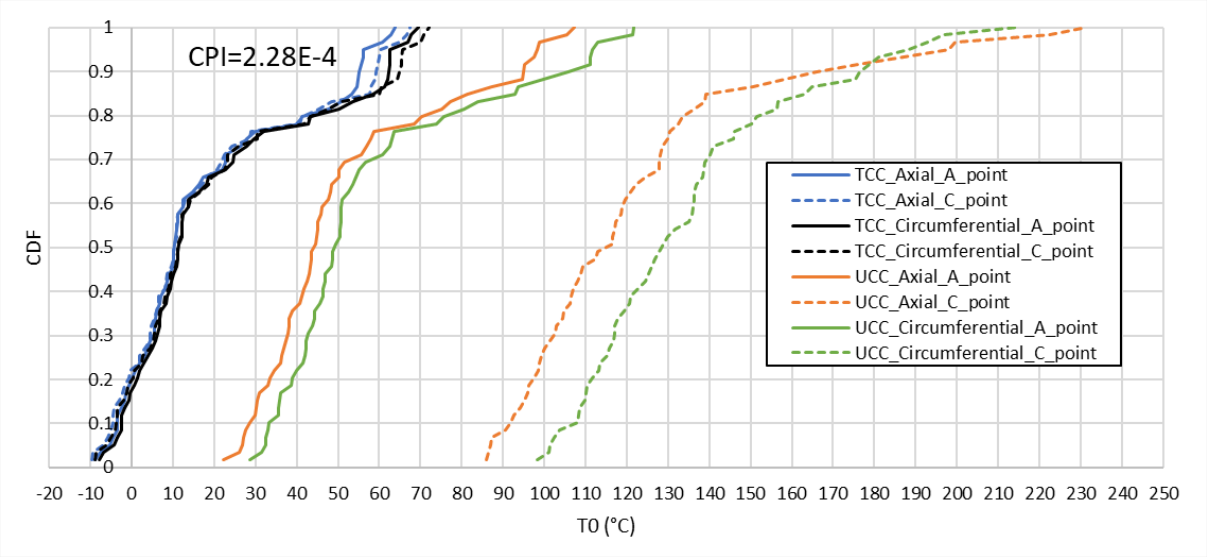

Figure 6.11: IRSN results for max. all. ART based on UJV Wilks data sets – T_0 concept

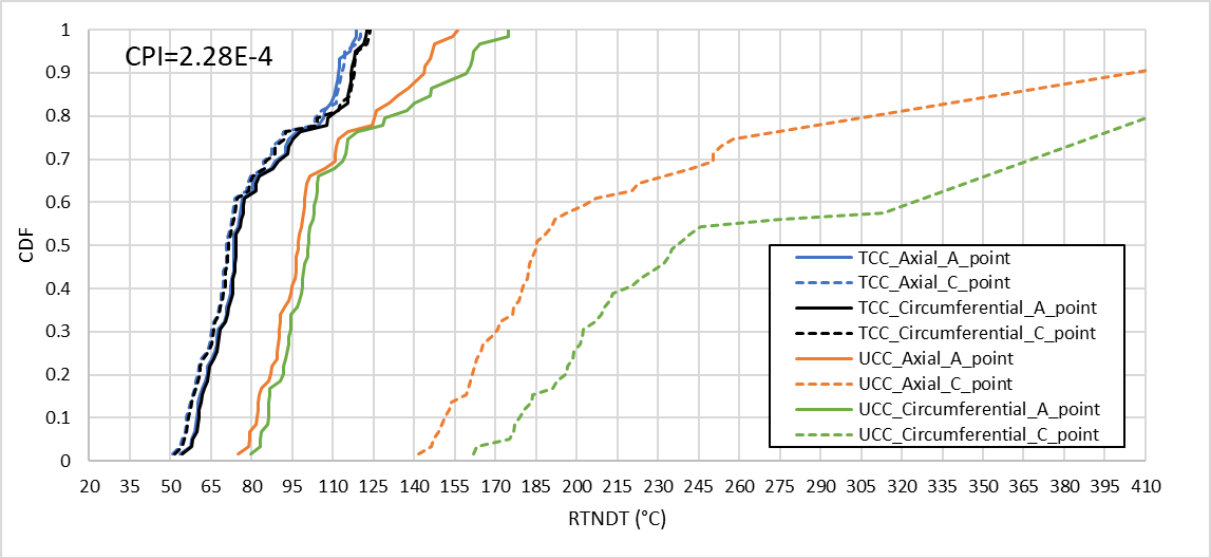

Figure 6.12: IRSN results for max. all. ART based on UJV Wilks data sets – RT_{NDT} concept

Table 6.12: IRSN results for max. all. ART based on UJV Wilks data sets – T_0 concept

			T_0				T_0		
			med (°C)	**min (°C)**	max(°C)	cov	BC	**CONS**	BE
TCC	Axial	A	17.65	**-8.98**	63.81	123%	-4.65	**-8.98**	8.45
		C	17.75	**-9.55**	67.35	130%	-6.02	**-9.08**	7.82
	Circum	A	19.73	**-7.83**	69.39	119%	-3.65	**-6.93**	9.52
		C	19.47	**-8.81**	72.05	125%	-5.11	**-7.33**	8.79
UCC	Axial	A	50.78	**22.30**	107.41	46%	25.52	**13.65**	39.73
		C	120.90	**86.08**	231.51	28%	86.80	**65.40**	105.78
	Circum	A	57.23	**28.62**	121.73	45%	31.24	**20.88**	45.28
		C	133.27	**98.25**	214.41	21%	102.73	**78.73**	122.81

Table 6.13: IRSN results for max. all. ART based on UJV Wilks data sets – RT_{NDT} concept

			RT_{NDT}				RT_{NDT}		
			med (°C)	**min (°C)**	max(°C)	cov	BC	**CONS**	BE
TCC	Axial	A	80.38	**53.81**	118.84	25%	59.07	**51.91**	71.95
		C	78.06	**51.06**	120.31	27%	55.48	**50.25**	68.73
	Circum	A	81.94	**54.52**	122.70	26%	59.73	**54.20**	72.62
		C	79.44	**51.70**	123.76	28%	56.06	**52.14**	69.36
UCC	Axial	A	103.51	**74.96**	156.25	22%	79.01	**67.07**	93.39
		C	258.99	**141.61**	>500	54%	152.32	**117.83**	184.70
	Circum	A	109.55	**79.70**	174.73	24%	83.32	**74.18**	97.62
		C	325.14	**162.04**	>500	45%	196.06	**131.50**	229.66

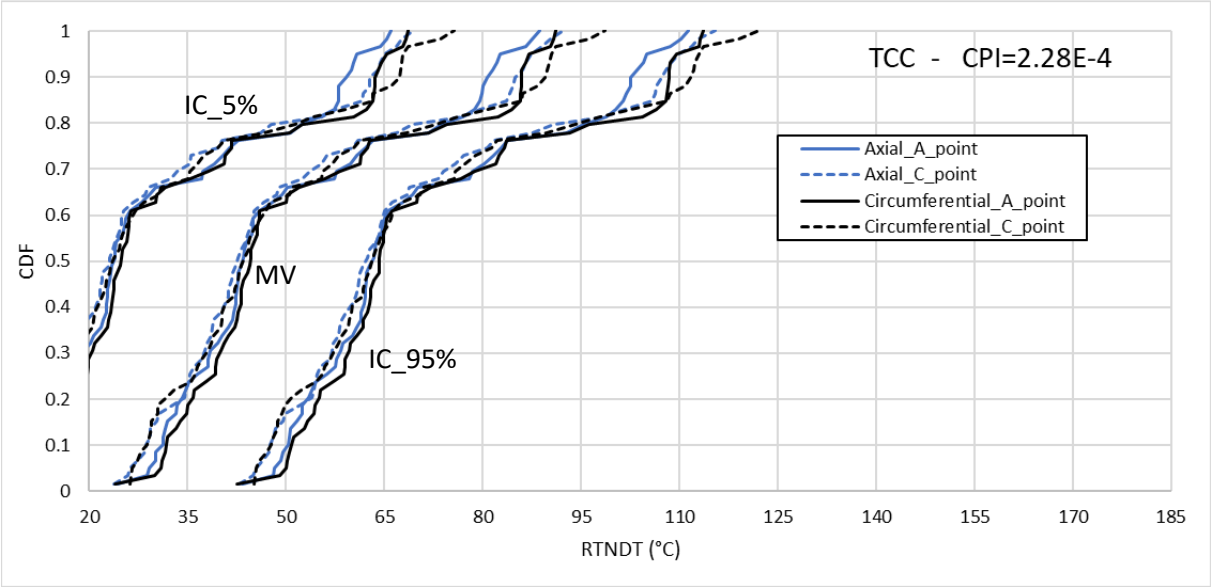

Figure 6.13: IRSN results for max. all. ART for TCC based on UJV Wilks data sets – RT_{NDT} concept (results are shown for RTNDT>20°C). The curves represent the empirical cumulative density functions for the median values and the confidence intervals at 5% and 95%.

Table 6.14: IRSN results for TCC and UCC (Age, RT_{NDT}) based on UJV Wilks data sets – RT_{NDT} concept

			Wilks									
			RTNDT(°C)									
			med	min	max	cov	std	cov std	IC_5%	cov_IC_5%	IC_95%	Cov_IC_95%
TCC	Axial	A	50.90	24.23	88.66	0.37	12.27	0.05	30.76	0.58	71.13	28.07%
		C	50.17	23.76	92.28	0.41	12.25	0.06	30.05	0.64	70.36	30.70%
	Circ	A	52.67	23.90	91.12	0.38	12.32	0.06	32.44	0.58	72.96	29.06%
		C	51.35	26.15	98.74	0.42	12.31	0.06	31.13	0.66	71.56	32.01%
UCC	Axial	A	80.88	53.29	153.31	0.31	13.38	0.08	58.89	0.39	102.92	26.03%
		C	-	-	-	-	-	-	-	-	-	-
	Circ	A	87.14	60.97	165.95	0.29	13.64	0.09	64.74	0.37	109.63	25.19%
		C	-	-	-	-	-	-	-	-	-	-

6.2.1.6 JSI

The TH-data cases used by JSI are the following:

- Base Case: reference case from T2.1 delivered in D2.1. This case used an input deck and a set of input parameters given for the task, and RELAP5 version 33lf.
- Best Estimate: reference case from T2.3 delivered in D2.3. This case used a modified input deck and effectively the same (but very slightly different) set of input parameters agreed for the task, and RELAP5 version 33lj.
- Wilks: Two independent Wilks' sets with 59 and 130 samples were assessed, respectively. These cases used the same input deck and RELAP5 version as the Best Estimate and are based on the best estimate case with random sampling of selected plant parameters and boundary conditions. The random parameters and sampling methodology are described in D2.3.

- Min.Bound.Case : TH run with a set of parameters leading to a less stringent transient for the structure. The same input deck and RELAP5 version as the Best Estimate was used.
- Max.Bound.Case : TH run with a set of parameters leading to a more stringent transient for the structure. The same input deck and RELAP5 version as the Best Estimate was used.

The assessed crack geometry is TCC circumferential point A (deepest point). The crack location is core weld inside plume (095-05). Both the tangent and the Max WPS approach were assessed. For the calculation of max. all. ART the RT_{NDT} concept, T_0 concept and the FAVOR-RT_{NDT} concept (in-house) were applied. The FAVOR-RT_{NDT} results were generated with an in-house implementation of the FAVOR-RT_{NDT} curve. The results are not from the FAVOR/CAPAL code. Stress and SIF calculations include crack face pressure and FAVOR weld residual stresses.

In Figure 6.14 an example is given to show how to read the JSI result plots. The lines correspond to results for given ART (0, 50, 100, 150 and 200°C), and the points correspond to results for the given CPI-target (2.28E-4). JSI used a 1°C accuracy in the search for ART given CPI-target, assuming ART >0°C. Lower accuracy would be required to improve the match of CPI-target by some of the samples, as seen by the ART results (dots) away from target. Note that in JSI calculations, the distributed fracture toughness (K_{IC}) does not affect convergence since, for given ART, the cpi(t) is obtained directly from the CDF of the distributed K_{IC} (without Monte Carlo). The results with tangent and Max WPS approaches for the two Wilks' sets (59 and 130 samples) and the three ART concepts are shown in Figure 6.15 to Figure 6.20. An overview of all results is given in Table 6.15.

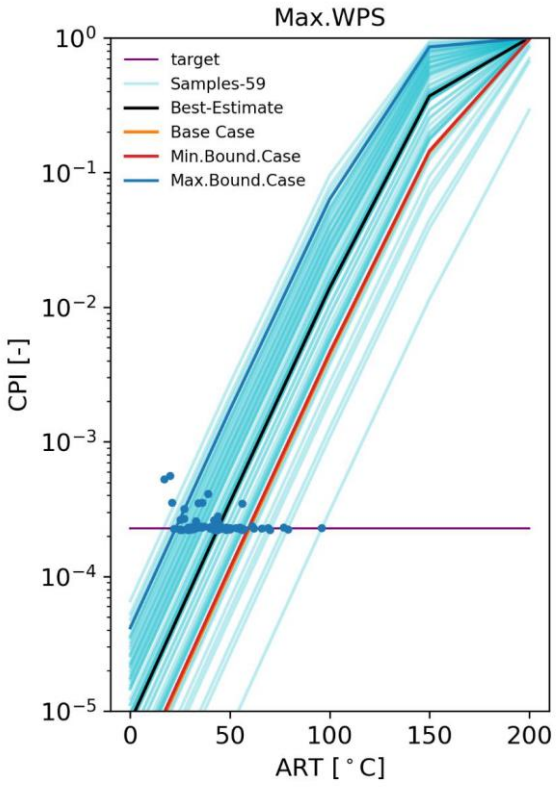

	ART_final_wps [°C]
mean	43
std	16
min	17
5%	22
50%	42
95%	71
max	96
Best-Est.59	44

Figure 6.14: Example (Master Curve T_0, Max. WPS, Wilks-59) how to read JSI result plots. Note that orange (Base Case) and red (Min.Bound.Case) lines overlap in this example.

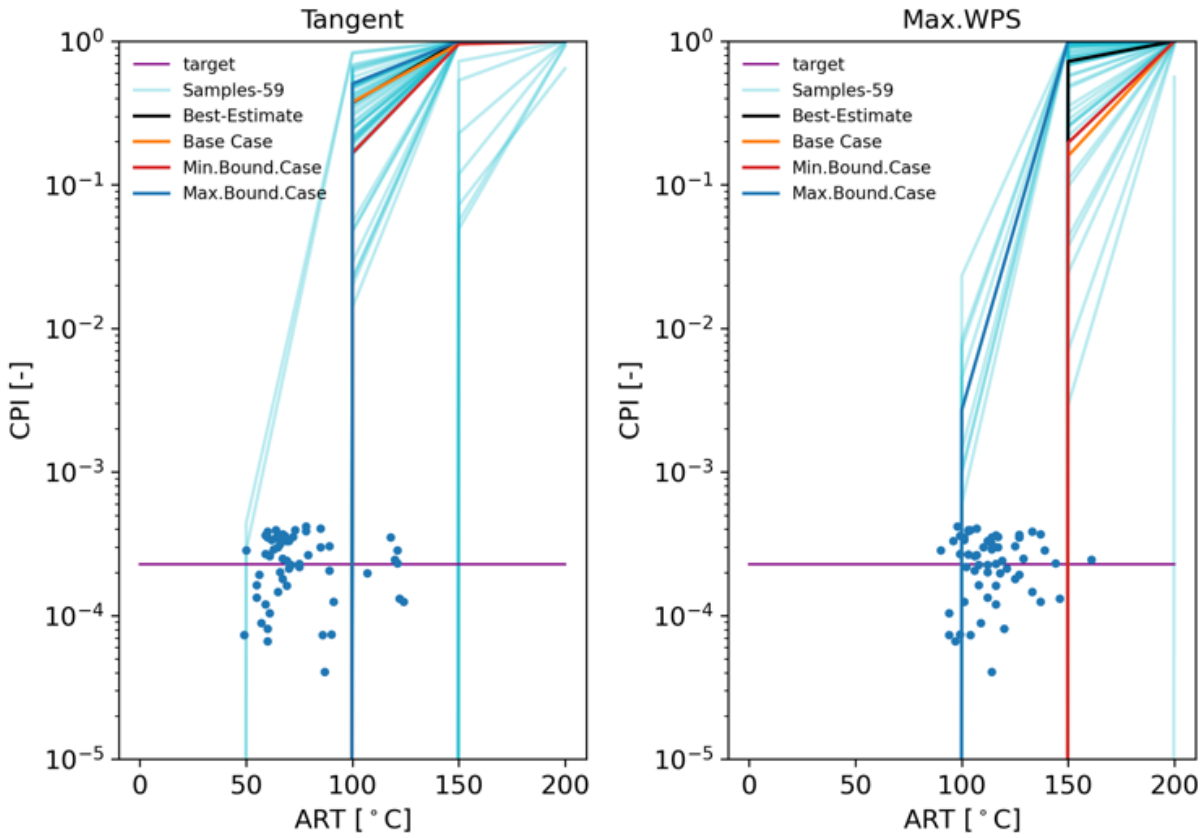

Figure 6.15: JSI results for Wilks-59 – ASME RT_{NDT} concept

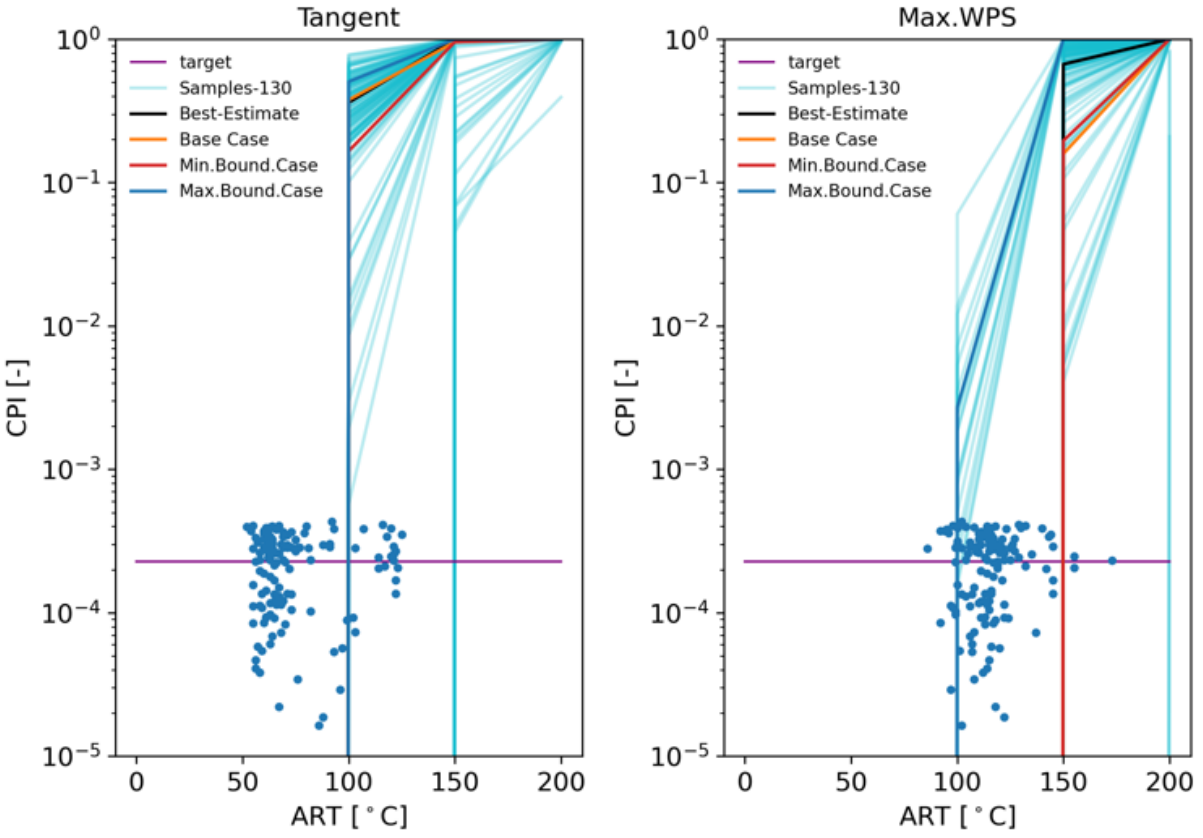

Figure 6.16: JSI results for Wilks-130 – ASME RT_{NDT} concept

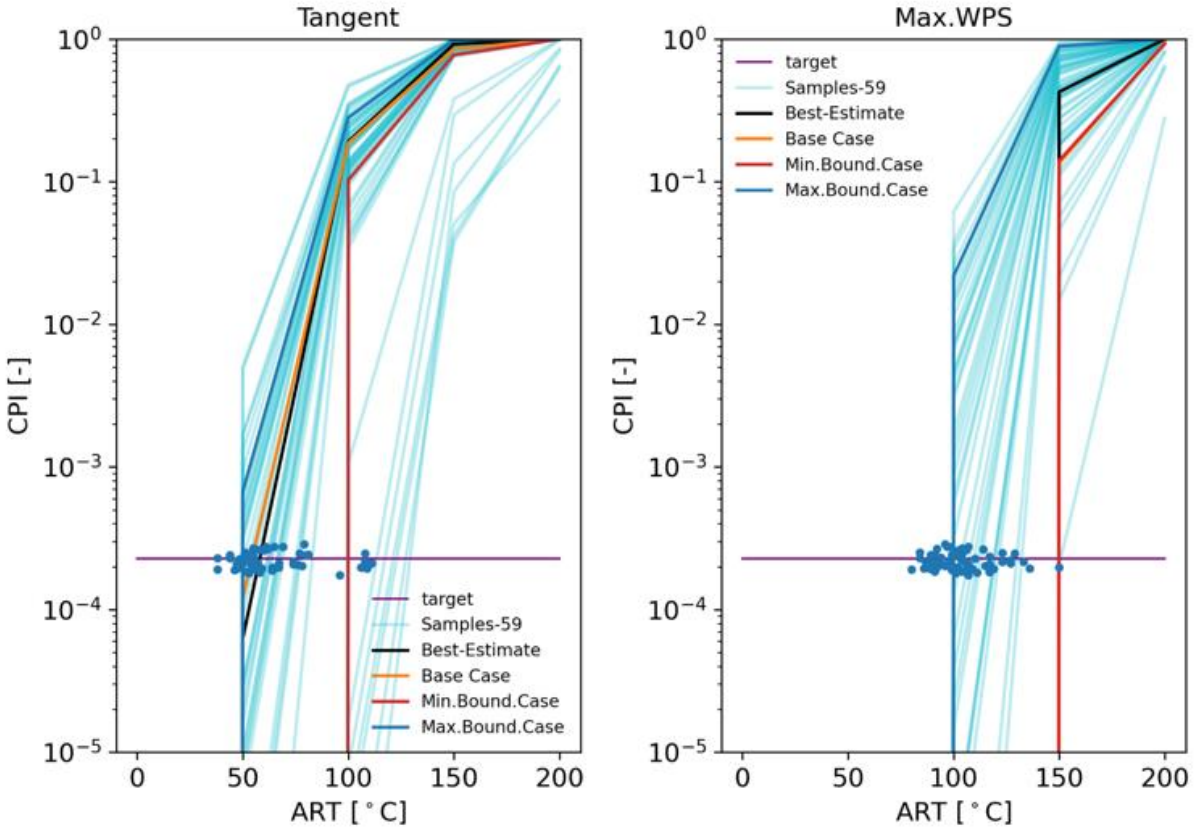

Figure 6.17: JSI results for Wilks-59 – FAVOR RT_{NDT} concept

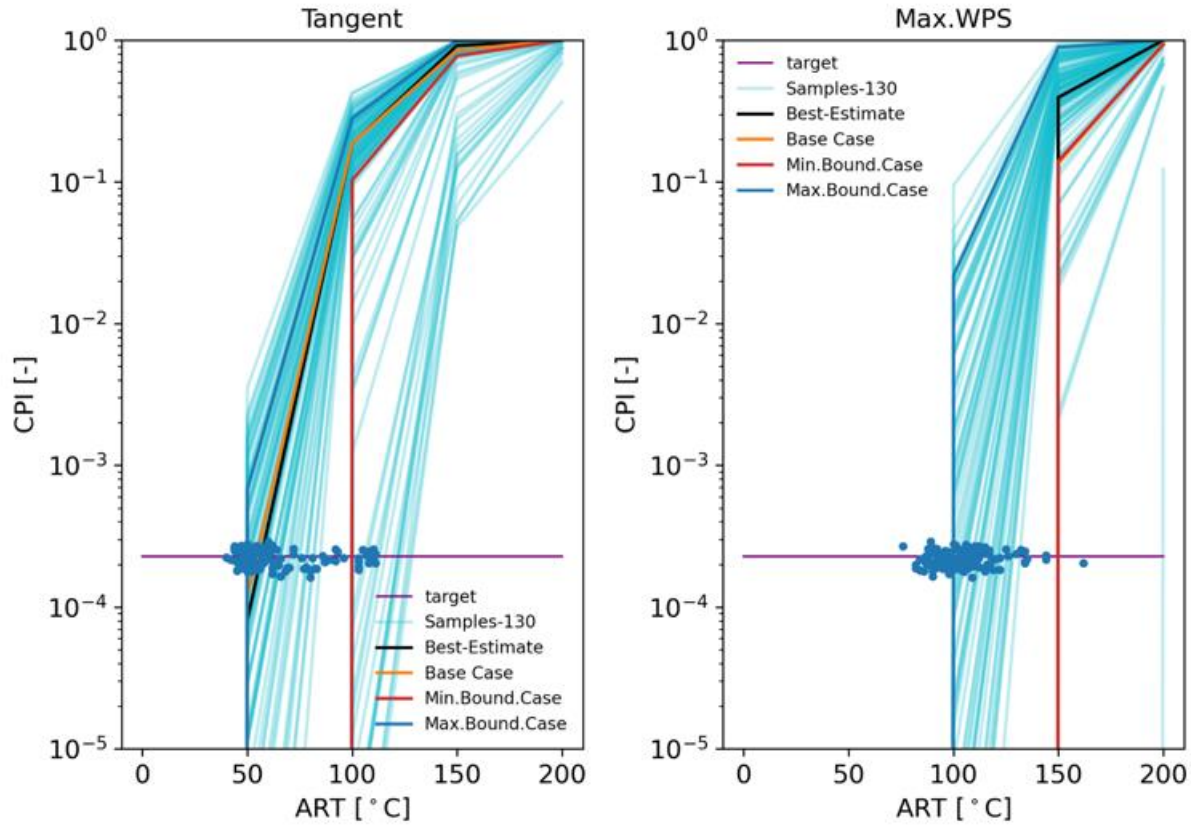

Figure 6.18: JSI results for Wilks-130 – FAVOR RT_{NDT} concept

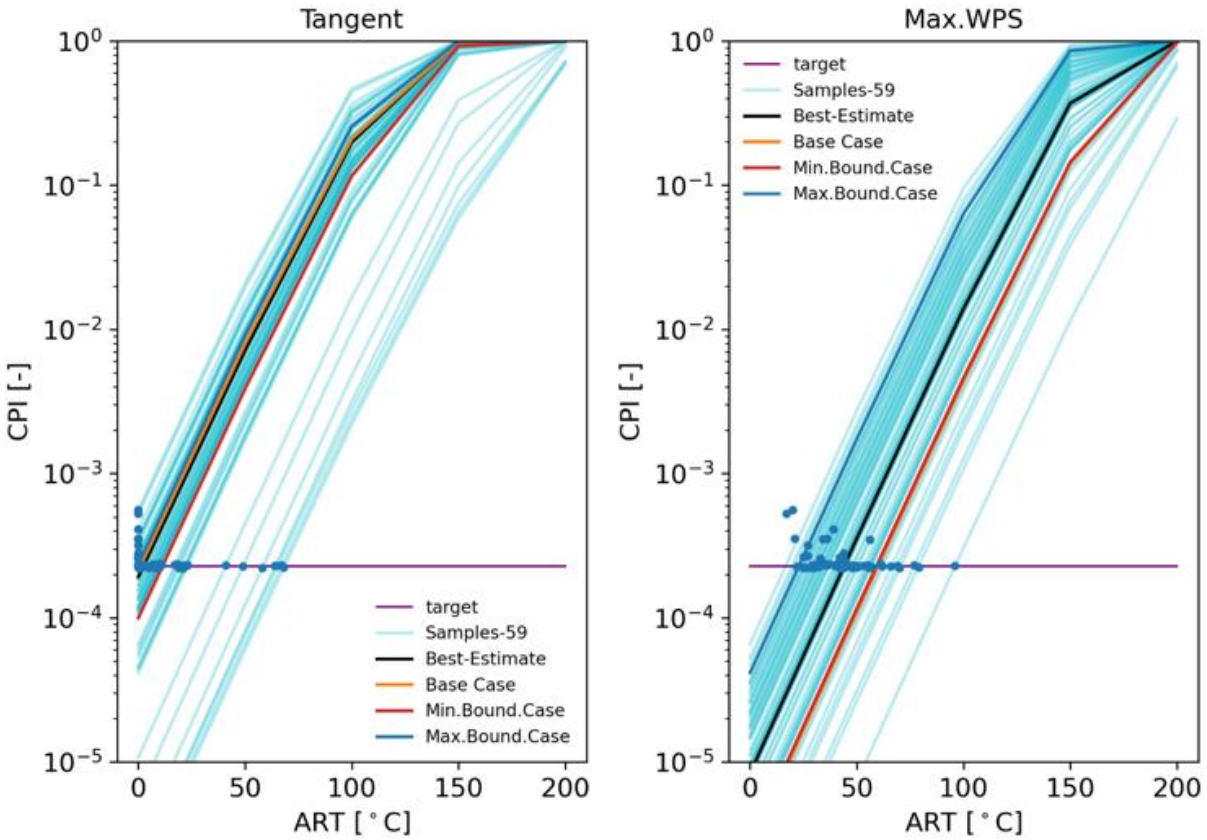

Figure 6.19: JSI results for Wilks-59 – MC-T_0 concept

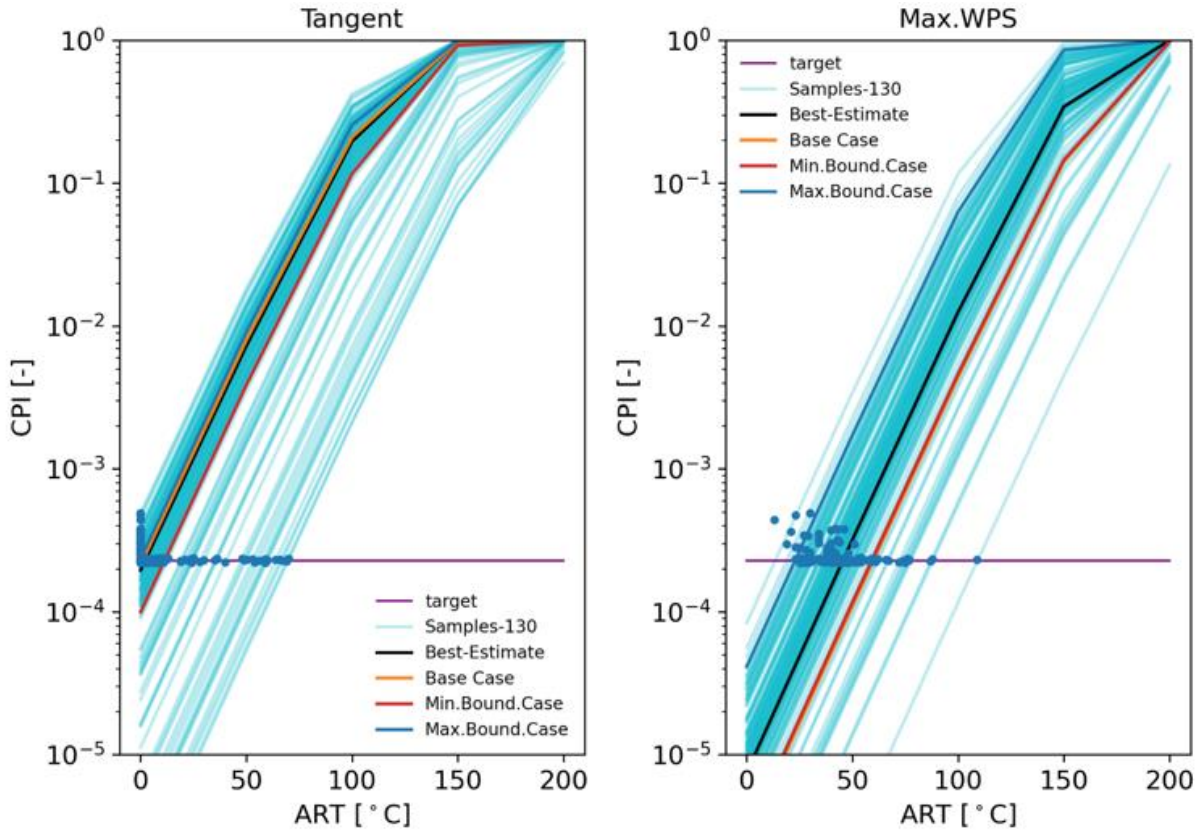

Figure 6.20: JSI results for Wilks-130 – MC-T_0 concept

Table 6.15: JSI statistics obtained from the distribution of max. all. ART results

	Tangent			Max.WPS		
	Max. all. ART final ASME	Max. all. ART final FAVOR	Max. all. ART final MC-T_0	Max. all. ART final ASME	Max. all. ART final FAVOR	Max. all. ART final MC-T_0
	wilks-59					
mean	74	63	13	114	104	43
std	19	19	19	15	14	16
min	49	38	0	90	80	17
95%	55	44	0	96	86	22
50%	68	57	7	112	103	42
5%	121	108	64	140	129	71
max	124	111	68	161	150	96
Best-Est.59	64	52	2	116	106	44
	wilks-130					
mean	75	63	13	115	105	44
std	20	20	19	14	14	15
min	52	40	0	86	76	13
95%	55	44	0	97	87	25
50%	67	55	4	114	105	42
5%	121	109	59	144	133	76
max	125	111	70	173	162	109
Best-Est.130	63	52	2	118	108	45
	other					
Base Case	63	51	1	130	120	60
Min.Bound.	74	63	11	127	117	59
Max.Bound.	59	46	0	97	87	23

6.2.1.7 KIWA

The results of KIWA include TCC and UCC, circumferential and axial orientation, deepest point and interface point. The max. all. ART was evaluated with the RT_{NDT} concept for both the tangent and the Max WPS approach. The PMA1 results are shown in Figure 6.21 and Figure 6.22. Kiwa analysed the full 59 Wilks sets for each case to locate the limiting transient. Figure 6.23 shows an example plot for point A of a circumferential TCC where the limiting transient is w45_wrs. The limiting transients for all cases are included in Table 6.16.

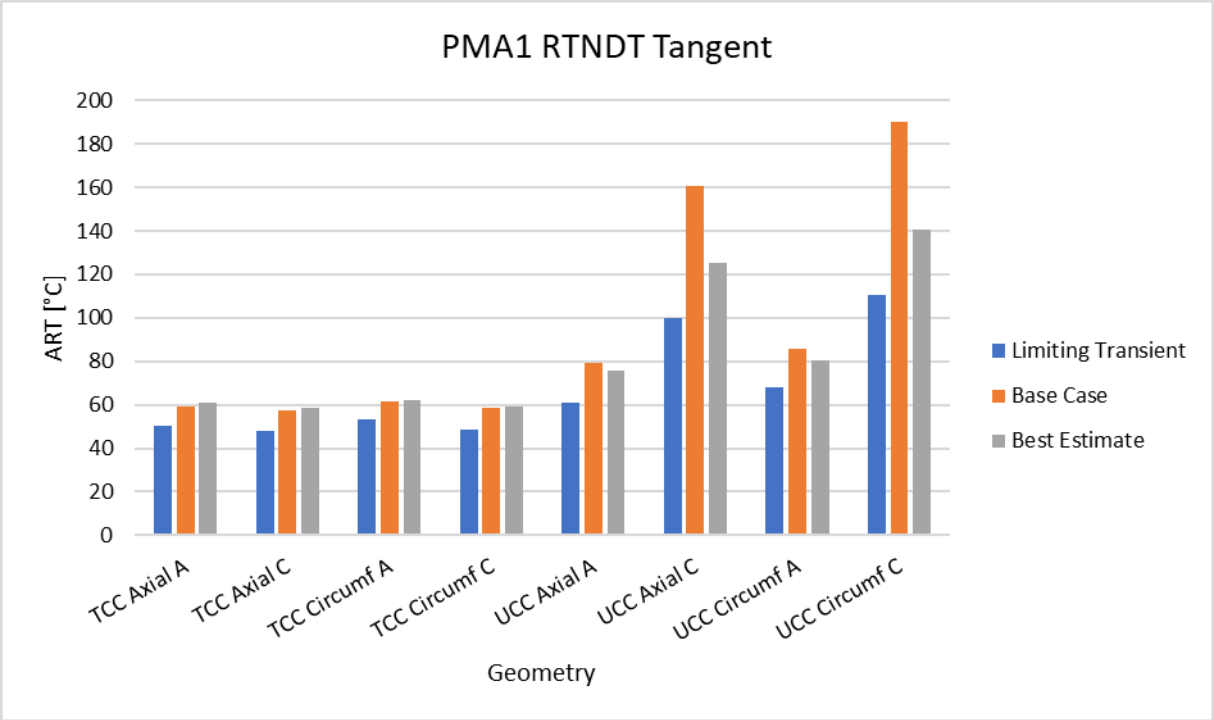

Figure 6.21: KIWA results for max. all. ART tangent approach – RT_{NDT} concept

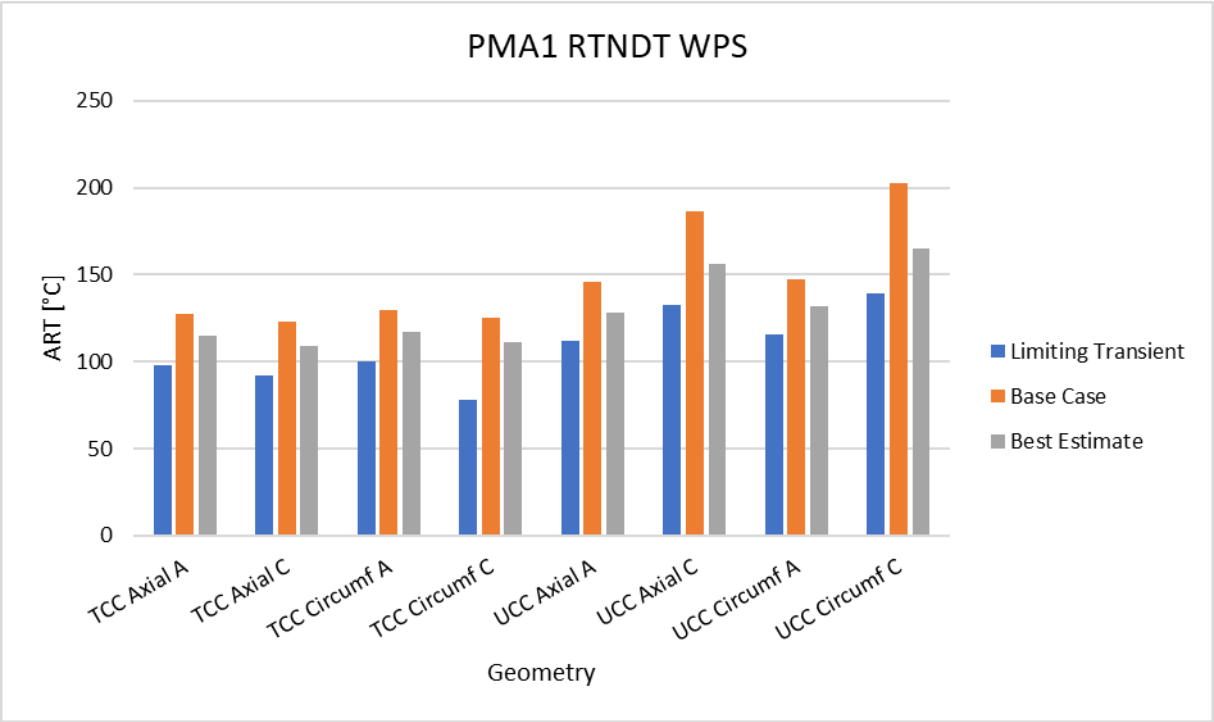

Figure 6.22: KIWA results for max. all. ART Max WPS approach – RT_{NDT} concept

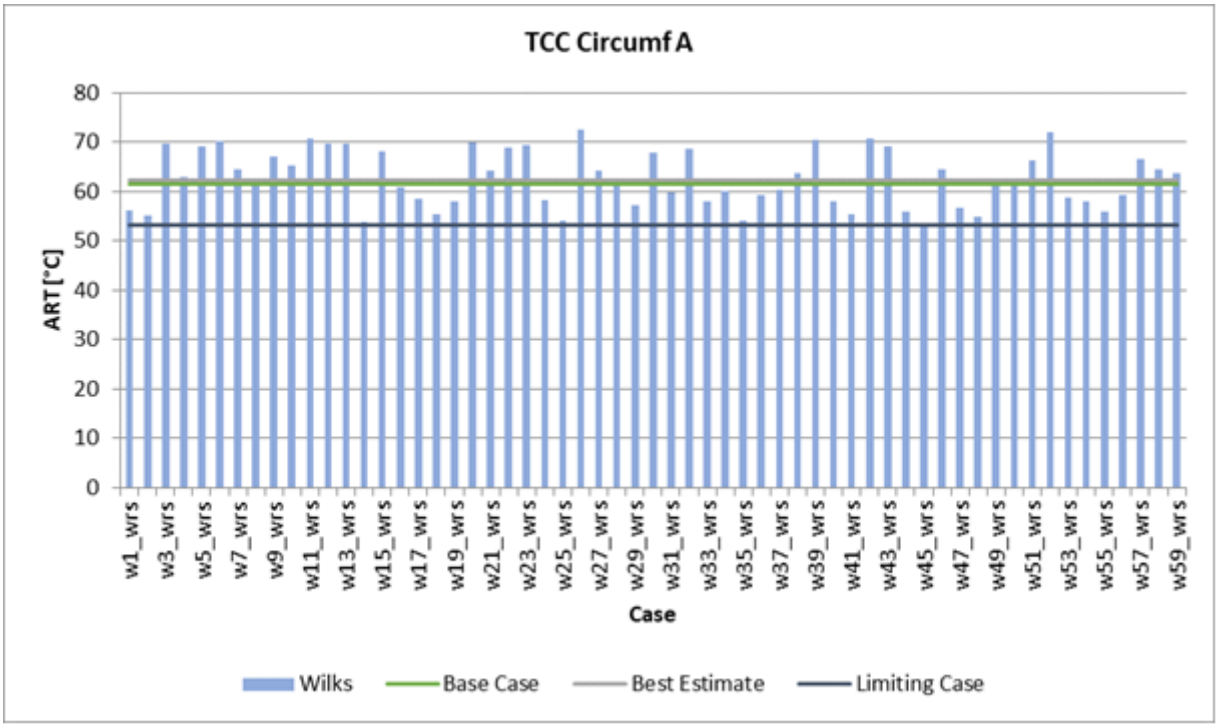

Figure 6.23: KIWA results for all Wilks sets for TCC circumferential, point A (deepest point)

Table 6.16: KIWA summary of all PMA1 results

Name	Margin Approach	Concept	Limit Condition	ART in °C	Limiting Transient	Base Case	Best Estimate
TCC Axial A	PMA1	RT_{NDT}	Tangent	50.4906	w45_wrs	59.2086	61.2183
TCC Axial C	PMA1	RT_{NDT}	Tangent	48.2021	w14_wrs	57.6909	58.4874
TCC Circ A	PMA1	RT_{NDT}	Tangent	53.1196	w45_wrs	61.4211	62.3684
TCC Circ C	PMA1	RT_{NDT}	Tangent	48.6199	w14_wrs	58.7387	59.1757
UCC Axial A	PMA1	RT_{NDT}	Tangent	61.0106	w35_wrs	78.9512	75.6197
UCC Axial C	PMA1	RT_{NDT}	Tangent	99.8104	w2_wrs	160.6272	125.3115
UCC Circ A	PMA1	RT_{NDT}	Tangent	68.0451	w35_wrs	85.933	80.4317
UCC Circ C	PMA1	RT_{NDT}	Tangent	110.4087	w17_wrs	190.3785	140.5883
TCC Axial A	PMA1	RT_{NDT}	max. WPS	98.1248	w33_wrs	127.1955	114.7603
TCC Axial C	PMA1	RT_{NDT}	max. WPS	92.3517	w33_wrs	122.9356	109.0043
TCC Circ A	PMA1	RT_{NDT}	max. WPS	100.0021	w33_wrs	129.3545	116.8597
TCC Circ C	PMA1	RT_{NDT}	max. WPS	77.693	w49_wrs	124.9451	110.9405
UCC Axial A	PMA1	RT_{NDT}	max. WPS	112.1069	w33_wrs	145.9651	128.1029
UCC Axial C	PMA1	RT_{NDT}	max. WPS	132.9418	w17_wrs	186.267	156.1545
UCC Circ A	PMA1	RT_{NDT}	max. WPS	115.6252	w33_wrs	147.194	132.055
UCC Circ C	PMA1	RT_{NDT}	max. WPS	138.9279	w17_wrs	202.9472	164.9592

6.2.1.8 Tecnatom

The Tecnatom results are all for TCC circumferential orientation at the deepest point. The assessed location is CW-IP, the used TH data is TRACE 59 Wilks set from PSI. The max. all. ART was evaluated with the FAVOR-RT_{NDT} concept for both the tangent and the Max WPS approach. All results were calculated with FAVOR/CAPAL. Tecnatom's probability results are conservative (i.e. lower values of maximum allowable RT_{NDT} or lifetime) because of the assumptions taken due to FAVOR limitations to consider the postulated cracks. An overview of all results is given in Table 6.17.
From all the transients included in the Wilks set, the most limiting transient from the deterministic analyses in Task 3.4 is evaluated using the probabilistic approach, i.e. the transient with the lowest value of max. allows RTNDT. For TCC circumferential with tangent approach it is the transient number 13, and for TCC circumferential with max. WPS approach it is the transient number 57.

Table 6.17: Overview of Tecnatom results for max. all. ART in °C – TCC circumferential, FAVOR-RT_{NDT} concept

	Base Case	Best Estimate	95% quantile
Tangent	33.5	39	16
Max WPS	79.5	110	42

6.2.1.9 UJV

The assessed cases for UJV include TCC circumferential orientation at the deepest point for the CW-CL location. The max. all. ART was evaluated with the RT_{NDT} concept for both the tangent and the Max WPS approach. An overview of the results for max. all. ART is given in Table 6.18.
The assessed Wilks transients are the UJV-59 transients calculated by RELAP. The full Wilks data set was analysed, and the lowest max. all. ART was taken as a resulting 95% quantile, separately for the tangent and Max WPS approach.
The dependence of CPI on the postulated value of RT_{NDT} is shown in Figure 6.24 and Figure 6.25 for the tangent and Max WPS approach, respectively. The Figures show CPI values for the Best Estimate transient, Conservative transient and for the transients with lowest max. all. ART (transient no. 36 for the tangent approach and transient no. 46 for the Max WPS approach).

Table 6.18: Overview of UJV results for max. all. ART in °C – TCC circumferential, RT_{NDT} concept

	Base Case	Best Estimate	Conservative	95% quantile
Tangent	59.7	72.2	54.6	54.5
Max WPS	143.5	138.9	138.8	69.8

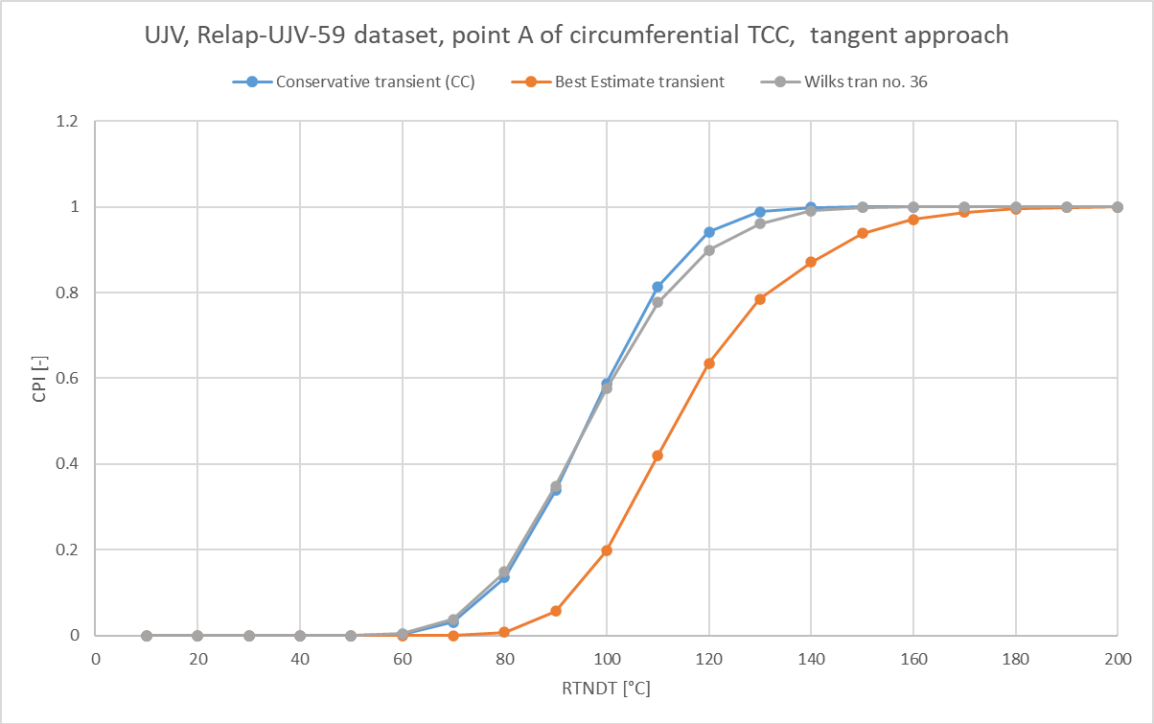

Figure 6.24: UJV results. Comparison of Conservative transient, Best Estimate transient and a transient with smallest value of max. all. ART from the UJV-59 wilks set for tangent approach – RT_{NDT} concept

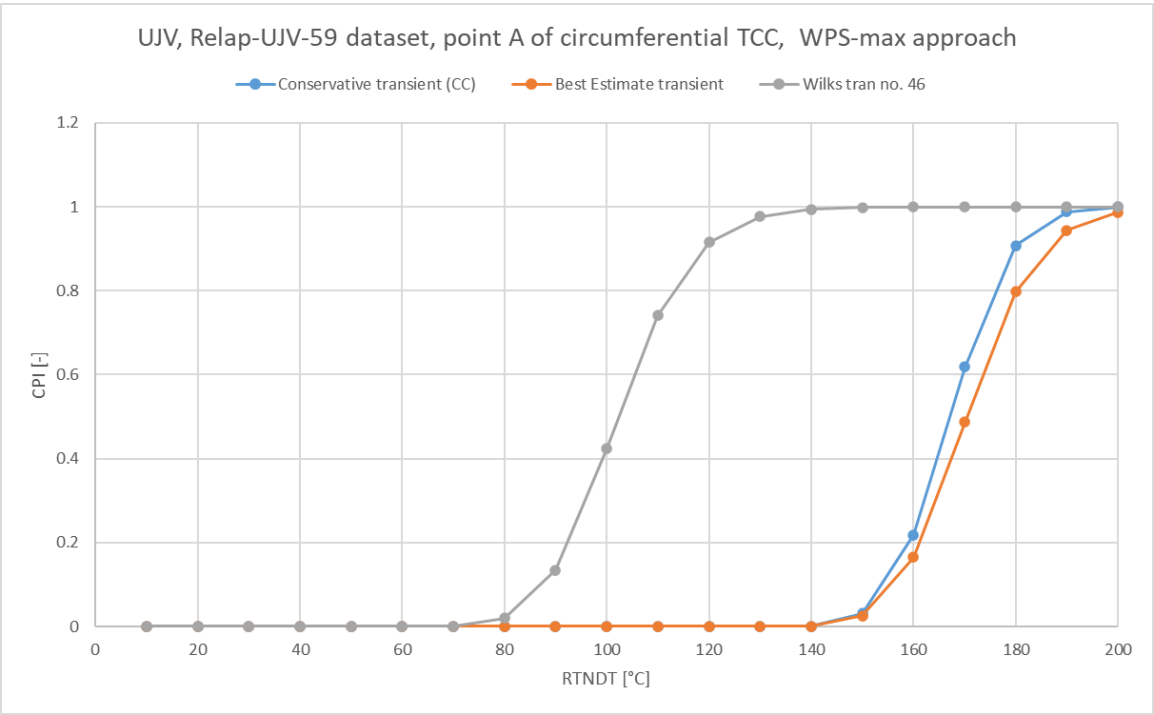

Figure 6.25: UJV results. Comparison of Conservative transient, Best Estimate transient and a transient with smallest value of max. all. ART from the UJV-59 wilks set for Max WPS approach – RT_{NDT} concept

6.2.2 Results overview for PMA2

6.2.2.1 GRS

The results provided by GRS are for TCC axial and circumferential orientation at the deepest point for the CW-IP location. The max. all. ART was evaluated with the RT_{NDT} concept for both the tangent and the Max WPS approach. The results were obtained by the FORM method. The assessed Wilks transients are the GRS transients calculated with ECC-MIX. The results for maximum allowable RVP age are shown in Figure 6.26 and their foundational CPIs are in Figure 6.27.

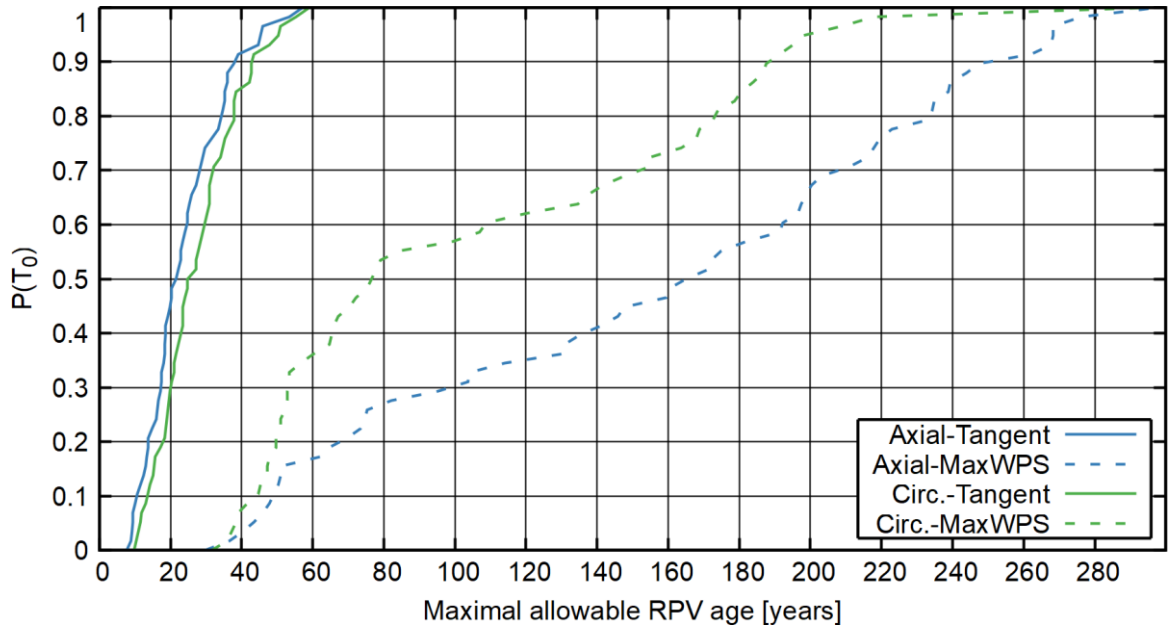

Figure 6.26: GRS results probability of max. all. RPV age – TCC, RT_{NDT} concept

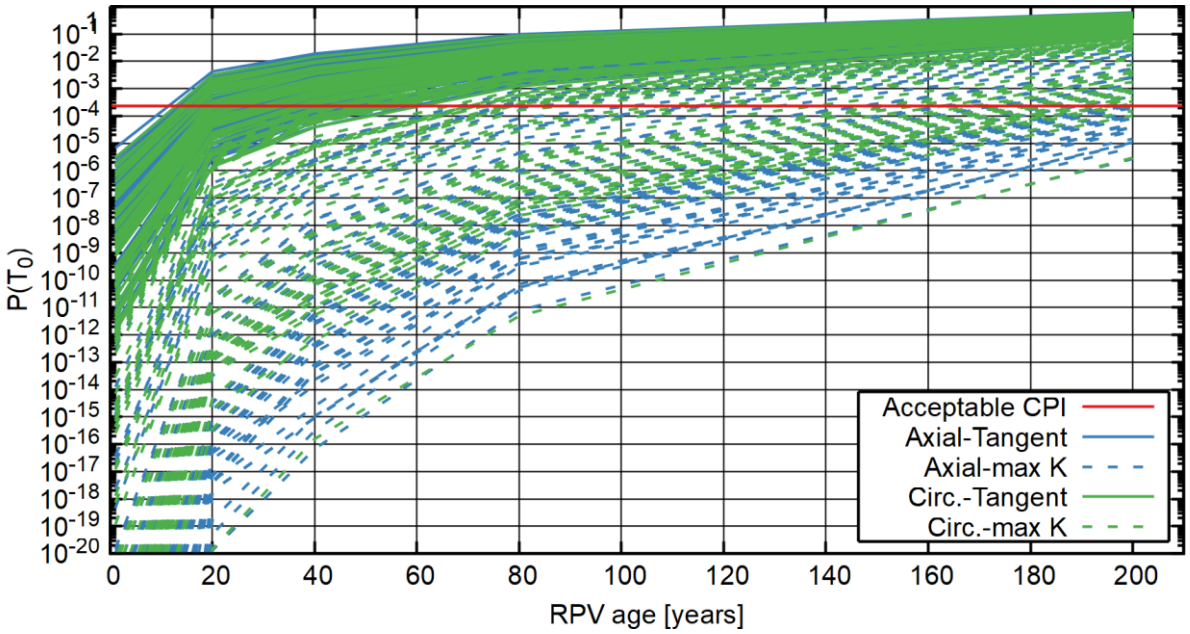

Figure 6.27: GRS results for CPI per RPV age – TCC, RT_{NDT} concept

6.2.2.2 IPP

The calculations of IPP are based on 59 transients which were generated considering the TH uncertainties. The RELAP computation by SSTC NRC was used. The calculations were performed using the IPP in-house tool SIF-Master with the SIF solutions of Marie & Chapuliot (2008) and plastic correction of Marie & Nedelec (2007). The initial data for the core weld position 95-5 inside plume are shown in Figure 6.4. The calculations for RR2 PMA2 were performed for UCC/TCC + axial/circumferential + deepest/surface point, always with WRS. The golden-section search method was used for both PMA1 and PMA2.

The results for the RT_{NDT} concept are shown in Figure 6.28, Figure 6.29, Table 6.19 and Table 6.20. The results for the Master Curve concept are shown in Figure 6.30, Table 6.21 and Table 6.22.

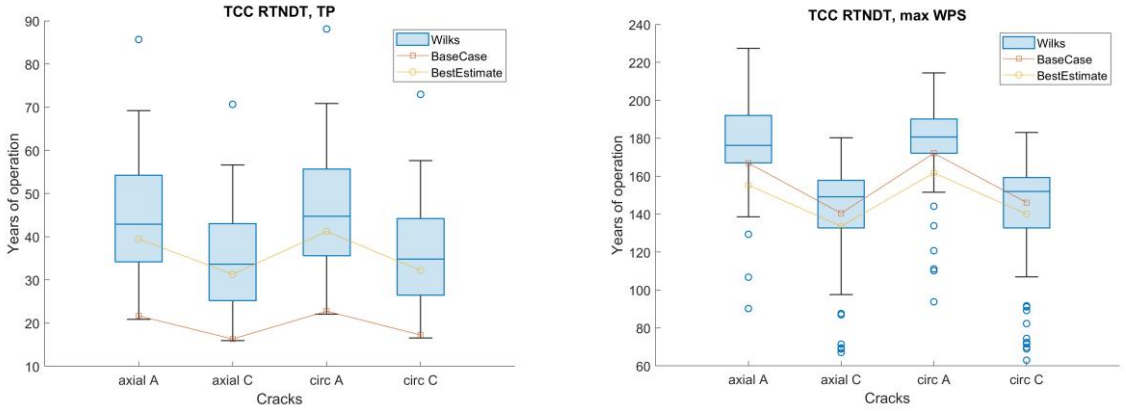

Figure 6.28: Final max. allowable RPV age results (IPP) for TCC, RT_{NDT} concept

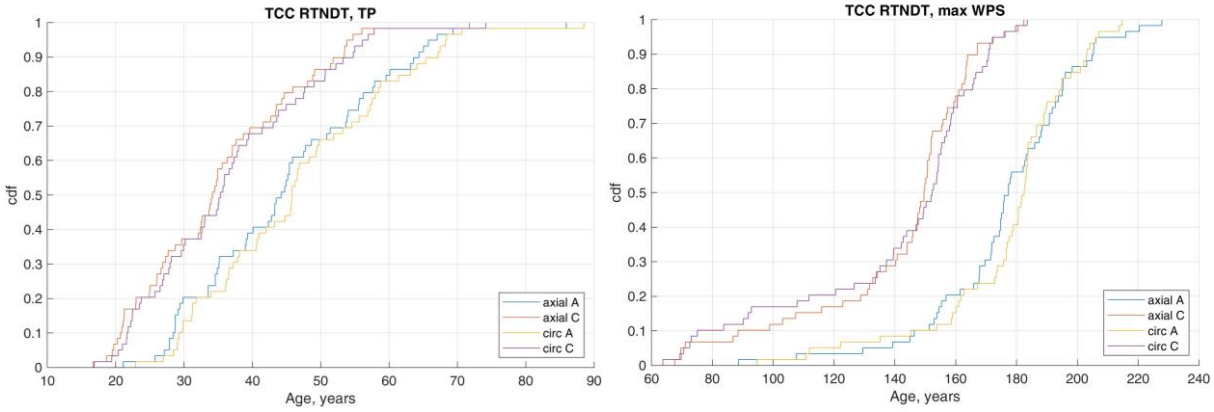

Figure 6.29: Statistical examination of final max. allowable ART results (IPP) for TCC, RT_{NDT} concept

Table 6.19: Final max. allowable RPV age results (IPP) for TCC crack, RT_{NDT} concept

	Axial Crack				Circumferential Crack			
	Deepest Point		Surface Point		Deepest Point		Surface Point	
	TP	maxWPS	TP	maxWPS	TP	maxWPS	TP	maxWPS
base case transient:	21.75	166.19	16.83	141.43	23.77	174.21	17.73	146.48
best estimate transient:	40.24	156.58	31.68	132.52	41.76	162.99	33.30	139.51
smallest value of Wilks set:	21.08	88.56	16.72	67.61	22.90	94.70	16.83	63.72
mean of Wilks set:	44.98	176.55	35.25	141.31	46.67	177.34	36.43	140.21
median from Wilks set:	44.20	177.34	34.15	149.60	45.76	182.48	35.31	152.30

Table 6.20: Final max. allowable RPV age results (IPP) for UCC crack, RT_{NDT} concept

	Axial Crack				Circumferential Crack			
	Deepest Point		Surface Point		Deepest Point		Surface Point	
	TP	maxWPS	TP	maxWPS	TP	maxWPS	TP	maxWPS
base case transient:	59.26	232.49	334.01	414.39	69.85	238.89	497.73	>500
best estimate transient:	90.61	261.71	448.92	>500	103.24	256.14	>500	>500
smallest value of Wilks set:	56.77	136.14	239.53	253.84	63.96	144.05	283.88	296.94
mean of Wilks set:	94.80	257.96	417.07	463.99	107.46	260.08	482.41	492.20
median from Wilks set:	92.84	257.76	432.08	481.95	107.60	259.16	>500	>500

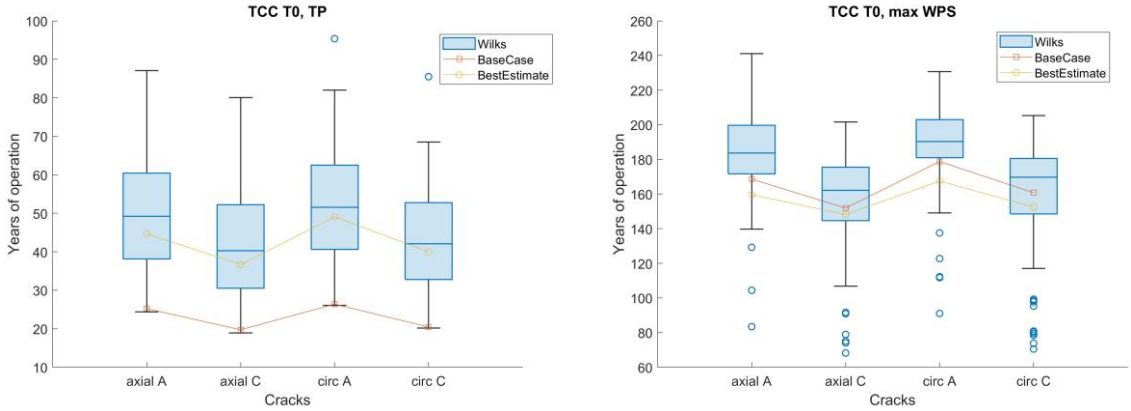

Figure 6.30: Final max. allowable RPV age results (IPP) for TCC, Master Curve concept

Table 6.21: Final max. allowable RPV age results (IPP) for TCC, Master curve concept

	Axial Crack				Circumferential Crack			
	Deepest Point		Surface Point		Deepest Point		Surface Point	
	TP	maxWPS	TP	maxWPS	TP	maxWPS	TP	maxWPS
base case transient:	26.86	170.78	21.25	157.50	28.84	179.89	22.68	162.64
best estimate transient:	47.67	161.19	40.81	146.49	51.40	165.45	39.46	156.58
smallest value of Wilks set:	25.37	85.94	20.44	70.85	27.81	93.22	22.01	69.35
mean of Wilks set:	52.55	183.98	43.62	155.73	54.45	188.27	45.63	157.10
median from Wilks set:	51.45	182.87	41.68	165.30	53.71	193.26	44.24	169.87

Table 6.22: Final max. allowable RPV age results (IPP) for UCC, Master curve concept

	Axial Crack				Circumferential Crack			
	Deepest Point		Surface Point		Deepest Point		Surface Point	
	TP	maxWPS	TP	maxWPS	TP	maxWPS	TP	maxWPS
base case transient:	80.47	267.63	231.46	459.14	90.87	274.84	292.24	>500
best estimate transient:	116.31	311.32	316.24	>500	133.39	306.61	379.64	>500
smallest value of Wilks set:	75.75	152.01	219.55	286.79	85.29	172.69	249.69	322.99
mean of Wilks set:	121.78	300.66	314.86	480.66	137.37	307.45	384.59	491.25
median from Wilks set:	118.48	300.31	316.56	499.63	136.53	307.45	392.73	>500

6.2.2.3 IRSN

The inputs used by IRSN were the 93 Wilks data sets "CW-CL-IP-180°" of Framatome and the 59 Wilks data sets CW + Base case + Conservative case + Best estimate from UJV. As for Task 4.3 RR2 the dichotomy method with precision of 0.01°C was applied. Convergence was achieved in less than 15 iterations. All results were calculated using the tangent approach.

Results based on Framatome 93 Wilks data sets

The results of IRSN for max. RPV age are shown in Figure 6.31, all the results for the Framatome Wilks data sets are given in Table 6.23.

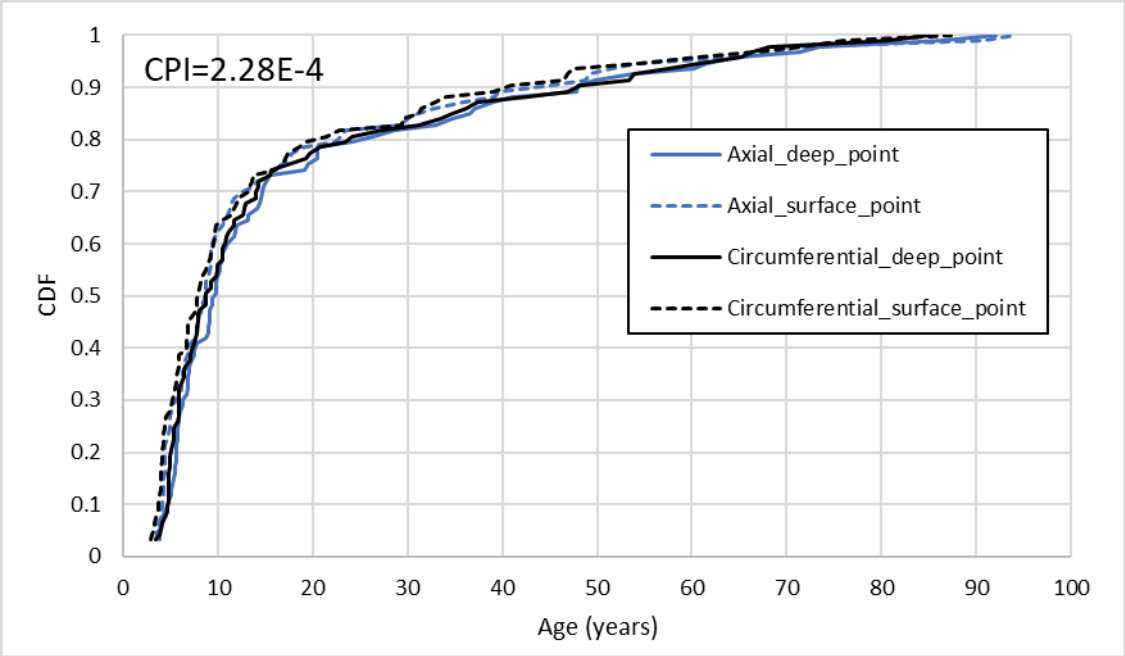

Figure 6.31: IRSN results for max. all. RPV age based on FRA 93 Wilks data sets – RT_{NDT} concept

Table 6.23: IRSN results for TCC (max. all. age, RT_{NDT}) based on FRA 93 Wilks data sets – RT_{NDT} concept

		Wilks			
		Age (years)			
		mean	min	max	cov
Axial	A	17.88	3.63	92.13	110.3%
	C	16.26	2.90	94.02	118.5%
Circ	A	17.07	2.90	84.87	111.3%
	C	15.35	2.41	87.31	117.3%

Results based on UJV 59 Wilks data sets + BC/CONS/BE

The results of IRSN for max. RPV age based on the UJV Wilks data sets are shown in Figure 6.32, all the results for the UJV Wilks data sets are given in Table 6.24.

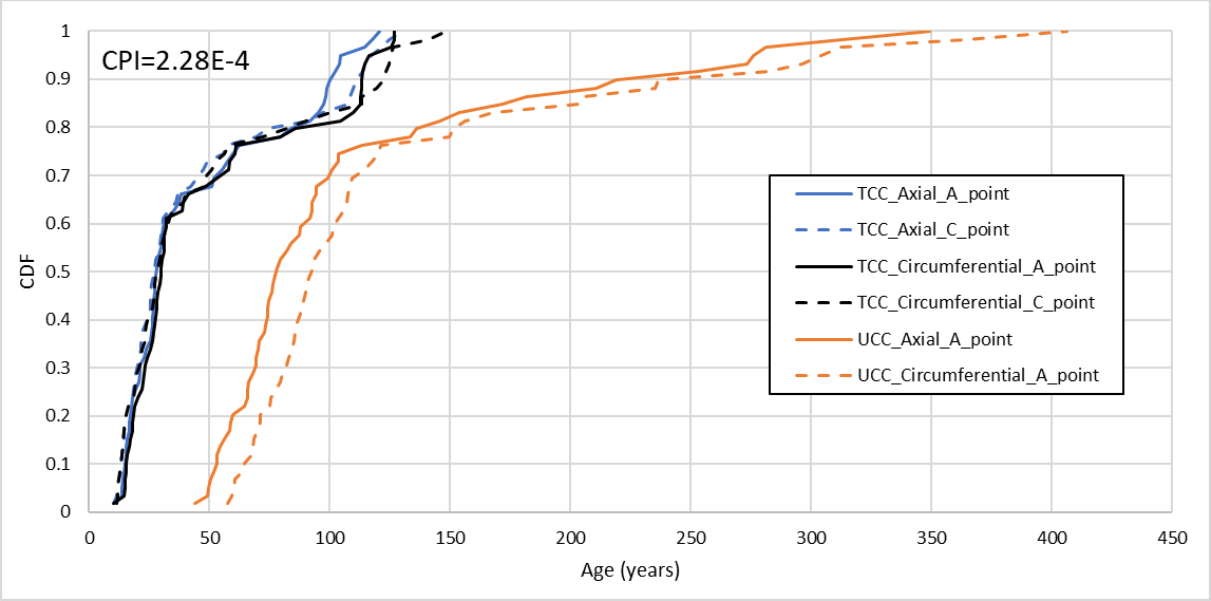

Figure 6.32: IRSN results for max. all. RPV age based on UJV 59 Wilks data sets – RT_{NDT} concept

Table 6.24: IRSN results for TCC and UCC (max. all. age, RT_{NDT}) based on UJV 59 Wilks data sets – RT_{NDT} concept

			Wilks			
			Age (years)			
			mean	min	max	cov
TCC	Axial	A	44.93	10.47	120.51	75.41%
		C	44.68	10.04	130.16	83.26%
	Circ	A	48.35	10.22	126.92	77.95%
		C	47.32	11.69	148.29	85.86%
UCC	Axial	A	108.99	43.91	349.40	66.90%
		C	-	-	-	-
	Circ	A	125.16	57.59	406.22	64.45%
		C	-	-	-	-

6.2.2.4 JSI

The same explanation of the JSI calculations for PMA1 given in chapter 6.2.1.6 applies here for PMA2. The results with tangent and Max WPS approaches for the two Wilks' sets (59 and 130 samples) and the three ART concepts are shown in Figure 6.33 to Figure 6.36. An overview of all results is given in Table 6.25.

In the figures, lines correspond to CPI results for given Age, and the points correspond to Age results for the given CPI-target (2.28E-4). JSI used a 1-year accuracy in the search for Age given CPI-target, assuming age >0. Lower accuracy could improve the match of CPI-target by some of the samples, as seen by the Age results (dots) away from target. However, it is also worth mentioning that the fluctuations in the curves (CPI not monotonically increasing for increasing Age) observed in Figure 6.33 to Figure 6.36 possibly reflect a not fully converged CPI obtained with 2000 and 1000 Monte Carlo trials, respectively, for the RT_{NDT} and Master Curve approaches. For JSI, the distributed fracture toughness (K_{IC}) does not affect convergence since, for given ART, the cpi(t) is obtained directly from the CDF of the distributed KIC (without Monte Carlo). The fluctuations in these curves, and therefore convergence, are only affected by the other distributed parameters (ART, fluence, weld chemical composition dictating ART shift), which could be suppressed with higher number of trials.

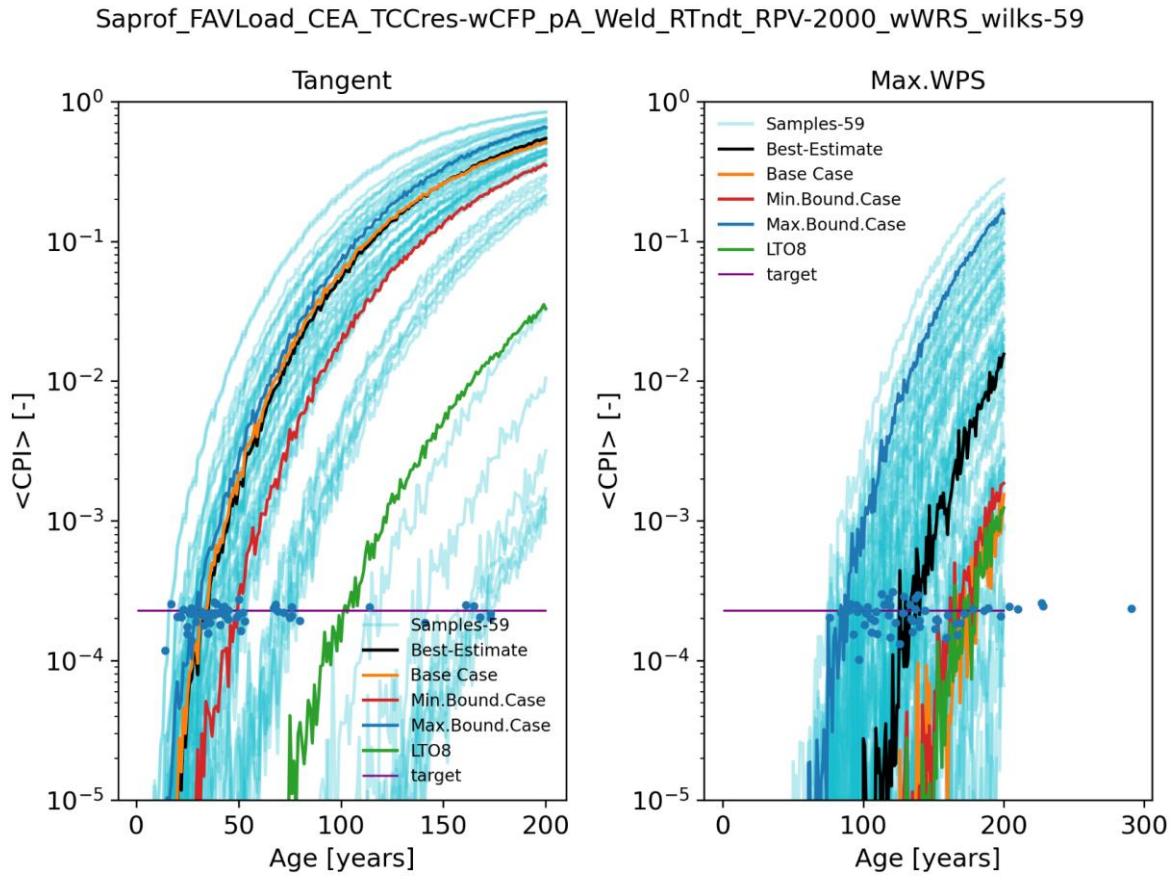

Figure 6.33: JSI results for Wilks-59 – ASME RT_{NDT} concept

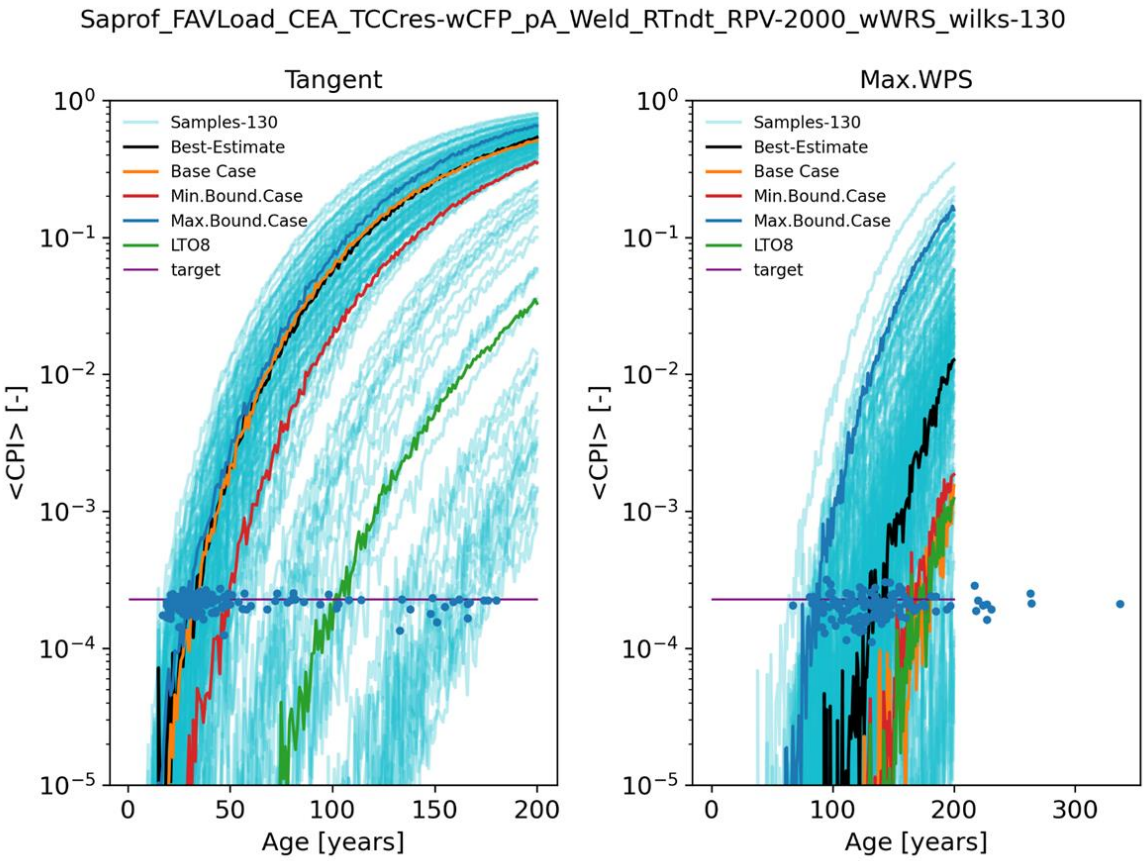

Figure 6.34: JSI results for Wilks-130 – ASME RT_{NDT} concept

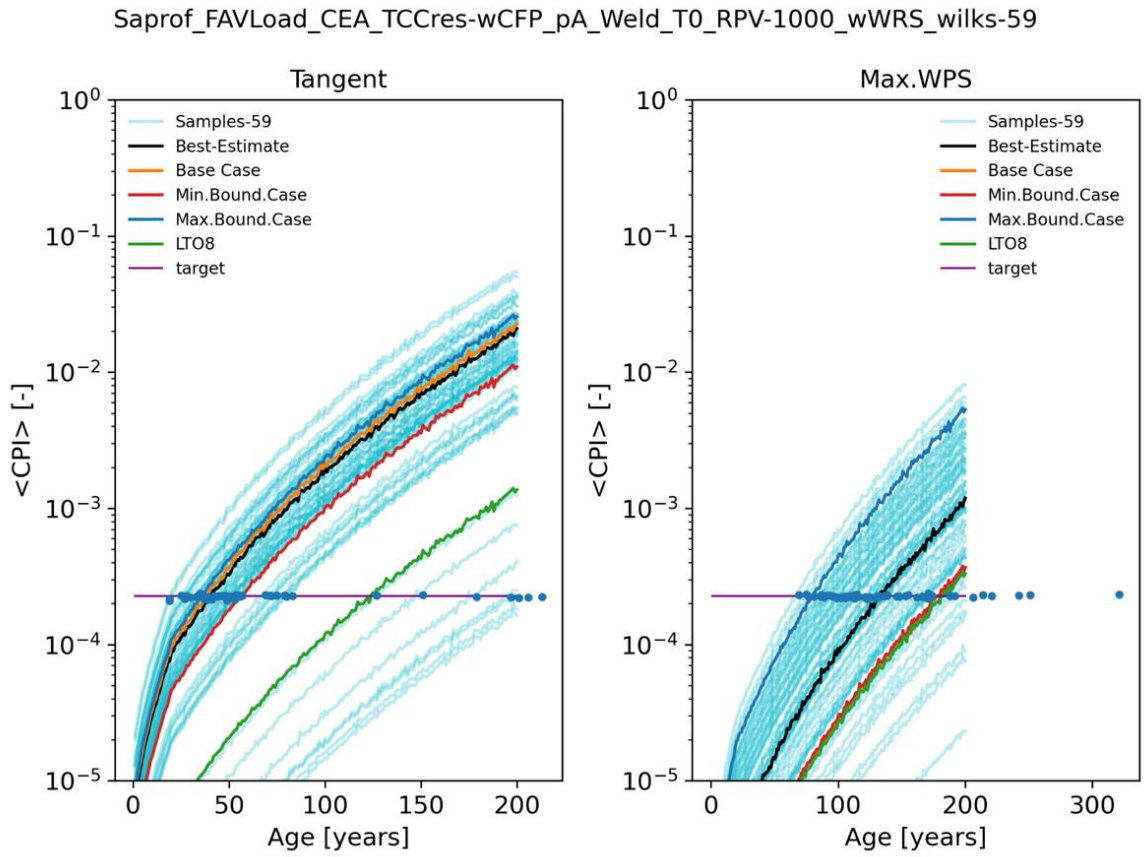

Figure 6.35: JSI results for Wilks-59 – MC-T_0 concept

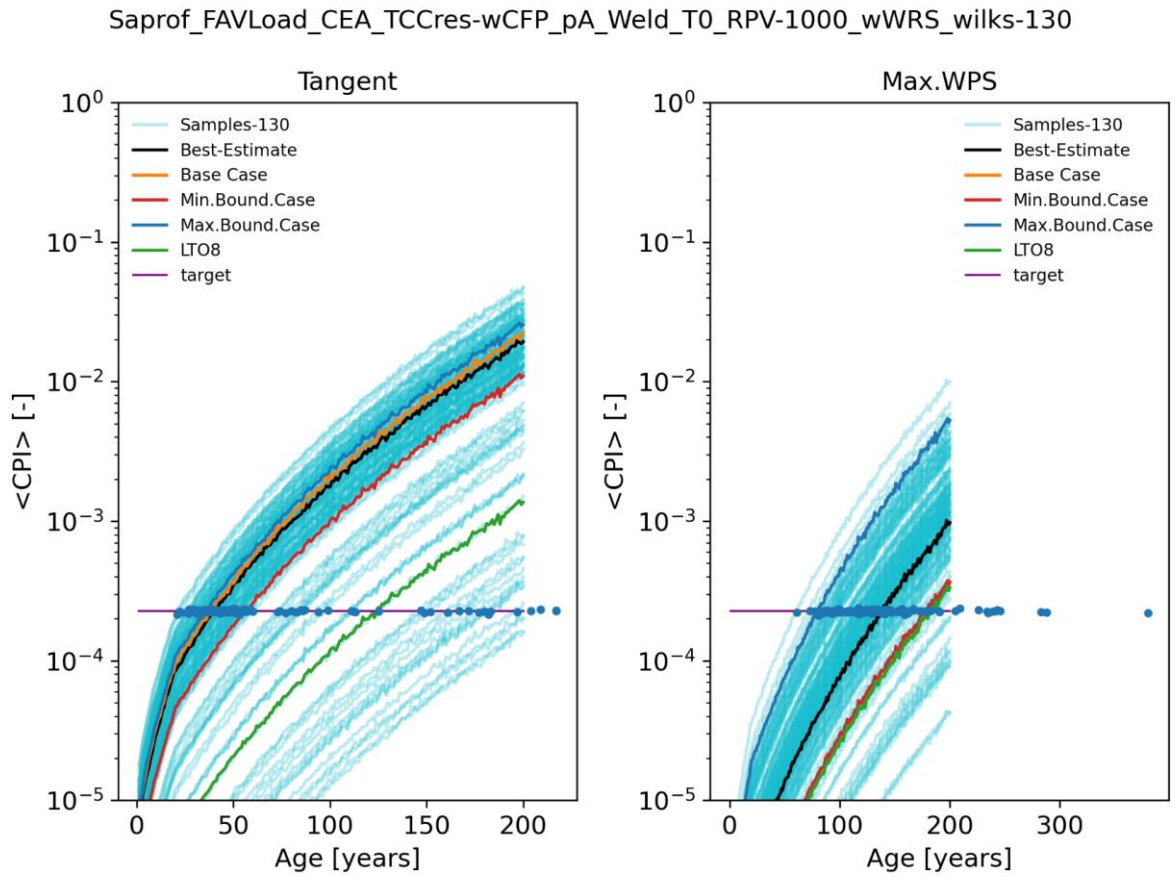

Figure 6.36: JSI results for Wilks-130 – MC-T_0 concept

Table 6.25: JSI statistics obtained from the distribution of max. all. RPV age results

	Tangent		Max.WPS	
	Age final ASME	Age final MC-T_0	Age final ASME	Age final MC-T_0
	wilks-59			
mean	54	63	136	135
std	42	48	42	48
min	14	19	76	69
95%	21	27	90	81
50%	39	49	128	129
5%	165	197	212	223
max	173	213	291	321
Best-Est.59	31	42	140	136
	wilks-130			
mean	54	63	138	138
std	42	47	40	47
min	17	21	67	61
95%	21	27	91	85
50%	37	45	135	132
5%	161	181	222	237
max	180	217	337	380
Best-Est.130	32	41	141	140
	other			
Base Case	31	39	175	185
Min.Bound.	49	57	178	181
Max.Bound.	29	37	89	82
LTO8	102	127	178	185

6.2.2.5 KIWA

The results of KIWA include TCC and UCC, circumferential and axial orientation, deepest point and interface point. The results were evaluated with the RT_{NDT} concept for both the tangent and the Max WPS approach. The PMA2 results are shown in Figure 6.37 and Figure 6.38. The exact values of all results are given in Table 6.26.

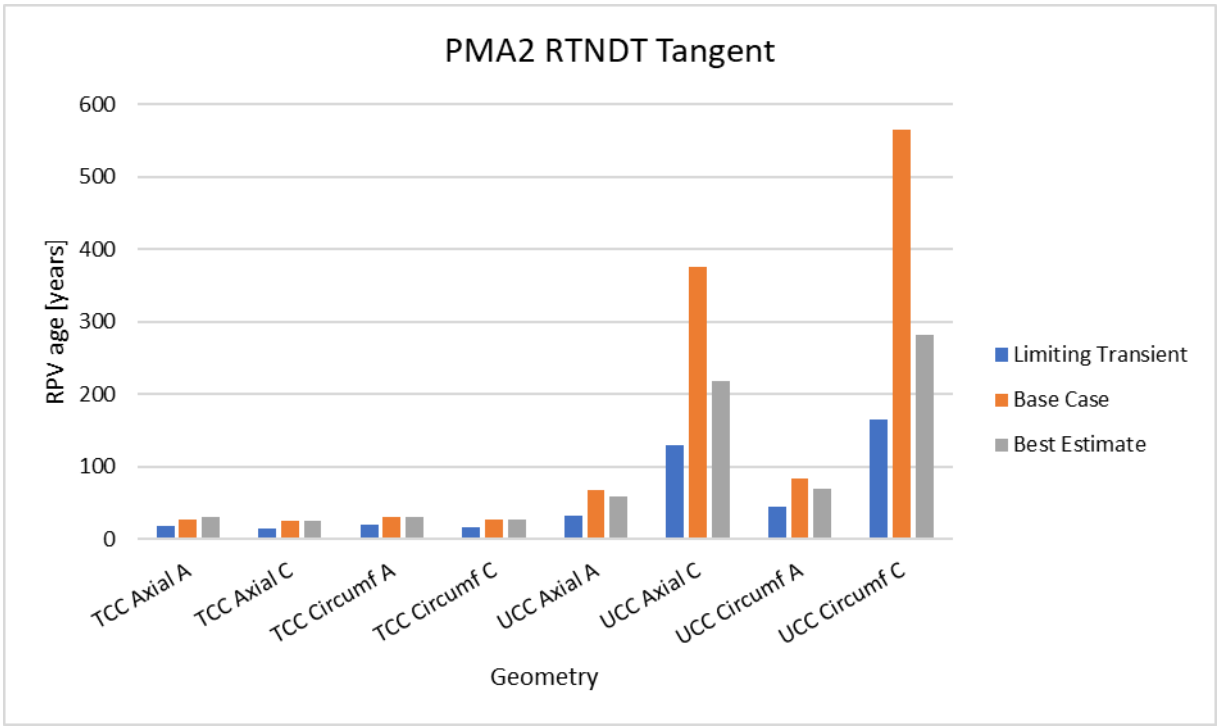

Figure 6.37: KIWA results for max. all. RPV age tangent approach – RT_{NDT} concept

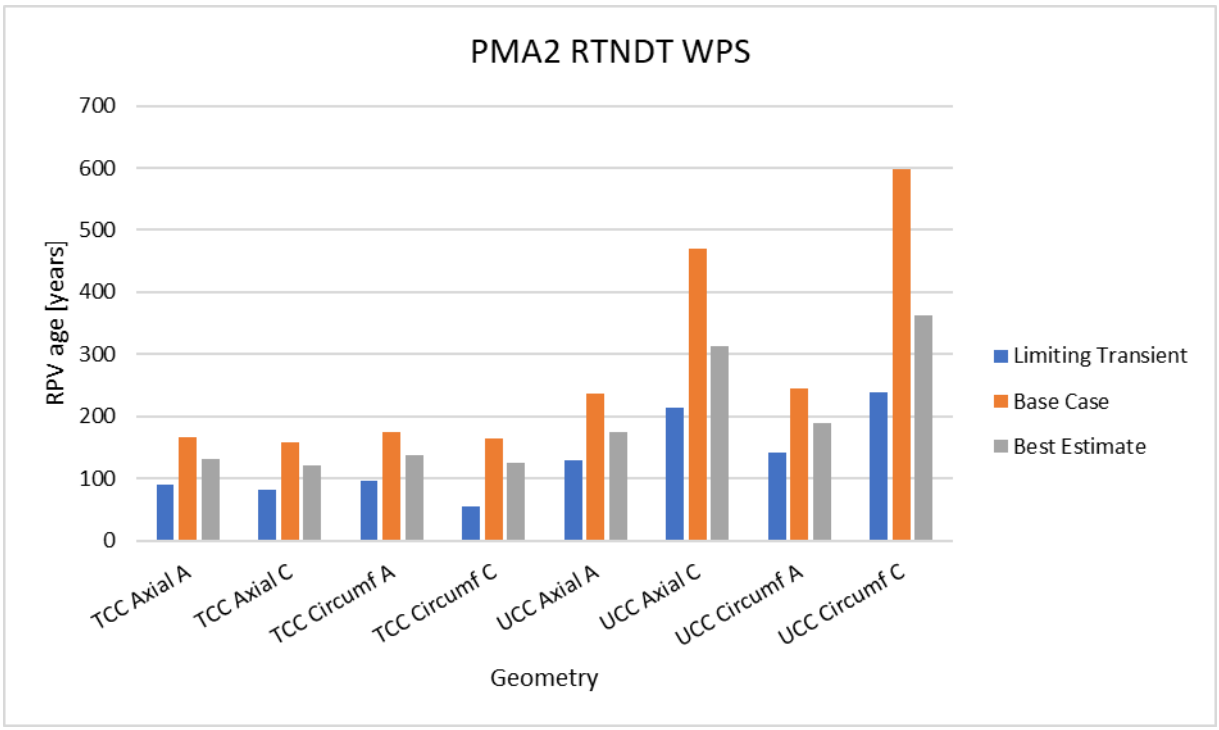

Figure 6.38: KIWA results for max. all. RPV age Max WPS approach – RT_{NDT} concept

Table 6.26: KIWA summary of PMA2 results – max. all. RPV age (years)

Name	Margin Approach	Concept	Limit Condition	RPV age	Limiting Transient	Base Case	Best Estimate
TCC Axial A	PMA2	RT_{NDT}	Tangent	17.8	w45_wrs	27.3	29.9
TCC Axial C	PMA2	RT_{NDT}	Tangent	15.2	w14_wrs	25.8	26.1
TCC Circ A	PMA2	RT_{NDT}	Tangent	19.4	w14_wrs	30.6	31.1
TCC Circ C	PMA2	RT_{NDT}	Tangent	16.1	w14_wrs	26.5	27.9
UCC Axial A	PMA2	RT_{NDT}	Tangent	33.1	w35_wrs	67.6	59.3
UCC Axial C	PMA2	RT_{NDT}	Tangent	130.1	w17_wrs	376.4	217.4
UCC Circ A	PMA2	RT_{NDT}	Tangent	45.5	w2_wrs	83.8	69.2
UCC Circ C	PMA2	RT_{NDT}	Tangent	164.8	w1_wrs	564.4	282.5
TCC Axial A	PMA2	RT_{NDT}	max. WPS	90.9	w33_wrs	166.5	130.8
TCC Axial C	PMA2	RT_{NDT}	max. WPS	81.4	w33_wrs	159.1	120.2
TCC Circ A	PMA2	RT_{NDT}	max. WPS	96.3	w33_wrs	174.3	137.6
TCC Circ C	PMA2	RT_{NDT}	max. WPS	54.9	w49_wrs	164.8	124.7
UCC Axial A	PMA2	RT_{NDT}	max. WPS	129.6	w17_wrs	236.5	174.1
UCC Axial C	PMA2	RT_{NDT}	max. WPS	213.9	w17_wrs	470.4	312.6
UCC Circ A	PMA2	RT_{NDT}	max. WPS	140.9	w17_wrs	244.6	189.7
UCC Circ C	PMA2	RT_{NDT}	max. WPS	237.8	w17_wrs	598.6	363.0

6.2.2.6 UJV

The assessed cases for UJV include TCC circumferential orientation at the deepest point for the CW-CL location. The results were evaluated with the RT_{NDT} concept for both the tangent and the Max WPS approach. An overview of the results for max. all. RPV age is given in Table 6.27.
The assessed Wilks transients are the UJV-59 transients calculated by RELAP. The full Wilks data set was analysed, and the lowest max. all. ART was taken as resulting 95% quantile.

The empirical CDF of RPV lifetime for PMA2 is shown in Figure 6.39 and Figure 6.40. for the tangent and Max WPS approach, respectively. The dependence of CPI on RPV lifetime for all analysed TH transients is shown in Figure 6.41 and Figure 6.42 for the tangent and Max WPS approach, respectively.

Table 6.27: Overview of UJV results for max. all. RPV age in years – TCC circumferential, RT_{NDT} concept

	Base Case	Best Estimate	Conservative	95% quantile
Tangent	27.4	47.2	21.8	20.6
Max WPS	218.6	204.0	201.5	40.7

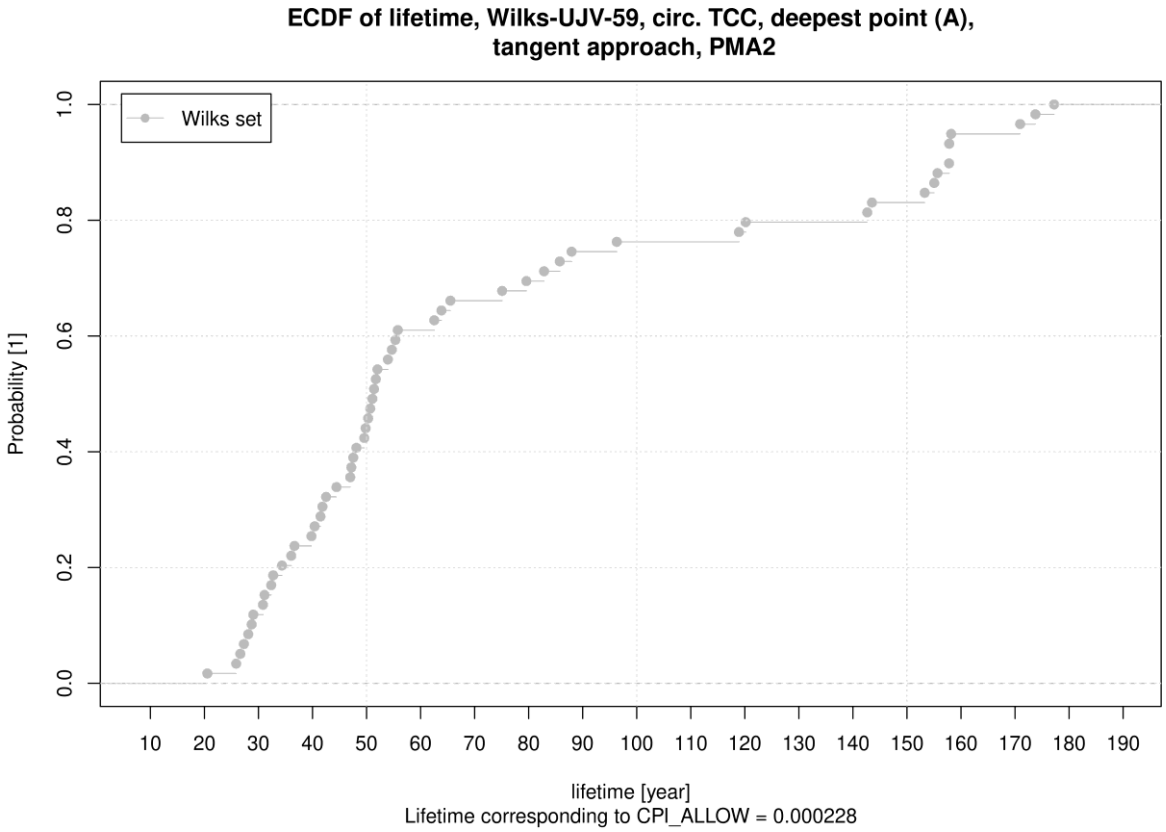

Figure 6.39: UJV results. Empirical cumulative distribution function of RPV lifetime for Relap-UJV-59 dataset, tangent approach, RT_{NDT} concept.

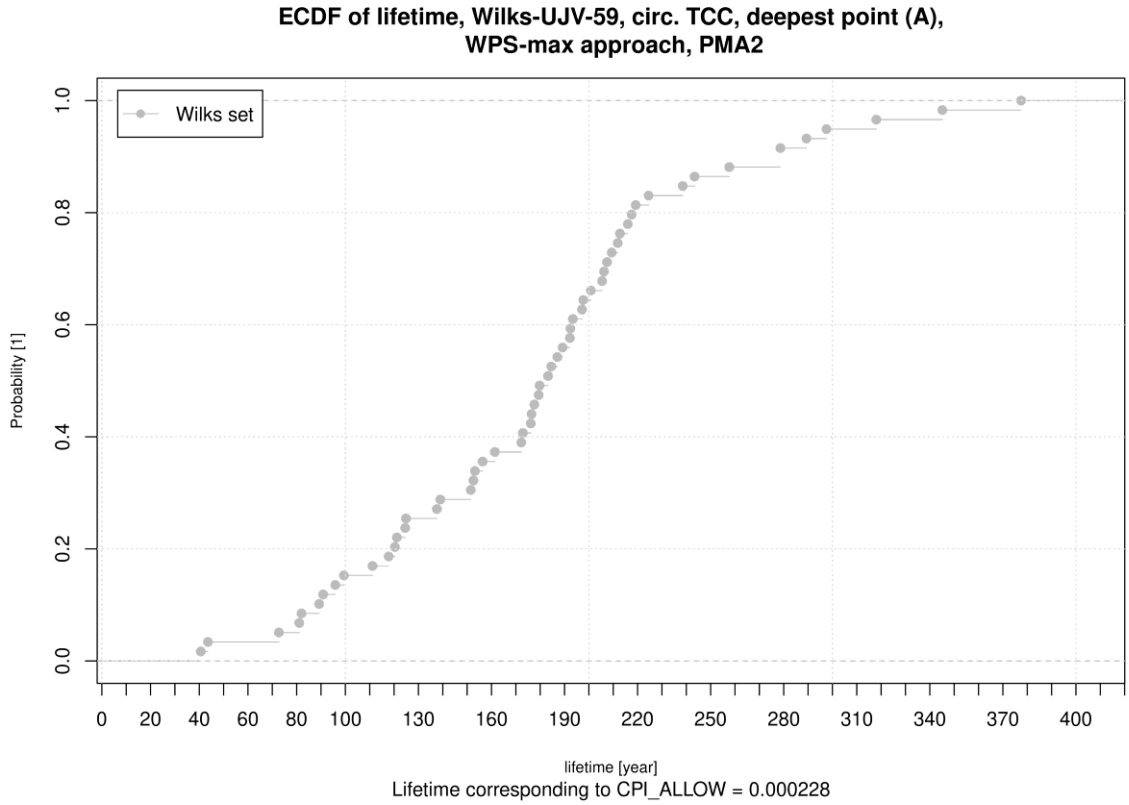

Figure 6.40: UJV results. Empirical cumulative distribution function of RPV lifetime for Relap-UJV-59 dataset, Max WPS approach, RT_{NDT} concept.

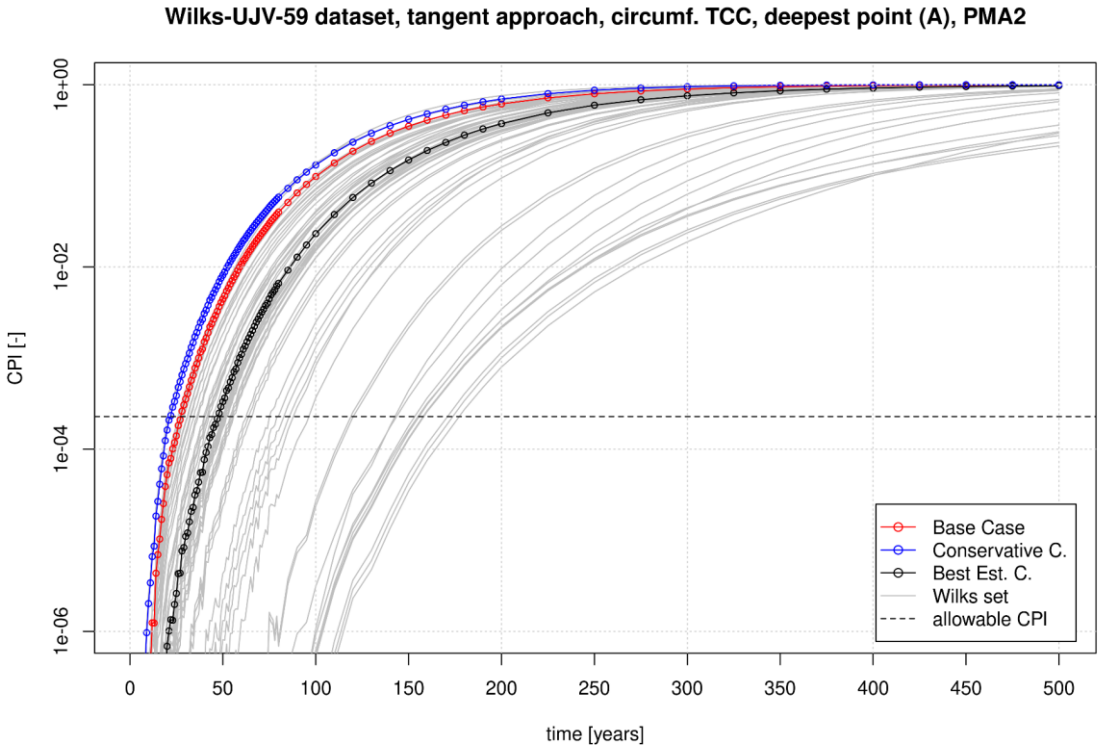

Figure 6.41: UJV results. CPI dependence on RPV lifetime for Base Case, Conservative Case, Best Estimate transient and for all transients from Relap-UJV-59 Wilks set. Tangent approach, RT_{NDT} concept.

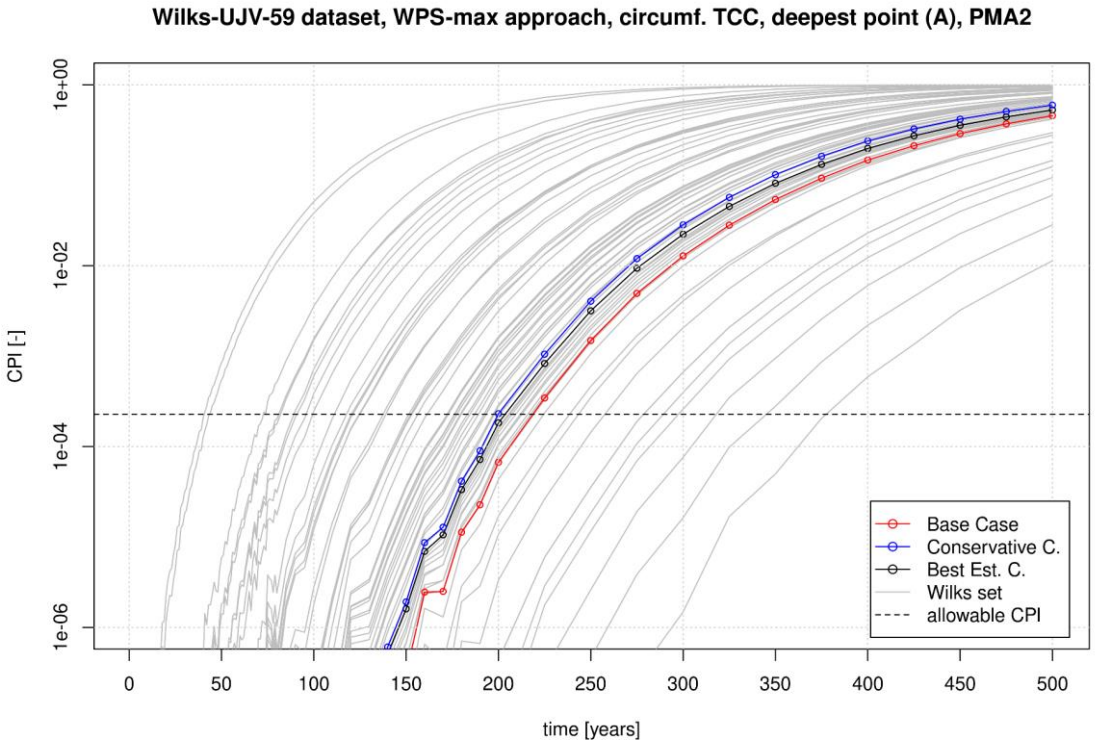

Figure 6.42: UJV results. CPI dependence on RPV lifetime for Base Case, Conservative Case, Best Estimate transient and for all transients from Relap-UJV-59 Wilks set. Max WPS approach, RT_{NDT} concept.

6.2.3 Plausibility checks

In Figure 6.43 the results for max. all. ART (PMA1) for the base-case and best-estimate transient are shown for each partner. In the plot only the results for TCC circumferential at the deepest point for the RT_{NDT} concept are included. The results of all partners are consistent regarding the following aspects: The results for the Max WPS approach are always higher than the results for the tangent approach. Also, the results are in the same order of magnitude for the same cases.
Further results (quantiles, mean and median) are summarised in Table 6.28.

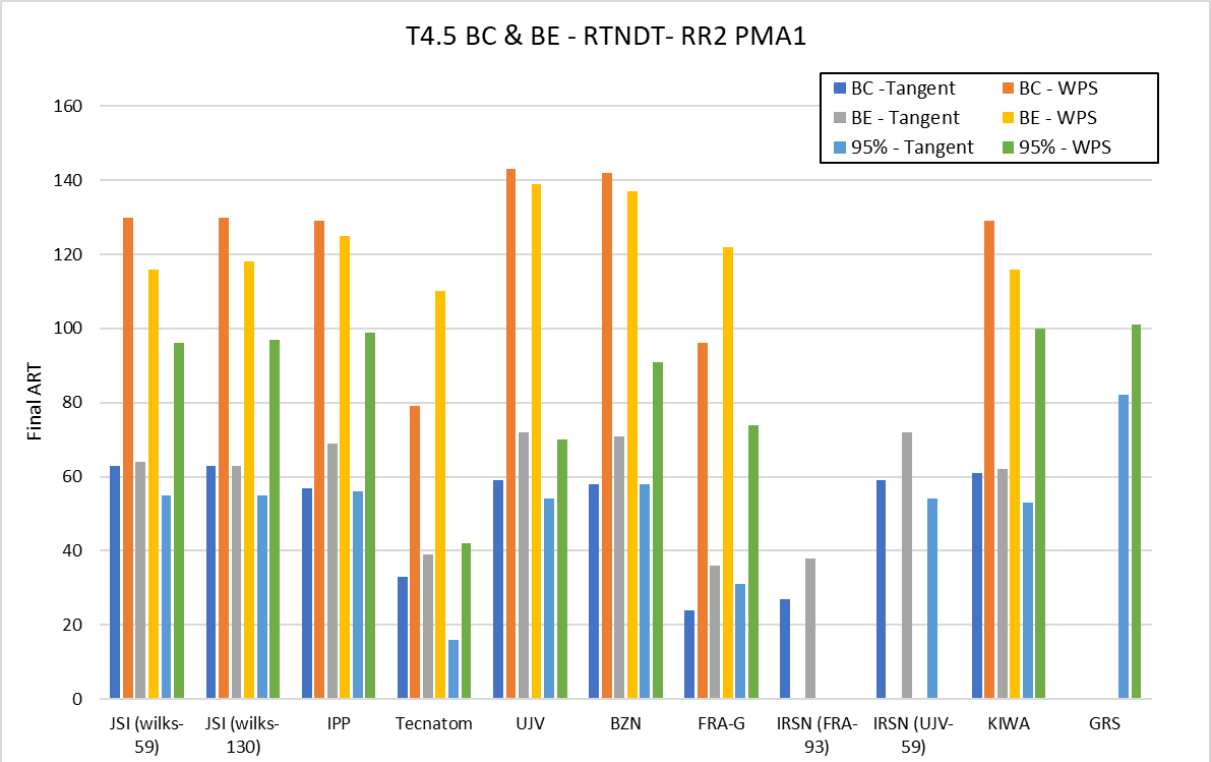

Figure 6.43: Summary of Base Case, Best Estimate and 95%-Quantile results for TCC circumferential at the deepest point, PMA1, RT_{NDT} concept

Table 6.28: Overview of all results for max. all. ART in °C for TCC circumferential deepest point PMA1, RT_{NDT} concept

	Base Case		Best Estimate		95%-Quantile		5%-Quantile		Mean		Median	
	Tang-ent	WPS	Tang-ent	WPS	Tang-ent	WPS	Tang-ent	WPS	Tang-ent	WPS	Tang-ent	WPS
JSI (wilks-59)	63	130	64	116	55	96	121	140	74	114	68	112
JSI (wilks-130)	63	130	63	118	55	97	121	144	75	115	67	114
IPP	57	129	69	125	56	99	93	142	71	130	71	132
Tecnatom	33	79	39	110	16	42						
UJV	59	143	72	139	54	70	123	184				
BZN	58	142	71	137	58	91						
FRA-G	24	96	36	122	31	74						
IRSN (FRA-93)	27		38								56	
IRSN (UJV-59)	59		72		54		119				80	
KIWA	61	129	62	116	53	100	72	155	63	117	62	116
GRS					82	101	116	166				

The comparison of the CPIs for TCC circumferential, deepest point, RT_{NDT} concept, for the best estimate and base case transients in dependency on ART for each partner is shown in Figure 6.44 for the tangent approach and in Figure 6.46 for the Max WPS approach. For an easier comparison with the max. all. CPI the plots are also presented with logarithmic scaling in Figure 6.45 and Figure 6.47.

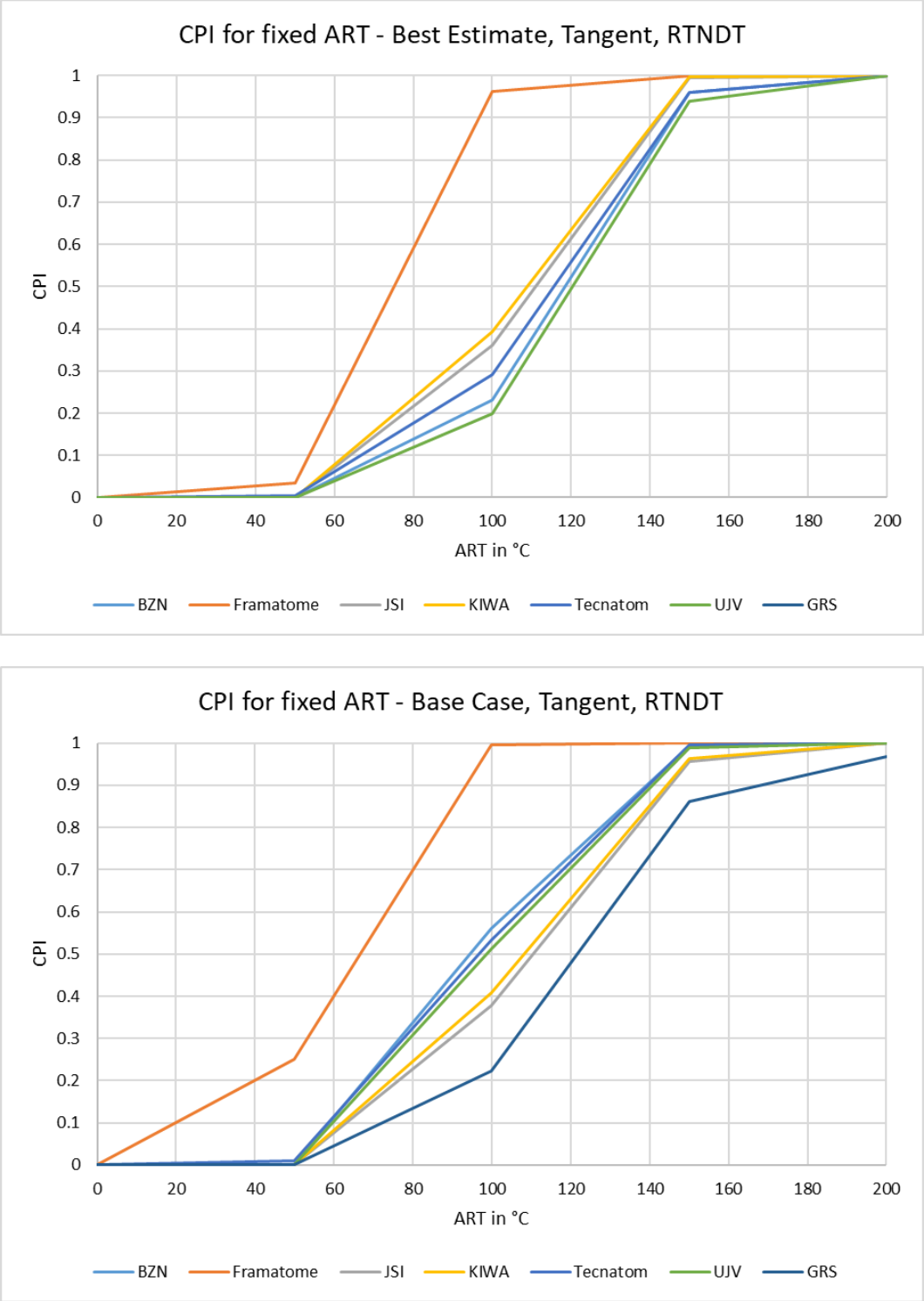

Figure 6.44: CPI in dependency of ART – TCC circumferential, deepest point, tangent approach, RT_{NDT} concept

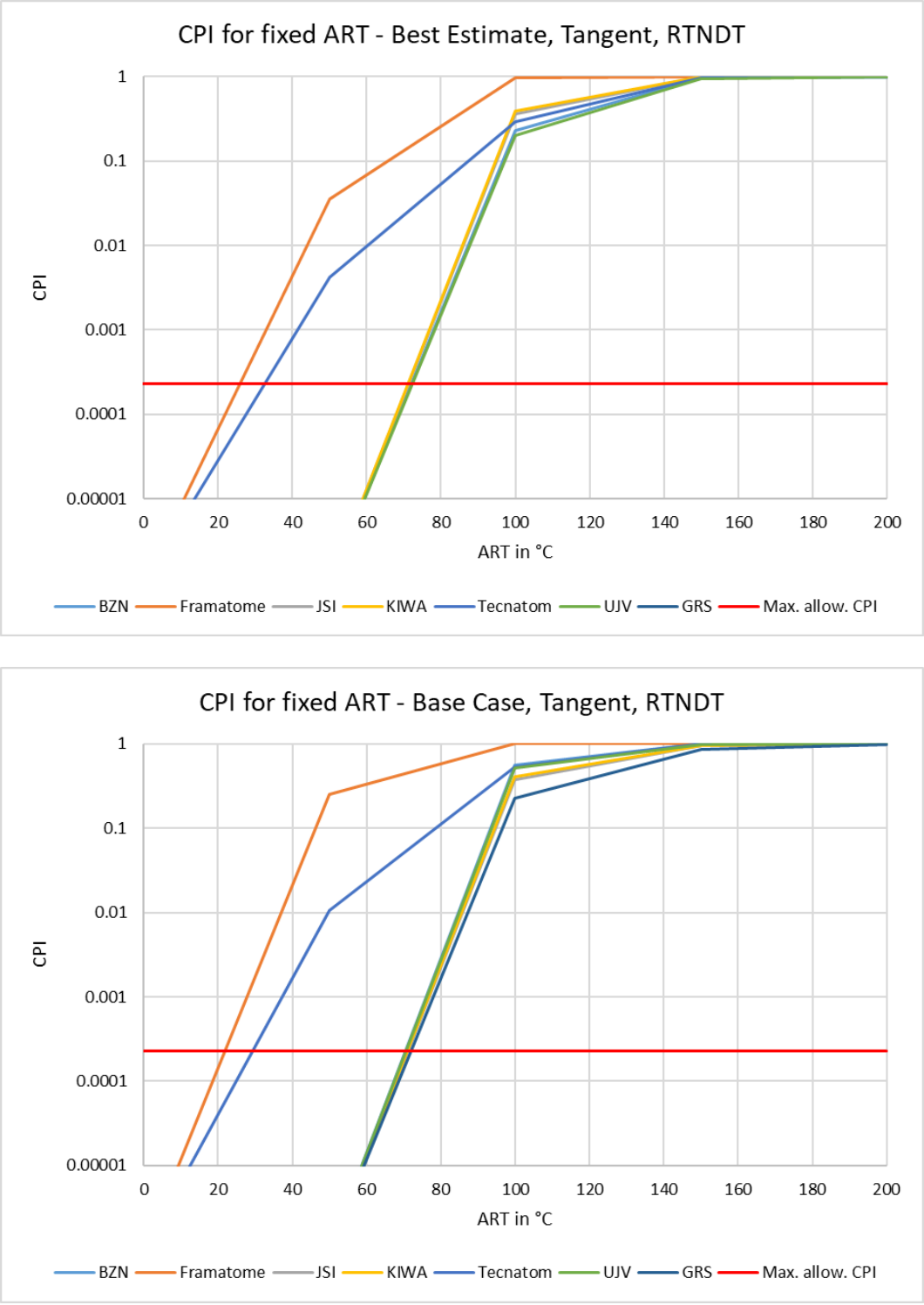

Figure 6.45: CPI in dependency on ART – TCC circumferential deepest point, tangent approach, RT_{NDT} concept (logarithmic)

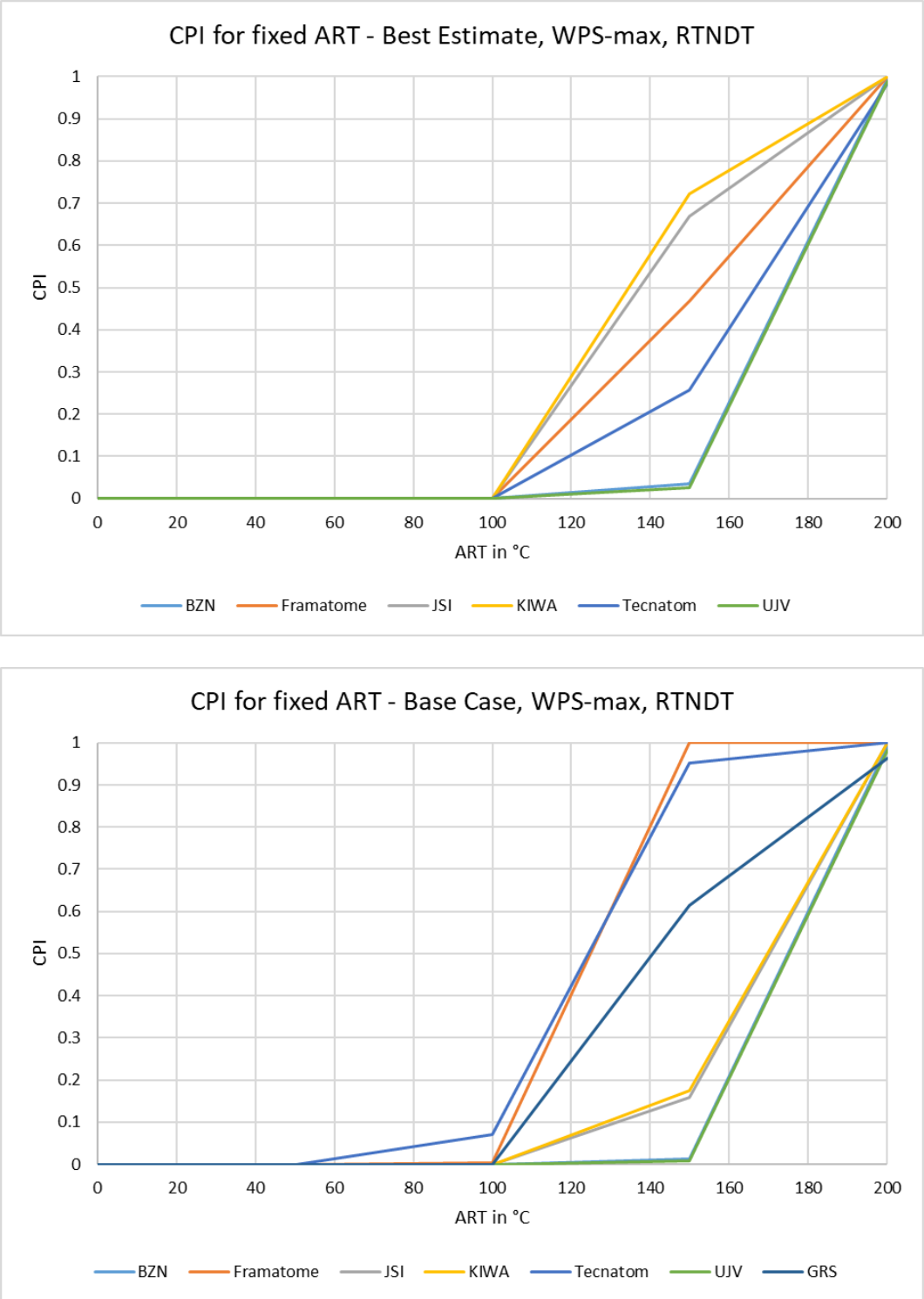

Figure 6.46: CPI in dependency on ART – TCC circumferential deepest point, Max WPS approach, RT_{NDT} concept

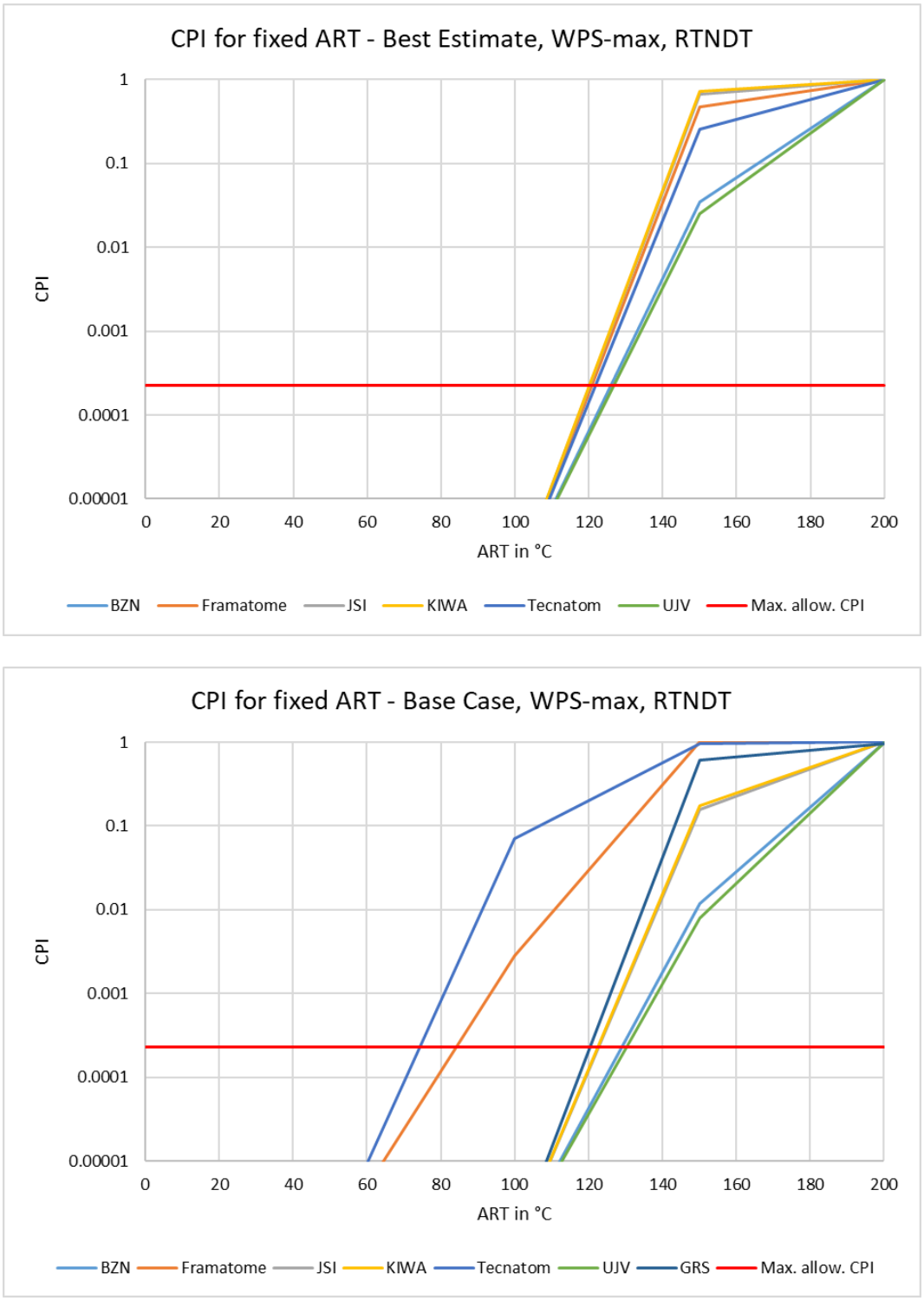

Figure 6.47: CPI in dependency on ART – TCC circumferential deepest point, Max WPS approach, RT_{NDT} concept (logarithmic)

Some partners also evaluated the Master Curve concept. These results are shown in Figure 6.48 and are listed in Table 6.29.

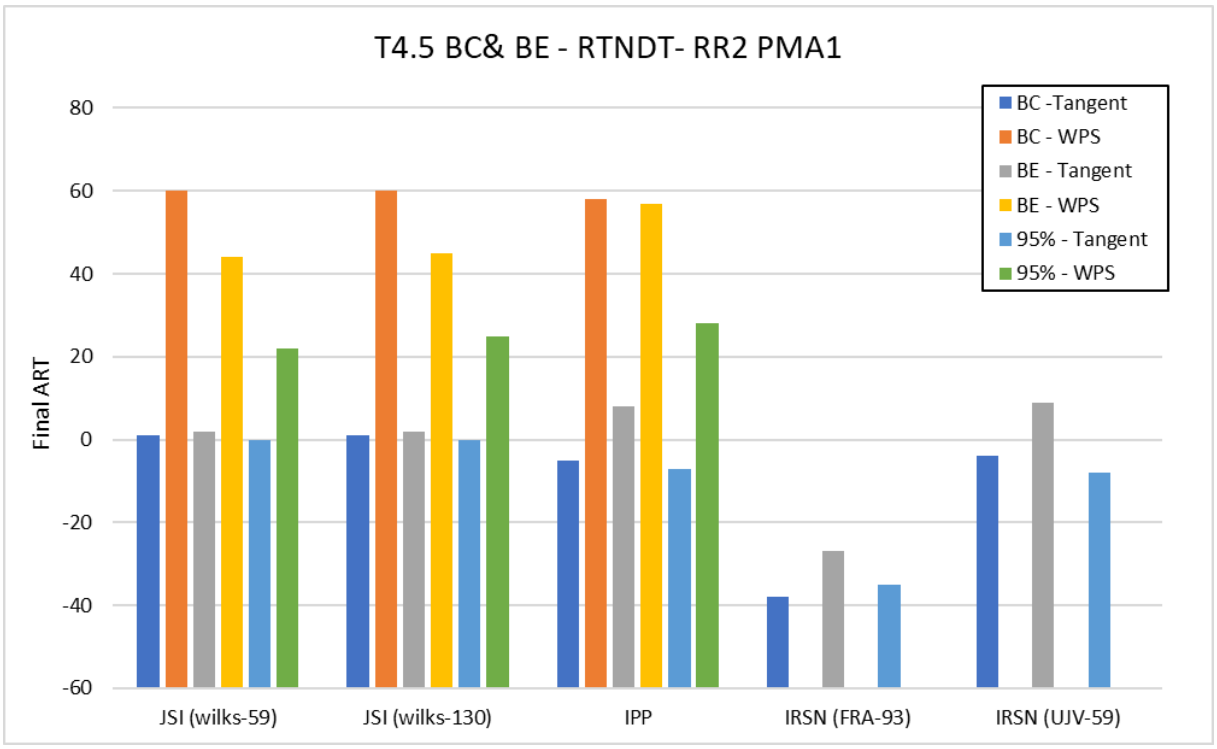

Figure 6.48: Summary of Base Case, Best Estimate and 95%-Quantile results for TCC circumferential, deepest point, PMA1, T_0 (Master Curve) concept

Table 6.29: Overview of results for max. all. ART in °C for TCC circumferential deepest point PMA1, T_0 (Master Curve) concept

	Base Case		Best Estimate		95%-Quantile		5%-Quantile		Mean		Median	
	Tang-ent	WPS	Tang-ent	WPS	Tang-ent	WPS	Tang-ent	WPS	Tang-ent	WPS	Tang-ent	WPS
JSI (wilks-59)	1	60	2	44	0	22	64	71	13	43	7	42
JSI (wilks-130)	1	60	2	45	0	25	59	76	13	44	4	42
IPP	-5	58	8	57	-7	28	28	74	9	61	9	62
IRSN (FRA-93)	-38		-27		-35		38		-12		-17	
IRSN (UJV-59)	-4		9		-8		69		20		11	

In Figure 6.49 the results for max. all. RPV age (PMA2) for the base-case, best-estimate, and 95%-Quantile transient are shown for each partner for the ASME RT_{NDT} concept. The results for the Master Curve concept are shown in Figure 6.50. In the plots only the results for TCC circumferential at the deepest point are included.

The results of all partners are consistent regarding the following aspects: The results for the Max WPS approach are always higher than the results with the tangent approach. Also, the results are in the same order of magnitude for the same cases. Further results (quantiles, mean and median) are summarised in Table 6.30 for ASME RT_{NDT} concept and in Table 6.31 for the Master Curve concept.

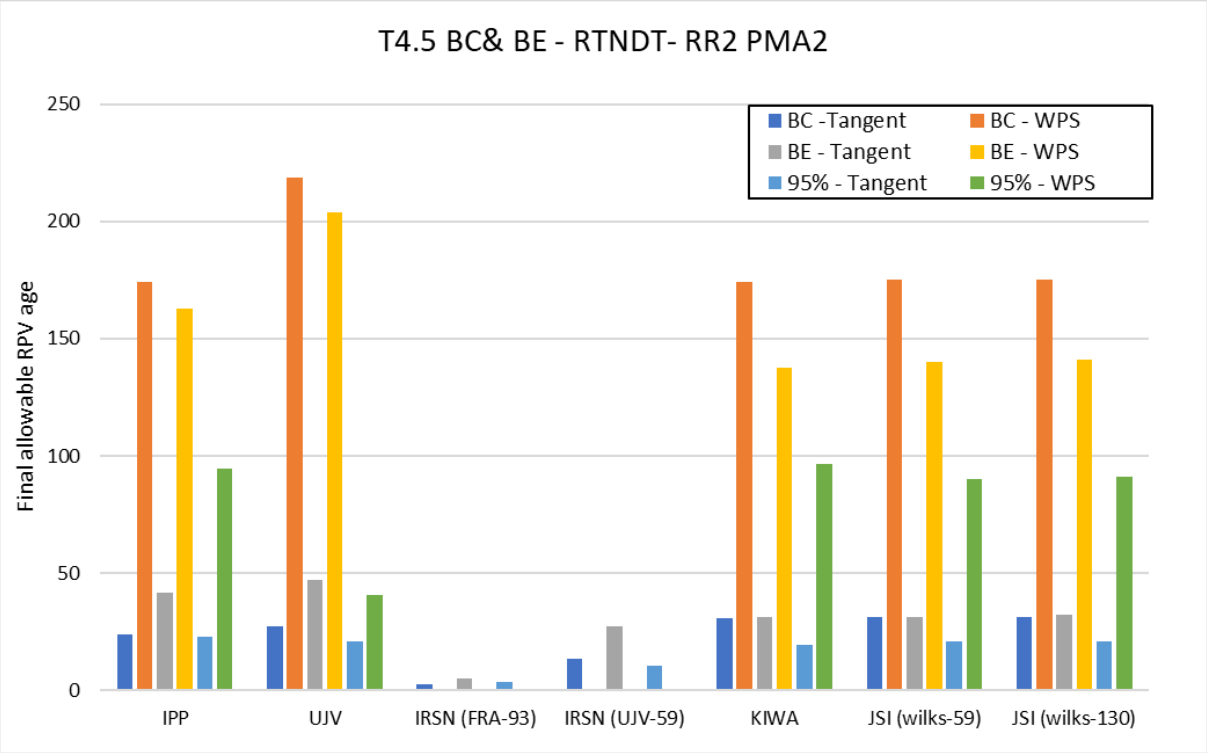

Figure 6.49: Summary of Base Case, Best Estimate and 95%-Quantile results for TCC circumferential deepest point PMA2 – RT_{NDT} concept

Table 6.30: Overview of results for max. all. RPV age for TCC circumferential, deepest point, PMA2 – RT_{NDT} concept

	Base Case		Best Estimate		95%-Quantile		5%-Quantile		Mean		Median	
	Tang-ent	WPS	Tang-ent	WPS	Tang-ent	WPS	Tang-ent	WPS	Tang-ent	WPS	Tang-ent	WPS
IPP	23.8	174.2	41.8	163	22.9	94.7			46.7	177.3	45.8	182.5
UJV	27.4	218.6	47.2	204	20.6	40.7	177.2	377.5	73.4	180.9	51.4	183.2
IRSN (FRA-93)	2.6		4.8		3.4		80.7		17.1		8.7	
IRSN (UJV-59)	13.6		27		10.2		126.9		29.9		48.4	
KIWA	30.6	174.3	31.1	137.6	19.4	96.3						
JSI (wilks-59)	31	175	31	140	21	90	165	212	54	136	39	128
JSI (wilks-130)	31	175	32	141	21	91	161	222	54	138	37	135

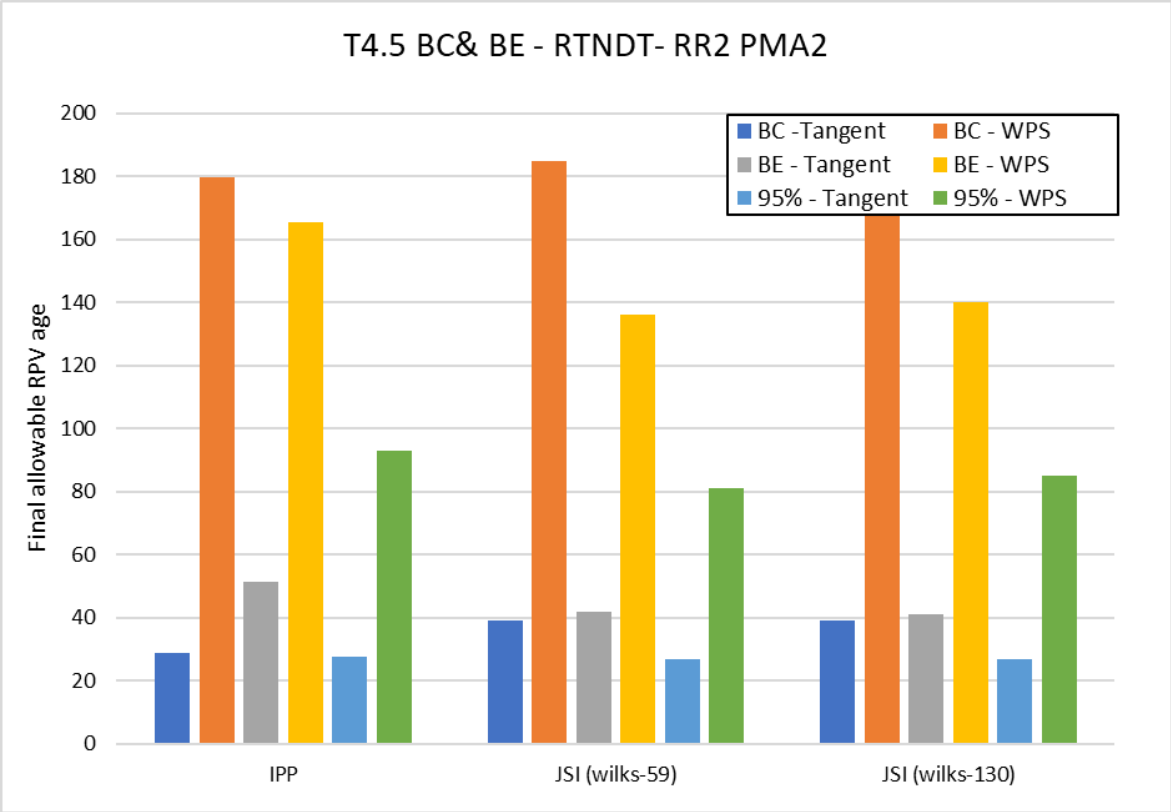

Figure 6.50: Summary of Base Case, Best Estimate and 95%-Quantile results for TCC circumferential, deepest point, PMA2 – Master Curve concept

Table 6.31: Overview of results for max. all. RPV age for TCC circumferential, deepest point, PMA2 – Master Curve concept

	Base Case		Best Estimate		95%-Quantile		5%-Quantile		Mean		Median	
	Tang-ent	WPS	Tang-ent	WPS	Tang-ent	WPS	Tang-ent	WPS	Tang-ent	WPS	Tang-ent	WPS
IPP	28.8	179.9	51.4	165.5	27.8	93.2			54.5	188.3	53.7	193.3
JSI (wilks-59)	39	185	42	136	27	81	197	223	63	135	49	129
JSI (wilks-130)	39	185	41	140	27	85	181	237	63	138	45	132

6.3 Discussion and main outcome

Within the WP4, Task 4.5 several probabilistic fracture-mechanics calculations related to the uncertainties in the thermal hydraulic data were performed by each partner. For a first comparison, the CPI for several fixed max. all. ART values were calculated. The results presented in chapter 6.2 were in good agreement, and the differences can be explained by the use of different TH input data, mainly by the differences between mixing and system (non-mixing) TH analyses.

For PMA1, the max. all. ART for a given allowable crack initiation frequency (CPI=2.28e-4) with ART being a fixed input parameter to PFM was determined. The preliminary comparison between the partners was done in terms of max. all. ART in chapter6.2.3. The quantiles and mean value for max. all. ART were calculated and compared. Within this task consistent results for all partners were obtained. The WPS approach has a big influence on the final result.

For PMA2, the max. all. lifetime (RPV age) for a given allowable crack initiation frequency (CPI=2.28e-4) was calculated. The lifetime of the RPV defines the ART shift (both the initial ART and the ART shift were treated as distributed parameters) as input for the PFM. In the end the correlation of a lifetime with CPI (from several probabilistic fracture mechanics analyses) was used to determine the maximum allowable lifetime. Within this task consistent results for all partners were obtained. The WPS approach has a big influence on the final result, even more than for PMA1.

In general, consistent results for all partners were obtained for all subtasks. Some differences between the partners are related to the differences in the thermohydraulic input, i.e. thermohydraulic input data and code used, especially the way of analysing the mixing. The consideration of WPS effect has a big influence for the final result. It is resulting in a large difference compared with the tangent approach for the max. all. ART results (PMA1) and even larger difference for the max. all. RPV age (PMA2).

7 Probabilistic margin assessment

7.1 Objectives

The main objective of APAL's task 4.6 is to quantify:

i. Increase (or decrease) of explicit margin by taking into account TH data sets related to LTO improvements or human factor (from task 2.1).
ii. Implicit margin related to the use of envelope TH data set. This will be done by comparison of results based on the envelope TH data set (determined from envelope TH input data) with results from best-estimate TH data set (determined from best-estimate TH input data).
iii. Verification of (ii) by assessing all TH data sets from Wilks method (from task 2.3): What is the best-estimate and envelope result for all TH data sets from Wilks method and compare it with results from (ii).

The assessment for (i) is illustrated in Figure 7.1 and for (ii)/(iii) in Figure 7.2, which are the same as Figure 5.1 and Figure 6.1. It has to be noted that "safety margin" is not always necessarily an explicit margin (i.e. comparison of allowable value with actual RPV value). The comparison can also be done in terms of allowable values, as this gives the increase of explicit margin.

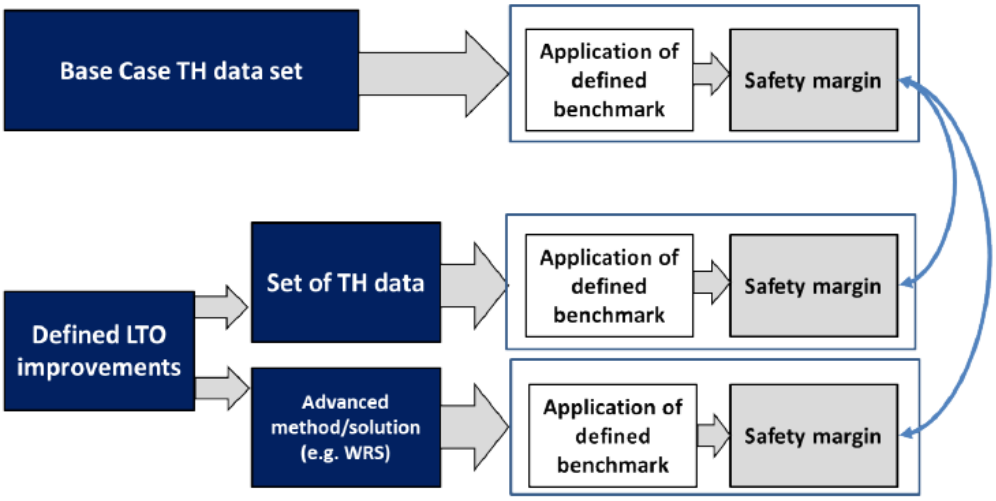

Figure 7.1: Comparison performed in Task 4.4.

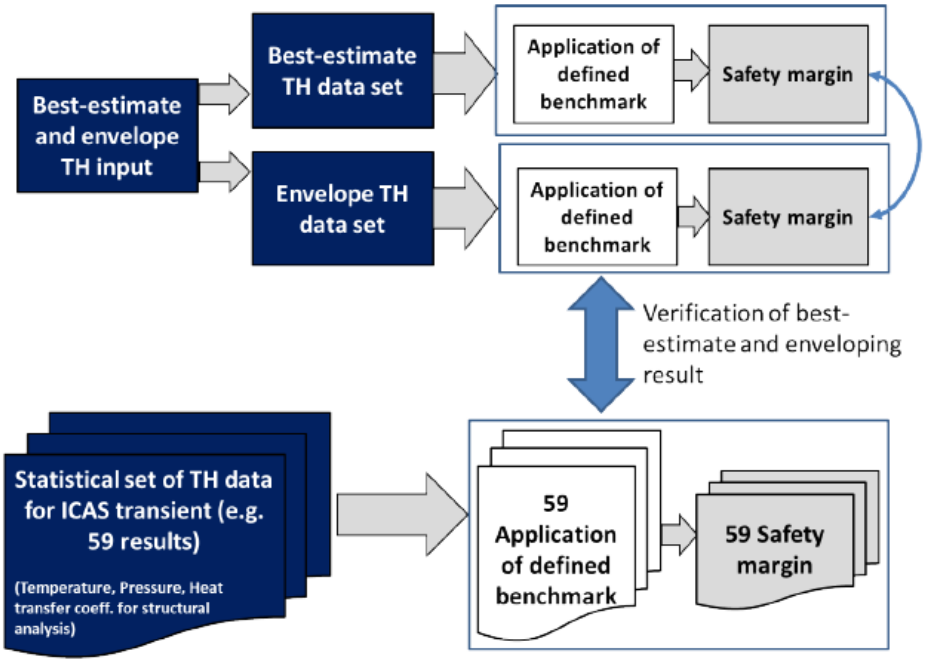

Figure 7.2: Comparison and verification performed in Task 4.5.

Within the APAL project, the probabilistic analysis of PTS by probabilistic fracture mechanics is one of the two main approaches (i.e., deterministic and probabilistic approach). This Section documents the margin assessment using several approaches to probabilistic assessment.

7.2 Introduction to margin concepts

In general, the margin measures the "distance" between the current state and the acceptance criterion, i.e., the limiting acceptable state. This concept represents an explicit margin, and in PTS analysis, the difference between material ART and maximum allowable ART is a good example of such an explicit margin.

In contrast to explicit margins, an implicit margin is a distance between acceptance criterion and actual failure (or crack initiation). Implicit margins might be present due to the imposed conditions, which may contain additional conservative settings which influence the actual margin. The investigation of thermal-hydraulic uncertainties within APAL represents the assessment of implicit margins.

7.3 Probabilistic Margins Concepts

Four probabilistic margin concepts are included in the APAL project. These four assessments are described in detail in the following subsections.

7.3.1 Assessment based on fracture toughness (PMA1)

In the assessment based on fracture toughness K_{Ic}, the only distributed parameter is the scaling of the fracture toughness, while all other parameters are deterministically treated.

$$K_{Ic}(T, RT_{NDT}) = f\ K_{Ic}^{\text{mean}}(T, RT_{NDT}) \quad (1)$$

The prefactor f in this case, as used in APAL (see D4.2 [2]), follows the normal distribution function with the standard deviation equal to 0.15 of mean value K_{Ic}^{mean}, truncated to three standard deviations. The K_{Ic}^{mean}-function is the ASME fracture toughness curve, divided by 0.7 (i.e., the standard ASME fracture toughness curve is supposed to be mean – 2 standard deviation "lower bound" of normal distribution of fracture toughness). Alternatively, the equation might be formulated in terms of the ASME fracture toughness curve with an adjusted prefactor.

In this assessment, as the transient is fixed, the probability of crack initiation (either at a given time, or during the whole transient) depends on the transition temperature. While the reference temperature is a material characteristic given in each specific case, it might also be treated as a variation parameter to quantify the safety margin. The maximum allowable reference temperature (MART) is implicitly defined by the crack initiation probability acceptance criterion (final allowable CPI, see [2]).

$$P(RT_{NDT} = MART) = 2.28 \cdot 10^{-4} \quad (2)$$

This approach has a very close relation to the deterministic margin for the maximum allowable reference temperature, since there is a relation between the quantiles of the K_{Ic} curve and the deterministic assessment, since the deterministic assessment curve is just imposed by a scaling factor. Therefore, the probabilistically determined PMA1 margin would be identical to the margin determined in the deterministic assessment for the allowable CPI of $\Phi(-2) \approx 2.28 \cdot 10^{-2}$, where Φ represents the cumulative distribution function of the standard normal distribution. This comparison is shown in Figure 7.3.

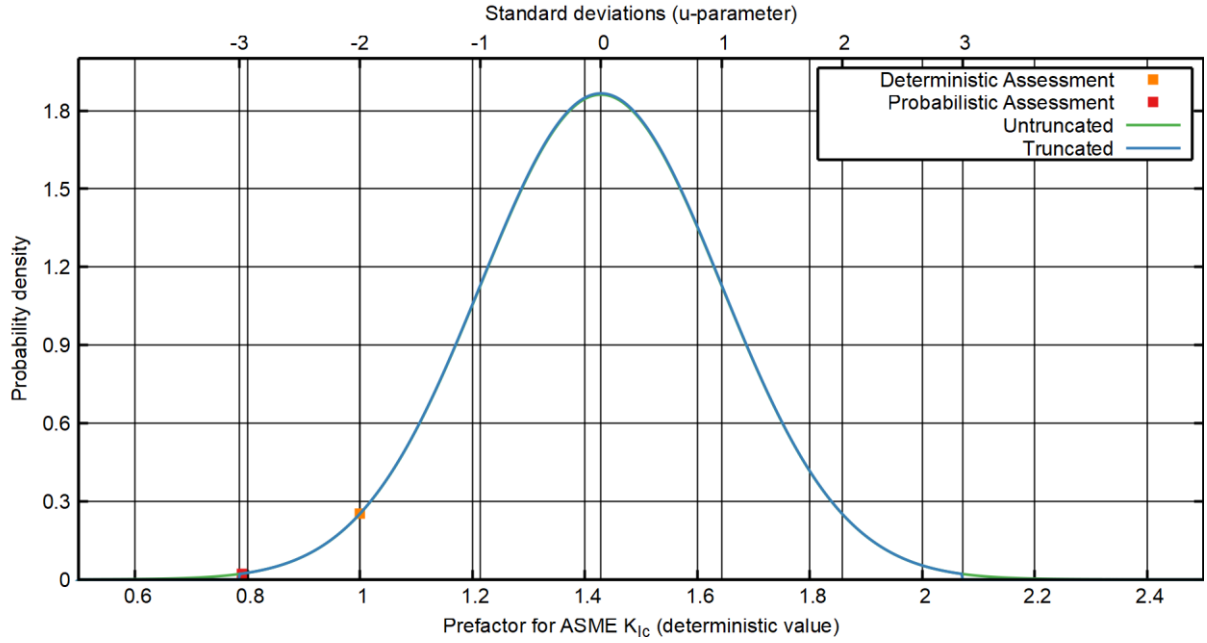

Figure 7.3: Comparison of the deterministic assessment and PMA1, based on the fracture toughness scaling function.

In this graphical comparison, it can be seen that the probabilistic acceptance criterion is very close to the truncation at -3 standard deviations, while the deterministic criterion is at -2 standard deviations. Therefore, it is expected that the PMA1 assessment leads systematically to more conservative results than the deterministic assessment, i.e. the probabilistic maximum allowable reference temperature is lower than the deterministic.

7.3.2 Assessment based on lifetime (PMA2)

The margin quantification uses the crack initiation acceptance criterion to quantify the allowable RPV age. The assessment based on lifetime assumes a relation between the fluence, φ, and the RPV age or years of reactor operation, L. This approach allows for the consideration of distributions of the embrittlement influencing parameters, i.e. parameters influencing fracture toughness including the initial ART and the ART shift dependencies on RPV material chemical composition and on neutron fluence (all are treated as distributed) as input for the PFM. All parameters are defined in Section 2.3.

7.3.3 Assessment based on failure frequency (PMA3)

Comparisons of PMA3 approach are not included in this deliverable; it is introduced here for completeness. The initiation frequency for a given transient and postulated crack gives also a quantification of the existing safety margin for a given RPV lifetime, especially when compared to the CPI frequency derived from the acceptance criterion.

$$PMA3 = CPI \times f_{\mathrm{occ}} - f_{\mathrm{accepted}} \quad (3)$$

In cases where only one transient is considered, the margin might be divided by the occurrence frequency f_{occ}. The analogous approach yields in case of failure frequency, with consideration of crack arrest. This assessment allows to use the reliability theory toolbox, which is explored in PMA4.

7.3.4 Assessment based on reliability theory (PMA4)

The assessment based on reliability theory quantifies the margin in terms of the position of the so-called most probable failure point (MPFP) in the standard normal space (u-space). This concept is briefly introduced in the following.

Given a probabilistic fracture-mechanics case, N independent distributed parameters $x_1, \dots, x_N$ form an N-dimensional space. The vector of parameters is denoted $x = (x_1, \dots, x_N)$. Each parameter x_i is described by a cumulative distribution function $F_i(x_i)$. The joint probability density function is denoted as $\rho(x)$. Given a failure assessment criterion which predicts failure or safety for each point, a continuous limit state function g is defined such that $g(x) > 0$ if x is safe, and $g(x) \leq 0$ if failure (or initiation, in the case of APAL) is predicted for x. With this definition, the CPI and/or failure frequency can be written as follows.

$$CPI = \int_{g(x)\leq 0} \rho(x)dx \quad (4)$$

Instead of computing in the space of parameters, it is convenient to transform the space to standard normal parameters, using the transformation

$$u_i = \Phi^{-1}[F_i(x_i)] \quad (5)$$

The origin of the u-space corresponds to the median value of all parameters. The limit state function g can be defined equally in the space of parameters ($g(x)$) or in the standard normal space ($g(u)$). The most probable failure point MPFP is defined as the point in the u-space closest to the median value, i.e. the point with $g \leq 0$ with the minimal distance to the origin.

$$MPFP = \arg\min\{\|u\| : g(u) \leq 0\} \quad (6)$$

Here, the symbol $\|u\|$ denotes the Euclidean norm in standard normal space, i.e., the geometrical distance to the median. The norm of the MPFP is denoted β, the reliability index.

$$\beta = \|MPFP\| \quad (7)$$

This index provides a characterization of the distance between the most probable parameter set leading to failure in terms of standard deviations (or its multi-dimensional generalization). Note that in the First Order Reliability Method (FORM), the probability of initiation/failure is approximated by $P = \Phi(-\beta)$, where Φ reprensents the cumulative distribution function of the standard normal distribution.

For the numerical computation of the MPFP, the classical FORM approach uses a numerical optimization algorithm that directly attempts to solve Eq. (6). However, it is also possible to approximate the MPFP based on a Monte Carlo sampling method.

$$MPFP_i \approx \frac{1}{|\mathcal{F}|} \sum_{x \in \mathcal{F}} \Phi^{-1}[F_i(x_i)] \qquad (8)$$

In this approach, $\mathcal{F}$ denotes the set of Monte Carlo Samples in the simulation that lead to initiation, and $|\mathcal{F}|$ denotes the number of these samples. This approximation corresponds to the centre of mass (in u-space) of Monte Carlo samples leading to initiation.

The advantage of the PMA4 approach is that additional information about the probabilistic case is gained. The distance of the MPFP from the origin (the median), the reliability index β, is directly related to the probability, which provides information similar as PMA3. In addition, the location of the MPFP is representative for "typical" failures, which can be expected to dominate statistically the failure frequency. This allows to interpret the role of different distributed parameters, and the relevance of the associated uncertainties for the final failure probability. The MPFP coordinates (in u-space) can be directly used, or enter in specific sensitivity measures, like the importance factors $|MPFP_i|/\beta$. The ranking of the importance factor allows for a ranking of the influence of the different uncertainties on the CPI: this sensitivity information is a benefit of the PMA4 approach.

7.4 Description of Activities

7.4.1 Common approaches for probabilistic assessment

The cases analysed in the Task 4.6 are based on the APAL standard example; the participants use different tools and approaches. The details are provided in other topical APAL deliverables, for instance in D4.3 [3], D4.4 [4], and D4.5 [5] which have been summarised in Sections4, 5 and 6, respectively.

The objectives of the activities performed in Task 4.6 and described in this report are:

- Assessment of different probabilistic margin approaches (see also Section 7.3: This will be done mainly for the baseline benchmark considering base-case transient. The main objectives are to quantify the bias due to the different probabilistic PTS assessments from the partners (different TH analysis, mixing analysis, codes for PFM, etc.), to compare the different probabilistic margin approaches and to gather recommendations for best-practice.
- Quantification of impact of LTO improvements: A comparison of explicit margin for the base-case (results from task 4.3) with explicit margin for selected LTO improvements (results from Task 4.4).
- Quantification of impact of TH uncertainties: A comparison of margin for the base-case (results from Task 4.3) with margin for 5% quantile and best-estimate TH data set (results from Task 4.5). Moreover, the selection of envelope TH data set (based on results from deterministic assessment in Task 3.5) and best-estimate TH data set will be verified with assessment of all TH data sets from Wilks analysis.
- Comparison of probabilistic and deterministic margin assessment: A comparison of the allowable ART from deterministic assessment and from PMA1 for base-case will be performed and conclusions will be drawn on the link between deterministic and probabilistic margin assessment. In addition, the impact of LTO improvements and TH uncertainties will be compared between deterministic assessment and PMA1.

7.4.2 Relation to other deliverables and tasks

Tasks 4.3, 4.4 and 4.5, described in Sections4, 5 and 6, respectively, are very similar from the methodological point of view. In all these tasks, the probabilistic assessments of certain PTS cases are performed. While the cases differ in the thermal-hydraulic conditions of the transients, the selection of postulated cracks (orientation and shape) and assessment procedures (regarding WPS) are defined uniformly in all tasks.

As all three tasks finally assess the probabilistic margin, this Section compares the probabilistic margins derived for the different cases. This approach allows to concentrate on the comparison of margin assessment methods and on the comparison of quantified margins in this Section, while the actual case description is provided in D4.3 [3], D4.4 [4], and D4.5 [5], respectively. The thermal-hydraulic foundation of these cases is provided in the deliverables D2.1 [10] and D2.2 [11], respectively, which have been summarised in WP2 Public Summary report [8]. The comparison of probabilistic margins and deterministic margins is especially of interest here for the LTO improvements and the thermal-hydraulic uncertainties. Therefore, a link to D3.4 [16] is also established.

7.4.3 Common template

A common template was created to report the results of the tasks 4.3, 4.4, and 4.5, respectively, in a similar way. For the probabilistic margin assessment based on the maximum allowable adjusted reference temperature, PMA1, the template requires variations of the pre-defined fixed ART. The results for fixed ART and the iterations to match the acceptance criterion are to be reported together with the simulation information. The template for PMA1 is shown in Table 7.1.

Table 7.1: PMA1 template

			Results for pre-defined fixed ART:					Add intermediate results (extend the table if necessary):				Final result
Fixed ART [°C]			0	50	100	150	200					
Final CPI for the transient												
Number of MC runs												
Convergence criterion used (y/n)												
Time in the transient (s)	Temp [°C]	KI [MPavm]	Instantaneous cpi (t)									
0												
…												
10000												

The template for PMA2 is similar, but the RPV lifetime, or equivalently the mean value of fluence at the inner surface (IS), is the varied parameter instead of the ART. The distribution of the ART is, in this case, dependent on the lifetime; the participants are expected to report mean value (MV), standard deviation (SD), and quantiles. The CPI in this case is not considered as a distribution, i.e. the point estimate regarding the fracture toughness is computed. The corresponding template for PMA2 is shown in Table 7.2.

Table 7.2: PMA2 template

			Results for pre-defined RPV age:					Add intermediate results (extend the table if necessary):				Final result
RPV age [year]			1	20	40	80	200					
Mean value of fluence IS (10^{23} n/m²)			1	5	7.5	12.5	27.5					
ART	MV											
	SD											
	5% Quantile											
	95% Quantile											
Final CPI for the transient												
Number of MC runs												
Convergence criterion used (y/n)												
Time in the transient (s)	Temp [°C]	KI [MPa√m]	Instantaneous CPI (t)									
0												
…												
10000												

The PMA4 template only requires the information for the fixed lifetimes of PMA2, and reports the coordinates of the most probable failure point. The corresponding template for PMA4 is shown in Table 7.3.

Table 7.3: PMA4 template.

	Results for pre-defined RPV age:				
RPV age	1	20	40	80	200
Mean value fluence IS (10^{23} n/m²)	1	5	7.5	12.5	27.5
Final CPI for the transient					
Reliability Index					

Most probable point of failure (MPF):

Initial Ref. Temp.	**Value**					
	u-value					
Cu	**Value**					
	u-value					
Ni	**Value**					
	u-value					
P	**Value**					
	u-value					
neutron fluence	**Value**					
	u-value					
ΔART error function	**Value**					
	u-value					
fracture toughness	**Value**					
	u-value					
Number of MC runs						
Convergence criterion used (y/n)						

In addition, the complete templates also contain fields for reporting participant information and the final results.

7.4.4 Case selection and connection points to D4.3, D4.4 and D4.5

The cases in the baseline probabilistic benchmark, the LTO improvements and thermal-hydraulic uncertainties were selected to allow an assessment of the differences between the probabilistic and deterministic approaches, the effectiveness of LTO improvements, and the importance of thermal-hydraulic uncertainties. In order to focus on the probabilistic margin quantification approaches, the mandatory cases were specifically reduced with regard to relevance, expected significance of results, and also code capabilities.

Given these circumstances, it is sufficient to assess for the cases beyond the baseline cases only one orientation, one geometry and one specific point of the postulated cracks at the crack front. Already this allows to draw convincing conclusions concerning the methodology. Single analyses have been performed for other variants including different crack types, crack orientation, and different point on the crack front, and no indication was found that this spoils the generality of the conclusions.

7.5 Probabilistic margin assessment

In this chapter, the computed margins of the participants are discussed and compared. As for WPS approaches, only results using tangent approach (i.e. no WPS) and the simplistic (max. K_I) WPS were delivered by the partners. In most cases, the partners delivered both types of results. Therefore, it

makes sense to interpret these two criteria as a pessimistic (tangent) or optimistic (simplistic WPS) extreme, and the realistic WPS approaches would lie in between. In this sense, the assessment with both criteria is visualised as bars in this chapter.

7.5.1 Probabilistic margin assessment for baseline probabilistic cases

7.5.1.1 Introduction

The baseline probabilistic benchmark (see Section 4) involves several preparatory steps and also sophisticated probabilistic computations. For the assessment of the probabilistic margins, this report focusses on the round robin RR2. A scheme of the case matrix is provided in Figure 7.4.

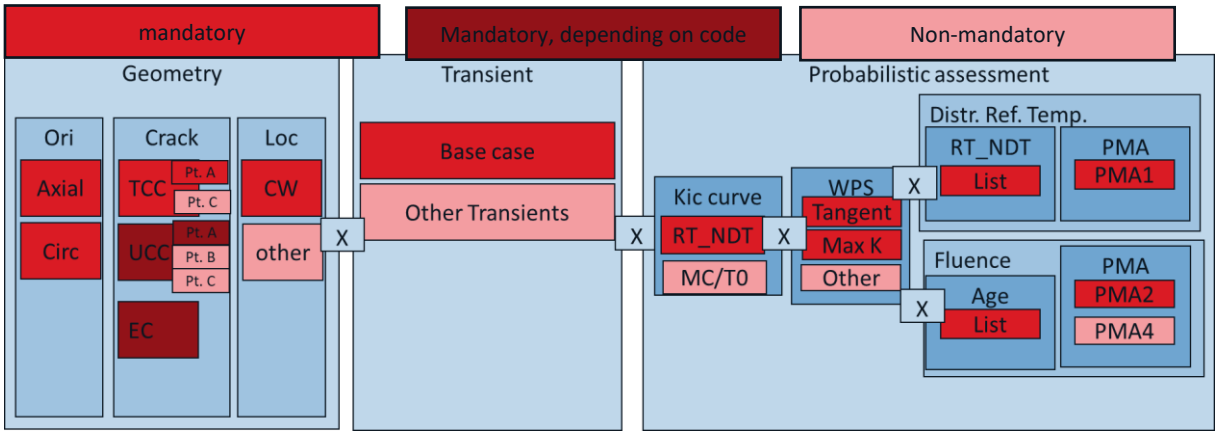

Figure 7.4: Case matrix for the round robin RR2 of the baseline probabilistic study.

In this section, the discussion of different probabilistic margin approaches is focussed on the methodological aspects in more depth than for the later benchmark tasks.

7.5.1.2 PMA1

The probabilistically determined maximum allowable reference temperature is computed for the baseline transient case and different postulated cracks. One single point on the crack front, the deepest point, is assessed. Some organizations submitted more than one base case analysis, for example originating from different thermal-hydraulic codes; in this case, both results are included separately. The resulting spans defined by tangent and max. K WPS criteria are compared in Figure 7.5. Upper and lower values of the spans are the results, respectively, with max WPS and tangent criteria. Few contributions only provide the tangent results, which is indicated by truncated bars.

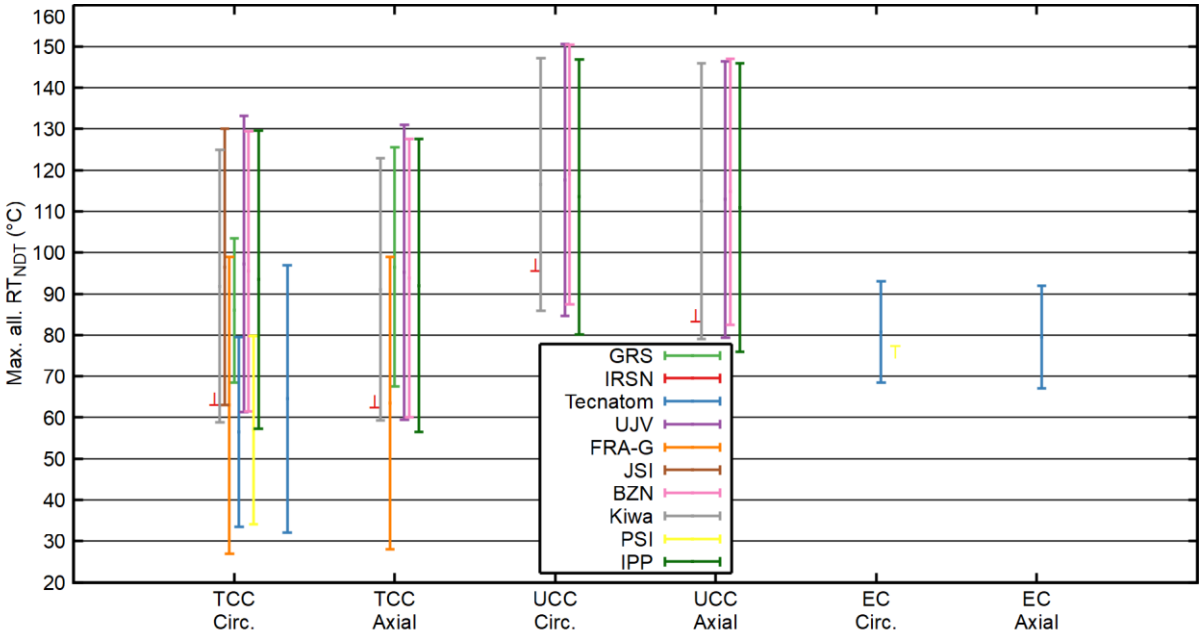

Figure 7.5: PMA1 of the base case, RR2. The bar represents the span between tangent- and max. K_I WPS criterion. Two different base cases, related to the LTO study, are included for Tecnatom.

This comparison shows that the deviations between different thermal-hydraulic data sets from different codes are similar to the deterministic benchmark. It can be seen that the differences between axial and circumferential orientations are very small. This supports the concentration on one orientation in subsequent tasks. Specific results are conservative (i.e. lower values of maximum allowable RT-NDT), for example because assumptions taken due to FAVOR limitations (Tecnatom contribution) or because of the consideration of the plume effect via a FE analysis (FRA-G).

Four partners submitted also results for an assessment with the Master Curve approach. The results for the maximum allowable T_0 are shown in Figure 7.6.

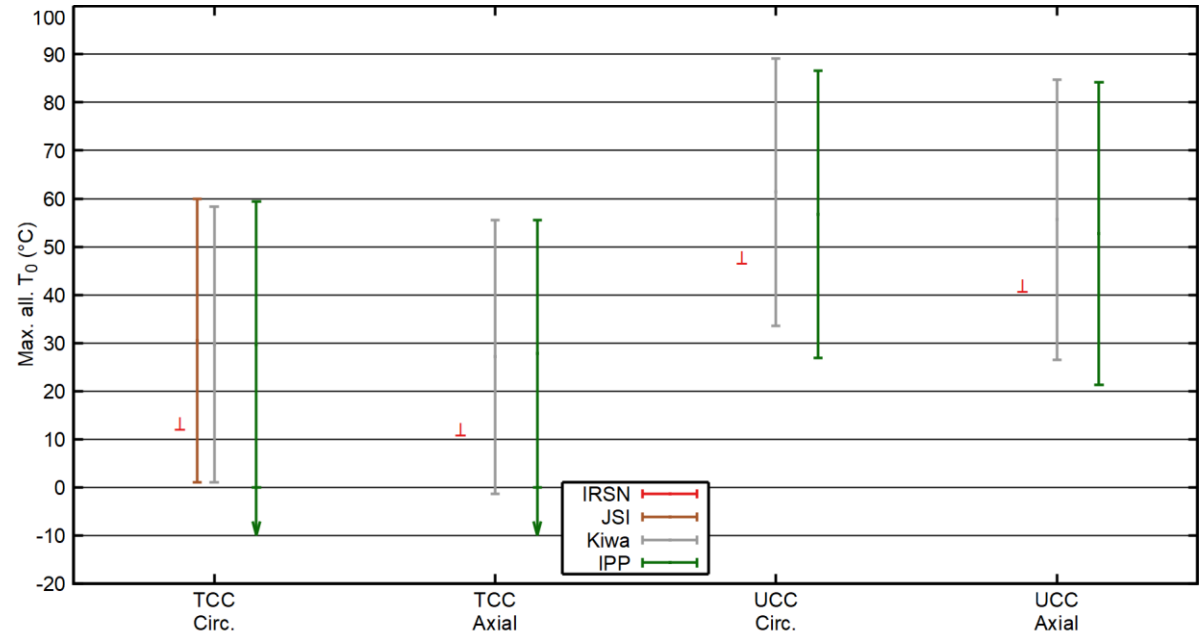

Figure 7.6: PMA1 of the baseline case, RR2, with the Master Curve approach. Arrows indicate that the lowest point is an upper limit bound.

When comparing the Master Curve result to the RT-NDT result, it is visible that both approaches have the same trend, and the comparison between the three included partners is consistent.

7.5.1.3 PMA2

This procedure is repeated for the lifetime-based assessment (PMA2). Similarly to PMA1, the different baseline cases for different crack assumptions are compared in Figure 7.7. The resulting spans defined by tangent and max. K_I WPS criteria are compared in Figure 7.7.

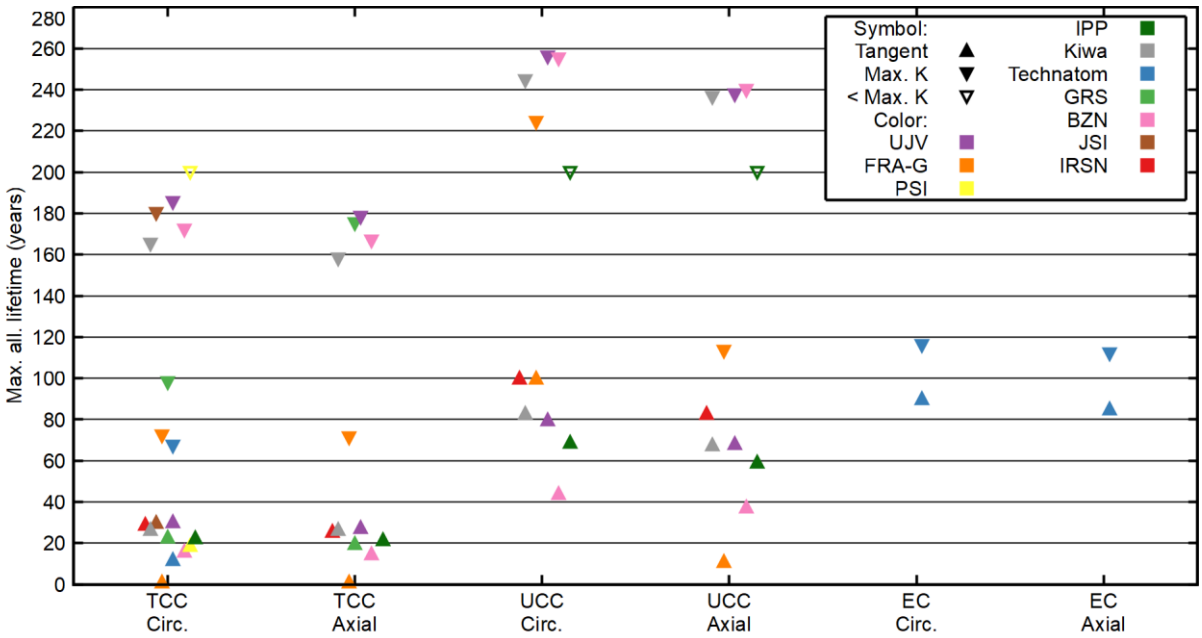

Figure 7.7: PMA2 of baseline cases, RR2.

Also for PMA2, the different orientations of cracks lead to very similar (but not equal) lifetimes. This again motivates the concentration on one configuration for the discussion of the suitability of different probabilistic margin assessments and influences on safety margins: Task 4.4 and Task 4.5 concentrate on one orientation. The selected criterion is again very important for the result: While the allowable RPV lifetime of the base case is below 40 years for the TCC crack and the tangent criterion, it is above 150 years for most other (except for FRA-G, GRS and Tecnatom). This underlines that long term operation improvements are most relevant for tangent criterion assessments. As for PMA1, specific results are conservative (i.e. lower values of lifetime) because of assumptions taken due to FAVOR limitations (e.g. Tecnatom).

Three participants provided PMA2 contributions based on the Master Curve approach. In contrast to the PMA1 approach, the T_0 parameter is not explicitly contained in the result – the lifetime based on the shift of the Master curve is depicted in Figure 7.8.

This result is similar to the RT-NDT curve regarding the influence of the crack orientation. The fact that both fracture toughness formulations lead finally to a maximum allowable lifetime allows for a comparison of the predicted lifetime. This is done graphically in Figure 7.9.

This comparison shows that the T_0 approach leads to longer allowable lifetimes than the RT-NDT approach (except for one case, where both are almost identical). The difference depends on the selection of the initial values of RTNDT and T0. In the benchmark, they were different, however, they were realistic. The difference is the largest for the UCC cracks, where the shift is more than 15 years.

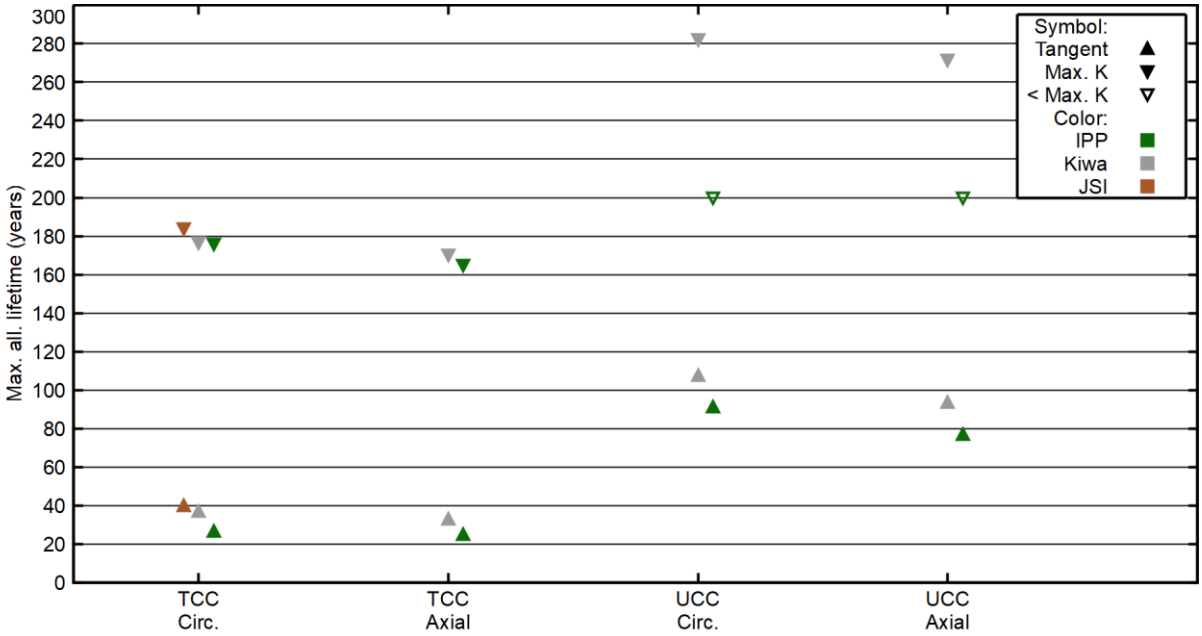

Figure 7.8: PMA2 of the baseline cases, using the Master Curve.

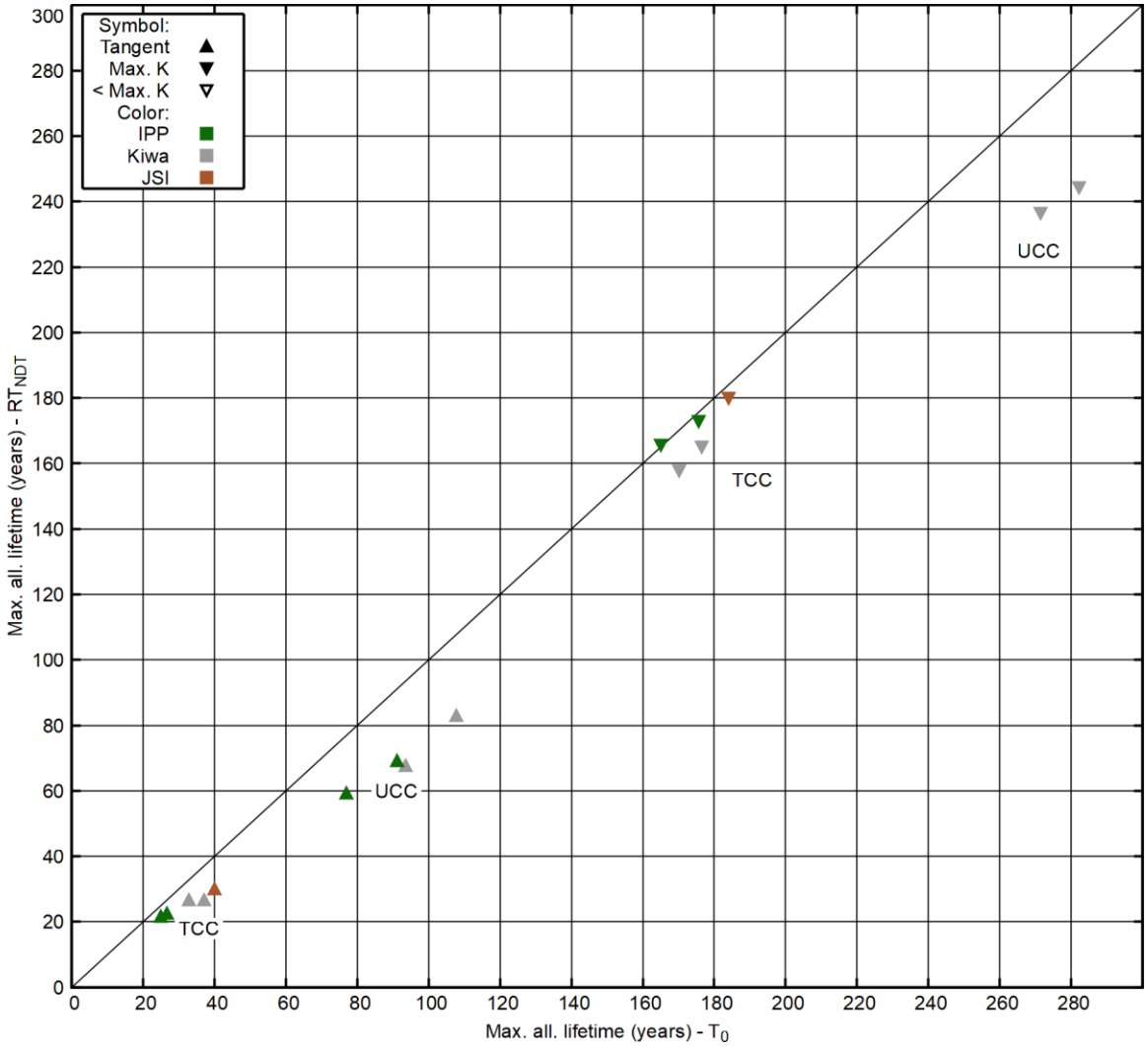

Figure 7.9: Comparison of the maximum allowable lifetimes with both fracture toughness approaches.

7.5.1.4 PMA4

The PMA4 task is analysed in this section; the axial TCC with the tangent criterion is selected. The CPI for the preselected years are listed in Table 7.4 (the GRS contribution is selected).

Table 7.4: CPI and reliability index for pre-selected years. GRS contribution for axial TCC.

RPV age	1	20	40	80	200
Final CPI for the transient	1.04E-08	2.31E-04	1.74E-03	1.96E-02	2.69E-01
Reliabilty Index	5.96	4	3.097	2.568	0.634

The location of the most probable failure point (MPFP) in the 7-dimensional space of random variables is not located close to a linear subspace throughout the lifetime: All coordinates of the MPFP are nonzero. Therefore, the MPFP is shown in a spider plot in Figure 7.10 as a visualization of the points in a 7-dimensional abstract space. For a normalization, the absolute values of the standard normal coordinates is chosen (all but the K_{Ic}-related standard normal coordinates are positive, as expected).

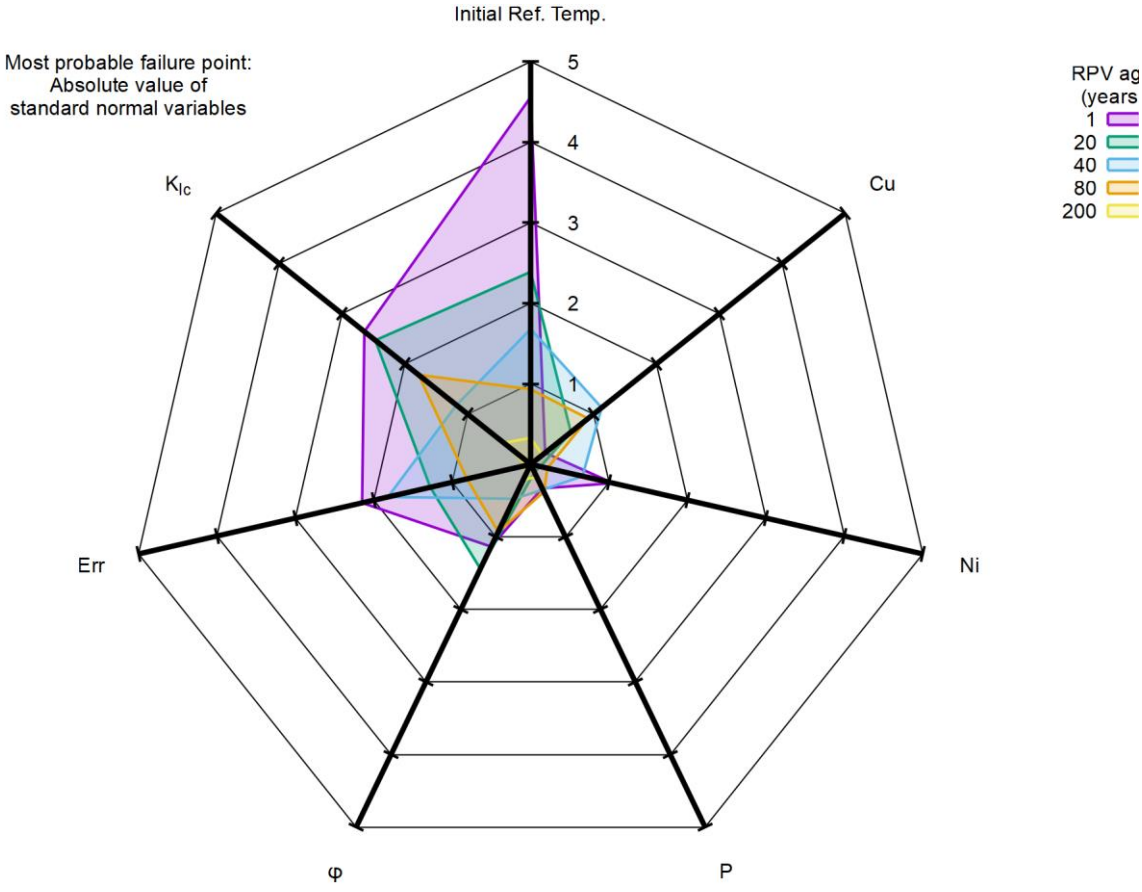

Figure 7.10: PMA4 assessment of the baseline case (axial TCC with tangent criterion). The coordinates (absolute values in standard normal space) of the most probable failure point for different RPV ages are indicated in the spider plot.

It can be seen that in the beginning of the lifetime, the MPFP is dominated by the initial reference temperature: The MPFP is located at about 4.6 standard deviation from its median for 1 year of operation. This means that the assumed distribution of the initial reference temperature strongly influences the CPI for this age. This equilibrates by the MPFP at 40 years, when the Fluence-Error and the fracture toughness scaling are equally important ($|u_i| \approx 1.7 - 1.8$), and even the Cu- and Ni-concentration show their influence. At 80 years, K_{Ic}, fluence and copper dominate, and for later ages,

the MPFP moves towards the median value. The least influential parameter throughout the lifetime is the P-concentration.

An alternative evaluation is the comparison of the importance factors, defined as $|u_i|/\beta$. The comparison of the importance factors for the FORM-computed GRS contribution (i.e. minimum in u-space) and the Monte Carlo-computed IPP contribution (i.e. center of mass) is shown in Figure 7.11.

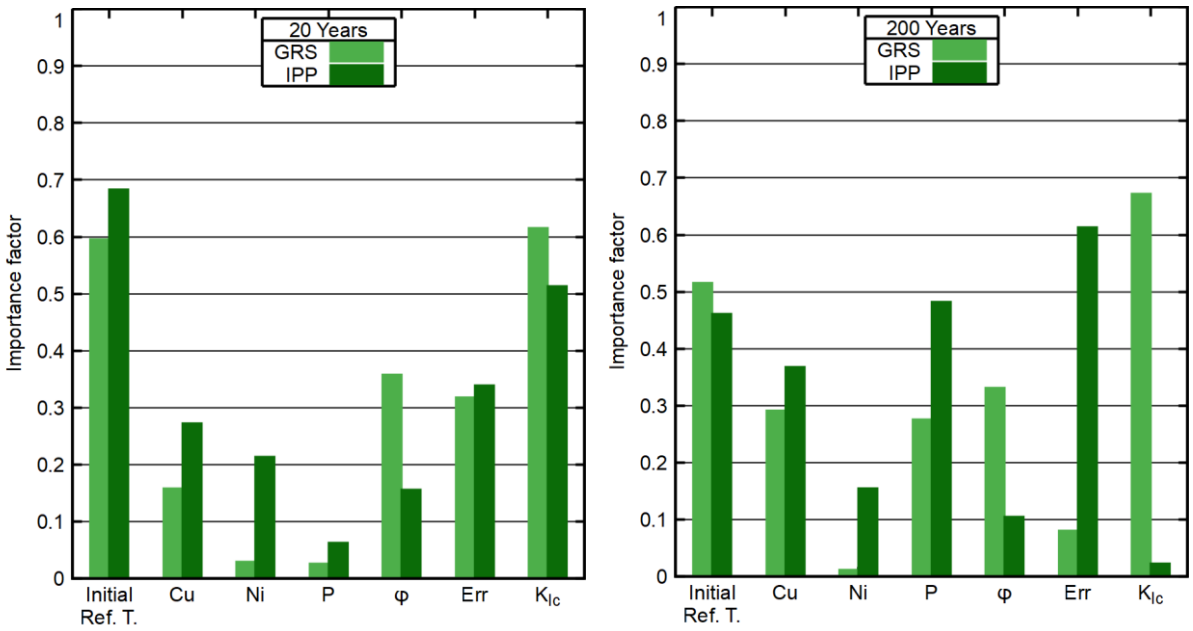

Figure 7.11: PMA4 assessment for axial TCC crack; comparison of the importance factors of GRS and IPP for 20 years (left) and 200 years (right).

This comparison shows that, for an RPV age of 20 years, the two parameters with the highest importance factors agree (initial reference temperature and fracture toughness), and also the parameter with the lowest importance factor is the same (phosphorus). For 200 years, it can be seen that the importance of the initial reference temperature is smaller for both contributions. Most probable parameter combination from both participants differ with respect to the highest importance factor: It is the fluence error or the fracture toughness. Given the high CPI larger than 10 % for 200 years, this difference might be attributed either to the differences in the thermal-hydraulic data or the different numerical approaches in the determination of the MPFP.

These findings can be related to the results of PROSIR [22] where also a similar analysis was performed and, for a specific case, the fracture toughness and the reference temperature were identified to have a larger impact than the chemical concentrations. Also the fact that all parameters have nonzero MPFP coordinates is similar to PROSIR.

7.5.2 Probabilistic margin assessment of LTO improvements

7.5.2.1 Introduction

The probabilistic assessments of LTO-improvements were done in Task 4.4 and scheme of the case matrix is provided in Figure 7.12. This section analyses the computed margins and provides a relation to the deterministic assessment in Task 3.4.

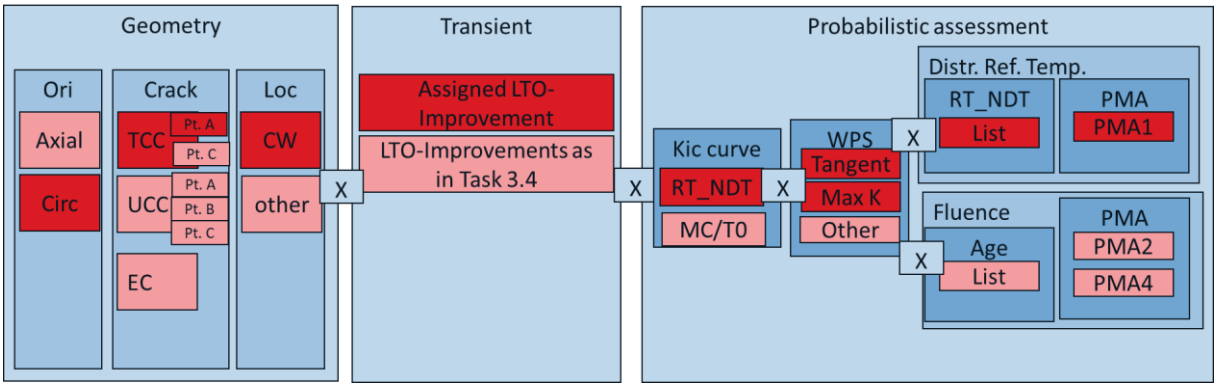

Figure 7.12: Case matrix for the probabilistic assessment of LTO improvements

As the focus is on the margin assessment methodology rather than on the individual improvements, the following subsections are ordered by the margin assessment approach. The individual LTO improvements and the assignment of LTO improvement tasks by the partners are described in detail in D3.4 [16]. As shown in Sec. 7.5.1.3, the lifetime obtained with the max. K WPS criterion are so high that a consideration of LTO improvements are not necessary, while they are required for the selected cases if the tangent criterion is used. Therefore, the tangent criterion is of specific importance in this section.

7.5.2.2 PMA1

In PMA1, the maximum allowable reference temperature is computed using the probabilistic acceptance criterion. The comparison of the maximum allowable reference temperature for the circumferential TCC postulate is shown in Figure 7.13. Note that Kiwa analysed the decrease in HPSI capacity in steps of 5% from 95% to 75% in LTO5. While an effect of the LTO improvement is visible, the differences induced by the different thermal-hydraulic codes used by the partners dominate the maximum allowable reference temperature (as also observed for the base case, see Sec. 7.5.1.2). This statement yields for the tangent criterion and the max. K WPS criterion, which, as in Sec. 7.5.1.2, are indicated by a bar.

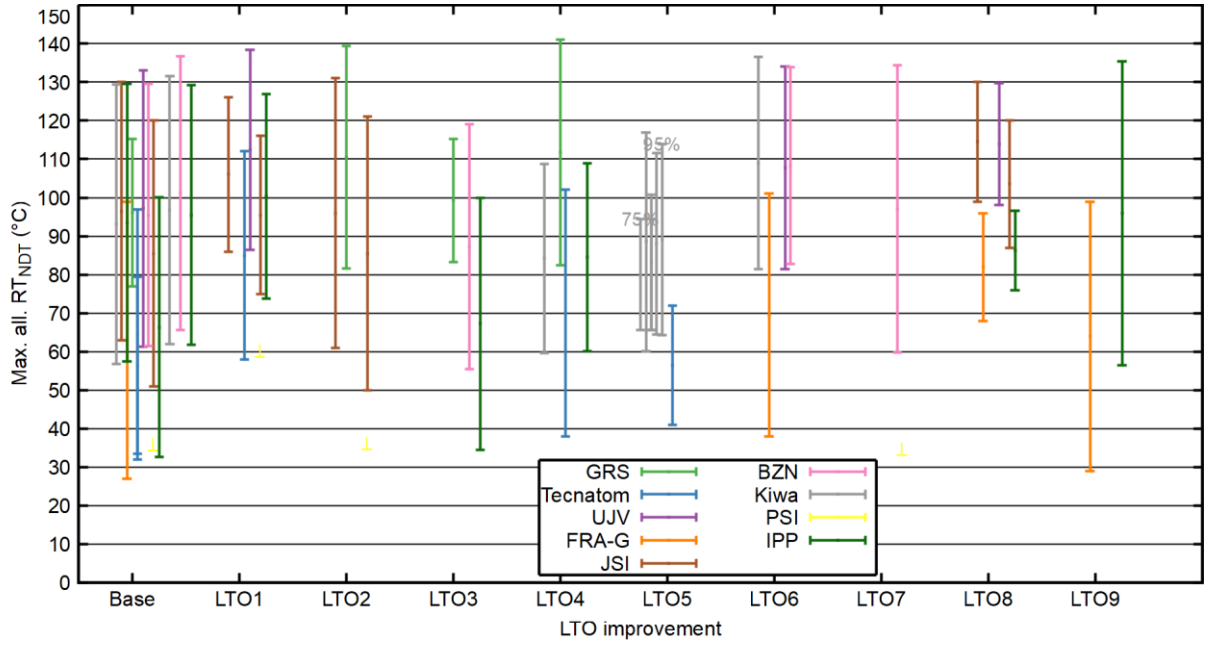

Figure 7.13: PMA1 results for the LTO improvements. The bar represents the span between tangent- and max. K_I WPS criterion. Circumferential TCC.

As the different thermal-hydraulic codes used by APAL partners lead to differences in the predicted baseline max. all. ART, the comparison between the APAL partners is preferably done regarding the shift in maximum allowable reference temperature (i.e. by the differences between LTO and base case). This comparison is shown in Figure 7.14.

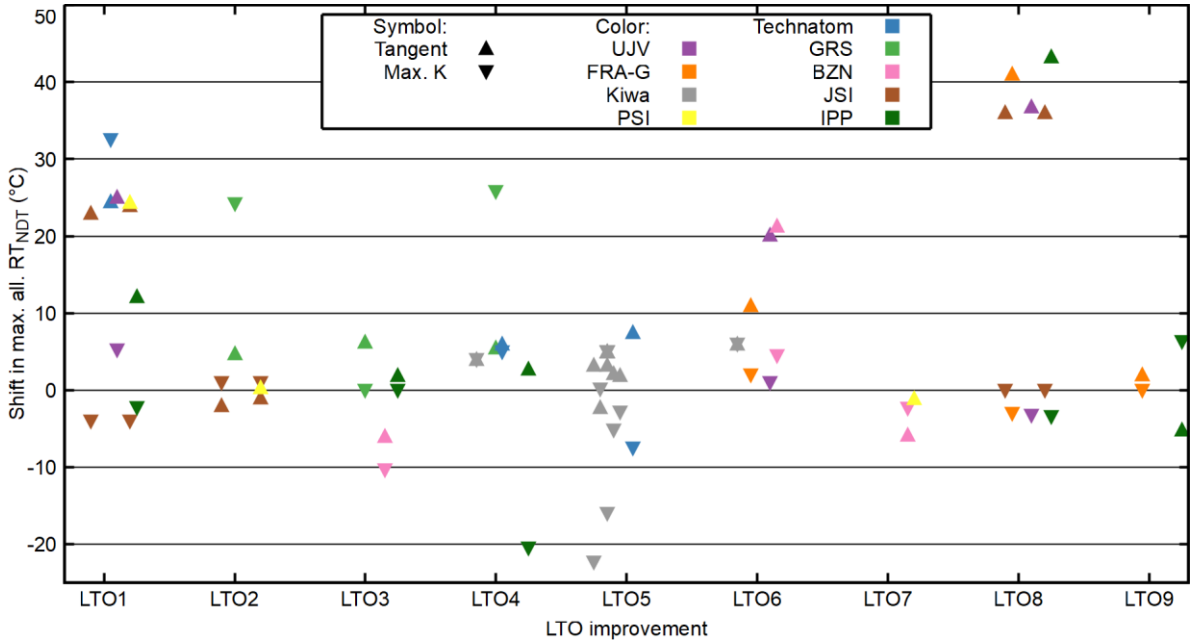

Figure 7.14: PMA1 of LTO-improvements: Predicted shift of maximum allowable RT-NDT by different LTO improvements computed by probabilistic approach.

The shift can be interpreted as the gain in safety margin. This comparison reveals that the different LTO improvement measures can have a different effect on the PTS analysis, and the PMA1 is able to quantify this. LTO1 and LTO8 provide a pronounced maximum allowable reference temperature shift (especially for the tangent criterion). The benefit of LTO3 is only small for the tangent approach for one single data set and has no or an adverse effect on the shift for all the other cases. These findings are in agreement with the deterministic assessment (see D3.4 [16]), where LTO8 and LTO1 have the strongest effect if the tangent criterion is used. The small effect of LTO3 is also seen in the deterministic assessment. The trend to conservative results for FAVOR users (Tecnatom) or the plume effect consideration (FRA-G) is similar as in Sec. 7.5.1.2 and Sec. 7.5.1.3, respectively.

The PMA1 assessment has a relation to the deterministic assessment; this relation is visualised in Figure 7.15. The deterministic max. all. ART is shown as a function of the probabilistic (PMA1) max. all. ART. It can be seen that there is a simple relation of a about an offset of 10 °C between the two approaches to safety margin definition. The lower max. all. ART of the probabilistic approach can be understood by the different quantiles (see 7.3.1).

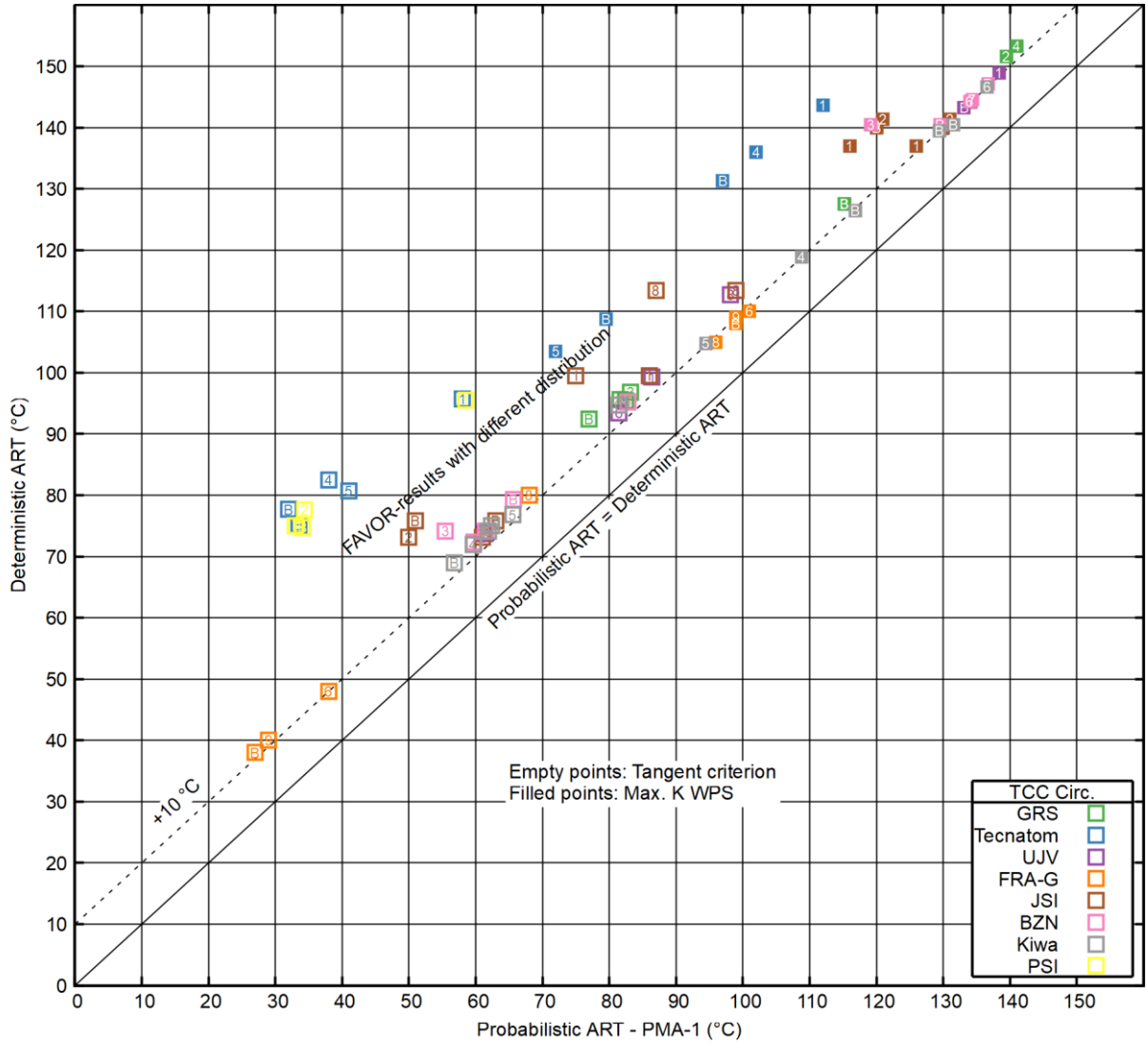

Figure 7.15: Comparison of PMA1 maximum allowable reference temperature of the LTO improvement with the deterministically computed maximum allowable reference temperature. The crack postulate is circumferential TCC. Numbers in the boxes mean numbers of LTO improvement, B mean the base case .max. all. ART.

From this comparison, it can be verified that the relation between the deterministic and the probabilistic max. all. ART is (almost) monotonic: A ranking of the effect of LTO improvements or specific transients seems to be possible even by starting from a deterministic assessment. As it can be seen, the FAVOR results (Tecnatom, PSI, FAVOR-analysis of JSI) are slightly off the others. This can be understood as the code uses different stress intensity factors, crack size inputs, but most important also a different distribution assumption for the fracture toughness (Weibull distribution instead of normal distribution). As this distribution is the only source of uncertainty in the probabilistic approach for PMA1, this difference has a significant impact. The conservative trend for the probabilistic results with the specific FAVOR settings is in line with the previous findings.

It is also instructive to study the relation between the probabilistic and deterministic shift in max. all. reference temperature. The comparison of these parameters is shown in Figure 7.16.

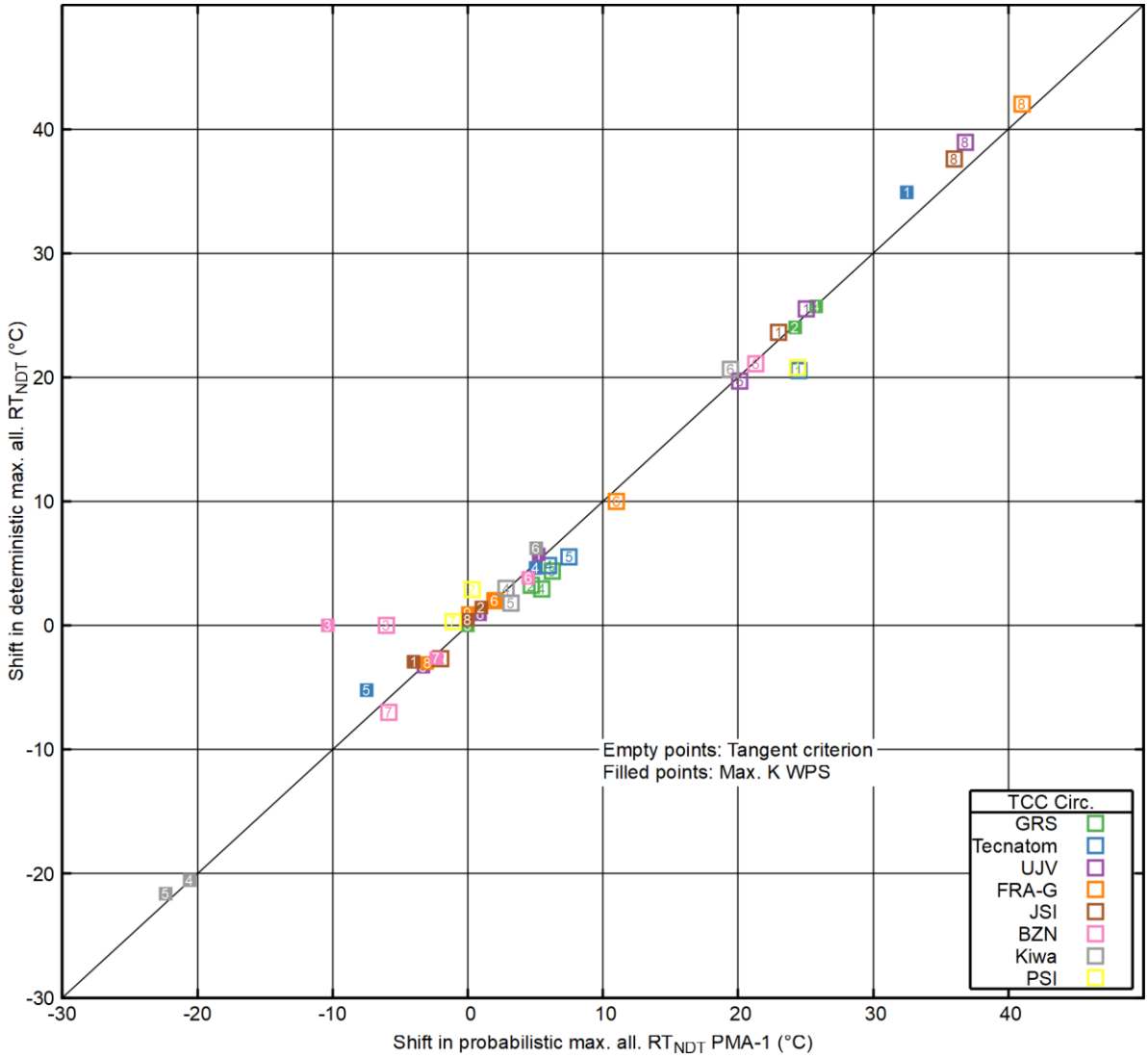

Figure 7.16: Comparison of the shift in the max. all. reference temperature by the LTO improvements (probabilistic vs. deterministic).

This investigation shows that the shifts are almost equal – a behaviour that is already expected from the investigation of the absolute values above. In this representation, also the ordering of the LTO effectiveness can be directly identified (LTO8 and LTO1 with the tangent criterion are the top right points, which implies that they are the most beneficial).

As non-mandatory cases, axial TCC cracks were examined. These results show only few differences compared to the circumferential cracks (see Figure 7.17).

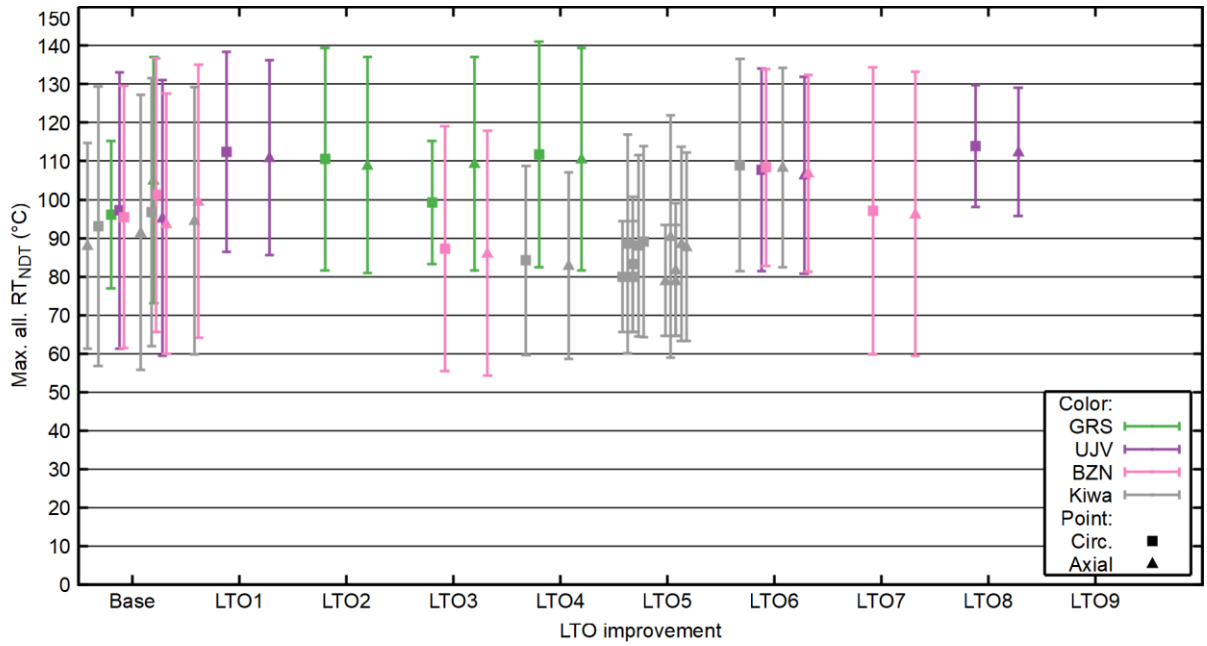

Figure 7.17: PMA1 for LTO improvements; comparison of axial and circumferential TCC orientation. The bar represents the span between tangent- and max. K_I WPS criterion.

The axial orientation exhibits a trend to slightly smaller values of max. all. reference temperature. Based on this evaluation, it can be concluded that for the purpose of determination of the LTO improvement impact, it is sufficient to concentrate on one crack orientation. No case was found where one specific orientation would show a completely different behaviour[3] than the other one.

7.5.2.3 PMA2

In PMA2, the allowable RPV lifetime is computed; the comparison between the obtained contributions is displayed in Figure 7.18. As for PMA1, the different allowable ages of the baseline cases of different codes differ due to the different thermal-hydraulic data sets which were used.

[3] This is caused by the fact, that 1D solution was used in the performed analyses, i.e. no cold plume effect was considered. Moreover, the value of inner pressure in the critical time was small. In other cases, crack orientation can affect the results more significantly.

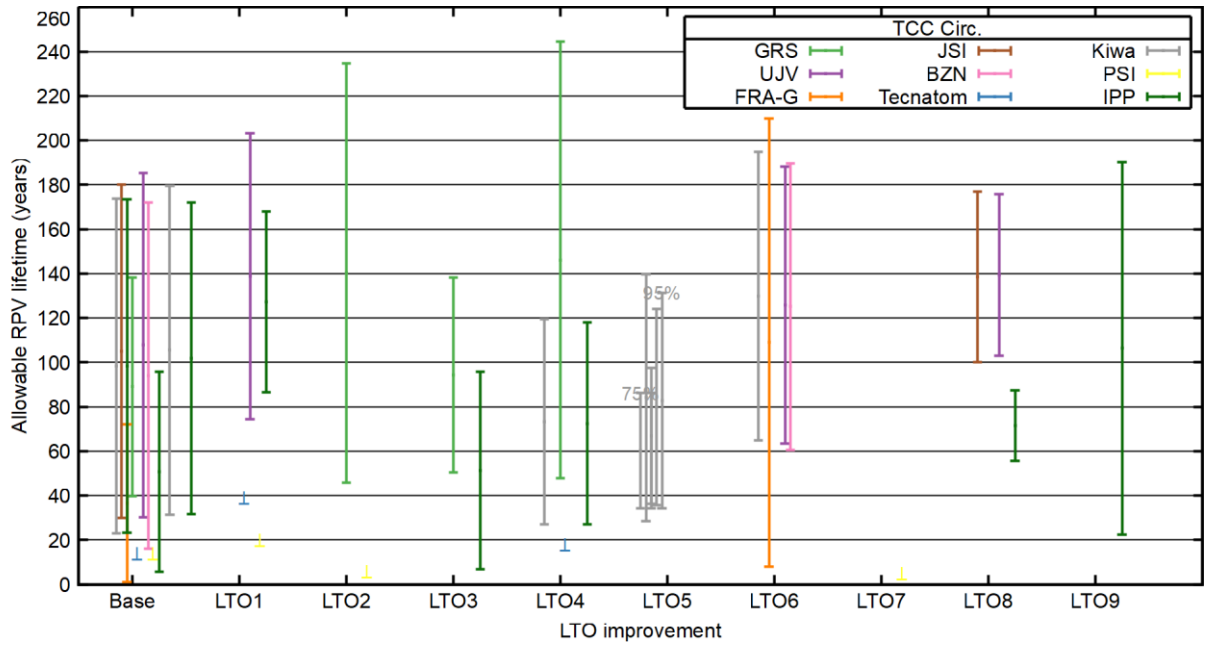

Figure 7.18: PMA2 of the LTO improvements: Predicted allowable RPV lifetime for the different LTO improvements. The bar represents the span between tangent- and max. K WPS criterion.

As there are different results for baseline case, the analysis of the effect of different LTO improvements ("lifetime prolongation") was performed, i.e. the change in allowable RPV lifetime compared to the baseline case was established. This comparison is shown in Figure 7.19.

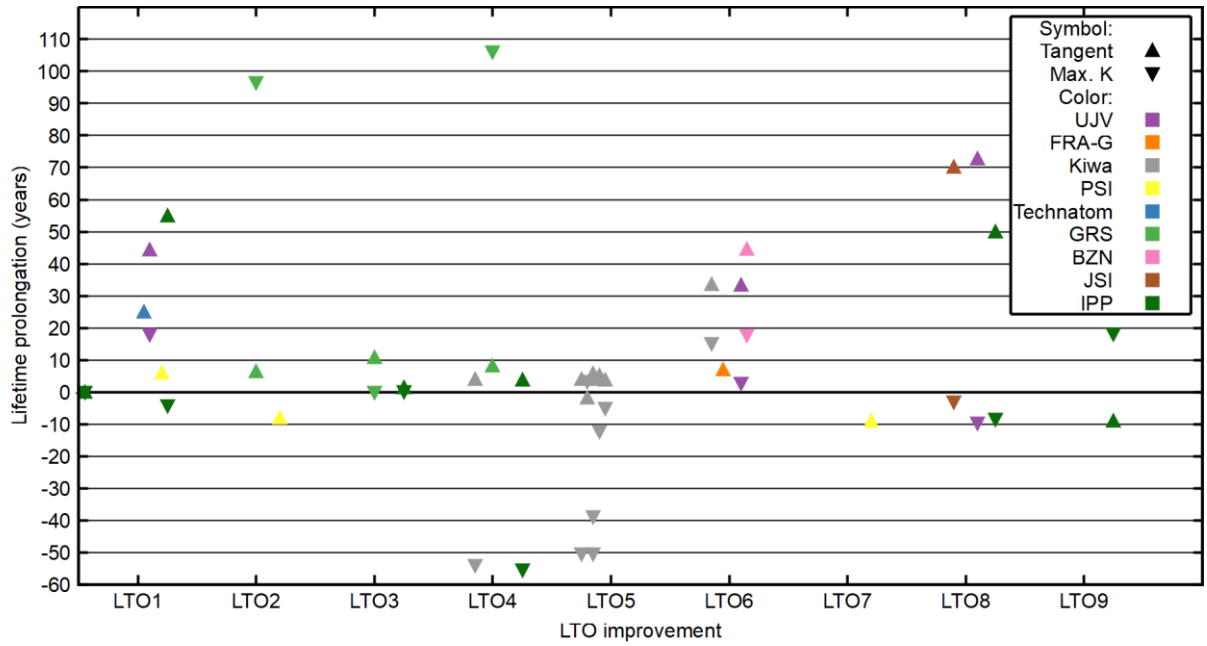

Figure 7.19: PMA2 of LTO-improvements: Predicted lifetime prolongation by different LTO improvements computed by probabilistic approach.

From this investigation, it is seen that LTO3 has only a very small effect; there is even no prolongation of lifetime for the WPS criterion. For LTO5, a small prolongation is found for the tangent criterion, and a reduction of lifetime for the max. K. assessment. However, there are also cases where a lifetime prolongation is found even with the WPS method, e.g. LTO2 (GRS) and LTO4 (GRS). Pronounced prolongations for the tangent criterion are found for LTO1, LTO6 and LTO8.

These results can be put in relation to the PMA1 results. For investigating the relation between PMA1 and PMA2, the maximum allowable RPV lifetime is shown as a function of the maximum allowable ART for the base cases and for the LTO improvements in Figure 7.20.

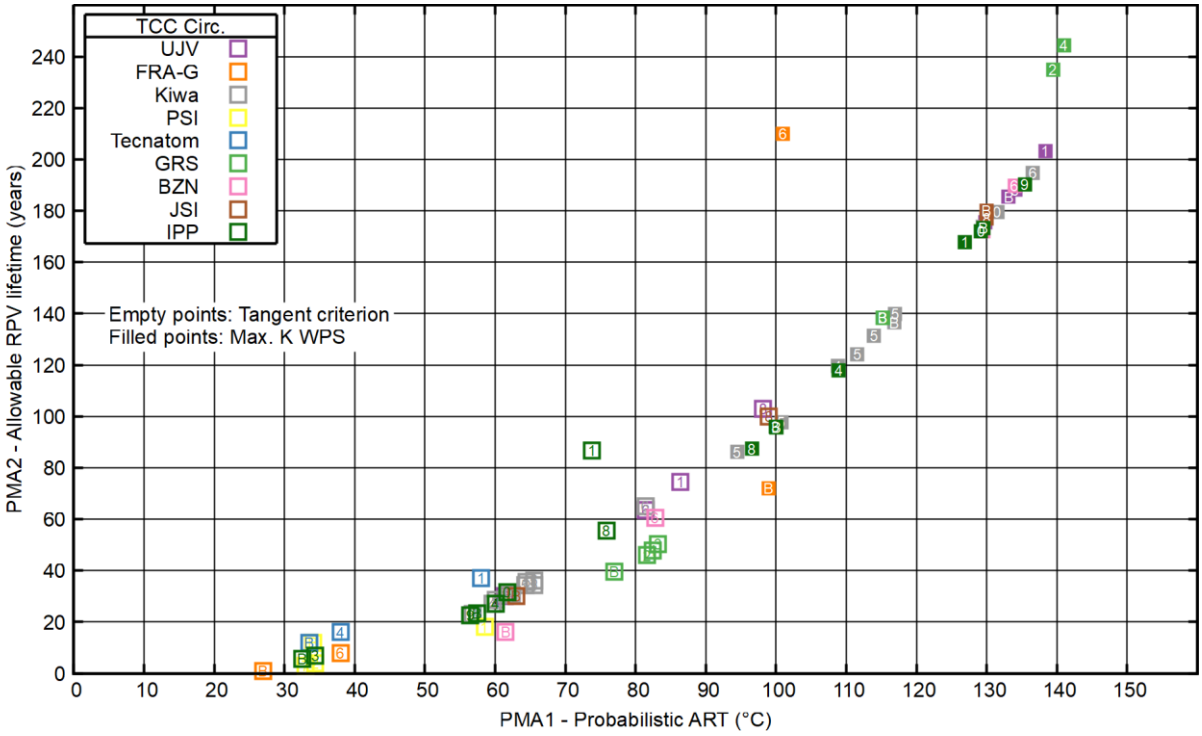

Figure 7.20: Maximum allowable RPV lifetime as a function of the probabilistically computed max. all. ART. Numbers in the boxes mean numbers of LTO improvement, B mean the base case.

This graph shows that the relation between PMA1 and PMA2 is more complex than between PMA1 and max. all. reference temperature in the deterministic assessment (see Figure 7.15). That means that the absolute lifetime prolongation effect cannot be solely determined based on PMA1. However, the relation appears to be monotonic, which means that the ranking of different improvements is the same for PMA1 and PMA2.

7.5.2.4 PMA4

The PMA4 approach allows to investigate in more detail the actual effect of the LTO improvement on the initiation probability. Therefore, PMA4 is investigated at 40 years lifetime, tangent criterion and max. K WPS criterion.

Table 7.5: CPI for 40 years, GRS contribution, TCC in circumferential orientation.

	Base	LTO2	LTO3	LTO4
Tangent	2.31e-4	8.85e-5	7.84e-5	1.066e-4
Max. K WPS	7.52e-9	5.56e-14	7.67e-9	1.96e-14

The coordinates of the MPFP are depicted in Figure 7.21 – as in Sec. 7.5.1.4, the seven coordinates are shown as the absolute values of the u-values.

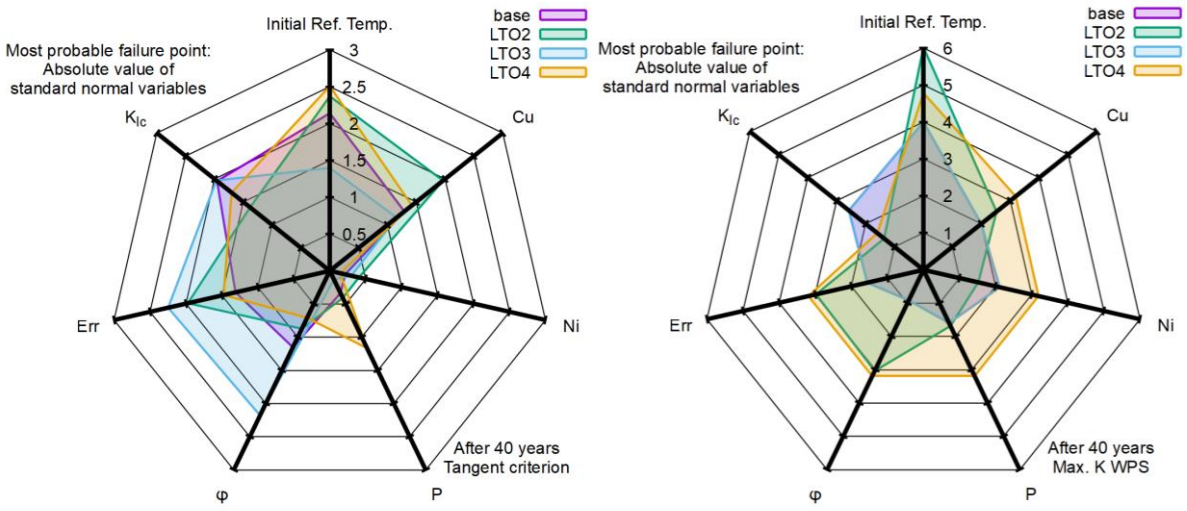

Figure 7.21: PMA4 analysis of LTO improvements LTO2, LTO3, and LTO4 after 40 years. Left: Tangent criterion, right: max. K WPS criterion.

This comparison shows that LTO2 and LTO4 differ significantly from the base case: There is a trend to higher initial reference temperatures for relevant samples, and the chemical composition plays a more important role. This can be deduced from the corresponding coordinates of the MPFPs. In contrast, LTO3 has the same MPFP as the base case for max. K WPS. Interestingly, the MPFP differs for the tangent criterion, although the lifetime prolongation effect is only small. Given the fact that the coordinates of the MPFP are related to the relevant uncertainties (see Sec. 7.3.4), this indicates that, if assessed for the tangent criterion, other uncertainties are more influential for LTO3 and the base case: While the total CPI change between the base case and LTO3 was not large, the PMA4 analysis showed that the LTO3 improvement does change the situation: Different uncertainties are relevant for the initiation probability. This insight can only be obtained by the PMA4 analysis, but not with the PMA2 analysis.

While this analysis again motivates the focus on the tangent criterion for LTO improvement assessment, it is instructive to compare the sensitivity information coded in PMA4 for different LTO improvements in a relevant age window. For this purpose, six different LTO improvements are compared for 40 years and 80 years of RPV age in the terms of importance factors in Figure 7.22.

LTO1 and LTO8 show only a small influence of the chemical composition, even for 80 years, while this is different for the other cases, especially for LTO2. This indicates that the improvements for long term operation as imposed by LTO1 and LTO8 successfully mitigate the ageing challenges. Also, it can be seen that the Copper and Nickel content for LTO2 are less relevant for an age of 40 years, but become very relevant for 80 years. (A similar statement can be made for Nickel and Phosphorus concerning LTO3).

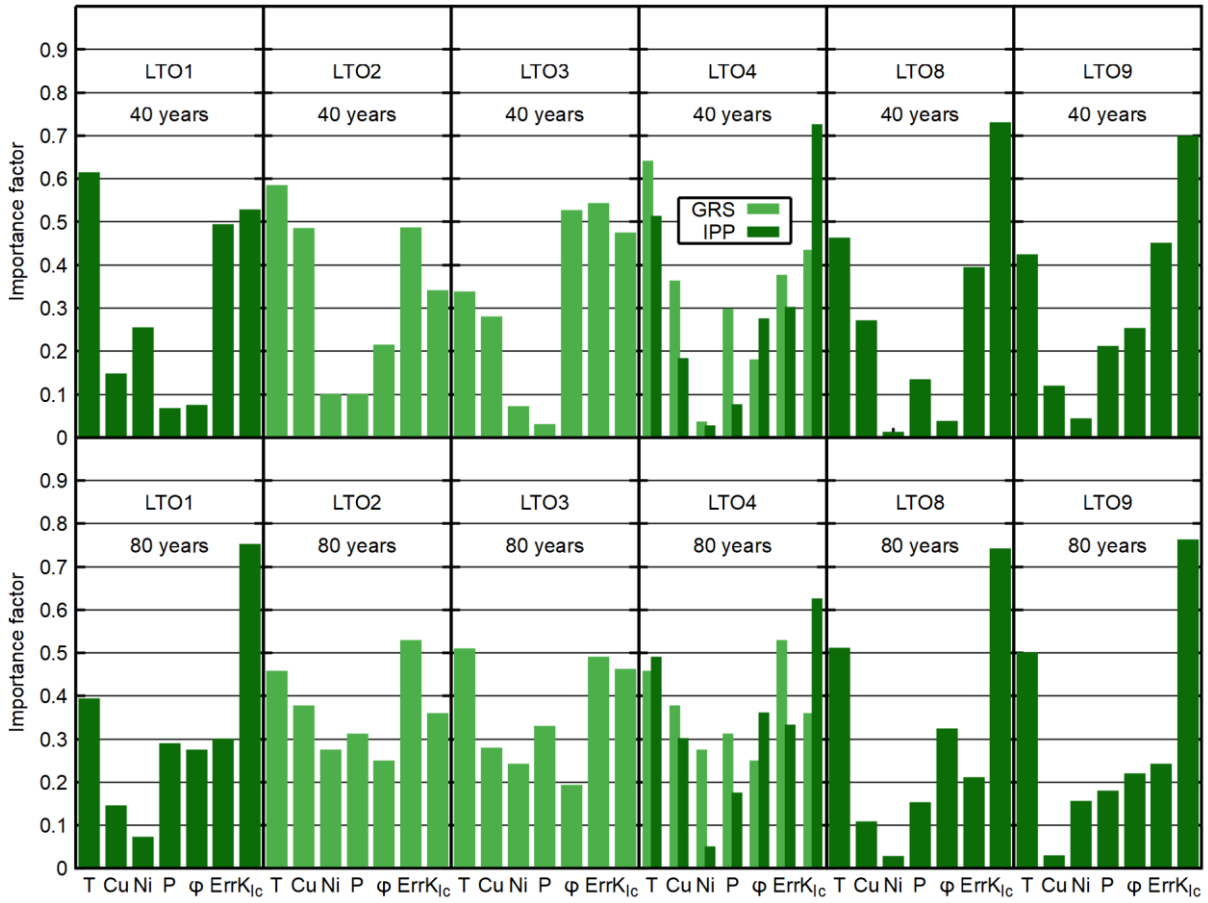

Figure 7.22: Importance factors for selected LTO improvements, TCC circ., tangent criterion, for 40 years (upper row) or 80 years (lower row) of operation.

7.5.3 Probabilistic margin assessment of thermal-hydraulic uncertainties

7.5.3.1 Introduction

The probabilistic assessment of thermal-hydraulic uncertainties is performed in Task 4.5. This section analyses the margins associated with these uncertainties and compares the results with the results of Task 3.5, where the uncertainties are considered in a deterministic fracture-mechanics assessment.

The treatment of thermal-hydraulic uncertainties in the probabilistic assessment is different than the treatment of structural uncertainties. The technical reason for this difference is that the transient set is generated by the external thermal-hydraulic code and restricted to the given “Wilks” set. The attempt of computing the CPI by “integrating out” the TH contribution by random sampling to the transient from this set has to be done with caution, since the Monte Carlo samples are from a small set, compared to the structural uncertainties and embrittlement uncertainties (see Figure 7.23). If CPI is very small (i.e. smaller than the inverse number of TH samples), it has to be conjectured that TH uncertainties contributing to this total CPI are overlooked by the restricted TH samples. Therefore, one focus of this task is the analysis of the specific contribution of TH uncertainties and the assessment of their relevance, rather than representing an integrated probabilistic PTS assessment with full consideration of TH uncertainties.

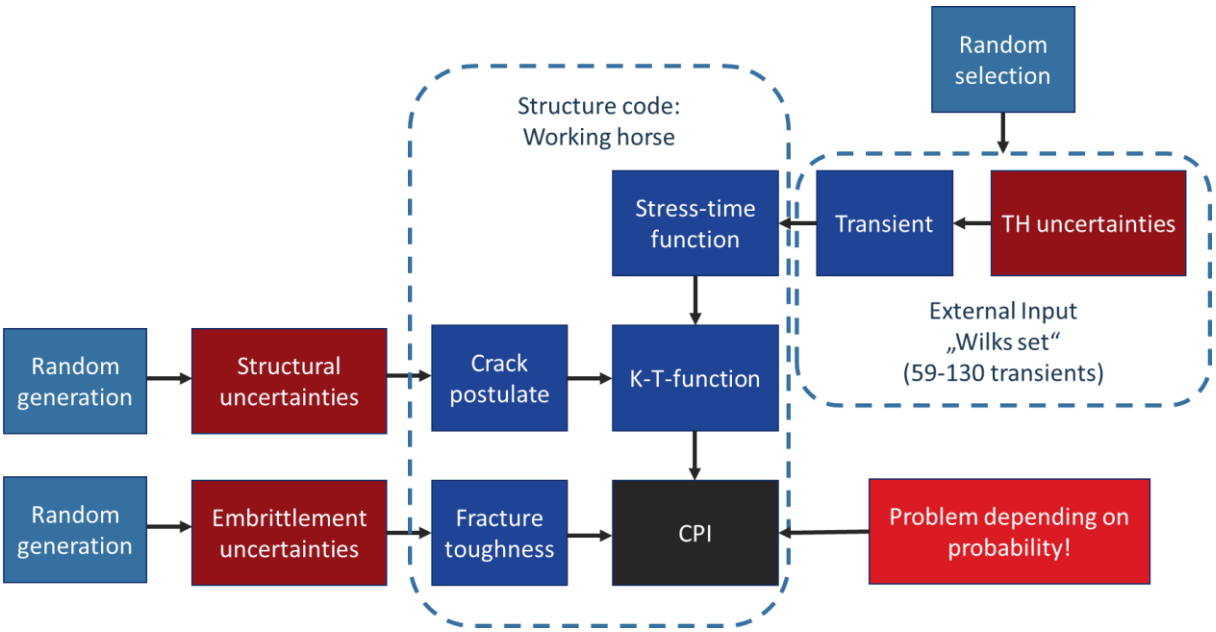

Figure 7.23: Hypothetical integration scheme for consideration of TH uncertainties in the CPI computation

As an alternative to the full probabilistic approach considering all uncertainties equally, the Wilks approach can be applied. Even the limited sample size can provide a lower or upper bound of the "figure of merit" with given confidence. Figure of merits may be either the conditional probability of initiation (CPI), or the probabilistically computed margins PMA1 or PMA2. In APAL, the most frequently used approach is to find 5% lower bound max. all. reference temperature with 95% confidence, which according to Wilks means to perform 59 samples of TH distributed parameters and the lowest value of max. all. reference temperature is the result.

As the processing of a larger set of transients requires practically the capability of scripting the fracture-mechanics code, the mandatory cases are limited. Therefore, the probabilistic fracture-mechanics assessment of the deterministically determined “bounding” (i.e. 95% quantile) transient (as identified in Task 3.4 [16])[4] is mandatory, and the probabilistic assessment of full “Wilks” set is optional. The case matrix is visualised in Figure 7.24.

[4] It was shown in WP3, that it is practically impossible to create a „bounding“ TH transient based only on TH data (pressure, temperature, HTC time variations) for the full Wilks data set. At least deterministic structural and fracture-mechanic assessment fort the full Wilks data set is needed to find the bounding transient.

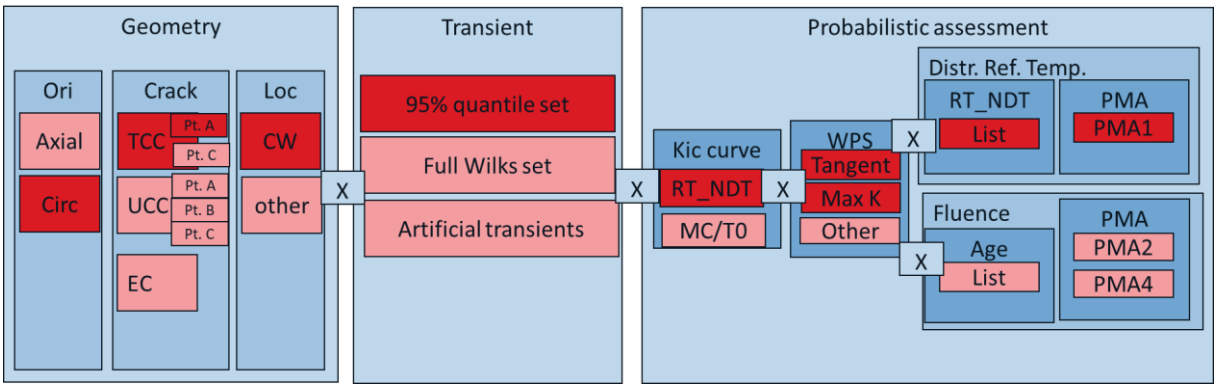

Figure 7.24: Case matrix for the probabilistic assessment of thermal-hydraulic uncertainties

Because of the interest in the full "Wilks" set analysis, the probabilistic margin assessment of the full Wilks data set is documented in detail.

7.5.3.2 PMA1

The PMA1 assessment was performed for best-estimate cases, partly for base cases, and for the deterministically determined bounding data sets. The comparison of the maximum allowable reference temperature is shown in Figure 7.25.

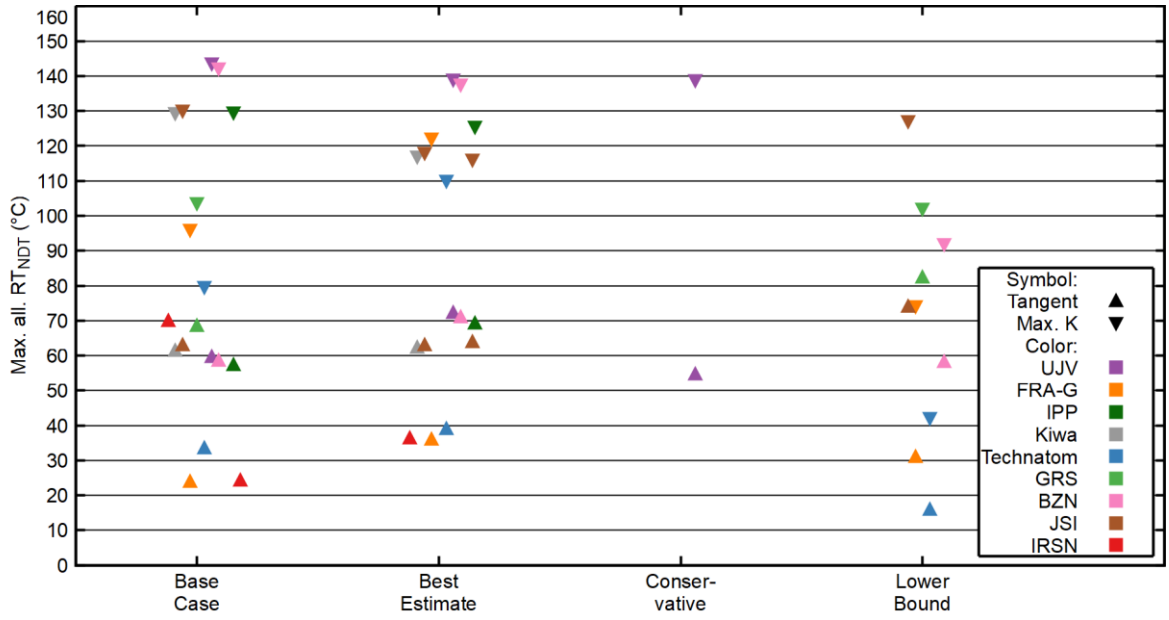

Figure 7.25: PMA1 assessment of thermal-hydraulic uncertainties; comparison of the base case, the best estimate case, and preselected bounding transients.

As seen from this figure for the tangent criterion, the best estimate case yields in general higher maximum allowable RT-NDT than the base case, as expected. This trend is not present for the max. K WPS criterion.

Several organizations submitted also the PMA1 analysis for the full Wilks set of transients. The empirical cumulative distribution functions for the circumferential TCC and the single assessments are shown together in Figure 7.26. The IRSN-93 was obtained from FRA-G with KWU-MIX, while the IRSN-59 are from UJV with RELAP.

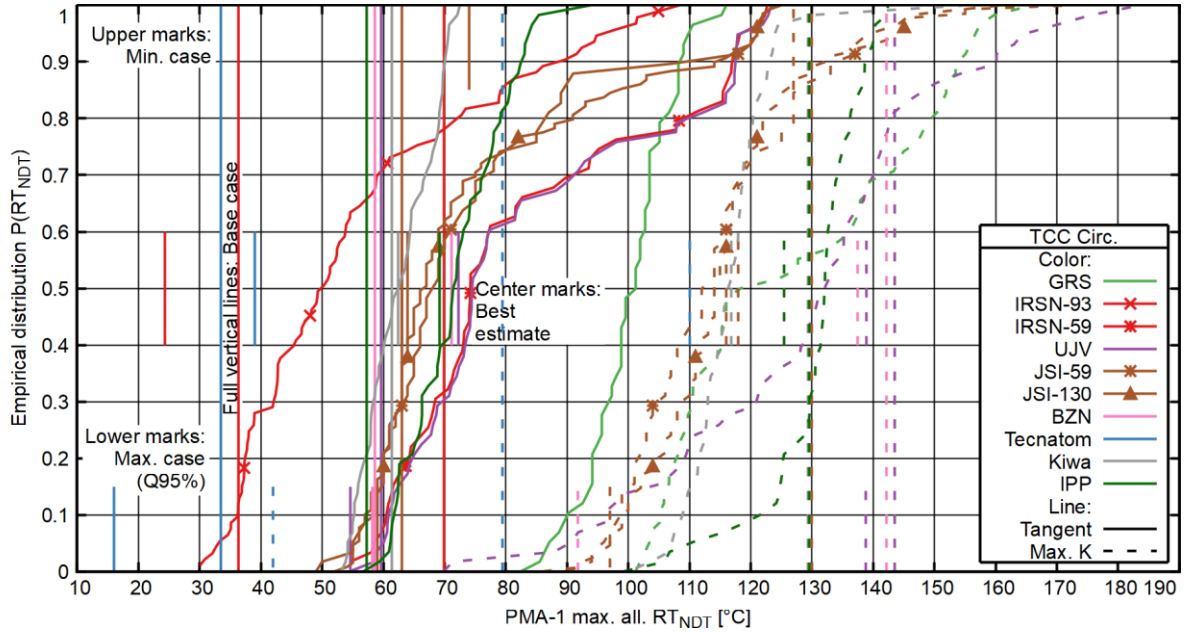

Figure 7.26: Empirical distribution function for the maximum allowable reference temperature.

Considering the results of the full "Wilks" sets, the participants derive an empirical distribution function with significant broadness, covering a range of about 33°C (ATHLET/GRS) to 80°C (RELAP/UJV/IRSN/JSI) for the tangent criterion, and even larger ranges above 100°C for the max. WPS criterion. This underlines the significance of thermal-hydraulic uncertainties in the PTS assessment. The analysis of two independent sets of different size (JSI) shows that both empirical distributions are very similar for both the tangent and the max. K WPS approach. This could imply that the larger set provides only small additional variability to the obtained results with the small set, i.e. the small set may already have a satisfying accuracy, depending on the application.

A systematic comparison of this probabilistic result with the deterministic assessment (see [16]) can also be provided. The dependence between both maximum allowable reference temperatures is visualised in Figure 7.27.

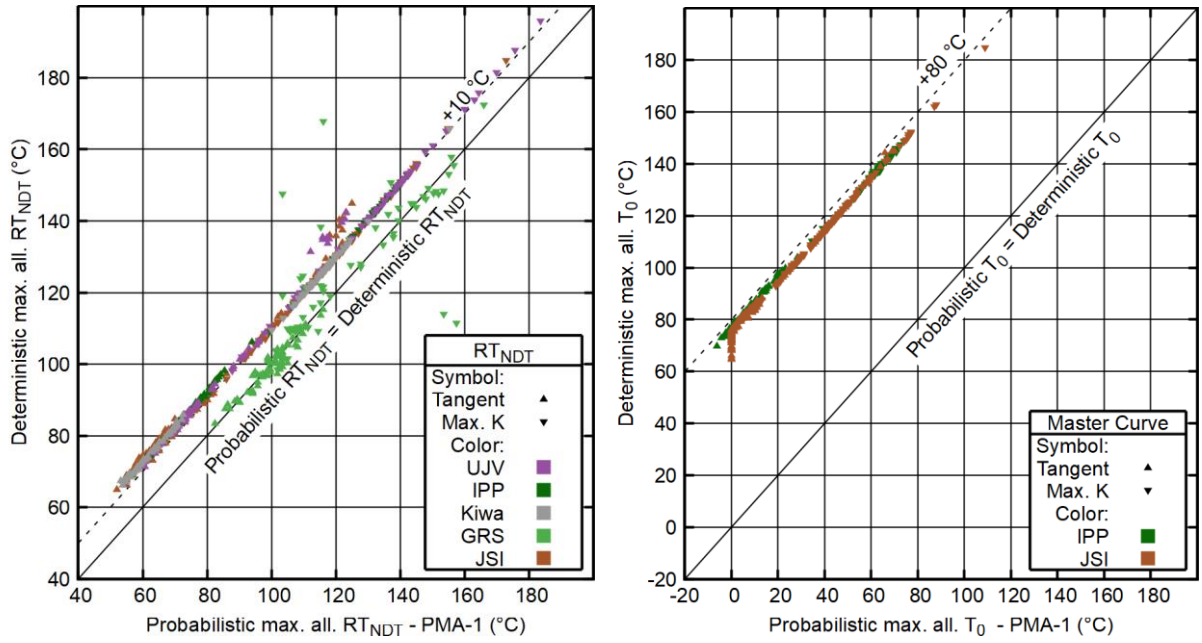

Figure 7.27: Relation between deterministic and probabilistic maximum allowable reference temperature. Left: RT-NDT approach, right: Master Curve approach.

This comparison shows that there is a clear dependence between both margins. For the RT-NDT approach, most results agree in a shift of the deterministic margin of 10°C from the probabilistic margin, except for GRS results, which are slightly lower. The Master curve result leads to significantly higher shifts of almost 80°C.

7.5.3.3 PMA2

As seen in the scheme in Figure 7.24, the PMA2 analysis is a non-mandatory task. The analysis of the maximum allowable lifetime for the base case, the best-estimate case, and the lower bound transient was provided by several participants. The comparison is shown in Figure 7.28 for the circumferential TCC postulate.

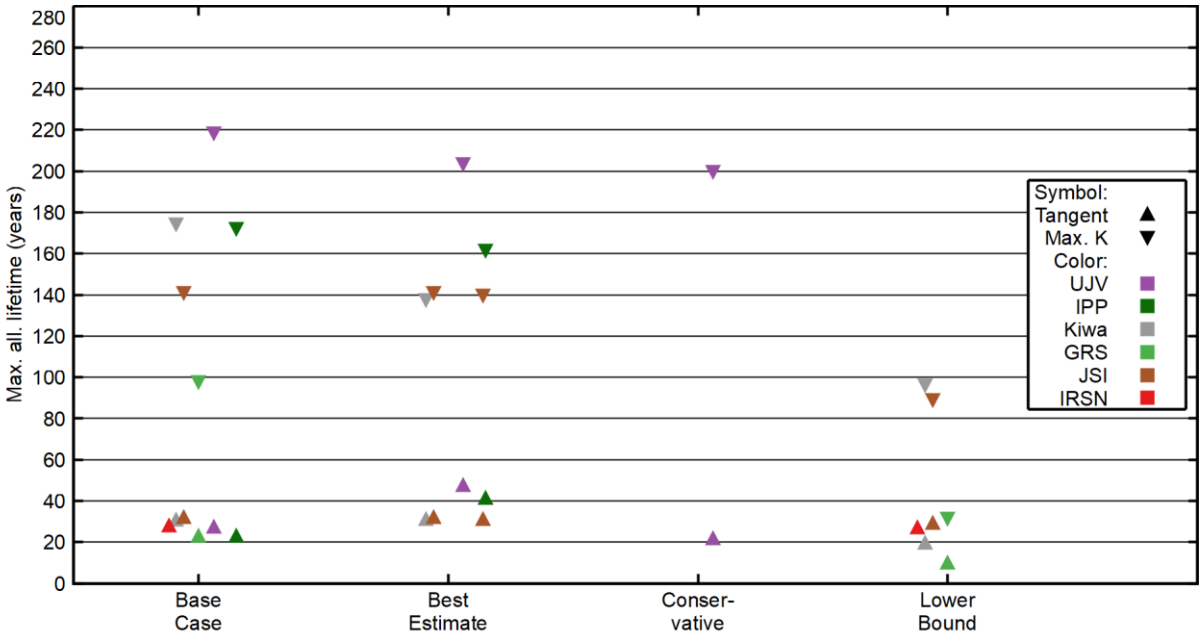

Figure 7.28: Comparison of the maximum allowable lifetime (PMA2) for the base case, the best estimate case, and the extremal transient set.

This comparison shows that the best estimate case leads to lifetimes above the base case for the tangent criterion, as expected, however this is not true for the max. K WPS method. The lower bound transient leads to smaller maximum allowable lifetimes than the base case.

The PMA2 assessment of the full set of transients provides the empirical distribution function for the maximum allowable age. The result for the circumferential TCC is shown in Figure 7.29. As stated before, the two IRSN-results are obtained from different thermal-hydraulic codes.

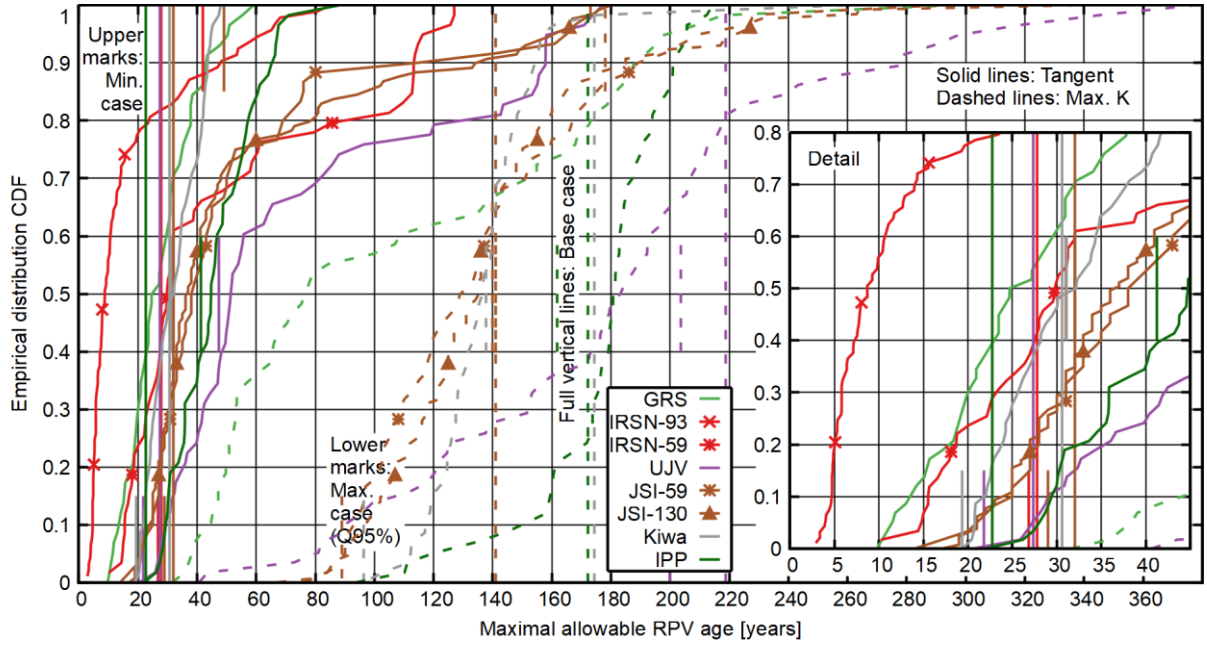

Figure 7.29: Empirical distribution function for the maximum allowable RPV age (mean value), for the circumferential TCC postulate.

The range of maximum allowable RPV ages varies between about 30 years (Kiwa, tangent approach) and about 220 years (UJV, max. K approach). The set corresponding to the 95 % confidence 5 % lower bound (rank-1 for 59 samples, rank-2 for 93 samples), is between about 1 year (IRSN) and 25 years (UJV) for the tangent approach. Again, the analysis of independent sets of different sizes (JSI) is in good agreement.

Besides the quantification of safety margin uncertainties due to the thermal hydraulic transient, this large data set can also be used to investigate the relation between PMA1 and PMA2. This comparison is done in Figure 7.30 for the RT-NDT approach, and also for the available Master Curve assessments.

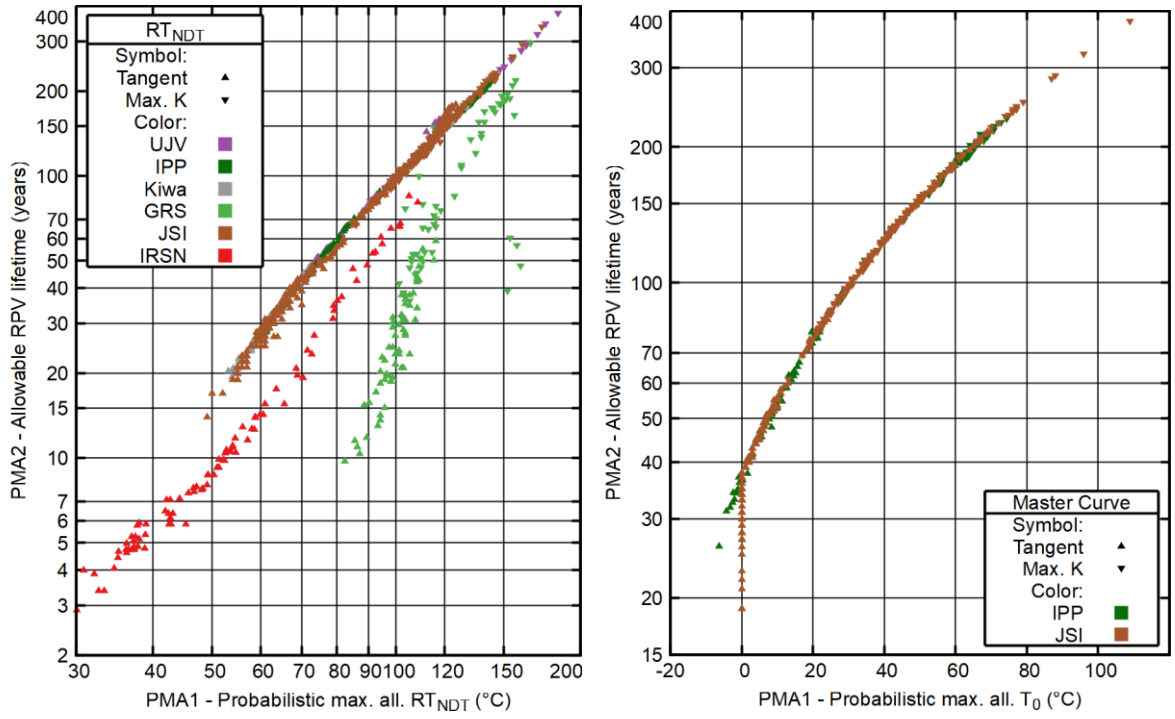

Figure 7.30: Comparison of PMA2 and PMA1 for RT-NDT (left) and Master Curve (T_0) (right) of the full Wilks sets. Note the different scales of the axes.

This investigation reveals a very strict and consistent relationship between PMA1 and PMA2 for the submissions by UJV, IPP, Kiwa, and JSI. The GRS and IRSN examples are systematically shifted, which might be related to different treatments of the distributions, or to the use of different thermal-hydraulic codes. Note the restriction to positive T_0 for JSI.

Likewise, the data can also be used to study the effect of the applied fracture toughness curve in the assessment, as the RT-NDT approach and the T_0 approach finally lead to a maximum allowable lifetime. The comparison of both predicted allowable lifetime is shown in Figure 7.31.

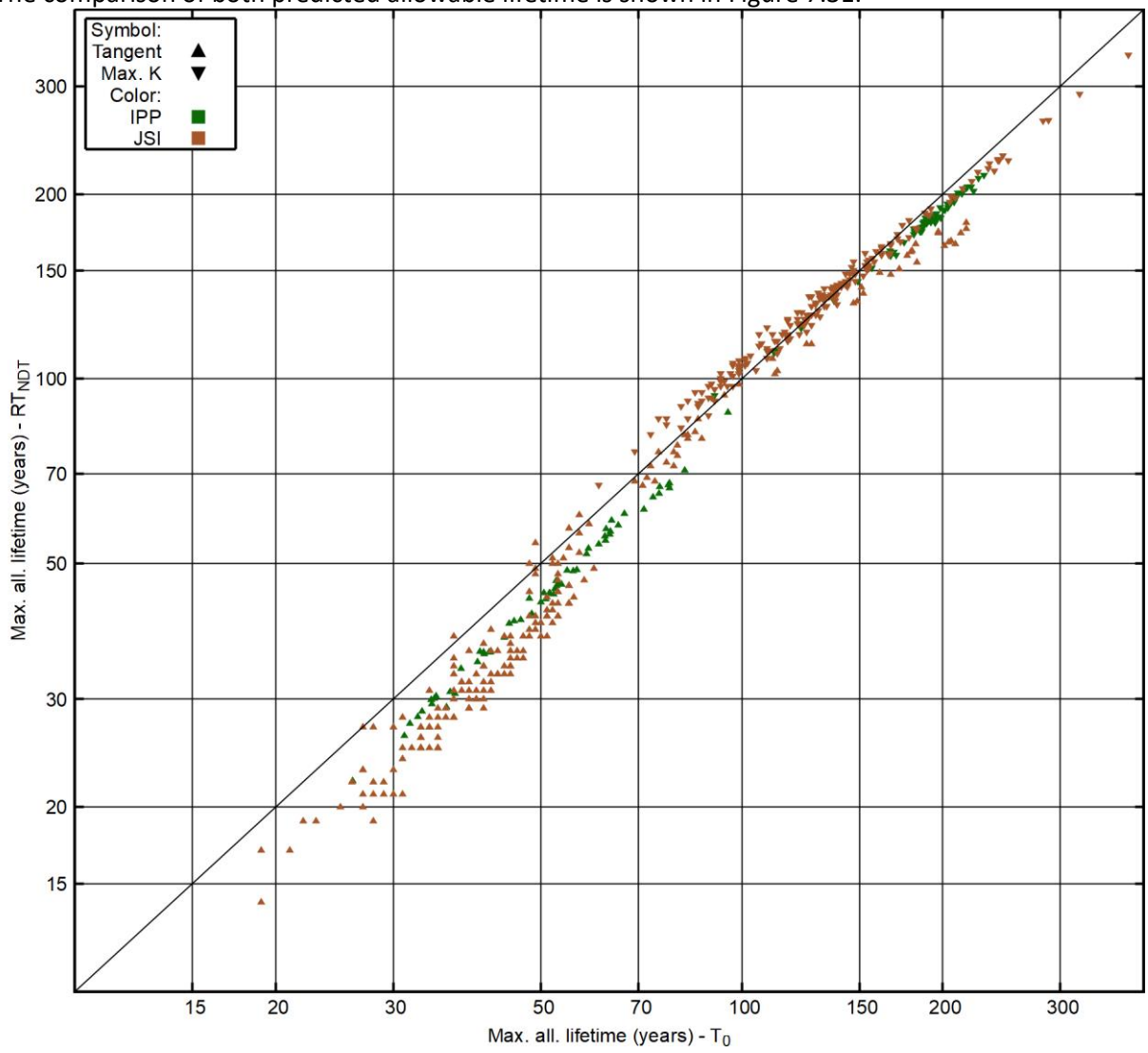

Figure 7.31: Comparison of the maximum allowable lifetime (PMA2) computed by the RT-NDT approach and the Master Curve.

This comparison shows that the Master Curve application leads in most cases to an allowable lifetime that is few years longer than the ASME curve, especially for small or large total lifetimes. However, in the range between about 50 to 160 years, also the RT-NDT curve might lead to longer allowable lifetimes. In summary, both approaches are not identical, but quite consistent. It should be noted that this result depends on the postulated initial value of RT-NDT and T_0, and also on the consideration of the crack front correction of the Master Curve.

7.6 Conclusion

Different probabilistic margin approaches were applied to probabilistic PTS assessments. Besides the baseline cases, the margin assessments for the LTO improvements and the thermal-hydraulic uncertainties are discussed.

From the methodology point of view, the PMA1 assessment in its simplest form (i.e. without additional uncertainties like crack size) offers a probabilistic quantification of safety margin with consideration of aleatoric fracture toughness uncertainties alone. It has been shown that in its simplest version this approach is strongly related to the deterministic computation of the maximum allowable reference temperature: It represents a consequent probabilistic equivalent, which also implies that it provides only limited additional information. Therefore, trends in LTO improvement effects and thermal hydraulic uncertainties can be assessed with PMA1, in a similar way as for deterministic assessments. It should be noted that the observed shift of 10°C between PMA1 and the deterministic assessment is a result of the chosen allowable CPI in this case and is therefore not necessary the same for all assessments.

The PMA2 assessment considers the interaction between uncertainties in fracture toughness, chemical composition, fluence, initial ART and potentially also additional influencing parameters. The probabilistically computed maximum allowable RPV lifetime allows a clear quantification of the safety margins of an RPV at different ages, and also the quantification of actual LTO improvement benefits and the relevance of thermal-hydraulic uncertainties.

The PMA4 approach is based on the same uncertainty consideration as PMA2 but allows for a better understanding of the mechanisms and individual risks due to specific uncertainties that are relevant. These insights can help to understand the evolution of a CPI of an ageing RPV, and to separate the different uncertainties, also for the effectiveness of LTO improvements.

The contributions of the participants differ due to different thermal-hydraulic input data sets and different fracture-mechanics codes. Thanks to the preparatory steps in the deterministic benchmarks, these differences are understood. Therefore, the present variations in the analysis results represent rather sensitivity studies with use of alternative data sets than the quantification of numerical problems. Indeed, several cases underline a good agreement when the thermal-hydraulic data set and the fracture-mechanics approach are identical.

The investigated base cases and the specific dimensions and positions of the postulated cracks show that the UCC assumption leads to the largest margins, and the TCC assumption to the smallest margins. Only few EC contributions are received (as substitute for UCC); they turn out to have smaller margins than UCC, but larger than TCC. The axial orientation leads typically to a slightly smaller margin than the circumferential orientation, which can be understood from the pressure influence (causing higher hoop stresses than axial stresses). The results for axial and circumferential crack orientations are similar because mostly 1D solution was used in the performed analyses, i.e. no cold plume effect was considered. Moreover, the value of inner pressure in the critical time was small. In other cases, crack orientation can affect the results more significantly.

In the comparison of LTO improvements, the probabilistic approach allows for a ranking of the effectiveness of the different proposed improvement measures. As the relation between PMA1, PMA2 and the deterministic margin is monotonic, it can be concluded that the ranking is identical to the deterministic approach. However, the quantification of the additional possible lifetime via PMA2 is a convincing result of this study. It makes sense to assess the LTO aspects with the tangent criterion only, due to less sensitivity and smaller scatter in the results by different partners. Also, with regard to the selected cases in this report, the very long possible lifetimes obtained with use of the max. K WPS criterion are typically beyond any expectations on RPV operation time. Focused on this, the lifetime prolongation ranges from few years (LTO2, LTO3, LTO4, LTO5) to some decades (LTO1 and LTO8, tangent criterion).

In the probabilistic quantification of thermal-hydraulic uncertainties, the most interesting result is the computation of the CPI for the full “Wilks” set, which was provided by six different participants for PMA1 and PMA2, respectively. This analysis allows for the derivation of an empirical cumulative distribution function of the MART, lifetime, or CPI, and for the identification of a value of a 5% lower bound value following the Wilks approach. The analysis confirms that the thermal-hydraulic uncertainties lead to a large scatter in maximum allowable reference temperature (PMA1) and maximum allowable RPV lifetime (PMA2), respectively. Moreover, it shows that the base case has typically higher margins than this 5% lower bound. This finding underlines that an expert-based pre-selection of transients might miss the most critical TH parameter set, and an assessment of a large set of transients with TH uncertainties included is a more appropriate approach. This effect is more pronounced when max K WPS approach is used. While the monotony of the margins (see above) promises that already a deterministic margin assessment might be a good guidance, the overall goal should be an integrated consideration of uncertainties from all sources for a probabilistic assessment. The conceptualization and the realization of the inclusion of the thermal-hydraulic uncertainties in the probabilistic assessment, despite challenges in software architecture and numerical techniques, is therefore the vision at the end of the probabilistic margin assessment within APAL.

This deliverable only considers the tangent approach and the max. K WPS approach. Observations can be made based on the sheer number of investigated cases. It can be concluded that the Max WPS approach is realistic (in the sense of a best-estimate), but it is less suitable for lifetime assessment of real nuclear power plants, because it is very sensitive to input thermal hydraulic data. The tangent approach (and possibly also other criteria) are more conservative and, at the same time, less sensitive to the TH inputs.

8 General conclusions of WP4

APAL (Advanced PTS Analysis for LTO) is a project funded by the EU within HORIZON 2020 programme. One of the most limiting safety assessments for the long-term operation (LTO) of nuclear power plants (NPPs) is the reactor pressure vessel (RPV) integrity assessment for pressurized thermal shock (PTS). The main objectives of APAL project are establishment of state-of-the-art of LTO improvements having an impact on PTS analysis, development of advanced deterministic and probabilistic PTS assessment methods including thermal hydraulic (TH) uncertainty analyses, the quantification of safety margins for LTO improvements and the development of best-practice guidance. The APAL project consists of 7 work packages (WP), which are listed in the Introduction chapter of this report.

This report summarises the work and results of **WP4 "Probabilistic margin assessment".** The main objective of the WP4 was to determine the impact of LTO improvements and uncertainties in thermal hydraulic (TH) data on the results of PTS analysis using probabilistic assessment. As a part of this assessment, probabilistic safety margins have been quantified and compared with deterministic safety margins. The WP4 (Probabilistic margin assessment) consisted of six tasks:

- Task 4.1: Structural assessment
- Task 4.2: Definition of a probabilistic benchmark
- Task 4.3: Baseline probabilistic benchmark
- Task 4.4: Probabilistic benchmark related to LTO improvements
- Task 4.5: Probabilistic benchmark related to uncertainties in the TH data
- Task 4.6: Probabilistic margin assessment

The detailed conclusions for main computational tasks (Tasks 4.3-4.6) have been presented in the respective Sections 4-7 of this report. This Section repeats the main findings and general conclusions per Task in a more structured way.

The **Task 4.3: Baseline probabilistic benchmark**, dealt with verification of probabilistic tools used by participants followed by testing and evaluation of a complete chain of probabilistic analyses through a series of round robin benchmarks. All analyses dealing with probabilistic tool verification and the first round robin benchmark have been performed by partners using the pre-defined common data.

Considering a complexity of probabilistic analyses along with a variety of used probabilistic tools, the tool verification using the pre-defined common data was an important and essential step before embarking on probabilistic analyses with partner-specific transient data. By comparing the results from different partners obtained from the tool verification analyses a performance and trustworthiness of used probabilistic tools was verified. Also, some ambiguities with interpretation of certain input data were identified and adjusted.

One of the challenges within the APAL project was related to developing a realistic flaw depth distribution for UCC cracks that can be used in probabilistic analyses. The PNNL flaw distribution model for UCC cracks was chosen as a basis, however the original PNNL model cannot be used directly with an arbitrary probabilistic code. The generic CDF for UCC flaw depth has been developed through a round-robin exercise where the involved partners individually interpreted, made necessary assumptions, and mathematically treated the PNNL flaw distribution model. Based on these results, the CDF for UCC flaw depth was defined for probabilistic assessments in APAL.

Also, treatment of certain input parameters described by truncated normal distributions has been investigated as a part of tool verification work. No significant differences have been observed between the partners as a result of truncation of distributions. It should be noted that the FAVOR users did not participate in this tools verification and thus, the truncation method used within FAVOR was not considered in the comparisons.

Calculation of CPI and cpi(t) for a pre-defined transient was also performed as a part of tool verification work. This subtask required several iterations for achieving similar results between the partners but was beneficial for testing a computational chain prior to the subsequent round robin analyses based on partner-specific transient data.

The first round robin analysis RR1 was based on the pre-defined common data and aimed at predicting ART-values for an increasing fluence level. The results indicated that ART-values have a clear correlation with fluence level, increasing with the RPV age. It was shown that the ART-values vary through the RPV wall thickness being highest at the inner surface of the RPV. It has also been observed that for shallow cracks the ART-values for welds were higher in comparison to base metal. However, the ART-values for base metal were governing for deeper cracks. This transition occurs at a deeper position through the RPV wall with increasing RPV operation times. The results from RR1 also demonstrated that a choice of shift function has a large influence on the calculated ART-values, where the shift function according to RSE-M governs the ART-values for shallow cracks. For deeper crack the base shift function takes over predicting the highest ART-values for base metal, while the 10CFR50.61a shift function governs the ART-values for welds.

The round robin analysis RR2 was based on partner-specific transient data, and thus some differences in results were expected. In general, the agreement between partners after some iterations was good and the differences can be explained by different transient data. The TCC gives the shortest lifetimes and in most cases, point C at the clad/base interface was limiting.

The RR3 analysis with a considered crack arrest was a non-mandatory extension of RR2. Only few partners participated in this subtask which made comparative verification difficult. Some benefits could be seen when considering crack arrest, especially for the FAVOR users, but crack arrest did not lead to longer lifetimes for all cases.

The RR4 analysis was similar to the RR2, but a distributed crack was considered in this assessment. It should be noted that even the largest crack size in the distribution was smaller than the crack used in RR2. Therefore, substantially higher max. all. ART-values and RPV ages were obtained for the RT_{NDT} and T_0 concepts, while the differences were much smaller for the FAVOR concept.

The RR5 analysis was a non-mandatory extension of RR4 where crack arrest was considered. Only IPP contributed with results for the RT_{NDT} and T_0 concept, while both JSI and Tecnatom contributed with results for a circumferential TCC2 using the FAVOR concept. For the RT_{NDT} concept, IPP gets a benefit from considering crack arrest for TCCs when using the tangent approach, while no gain is seen for the max WPS approach. The results are similar for the T_0 concept, with the addition that a small benefit for TCCs is seen for the max WPS approach as well. For the FAVOR concept, a benefit from considering crack arrest is seen for all cases studied.

The **Task 4.4: Probabilistic benchmark related to LTO improvements**, has focused on probabilistic fracture mechanics calculations of the LTO improvements identified in WP2 [8]. In general, the results for the mandatory case were consistent and reasonable when compared to the deterministic results from WP3 [7], although the initiation frequency (CPI) used in the deterministic and probabilistic assessments are different. Most of the differences between the partners can be attributed to either the source of the TH input data or the code used in the probabilistic assessments. The partners who used FAVOR in their probabilistic calculations have used a crack size different from that defined for the benchmark due to certain limitations in the FAVOR code when performing PMA1.

The **Task 4.5: Probabilistic benchmark related to uncertainties in the TH data**, has dealt with several probabilistic fracture-mechanics calculations related to the uncertainties in the thermal hydraulic data. For a first comparison, the CPI for several fixed max. all. ART values were calculated. The results were shown to be in good agreement, and the differences can be explained by the use of different TH input data, mainly by the differences between mixing and system (non-mixing) TH analyses.

For PMA1, the max. all. ART for a given allowable crack initiation frequency (CPI=2.28e-4) with ART being a fixed input parameter to PFM was determined. The preliminary comparison between the partners was done in terms of max. all. ART. The quantiles and mean value for max. all. ART were calculated and compared. Within this task consistent results for all partners were obtained. The WPS approach has a big influence on the final result.

For PMA2, the max. all. lifetime (RPV age) for a given allowable crack initiation frequency (CPI=2.28e-4) was calculated. The lifetime of the RPV defines the ART shift (both the initial ART and the ART shift were treated as distributed parameters) as input for the PFM. In the end the correlation of a lifetime with CPI (from several probabilistic fracture mechanics analyses) was used to determine the maximum allowable lifetime. Within this task consistent results for all partners were obtained. The WPS approach has a big influence on the final result, even more than for PMA1.

In general, consistent results for all partners were obtained for all subtasks. Some differences between the partners are related to the differences in the thermohydraulic input, i.e. thermohydraulic input data and code used, especially the way of analysing the mixing. The consideration of WPS effect has a big influence for the final result. It is resulting in a large difference compared with the tangent approach for the max. all. ART results (PMA1) and even larger difference for the max. all. RPV age (PMA2).

In the **Task 4.6: Probabilistic margin assessment**, different probabilistic margin approaches were applied to probabilistic PTS assessments performed for the baseline cases, the LTO improvements and the thermal-hydraulic uncertainties.

From the methodology point of view, the PMA1 assessment in its simplest form (i.e. without additional uncertainties like crack size) offers a probabilistic quantification of safety margin with consideration of aleatoric fracture toughness uncertainties alone. It has been shown that in its simplest version this approach is strongly related to the deterministic computation of the maximum allowable reference temperature: It represents a consequent probabilistic equivalent, which also implies that it provides only limited additional information. Therefore, trends in LTO improvement effects and thermal hydraulic uncertainties can be assessed with PMA1, in a similar way as for deterministic assessments. It should be noted that the observed shift of 10°C between PMA1 and the deterministic assessment is a result of the chosen allowable CPI in this case and is therefore not necessary the same for all assessments.

The PMA2 assessment considered the interaction between uncertainties in fracture toughness, chemical composition, fluence, initial ART and potentially also additional influencing parameters. The probabilistically computed maximum allowable RPV lifetime allowed for a clear quantification of the safety margins of an RPV at different ages, and also the quantification of actual LTO improvement benefits and the relevance of thermal-hydraulic uncertainties.

The PMA4 approach was based on the same uncertainty consideration as PMA2 but allowed for a better understanding of the mechanisms and individual risks due to specific uncertainties that are relevant. These insights can help to understand the evolution of a CPI of an ageing RPV, and to separate the different uncertainties, also for the effectiveness of LTO improvements.

The contributions of the participants differed due to different thermal-hydraulic input data sets and different fracture-mechanics codes. Thanks to the preparatory steps in the deterministic benchmarks, these differences were understood. Therefore, the present variations in the analysis results represent rather sensitivity studies with use of alternative data sets than the quantification of numerical problems. Indeed, several cases underline a good agreement when the thermal-hydraulic data set and the fracture-mechanics approach are identical.

The investigated base cases and the specific dimensions and positions of the postulated cracks show that the UCC assumption leads to the largest margins, and the TCC assumption to the smallest margins. Only few EC contributions are received (as substitute for UCC); they turn out to have smaller margins

than UCC, but larger than TCC. The axial orientation leads typically to a slightly smaller margin than the circumferential orientation, which can be understood from the pressure influence (causing higher hoop stresses than axial stresses). The results for axial and circumferential crack orientations are similar because mostly 1D solution was used in the performed analyses, i.e. no cold plume effect was considered. Moreover, the value of inner pressure in the critical time was small. In other cases, crack orientation can affect the results more significantly.

In the comparison of LTO improvements, the probabilistic approach allows for a ranking of the effectiveness of the different proposed improvement measures. As the relation between PMA1, PMA2 and the deterministic margin is monotonic, it can be concluded that the ranking is identical to the deterministic approach. However, the quantification of the additional possible lifetime via PMA2 is a convincing result of this study. It makes sense to assess the LTO aspects with the tangent criterion only, due to less sensitivity and smaller scatter in the results by different partners. Also, with regard to the selected cases in this report, the very long possible lifetimes obtained with use of the max. K WPS criterion are typically beyond any expectations on RPV operation time. Focused on this, the lifetime prolongation ranges from few years (LTO2, LTO3, LTO4, LTO5) to some decades (LTO1 and LTO8, tangent criterion).

In the probabilistic quantification of thermal-hydraulic uncertainties, the most interesting result is the computation of the CPI for the full “Wilks” set, which was provided by six different participants for PMA1 and PMA2, respectively. This analysis allowed for the derivation of an empirical cumulative distribution function of the MART, lifetime, or CPI, and for the identification of a value of a 5% lower bound value following the Wilks approach. The analysis confirmed that the thermal-hydraulic uncertainties lead to a large scatter in maximum allowable reference temperature (PMA1) and maximum allowable RPV lifetime (PMA2), respectively. Moreover, it showed that the base case had typically higher margins than this 5% lower bound. This finding underlines that an expert-based pre-selection of transients might miss the most critical TH parameter set, and an assessment of a large set of transients with TH uncertainties included would be a more appropriate approach. This effect is more pronounced when max WPS approach is used. While the monotony of the margins promises that already a deterministic margin assessment might be a good guidance, the overall goal should be an integrated consideration of uncertainties from all sources for a probabilistic assessment. The conceptualization and the realization of the inclusion of the thermal-hydraulic uncertainties in the probabilistic assessment, despite challenges in software architecture and numerical techniques, is therefore the vision at the end of the probabilistic margin assessment within APAL.

For the probabilistic margin assessments only the tangent approach and the max WPS approach were considered. Observations can be made based on the sheer number of investigated cases. It can be concluded that the max WPS approach is realistic (in the sense of a best-estimate), but it is less suitable for lifetime assessment of real nuclear power plants, because it is very sensitive to input thermal hydraulic data. The tangent approach (and possibly also other criteria) are more conservative and, at the same time, less sensitive to the TH inputs.

9 Lessons-learned in WP4

During the work performed within the WP4 in the APAL project several important lessons learned topics have been identified and described below.

9.1 Tool verification and round robin analyses

In the context of performed tool verifications and initial round robin analyses, the following important and interesting findings can be highlighted as lessons-learned:

- Considering a complexity of probabilistic analyses along with a variety of used probabilistic tools, verification of different tools and methods based on the pre-defined common data was shown to be an important and essential prerequisite in APAL before embarking on probabilistic analyses with partner-specific transient data. By comparing the results from different partners obtained from the tool verification analyses a performance and trustworthiness of used probabilistic tools was verified. Also, some ambiguities with interpretation of certain input data were identified and adjusted.

- For crack depth positions closer to the inner surface (i.e. for shallow cracks), the ART-values for welds were shown to be higher in comparison to the ART-values for base metal. However, for crack depth positions located deeper in the RPV wall the ART-values for base metal become governing instead. The depth through the RPV wall at which this transition occurs was found to increase with longer operation times (see Figure 4.50 in Section 4.3.1). It has to be noted, that this finding is relevant for APAL benchmark, as it is strongly dependent on the initial value of ART and the irradiation embrittlement formulae used.

- A choice of ART shift function was shown to have a large influence on the calculated ART-values as demonstrated by the calculation results in RR1 (see Section 4.3.1).

- For verifying calculations and finding reasons for deviances between results, Kiwa performed analyses using the transient data from other partners for several cases within RR2 (see Section 4.3.2.3). During this work, the results for PMA1 could directly be verified while the more complex PMA2 calculations required some iterations in order to obtain good agreement in results. In conclusion, performing the analyses of the same case using a full set of available probabilistic tools may be useful to identify inherent code differences and investigate the influence of taken assumptions.

9.2 Probabilistic analyses and margin assessments

Based on performed probabilistic analyses for LTO improvements and TH uncertainties, the following important and interesting findings can be highlighted as lessons-learned:

- PMA1 assessment offers a probabilistic quantification of safety margin with consideration of aleatoric fracture toughness uncertainties alone as distributed parameter. It was shown that PMA1 in its simplest version is strongly related to the deterministic computation of the max. all. ART providing only limited additional information. Thus, trends in LTO improvement effects and TH uncertainties can be assessed with PMA1, in a similar way as for deterministic assessments.

- PMA2 assessment takes into account the interaction between uncertainties in fracture toughness, chemical composition, fluence, initial ART and potentially also additional influencing parameters. The probabilistically computed max. all. RPV lifetime allowed for a

clear quantification of the safety margins of an RPV at different ages, and also the quantification of actual LTO improvement benefits and the relevance of TH uncertainties.

- PMA4 approach was based on the same statistically distributed input parameters as PMA2 but allowed for a better understanding of the mechanisms and individual risks due to the use of reliability theory quantifying the margins in terms of the position of the most probable failure point (MPFP). This approach can help to understand the evolution of a CPI of an ageing RPV, and to separate the different uncertainties, also for the effectiveness of LTO improvements.

- Probabilistic approach allowed for a ranking of the effectiveness of the different proposed LTO improvement measures. The tangent approach was shown to provide consistent results with a smaller scatter between the partners. However, quantification of the additional possible lifetime via PMA2 obtained with max WPS approach provided a substantial gain in RPV operation time.

- Performed probabilistic margin assessments confirmed that the TH uncertainties propagate to „wide“ CDFs of max. all. ART (PMA-1) and max. all. RPV lifetime (PMA-2). Moreover, it was also shown that the base case transient had typically higher margins than the 5% lower bound case. This finding underlines that an expert-based pre-selection of transients might miss the most critical TH parameter set, and an assessment including a large set of transients with TH uncertainties using Wilks approach would be a more appropriate approach. This feature is more pronounced, when max WPS approach is used.

- Investigation of deterministic and probabilistic margins showed that a monotonic relation between both approaches can be established. This indicates that a deterministic margin assessment might solely provide a good guidance for selection of most critical transient or TH uncertainty parameter set, however the overall goal should be an integrated consideration of uncertainties from all sources (i.e. thermal-hydraulic and fracture mechanics parameters) for a probabilistic assessment. The conceptualization and the realization of the inclusion of the TH uncertainties in the probabilistic assessment, despite challenges in software architecture and numerical techniques, is therefore the vision at the end of the probabilistic margin assessment within APAL.

- Consideration of WPS effect was shown to have a substantial influence compared with the tangent approach for the max. all. ART results (PMA1) and even larger difference for the max. all. RPV age (PMA2). It is concluded that the max WPS approach is realistic (in the sense of a best-estimate), but it is less suitable for lifetime assessment of real nuclear power plants, because it is very sensitive to input thermal hydraulic data. The tangent approach (and possibly also other WPS approaches) are more conservative and, at the same time, less sensitive to the TH inputs.

10 References

[1] APAL Deliverable No. 4.1. Stress and temperature distributions to be to be used in the probabilistic assessment. APAL Project. November 2023.

[2] APAL Deliverable No. 4.2. Baseline probabilistic benchmark definition. APAL Project. November 2022.

[3] APAL Deliverable No. 4.3. Baseline probabilistic benchmark. APAL Project. June 2024.

[4] APAL Deliverable No. 4.4. Probabilistic benchmark related to LTO improvements. APAL Project. June 2024.

[5] APAL Deliverable No. 4.5. Probabilistic benchmark related to uncertainties in the thermal hydraulic data. APAL Project. June 2024.

[6] APAL Deliverable No. 4.6. Probabilistic Margin Assessment. APAL Project. June 2024.

[7] APAL Deliverable No. 3.5. Public Summary report of WP3. APAL Project. July 2024.

[8] APAL Deliverable No. 2.4. Public Summary report of WP2. APAL Project. March 2023.

[9] APAL Deliverable No. 1.6. Public Summary report of WP1. APAL Project. December 2021.

[10] APAL Deliverable No. 2.1. Results of TH analysis for selected LTO improvements. APAL Project. December 2021.

[11] APAL Deliverable No. 2.2. Evaluation of uncertainties in TH analysis related to computer code models, plant parameters and human factors. APAL Project. May 2022.

[12] APAL Deliverable No. 2.3: Results of TH Analysis Related to TH Uncertainties. APAL Project. December 2022.

[13] APAL Deliverable No. 3.1. Stress and temperature distributions for benchmark performance. APAL project. May 2023.

[14] APAL Deliverable No. 3.2. Benchmark definition. APAL project. September 2022.

[15] APAL Deliverable No. 3.3. First Benchmark Performance. APAL project. December 2023.

[16] APAL Deliverable No. 3.4. Safety margin related to LTO improvements and TH uncertainties. APAL project. June 2024.

[17] APAL Deliverable No. 1.4. State-of-the-art of probabilistic PTS analysis and relevant statistical tools. APAL project. September 2021.

[18] https://en.wikipedia.org/wiki/Mersenne_Twister

[19] ICAS project. https://www.grs.de/sites/default/files/2021-06/GRS-152.pdf

[20] DEFI-PROSAFE D6.9.1 “Approach adopted for safety margin evaluation based on probabilistic” V4/270816.

[21] Regulatory Guide 1.230, Revision 0. Regulatory Guidance on the Alternate Pressurized Thermal Shock Rule. (RG 1.230, "Regulatory Guidance on the Alternate Pressurized Thermal Shock Rule." (nrc.gov))

[22] NEA/CSNI/R(2016)12. Probabilistic Structural Integrity of a Pressurised Water Reactor Pressure Vessel (PROSIR). Final Report, December 2016.

[23] P. T. William, et al., Fracture Analysis of Vessels – Oak Ridge FAVOR, v16.1, Computer Code: Theory and Implementation of Algorithms, Methods, and Correlations, ORNL/LTR-2016/309, 2016.

[24] B. R. Bass, P. T. William, CAPAL (Code for Advanced PTS Analysis for Long-Term Operation of RPVs) Ver. 23.3: User's Guide, OCI/ 2023/05-REV 0, OCI - Oakridge Consulting International, Inc., Oak Ridge, Tennessee USA, 2023.

[25] EriksonKirk, M.T., Dickson, T.L. "Recommended Screening Limits for Pressurized Thermal Shock (PTS)," NUREG-1874, 2010.

[26] https://en.wikipedia.org/wiki/Truncated_normal_distribution

[27] B. R. Bass, P. T. William, P. Dillström, R. Tiete, S. Blasset, and V. Pistora. Probabilistic fracture mechanics framework for the APAL project. PVP2024-121814. Proceedings of the ASME Pressure Vessels & Piping Conference, Bellevue, Washington, USA, 2024.